THE SYNTHESIS AND COORDINATION CHEMISTRY OF BULKY β-TRIKETIMINES AND APPLICATION OF THEIR NICKEL(II) DERIVATIVES AS ETHYLENE POLYMERISATION CATALYSTS

A thesis submitted to the University of Manchester for the degree of Doctor of Philosophy in the Faculty of Engineering and Physical Sciences

2010

ANDREW JOLLEYS

SCHOOL OF CHEMISTRY

Contents

Abstract

The University of Manchester
Andrew Jolleys
Doctor of Philosophy

The Synthesis and Coordination Chemistry of Bulky β-Triketimines and Application of their Nickel(II) Derivatives as Ethylene Polymerisation Catalysts

December 2010

The reaction of imidoyl chlorides **IMC$^{1-9}$** with lithium β-diketiminates **Li(BDK^{x})** (**x** = **^{i}Pr, ^{i}Pr$_2$, ^{t}Bu, Me$_3$, ^{i}Pr$_2$/OMe**) yields β-triketimines **L$^{1-16}$** which represent a new class of facially-coordinating neutral tridentate nitrogen ligands. The synthetic route is highly modular, allowing for wide variation of substitution patterns and thus fine control over the steric demands of the ligands. In all but two examples (**L^{11}** and **L^{12}**) the β-triketimines exist in solution either solely as their enamine-diimine tautomers, or as equilibrium mixtures of the two. The processes of solution-phase equilibration have been studied by NMR spectroscopy. The molecular structures of **L^{1}**, **L^{10}** and **L^{11}** are presented, and for each case a single differing tautomer or isomer is observed exclusively. The majority of the ligands yield ***fac*-(L)M(CO)$_3$** adducts upon reaction with group 6 metal carbonyls, except in cases of extreme steric bulk. The β-triketimines are relatively weak σ-donors, as determined by the CO stretching frequencies in **(L)M(CO)$_3$**. The molecular structures of the isomorphous pair **(L^{1})M(CO)$_3$** (M = Cr, Mo) reveal porous infinite network arrangements generated by aryl-aryl and CH---OC interactions. The direct reaction of β-triketimines with $ZnCl_2$ in most cases gives **[(L)ZnCl]$_2$[Zn$_2$Cl$_6$]** complexes, whilst in the presence of either $NaBAr^F_4$ or AgOTf the corresponding **[(L)ZnCl][BAr$^F_4$]** and **[(L)ZnCl][OTf]** species are obtained. The complexes invariably feature four-coordinate, cationic zinc centres, except in the case of **[(η^4-L^{16})ZnCl][BAr$^F_4$]** where a five-coordinate complex is formed by additional coordination of a single ligand methoxy group. The reaction of **[(L)ZnCl][BAr$^F_4$]** with TlOEt yielded not the desired zinc alkoxides, but novel **[(L)Tl][BAr$^F_4$]** complexes, the solid-state structures of which display thallophilic interactions. The direct reaction of **L^{8}** and **L$^{10-12}$** with $NiBr_2$(DME) gives the corresponding four-coordinate **[(L)NiBr]$_2$[NiBr$_4$]** complexes, whereas the products obtained with weakly-coordinating anions are dependent on the ligand bulk and the size of the anion. With the large $BAr^F_4^-$ ion the formation of the five-coordinate dimeric **[{(L)Ni(μ-Br)}$_2$][BAr$^F_4$]$_2$** (**L** = **L^{1}**, **L^{3}**, **L^{5}**, **L^{7}**, **L^{8}**, **L^{12}**) is strongly favoured, except for the bulkiest ligands where the four-coordinate **[(L)NiBr][BAr$^F_4$]** (**L** = **L^{10}**, **L^{11}**) are obtained. The smaller triflate ion generally favours the formation of **[(L)NiBr][OTf]** (**L^{1}**, **L^{8}**, **L$^{10-12}$**) except in the case of **[{(L)Ni(μ-Br)}$_2$][OTf]$_2$** (**L** = **L^{3}**, **L^{5}**). **L^{15}** and **L^{16}** act invariably as tetradentate donors to Ni(II), yielding the five-coordinate **[(η^4-L)NiBr][X]** (**X** = **BAr$^F_4$**, **OTf**) and **[(η^4-L^{16})NiBr]$_2$[NiBr$_4$]**. The very bulky **L^{6}** coordinates in a bidentate mode to Ni(II), giving the four-coordinate **[(η^2-L^{6})NiBr(THF)][BAr$^F_4$]** and **(η^2-L^{6})NiBr$_2$**. **[{(L)Ni(μ-Br)}$_2$][BAr$^F_4$]$_2$** (**L** = **L^{3}**, **L^{5}**, **L^{7}**), **[{(L)Ni(μ-Br)}$_2$][OTf]$_2$** (**L** = **L^{3}**, **L^{5}**), **[(η^2-L^{6})NiBr(THF)][BAr$^F_4$]** and **(η^2-L^{6})NiBr$_2$** show moderate catalytic activity for the polymerisation of ethylene in combination with MAO. All other complexes tested are inactive, either due to steric factors or the inability of certain β-triketimines to support catalytically active square-planar Ni(II) species. A proposed mechanism for catalyst activation is presented. Elastomeric polyethylene of very low crystallinity is obtained, with branching rates in the range 43-84 branches per 1000 C. ^{13}C NMR spectroscopy reveals the presence of all short-chain branches from methyl to hexyl, as well as longer branches and pairs of branches.

Declaration

No portion of the work referred to in the thesis has been submitted in support of an application for another degree or qualification of this or any other university or other institute of learning.

Copyright

Acknowledgements

I would like to thank first and foremost my supervisor, Dr. Frank Mair, for giving me the opportunity to undertake this research, and for the boundless assistance, encouragement and highly informative discussions he has provided. I have been very fortunate to work for someone who is always willing to listen and offer advice, no matter how busy he is, and for this I am extremely grateful. And thanks for putting up with me when things went a little awry towards the end!

I would also like to thank Drs. Chris Muryn and Robin Pritchard for instructing me in the ways of X-ray crystallography, Dr Madeleine Helliwell for solving a fiendishly large crystal structure, and Mr Martin Jennings for carrying out the DSC measurements.

My thanks go to all the people who have made the last four-and-a-half years a thoroughly enjoyable experience, in particular anyone who has ever worked in offices 1.075 and 3.08.

I would like to thank all of my friends from outside of university (especially the Brothers Gillespie), my mum Aileen and my brother Matthew.

Finally, I would like to thank the most special person in my life, Siân, without whose love, kindness and support I would not be where I am today.

List of Abbreviations

acac	acetylacetonate
Ar	aryl
BAr^F_4	tetrakis(3,5-bis(trifluoromethyl)phenyl)borate
BIAN	bis(imino)acenaphthene
bipy	bipyridyl
BDK	β-diketiminate
Bzd-Tach	*cis*,*cis*-1,3,5-tris((*E*)-benzylideneamino)cyclohexane
CFSE	Crystal Field Stabilisation Energy
dbc	3,5-di-*tert*-butylcatecholate
DCM	dichloromethane
dien	diethylenetriamine
DME	1,2-dimethoxyethane
DMF	*N,N*-dimethylformamide
DMSO	dimethylsulfoxide
DSC	Differential Scanning Calorimetry
en	ethylenediamine
ESI	Electrospray Ionisation
Et_2O	diethyl ether
HBDK	neutral β-iminoenamine/β-diketimine
HDPE	High-Density Polyethylene
Him	imidazole
Hpz	pyrazole
IMC	imidoyl chloride
LDPE	Low-Density Polyethylene
LLDPE	Linear Low-Density Polyethylene
MALDI	Matrix-Assisted Laser Desorption Ionisation

MAO	methylaluminoxane
Mes	mesityl (2,4,6-trimethylphenyl)
MLCT	Metal to Ligand Charge Transfer
MMAO	modified methylaluminoxane (obtained by partial hydrolysis of a mixture of trimethylaluminium (70%) and triisobutylaluminium (30%); alkane soluble)
NMR	Nuclear Magnetic Resonance
OTf	triflate (trifluoromethanesulfonate)
Pro-Tach	*cis*,*cis*-1,3,5-tris((*E*,*E*)-phenylpropenylideneamino)cyclohexane
pz	pyrazolate
Tach	*cis*,*cis*-1,3,5-triaminocyclohexane
terpy	2,2′:6′,2″-terpyridine
Tbt	tris(1,2,3-benzotriazol-1-yl)borate
THF	tetrahydrofuran
θ_T	aryl/imine interplanar torsion angle
^{2}Tim	tris(imidazol-2-yl)methane
^{4}Tim	tris(imidazol-4-yl)methane
^{2}Tip	tris(imidazol-2-yl)phosphine
^{4}Tip	tris(imidazol-4-yl)phosphine
^{4}Tipo	tris(imidazol-4-yl)phosphine oxide
Tm	tris(2-thioimidazol-3-yl)borate
T_m	temperature of melting
Tob	tris(oxazolin-2-yl)borate
TOF	Turnover Frequency
Tom	tris(oxazolin-2-yl)methane
Tp	tris(pyrazolyl)borate
Tpa	tris(pyrazolyl)aluminate
Tpg	tris(pyrazolyl)gallate

Tpm	tris(pyrazolyl)methane
Tpms	tris(pyrazolyl)methanesulfonate
Tpp	tris(pyrazolyl)phosphine
Tppo	tris(pyrazolyl)phosphine oxide
Tps	tris(pyrazolyl)silane
Ttz	tris(1,2,4-triazol-1-yl)borate
X_c	crystallinity

Key to β-Triketimine Ligands

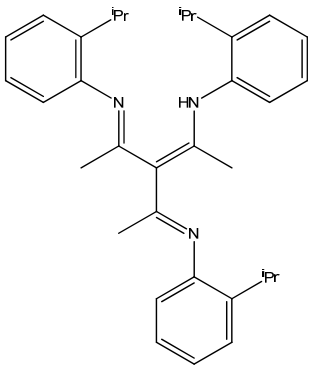

L[1]

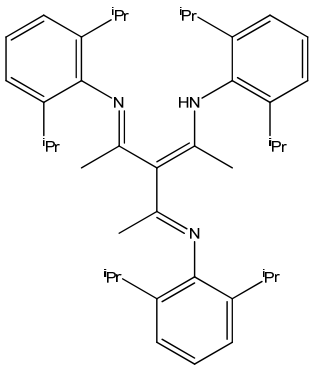

L[2]

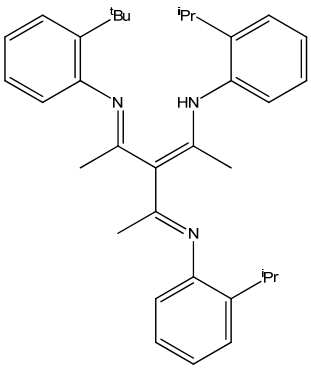

L[3]

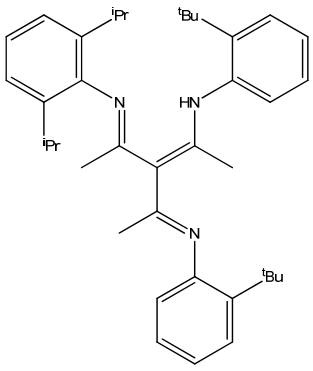

L[4]

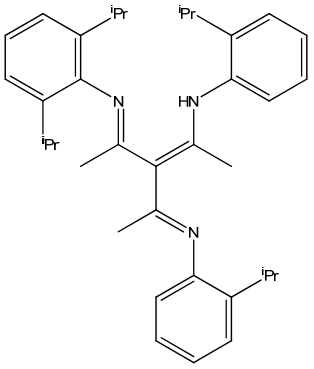

L[5]

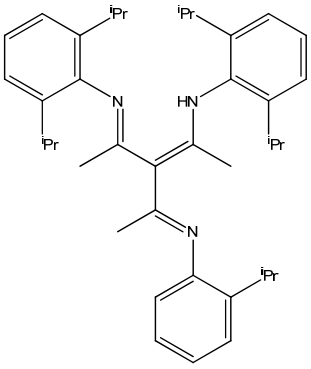

L[6]

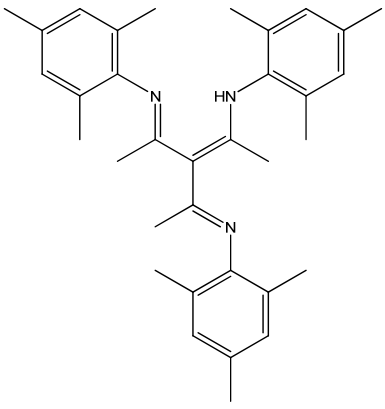

L[7]

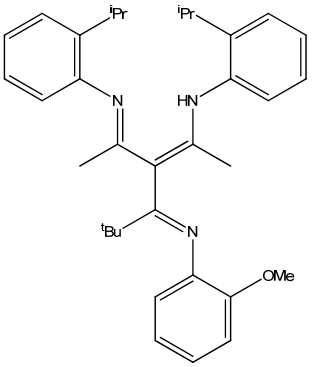

L[8]

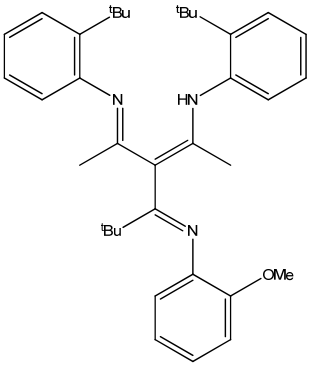

L[9]

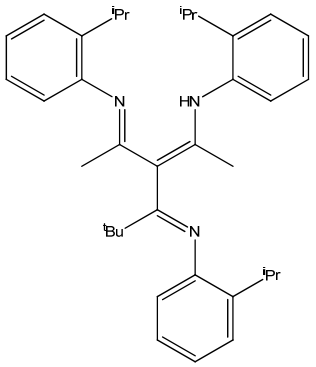

L^{10}

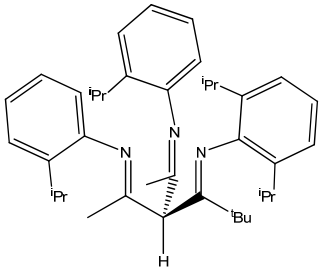

L^{11}

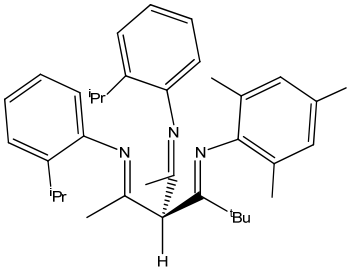

L^{12}

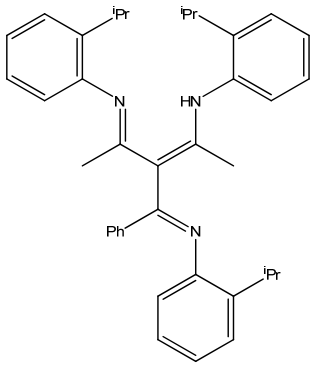

L^{13}

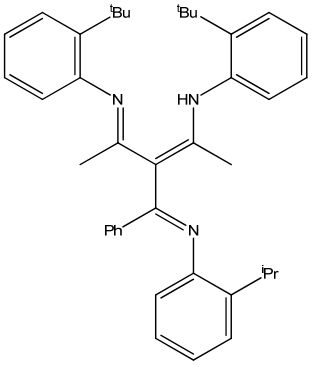

L^{14}

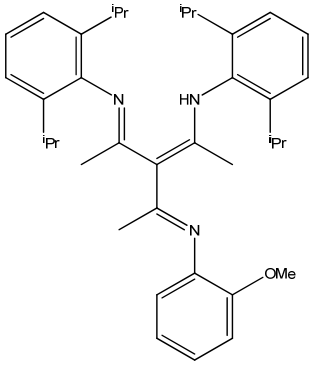

L^{15}

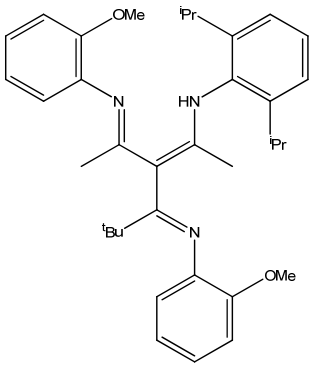

L^{16}

1. Introduction

1.1 General Introduction

The development of new ligand systems is an essential driving force behind novel discoveries in coordination chemistry. In particular, the use of chelating ligands with large, sterically demanding substituent groups will often allow for the preparation of metal complexes of low coordination number, an attribute which in turn is likely to yield interesting reactive properties such as activity towards both catalytic and stoichiometric transformations, as well as the activation of normally inert small molecules such as N_2. Bulky chelating ligands may also be used to stabilise highly reactive species, such as metal-dioxygen adducts and complexes of metals in unusually low formal oxidation states (Zn^I, Mg^I, Ga^I, M^0 etc.; M = transition element), as well as allowing for the isolation of complexes featuring relatively rare coordination environments, for example transition metals in a three-coordinate, planar geometry. In all instances the presence of large, sterically encumbering moieties in close proximity to the donor atoms is paramount to the aforementioned properties.

1.2 Polydentate Nitrogen Ligands

Metal complexes of chelating nitrogen donor ligands, the simplest such ligand being ethylenediamine, have been known for over 100 years.[1] This, along with other simple bidentate nitrogen ligands such as 1,2-phenylenediamine, 2,2′-bipyridine and phenanthroline, as well as tridentate chelators such as diethylenetriamine and 2,2′:6′,2″-terpyridine, have been used to form innumerable complexes with the vast majority of metallic elements. However, the lack of steric bulk provided by these unsubstituted ligand systems offers little or no control over the coordination number of the obtained complexes. Instead, this is determined by the nature of the metal centre, and also by the nature of any other ancillary ligands. As such, the overwhelming preference of the majority of first-row d-block metal ions is for the formation of octahedral tris- or bis-chelates such as $[M(en)_3]^{n+}$ or $[M(terpy)_2]^{n+}$. Bidentate nitrogen ligands with imine donor functionalities, specifically the α-diimines (**1**, also known as diazadienes), and β-iminoenamines (**2**, usually found coordinated as their monoanionic β-diiminate derivatives) have been known since 1951[2] and 1968[3] respectively.

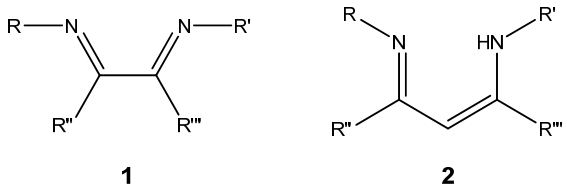

Figure 1.1 Generic structures of free α-diimines (1) and β-iminoenamines (2) (R, R′, R″, R‴ = e.g. H, aryl, 1° alkyl, 2° alkyl, 3° alkyl, trialkylsilyl etc.)

Though there are a few examples reported prior to the mid-1990s of both classes of ligand being used to prepare low-coordinate (<6) first-row transition metal complexes (for example **3**,[4] **4**[5] and **5**[6]), the majority of other such complexes are either organometallic, zerovalent or homoleptic derivatives (e.g. **6**,[7] **7**[8] and **8**[3,9] respectively), and these can reasonably be regarded as simple curiosities.

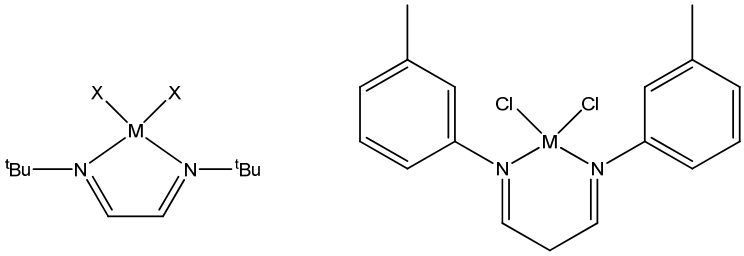

Figure 1.2 Low-coordinate metal-halide derivatives of α-diimines (3, 4) and β-iminoenamines (5)

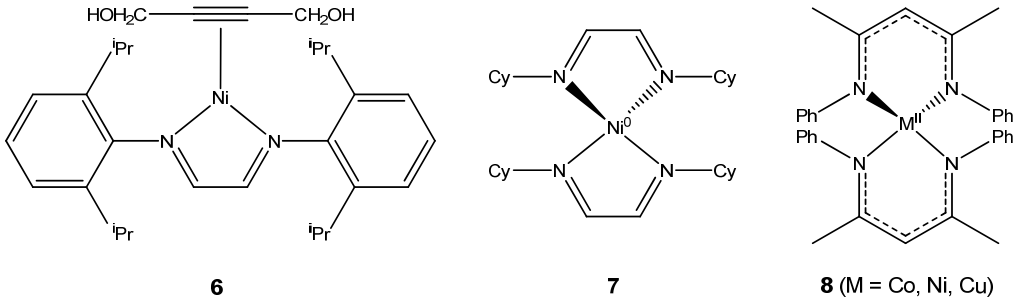

Figure 1.3 Organometallic (6) and zerovalent (7) derivatives of α-diimines; homoleptic β-iminoenamine complexes (8)

In a demonstration of the vast importance of ligand steric bulk with respect to the development of new coordination chemistry, these two ligand classes each experienced an explosion in research activity following the publication of two seminal independent reports, both of which were concerned with the application of nickel(II) complexes in olefin polymerisation catalysis. The first,[10] published by Brookhart and co-workers in 1995, described the preparation of a nickel dibromide complex (**9**) of the very bulky, strongly π-

accepting ligand 1,2-bis(2,6-diisopropylphenylimino)acenaphthene (BIAN^{iPr2}), the synthesis of which had been reported the previous year by Elsevier *et al.*[11] The second,[12] published in 1997 by Feldman *et al.* described the synthesis of 2-(2,6-diisopropyl)phenylamino-4-(2,6-diisopropyl)phenyliminopent-2-ene (HBDK^{iPr2}) and the preparation of its nickel dibromide derivative (**10**). It should be noted here that whilst free HBDK^{iPr2} exists solely as the β-iminoenamine isomer, upon coordination to a metal centre it tautomerises to the β-diimine form. In the vast majority of subsequently reported complexes the HBDK^{iPr2} ligand has actually been employed as its monodeprotonated β-diketiminate congener (BDK^{iPr2}), the first complex of which was a potassium derivative (**11**) described by Mair *et al.* in 1998.[13] To further illustrate the impact of the two independent publications by Feldman and Mair, 89% of the reports regarding β-diiminate/β-diimine complexes in the scientific literature were published post-1997.[14] Metal complexes of β-diketiminates and their synthetic elaboration to compounds with an modified ligand framework will be discussed further in **chapter 2**, whereas nickel derivatives of α-diimines will be discussed in **chapter 4**.

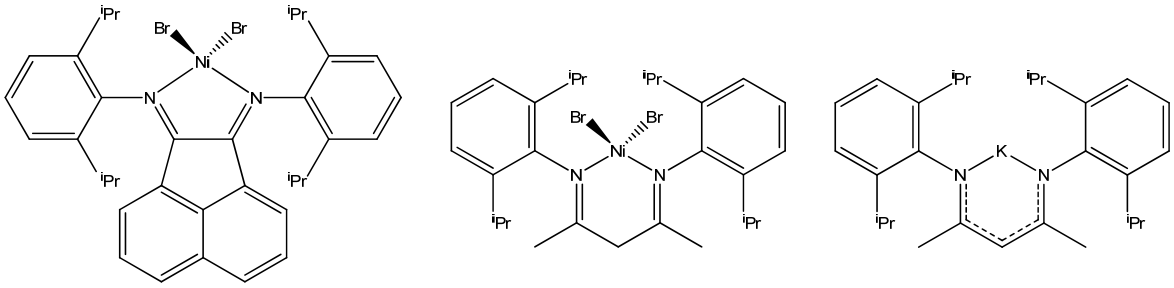

9 **10** **11**

Figure 1.4 Nickel dibromide derivatives of BIAN^{iPr2} (9) and HBDK^{iPr2} (10); potassium complex of BDK^{iPr2} (11)

The remainder of this introductory chapter shall focus on tripodal trinitrogen ligands. Firstly, the coordination chemistry of the tris(pyrazolyl)borates, which are by far the most widely studied tripodal nitrogen ligands, will be reviewed. There then follows a discussion of the general characteristics of tripodal ligands, with other such ligands reviewed in turn, in order to place in context the following chapters which introduce a new member of this family, the β-triketimines.

1.3 Tris(pyrazolyl)borates

The monoanionic tris(pyrazolyl)borates, first introduced by Trofimenko in 1966,[15] have a molecular framework which consists of three pyrazolyl moieties bound to a central B-H unit (**12**). These ligands have found widespread application in coordination chemistry, forming stable complexes with the majority of metal (and some non-metal) centres. Due to their relatively low steric bulk, the parent ligand hydrotris(pyrazolyl)borate (Tp) and its slightly more bulky derivative hydrotris(3,5-dimethylpyrazolyl)borate (Tp*) usually favour the formation of homoleptic, octahedral bis-Tp^x ('sandwich') complexes (**13**) with the majority of the first-row d-block metals. By inspecting the mode of coordination of the three pyrazolyl rings, it is easy to see why ligands of this type have been christened 'scorpionates', if one considers two of the pyrazolyl donors as 'claws' and the other as the 'sting'. Scorpionate chemistry has been subject to a number of comprehensive reviews; this review shall seek to update these, whilst still including many of the most important achievements.[16]

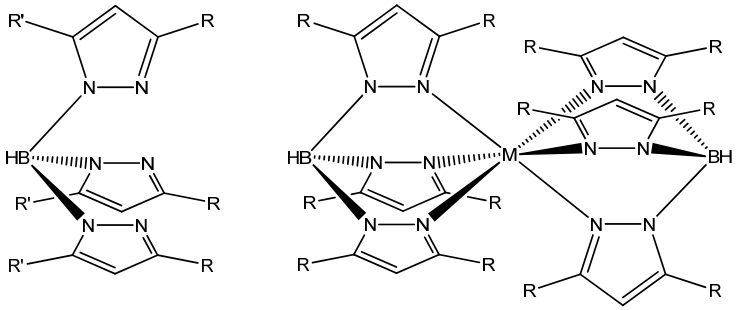

12 **13**

Figure 1.5 Generic structure of 3,5-disubstituted tris(pyrazolyl)borate ligands (12); sandwich complexes (13) of Tp (R = H) and Tp* (R = Me)

Due to their preference for higher oxidation states, mono-ligand complexes of Tp and Tp* are more common for the earlier first-row transition metals, particularly Ti and V, though these are usually six-coordinate species such as $(Tp^*)TiCl_3$,[17] $(Tp^*)VOCl_2$[18] and $(Tp)CrCl_2(THF)$.[19] A few sandwich complexes such as $(Tp)_2Ti$,[20] $(Tp)_2V$[21] and $(Tp)_2Cr$[22] are known but show high reactivity due to the relative instability of the +2 oxidation state; unsurprisingly the Cr(III) derivative $[(Tp)_2Cr][PF_6]$ shows much higher stability.[23] For the remainder of the first-row d-block metals, the high relative stability of the +2 oxidation state (and the +3 oxidation state for the elements Cr-Co) means that octahedral sandwich complexes of general formula $[(Tp)_2M]^{n+}$ (n = 0,1) are usually formed with the ligands Tp

and Tp*. Sandwich complexes of Mn(IV) such as $[(Tp)^*_2Mn][ClO_4]_2$ are also known, the octahedral d^3 electron configuration likely being a contributing factor in their formation.[24]

Coordination numbers lower than six are rare for first-row complexes of Tp and Tp*, except in the case of Cu(I) for which the inherent nature of the metal ion favours the formation of four-coordinate complexes such as (Tp)Cu(CO),[25] $(Tp)Cu(PPh_3)$[26] and $K[(Tp^*)Cu(SC_6H_4\text{-}4\text{-}NO_2)]$.[27] Examples of other four-coordinate derivatives of Tp* include $(Tp^*)Co(SR)$ ($R = C_6F_5$, 2,6-$Me_2C_6H_3$),[28] $(Tp^*)ZnX$ (X = Cl, OAc)[29] and $(Tp^*)NiX$ (X = Cl, Br).[30] Monomeric five-coordinate derivatives of Tp and Tp* are similarly uncommon; some structurally characterised examples include $(Tp)Zn(\eta^2\text{-}NO_3)$,[31] $(Tp^*)Cu(\eta^2\text{-}NO_2)$,[32] $(Tp^*)Ni(\eta^2\text{-}OAc)$[33] and $[NEt_4][(Tp^*)M(CN)_2]$ (M = Cr, Co, Ni).[34] Somewhat more common are bridged five-coordinate dimeric species, such as $\{(Tp)Cu(\mu\text{-}X)\}_2$ (X = Cl, N_3),[35] $\{(Tp^*)Cu(\mu\text{-}OH)\}_2$,[36] $\{(Tp^*)Ni(\mu\text{-}O_2P(OR)_2)\}_2$ (R = Me, Ph)[37] and $\{(Tp^*)Cu(\mu\text{-}1,2\text{-}pz)\}_2$.[38] The aforementioned $\{(Tp^*)Cu(\mu\text{-}OH)\}_2$ reacts with H_2O_2 to give the side-on peroxo-bridged species $\{(Tp^*)Cu\}_2(\mu\text{-}\eta^2\text{:}\eta^2\text{-}O_2)$ (**14**), which is a synthetic model for the oxidised form of the dioxygen transport protein haemocyanin.[36] However, in this case the low bulk of the Tp* ligand precluded crystallographic characterisation of this complex owing to its very high reactivity. Monomeric octahedral non-sandwich complexes of Tp and Tp* with the later d-block metals are usually restricted to organometallic species such as $(Tp)Mn(CO)_3$,[39] or complexes of strong-field ligands such as $[NEt_4][(Tp^*)Fe(CN)_3]$.[40] There are a few exceptions however, an example being $(Tp^*)Ni(\eta^2\text{-}NO_2)(MeOH)$.[41] Dinuclear six-coordinate derivatives of Tp are numerous, particularly for Mn and Fe, and complexes of the general formula $\{(Tp)M^{III}\}_2(\mu\text{-}O_2CR)_2(\mu\text{-}O)$ (M = Fe (**15**), Mn (**16**)), first prepared by Lippard and colleagues, have been widely studied as synthetic models for the active sites of dinuclear metalloproteins such as haemerythrin (Fe) and manganese catalase.[42]

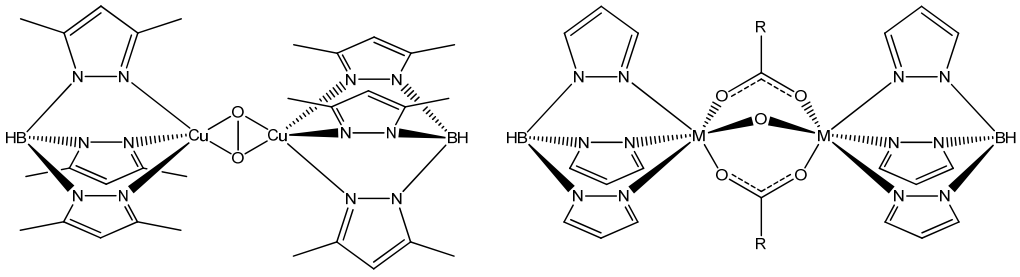

14

15 (M = Fe, R = H, Me, Et, Ph);
16 (M = Mn, R = H, Me, Et)

Figure 1.6 Structures of $\{(Tp^*)Cu\}_2(\mu\text{-}\eta^2\text{:}\eta^2\text{-}O_2)$ (14) and $\{(Tp)M^{III}\}_2(\mu\text{-}O_2CR)_2(\mu\text{-}O)$ (15, 16)

1.4 Complexes of Sterically Bulky Tris(pyrazolyl)borate Ligands

The steric demands of tris(pyrazolyl)borate ligands can be varied widely by the presence of substituent groups on the pyrazolyl rings, in particular those at the 3-position. The first Tp ligands to feature sterically bulky substituents at the 3-position were hydrotris(3-*tert*-butylpyrazolyl)borate (Tp^{tBu}) and hydrotris(3-phenylpyrazolyl)borate (Tp^{Ph}), cobalt(II) complexes of which were reported in 1986 by Thompson *et al.* Due to the very high steric demand of Tp^{tBu}, complexation to $Co(NCS)_2$ in THF allows only for formation of the tetrahedral complex (Tp^{tBu})Co(NCS) (**17**), whereas the less bulky Tp^{Ph} yields the five-coordinate (Tp^{Ph})Co(NCS)(THF) (**18**). In the former case, the formation of a bis-Tp^{tBu} adduct is extremely disfavoured due to the very large steric clash which would result between the *tert*-butyl groups of the two ligand molecules in such a complex.[43]

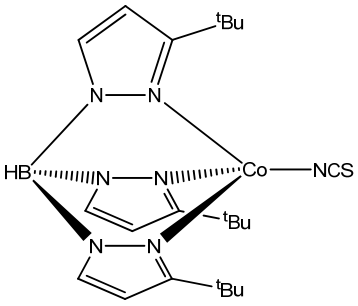

17

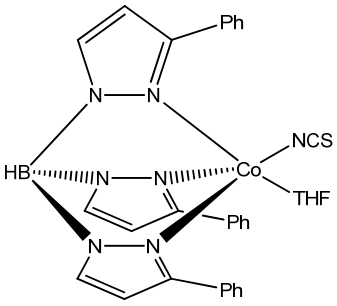

18

Figure 1.7 Structures of (Tp^{tBu})Co(NCS) (17) and (Tp^{Ph})Co(NCS)(THF) (18)

1.4.1 Complexes of Tp^{tBu}

The large steric bulk of the Tp^{tBu} ligand was also employed to prepare a whole series of tetrahedral (Tp^{tBu})MX (M = Mn, Fe, Co, Ni, Cu, X = Cl; M = Co, Ni, Zn, X = NCS, NCO, N_3; M = Cu, X = NCO) derivatives;[43(b),44] attempts to form three-coordinate cationic species via halide abstraction from the complexes (Tp^{tBu})MCl (M = Fe, Co) with $AgBF_4$ yielded only (Tp^{tBu})MF (M = Fe, Co) derivatives resulting due to fluoride abstraction from the BF_4^- ion.[44] Other novel compounds prepared using the Tp^{tBu} ligand include the first structurally characterised monomeric copper nitrosyl adduct, (Tp^{tBu})Cu(NO) (**19**),[45] and the five-coordinate nitrito-copper(II) species (Tp^{tBu})Cu(η^2-NO_2) (**20**).[46]

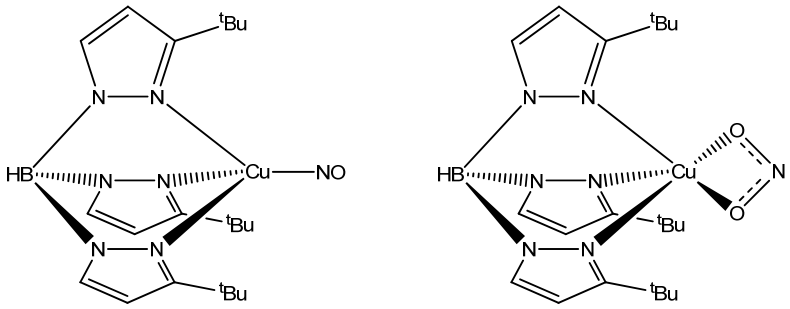

19 **20**

Figure 1.8 Structures of (Tp^{tBu})Cu(NO) (19) and (Tp^{tBu})Cu(η^2-NO_2)

Both of the aforementioned copper complexes can be regarded as structural models for intermediates in the reduction of NO_2^- to NO by bacterial nitrite reductase enzymes. In 1990 the groups of Parkin[47] and Vahrenkamp[48] independently reported the synthesis of the neutral monomeric methylzinc derivative (Tp^{tBu})ZnMe (**21a**); Parkin and co-workers then subsequently described the first example of a structurally characterised monomeric zinc hydride complex, (Tp^{tBu})ZnH (**21b**).[49] The Tp^{tBu}-derived ligand phenyltris(3-*tert*-butylpyrazolyl)borate ($PhTp^{tBu}$) was used to prepare the monomeric, tetrahedral derivatives ($PhTp^{tBu}$)FeMe (**22**) and ($PhTp^{tBu}$)Fe(CO) (**23**), both of which were structurally characterised. In comparison to the Tp^{tBu} ligand, the presence of the phenyl substituent on the central boron atom in $PhTp^{tBu}$ has a negligible effect on the steric requirements of the ligand. However, the researchers opted to use the $PhTp^{tBu}$ ligand so as to avoid any potential deleterious reactions of the B-H moiety with the highly reactive 14-electron methyliron fragment.[50] With the benefit of hindsight, this can now be regarded as overcautious, as the Tp^{tBu} ligand was subsequently used to prepare the analogous cobalt(II) derivative (Tp^{tBu})CoMe (**24**), which was also structurally characterised.[51]

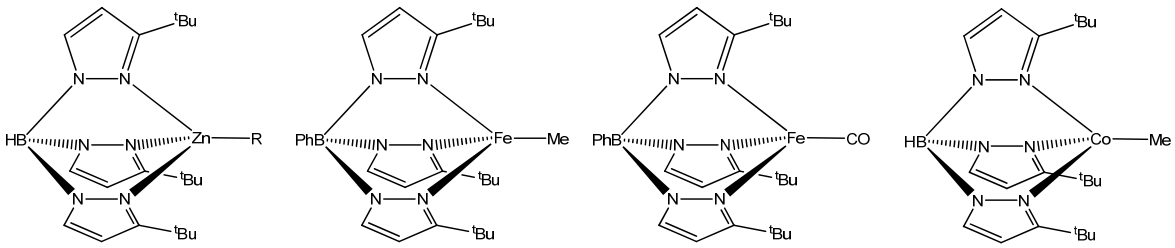

21a (R = Me);
21b (R = H) **22** **23** **24**

Figure 1.9 Structures of (Tp^{tBu})ZnR (21), ($PhTp^{tBu}$)FeMe (22), ($PhTp^{tBu}$)Fe(CO) (23) and (Tp^{tBu})CoMe (24)

1.4.2 Complexes of $Tp^{tBu,Me}$

The presence of additional substituent groups other than hydrogen at the 5-position of the pyrazolyl rings in Tp^x ligands causes a slight increase in steric bulk (in comparison to the analogous 5-unsubstituted ligands) due both to the repulsion between the 5-substituents and the central B-H unit, as well as that between the individual 5-substituents themselves. Additionally, the presence of substituent groups at the 5-position serves also to protect the ligand B-N bonds from degradative reaction, thus increasing the kinetic stability of derived metal complexes. This concept is exemplified by the coordination chemistry of hydrotris(3-*tert*-butyl-5-methylpyrazolyl)borate ($Tp^{tBu,Me}$), which was first reported in 1990 and used to prepare the dioxygen adduct $(Tp^{tBu,Me})Co(\eta^2\text{-}O_2)$ (**25**), the first example of a transition metal complex featuring a symmetrical, side-on bound superoxide ion. $(Tp^{tBu,Me})Co(\eta^2\text{-}O_2)$ was synthesised by addition of dioxygen to the cobalt(I) dinitrogen complex $(Tp^{tBu,Me})Co(N_2)$, itself prepared via magnesium reduction of the halide derivatives $(Tp^{tBu,Me})CoX$ (X = Cl, I) under an atmosphere of N_2.[52] Reaction of $(Tp^{tBu,Me})Co(N_2)$ with H_2O furnished the novel monomeric, four-coordinate cobalt(II) hydroxide $(Tp^{tBu,Me})CoOH$ (**26**),[52] though the molecular structure of the latter complex was not determined until 2003.[53] The structural nature of the dinitrogen adduct could not be determined crystallographically, but the related compound $\{(Tp^{Np})Co\}_2(\mu\text{-}\eta^1\text{:}\eta^{1'}\text{-}N_2)$ (**27**, Tp^{Np} = hydrotris(3-neopentylpyrazolyl)borate) was found to feature a dimeric arrangement of two four-coordinate cobalt(I) centres bridged by a single dinitrogen molecule.[54] The fact that Tp^{Np} is somewhat less bulky (the sandwich complexes $(Tp^{Np})_2M$ (M = Fe, Co, Ni) were isolated and structurally characterised for M = Ni)[55] than the $Tp^{tBu,R}$ ligands, yet provides a hydrophobic pocket which extends further from the coordinated metal centres, offers some explanation as to why this dimeric species is formed, rather than a monomeric N_2 adduct. The N-N stretching vibration in $\{(Tp^{Np})Co\}_2(\mu\text{-}\eta^1\text{:}\eta^{1'}\text{-}N_2)$ was found to be much less intense, and shifted to slightly higher frequency in comparison to that observed for $(Tp^{tBu,Me})Co(N_2)$, supporting the description of the latter species as a monomeric dinitrogen adduct.[54]

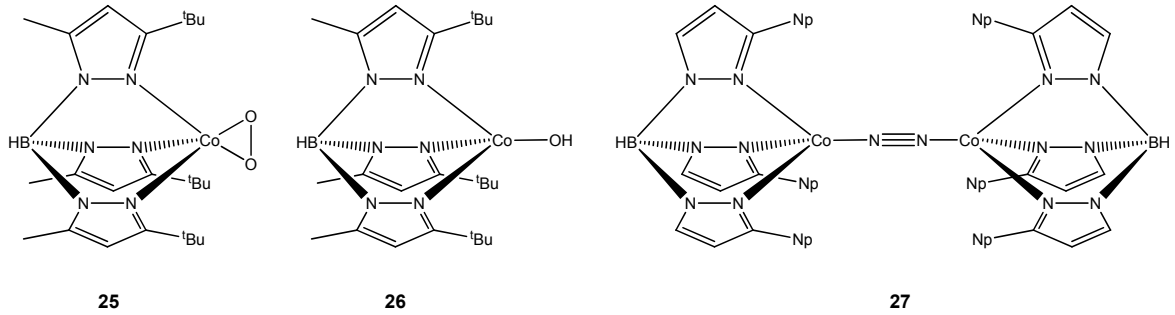

25 **26** **27**

Figure 1.10 Structures of $Tp^{tBu,Me}Co(\eta^2\text{-}O_2)$ (25), $Tp^{tBu,Me}CoOH$ (26) and $\{(Tp^{Np})Co\}_2(\mu\text{-}\eta^1\text{:}\eta^{1'}\text{-}N_2)$ (27)

Treatment of $(Tp^{tBu,Me})Co(N_2)$ with CO yielded $(Tp^{tBu,Me})Co(CO)$, which upon subsequent reduction with Mg metal gave the trimetallic magnesium(II)-dicobalt(0) species $\{(Tp^{tBu,Me}Co)(\mu\text{-}C,O\text{-}CO)\}_2Mg(THF)_4$ (**28**).[54] Treatment of $(Tp^{tBu,Me})CoI$ with organolithium reagents gave the series of cobalt(II) alkyls $Tp^{tBu,Me}CoR$ (**29a**, R = Me, Et, *n*-Bu), though unlike $(Tp^{tBu})CoMe$, none of these gave crystals suitable for X-ray diffraction. Also described in this report was the preparation of $(Tp^{tBu,Me})CoH$ (**29b**), formed by exposure of a hydrocarbon solution of $(Tp^{tBu,Me})Co(N_2)$ to H_2, as well as the cobalt(I) alkene adducts $(Tp^{tBu,Me})Co(C_2H_3R)$ (**30**, R = H, Me) which were prepared in an analogous manner by exposure of $(Tp^{tBu,Me})Co(N_2)$ to ethylene/propylene.[51]

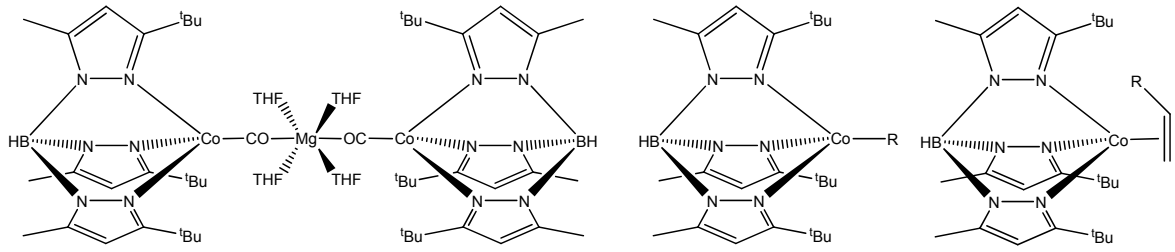

28 **29a** (R = Me, Et, ^{n}Bu); **29b** (R = H) **30** (R = H, Me)

Figure 1.11 Structures of $\{(Tp^{tBu,Me}Co)(\mu\text{-}C,O\text{-}CO)\}_2Mg(THF)_4$ (28), $Tp^{tBu,Me}CoR$ (29) and $(Tp^{tBu,Me})Co(C_2H_3R)$ (30)

Reaction of $(Tp^{tBu,Me})Co(N_2)$ with adamantyl azide furnished the cobalt(III) derivative $(Tp^{tBu,Me})Co(NAd)$ (**31**), which is one of only three structurally characterised imido-cobalt complexes reported to date. Thermal decomposition of this complex resulted in insertion of the imidoadamantyl moiety into a C-H bond of one of the ligand 3-*tert*-butyl groups, yielding a four-coordinate cobalt(I) amine complex (**32**) (**Scheme 1.1**).[56]

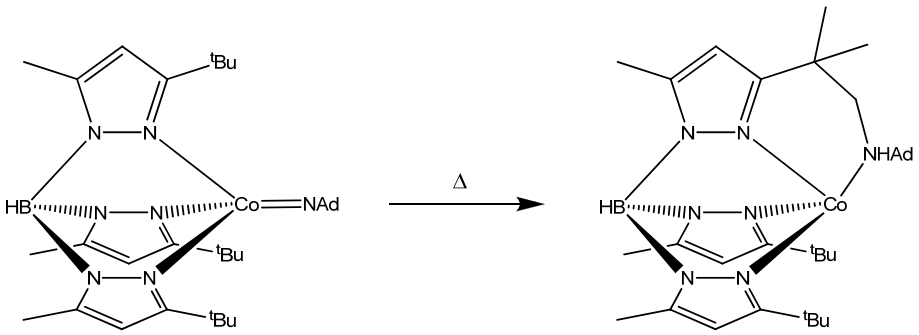

Scheme 1.1 Thermal decomposition of ($Tp^{tBu,Me}$)Co(NAd) (31)

The $Tp^{tBu,Me}$ ligand was also used to prepare the first structurally characterised monomeric four-coordinate zinc hydroxide complex, ($Tp^{tBu,Me}$)ZnOH (**33**).[57] The facile preparation of this stable complex illustrates the effectiveness of the 5-methyl substituents in preventing ligand degradation, as the preparation of the analogous Tp^{tBu} derivative had previously been attempted, yet the only product that could be isolated was the hydroxo-bridged species [{(3-*tert*-butylpyrazole)$_3$Zn}$_2$(μ-OH)][ClO_4]$_3$ resulting from decomposition of the Tp^{tBu} ligand.[48] ($Tp^{tBu,Me}$)ZnOH represents a highly effective structural model for the active site of the metalloenzyme carbonic anhydrase, which is responsible for the biocatalytic conversion of CO_2 to bicarbonate. The active site consists of a tetrahedral zinc ion bound by the imidazole donors of the three histidine residues, with the fourth coordination site occupied by a molecule of water, an arrangement which can be regarded as the inert or 'resting' state of the enzyme. Deprotonation of the coordinated water molecule under biological conditions gives the active hydroxo-zinc species, which reacts with CO_2 to produce a zinc bicarbonate species. The bicarbonate ion is then subsequently displaced by H_2O, thereby completing the catalytic cycle. Following exposure of ($Tp^{tBu,Me}$)ZnOH to an atmosphere of CO_2, it was possible to isolate and structurally characterise the dinuclear carbonate-bridged complex {($Tp^{tBu,Me}$)Zn}$_2$(μ-η^1:$\eta^{1'}$-CO_3) (**34**), which contains two four-coordinate zinc centres.[58] The intermediate bicarbonate complex was too unstable to be isolated but could be observed by IR spectroscopy.[59] Upon addition of H_2O to {($Tp^{tBu,Me}$)Zn}$_2$(μ-η^1:$\eta^{1'}$-CO_3), the starting hydroxo-complex is regenerated, concomitant with release of CO_2 (**scheme 1.2**).[58] Therefore, $Tp^{tBu,Me}$ZnOH can be regarded as not only an accurate *structural* model for carbonic anhydrase, but also as an accurate *functional* model which is able to replicate the reactivity and assumed catalytic cycle of the natural enzyme.

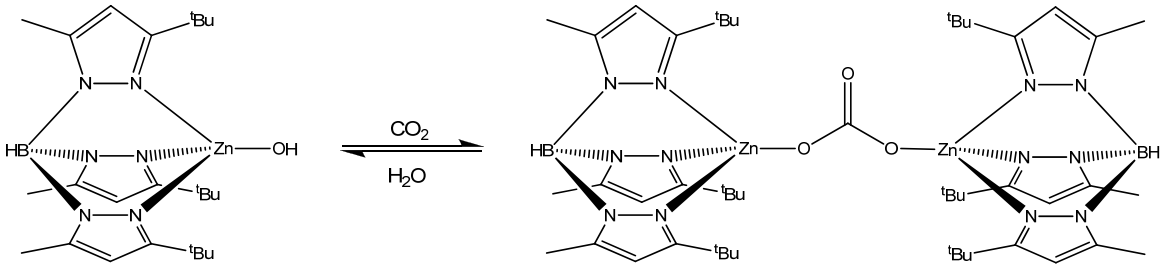

Scheme 1.2 Interconversion between ($Tp^{tBu,Me}$)ZnOH (33) and {($Tp^{tBu,Me}$)Zn}$_2$(μ-η^1:$\eta^{1'}$-CO_3) (34)

Although a species of the form $[LZn(OH_2)]^{n+}$ (L = tridentate ligand) remained elusive for some time, in 1999 Parkin and co-workers were able to isolate the cationic zinc-aqua complex $[(Tp^{tBu,Me})Zn(OH_2)][HOB(C_6F_5)_3]$ (**35**), which is stabilised by a hydrogen-bonding interaction between one hydrogen atom of the bound water molecule and the oxygen atom of the anion. As would be expected from the inactivity of the enzymatic aqua-complex, this species was also found to be completely unreactive towards CO_2. The hydrogen-bonding interaction observed in this complex mimics that seen in the structurally characterised enzyme, namely the interaction between the zinc-bound H_2O/OH and the hydroxyl moiety of a threonine residue.[53,60] The analogous cobalt(II) complex (**36**) was also prepared by the same researchers, and was found to show very similar properties to the zinc compound. This is concurrent with the fact that cobalt-substituted carbonic anhydrase shows similar activity to the natural zinc enzyme.[53] Zinc complexes of various Tp^x ligands and their application in the modelling of metalloenzyme active sites shall be discussed further in **chapter 3**.

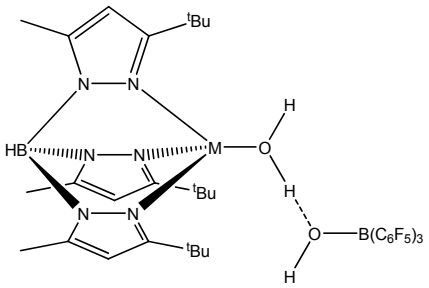

35 (M = Zn);
36 (M = Co)

Figure 1.12 Structure of $[(Tp^{tBu,Me})Zn(OH_2)][HOB(C_6F_5)_3]$ (35)

In 1997 Theopold and colleagues reported the synthesis of the four-coordinate chromium(II) complex ($Tp^{tBu,Me}$)CrCl, and its elaboration to the alkyl derivatives ($Tp^{tBu,Me}$)CrR (R = Et, Ph, CH_2SiMe_3) through reaction with the corresponding Grignard

reagents.[61] Rather than the expected tetrahedral geometry, all these compounds display a highly unusual '*cis*-divacant octahedral' geometry; that is, one formally derived from regular octahedral through removal of two *cis*-ligands. The same researchers were also successful in preparing and structurally characterising a number of interesting chromium-oxygen derivatives, such as the neutral oxo-chromium(IV) species ($Tp^{tBu,Me}$)CrO(OPh) (**38**), formed by dioxygen insertion in the Cr-C bond of ($Tp^{tBu,Me}$)CrPh (**37**) (**scheme 1.3**).[62]

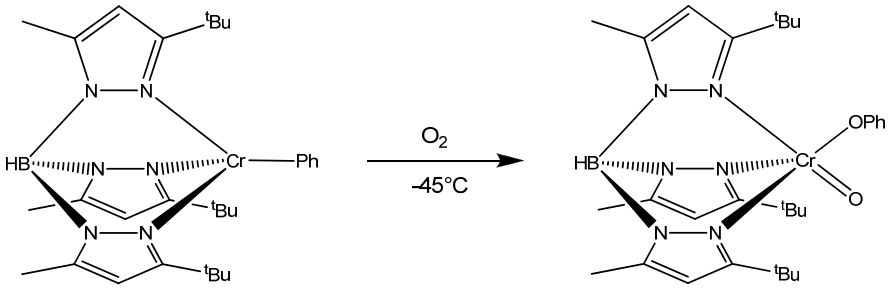

37 **38**

Scheme 1.3 Reaction of ($Tp^{tBu,Me}$)CrPh (37) with O_2

Treatment of ($Tp^{tBu,Me}$)CrCl($Hpz^{tBu,Me}$) (**39**) with sodium tetrakis(3,5-bis(trifluoromethyl)phenyl)borate ($NaBAr^F_4$) yielded [($Tp^{tBu,Me}$)Cr($Hpz^{tBu,Me}$)][BAr^F_4] (**40**), which upon exposure to O_2 in Et_2O solution at -78°C gave access to the first example of a structurally characterised side-on bound chromium(III) superoxide complex, [($Tp^{tBu,Me}$)Cr(η^2-O_2)($Hpz^{tBu,Me}$)][BAr^F_4] (**41**) (**scheme 1.4**).[63] The latter compound was subsequently shown to react with its precursor (**40**) in Et_2O at room temperature to furnish the hydroxide complex [($Tp^{tBu,Me}$)CrOH($Hpz^{tBu,Me}$)][BAr^F_4] (**42**), whereas direct reaction of **40** with PhIO in DCM gave the cationic oxo-chromium(IV) complex [($Tp^{tBu,Me}$)CrO($Hpz^{tBu,Me}$)][BAr^F_4] (**43**).[64] Many of the aforementioned chromium compounds are rare examples of 'true' five-coordinate d-block metal complexes of $Tp^{tBu,Me}$ (i.e. as opposed to those featuring small bidentate ancillary ligands such as O_2^-, AcO^- and NO_2^-).

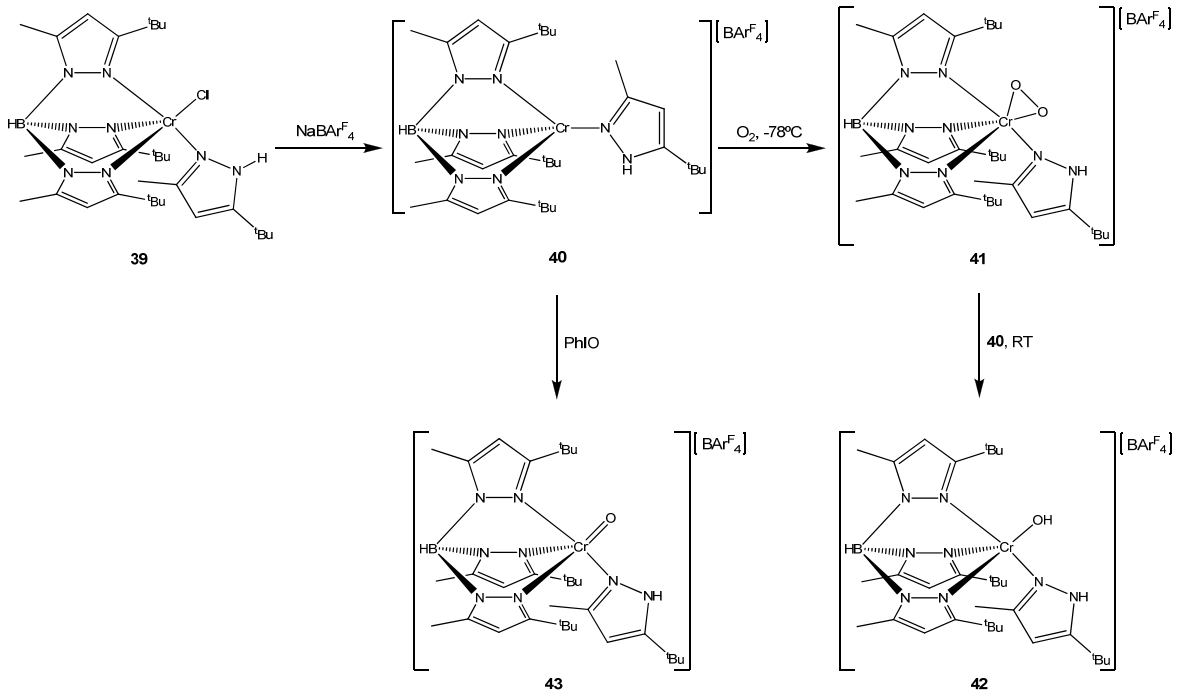

Scheme 1.4 Preparation of novel chromium-Tp^{tBu,Me} complexes

1.4.3 Complexes of Tp^{tBu,iPr}

An extreme of steric encumbrance is achieved with hydrotris(3-*tert*-butyl-5-isopropylpyrazolyl)borate (Tp^{tBu,iPr}), which has been used by Kitajima, Fujisawa, Moro-Oka and others to prepare a number of novel derivatives such as the first (and to date only) structurally characterised superoxo-copper(II) complex (Tp^{tBu,iPr})Cu(η^2-O$_2$) (**44**). This compound was prepared by direct addition of O$_2$ to the corresponding four-coordinate Cu(I)-DMF adduct and is a structural model for copper oxygenase enzymes that feature a monomeric active site, representing initial O$_2$ binding by the metalloenzyme before substrate oxidation occurs. The formation of a dimeric peroxo-bridged species as observed for other Tp^x ligands is, in this instance, disfavoured by the sheer magnitude of the ligand steric bulk.[65] A related compound is the monomeric (Tp^{tBu,iPr})CuOH (**45**), which is a rare example of a hydroxo-copper(II) complex of a tridentate ligand that eschews the formation of a dimeric {Cu(μ-OH)}$_2$ unit.[66] The tetrahedral alkylperoxo-complexes (Tp^{tBu,iPr})M(OOCMe$_2$Ph) (**46**, M = Mn(**a**)[67], Co(**b**)[68]) were prepared by reaction of the corresponding hydroxo-derivatives with cumyl hydroperoxide. Both complexes were structurally characterised, and represent the first alkylperoxo derivatives of Mn and Co in the +2 oxidation state. (Tp^{tBu,iPr})Mn(OOCMe$_2$Ph) remains to date the only alkylperoxo complex of manganese for which the molecular structure has been determined by X-ray

diffraction. These complexes decompose slowly at room temperature, and are relatively inert towards oxidation of substrates such as PPh_3.[67,68]

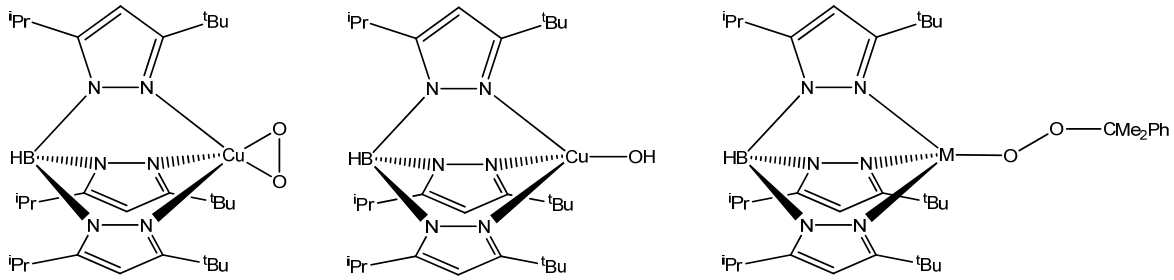

44 **45** **46a** (M = Mn); **46b** (M = Co)

Figure 1.13 Structures of ($Tp^{tBu,iPr}$)Cu(η^2-O_2) (44), ($Tp^{tBu,iPr}$)CuOH (45) and ($Tp^{tBu,iPr}$)M($OOCMe_2Ph$) (46)

The same researchers prepared a monomeric hydroxo-complex of iron(II) analogous to that described above for copper, by the treatment of ($Tp^{tBu,iPr}$)Fe(OAc) with aqueous NaOH. ($Tp^{tBu,iPr}$)FeOH was then further reacted with benzoylformic acid to give the benzoylformato-iron(II) complex ($Tp^{tBu,iPr}$)Fe(O_2CCOPh). This compound was found to display thermochromism, with a colourless tetrahedral form (**47a**) featuring a monodentate benzoylformate ligand isolated at 4°C. Upon cooling of a solution of ($Tp^{tBu,iPr}$)Fe(O_2CCOPh) to -78°C followed by warming to -20°C, a purple-blue trigonal-bipyramidal species (**47b**) was also obtained in which the benzoylformate anion was found to act as a bidentate chelating ligand, with the α-keto moiety acting as a donor in addition to the carboxylate oxygen. The former species can be considered a structural model for the active site of the enzyme soybean lipogenase, though rather than tetrahedral the coordination geometry of the enzymatic iron centre is described more accurately as the aforementioned *cis*-divacant octahedral. The trigonal-bipyramidal N_3O_2 coordination environment of the low-temperature species replicates that observed in the active site of iron superoxide dismutase. However, in the metalloenzyme the iron centre is coordinated by three histidine residues and a monodentate glutamate residue, with the fifth coordination site occupied by either a hydroxide ion or water molecule.[69] ($Tp^{tBu,iPr}$)Fe(OAc) and ($Tp^{tBu,iPr}$)FeOH were found to be unreactive towards O_2, whereas the reaction of ($Tp^{tBu,iPr}$)FeOH with alkyl hydroperoxides gave high-spin iron(III) alkylperoxo species which were stable enough to be characterised by various spectroscopic methods.[70]

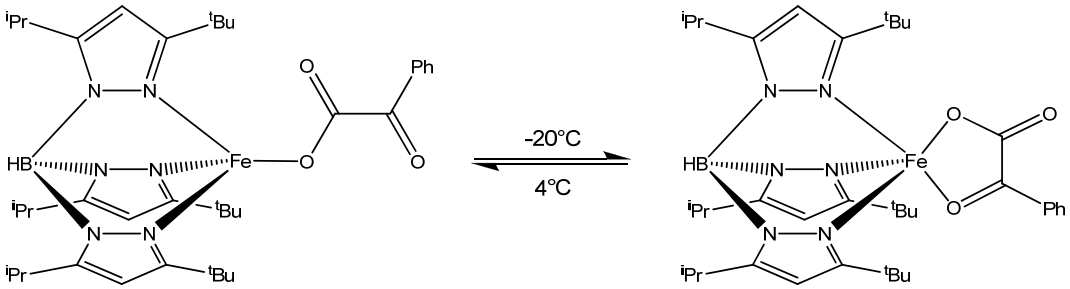

Figure 1.14 Thermochromic behaviour of $(Tp^{tBu,iPr})Fe(O_2CCOPh)$

The manganese(II) complexes $(Tp^{tBu,iPr})MnX$ (X = Br, Cl, NO_3) were found to show high catalytic activity towards the polymerisation of ethylene when activated with $Al^iBu_3/[Ph_3C][B(C_6F_5)_4]$. In particular, $(Tp^{tBu,iPr})MnCl$ gave an activity of 920 $kgmol^{-1}h^{-1}$, which was substantially higher than the activities observed for the bromo- and nitrato-anaologues, implying that the nature of the coordinated anions has an influence on the catalyst efficacy.[71] Though a number of other manganese(II) complexes of various Tp^x ligands have been screened for catalytic activity, they are all less active than $(Tp^{tBu,iPr})MnCl$.[72]

1.4.4 Complexes of Tp^{tBu2}

The ligand hydrotris(3,5-di-*tert*-butylpyrazoyl)borate (Tp^{tBu2}) is known, yet there is only a single report of it being used to form complexes of d-block metal ions, namely $(Tp^{tBu2})MI$ (M = Zn, Cd). The molecular structures of these complexes show that in both cases the Tp^{tBu2} ligand adopts a highly twisted conformation, with a large deviation from effective C_{3v} symmetry.[73] Aside from the thallium(I), potassium and caesium derivatives also described in the aforementioned paper, all other reports regarding the coordination chemistry of Tp^{tBu2} have been concerned with the preparation of indium and gallium derivatives such as $(Tp^{tBu2})M^I$ (M = Ga, In),[74] $(Tp^{tBu2})InI_2$[75] and $(Tp^{tBu2})GaE$ (E = S, Se, Te).[76]

1.4.5 Complexes of Tp^{iPr} and $Tp^{iPr,Me}$

Due to their overwhelming preference for the formation of four co-ordinate metal complexes, Tp^x ligands with 3-*tert*-butyl substituents have been described as 'tetrahedral enforcers'.[43(b)] 3-isopropyl substituted ligands are somewhat more flexible, being equally able to support four-, five- and six-coordinate complexes. For example, hydrotris(3-

isopropylpyrazolyl)borate (Tp^{iPr}) was used to prepare a series of tetrahedral (Tp^{iPr})MX (M = Co, Zn, X = NCS, NCO; M = Ni, X = NCO; M = Zn, X = N_3) complexes, as well as the five-coordinate dimeric {(Tp^{iPr})Ni(μ-*N,S*-NCS)}$_2$.[77] The sandwich complexes (Tp^{iPr})$_2$M (M = Fe, Co, Ni, Cu, Zn) were also prepared, but in the case of M = Fe, Co, Ni the Tp^{iPr} ligand was found to have undergone a structural rearrangement to its hydrobis(3-isopropylpyrazolyl)(5-isopropylpyrazolyl)borate (Tp^{iPr*}) isomer, giving only (Tp^{iPr*})$_2$M. For M = Cu and Zn, the products were found to be a mixture of (Tp^{iPr})$_2$M (**48a**) and (Tp^{iPr*})$_2$M (**49a**).[77(a)] This type of rearrangement reaction is relatively common for 3-monosubstitued Tp^x ligands, giving access to less sterically congested metal complexes. Indeed, similar behaviour was also observed for hydrotris(3-isopropyl-5-methylpyrazolyl)borate ($Tp^{iPr,Me}$), which is unsurprising when considering that, unlike Tp^{iPr}, the free $Tp^{iPr,Me}$ ligand could not be prepared in a regiochemically pure form. Instead, the crude ligand was found to consist of a mixture of $Tp^{iPr,Me}$ and hydrobis(3-isopropyl-5-methyl)(3-methyl-5-isopropyl)borate ($Tp^{iPr,Me*}$) in an approximately 4:1 ratio respectively. The desired products ($Tp^{iPr,Me}$)MX (M = Co, Ni, X = NCO; M = Co, Zn, X = NCS; M = Zn, X = N_3) and {($Tp^{iPr,Me}$)Ni(μ-*N,S*-NCS)}$_2$ could be isolated by fractional crystallisation, whereas the octahedral sandwich complexes existed as inseparable mixtures of ($Tp^{iPr,Me}$)$_2$M (**48b**) and ($Tp^{iPr,Me*}$)$_2$M (**49b**) (M = Fe, Co, Ni, Zn).[78]

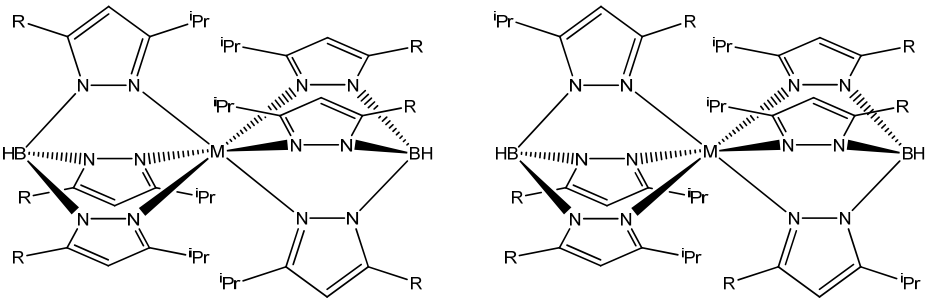

48a (R = H, M = Cu, Zn);
48b (R = Me, M = Fe, Co, Ni, Zn)

49a (R = H, M = Fe, Co, Ni, Cu, Zn);
49b (R = Me, M = Fe, Co, Ni, Zn)

Figure 1.15 Structures of complexes 48 and 49

Using an unusual 'inverse recrystallisation' procedure (i.e. cooling of a suspension to yield a solution followed by crystallisation on slow warming), the complex ($Tp^{iPr,Me}$)CoI (**50**) was obtained as a regiochemically pure material.[79] This complex was then used as a starting material for the preparation (**scheme 1.5**) of the spectroscopically characterised superoxo-adduct ($Tp^{iPr,Me}$)Co(η^2-O_2) (**52**) via the intermediate ($Tp^{iPr,Me}$)Co(CO) (**51**), in analogy to the chemistry described above regarding the $Tp^{tBu,Me}$ ligand. In contrast to this

however, treatment of the dinitrogen adduct $\{(Tp^{iPr,Me})Co\}_2(\mu\text{-}\eta^1\text{:}\eta^{1'}\text{-}N_2)$ with O_2 gave a transient species which decomposed rapidly via ligand hydrogen abstraction. Unlike the stable and structurally characterised $(Tp^{tBu,Me})Co(\eta^2\text{-}O_2)$, $(Tp^{iPr,Me})Co(\eta^2\text{-}O_2)$ decomposed rapidly in solution at room temperature giving the aforementioned unstable dimeric complex.[80] This illustrates the insufficient steric shielding of the highly reactive cobalt-superoxo adduct by the $Tp^{iPr,Me}$ ligand in comparison to the bulkier $Tp^{tBu,Me}$. Though it could be isolated as a solid material, single crystals of $(Tp^{iPr,Me})Co(\eta^2\text{-}O_2)$ could not be obtained due to its low stability in solution. However, from a low temperature solution it was possible to isolate crystals of the dimeric bis-(μ-superoxo) adduct $\{(Tp^{iPr,Me})Co(\mu\text{-}\eta^1\text{:}\eta^{1'}\text{-}O_2)\}_2$ (**53**).[81]

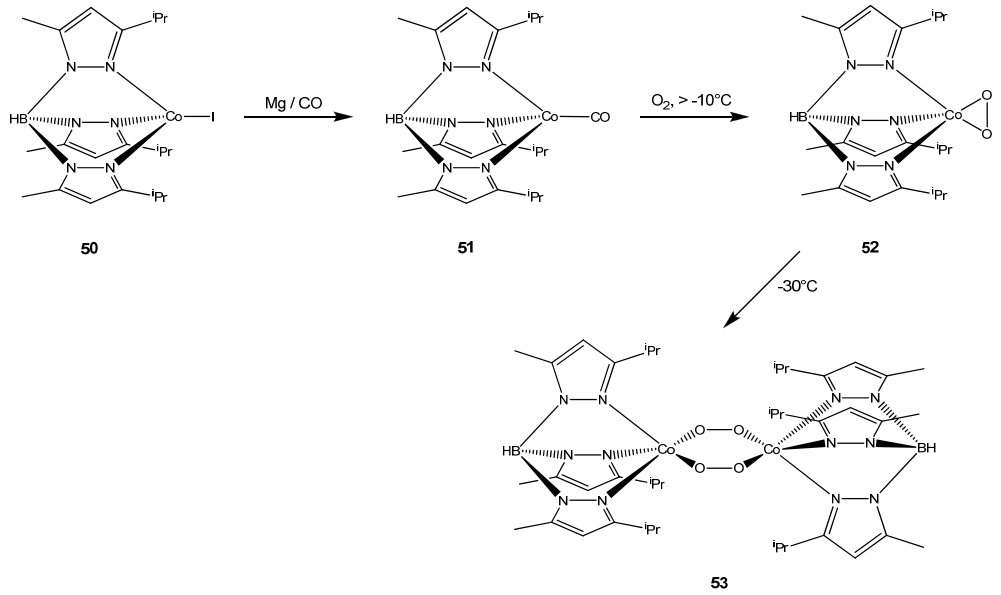

Scheme 1.5 Formation of Co(II)-dioxygen adducts

It should be noted that $\{(Tp^{iPr,Me})Co(\mu\text{-}\eta^1\text{:}\eta^{1'}\text{-}O_2)\}_2$ is the only structurally characterised dicobalt μ-O_2 complex reported to date in which the cobalt ions are less than six-coordinate, though the vast majority of other such examples are μ-peroxo complexes in which the cobalt atoms are in the +3 oxidation state, for which octahedral coordination is strongly favoured. Exposure of $\{(Tp^{iPr,Me})Co\}_2(\mu\text{-}\eta^1\text{:}\eta^{1'}\text{-}N_2)$ to a high pressure of CO gave the diamagnetic, square-pyramidal $(Tp^{iPr,Me})Co(CO)_2$, which was structurally characterised. In solution this species spontaneously loses CO, forming the paramagnetic tetrahedral $(Tp^{iPr,Me})Co(CO)$, while if excess CO is present in solution the two complexes are in equilibrium.[82]

In an attempt to prepare an imido-cobalt complex prior to the successful isolation of ($Tp^{tBu,Me}$)Co(NAd), {($Tp^{iPr,Me}$)Co}$_2$(μ-η^1:$\eta^{1'}$-N_2) (**54**) was reacted with trimethylsilylazide (**scheme 1.6**). However, the molecular structure of the reaction product revealed that one isopropyl group from each of two ligands had coupled to furnish a dinuclear cobalt(II) amido complex (**55**). Conversely, the reaction of ($Tp^{tBu,Me}$)Co(N_2) (**56**) with Me_3SiN_3 gave a monomeric cobalt(III) amido complex (**57**) in which a single monodeprotonated 3-*tert*-butyl group of the $Tp^{tBu,Me}$ ligand is also bound to the cobalt atom (**scheme 1.6**).[83] The fact that Me_3SiN_3 failed to yield imido-cobalt complexes, whereas the aforementioned ($Tp^{tBu,Me}$)Co(NAd) could be isolated illustrates the fact then when attempting to form such compounds, correct choice of substrate is as important as the choice of ligand.

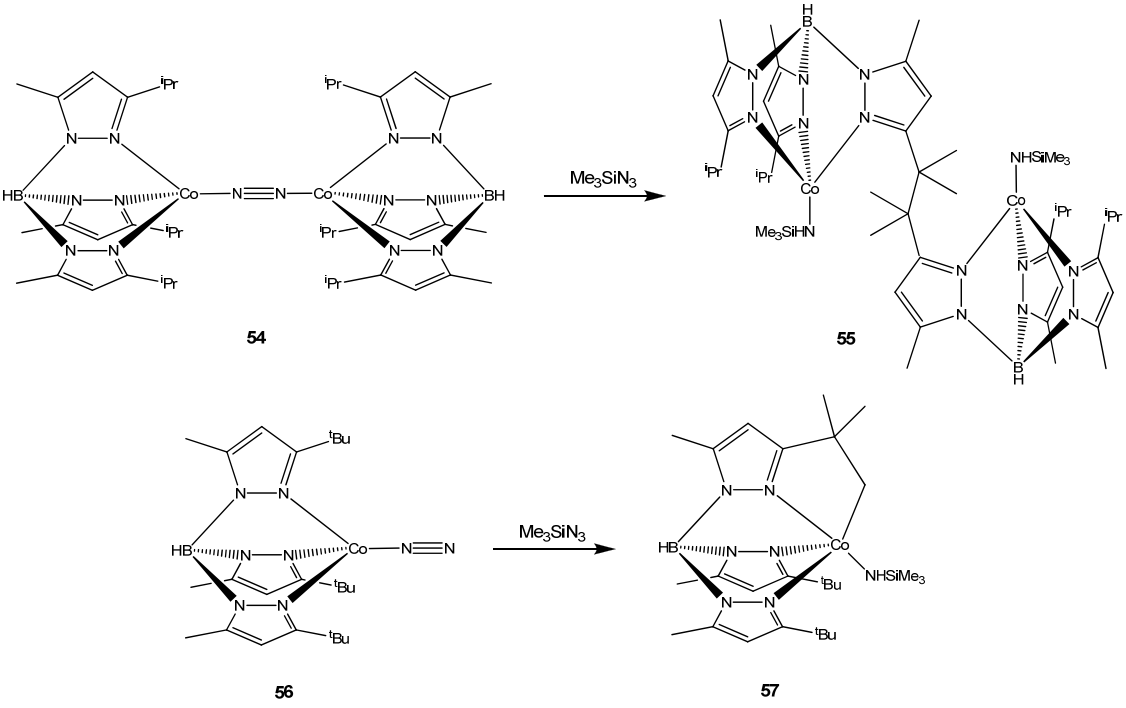

Scheme 1.6 Reaction of {($Tp^{iPr,Me}$)Co}$_2$(μ-η^1:$\eta^{1'}$-N_2) (54) and ($Tp^{tBu,Me}$)Co(N_2) (56) with Me_3SiN_3

1.4.6 Complexes of Tp^{iPr2}

The most widely studied tris(pyrazolyl)borate ligand, excluding Tp and Tp*, is hydrotris(3,5-diisopropylpyrazolyl)borate (Tp^{iPr2}). This ligand has been used to generate with equal propensity four-, five- and six-coordinate complexes of the first-row d-block metals, a fact which again illustrates the highly versatile nature of 'intermediate-bulk' Tp^x ligands. Once again, researchers such as Kitajima, Fujiwasa, Moro-Oka and Akita have applied the Tp^{iPr2} ligand to prepare a myriad of novel first-row d-block derivatives. Although {(Tp*)Cu}$_2$(μ-η^2:η^2-O_2) had previously been identified spectroscopically as a

side-on peroxo-bridged species, the increased bulk of the Tp^{iPr2} ligand allowed for the structural characterisation of the analogous $\{(Tp^{iPr2})Cu\}_2(\mu\text{-}\eta^2\text{:}\eta^2\text{-}O_2)$ (**59**), therefore definitively confirming for the first time the presence of this structural motif. $\{(Tp^{iPr2})Cu\}_2(\mu\text{-}\eta^2\text{:}\eta^2\text{-}O_2)$ could be prepared (**scheme 1.7**) either by H_2O_2 oxidation of $\{(Tp^{iPr2})Cu(\mu\text{-}OH)\}_2$ (**58**), itself prepared by addition of aqueous hydroxide to $(Tp^{iPr2})CuBr$, or alternatively by addition of O_2 to the highly reactive complex $(Tp^{iPr2})Cu$ (**60**).[84]

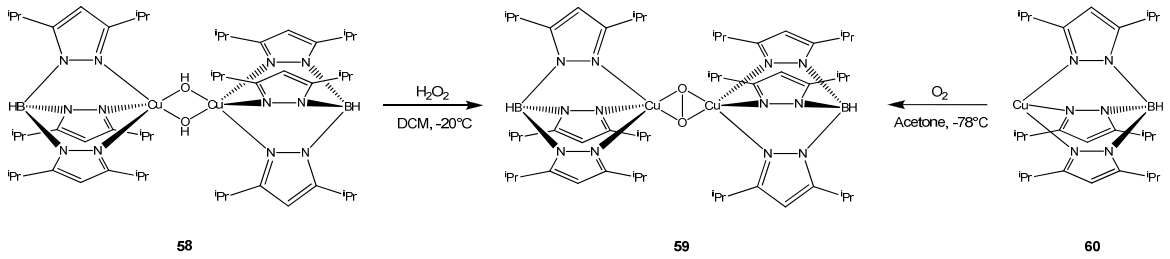

Scheme 1.7 Formation of $\{(Tp^{iPr2})Cu\}_2(\mu\text{-}\eta^2\text{:}\eta^2\text{-}O_2)$ (59)

$\{(Tp^{iPr2})Cu(\mu\text{-}OH)\}_2$ was also shown to react with aryl- and alkylthiols to furnish the monomeric, copper(II) thiolates $(Tp^{iPr2})Cu(SR)$ (**61**, R = C_6F_5, ^{t}Bu, CPh_3).[85] The molecular structure for R = C_6F_5 was determined, and showed the copper(II) centre to be in a substantially flattened tetrahedral geometry. The level of flattening is to a markedly greater extent than observed in the related $(Tp^{iPr2})CuCl$,[86] and therefore it is unsurprising that the spectroscopic properties of the $(Tp^{iPr2})Cu(SR)$ complexes were found to closely resemble those of type 1 and 2 blue copper proteins, in which the copper atoms are ligated by a N_2S_2 donor set in a highly distorted tetrahedral geometry.[85] The structural properties of the copper(I) congener $K[(Tp^{iPr2})Cu(SC_6F_5)]$ were found to be very similar to those of $Tp^{iPr2}Cu(SC_6F_5)$, just as little change in structure would be expected to occur in the enzymatic site when undergoing redox processes.[87] Thermal decomposition of $(Tp^{iPr2})Cu(SCPh_3)$ yielded the side-on disulfido-bridged $\{(Tp^{iPr2})Cu\}_2(\mu\text{-}\eta^2\text{:}\eta^2\text{-}S_2)$ (**62**),[88] the molecular structure of which is analogous to that of $\{(Tp^{iPr2})Cu\}_2(\mu\text{-}\eta^2\text{:}\eta^2\text{-}O_2)$.

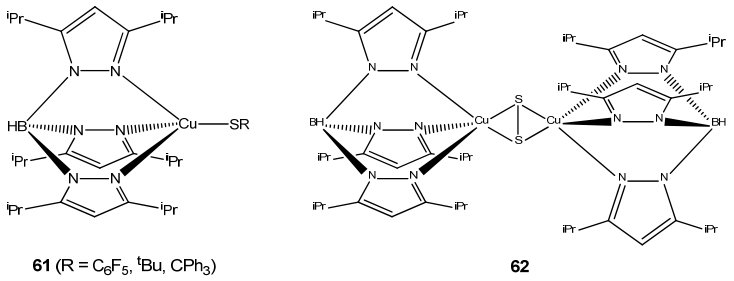

Figure 1.16 Structures of $(Tp^{iPr2})Cu(SR)$ (61) and $\{(Tp^{iPr2})Cu\}_2(\mu\text{-}\eta^2\text{:}\eta^2\text{-}S_2)$ (62)

Reaction of $\{(Tp^{iPr2})Cu(\mu\text{-}OH)\}_2$ with substituted phenols furnished the complexes $(Tp^{iPr2})Cu(OAr)$ (Ar = 4-FC_6H_4, 2,6-$Me_2C_6H_3$ (**63a**), 2,6-$^tBu_2C_6H_3$ (**63b**)). Whilst $(Tp^{iPr2})Cu(OC_6H_4\text{-}4\text{-}F)$ displayed high stability and was crystallographically characterised, the 2,6-dialkyl-substituted phenolato-copper(II) compounds both reacted spontaneously with O_2 (**scheme 1.8**) to give mixtures of the corresponding benzoquinone and oxidatively-coupled diphenoquinone decomposition products. Even when $(Tp^{iPr2})Cu(OAr)$ (Ar = 2,6-$Me_2C_6H_3$, 2,6-$^tBu_2C_6H_3$) were stored under argon at room temperature slow decomposition was observed, though in the absence of oxygen the diphenoquinone products are obtained exclusively.[89]

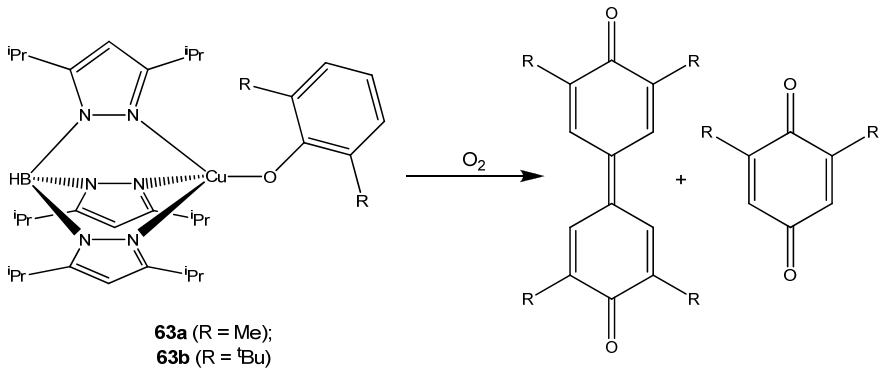

63a (R = Me);
63b (R = ^{t}Bu)

Scheme 1.8 Reaction of 63 with O_2

The analogous reaction of $\{(Tp^{iPr2})Cu(\mu\text{-}OH)\}_2$ with alkylhydroperoxides gave the monomeric alklyperoxo-copper(II) derivatives $(Tp^{iPr2})Cu(OOR)$ (R = ^{t}Bu, CMe_2Ph), and the molecular structure was determined for R = CMe_2Ph. These alkylperoxo adducts are stable at low temperature, but decompose rapidly at room temperature via a radical mechanism, which is implied by the observed formation of products arising from attack on the hydrocarbon solvent.[90] Treatment of $\{(Tp^{iPr2})Cu(\mu\text{-}OH)\}_2$ with hydrazine and 1,2-dimethylhydrazine gave the corresponding dinuclear diazene-bridged products $\{(Tp^{iPr2})Cu\}_2(\mu\text{-}\eta^1\text{:}\eta^{1\prime}\text{-}RN{=}NR)$ (**64**, R = H, Me), resulting from the oxidation of the respective hydrazines to diazenes with concomitant reduction of the copper(II) centres to copper(I).[91] However, the reaction of monomeric $(Tp^{tBu,iPr})CuOH$ with hydrazine furnished only the copper(I) hydrazine adduct $(Tp^{tBu,iPr})Cu(\eta^1\text{-}N_2H_4)$ (**65**), illustrating both the extreme reluctance of the $Tp^{tBu,iPr}$ ligand to form dimeric complexes, as well as the unstable nature of terminal diazene complexes.[92] Using the more sterically hindered phenylhydrazine and 1,1-diphenylhydrazine, it was also possible to isolate the monomeric $(Tp^{iPr2})Cu(N{=}NPhR)$ (**66**, R = H, Ph), though only in the case of R = Ph could crystals suitable for X-ray diffraction be obtained.[92]

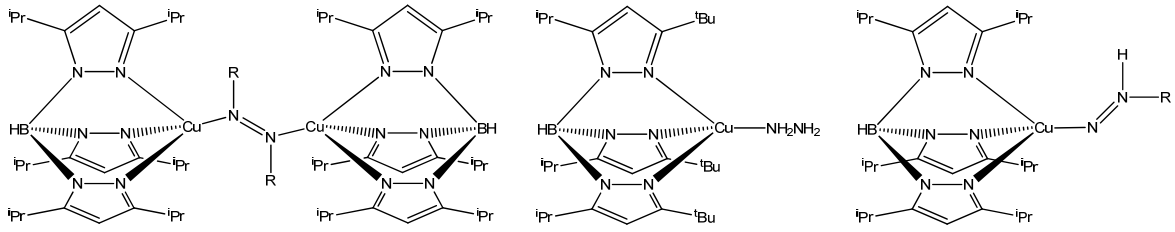

64 (R = H, Me) **65** **66** (R = H, Me)

Figure 1.17 Structures of $\{(Tp^{iPr2})Cu\}_2(\mu\text{-}\eta^1\text{:}\eta^{1'}\text{-RN=NR})$ (64), $(Tp^{tBu,iPr})Cu(\eta^1\text{-}N_2H_4)$ (65) and $(Tp^{iPr2})Cu(N{=}NPhR)$ (66)

As described above for the analogous copper(II) complexes, the dimeric species $\{(Tp^{iPr2})M(\mu\text{-}OH)\}_2$ (M = Mn, Co, Ni)[93] - formed by treatment of the corresponding monomeric halo- or acetato-derviatives with aqueous NaOH - are also of considerable synthetic utility. The corresponding iron(II) complex, $\{(Tp^{iPr2})Fe(\mu\text{-}OH)\}_2$, is also known but due to its extremely high sensitivity to oxygen it is of rather less use with respect to further synthetic derivation.[93] By anaerobic oxidation of $\{(Tp^{iPr2})Mn(\mu\text{-}OH)\}_2$ (**67**) with $KMnO_4$ (**scheme 1.9**), it was possible to obtain the dimanganese(III) oxo-bridged species $\{(Tp^{iPr2})Mn(\mu\text{-}O)\}_2$ (**68**). The latter complex could also be prepared by simple exposure of $\{(Tp^{iPr2})Mn(\mu\text{-}OH)\}_2$ to an atmosphere of dioxygen, but in this case the reaction was also accompanied by oxidation of the Tp^{iPr2} ligand (**scheme 1.9**).[94] The oxidation product (**69**) was subsequently isolated and structurally characterised, revealing the presence of a dimeric complex in which a single isopropyl CH moiety from each of the two Tp^{iPr2} ligands had been oxidised to give alkoxides which act as additional donors to each manganese ion, with the two manganese centres bridged by a single oxo anion.[95]

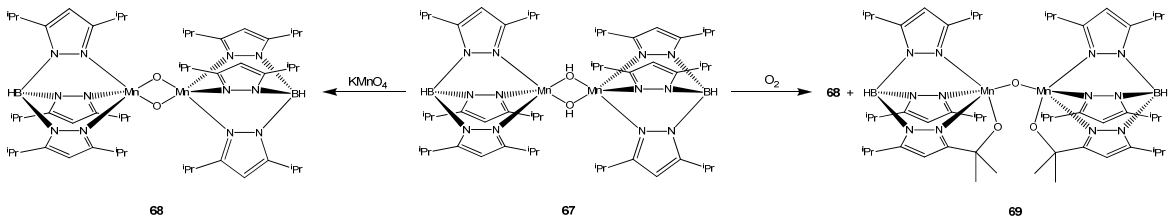

68 **67** **69**

Scheme 1.9 Reaction of $\{(Tp^{iPr2})Mn(\mu\text{-}OH)\}_2$ (67) with $KMnO_4$ and O_2

Likewise, when $\{(Tp^{iPr2})M(\mu\text{-}OH)\}_2$ (M = Co, Ni) were treated with H_2O_2, the oxo-bridged dimers $\{(Tp^{iPr2})M(\mu\text{-}O)\}_2$ (M = Co, Ni) were obtained, though both of these complexes were too unstable to provide crystals suitable for X-ray diffraction.[96] Crystalline ligand-oxidized products were obtained (**scheme 1.10**) as in the case of the aforementioned manganese complex, though the identity of these decomposition products is dependent on the identity of the metal ion, as well as the stoichiometry of the reactants. For example,

when $\{(Tp^{iPr2})Co(\mu\text{-}OH)\}_2$ (**70**) was reacted with one equivalent of H_2O_2, a μ-hydroxo μ-alkoxo complex (**71**) was obtained, in which the methine function of a single isopropyl group has been oxygenated and acts as an additional bridging ligand. When H_2O_2 is present in excess, a mixture of crystalline products is obtained consisting of a di-oxygenated bis(μ-alkoxo) complex (**72**), and a monomeric hydroxo complex (**73**) in which all of the ligand isopropyl CH units have been oxygenated and one acts as an alkoxo donor.[68,97]

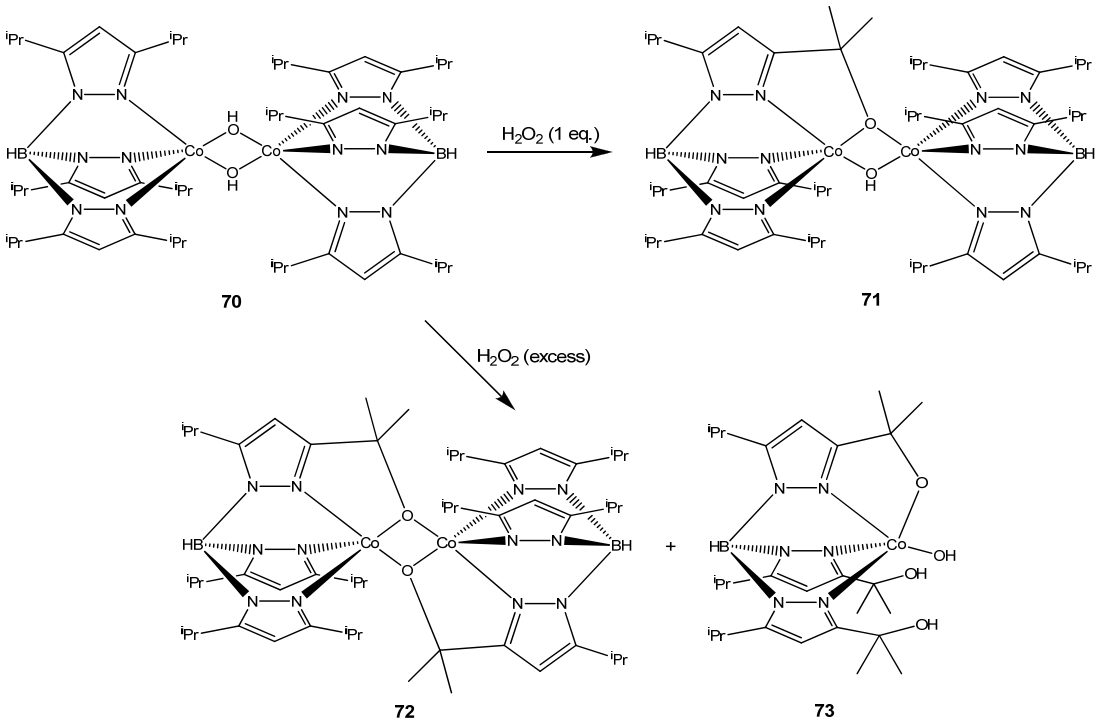

Scheme 1.10 Oxidation of $\{(Tp^{iPr2})Co(\mu\text{-}OH)\}_2$ (70) with H_2O_2

Complex **72** could also be obtained exclusively through the decomposition of the thermally unstable complexes $(Tp^{iPr2})Co(OOR)$ (R = ^{t}Bu, CMe_2Ph), formed by the reaction of $\{(Tp^{iPr2})Co(\mu\text{-}OH)\}_2$ with the corresponding alkyl hydroperoxides.[68] Reaction of $\{(Tp^{iPr2})Ni(\mu\text{-}OH)\}_2$ with an excess of H_2O_2 gave a single crystalline product, which was found to be a bis(enolato)-bridged dimer (**74**), in which dehydrogenation of one of the isopropyl groups of each ligand has occurred in addition to oxygenation at the methyl carbon atoms.[97] Treatment of $\{(Tp^{iPr2})Ni(\mu\text{-}OH)\}_2$ with ^{t}BuOOH furnished the novel monomeric $(Tp^{iPr2})Ni(OO^tBu)$ (**75**), the molecular structure of which showed the alkylperoxo ligand to be bound in a mode intermediate between η^1 and η^2.[98]

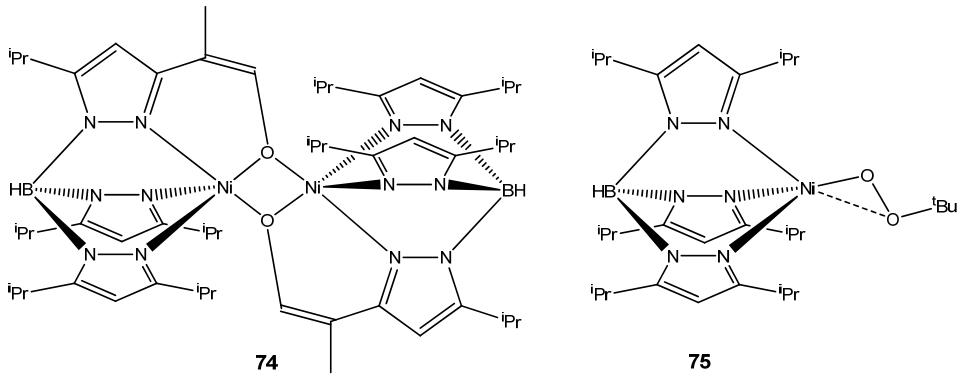

Figure 1.18 Structures of 74 and (Tp^{iPr2})Ni(OO^{t}Bu) (75)

{(Tp^{iPr2})Co(μ-OH)}$_2$ was also found to be sufficiently basic to deprotonate a series of terminal alkynes, generating the monomeric, tetrahedral (Tp^{iPr2})Co(C≡CR) (**76**, R = H, ^{t}Bu, Ph, $SiMe_3$, $SiEt_3$, COMe, CO_2Me, CO_2Et) derivatives (**scheme 1.11**). The reaction of {(Tp^{iPr2})Co(μ-OH)}$_2$ with triphenylsilylacetylene did not produce an alkynyl complex, instead forming the siloxo-cobalt(II) species (Tp^{iPr2})Co($OSiPh_3$) (**77**) arising from nucleophilic attack of OH^- at the silicon atom. When (Tp^{iPr2})Co(C≡CCO_2Me) was heated to reflux in benzene in the presence of an excess of free methyl propiolate, an unusual stereospecific trimerisation reaction of the alkyne occurred (**scheme 1.11**).[99]

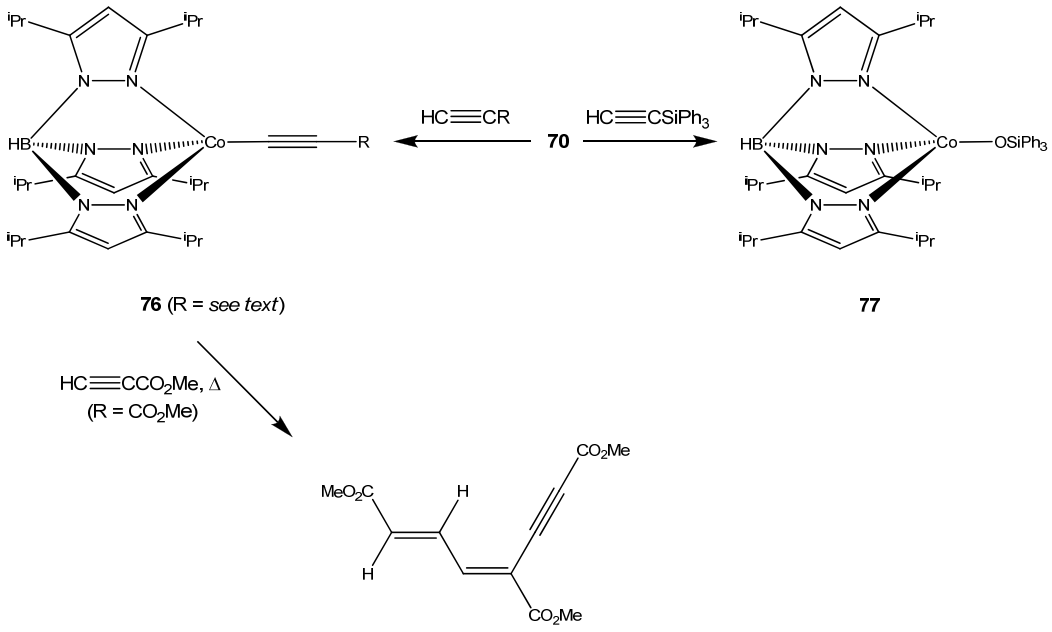

Scheme 1.11 Preparation and reactivity of (Tp^{iPr2})Co(C≡CR) (76); preparation of (Tp^{iPr2})Co($OSiPh_3$) (77)

When {(Tp^{iPr2})Mn(μ-OH)}$_2$ was treated with 3,5-diisopropylpyrazole (Hpz^{iPr2}) and a large excess of H_2O_2, the monomeric side-on peroxo adduct (Tp^{iPr2})Mn(η^2-O_2)(Hpz^{iPr2}) (**78**) was obtained. Two crystalline thermochromic congeners of this complex were isolated from

different solvent systems: a brown form (**78a**) at -20°C in acetonitrile; and a blue form (**78b**) at -78°C in toluene or diethyl ether. The molecular structures of these two species were found to be very similar, differing only by the presence of an intramolecular hydrogen bonding interaction between one of the peroxide oxygens and the NH of the bound pyrazole in the blue form, and the absence of this interaction in the brown form.[100] The molecular structure of a related compound in which the Hpz^{iPr2} ligand was substituted by 2-methylimidazole, $(Tp^{iPr2})Mn(\eta^2\text{-}O_2)(Him^{Me})$ (**79**), displayed a similar but stronger *intermolecular* hydrogen bonding interaction which gives rise to a cyclic tetranuclear arrangement in the solid-state.[101]

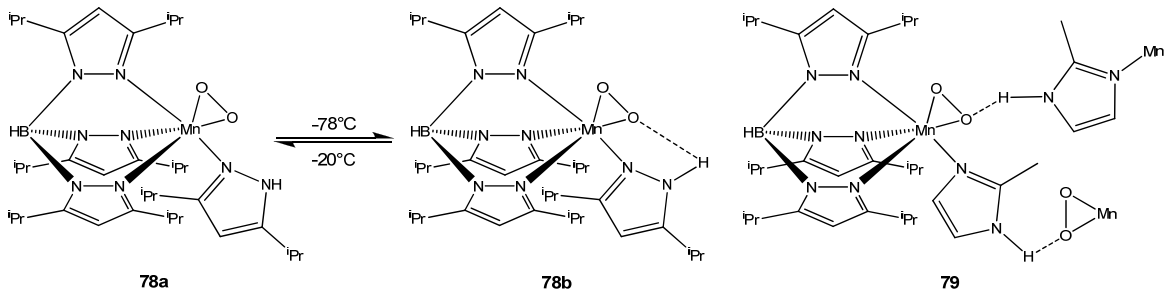

Figure 1.19 Thermochromic behaviour of $(Tp^{iPr2})Mn(\eta^2\text{-}O_2)(Hpz^{iPr2})$ (78); simplified depiction of hydrogen bonding in $(Tp^{iPr2})Mn(\eta^2\text{-}O_2)(Him^{Me})$ (79)

Reaction of $\{(Tp^{iPr2})Mn(\mu\text{-}OH)\}_2$ with one equivalent of acetic acid was shown to give the asymmetrically bridged dimer $\{(Tp^{iPr2})Mn\}_2(\mu\text{-}OH)(\mu\text{-}OAc)$ (**80**), which upon further treatment with either H_2O_2 or dioxygen (**scheme 1.12**) produced a mixture of the mono- and di-oxo bridged dimers $[\{(Tp^{iPr2})Mn^{III}\}_2(\mu\text{-}O)(\mu\text{-}OAc)]^+$ (**81**, the anion was not identified and this complex was not subjected to X-ray diffraction studies) and $(Tp^{iPr2})_2Mn^{III}Mn^{IV}(\mu\text{-}O)_2(\mu\text{-}OAc)$ (**82**). The former cationic species could also be prepared as its BF_4^- salt by addition of one equivalent each of acetic acid and HBF_4 to $\{(Tp^{iPr2})Mn(\mu\text{-}O)\}_2$, which provided the basis for its identification by spectroscopy.[102]

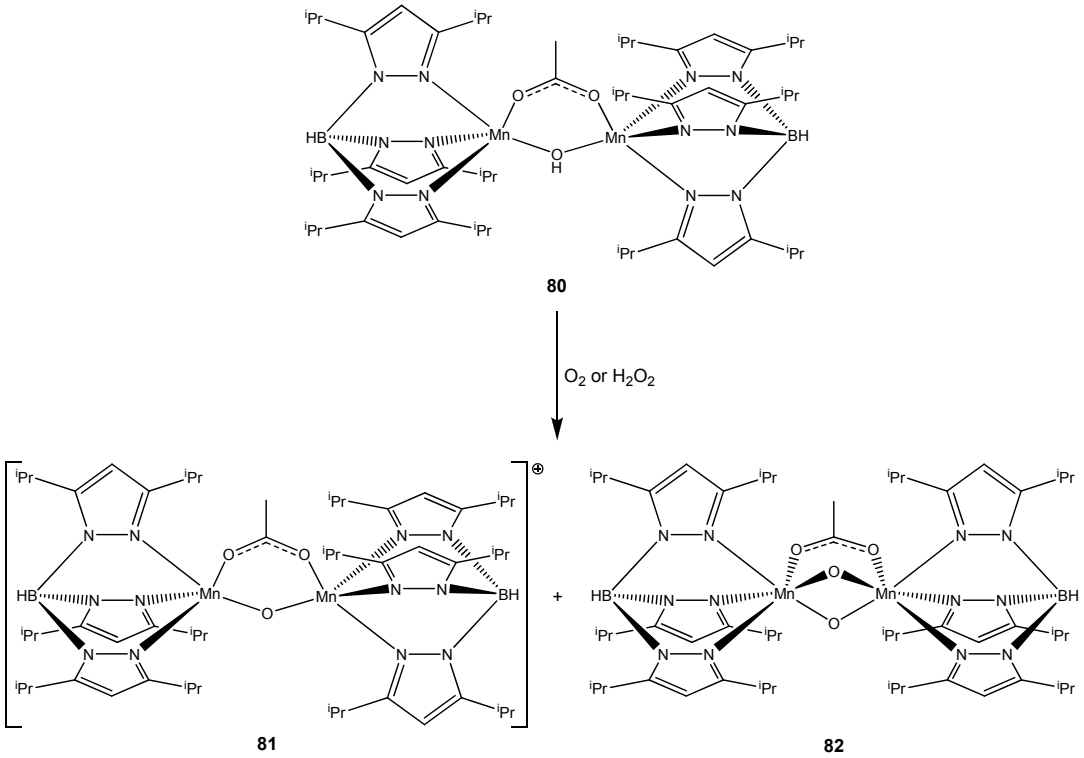

Scheme 1.12 Oxidation of $\{(Tp^{iPr2})Mn\}_2(\mu\text{-OH})(\mu\text{-OAc})$ (80)

Addition of 4-nitrobenzenethiol to $\{(Tp^{iPr2})Mn(\mu\text{-OH})\}_2$ yielded the monomeric manganese(II) thiolate $(Tp^{iPr2})Mn(SC_6H_4\text{-}4\text{-}NO_2)$, which reacted readily with O_2 to give a mixture of $\{(Tp^{iPr2})Mn(\mu\text{-O})\}_2$, the aforementioned ligand-oxidized product (**69**), and the disulfide $(4\text{-}NO_2C_6H_4)_2S_2$.[103] The series of analogous $(Tp^{iPr2})M(SC_6F_5)$ (M = Mn, Fe, Co, Ni, Zn) complexes were also prepared, either by means of the direct addition of pentafluorobenzenethiol to $\{(Tp^{iPr2})M(\mu\text{-OH})\}_2$ (M = Mn, Co, Ni), or alternatively through the reaction of $(Tp^{iPr2})MX$ (M = Fe, X = Cl; M = Zn, X = Br) with $NaSC_6F_5$. The molecular structures of $(Tp^{iPr2})M(SC_6F_5)$ (M = Mn, Fe, Co, Ni, Zn) were found to be very similar to the highly distorted tetrahedral arrangement observed for the aforementioned $(Tp^{iPr2})Cu(SC_6F_5)$, with the degree of flattening highest for the iron complex.[104] The zinc thiolates $(Tp^{iPr2})Zn(SR)$ (**83**, R = Bn, Cy, ^{t}Bu) were also prepared by Warren *et al.*, and were found to undergo reversible transnitrosation reactions with *S*-nitrosothiols (**scheme 1.13**). The molecular structure of $(Tp^{iPr2})Zn(S^tBu)$ was determined, and upon reaction of this compound with NO_2 (or a mixture of NO/O_2), $(Tp^{iPr2})Zn(\eta^2\text{-}NO_3)$ and ^{t}BuSNO were formed. ^{t}BuSNO was also produced in the reaction of $(Tp^{iPr2})Zn(S^tBu)$ (**84**) with $[NO][BF_4]$, in addition to $(Tp^{iPr2})Zn(\eta^{2\text{-}}BF_4)$ (**85**), the molecular structure of which shows a coordinated tetrafluoroborate ion bound in a bidentate fashion.[105]

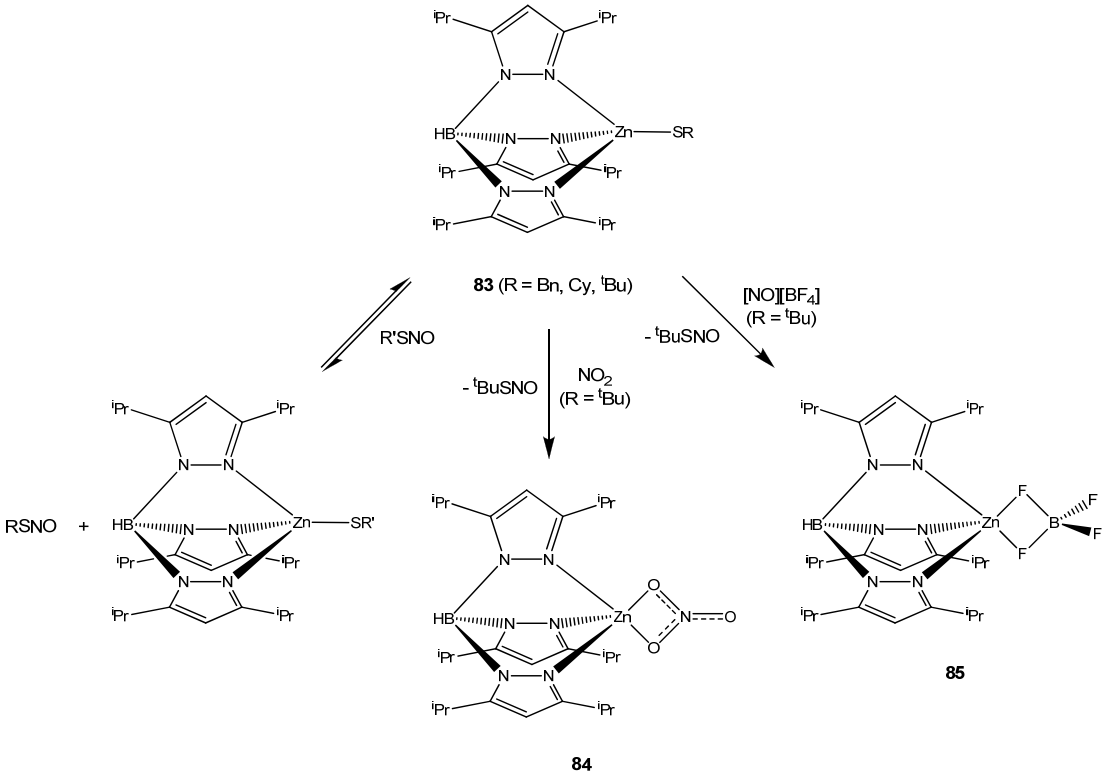

Scheme 1.13 Reactions of $(Tp^{iPr2})Zn(SR)$ (83)

In analogy with the chemistry of $(Tp^{tBu,Me})ZnOH$, all of the $\{(Tp^{iPr2})M(\mu\text{-}OH)\}_2$ (M = Mn, Fe, Co, Ni, Cu) compounds, in addition to the related $(Tp^{iPr2})ZnOH$, react with CO_2 to furnish the dimeric $\{(Tp^{iPr2})M\}_2(\mu\text{-}CO_3)$ (**86**, M = Mn, Fe, Co, Ni, Cu; **87**, M = Zn) derivatives. For M = Mn, Fe, Co, Ni, Cu, the bonding mode of the carbonate is bis-bidentate ($\mu\text{-}\eta^2\text{:}\eta^{2'}$), and hence both of the metal centres are five-coordinate.[93] However, the molecular structure of $\{(Tp^{iPr2})Zn\}_2(\mu\text{-}\eta^2\text{:}\eta^{1'}\text{-}CO_3)$ (**87**) revealed that in this case the carbonate ligand is bound in a bidentate fashion to one of the zinc ions, and monodentately to the other.[58(b),59,93] This is in contrast to the structure of $\{(Tp^{tBu,Me})Zn\}_2(\mu\text{-}\eta^1\text{:}\eta^{1'}\text{-}CO_3)$ (**section 1.4.2**), in which the carbonate anion is bound to both zinc centres in a monodentate fashion, and illustrates the effect of the reduction in bulk of the Tp^{iPr2} ligand in comparison to $Tp^{tBu,Me}$. Additionally, whereas $\{(Tp^{tBu,Me})Zn\}_2(\mu\text{-}\eta^1\text{:}\eta^{1'}\text{-}CO_3)$ is readily hydrolysed to the starting hydroxo-complex, $\{(Tp^{iPr2})Zn\}_2(\mu\text{-}\eta^2\text{:}\eta^{1'}\text{-}CO_3)$ does not react at all with H_2O. This implies that the bidentate coordination mode of carbonate is inhibitive with respect to reversible carbonic anhydrase-like activity.[59,93]

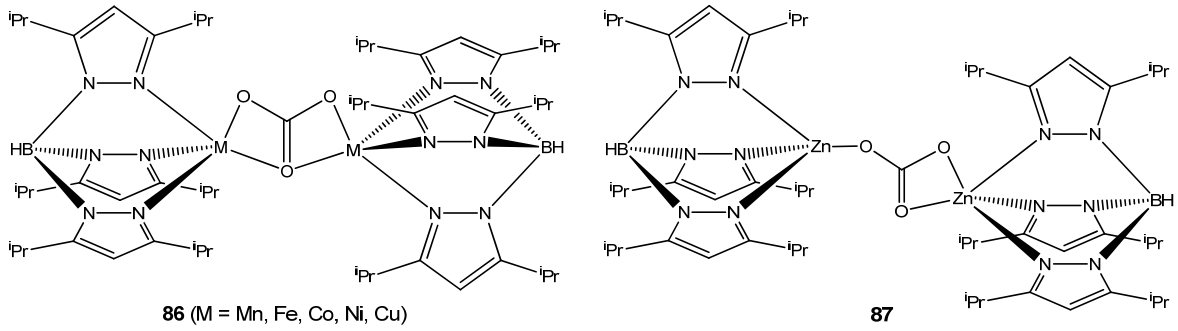

Figure 1.20 Structures of $\{(Tp^{iPr2})M\}_2(\mu\text{-}CO_3)$ (86) and $\{(Tp^{iPr2})Zn\}_2(\mu\text{-}\eta^2\text{:}\eta^{1'}\text{-}CO_3)$ (87)

A series of monomeric iron(II) carboxylates $(Tp^{iPr2})Fe(O_2CR)$ (R = Me, Et, ^{i}Pr, ^{t}Bu, Ad, Ph, 4-substituted Ph) were prepared and their reactivity towards dioxygen was investigated. Except in the case of R = ^{i}Pr, ^{t}Bu, Ad, all were found to react with O_2 in toluene solution at temperatures below -20°C to give a blue-green dioxygen adduct. In particular, the spectroscopic properties of the adduct obtained from O_2 addition to $(Tp^{iPr2})Fe(O_2CPh)$ were investigated in detail and its structure was determined to be the iron(III) peroxo-bridged dimer $\{(Tp^{iPr2})Fe\}_2(\mu\text{-}O_2CPh)_2(\mu\text{-}\eta^1\text{:}\eta^{1'}\text{-}O_2)$, though single crystals of this complex suitable for X-ray diffraction could not be obtained.[106] $\{(Tp^{iPr2})Fe\}_2(\mu\text{-}O_2CPh)_2(\mu\text{-}\eta^1\text{:}\eta^{1'}\text{-}O_2)$ decomposes at temperatures above -20°C, though the identity of the resultant product(s) could not be determined. However, thermal decomposition of the peroxo-adduct of the related $(Tp^{iPr2})Fe(\eta^2\text{-acac})$ in acetonitrile solution furnished crystals of the novel asymmetric triiron(III) complex $(Tp^{iPr2})Fe(\mu\text{-}O)(\mu\text{-}OAc)_2Fe(\mu\text{-}OH)(\mu\text{-}OAc)_2Fe(Tp^{iPr2})$ (**88**). Isotopic labelling experiments with $^{18}O_2$ showed that the acetate ligands arise from the acetylacetonate moiety in the starting material. Although the molecular structure appeared to show a symmetric mixed-valence $Fe^{II}/(Fe^{III})_2$ complex with two hydroxo bridges, spectroscopic and magnetic measurements ruled out the presence of an iron(II) centre, and the apparent symmetry was ascribed to crystallographic disorder.[107] By employing phenylacetate as the carboxylate ligand, the group of Lippard *et al.* were eventually successful in crystallographically characterising $\{(Tp^{iPr2})Fe\}_2(\mu\text{-}O_2CBn)_2(\mu\text{-}\eta^1\text{:}\eta^{1'}\text{-}O_2)$ (**89**), which unequivocally confirmed the prior structural assignment. Such complexes are accurate structural models for the oxygenated diferric site of metalloenzymes such as methane monooxygenase and ribonucleotide reductase.[108]

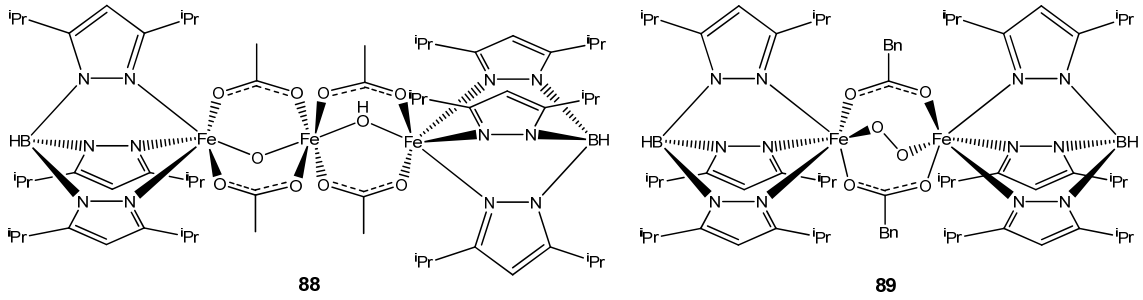

Figure 1.21 Structures of $(Tp^{iPr2})Fe(\mu\text{-}O)(\mu\text{-}OAc)_2Fe(\mu\text{-}OH)(\mu\text{-}OAc)_2Fe(Tp^{iPr2})$ (88) and $\{(Tp^{iPr2})Fe\}_2(\mu\text{-}O_2CBn)_2(\mu\text{-}\eta^1{:}\eta^{1'}\text{-}O_2)$ (89)

The aryloxo-iron(II) complexes $(Tp^{iPr2})Fe(OAr)$ (Ar = Ph, C_6F_5, 4-$NO_2C_6H_4$, 4-ClC_6H_4, 4-FC_6H_4, 4-MeC_6H_4, 2,6-$Cl_2C_6H_3$) were synthesised by reaction of $(Tp^{iPr2})FeCl$ with the corresponding sodium aryloxides, and upon exposure to O_2 furnished the bis-aryloxo-iron (III) derivatives $(Tp^{iPr2})Fe(OAr)_2$ (Ar = Ph, C_6F_5, 4-$NO_2C_6H_4$, 4-ClC_6H_4, 4-FC_6H_4, 4-MeC_6H_4, 2,6-$Cl_2C_6H_3$).[109] Treatment of $(Tp^{iPr2})Fe(OC_6H_4\text{-}4\text{-}R)_2$ (**90**, R = NO_2, Cl, F, Me) with 3-chloroperbenzoic acid at low temperature (**scheme 1.14**) produced the corresponding iron(III) η^1-catechol derivatives (**91**) by means of an acylperoxo-iron(III) intermediate. This reactivity is similar to the biological function of the iron enzyme tyrosine hydroxylase, responsible for the biocatalytic oxidation of tyrosine to 3,4-dihydroxyphenylalanine.[109(a)]

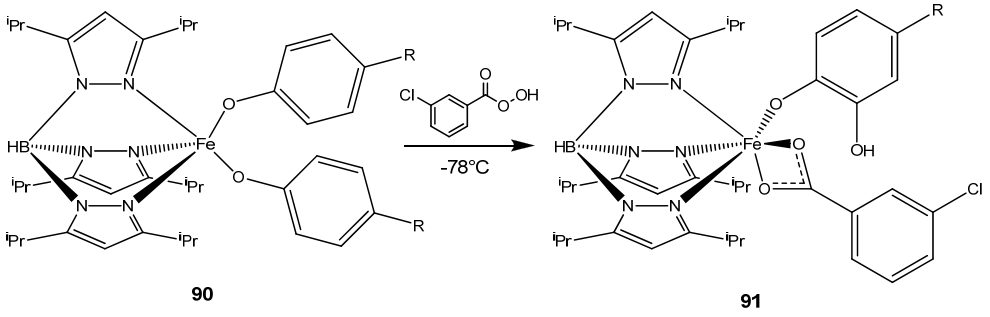

Scheme 1.14 Reaction of $(Tp^{iPr2})Fe(OC_6H_4\text{-}4\text{-}R)_2$ (90) with 3-chloroperbenzoic acid

The related six-coordinate catecholate complex $(Tp^{iPr2})Fe^{III}(\eta^2\text{-dbc})(NCMe)$ (**92**, H_2dbc = 3,5-di-*tert*-butylcatechol) was also prepared and again reacted with O_2, which resulted in cleavage of the catecholate moiety in both an *extradiol* and *intradiol* manner (**scheme 1.15**), thereby mimicking the reactivity of catechol dioxygenase enzymes.[110] Dissociation of the weakly-bound acetonitrile ligand in solution to give a square-pyramidal complex with a single free coordination site available for binding of O_2 was implied to be essential for this reactivity, as the related trigonal-bipyramidal $(Tp^{tBu,iPr})Fe^{III}(\eta^2\text{-dbc})$ showed no analogous cleavage of the bound catecholate upon exposure to O_2.[110]

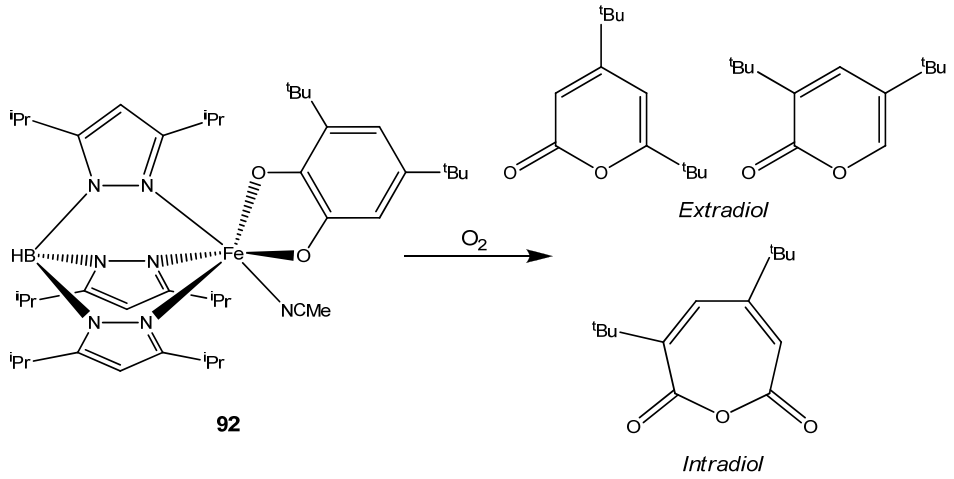

Scheme 1.15 Reaction of $(Tp^{iPr2})Fe^{III}(\eta^2\text{-dbc})(NCMe)$ (92) with O_2

Tp^{iPr2} was also used to prepare a number of interesting organometallic derivatives of the late first-row transition elements, namely $(Tp^{iPr2})M(C_3H_5)$ (**93**, M = Co, Ni; **94**, M = Fe), $(Tp^{iPr2})M(CH_2C_6H_4\text{-}4\text{-}Me)$ (**95**, M = Fe, Co) and $(Tp^{iPr2})MEt$ (**96**, M = Fe, Co). The structures of the allyl complexes for M = Co (17 valence electrons) and Ni (18 valence electrons) show the expected coordinatively saturated species in which the allyl ligand is η^3-bound. However, in the case of $(Tp^{iPr2})Fe(C_3H_5)$, the molecular structure revealed the allyl ligand to be η^1-bound to a coordinatively unsaturated, 14 valence electron tetrahedral iron centre. As expected, theoretical calculations supported the formation of a η^3-allyl complex, and the researchers could offer no explanation as to why the η^1 adduct was formed preferentially. Likewise, the 4-methylbenzyl ligands in $(Tp^{iPr2})M(CH_2C_6H_4\text{-}4\text{-}Me)$ (M = Fe, Co) were also found to bind in a η^1 manner to give 14- and 15-valence electron species respectively.[111]

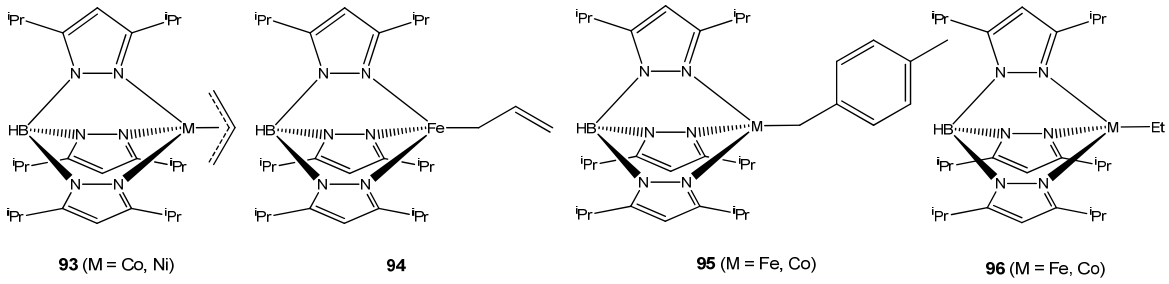

Figure 1.22 Structures of $(Tp^{iPr2})M(C_3H_5)$ (93, 94), $(Tp^{iPr2})M(CH_2C_6H_4\text{-}4\text{-}Me)$ (95) and $(Tp^{iPr2})MEt$ (96)

The ethyl complexes are remarkable in that they are rare examples of coordinatively unsaturated organotransition metal alkyls which are stable with respect to β-hydrogen elimination. The cobalt complex is stable at 60°C but decomposes completely at 120°C to give a single unidentified product, whereas the iron complex underwent no change upon

heating at 110°C for extended periods. Attempts to form the analogous ethylnickel and 4-methylbenzylnickel complexes by reaction of (Tp^{iPr2})NiCl with ethylmagnesium bromide and 4-methylbenzylmagnesium chloride respectively resulted in rapid decomposition in both cases. The ethylnickel complex was stable in solution at -78°C, but underwent decomposition via β-hydrogen elimination upon warming to room temperature, as confirmed by detection of the liberated C_2H_4. The unstable (Tp^{iPr2})NiEt (**97**) could however be trapped (**scheme 1.16**) by addition of CO at -78°C to give the acylnickel complex (Tp^{iPr2})Ni(CO)(COEt) (**98**), which was structurally characterised.[111]

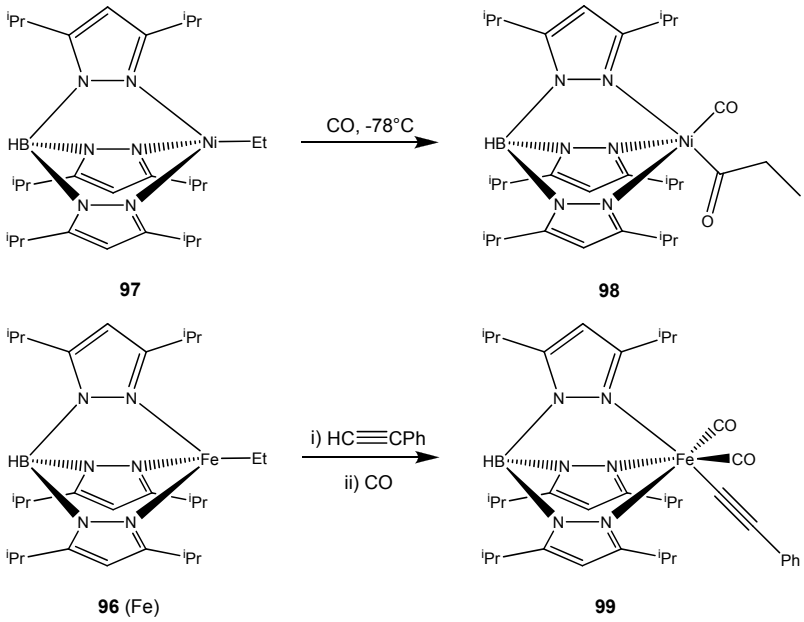

Scheme 1.16 Reaction of (Tp^{iPr2})NiEt (97) with CO; Reaction of Tp^{iPr2}FeEt with phenylacetylene and CO

Theoretical calculations suggested that the stability of the iron and cobalt alkyls could be ascribed to the fact that all the frontier molecular orbitals are occupied by either a single electron or electron pairs, due to the high spin configurations of the metal ions, and as such there are no vacant d-orbitals available for the coordination of further ligands. The reaction of (Tp^{iPr2})MEt (M = Fe, Co) with a variety of unsaturated organic substrates was also investigated, yet of these only phenylacetylene showed any reactivity yielding the corresponding unstable alkenyl (Co) and alkynyl (Fe) species at elevated temperature. Treatment of the latter iron-phenylacetylide with CO (**scheme 1.16**) gave the complex (Tp^{iPr2})Fe$(CO)_2$(C≡CPh) (**99**), which could be isolated. Although (Tp^{iPr2})MEt (M = Fe, Co) did not react directly with ethylene, polyethylene was produced in the presence of a large excess of methylaluminoxane, though the catalytic activities were low.[111]

1.4.7 Complexes of Tp^{Ph}

Like the aforementioned 3-isopropyl substituted ligands, 3-phenyl substituted Tp^{x} ligands can also be considered to be of 'intermediate bulk'. The coordination number of the derived complexes is hence determined more by the nature of the metal centre and the ancillary ligands, rather than by the steric demands of the 3-phenyl substituted Tp^{x} ligands. In contrast to the behaviour of Tp^{iPr} and $Tp^{iPr,Me}$, the reaction of $M(OTf)_2$ (M = Mn, Fe) with Tp^{Ph} in THF produced $(Tp^{Ph})_2M$ (**100**, M = Mn, Fe) as the only isolable product, regardless of the stoichiometry of the reactants. No rearrangement of the pyrazolyl substituents was observed, and through examination of the molecular structures of $(Tp^{Ph})_2M$ (M = Mn, Fe) it is obvious that π-stacking interactions between the phenyl groups of the two Tp^{Ph} ligands have a significant influence on the formation of the sandwich complexes.[112] With more strongly donating ancillary ligands, complexes such as the six-coordinate $(Tp^{Ph})Fe^{III}(\eta^2\text{-}NO_3)(\eta^1\text{-}NO_3)$ (**101**) and five-coordinate $(Tp^{Ph})Fe(NCS)(THF)$ could be isolated,[113] the latter in analogy to the previously described $(Tp^{Ph})Co(NCS)(THF)$.

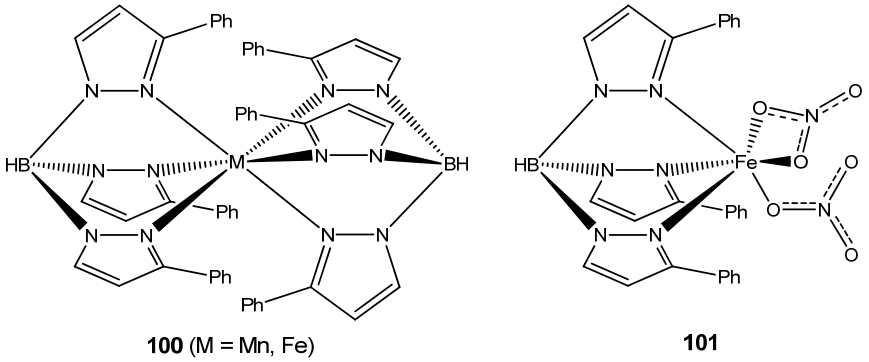

100 (M = Mn, Fe) **101**

Figure 1.23 Structures of $(Tp^{Ph})_2M$ (100) and $(Tp^{Ph})Fe^{III}(\eta^2\text{-}NO_3)(\eta^1\text{-}NO_3)$ (101)

Bis-Tp^{Ph} complexes were obtained for cobalt and zinc, though interestingly neither of these was found to have an octahedral coordination environment. The molecular structure of $(\eta^3\text{-}Tp^{Ph})(\eta^2\text{-}Tp^{Ph})Co$ (**102**)[114] showed a five-coordinate cobalt centre with one Tp^{Ph} ligand bound in the regular tridentate fashion and the other coordinated bidentately, whereas the structure of $(\eta^2\text{-}Tp^{Ph})_2Zn$ (**103**) was found to show a bis(bidentate) tetrahedral arrangement.[115] The fact that Co(II) and Zn(II) do not form octahedral sandwich complexes with Tp^{Ph} may be due to their relatively smaller ionic radii in comparison to Mn(II) and Fe(II).

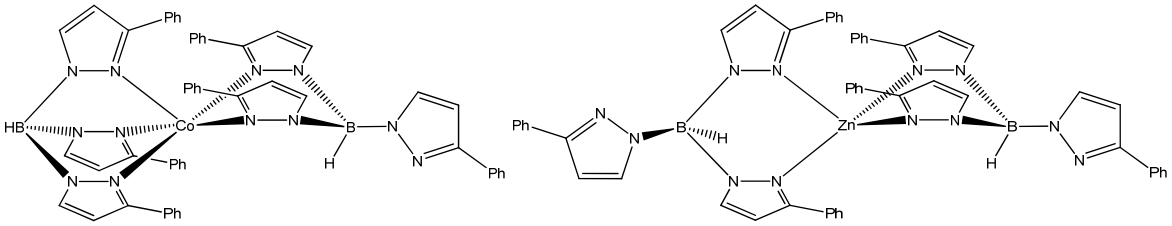

102 103

Figure 1.24 Structures of (η^3-Tp^{Ph})(η^2-Tp^{Ph})Co (102) and (η^2-Tp^{Ph})$_2$Zn (103)

Tetrahedral complexes of the form (Tp^{Ph})MX (M = Co, Zn, X = Cl, Br, N_3, NCS, NCO; M = Ni, X = NCS) were also easily accessible,[43(b),114,115] and the (Tp^{Ph})MCl (M = Co, Zn) derivatives were elaborated to the corresponding carboxylate adducts (Tp^{Ph})M(O_2CR) (R = Me, Ph, 4-F-C_6H_4, 4-NO_2-C_6H_4) by metathesis with the appropriate silver or potassium carboxylate. None of these complexes were structurally characterised, though the molecular structures of the related five-coordinate anthranilate (**104**) and acetylacetonate (**105**) derivatives were determined.[114] The organometallic complex (η^2-Tp^{Ph})Ni(*o*-tol)(PPh_3) (**106**) was found to show high catalytic activity towards the copolymerisation of ethylene and carbon monoxide. The bidentate bonding mode of the Tp^{Ph} is observed due to the fact that square-planar 16-electron species are favoured for organometallic nickel(II) complexes of strongly σ-donating ligands such as *o*-tolyl.[116]

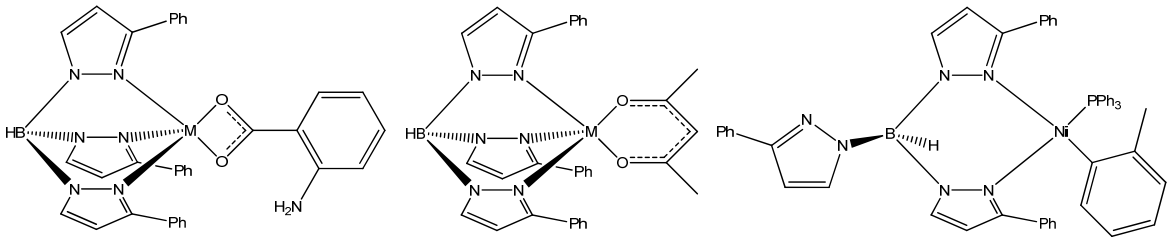

104 (M = Co, Zn) **105** (M = Co, Zn) **106**

Figure 1.25 Structures of 104, 105 and (η^2-Tp^{Ph})Ni(*o*-tol)(PPh_3) (106)

Halcrow and co-workers prepared a series of square-pyramidal complexes of the form (Tp^{Ph})Cu(L), where L is a bidentate, monoanionic substituted salicylaldehyde or salicylaldiminate derivative. These complexes were shown to undergo one-electron ligand oxidation reactions, yielding the radical species (Tp^{Ph})Cu($L^{\cdot+}$) which were stable in solution for a number of hours.[117] The oxidation processes were irreversible, except for when HL = 2-hydroxy-3-methylthio-5-methylbenzaldehyde (**107**). In this case, the UV-Vis-NIR spectrum of the oxidised product was found to strongly resemble that of the active form of

galactose oxidase, a fungal metalloenzyme responsible for the catalytic oxidation of alcohols to aldehydes.[117]

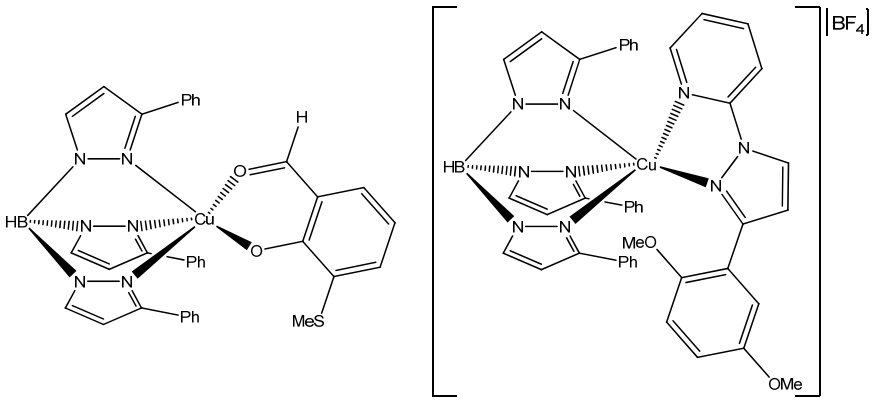

Figure 1.26 Structures of 107 and [(Tp^{Ph})Cu(L)][BF_4] (108)

The use of salicylaldehyde ligands containing bulky *tert*-butyl substituents gave rise to radical species with significantly shorter lifetimes, a phenomenon attributed to unfavourable steric interactions between the salicylaldehyde *tert*-butyl groups and the phenyl groups of the Tp^{Ph} ligand.[118] Similarly, the cationic complex [(Tp^{Ph})Cu(L)][BF_4] (**108**, L = η^2-*N,N'*-3-(2,5-dimethoxyphenyl)-1-(2-pyridyl)pyrazole) gave a one-electron oxidised derivative upon electrochemical oxidation, the stability of which was originally attributed to favourable π-π interactions between one of the Tp^{Ph} phenyl groups and the dimethoxyphenyl function of the ancillary ligand.[119] However, as the lifetime of the one-electron oxidised form of the related complex [(Tp^{Cy})Cu(L)][BF_4] (Tp^{Cy} = hydrotris(3-cyclohexylpyrazolyl)borate, L = η^2-*N,N'*-3-(2,5-dimethoxyphenyl)-1-(2-pyridyl)pyrazole) was found to be almost identical, this hypothesis was subsequently proven to be incorrect.[120] A series of square-pyramidal complexes of the general form [(Tp^{Ph})M(L)][ClO_4] (M = Co, Ni, Cu, Zn, L = phenanthroline (**109**), dipyridoquinoxaline (**110**)) were prepared by Chakravarty *et al.*, and these were screened for their efficacy as sensitisers for the photoinduced cleavage of DNA. All of the dipyridoquinoxaline complexes were found to efficiently cleave DNA upon irradiation with UV-A light, whereas only the cobalt and copper dipyridoquinoxaline complexes showed similar activity when irradiated with visible light. The Tp^{Ph} ligand provides steric shielding against quenching of the triplet excited state arising upon irradiation of these complexes. This excited state in turn is responsible for the generation of singlet oxygen, which is the actual species responsible for the cleavage of DNA.[121]

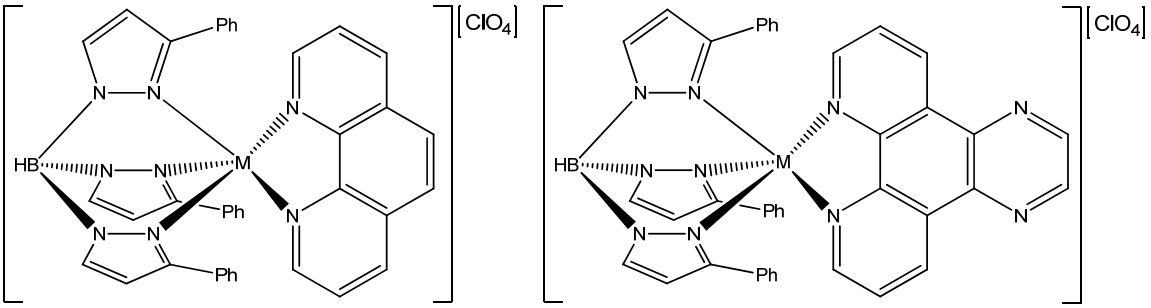

109 (M = Co, Ni, Cu, Zn) **110** (M = Co, Ni, Cu, Zn)

Figure 1.27 Structures of [(Tp^{Ph})M(L)][ClO$_4$] (109, 110)

1.4.8 Complexes of Tp^{Ph,Me}

The chemistry of the hydrotris(3-phenyl-5-methylpyrazolyl)borate (Tp^{Ph,Me}) ligand was found to be very similar to that of Tp^{Ph}. Octahedral (Tp^{Ph,Me})$_2$M (M = Fe, Co, Zn) complexes were obtained, as well as the tetrahedral (Tp^{Ph,Me})MX (M = Co, Ni, X = NCS; M = Zn, X = Cl, I, NCS) derivatives.[122] (Tp^{Ph,Me})NiCl was reacted with ethylcysteine (HCysEt) in basic solution to give the trigonal-bipyramidal (Tp^{Ph,Me})Ni(η^2-*N,S*-CysEt) (**111a**), which was found to be much less reactive towards O_2 than the related (Tp*)Ni(η^2-*N,S*-CysEt) (**111b**), a property attributed to a combination of the decreased steric bulk and increased electron donating ability of Tp* in comparison to Tp^{Ph,Me}.[123] Treatment of (Tp^{Ph,Me})MCl (M = Co, Ni) with AgOTf in acetonitrile furnished the cationic, octahedral [(Tp^{Ph,Me})M(NCMe)$_3$][OTf] (**112**, M = Co, Ni). Subsequent derivation of these tris-acetonitrile adducts with strong donor ligands such as pyridine, 2,2′-bipyridine, 4,4′-bipyridine, 1,4-dicyanobenzene, 1,2-dicyanoethane and various bidentate phosphines afforded a plethora of cationic complexes, the most interesting of which were polymetallic species such as the dinuclear [{(Tp^{Ph,Me})Ni(NCMe)}$_2$(μ-NCC$_6$H$_4$CN)][OTf]$_2$ and polymeric {[(Tp^{Ph,Me})M(μ-4,4′-bipy)][OTf]}$_n$.[124]

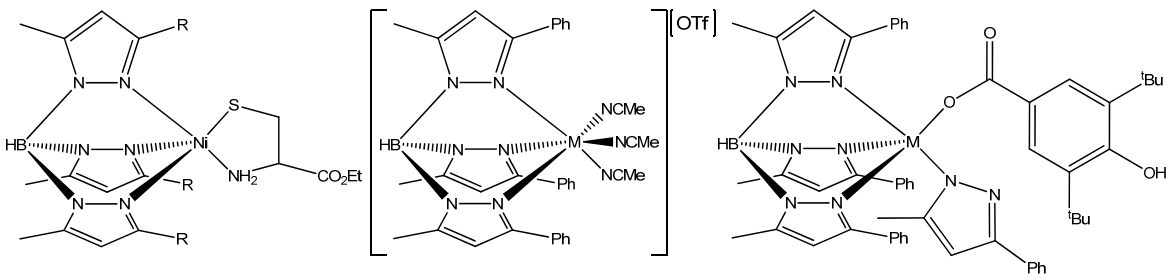

111a (R = Ph)
111b (R = Me)

112 (M = Co, Ni)

113 (M = Mn, Co, Ni)

Figure 1.28 Structures of (Tp^{R,Me})Ni(η^2-*N,S*-CysEt) (111), [(Tp^{Ph,Me})M(NCMe)$_3$][OTf] (112) and (Tp^{Ph,Me})M(η^1-dbcp)(Hpz^{Ph,Me}) (113)

Chemical oxidation of the five-coordinate ($Tp^{Ph,Me}$)M(η^1-dbcp)($Hpz^{Ph,Me}$) (**113**, M = Mn, Co, Ni, dbcp = 2,6-di-*tert*-butyl-4-carboxyphenol) with PbO_2 gave persistent phenoxyl radical species and attendant slow formation of the corresponding diphenoquinone, except in the case of M = Mn where formation of the diphenoquinone was very rapid and no radical species could be detected.[125] The structural and spectroscopic properties of the arylthiolate nickel(II) complexes ($Tp^{Ph,Me}$)Ni(SR) (R = Ph, mes, xyl) were investigated by Jensen and co-workers. These properties were found to be highly dependent on the nature of the arylthiolate ligand, as an increase in the steric bulk of the arythiolate causes a decrease in the degree of covalency of the Ni-S bond.[126] The same researchers also prepared a series of nickel complexes of the general form ($Tp^{Ph,Me}$)Ni(η^2-S_2CR) (R = NEt_2, NPh_2, OEt), all of which were structurally characterised. The coordination geometry of these complexes was dependent on both the steric demand and electron donor strength of the $[S_2CR]^-$ ligand. For example, the small and relatively weakly donating ethylxanthate anion gave the square-pyramidal complex (η^3-$Tp^{Ph,Me}$)Ni(η^2-S_2COEt) (**114**) in which the $Tp^{Ph,Me}$ ligand is bound tridentately. Conversely, the bulkier and more strongly electron-donating *N*,*N*-diethyldithiocarbamate and *N*,*N*-diphenyldithiocarbamate ligands gave the square-planar complexes (η^2-$Tp^{Ph,Me}$)Ni(η^2-S_2CR) (**115**, R = NEt_2, NPh_2) in which the $Tp^{Ph,Me}$ ligand is coordinated to the nickel centre in a bidentate fashion.[127]

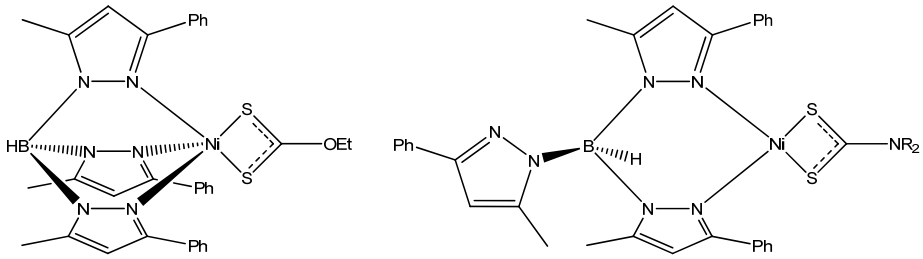

114 **115** (R = Et, Ph)

Figure 1.29 Structures of (η^3-$Tp^{Ph,Me}$)Ni(η^2-S_2COEt) (114) and (η^2-$Tp^{Ph,Me}$)Ni(η^2-S_2CR) (115)

1.4.9 Complexes of $Tp^{Cum,Me}$

Hydrotris(3-(*p*-cumenyl)-5-methylpyrazolyl)borate ($Tp^{Cum,Me}$) imparts a similar level of steric encumbrance to $Tp^{Ph,Me}$, yet also provides a hydrophobic pocket around the remaining coordination sites of the bound metal atom which extends substantially further than in complexes of $Tp^{Ph,Me}$. This property has led to the extensive use of $Tp^{Cum,Me}$ in the area of biomimetic zinc chemistry, and this will be discussed later. Ruf and colleagues described the synthesis of the semiquinonate complexes ($Tp^{Cum,Me}$)M(η^2-dbsq) (**116**, M =

Co, Cu, Zn, dbsq = 3,5-di-*tert*-butylsemiquinonate), which were prepared by the aerial oxidation of solutions of either 3,5-di-*tert*-butylcatechol (H_2dbc) and ($Tp^{Cum,Me}$)MOH (M = Cu, Zn), or H_2dbc and ($Tp^{Cum,Me}$)$_2$Co. The coordination geometry in each of these complexes was found to be intermediate between square-pyramidal and trigonal-bipyramidal, and their magnetic (M = Cu) and electrochemical (M = Co) properties were subjected to a detailed investigation.[128]

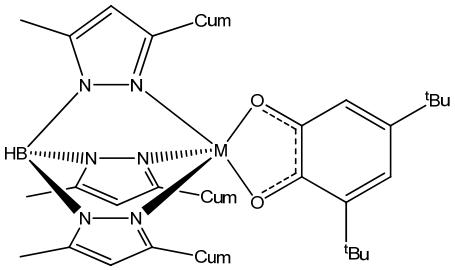

116 (M = Co, Cu, Zn)

Figure 1.30 Structure of ($Tp^{Cum,Me}$)M(η^2-dbsq) (116)

The same researchers were also able to prepare the unusual trinuclear ($Tp^{Cum,Me}$)Cu(μ-OMe)$_2$Cu(μ-OMe)$_2$Cu($Tp^{Cum,Me}$) (**117**), simply by the reaction of $Cu(ClO_4)_2$ and $Tp^{Cum,Me}$ in a DCM/methanol mixed solvent.[129] Upon treatment of this highly basic complex with 2-(methylthio)phenol (Hmtp) (**scheme 1.17**), the square-pyramidal ($Tp^{Cum,Me}$)Cu(η^2-mtp) (**118**) was obtained,[129] which was postulated as a synthetic model for galactose oxidase in analogy with the aforementioned Cu(II) complexes of Tp^{Ph}. Kirk, Schultz, and others have also prepared a wide range of $Tp^{Cum,Me}$-supported manganese, cobalt, nickel, copper and zinc complexes of a variety of semiquinonates, with regard to detailed analysis of their magnetic properties.[130]

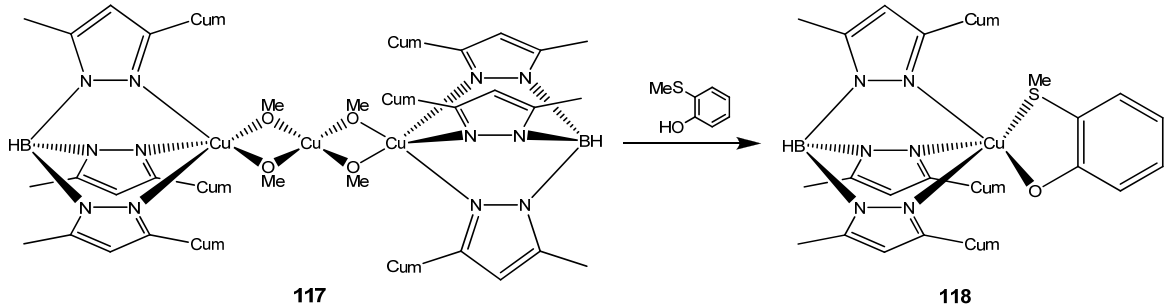

117 **118**

Scheme 1.17 Reaction of ($Tp^{Cum,Me}$)Cu(μ-OMe)$_2$Cu(μ-OMe)$_2$Cu($Tp^{Cum,Me}$) (117) with 2-(methylthio)phenol

1.4.10 Complexes of Tp^{Ph2}

Despite the increased propensity of 3-phenyl substituted Tp^{x} ligands to form bis-ligand sandwich complexes in comparison to the equivalent 3-*tert*-butyl or 3-isopropyl substituted ligands, it is still perhaps unsurprising that no such compounds are known for hydrotris(3,5-diphenylpyrazolyl)borate (Tp^{Ph2}), a fact likely due to the extreme steric crowding which would result. Additionally, in contrast to Tp^{iPr2}, no 'true' six-coordinate complexes of Tp^{Ph2} have ever been reported (see exception below), which again shows the high level of steric encumbrance imparted by this ligand. The tetrahedral adduct $(Tp^{Ph2})CuCl$ was found to act as a catalyst towards the oxidative polymerisation of 4-phenoxyphenol, giving polyphenylene oxide with a high degree of crystallinity.[131] With similar aims to their work with Tp^{Ph} complexes of copper(II) as models for galactose oxidase, Halcrow and co-workers prepared the complexes $(Tp^{Ph2})M(\eta^2\text{-L})$ (M = Cu, Zn, HL = 2-hydroxy-5-methyl-1,4-benzoquinone). The molecular structure of the copper(II) compound (**119**) revealed a square-pyramidal coordination environment, whereas in the case of the zinc complex (**120**) the coordination geometry was found to be essentially trigonal-bipyramidal, but with a highly elongated interaction between the zinc centre and the carbonyl donor of the quinone in comparison to that observed in the Cu complex. $(Tp^{Ph2})Cu(\eta^2\text{-L})$ (HL = 2-hydroxy-5-methyl-1,4-benzoquinone) is a synthetic model for the active site of copper amine oxidase enzymes, in which the tris-histidine bound copper centre is either in close proximity to, or directly bound by, the cofactor TPQ (2-hydroxy-5-(2-alaninyl)-1,4-benzoquinone).[132]

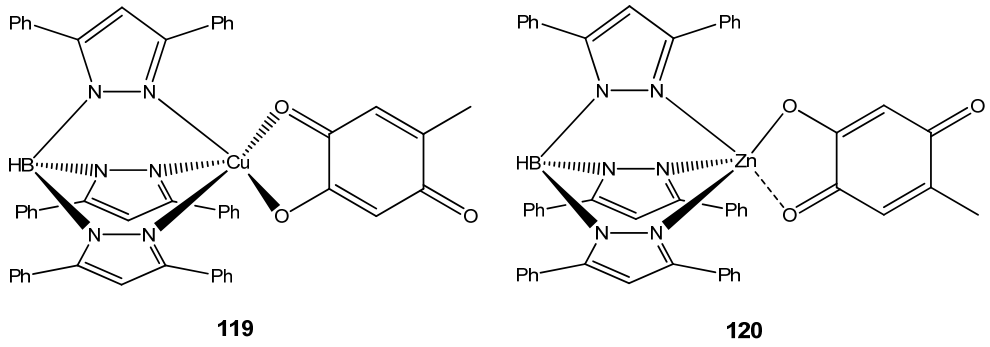

119 **120**

Figure 1.31 Structures of $(Tp^{Ph2})M(\eta^2\text{-L})$ (119, 120)

In a detailed modelling study of α-ketoacid-dependent iron oxygenase enzymes, Que and co-workers prepared the iron(II) carboxylate complexes $(Tp^{Ph2})Fe(\eta^2\text{-OBz})$ and $(Tp^{Ph2})Fe(\eta^1\text{-OAc})(Hpz^{Ph2})$, as well as the pyruvate and benzoylformate complexes $(Tp^{Ph2})Fe(\eta^2\text{-}O_2CCOR)$ (R = Me, Ph) in which the α-ketocarboxylate ligands are bound in

a bidentate manner via the α-carbonyl donor in addition to a single carboxylate oxygen. All of these complexes were shown to react rapidly with dioxygen to effect oxygenation of the ortho-position of a single phenyl group of the Tp^{Ph2} ligand (**scheme 1.18**), with attendant oxidative decarboxylation of the α-ketocarboxylate ligand in the case of the pyruvate and benzoylformate complexes. For $(Tp^{Ph2})Fe(\eta^1\text{-}OAc)(Hpz^{Ph2})$ (**121**), the molecular structure of the oxygenation product (**122**) was determined crystallographically, and showed an octahedral iron(III) centre bound by an monodentate acetate ligand, which was hydrogen-bonded to the coordinated Hpz^{Ph2}. The remaining four coordination sites are occupied by the three pyrazole nitrogen donors of the Tp^{Ph} ligand, and the additional phenoxide donor moiety arising from oxygenation of one the 3-phenyl groups of Tp^{Ph2}.[133]

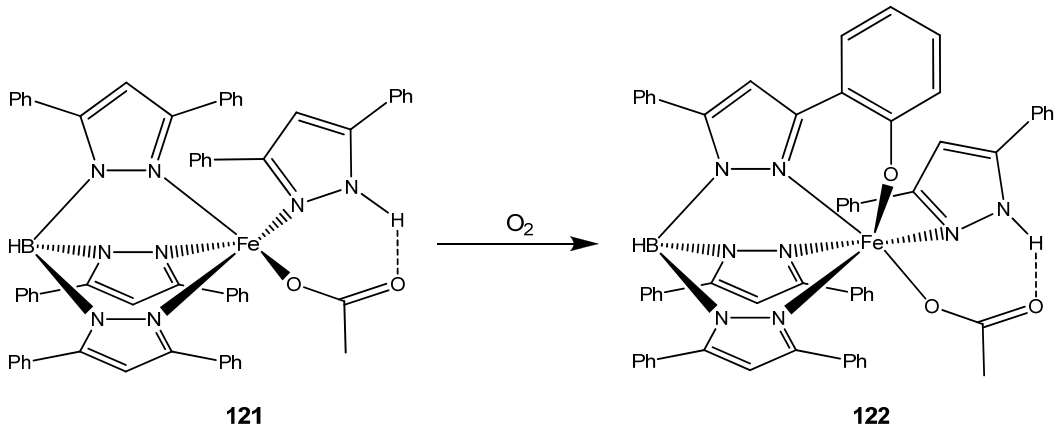

121 **122**

Scheme 1.18 Reaction of $(Tp^{Ph2})Fe(\eta^1\text{-}OAc)(Hpz^{Ph2})$ (121) with O_2

The α-ketocarboxylate complexes can therefore be considered as excellent functional models for α-ketoglutarate-dependent iron dioxygenase enzymes, the active sites of which usually contain five-coordinate iron centres bound by two histidine residues, one carboxylate residue and a bidentate α-ketoglutarate cofactor. Isotopic labelling studies with $^{18}O_2$ (**scheme 1.19**) showed that, in the case of the α-ketocarboxylate complexes, one oxygen atom derived from $^{18}O_2$ is incorporated into the aromatic phenoxide moiety, while the other becomes part of the derived carboxylate ligand in the case of the α-ketocarboxylate complexes, a distribution which is consistent with that observed in the natural system. Additionally, the α-ketocarboxylate complexes reacted with O_2 two orders of magnitude faster than the carboxylate derivatives, an observation which highlights the importance of the α-ketoglutarate cofactor in the activation of dioxygen by these metalloenzymes. The effectiveness of these systems as *structural* models is somewhat limited, due to the fact that the N_3 coordination environment provided by the Tp^{Ph2} does not

accurately replicate the 2-His-1-Carboxylate coordination observed in the metalloenzyme, though their prowess as functional models easily compensates for this.[133,134]

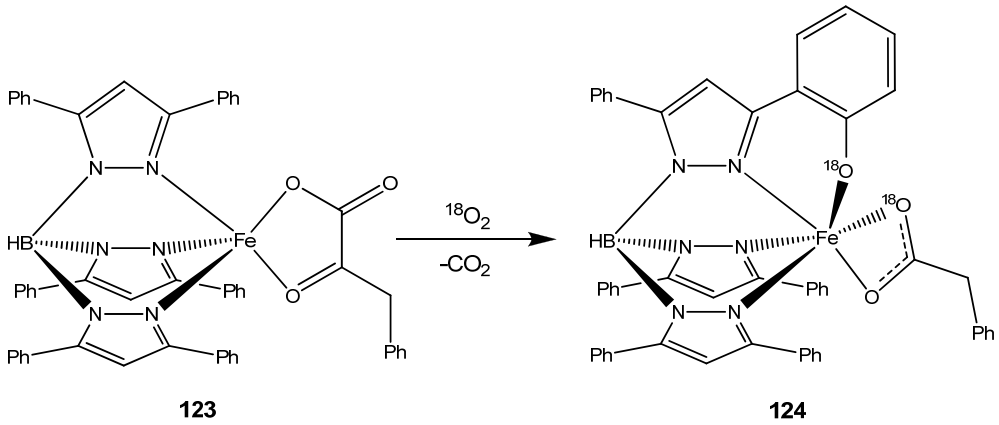

123 **124**

Scheme 1.19 Depiction of oxygen distribution in product (124) arising from oxidation of (Tp^{Ph2})Fe(O_2CCOBn) (123).

In certain rare examples, such as the enzyme 4-hydroxyphenylpyruvate dioxygenase, the α-ketoacid functionality is also the substrate, in this example being oxidised to 2,5-dihydroxyphenylacetate and CO_2. In an attempt to mimic this reactivity, the same researchers prepared the phenylpyruvate complex (Tp^{Ph2})Fe(O_2CCOBn) (**123**). However, upon reaction with O_2 (**scheme 1.19**), no oxygenation of the phenylpyruvate moiety was observed. As previously, an iron(III) complex (**124**) consisting of a tetradentate mono-oxygenated Tp^{Ph2} ligand, as well as a coordinated phenylacetate ligand arising from decarboxylation of the phenylpyruvate, was obtained as the only product (in addition to CO_2).[134]

The oxidative ability of (Tp^{Ph2})Fe(O_2CCOPh) towards a variety of substrates in the presence of O_2 was also investigated. With organosulfides, the corresponding sulfoxide iron(II) complexes were obtained without ligand oxidation, whereas cyclohexene was oxidised to 1,3-cyclohexadiene with concomitant formation of an unidentified diiron (III) by-product. Reactivity towards cycloalkanes was found to show evidence of shape-selectivity; cyclohexane showed no evidence of reaction, whereas cyclopentane and cyclooctane were found to undergo oxidation, albeit at a much slower rate than cyclohexene. Surprisingly, no oxygenation of hydrocarbon substrates was observed, a fact attributed to the alkyl radical (formed by interaction of the substrate and the putative oxo-iron(IV) intermediate) being too distant from the iron centre due to steric constraints to allow oxygen transfer to occur. Instead, one-electron oxidation of the alkyl radical to a carbocation is followed by rapid dehydrogenation.[135]

The formally six-coordinate (Tp^{Ph2})Fe(BH_4) (**125**) was also prepared by Que *et al.*, and is a rare example of a structurally characterised, monomeric late transition metal borohydride complex in which the BH_4^- anion is bound in a tridentate fashion. The short Fe-B distance, coupled with evidence from theoretical calculations, implies a significant bonding interaction between the Fe and B centres, and as such the bonding mode of the borohydride ligand may be reasonably described as η^4.[136] Harding and colleagues have prepared the series of cobalt(II) derivatives (Tp^{Ph2})Co(X) (X = Cl, Br, NO_2, NO_3, N_3, NCS), as well as (Tp^{Ph2})Co(η^1-OAc)(Hpz^{Ph2}) which was formed by the direct reaction of KTp^{Ph2} with $Co(OAc)_2$. Reaction of Tp^{Ph2}Co(η^1-OAc)(Hpz^{Ph2}) with acetylacetone, hexafluoroacetylacetone, dibenzoylmethane and 2,2,6,6-tetramethylheptane-3,5-dione in the presence of sodium methoxide gave the corresponding square-pyramidal β-diketonate complexes (**126**).[137] The same researchers also synthesised a series of (Tp^{Ph2})NiX (X = Br, OAc, NO_3, η^2-acac) derivatives, in addition to (Tp^{Ph2})NiCl(Hpz^{Ph2}) and (Tp^{Ph2})Ni(NO). The latter complex was prepared by reaction of KTp^{Ph2} with NiBr(NO)(PPh_3)$_2$, and as expected the nitrosyl ligand was determined by spectroscopy to exhibit a linear bonding mode, giving an 18-electron complex with a formally Ni(0) centre.[138]

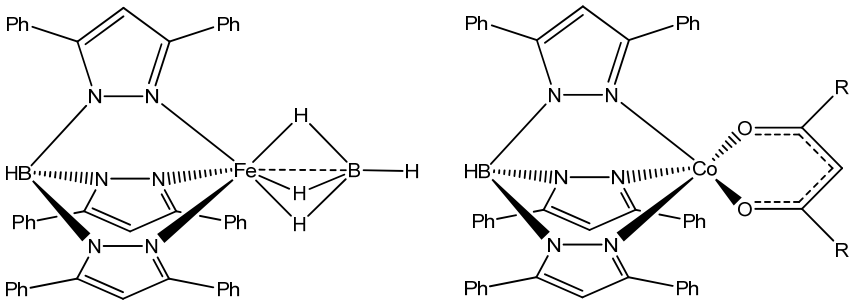

125 **126** (R = Me, CF_3, Ph, ^{t}Bu)

Figure 1.32 Structures of (Tp^{Ph2})Fe(BH_4) (125) and 126

1.5 Characteristic Features of Tripodal Nitrogen Ligands

Tris(pyrazolyl)borates are one of the archetypal members of a class of tridentate ligands known collectively as 'tripodal' ligands. A tripodal ligand can be defined as one which, due to its inherently restricted molecular geometry, may only coordinate to a metal ion in a facial (*fac*) manner (**figure 1.33**, (**i**)); i.e. to a single face of an octahedron (or tetrahedron).[139] An essential feature of all tripodal ligands is the presence of three donor functionalities ('legs'), each bound to a central structural scaffold. In the case of tris(pyrazolyl)borates, the three pyrazolyl donor legs are attached to a central BH scaffold, forming the tripod-like arrangement. In certain cases, such as $N(CH_2PPh_2)_3$, the central unit may also be a donor atom, giving potentially tetradentate ligands, many of which do indeed often behave in this manner. As this review shall be concerned primarily with tridentate tripodal nitrogen ligands, these tetradentate donors will not be considered further. The strictly *fac*-coordinating nature is unique to tripodal ligands; planar tridentate ligands such as terpyridine display only meridional (*mer*) coordination (i.e. to two coplanar edges of an octahedron) (**figure 1.33**, (**ii**)),[139] whereas non-rigid ligands like diethylenetriamine show no preference for either geometry and as such are unreliable when a specific coordination environment is required.

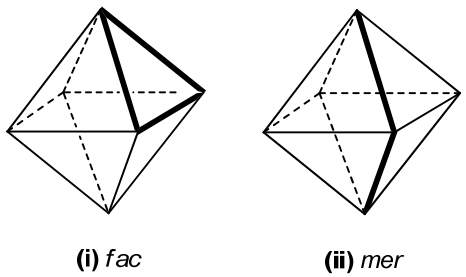

Figure 1.33 Schematic representation of an octahedral metal centre: (i) facially coordinated by a tripodal ligand; (ii) meridionally coordinated by a planar tridentate ligand.[139]

As can been seen from the aforementioned comments on the coordination chemistry of tris(pyrazolyl)borates, in the case of a four-coordinate metal centre, tetrahedral geometry (or some distortion of) is the only possible arrangement when bound to a tripodal ligand. Square-planar geometry, possible for metal complexes of non-rigid ligands and highly favoured by planar tridentate ligands, is an essentially impossible arrangement for four-coordinate complexes of tripodal ligands (unless the ligand binds in a bidentate fashion). As previously discussed, tripodal nitrogen donor ligands (especially those which contain heterocyclic donor functionalities) are extremely useful in replicating the tris-histidine

coordination sphere observed in the active sites of numerous metalloenzymes. This, coupled with the fact that nitrogen is an intermediate hard/soft Lewis base and as such forms complexes readily with metals from across the periodic table, has led to the preparation of a vast array of tripodal nitrogen ligands, each class displaying its own intrinsic coordination chemistry.

1.6 Ligands Based on a Tris(pyrazolyl)methane Architecture

1.6.1 Tris(pyrazolyl)methanes

Tris(pyrazolyl)methanes (Tpm^x) are the neutral analogues of Tp^x ligands, formally derived by the replacement of the BH^- group with an isoelectronic CH moiety. The parent ligand, tris(pyrazolyl)methane (Tpm), was first reported in 1937,[140] yet remained dormant with respect to coordination chemistry until 1966.[141] In analogy to the behaviour of the corresponding Tp^x ligands, the chemistry of Tpm and tris(3,5-dimethylpyrazolyl)methane (Tpm*) with respect to the first row d-block metals is dominated by the formation of octahedral bis-ligand complexes. In comparison to the Tp^x ligands, the chemistry of the tris(pyrazolyl)methanes has been little studied, and to date remains highly underdeveloped. This is mainly due to the synthetic difficulties and very low yields associated with the preparation of Tpm^x ligands in which the substituents on the pyrazolyl rings are larger than methyl. Until the development of an improved synthetic strategy by Elguero in 1984,[142] and its subsequent application in the generation of Tpm^x ligands bearing bulky substituents by the groups of Vahrenkamp[143] and Reger[144] in 1995 and 1996 respectively, there were only 15 reports pertaining to first-row d-block metal complexes of Tpm. Of these, only six described the synthesis of non-homoleptic complexes, such as $(Tpm)FeCl_3$,[145] $(Tpm)Fe(NCS)_2$,[146] $(Tpm)NiX_2(H_2O)$ (X = Cl, OAc)[147] and the organometallic mixed-sandwich species $[(Tpm)Co(L)][X]$ (L = η^5-C_5H_5, X = I; L = η^5-C_5Me_5, η^4-C_4Ph_4, X = PF_6).[148] The mono-Tpm derivatives $(Tpm)CuX_2$ (X = Cl, Br, OAc)[149] and $(Tpm)ZnX_2$[150] were also reported, but the authors gave little or no suggestion regarding the nature of their solid state structures.

Prior to 1995, the coordination chemistry of Tpm^x ligands was overwhelmingly dominated by second- and third-row d-block derivatives, which eschew the formation of sandwich complexes and instead usually form six-coordinate mono-Tpm^x derivatives. This

behaviour is identical to that observed for second- and third-row metal complexes of Tp^x and various other tripodal ligands, where bis-tripod complexes are very uncommon and restricted to a few adducts of certain d^0, d^6 and d^{10} ions. Four-coordinate complexes of tridentately coordinated tripodal ligands with the 4d and 5d elements are restricted to d^0 and d^{10} electron configurations, as are the related five-coordinate complexes except for a few highly distorted examples formed with d^8 metal ions. As such, in comparison to the related first-row metal complexes, the steric demands of the tripodal ligands have much less influence in dictating the geometry of the obtained adducts, which are far more dependent on the nature of the metal centre. The subsequent discussion will therefore concern non-sandwich complexes of the first-row d-block elements with Tpm^x ligands of varying steric bulk.

With an aim towards preparing biologically-relevant cationic zinc complexes in analogy to their work with neutral species such as $(Tp^{tBu,Me})ZnOH$, the 1995 report by Varhenkamp *et al.* described the synthesis five new bulky Tpm^x ligands, namely tris(3-*tert*-butyl-5-methylpyrazolyl)methane ($Tpm^{tBu,Me}$), tris(3-isopropyl-4,5-trimethylenepyrazolyl)methane ($Tpm^{iPr,(CH2)3}$), tris(3-*tert*-butyl-4,5-trimethylenepyrazolyl)methane ($Tpm^{tBu,(CH2)3}$), tris(3-phenyl-4,5-trimethylenepyrazolyl)methane ($Tpm^{Ph,(CH2)3}$) and tris(3-(*p*-cumenyl)-4,5-trimethylenepyrazolyl)methane ($Tpm^{Cum,(CH2)3}$). However, of these only $Tpm^{iPr(CH2)3}$, as well as the already known tris(3,4,5-trimethylpyrazolyl)methane (Tpm^{Me3}), gave ligand-containing products upon reaction with a variety of zinc salts. For example, in the case of $Tpm^{tBu,Me}$, $Tpm^{tBu,(CH2)3}$ and $Tpm^{Ph,(CH2)3}$, the Tpm^x ligands underwent hydrolysis in the presence of zinc salts to give the corresponding pyrazolyl zinc complexes, whereas $Tpm^{Cum,(CH2)3}$ was found to be completely unreactive towards the chloride, bromide, acetate and perchlorate salts of zinc. In the reaction of Tpm^{Me3} with $Zn(ClO_4)_2$, the sandwich compound $[(Tpm^{Me3})_2Zn][ClO_4]_2$ was formed as the only product, regardless of the stoichiometry of the reactants. Although $Tpm^{iPr,(CH2)3}$ did form 1:1 adducts with $ZnCl_2$ and $ZnBr_2$, the solid-state structures of $(\eta^2\text{-}Tpm^{iPr,(CH2)3})ZnX_2$ (**127**, X = Cl, Br) revealed the presence of bidentately coordinated $Tpm^{iPr,(CH2)3}$ ligands. Conversely, the bonding mode of $Tpm^{iPr,(CH2)3}$ in the octahedral $(Tpm^{iPr,(CH2)3})Zn(\eta^2\text{-}NO_3)(\eta^1\text{-}NO_3)$ (**128**) was found to be tridentate, a fact likely attributable to the reduced electron donating ability of the nitrate anion in comparison to halides.[143]

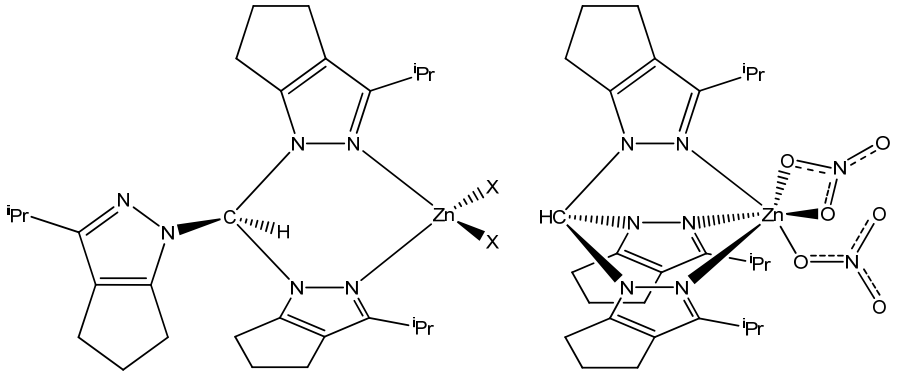

Figure 1.34 Structures of (η^2-Tpm$^{iPr,(CH2)3}$)ZnX_2 (127) and (Tpm$^{iPr,(CH2)3}$)Zn(η^2-NO_3)(η^1-NO_3) (128)

Removal of one of the bromide ligands in (η^2-Tpm$^{iPr(CH2)3}$)$ZnBr_2$ by metathesis with a single equivalent of silver perchlorate gave the rather unstable complex [(Tpm$^{iPr(CH2)3}$)ZnBr][ClO_4], whereas treatment with two equivalents of Ag(ClO_4) produced the highly unstable [(Tpm$^{iPr(CH2)3}$)Zn(OH_2)][ClO_4]$_2$. Though neither of these cationic complexes was stable enough to be crystallised, spectroscopic analysis supported the description of both as tetrahedral zinc compounds featuring tridentately coordinated Tpm$^{iPr,(CH2)3}$.[143] Tpm^{Me3} was also used by Pettinari and co-workers to prepare the 1:1 adducts (Tpm^{Me3})ZnX_2 (X = Cl, OAc), which were postulated to be either five-coordinate in the solid-state, or six-coordinate in the presence of coordinating solvents.[151] The fact that neither compound was subjected to X-ray structural analysis, coupled with the observed behaviour of the Tp$^{iPr,(CH2)3}$ ligand, makes the former assumption seem rather unlikely. Due to the apparent incompatibility of certain Tpm^x ligands with zinc salts, as well as the unpredictable nature of the few obtained complexes, it is perhaps unsurprising that very few such compounds have ever been reported.

In their aforementioned 1996 paper, Reger and co-workers reported the synthesis of tris(3-*tert*-butylpyrazolyl)methane (Tpm^{tBu}) and tris(3-phenylpyrazolyl)methane (Tpm^{Ph}), and the subsequent use of these ligands in addition to Tpm* to prepare the corresponding [(Tpm^x)Cu(NCMe)][PF_6] (**129**) adducts. Treatment of each of the copper(I) complexes with carbon monoxide was shown to give the corresponding carbonyl derivatives [(Tpm^x)Cu(CO)][PF_6] (**130**).[144]

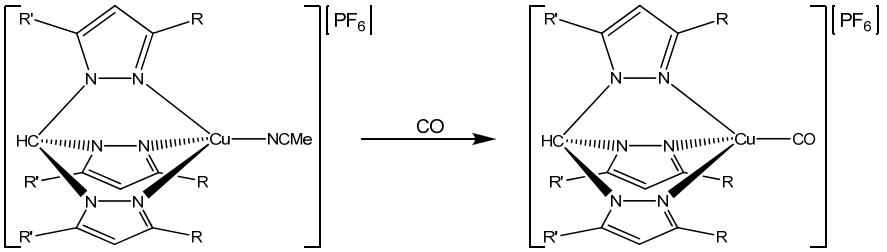

129 (R = R' = Me; R = ^{t}Bu, R' = H; R = ^{i}Pr, R' = H)

130 (R = R' = Me; R = ^{t}Bu, R' = H; R = ^{i}Pr, R' = H)

Scheme 1.20 Reaction of [(Tpm^{x})Cu(NCMe)][PF$_6$] (129) with CO

The carbonyl stretching vibrations observed for [(Tpm^{x})Cu(CO)][PF$_6$] are shifted to higher frequency in comparison to the analogous (Tp^{x})Cu(CO) complexes, due to the fact that the less electron-rich copper centres of [(Tpm^{x})Cu(CO)][PF$_6$] have a reduced propensity for π-backbonding to the CO ligand. This observation implies that the Tpm^{x} ligands are weaker electron donors than Tp^{x}, which is exactly as would be expected when comparing a charge-neutral ligand to a monoanionic one. In contrast to the behaviour of Tp^{x}-copper(I) adducts, it was reported that exposure of solutions of [(Tpm^{x})Cu(NCMe)][PF$_6$] to dioxygen at low temperature did not give the deep-purple colouration characteristic of the formation of a μ-η^2:η^2 peroxo-bridged dimer.[144] This observation was later proven to be erroneous, as Murray *et al.* reported that [(Tpm*)Cu(NCMe)][PF$_6$] did indeed react with O$_2$ (**scheme 1.21**) in DCM solution to give a purple-coloured species which was stable up to 7°C.[152]

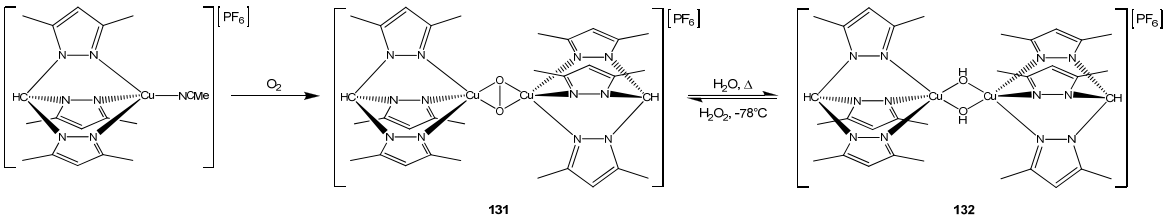

131 **132**

Scheme 1.21 Formation and decomposition of [{(Tpm*)Cu}$_2$(μ-η^2:η^2-O$_2$)][PF$_6$]$_2$ (131)

Although this dioxygen adduct could not be crystallised, spectroscopic analysis confirmed its identity as the peroxo-bridged dication [{(Tpm*)Cu}$_2$(μ-η^2:η^2-O$_2$)][PF$_6$]$_2$ (**131**), and the molecular structure of its decomposition product [{(Tpm*)Cu(μ-OH)}$_2$][PF$_6$]$_2$ (**132**) was determined by X-ray diffraction. Like the corresponding Tp^{x}-supported peroxo dicopper adducts, [{(Tpm*)Cu}$_2$(μ-η^2:η^2-O$_2$)][PF$_6$]$_2$ could also be regenerated by treatment of [{(Tpm*)Cu(μ-OH)}$_2$][PF$_6$]$_2$ with H$_2$O$_2$ at -78°C (**scheme 1.21**).[152] Kaim and co-workers prepared the similar compound [{(Tp$^{iPr(CH2)3}$)Cu}$_2$(μ-η^2:η^2-O$_2$)][BF$_4$]$_2$, which again was too

unstable to allow for crystallographic characterisation, but did form the crystalline decomposition product [{(Tpm$^{iPr(CH2)3}$)Cu(μ-OH)}$_2$][BF$_4$]$_2$.[153]

Fujisawa and co-workers prepared the ligand tris(3,5-diisopropylpyrazolyl)methane (Tpm^{iPr2}) and described the two five-coordinate copper(II) complexes, (Tpm^{iPr2})CuCl$_2$ (**133**) and (Tpm^{iPr2})Cu(η^1-NO$_3$)$_2$ (**134**).[154] (Tpm^{iPr2})CuCl$_2$ was subsequently reacted with two equivalents of sodium nitrite to give the very unusual five-coordinate (Tpm^{iPr2})Cu(η^1-*O*-NO$_2$)(η^1-*N*-NO$_2$) (**135**).[155] Mononuclear copper(II) complexes which feature N-bound nitrite ligands are relatively rare, while bis-nitrite complexes with mixed N/O coordination are exceptionally so. This behaviour is in stark contrast to that observed for (Tp^{iPr2})Cu(η^2-NO$_2$), which features a single nitrite ligand bound in the much more common bidentate *O,O′* mode.[155]

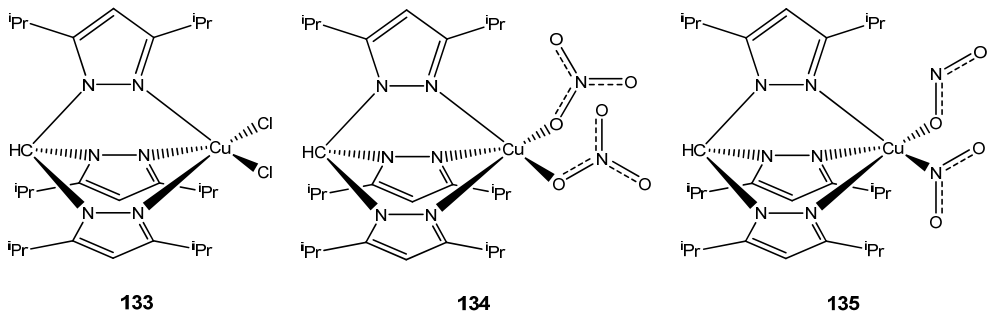

Figure 1.35 Structures of (Tpm^{iPr2})CuCl$_2$ (133), (Tpm^{iPr2})Cu(η^1-NO$_3$)$_2$ (134) and (Tpm^{iPr2})Cu(η^1-*O*-NO$_2$)(η^1-*N*-NO$_2$) (135).

Tris(3-*tert*-butyl-5-methylpyrazolyl)methane (Tpm^{tBu,Me}) was also employed by the same researchers to prepare [(Tpm^{tBu,Me})Cu(η^2-NO$_3$)][X] (**136**, X = ClO$_4$, ½Cu(NO$_3$)$_4$) and [(Tpm^{tBu,Me})CuCl][ClO$_4$] (**137**), which contain square-pyramidal and tetrahedral copper(II) centres respectively in the solid-state.[156] In this case, the obtained complexes are analogous in nature to their Tp^{tBu,Me} congeners, namely (Tp^{tBu,Me})CuCl[157] and (Tp^{tBu,Me})Cu(η^2-NO$_3$).[158]

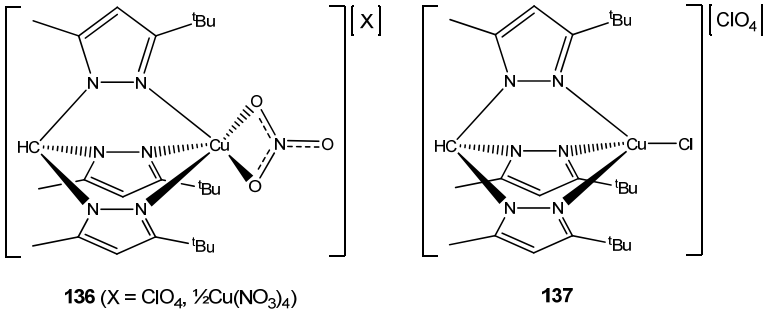

Figure 1.36 Structures of [(Tpm^{tBu,Me})Cu(η^2-NO$_3$)][X] (136) and [(Tpm^{tBu,Me})CuCl][ClO$_4$] (137)

A detailed investigation was also carried out into the structural and spectroscopic properties of the copper(I) adducts (Tpm^{iPr2})CuX (X = Cl, ClO_4), [(Tpm^{iPr2})Cu(L)][X] (L = NCMe, CO, X = PF_6, ClO_4), ($Tpm^{tBu,iPr}$)CuCl and [($Tpm^{tBu,iPr}$)Cu(NCMe)][PF_6] ($Tpm^{tBu,iPr}$ = tris(3-*tert*-butyl-5-isopropylpyrazolyl)methane). (Tpm^{iPr2})Cu(ClO_4) was found to react rapidly with O_2 to give the corresponding peroxo-bridged copper(II) dimer, whereas the reaction of [(Tpm^{iPr2})Cu(NCMe)][X] (X = PF_6, ClO_4) with O_2 was extremely sluggish. The carbonyl adducts were completely unreactive towards O_2, as was the very sterically encumbered [($Tpm^{tBu,iPr}$)Cu(NCMe)][PF_6].[159] The nitrosyl adduct [($Tpm^{tBu,iPr}$)Cu(NO)][ClO_4] (**138**) and the closely related ($Tp^{tBu,iPr}$)Cu(NO) were prepared and fully characterised as part of a highly detailed investigation into the nature of the bonding mode of NO in the NO-bound form of copper nitrite reductase enzymes.[160] With similar motivations, Fujii *et al.* used Tpm*, Tpm^{iPr2} and tris(3,5-diethylpyrazolyl)methane (Tpm^{Et2}) to prepare the corresponding (Tpm^{x})Cu(η^1-*N*-NO_2) (**139**) complexes, which are synthetic models for the nitrite-bound form of nitrite reductase. All the model complexes are four-coordinate in the solid state and feature N-bound nitrite ligands, as is commonly observed for such copper(I) adducts.[161]

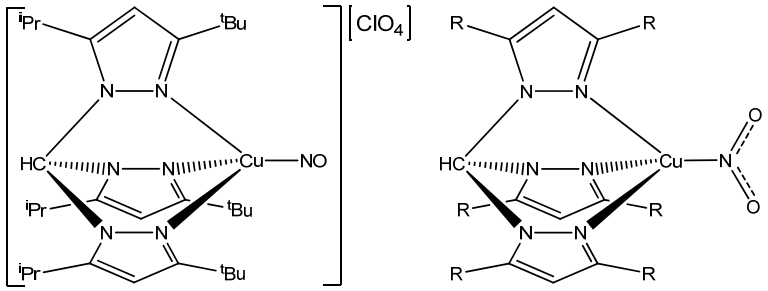

138 **139** (R = Me, Et, ^{i}Pr)

Figure 1.37 Structures of [($Tpm^{tBu,iPr}$)Cu(NO)][ClO_4] (138) and (Tpm^{x})Cu(η^1-*N*-NO_2) (139)

Using the apical *C*-functionalised ligands 2,2,2-tris(pyrazolyl)ethanol ($HOCH_2$Tpm) and 2,2,2-tris(pyrazolyl)ethyl methanesulfonate ($CH_3SO_3CH_2$Tpm), Pombeiro *et al.* prepared (η^3-*N,N′,N″*-$HOCH_2$Tpm)$CuCl_2$ (**140**) and {(η^2-*N,N′*-$CH_3SO_3CH_2$Tpm)$CuCl_2$}$_2$ (**141**), both of which show a high degree of solubility in water. These compounds were both shown to act as catalysts for the oxidation of cyclohexane to cyclohexanol and cyclohexanone by aqueous H_2O_2. Due to their high aqueous solubility, these systems are catalytically active in the absence of any organic solvent, albeit to a lesser degree than when acetonitrile is also present in the reaction mixture.[162]

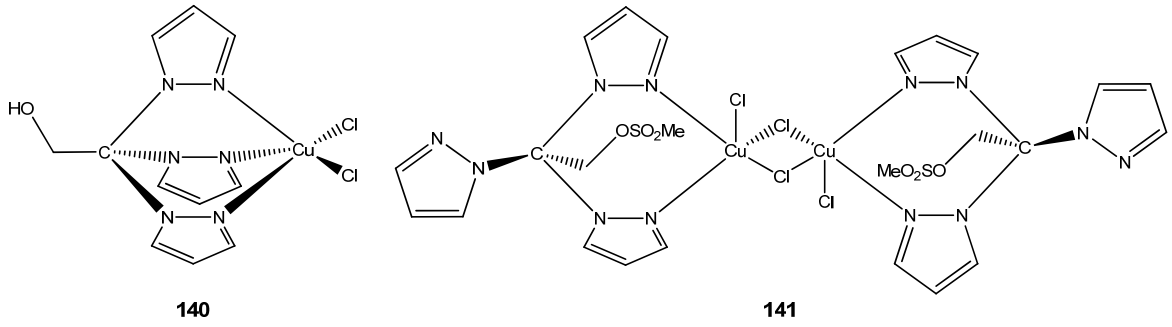

Figure 1.38 Structures of (η^3-*N,N',N''*-$HOCH_2Tpm$)$CuCl_2$ (140) and {(η^2-*N,N'*-$CH_3SO_3CH_2Tpm$)$CuCl_2$}$_2$ (141)

In 2000 Reger and co-workers reported the synthesis of tris(3-isopropylpyrazolyl)methane (Tpm^{iPr}) and $HOCH_2Tpm$, and used these ligands in addition to Tpm, Tpm* and Tpm^{Ph} to form the corresponding manganese(I) carbonyl adducts [(Tpm^x)$Mn(CO)_3$][OTf]. Unsurprisingly, Tpm^{tBu} did not coordinate to the $[Mn(CO)_3]^+$ fragment, again showing in analogy with the related $Tp^{tBu,R}$, the extreme reluctance of such 3-*tert*-butyl substituted ligands to form six-coordinate complexes.[163] The related [(Tpm)$Mn(CO)_3$][PF_6] has since been found to show photoinduced cytotoxicity towards colon cancer cells, to a degree comparable with the established chemotherapeutic 5-fluorouracil. Upon irradiation with UV light, [(Tpm)$Mn(CO)_3$][PF_6] undergoes photoinduced release of CO, which in turn is responsible for the resultant cytotoxicity. Due to the selective nature of CO toxicity, such CO-releasing compounds have potential advantages over those currently used in photodynamic therapy, which usually generate singlet oxygen as a non-specific destructive species.[164] Synthetic elaboration of $HOCH_2Tpm$ to 2,2,2-tris(pyrazolyl)ethyl propargyl ether ($HC{\equiv}CCH_2OCH_2Tpm$, **142**) allowed for further attachment of the Tpm moiety to functionalised amino acids and pentapeptides, either via 1,3-dipolar cycloaddition ('click') reactions of the alkyne group with azides, or through analogous Sonogashira cross-coupling reactions of the alkyne moiety with aryl iodides (**scheme 1.22**). The derived $[Mn(CO)_3]^+$ adducts showed identical photoinduced CO-releasing properties to [(Tpm)$Mn(CO)_3$][PF_6], and therefore such bioconjugate molecules may allow for targeted cellular delivery of the manganese tricarbonyl moiety.[165] It has been shown recently that the uptake and distribution of [(Tpm)$Mn(CO)_3$][Cl] in cancer cells can be studied by Raman microspectroscopy, making use of the characteristic CO vibrations as markers for the concentration of metal complex throughout the cell.[166]

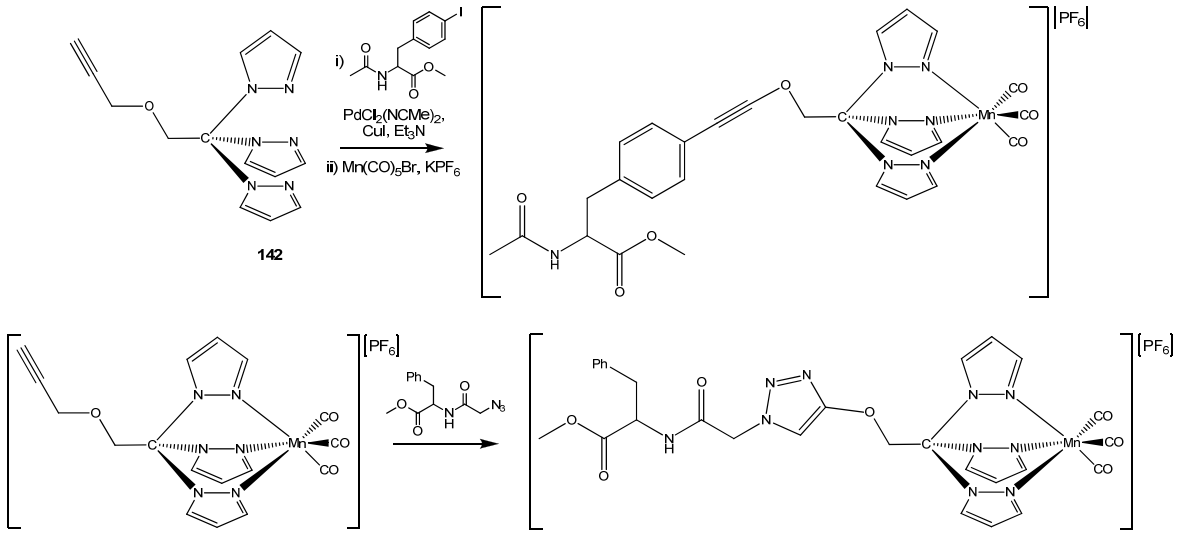

Scheme 1.22 Preparation of amino acid-[(Tpm)Mn(CO)$_3$]$^+$ conjugates

Fujisawa *et al.* also reported the preparation of (Tpm^{iPr2})MnCl$_2$ (**143**) and [(Tpm^{iPr2})Mn(Br)(MeOH)$_2$][Br] (**144**), and their subsequent application as precatalysts for the polymerisation of ethylene.[167] Both complexes show high activity upon activation with Al^{i}Bu$_3$/[Ph$_3$C][B(C$_6$F$_5$)$_4$]; in comparison to (Tp^{tBu,iPr})MnCl the activity of (Tpm^{iPr2})MnCl$_2$ is an order of magnitude greater, whereas for [(Tpm^{iPr2})Mn(Br)(MeOH)$_2$][Br] it is slightly lower. For both precatalyst systems the polyethylene produced had a much higher molecular weight than that obtained with (Tp^{tBu,iPr})MnCl, though the molecular weight distribution in both cases was much broader than that observed with the (Tp^{tBu,iPr})MnCl system.

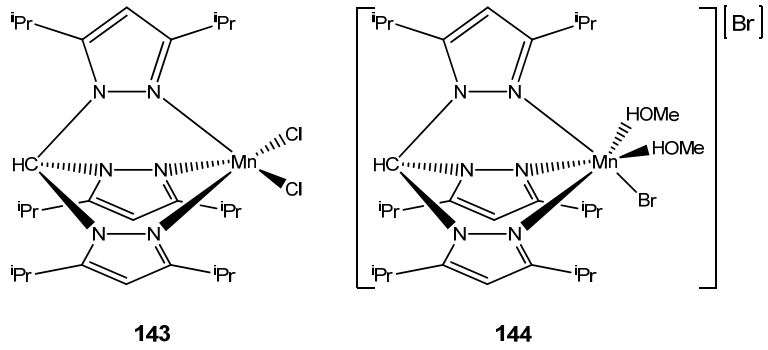

Figure 1.39 Structures of (Tpm^{iPr2})MnCl$_2$ (143) and [(Tpm^{iPr2})Mn(Br)(MeOH)$_2$][Br] (144)

The iron(II) complex [(Tpm)Fe(H$_2$O)$_3$][BF$_4$]$_2$ was the first non-sandwich iron-Tpm^x species for which the molecular structure was determined by X-ray diffraction. This compound was prepared using the iron(II) precursor [Fe(H$_2$O)$_6$][BF$_4$]$_2$, though as the reaction with Tpm was carried out using acetonitrile as the solvent, it is rather surprising that the tris-aqua adduct rather than the tris-acetonitrile complex was obtained.[168] By employing Tpm*

and Tpm^{Ph} in combination with $[M(NCMe)_6][BF_4]_2$ (M = Fe, Co), it was possible to prepare the octahedral iron(II) and cobalt(II) tris-acetonitrile adducts $[(Tpm^x)M(NCMe)_3][BF_4]_2$ (M = Fe, Co). All these complexes are high-spin paramagnetic species, as determined by magnetic measurements and examination of the M-N bond distances. In the case of the Tpm^{Ph} complexes, the average $M\text{-}N_{NCMe}$ bond lengths are shorter than the average $M\text{-}N_{Tpm}$ distances, an observation which suggests that the Tpm^{Ph} ligand is a weaker σ-donor than acetonitrile, though this may also be due to steric considerations. When $[(Tpm^x)M(NCMe)_3][BF_4]_2$ (M = Fe, Co) are treated with bidentate phosphine ligands such as 1,2-bis-(diphenylphosphino)ethane (dppe), the Tpm^x ligands are displaced yielding octahedral adducts of the general form $[M(NCMe)_2(dppe)_2][BF_4]_2$. This behaviour also supports the description of the Tpm^x ligands as relatively weak σ-donors.[169]

The dicyanamide-bridged iron(II) complex $\{(Tpm)Fe(\eta^1\text{-NCNCN})(\mu_{1,5}\text{-NCNCN})\}_2$ (**145**) was prepared by Murray and colleagues, as part of a study with the aim of producing dinuclear complexes in which one or both of the iron centres undergo 'spin-crossover', i.e. a change from high-spin to low-spin configuration or vice-versa in response to a change in temperature. However, both of the iron centres in $\{(Tpm)Fe(N\text{-NCNCN})(\mu_{1,5}\text{-NCNCN})\}_2$ were found to remain in the high-spin state across a wide temperature range of temperatures.[170]

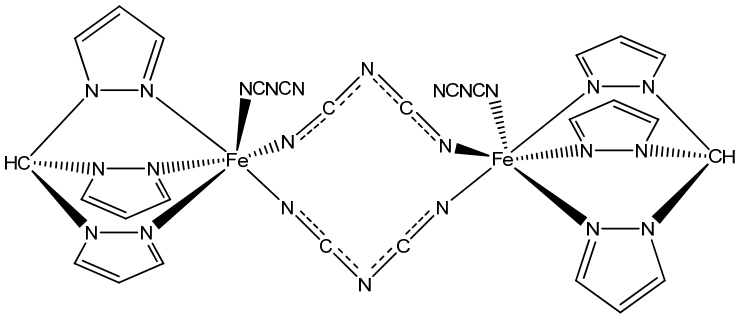

145

Figure 1.40 Structure of $\{(Tpm)Fe(\eta^1\text{-NCNCN})(\mu_{1,5}\text{-NCNCN})\}_2$ (145)

Similarly, the dimeric $\{(Tpm^*)Fe(NCE)(\mu\text{-NCE})\}_2$ (E = S, Se) were reported by Halcrow and co-workers. Neither of these complexes was sufficiently soluble in non-donating solvents to provide crystals suitable for X-ray diffraction, and as such the structural assignment was based purely on spectroscopic measurements. However, upon recrystallisation from acetonitrile, single crystals of the monomeric six-coordinate $(Tpm^*)Fe(NCE)_2(NCMe)$ (**146**, E = S, Se) were obtained. The acetonitrile molecules in

these complexes could be substituted by pyridine and imidazole to give (Tpm*)Fe(NCE)$_2$(py) (E = S, Se) and (Tpm*)Fe(NCS)$_2$(im) respectively, whilst reaction with 4,4'-bipyridine (**scheme 1.23**) yielded the bridged complexes {(Tpm*)Fe(NCE)$_2$}$_2$(μ-4,4'-bipy) (**147**, E = S, Se). (Tpm*)Fe(NCS)$_2$(py) could also be prepared through the direct reaction of Tpm* with Fe(NCS)$_4$(py)$_2$ in DCM, whereas the analogous reaction using Tpm in place of Tpm* gave the mixed-valence species [(Tpm)$_2$Fe^{II}][Fe^{III}(NCS)$_5$(py)]. The magnetic properties of (Tpm*)Fe(NCE)$_2$(py), (Tpm*)Fe(NCS)$_2$(im) and {(Tpm*)Fe(NCE)$_2$}$_2$(μ-4,4'-bipy) were investigated, yet none of these showed any evidence of spin-crossover behaviour.[171]

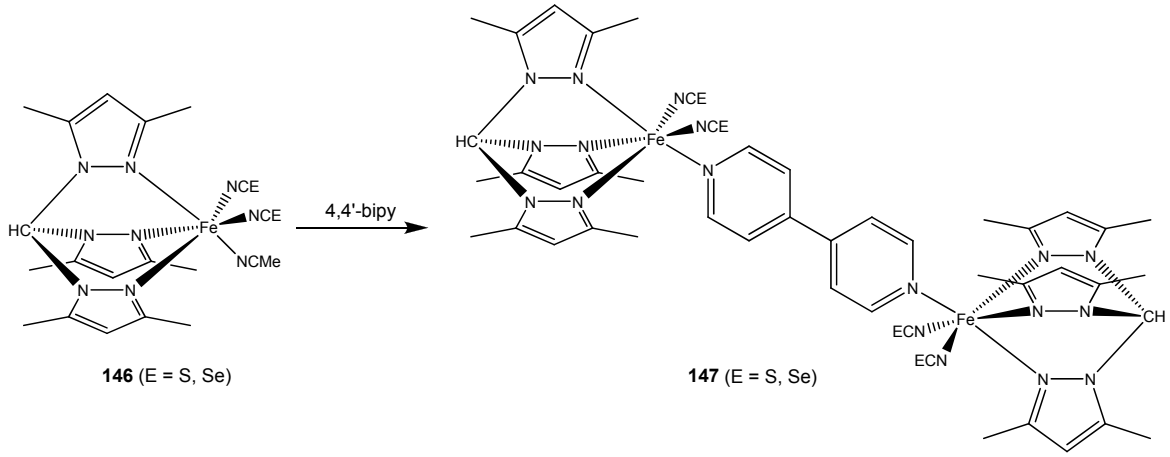

Scheme 1.23 Reaction of (Tpm*)Fe(NCE)$_2$(NCMe) (146) with 4,4'-bipy

Upon treatment of the iron trichloride adducts of Tpm, Tpm* and Tpm^{iPr} ((Tpm^x)FeCl$_3$, **148**) with H$_2$dbc in the presence of Et$_3$N and O$_2$ (**scheme 1.24**), 3,5-di-*tert*-butyl-2-hydroxy-1,4-benzoquinone was obtained as the major product, in addition to small amounts of the corresponding intradiol and extradiol oxidation products. This is in marked contrast to the aforementioned reactivity of (Tp^{iPr2})Fe(η^2-dbc)(NCMe), where approximately equal quantities of the intradiol and each of the two extradiol cleavage products were obtained, with the complete absence of any benzoquinone.[172] The efficacy of the Tpm^x complexes as functional models for catechol dioxygenases is therefore very poor in comparison to the (Tp^{iPr2})Fe(η^2-dbc)(NCMe) system. It was also reported that the yield of oxidation products decreases with increasing ligand steric bulk, which is concurrent with the observation that (Tp^{tBu,iPr})Fe(η^2-dbc) is totally inert with respect to oxidative cleavage of the dbc moiety.

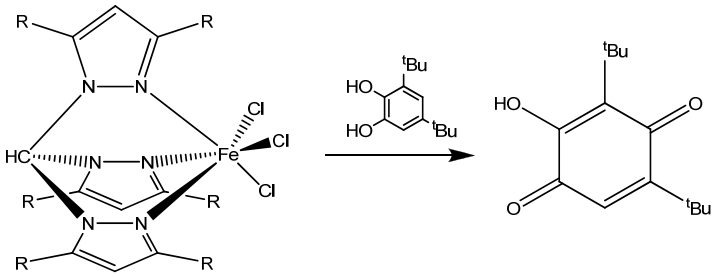

148 (R = R' = H;
R = R' = Me;
R = ^{i}Pr, R' = H)

Scheme 1.24 Oxidation of H_2dbc mediated by (Tpm^x)$FeCl_3$ (148)

Like the aforementioned chemistry of Tpm^x-zinc complexes, the coordination chemistry of nickel and cobalt with the Tpm^x ligands remains woefully underdeveloped. Aside from a number of Tp^x/Tpm^x supported mixed-Fe/Ni/Co clusters,[173] non-sandwich Tpm^x complexes of cobalt are limited to those already described above, whilst there are only four reports regarding non-sandwich derivatives of nickel. Zargarian *et al.* reported the synthesis and structural characterisation of (Tpm*)Ni(η^2-NO_3)(η^1-NO_3),[174] and a detailed analysis of its electronic absorption spectrum was described in a separate report.[175] The pyrazolate-bridged dimer [{(Tpm)Ni}$_2$(μ-1,2-pz)$_3$][OH] was prepared by Cheng and co-workers,[176] and recently Desrochers *et al.* have described a novel synthetic method which reliably gives access to simple non-sandwich nickel(II) complexes of Tpm. The appropriate nickel dihalide is treated (**scheme 1.25**) with the corresponding tetra-*n*-butylammonium salt in nitromethane to give the tetrahalonickelate salt *in situ*, then Tpm is added generating the octahedral (Tpm)$NiX_2(OH_2)$ (**149**, X = Cl, Br). These complexes are indefinitely stable in the solid-state, yet in solution they are rapidly converted to the corresponding [(Tpm)$_2$Ni][X]$_2$ species. Additionally, it was shown that (Tpm*)$NiCl_2(H_2O)$ can be obtained simply by direct reaction of a slight excess of Tpm* with $NiCl_2.6H_2O$ in acetone.[177]

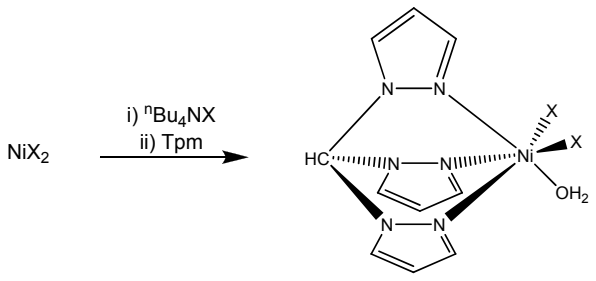

149 (X = Cl, Br)

Scheme 1.25 Preparation of (Tpm)$NiX_2(OH_2)$ (149)

The ligand 1,1,1-tris(pyrazolyl)ethane (MeTpm) was synthesised by Quijada and co-workers, and used alongside Tpm, Tpm*, $HOCH_2Tpm$, and $CH_3SO_3CH_2Tpm$ to form the corresponding $(Tpm^x)CrCl_3$ (**150**) adducts. Following activation with MAO, all of these complexes were found to show high activities as catalysts for the polymerisation of ethylene, except in the case of $(HOCH_2Tpm)CrCl_3$ which only displayed moderate activity. The presence of the relatively acidic hydroxy group in $(HOCH_2Tpm)CrCl_3$ likely accounts for its reduced activity, as in the presence of the strongly basic MAO the HO moiety is most probably deprotonated. This may in turn induce deleterious side-reactions, and thus cause a reduction in the efficacy of the catalyst. The generated alkoxide also has the potential to bind strongly to another Cr centre or an Al centre of the MAO cocatalyst, a factor which may also influence its activity. Similar considerations may account for the fact that $(MeTpm)CrCl_3$ displays an activity over four times greater than $(Tpm)CrCl_3$, due to the presence of the relatively acidic apical methine proton in Tpm.[178]

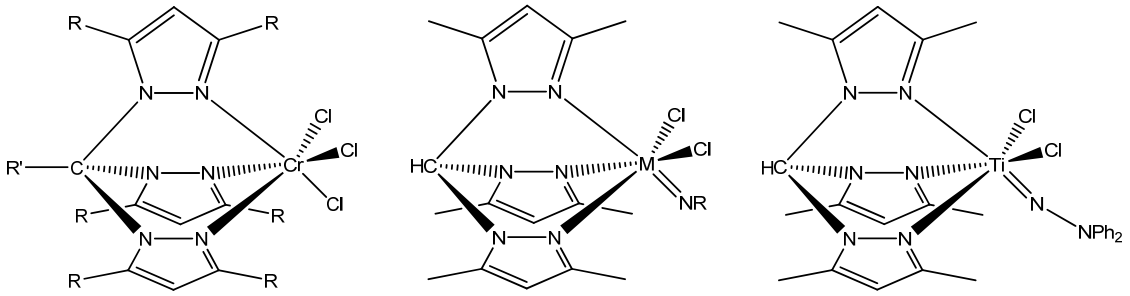

150 (R = R' = H; R = H, R' = Me; R = Me, R' = H; R = H, R' = CH_2OH; R = H, R' = CH_2O_3SMe)

151a (M = Ti, R = *see text*); **151b** (M = V, R = *see text*)

152

Figure 1.41 Structures of $(Tpm^x)CrCl_3$ (150), $(Tpm^*)MCl_2(NR)$ (151) and $(Tpm^*)TiCl_2(NNPh_2)$ (152)

Perhaps the most significant achievement in the field of first-row transition metal Tpm^x chemistry is represented by the work of Mountford and colleagues, which has involved the preparation of a wide range of six-coordinate imido-derivatives of titanium(IV) with the general formula $(Tpm^*)TiCl_2(NR)$ (**151a**, R = 1° alkyl, 2° alkyl, 3° alkyl, aryl).[179] The titanium complexes all show activity as precatalysts for the polymerisation of ethylene, especially at elevated temperatures, though the activities are highly dependent on the nature of the imido N-substituent. For example, at 100°C with an ethylene pressure of 7 bar, $(Tpm^*)TiCl_2(NC_6H_4\text{-}2\text{-}^tBu)$ shows an extremely high activity of 152,500 $kgmol^{-1}h^{-1}bar^{-1}$, whereas the slight reduction of steric bulk in $(Tpm^*)TiCl_2(NC_6H_4\text{-}2\text{-}^iPr)$ gives rise to a catalyst system with very low activity.[179(b)] The vanadium analogues $(Tpm^*)VCl_2(NR)$

(**151b**, R = ^{t}Bu, Ad, 2,6-$^{i}Pr_2C_6H_3$, 2-$^{t}BuC_6H_4$, 2-$CF_3C_6H_4$) also function as precatalysts for the polymerisation of ethylene, though the activities are several orders of magnitude lower than those observed for the most active titanium compounds.[180] The related hydrazido derivative (Tpm*)$TiCl_2(NNPh_2)$ (**152**) was also prepared by the same researchers and subjected to an extremely detailed theoretical analysis, though nothing pertaining to its efficacy with regards to catalysis was discussed.[181]

1.6.2 Tris(pyrazolyl)methanides

The research into (Tpm*)$TiCl_2(NR)$ complexes has also led to the isolation of the zwitterionic tris(3,5-dimethylpyrazolyl)methan*ide* complex {C(pz*)$_3$}TiCl(N^{t}Bu)(THF) (**153**), formed by treatment of (Tpm*)$TiCl_2$(N^{t}Bu) with methyllithium in THF and subsequent elimination of LiCl (**scheme 1.26**). The crystal structure of {C(pz*)$_3$}TiCl(N^{t}Bu)(THF) shows the presence of a 'naked' pyramidal carbanion, an unprecedented structural feature arising from deprotonation of the apical Tpm* methine carbon.[179(a)] Incidentally, {C(pz*)$_3$}TiCl(NC_6H_4-2-^{t}Bu)(THF), the zwitterionic analogue of (Tpm*)$TiCl_2$(NC_6H_4-2-^{t}Bu), also displayed high catalytic activity towards the polymerisation of ethylene, though this was slightly lower than that observed for the non-zwitterionic system. The molecular weight distribution of the polyethylene produced with {C(pz*)$_3$}TiCl(NC_6H_4-2-^{t}Bu)(THF) was also found to be very different to that of the polymer obtained with (Tpm*)$TiCl_2$(NC_6H_4-2-^{t}Bu), which implies that the actual catalytic species derived from the two systems are far from identical.[179(b)]

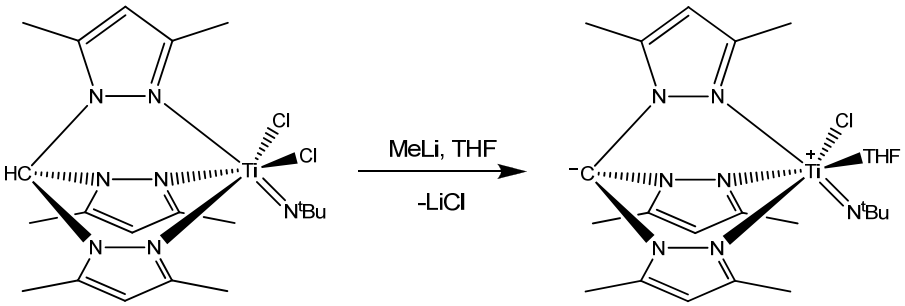

Scheme 1.26 Preparation of {C(pz*)$_3$}TiCl(N^{t}Bu)(THF) (153)

The analogous lithium complex {C(pz*)$_3$}Li(THF) (**154**) was obtained through treatment of free Tpm* with methyllithium, and was again found to contain a pyramidal carbanion in the solid state.[182] {C(pz*)$_3$}Li(THF) has proven to be a useful reagent for transfer of the {C(pz*)$_3$}$^{-}$ moiety to other metal centres, by means of metathesis with a series of copper(I),

silver (I) and gold (I) precursors (**scheme 1.27**). In $\{C(pz^*)_3\}Cu(PPh_3)$ (**155**) and $\{C(pz^*)_3\}Ag(PPh_3)$ (**156**), the $\{C(pz^*)_3\}^-$ ligand is N_3-coordinated and the complexes adopt a zwitterionic structure, whereas $(PPh_3)Au\{C(pz^*)_3\}$ (**157**) features a linear two-coordinate gold atom covalently bonded to the carbanionic centre. This illustrates the well-known preference of very large monocations such as gold(I) to favour coordination of 'soft' bases (e.g. carbanions) over harder donors like nitrogen.[183]

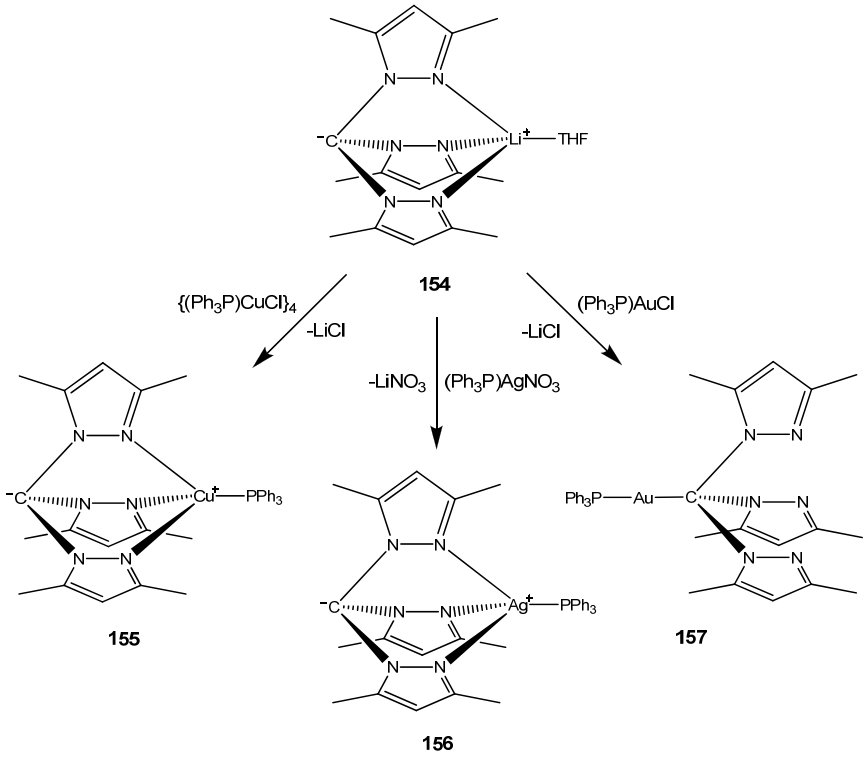

Scheme 1.27 Metathesis reactions of $\{C(pz^*)_3\}Li(THF)$ (154)

Complexes of $\{C(pz^*)_3\}^-$ may also be obtained through the reaction of Tpm* with highly basic metal compounds such as amide complexes, Grignard reagents and other organometallics. For example, reaction of Tpm* with MeMgX (X = Cl, Br) furnishes the tetrahedral adducts $\{C(pz^*)_3\}MgX$ (**158**, X = Cl, Br), while treatment of Tpm* with one equivalent of $MgPh_2$ in THF gives the five-coordinate $\{C(pz^*)_3\}MgPh(THF)$ (**159**). The neutral sandwich complex $\{C(pz^*)_3\}_2Mg$ (**160**) could be obtained by reaction of Tpm* with a half-equivalent of either $MgPh_2$ or Mg^nBu_2 in the absence of THF, whereas reaction of Tpm* with an excess of $ZnMe_2$ gave $\{C(pz^*)_3\}ZnMe$ (**161**).[184]

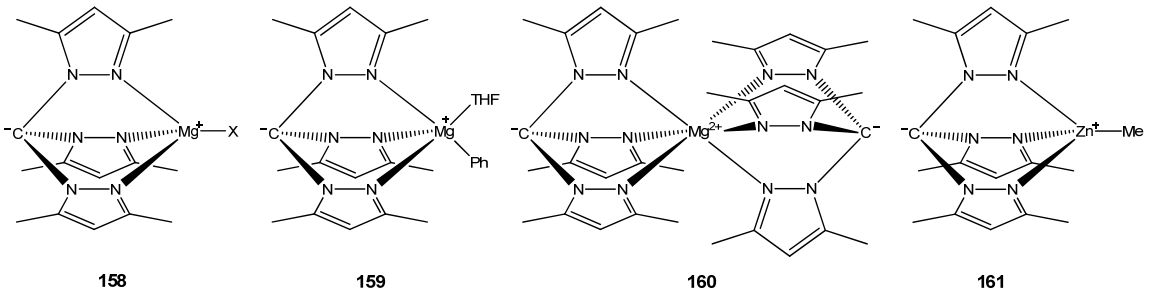

Figure 1.42 Structures of {C(pz*)$_3$}MgX (158), {C(pz*)$_3$}MgPh(THF) (159), {C(pz*)$_3$}$_2$Mg (160) and {C(pz*)$_3$}ZnMe (161)

The amides M(NSiMe$_3$)$_2$ (M = Mg, Ca, Cd) have been used to prepare a variety of {C(pz*)$_3$}$^-$ derivatives of group 2 and group 12 metals, as detailed in **scheme 1.28**. Conversely, Tpm* was unreactive towards Zn(N(SiMe$_3$)$_2$)$_2$, though metathesis of {C(pz*)$_3$}Li(THF) with ZnCl$_2$ gave {C(pz*)$_3$}ZnCl or {C(pz*)$_3$}$_2$Zn depending on the stoichiometry. Subsequent reaction of {C(pz*)$_3$}ZnCl with M(NSiMe$_2$R) (M = Li, R = H; M = Na, R = Me) gave access to the corresponding amido zinc complex (**scheme 1.28**). The molecular structure of {C(pz*)$_3$}Cd{C(pz)$_3$} is very unusual; the {C(pz*)$_3$}$^-$ ligand is bound in the regular zwitterionic fashion, whereas {C(pz)$_3$} is coordinated in a η^1-*C*,η^2-*N*,*N'* mode.[185]

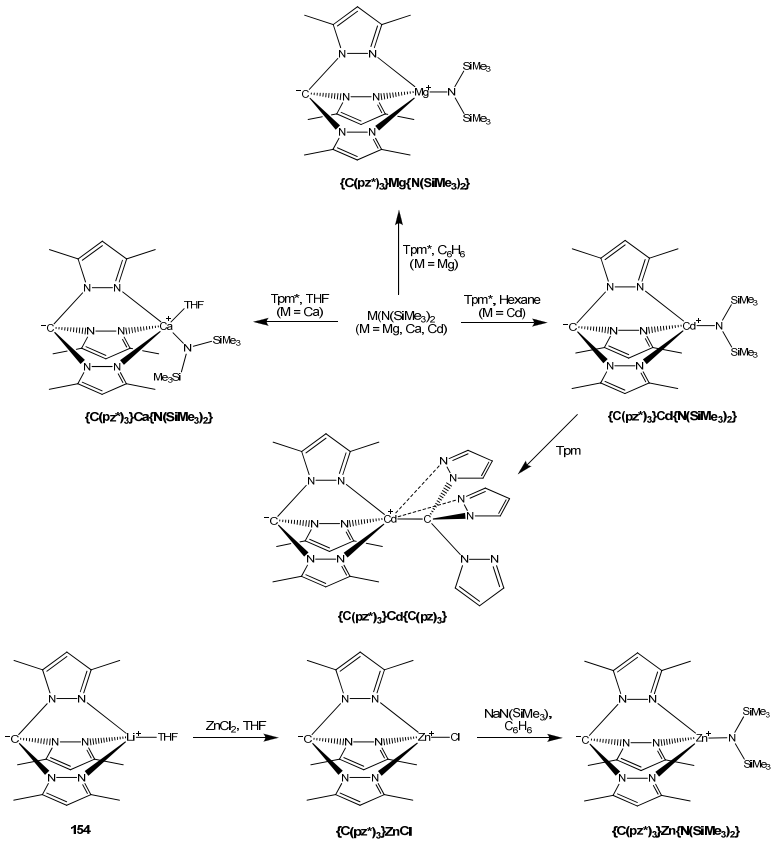

Scheme 1.28 Preparation of {C(pz*)$_3$}$^-$ complexes

The transition metal sandwich complexes $\{C(pz^*)_3\}_2M$ (M = Fe, Co) were prepared by simple deprotonation of $[(Tpm^*)_2M][OTf]_2$ (M = Fe, Co) with $Na(N(SiMe_3)_2)$, which were subsequently treated with ferrocenium hexafluorophosphate yielding the trivalent species $[\{C(pz^*)_3\}_2M][PF_6]$ (M = Fe, Co). The molecular structures of $\{C(pz^*)_3\}_2M$ (M = Fe, Co) were determined by X-ray diffraction, whereas the trivalent compounds were too insoluble to allow for the formation of single crystals.[186]

1.6.3 Tris(pyrazolyl)methanesulfonates

If a lithiated Tpm^x ligand is quenched with sulfur trioxide trimethylamine complex, the lithium salt of the corresponding tris(pyrazolyl)methanesulfonate ($Tpms^x$) ligand is obtained. The hydrophilic nature of these ligands and their derived complexes makes them potentially very useful in the area of enzyme modelling, due to the fact that in order for a model complex to truly replicate a biological system, it must be water soluble and also be able to function in an aqueous environment. This may be also important in the area of catalysis, where systems which operate in aqueous solution are actively sought after due to the inherently 'green' nature of being able to avoid the use of environmentally-harmful organic solvents.

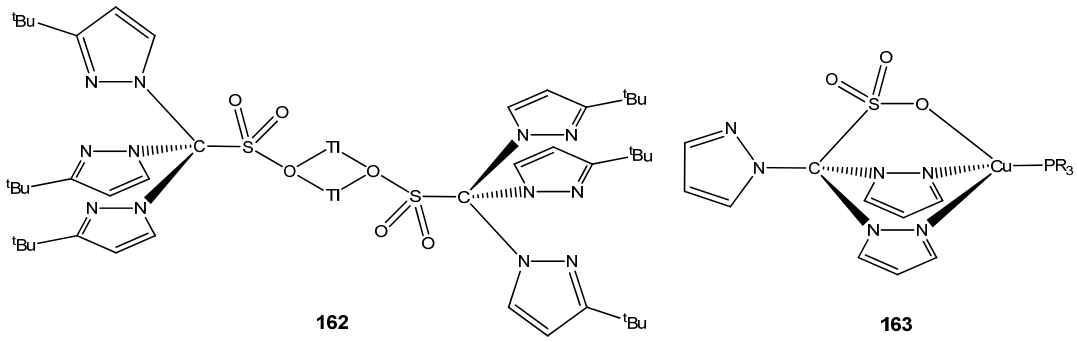

Figure 1.43 Structures of $\{(\mu\text{-}\eta^1\text{-}O\text{-}Tpms^{tBu})Tl\}_2$ (162) and $(\eta^3\text{-}N,N',O\text{-}Tpms)Cu(L)$ (163)

In 2000 Klaüi and co-workers reported the synthesis of the parent ligand tris(pyrazolyl)methanesulfonate (Tpms), as well as the much more bulky tris(3-*tert*-butylpyrazolyl)methanesulfonate, yet the only metal complex described (excluding the lithium and potassium salts) was the thallium(I) derivative of $Tpms^{tBu}$. The molecular structure of $\{(\mu\text{-}\eta^1\text{-}O\text{-}Tpms^{tBu})Tl\}_2$ (**162**) showed that the two thallium ions were both two-coordinate, bound only by a single sulfonate oxygen atom of the $Tpms^{tBu}$ ligand, and formed a square-shaped dimer with the donor oxygen acting as bridge to the other thallium centre.[187] The same researchers subsequently prepared the rhodium(I) adducts (η^2-*N,N'*-

Tpms)Rh(CO)$_2$, (η^2-*N,N′*-Tpms)Rh(cod)$_2$, (η^3-*N,N′,N″*-Tpms)Rh(nbd)$_2$ (nbd = norbornadiene) and (η^2-*N,N′*-Tpms)Rh(CO)(L) (L = PMe_3, PPh_3, PCy_3, $PPh_2(C_6H_4$-4-$SO_3K)$); all of these compounds feature the Tpms ligand bound either in a bidentate or tridentate fashion, and exclusively through the pyrazolyl N-donors.[188] However, when LiTpms was reacted with CuCl in the presence of a tertiary phosphine, the complexes (η^3-*N,N′,O*-Tpms)Cu(L) (**163**, L = PPh_3, $P(C_6H_4$-4-$CH_3)_3$) were obtained. In addition to the asymmetric coordination mode of the Tpms ligand being present in the solid state, low-temperature NMR studies confirmed that this bonding mode is maintained in solution.[189] The superoxide-scavenging abilities of the related (Tpms)Cu{$PPh_2(C_6H_4$-4-$CO_2H)$} and (Tpms)Cu{$P(C_6H_4$-3-$SO_3Na)_3$} were investigated and compared to that of the superoxide dismutase enzyme. Though their activities were found to be much lower than that of the enzymatic system, they were comparable to that of Cu_2(aspirinate)$_4$, an approved antioxidant drug. This degree of activity, coupled with the high water solubility imparted by the hydrophilic phosphine and Tpms ligands, means that such complexes therefore have potential application as pharmaceutical antioxidants.[190]

Tpms^{tBu} was employed to prepare a series of first-row d-block metal derivatives, and the bonding mode of the ligand was again found to be variable, being dependent on the nature of the metal centre. For example, the tetrahedral adducts (Tpms^{tBu})ZnX (X = Cl, Br) exist in solution as an equilibrium mixture of the *N,N′,N″* (**164**) and *N,N′,O* (**165**) isomers, yet both crystallise exclusively in the latter form. Conversely, the ^{1}H NMR spectrum of (Tpms^{tBu})ZnI shows no evidence of the *N,N′,N″* isomer, even at low temperature.[191]

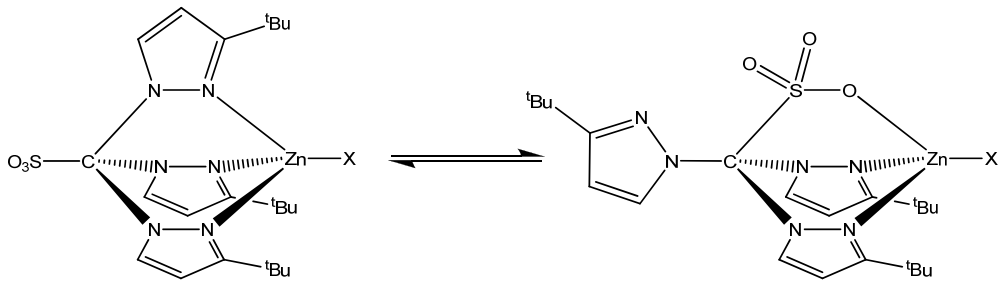

164 (X = Cl, Br) **165** (X = Cl, Br)

Figure 1.44 Different bonding modes of Tpms^{tBu} in (Tpms^{tBu})ZnX

In marked contrast to the behaviour of the (Tpms^{tBu})ZnX compounds, (Tpms^{tBu})NiX (**166**, X = Cl, Br) display *N,N′,N″* coordination exclusively, both in solution and in the solid state. When Tpms^{tBu} was reacted with $CoCl_2$ in methanol, the five-coordinate (η^3-*N,N′,O*-Tpms^{tBu})CoCl(Hpz^{tBu}) (**167**), featuring a free 3-*tert*-butylpyrazole ligand arising from

hydrolysis of the Tpms^{tBu} ligand, was obtained as the only product. By adopting the *N,N′,O* bonding mode, the Tpms^{tBu} ligand allows for five-coordination at the cobalt centre, an arrangement which would likely be highly disfavoured in the case of exclusive *N,N′,N″* binding. This behaviour also implies a slightly higher preference of cobalt(II), in comparison to nickel(II) and zinc(II), for the formation of five-coordinate complexes over four-coordinate ones.[191]

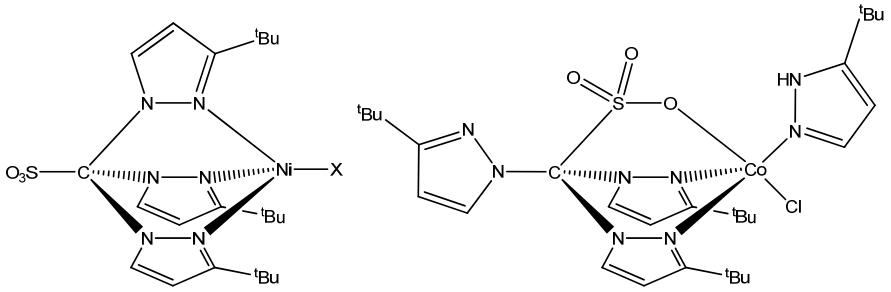

Figure 1.45 Structures of (Tpms^{tBu})NiX (166) and Tpms^{tBu})CoCl(Hpz^{tBu}) (167)

The acetate complex (Tpms^{tBu})Zn(OAc) was prepared in a rather unusual manner, through the reaction of (Tpms^{tBu})ZnEt with one equivalent of acetic acid in THF. However, when (Tpms^{tBu})ZnEt was reacted with a half-equivalent of acetic acid in benzene, the asymmetric dinuclear complex (η^2-*N,O*-Tpms^{tBu})Zn(μ-OH)(μ-OAc)Zn(η^3-*N,N′,O*-Tpms^{tBu}) (**168**) was obtained as the only product. The bridging hydroxide likely originates from trace water present in the solvent or acetic acid, and due to its small size gives rise to an asymmetrical bridge between the two zinc centres. This in turn causes the dimer to adopt a folded structure, and as such one of the Tpms^{tBu} ligands is only able to bind in a bidentate fashion. (η^2-*N,O*-Tpms^{tBu})Zn(μ-OH)(μ-OAc)Zn(η^3-*N,N′,O*-Tpms^{tBu}) is a structural model for the active sites of dizinc enzymes such as phospholipase and phosphodiesterase, which contain two N,N,O bound zinc centres linked by a bridging hydroxide and a bridging carboxylate ligand.[191]

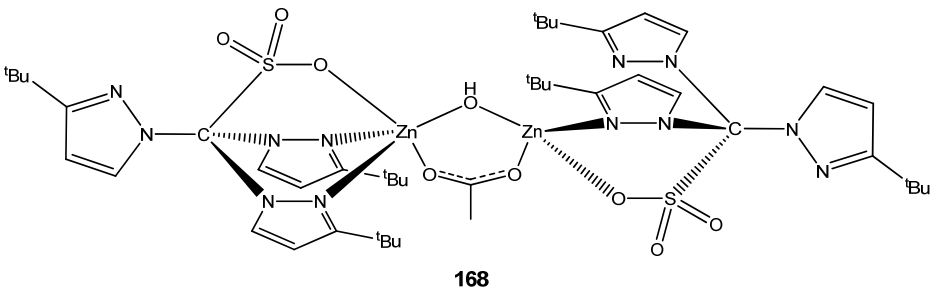

Figure 1.46 Structure of (η^2-*N,O*-Tpms^{tBu})Zn(μ-OH)(μ-OAc)Zn(η^3-*N,N′,O*-Tpms^{tBu}) (168)

The reaction of lithium tris(3-isopropylpyrazolyl)methane sulfonate (LiTpms^{iPr}) with a variety of first-row d-block metal precursors gave exclusively the sandwich complexes (η^3-*N,N′,O*-Tpms^{iPr})$_2$M (**169**, M = Fe, Co, Ni, Cu, Zn), except for when $ZnCl_2$ was reacted with LiTpms^{iPr} and the product was recrystallised from THF/cyclohexane. In this case the isolated product was (η^2-*N,N′*-LiTpms^{iPr})$ZnCl_2$ (**170**), in which the LiTpms^{iPr} precursor had failed to undergo a metathesis reaction with $ZnCl_2$. In an attempt to prepare a tetrahedral zinc hydroxo complex, (η^3-*N,N′,O*-Tpms)$_2$Zn was reacted with NaOH, yet the only crystalline product that could be isolated was NaTpms^{iPr}. Due to the seeming preference for *N,N′,O* coordination of Tpms^x ligands towards the first row d-block ions, the presence of only two isopropyl groups close to the metal centres in adducts of Tpms^{iPr} provides insufficient steric shielding to prevent the formation of octahedral bis-Tpms^{iPr} complexes.[192]

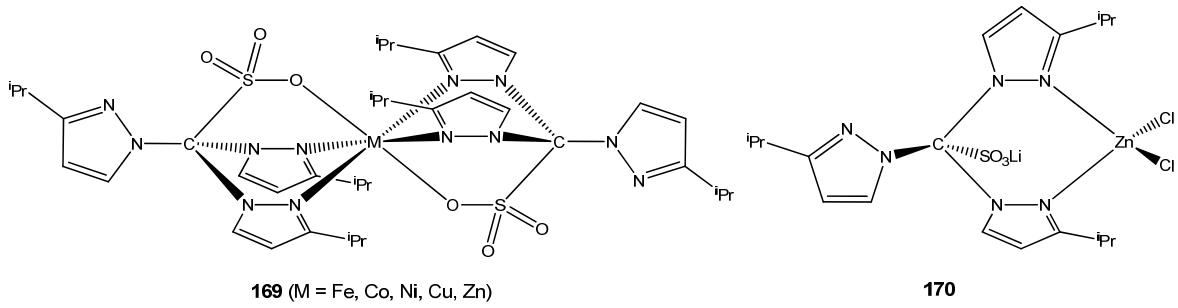

Figure 1.47 Structures of (η^3-*N,N′,O*-Tpms^{iPr})$_2$M (169) and (η^2-*N,N′*-LiTpms^{iPr})$ZnCl_2$ (170)

Tris(3-phenylpyrazolyl)methanesulfonate (Tpms^{Ph}) was used by Pombeiro *et al.* to prepare the copper(I) complexes (η^3-*N,N′,O*-Tpms^{Ph})Cu(L) (**171**, L = NCMe, hexamethylenetetramine (hmt)), (η^3-*N,N′,N″*-Tpms^{Ph})Cu(*P*-pta) (**172**, pta = 1,3,5-triaza-7-phosphaadamantane) and [(η^3-*N,N′,N″*-Tpms^{Ph})Cu(*P*-mpta)][PF_6] (**173**, mpta = *N*-methyl-1,3,5-triaza-7-phosphaadamantane), for which the bonding mode of the Tpms^{Ph} ligand was found to be dependent on the nature of the ancillary ligand.[193]

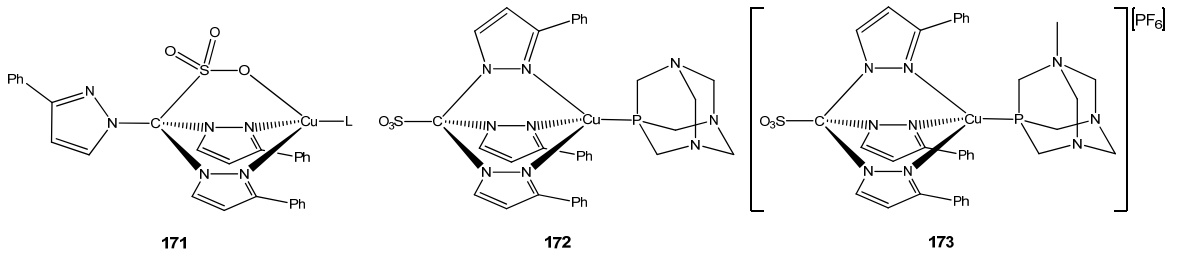

Figure 1.48 Structures of (η^3-*N,N′,O*-Tpms^{Ph})Cu(L) (171), (η^3-*N,N′,N″*-Tpms^{Ph})Cu(*P*-pta) (172) and [(η^3-*N,N′,N″*-Tpms^{Ph})Cu(*P*-mpta)][PF_6] (173)

In the case of the solely σ-donating acetonitrile and hexamethylenetetramine ligands, the copper(I) centre favours the more weakly electron-donating *N,N′,O* bonding mode of the $Tpms^{Ph}$. However, in combination with π-accepting phosphine ligands, the metal seems to favour the more strongly electron-releasing *N,N′,N″* configuration, despite the increase in steric repulsion that this entails.[193] The same researchers also prepared (Tpms)VCl_3, (Tpms)CuCl and [Li][(Tpms)$FeCl_2$], and although no crystal structures were obtained the authors assigned an *N,N′,N″* coordination mode of Tpms in all the complexes, though there was scant discussion of evidence for this. [Li][(Tpms)$FeCl_2$] was found to be an effective precatalyst for the oxidation of cyclohexane, in analogy with the Tpm^x-copper(II) compounds described in **section 1.6.1**. The high water solubility of [Li][(Tpms)$FeCl_2$] enabled it to operate using only water as a solvent, though once again the activity was increased in the presence of acetonitrile.[194] Similarly, (η^3-*N,N′,O*-Tpms)VOCl(DMF) was found by McLauchlan *et al.* to be catalytically active towards the oxidation of 3,5-di-*tert*-butylcatechol to 3,5-di-*tert*-butyl-1,2-benzoquinone.[195]

1.7 Other Tris(pyrazolyl) Ligands

1.7.1 Tris(pyrazolyl)phosphines

A number of other ligand systems based on a tris-pyrazolyl framework which contain core atoms other than boron or carbon are known, though most of these are restricted to very small numbers of reports regarding their coordination chemistry. For example, the neutral tris(3,5-dimethylpyrazolyl)phosphine (Tpp*) ligand and its oxide (Tppo*) have been used to prepare octahedral carbonyl adducts such as (Tpp*)$M(CO)_3X$ (**174**, M = Mn, X = Cl; M = Re, X = Br),[196] Tpp*$M(CO)_3$ (**175**, M = Mo, W)[197] and (Tppo*)$Mo(CO)_3$.[198] As would be expected for metal carbonyl derivatives of charge-neutral ligands, the carbonyl stretching vibrations are shifted to higher mean frequencies relative to the analogous Tp* complexes.

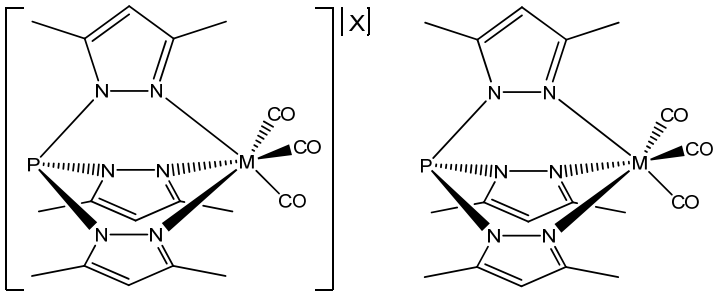

174 (M = Mn, X = Cl; M = Re, X = Br)

175 (M = Mo, W)

Figure 1.49 Structures of (Tpp*)M(CO)$_3$X (174) and Tpp*M(CO)$_3$ (175)

The chiral ligand OP(pz^{Camph})$_3$ represented the first example of a tris-pyrazolyl compound to be prepared in an enantiomerically pure form, and was used to generate the optically active tetrahedral complexes [{η^3-OP(pz^{Camph})$_3$}Cu(NCMe)][BF$_4$] (**176**), {η^3-OP(pz^{Camph})$_3$}CuX (**177**, X = Cl, OTf) and {η^2-OP(pz^{Camph})$_3$}ZnCl$_2$ (**178**). When [{η^3-OP(pz^{Camph})$_3$}Cu(NCMe)][BF$_4$] was employed as a catalyst in the cyclopropanation of styrene by ethyl diazoacetate, the *cis*-product was obtained in up to 60% enantiomeric excess (ee).[199]

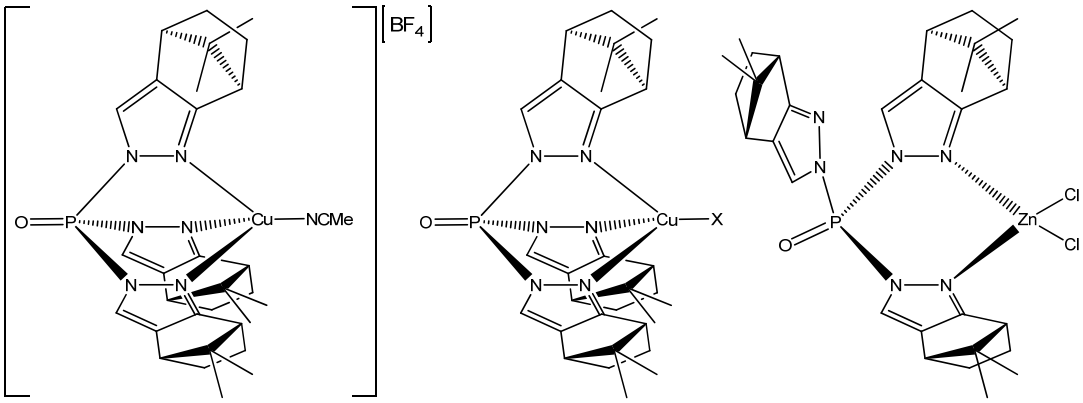

176 **177** (X = Cl, OTf) **178**

Figure 1.50 Structures of [{η^3-OP(pz^{Camph})$_3$}Cu(NCMe)][BF$_4$] (176), {η^3-OP(pz^{Camph})$_3$}CuX (177) and {η^2-OP(pz^{Camph})$_3$}ZnCl$_2$ (178)

1.7.2 Tris(pyrazolyl)gallates and Tris(pyrazolyl)aluminates

Methyltris(pyrazolyl)gallate (MeTpg) and methyltris(3,5-dimethylpyrazolyl)gallate (MeTpg*) are heavier group 13 analogues of Tp and Tp* respectively, and behave in a very similar fashion to their lighter congeners. Upon reaction of MeTpg with a series of first-row d-block metal halides, the neutral sandwich complexes (MeTpg)$_2$M (**179**, M = Mn, Fe, Co, Ni, Cu, Zn) were obtained.[200] Both MeTpg and MeTpg* were also found to react with Ni(NO)I to give the corresponding four-coordinate (Tpg^x)Ni(NO) (**180**) species.[201] The

mean carbonyl stretching frequencies observed for (MeTpg)Mn(CO)$_3$[200] and (MeTpg*)Mn(CO)$_3$[202] are shifted to lower energy by approximately 10 cm^{-1} in comparison to their Tp^x analogues, which implies that the MeTpg^x ligands are slightly stronger σ-donors, and thus give rise to more electron-rich metal centres. The related methyltris(3,5-di-*tert*-butylpyrazolyl)aluminate (MeTpa^{tBu2}) has been reported as the sodium adduct (MeTpa^{tBu2})Na(THF), which was obtained from the reaction of polymeric [Na{Al(pz^{tBu2})Me$_3$}$_3$(THF)$_2$]$_n$ with two further equivalents of Hpz^{tBu2}. The molecular structure of (MeTpa^{tBu2})Na(THF) (**181**) shows that, in addition to regular η^3-coordination, there is further strong bonding interaction between the sodium ion and a single pyrazole boron-bound nitrogen atom.[203] No attempts regarding subsequent transmetallation reactions of this complex, for example with transition metal halides, have been reported.

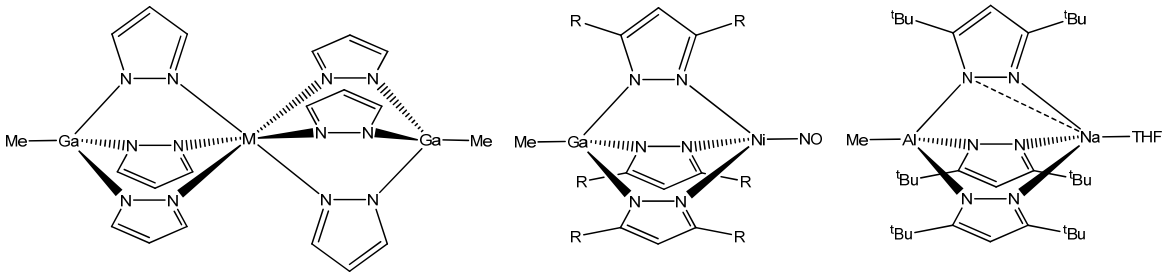

179 (Mn, Fe, Co, Ni, Cu, Zn) **180** (R = H, Me) **181**

Figure 1.51 Structures of (MeTpg)$_2$M (179) and (Tpg^x)Ni(NO) (180)

1.7.3 Tris(pyrazolyl)silanes

Tris(pyrazolyl)silanes, such as methyltris(3,5-dimethylpyrazolyl)silane (MeTps*) and methyltris(3-*tert*-butylpyrazolyl)silane (MeTps^{tBu}) do not suffer from the same synthetic difficulties associated with the related Tpm^x ligands, and can be prepared in high yield and purity through the reaction of methyltrichlorosilane with the appropriate alkali metal pyrazolate.[204] Even so, there are still only a handful of reports regarding their coordination chemistry. Rabinovich and co-workers used MeTps* and MeTps^{tBu} to prepare the corresponding [(MeTps^x)Cu(NCMe)][PF$_6$] (**182**) complexes,[205] as well as the carbonyl adducts (MeTps*)M(CO)$_3$ (**183**, M = Cr, Mo, W).[206] Whilst the spectroscopic and structural data for the carbonyl complexes show that the Tps* ligand is electronically very similar to Tpm*, inspection of the solid-state structures also implies that it is somewhat bulkier, in fact to a degree comparable to Tp^{tBu}.[206]

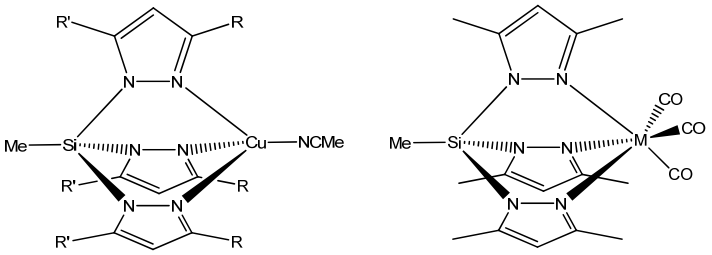

Figure 1.52 Structures of $[(MeTps^{x})Cu(NCMe)][PF_6]$ (182) and $(MeTps^{*})M(CO)_3$ (183)

In addition to their preparation of $(MeTps^{*})MCl_3$ (M = Sc, Y),[207] Mountford and colleagues also reported that upon reaction with $\{(THF)_2ZrCl_2(\mu\text{-}NAr)\}_2$ (Ar = 2,6-$^{i}Pr_2C_6H_3$), the MeTps* ligand undergoes a decomposition (**scheme 1.29**) reaction to give the octahedral $\{MeSi(pz^{*})_2(NAr)\}ZrCl_3$ (**184,** Ar = 2,6-$^{i}Pr_2C_6H_3$). This complex features a novel anionic tripodal nitrogen ligand arising from the cleavage of one of the pyrazolyl groups of MeTps* and its replacement with an amido function provided by the zirconium complex. As is commonly observed for such zirconium compounds, $\{MeSi(pz^{*})_2(NAr)\}ZrCl_3$ was found to be highly active as a precatalyst for the polymerisation of ethylene.[208]

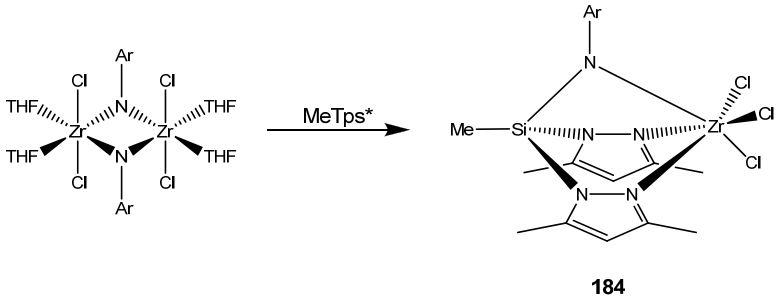

Scheme 1.29 Reaction of MeTps* with $\{(THF)_2ZrCl_2(\mu\text{-}NAr)\}_2$

1.7.4 Tris(pyrazolyl)silanides, Tris(pyrazolyl)germanides and Tris(pyrazolyl)stannides

Recently Breher *et al.* reported that when the related $Si(pz^{*})_4$ was reduced with lithium metal (**scheme 1.30**), a hydrocarbon-insoluble precipitate was obtained, which upon cooling to -30°C in THF solution furnished crystals of the tris(3,5-dimethylpyrazolyl)silanide complex $\{Si(pz^{*})_3\}Li(THF)$ (**185**). This complex was then further reacted with the electrophiles Me_3SiCl, Me_3SnCl and Ph_3SnCl to yield $RSi(pz^{*})_3$ (**186**, R = $SiMe_3$, $SnMe_3$, $SnPh_3$), all of which have potential application as neutral tripodal ligands.[209]

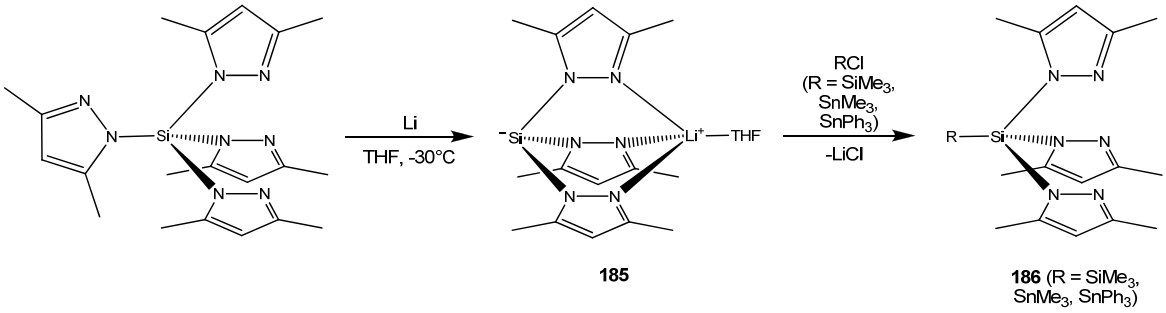

Scheme 1.30 Formation of {Si(pz*)$_3$}Li(THF) (185) and subsequent reaction with RCl

Additionally, {Si(pz*)$_3$}Li(THF) has the potential to be used as a metathesis reagent for the preparation of other complexes of {Si(pz*)$_3$}$^-$, in a manner analogous to {C(pz*)$_3$}Li(THF). The related tris(pyrazolyl)germanide and is also known in the compound {Ge(pz)$_3$}Na(THF)$_3$ (**187**), which was obtained from the reaction of $GeCl_2$ with sodium pyrazolate.[210] Reaction of Ba(pz)$_2$ with $GeCl_2$ gave the sandwich complex {Ge(pz)$_3$}$_2$Ba (**188**), in which one of the pyrazolyl moieties from each of the ligands is bound to the barium centre in a η^4 fashion, while the other two are coordinated in the regular η^1 mode.[211] The series of lithium adducts {E(pz*)$_3$}Li(THF) (E = C, Si, Ge, Sn) have been used as part of a study into a ^{7}Li,^{15}N 2D heteronuclear multiple quantum correlation (HMQC) NMR experiment, though no information regarding the synthesis of the germanium and tin compounds was provided.[212]

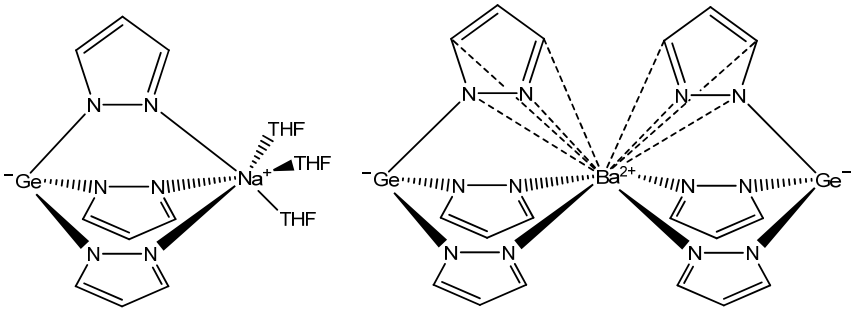

Figure 1.53 Structures of {Ge(pz)$_3$}Na(THF)$_3$ (187) and {Ge(pz)$_3$}$_2$Ba (188)

1.8 Tris(triazolyl) Ligands

1.8.1 Tris(1,2,4-triazolyl)borates

Formal replacement of the pyrazole donor moieties of Tp with 1,2,4-triazole gives the hydrotris(1,2,4-triazol-1-yl)borate ligand (Ttz), which displays a high level of aqueous solubility, in marked contrast to the Tp^x ligands which are essentially insoluble in water. This property of Ttz is due to the propensity of the nitrogen atoms in the 4-position of the triazole rings to engage in hydrogen bonding interactions with solvent water molecules, an attribute which also imparts a degree of water solubility to derived metal complexes. The sandwich complexes $(Ttz)_2M$ (M = Mn, Fe, Co, Ni, Cu, Zn) have been extensively studied,[213-217] and many of these show interesting solvated structures in the solid state. For example, when $(Ttz)_2M$ (**189**, M = Fe, Co, Ni, Zn) are crystallised from water, clathrated species are obtained, the molecular structures of which show two-dimensional layers of water molecules bound in between layers of complex molecules. These layered structures are generated by hydrogen bonding interactions between the exodentate triazole nitrogen atoms and water, as well as between individual molecules of water.[214,215,217] Structural and spectroscopic data for $[N(PPh_3)_2][(Ttz)Mo(CO)_3]$[218] and $[NEt_4][(Ttz^*)Mo(CO)_3]$ (Ttz* = hydrotris(3,5-dimethyl-1,2,4-triazol-1-yl)borate)[219] show that the Ttz^x ligands are slightly weaker σ-donors than the analogous Tp^x, which can be attributed to the electron-withdrawing effect of the additional ring nitrogen atoms in Ttz^x.

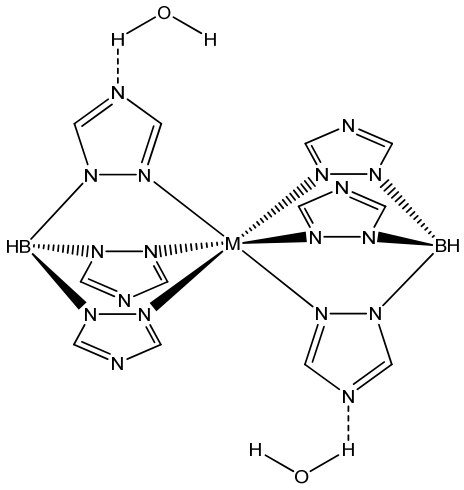

189 (M = Fe, Co, Ni, Zn)

Figure 1.54 Structure of $(Ttz)_2M$ (189) with simplified depiction of hydrogen-bonding interactions

The only examples of bulky Ttz^{x} ligands are hydrotris(3-*tert*-butyl-5-methyl-1,2,4-triazol-1-yl)borate (Ttz^{tBuMe}) and hydrotris(3-phenyl-5-methyl-1,2,4-triazol-1-yl)borate ($Ttz^{Ph,Me}$), prepared by the group of Papish and colleagues. Aside from the increased level of aqueous solubility, the properties of ($Ttz^{tBu,Me}$)CoCl (**190**), ($Ttz^{tBu,Me}$)Co(η^2-NO_3) (**191**) and ($Ttz^{tBu,Me}$)Zn(η^2-OAc) (**192**) were found to be very similar to their $Tp^{tBu,Me}$ analogues.[220]

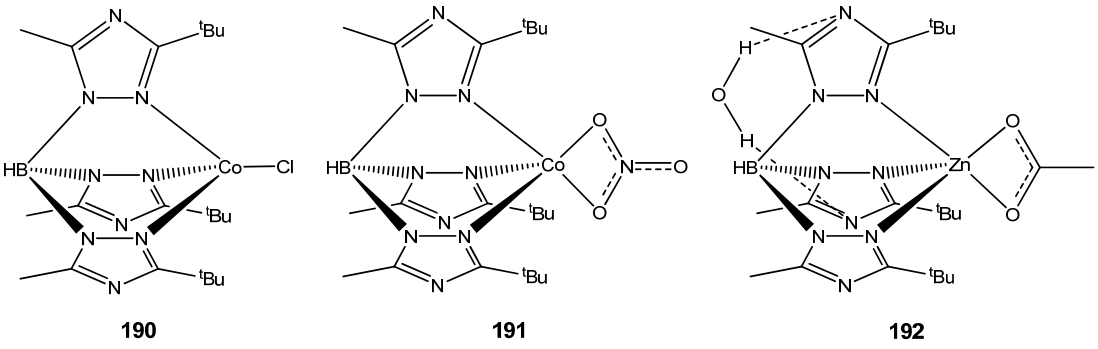

190 **191** **192**

Figure 1.55 Structures of ($Ttz^{tBu,Me}$)CoCl (190), ($Ttz^{tBu,Me}$)Co(η^2-NO_3) (191) and ($Ttz^{tBu,Me}$)Zn(η^2-OAc) (192)

Despite the fact that the molecular structure of ($Ttz^{Ph,Me}$)ZnCl (**193**) shows the presence of a weak hydrogen-bonding interaction with a methanol solvent molecule, this compound is only slightly soluble in methanol and insoluble in methanol/water mixtures.[221] This implies that the $Ttz^{Ph,Me}$ ligand is significantly more hydrophobic than $Ttz^{tBu,Me}$, which gives complexes that are highly methanol soluble and also have sparing solubility in pure water.[220] The carbonyl stretching frequency observed for ($Ttz^{tBu,Me}$)Cu(CO)[222] is shifted to a higher energy relative to ($Tp^{tBu,Me}$)Cu(CO),[223] again showing the Ttz^{x} ligands to be weaker electron donors than the analogous Tp^{x}, in concurrence with the previously described research. Interestingly, this information also implies that the electron-donating ability of $Ttz^{tBu,Me}$ is identical to that of Tp^{Ph2}, which gives an indication of the effect that the substituent groups, in addition to the nature of the heterocyclic moieties, have on the properties of such ligands.[222]

Treatment of Tl($Ttz^{tBu,Me}$) and Tl($Ttz^{Ph,Me}$) with ZnR_2 (R = Me, Et) gave the corresponding four-coordinate alkylzinc complexes ($Ttz^{tBu,Me}$)ZnR (**194**, R = Me, Et) and ($Ttz^{Ph,Me}$)ZnEt (**195**). The molecular structures of crystals of ($Ttz^{tBu,Me}$)ZnR (R = Me, Et) obtained from DCM/hexane under inert conditions both revealed the presence of a single molecule of adventitious water per complex unit, which is hydrogen bonded to one of the $Ttz^{tBu,Me}$ 4-N donors. The remarkable co-crystallisation of an alkylzinc adduct with a molecule of water is, unsurprisingly, unprecedented in the literature. Recrystallisation of ($Ttz^{Ph,Me}$)ZnEt

under the same conditions gave only $(Ttz^{Ph,Me})_2Zn$, presumably resulting from the hydrolysis of $(Ttz^{Ph,Me})ZnEt$ to $(Ttz^{Ph,Me})ZnOH$ and its subsequent disproportionation to the sandwich complex and $Zn(OH)_2$.[224]

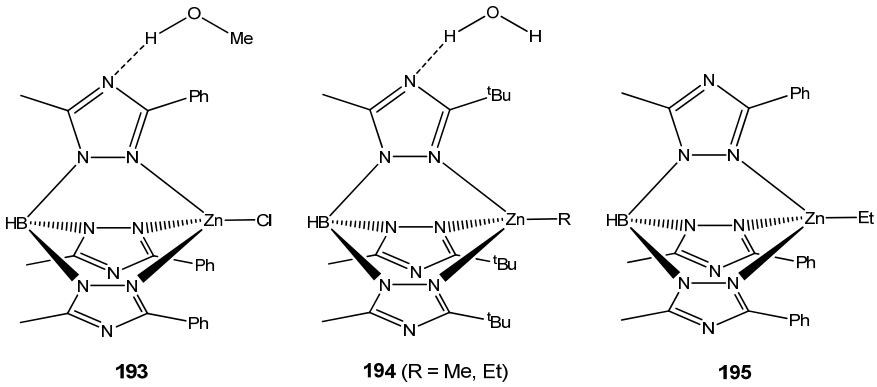

Figure 1.56 Structures of $(Ttz^{Ph,Me})ZnCl$ (193) and $(Ttz^{tBu,Me})ZnR$ (194) with simplified depictions of hydrogen-bonding; structure of $(Ttz^{Ph,Me})ZnEt$ (195)

1.8.2 Other Tris(triazolyl) Ligands

The isomeric hydrotris(1,2,3-benzotriazol-1-yl)borate (Tbt) ligand is also known, yet due to the presence of an additional nitrogen atom adjacent to the donor nitrogen there is no capacity for the introduction of sterically demanding groups into this ligand system that would have any significant influence on the coordination environment of a bound metal centre. As such, the Tbt ligand remains a relative curiosity, and only a few reports of its coordination chemistry have appeared. Known complexes include $(Tbt)_2M$ (M = Mn, Fe, Co, Ni, Cu, Zn, Cd),[225] $(Tbt)Cu\{PPh_2(C_6H_4\text{-}4\text{-}CO_2H)\}$ (**196**),[226] as well as $[NEt_4][(Tbt)Mo(CO)_3]$ (**197**)[227] and its derived adducts. $(Tbt)Cu\{PPh_2(C_6H_4\text{-}4\text{-}CO_2H)\}$ shows similar antioxidant activity to the analogous copper(I) complexes of Tpms discussed in **section 1.6.3**.

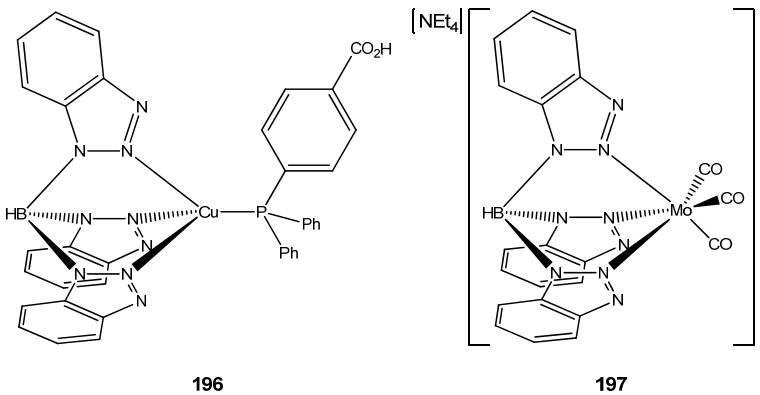

Figure 1.57 Structures of $(Tbt)Cu\{PPh_2(C_6H_4\text{-}4\text{-}CO_2H)\}$ (196) and $[NEt_4][(Tbt)Mo(CO)_3]$ (197)

Tris(1-phenyl-1,2,3-triazol-4-yl)phosphine oxide ($OP(tz^{Ph})_3$) (**198**) was recently synthesised by means of a 'click' reaction between tris(ethynyl)phosphine oxide and three equivalents of phenyl azide, and was used to prepare the adduct $\{OP(tz^{Ph})_3\}RhCl_3$ (**199**) in which the ligand was seen to act as a regular tripodal N_3 donor ligand (**scheme 1.31**). Reduction of $OP(tz^{Ph})_3$ with $PhSiH_3$ furnished tris(1-phenyl-1,2,3-triazol-4-yl)phosphine ($P(tz^{Ph})_3$), which upon stepwise reaction with $W(CO)_5(NCMe)$ followed by $(C_7H_8)Mo(CO)_3$ gave access to the heterobimetallic complex $(OC)_5W\{P(tz^{Ph})_3\}Mo(CO)_3$ (**200**).[228]

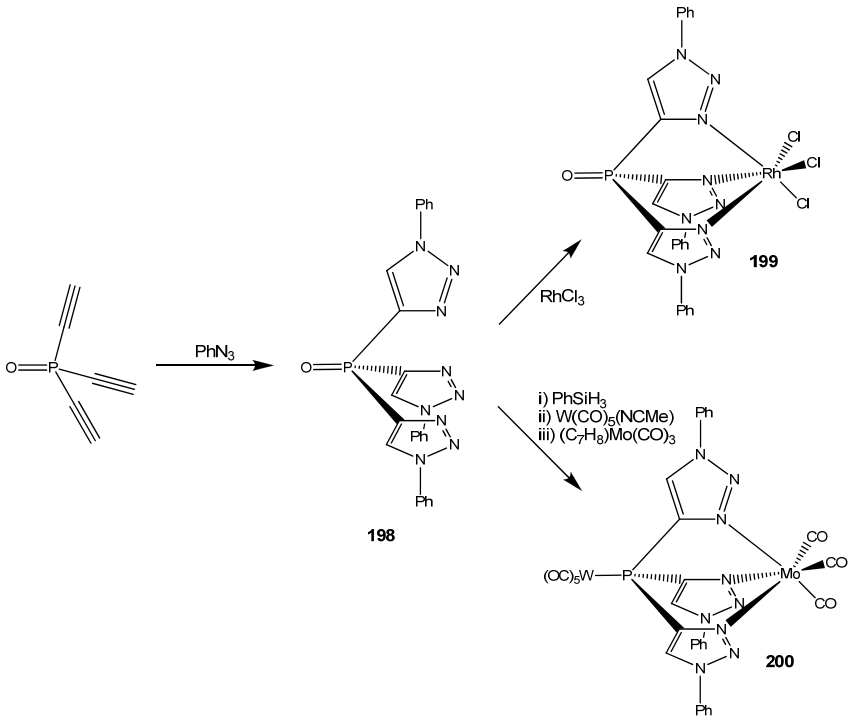

Scheme 1.31 Preparation and reactivity of $(OP(tz^{Ph})_3)$ (198)

1.9 Tris(imidazolyl) Ligands

When attempting to prepare model complexes which accurately replicate the tris-histidine sites in metalloenzymes, one drawback associated with the aforementioned pyrazole- and triazole-containing ligands is the fact that such donor moieties are not identical to the imidazole functionalities present in histidine residues. This has therefore motivated the synthesis of a number of ligands that are based on either a tris(imidazol-2-yl) or tris(imidazol-4-yl) framework, with an aim towards the preparation of complexes with increased bio-relevance.

1.9.1 Tris(imidazolyl)methanes

Tris(*N*-methylimidazol-2-yl)methyl methyl ether ($MeO^2Tim^{N\text{-}Me}$) was used to prepare the dimer $[\{(MeO^2Tim^{N\text{-}Me})Cu\}_2][PF_6]_2$ (**201**), in which the copper(I) centres both have a trigonal-planar geometry, with each ligand binding bidentately to one copper centre and monodentately to the other (i.e. in a μ-{η^2-*N,N′*:η^1-*N″*} fashion). Reaction of this complex with CO gave the corresponding carbonyl adduct, and although this was not crystallised, the monomeric four co-ordinate structure of $[(MeO^2Tim^{N\text{-}Me})Cu(CO)][PF_6]$ was confirmed by spectroscopy.[229] It was shown by Cavell and co-workers that $(MeO^2Tim)CrCl_3$ is a highly active precatalyst for the oligomerisation of ethylene, producing linear 1-alkenes with a 79% selectivity.[230] The related ligands tris(imidazol-2-yl)methanol (HO^2Tim) and tris(*N*-methylimidazol-2-yl)methanol ($HO^2Tim^{N\text{-}Me}$) have also been used to prepare octahedral sandwich complexes, namely $[(HO^2Tim)_2M][NO_3]_2$ (**202a**, M = Co, Ni),[231] $[(HO^2Tim^{N\text{-}Me})_2M][X]_2$ (**202b**, M = Co, Ni, X = Cl, NO_3)[231] and $[(HO^2Tim)_2Fe][FeCl_4]_nCl_n$ (n = 0, 1). As expected, both the iron(II) and iron (III) complexes were found to have magnetic properties representative of low-spin cations and high-spin anions.[232]

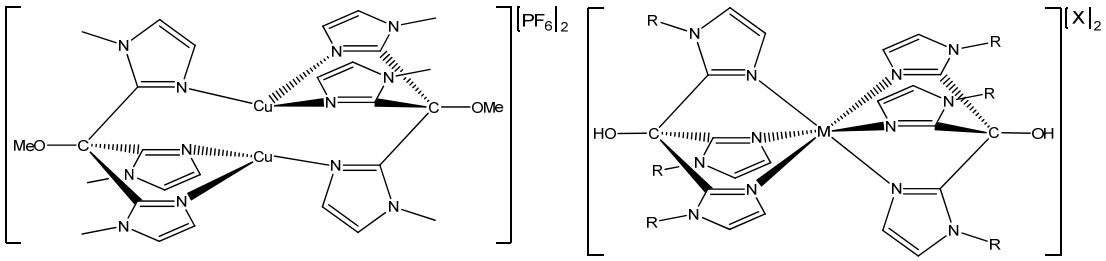

201

202a (R = H, M = Co, Ni, X = NO_3)
202b (R = Me, M = Co, Ni, X = Cl, NO_3)

Figure 1.58 Structures of $[\{(MeO^2Tim^{N\text{-}Me})Cu\}_2][PF_6]_2$ (201), $[(HO^2Tim)_2M][NO_3]_2$ (202a) and $[(HO^2Tim^{N\text{-}Me})_2M][X]_2$ (202b)

Nicholas and co-workers employed the series of ligands tris(*N*-methyl-4,5-diphenylimidazol-2-yl)methane ($^2Tim^{Ph2,N\text{-}Me}$), tris(*N*-methyl-4,5-diphenylimidazol-2-yl)methanol ($HO^2Tim^{Ph2,N\text{-}Me}$) and tris(*N*-methyl-4,5-diphenylimidazol-2-yl)methyl methyl ether ($MeO^2Tim^{Ph2,N\text{-}Me}$) to prepare the corresponding dimeric $[\{(^2Tim^x)Cu\}_2][PF_6]_2$ (**203**) adducts, all of which are structurally analogous to $[\{(MeO^2Tim)Cu\}_2][PF_6]_2$. The $[\{(^2Tim^x)Cu\}_2][PF_6]_2$ species all react with MeCN and CO to give the corresponding monomeric $[(^2Tim^x)Cu(L)][PF_6]$ (L = NCMe, CO) adducts, whereas the nature of the products obtained from the reaction of $[\{(^2Tim^x)Cu\}_2][PF_6]_2$ with *tert*-butyl isocyanide is dependent on the identity of the ligand (**scheme 1.32**).[233]

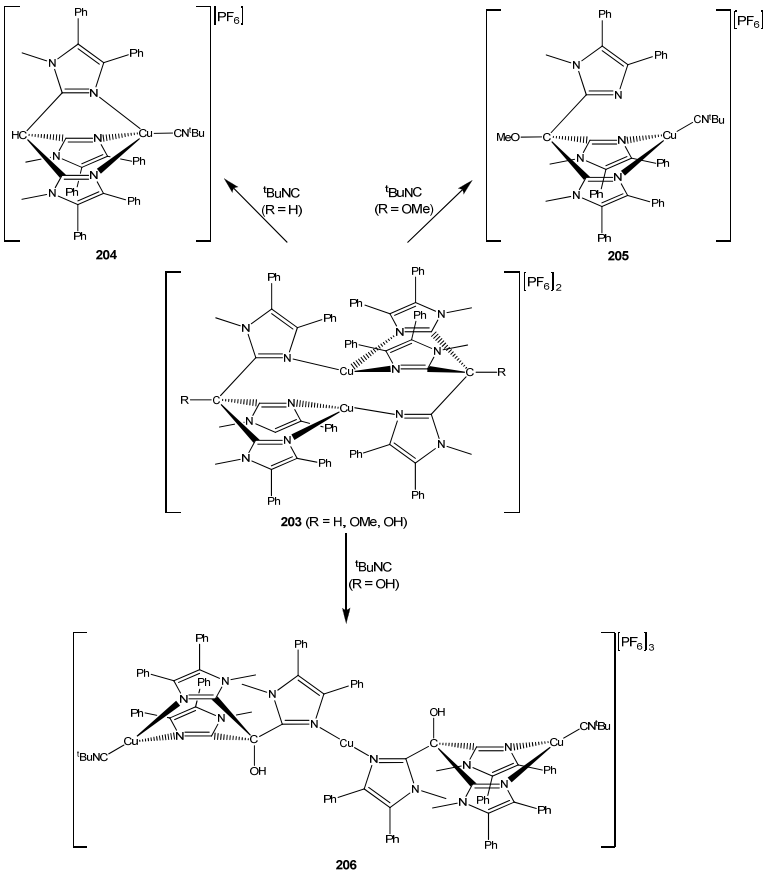

Scheme 1.32 Reactions of $[\{(^{2}Tim^{x})Cu\}_{2}][PF_{6}]_{2}$ (203) with $^{t}BuNC$

$[(\eta^{3}\text{-}^{2}Tim^{Ph2,N\text{-}Me})Cu(CN^{t}Bu)][PF_{6}]$ (**204**) shows the expected tetrahedral geometry, while $[(\eta^{2}\text{-}N,N'\text{-}MeO^{2}Tim^{Ph2,N\text{-}Me})Cu(CN^{t}Bu)][PF_{6}]$ (**205**) contains a three-coordinate planar copper(I) centre. Upon reaction of $[\{(HO^{2}Tim^{Ph2,N\text{-}Me})Cu\}_{2}][PF_{6}]_{2}$ with $^{t}BuNC$, the trinuclear complex $[(HO^{2}Tim^{Ph2,N\text{-}Me})_{2}Cu_{3}(CN^{t}Bu)_{2}][PF_{6}]_{3}$ (**206**) was isolated, the molecular structure of which shows two trigonal-planar copper(I) centres, each with one co-ordinated $^{t}BuNC$ molecule. These two copper centres are also bound bidentately by one each of the $HO^{2}Tim^{Ph2,N\text{-}Me}$ ligands, with the remaining free imidazole donors of each ligand attached to a bridging two-coordinate copper centre. Attempts to prepare peroxo-bridged dimeric species by reaction of $[\{(^{2}Tim^{x})Cu\}_{2}][PF_{6}]_{2}$ with O_{2} were met with failure, with no observable change occurring even after 20 hours under an O_{2} atmosphere in DCM solution at room temperature.[233] No mention was made of any investigation into reaction of the $[\{(^{2}Tim^{x})Cu\}_{2}][PF_{6}]_{2}$ complexes with O_{2} at low temperature, an experimental condition which is often vital to the generation and subsequent isolation of peroxo-dicopper species. However, exposure of a solution of $^{2}Tim^{Ph2,N\text{-}Me}$ and $[Cu(NCMe)_{4}][PF_{6}]$ in acetone to O_{2} for a period of 24 hours did furnish the five-coordinate copper(II) complex $[(^{2}Tim^{Ph2,N\text{-}Me})Cu(CH_{3}COCH_{3})(H_{2}O)][PF_{6}]_{2}$.[233] The very low reactivity of these adducts towards

dioxygen was ascribed by the researchers to a combination of steric shielding and reduced electron-donicity of the $^{2}Tim^{x}$ ligands in comparison to anionic donors such as Tp^{x}, though the latter explanation seems insufficient when copper(I) complexes of similarly weakly-donating ligands such as Tpm^{x} have been shown to form peroxo-bridged adducts. In fact, the carbonyl stretching frequency observed for $[(^{2}Tim^{Ph2,N\text{-}Me})Cu(CO)][PF_6]$ is approximately 20 cm^{-1} lower than those reported for the $[(Tpm^{x})Cu(CO)][PF_6]$ adducts, which implies that the $^{2}Tim^{x}$ ligands are actually somewhat more strongly electron donating than the Tpm^{x} ligands.[233] However, due to the different arrangement of the ring nitrogen atoms, and of the substituent groups, direct comparison of individual $^{2}Tim^{x}$ and Tpm^{x} ligands is rather difficult.

Isomeric ligands based on the tris(imidazol-4-yl)methane ($^{4}Tim^{x}$) skeleton are also known, yet their coordination chemistry is limited to a total of only four reports. Tris(imidazol-4-yl)methanol ($HO^{4}Tim$) was used to prepare the sandwich complex $[(HO^{4}Tim)_2Fe][Cl]_3$ (**207**),[234] the structural parameters of which were found to be very similar to those of the related complexes of $HO^{2}Tim$. The bulkier ligands tris(*N*-methyl-2-phenylimidazol-4-yl)methanol ($HO^{4}Tim^{Ph,N\text{-}Me}$), tris(*N*-methyl-2-isopropylimidazol-4-yl)methanol ($HO^{4}Tim^{iPr,N\text{-}Me}$) and tris(*N*-methyl-2-ethylimidazol-4-yl)methanol ($HO^{4}Tim^{Et,N\text{-}Me}$) were employed by Fujii and colleagues to prepare the corresponding copper(I) adducts $[(HO^{4}Tim^{x})Cu(L)][ClO_4]$ (**208**, L = NCMe, CO). In concurrence with the aforementioned remarks on the electron-donating ability of the $^{2}Tim^{x}$ ligands, the CO stretching frequencies observed for $[(HO^{4}Tim^{x})Cu(CO)][ClO_4]$ suggest that the $^{4}Tim^{x}$ ligands are stronger electron donors than other related neutral tripodal ligands such as Tpm^{x}.[235]

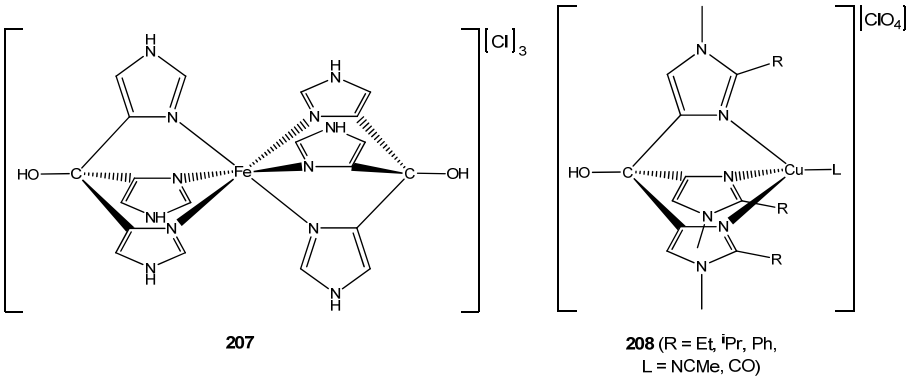

207 **208** (R = Et, ^{i}Pr, Ph, L = NCMe, CO)

Figure 1.59 Structures of $[(HO^{4}Tim)_2Fe][Cl]_3$ (207) and $[(HO^{4}Tim^{x})Cu(L)][ClO_4]$ (208)

1.9.2 Tris(imidazolyl)phosphines

The prevalence of tris(imidazolyl)phosphine ligands (Tip^x) in coordination chemistry is somewhat greater than the tris(imidazolyl)methanes, and similarly the imidazol-2-yl isomers have been much more widely studied than their imidazol-4-yl congeners. Kurtz and co-workers used tris(imidazol-2-yl)phosphine (^2Tip) and tris(*N*-methylimidazol-2-yl)phosphine ($^2Tip^{N\text{-}Me}$) to prepare the corresponding dimeric μ-oxo bis-μ-carboxylate iron(III) and manganese(III) complexes $[\{(^2Tip^x)M\}_2(\mu\text{-}O)(\mu\text{-}O_2CR)_2][X]_2$ (**209**, M = Fe, R = Et, Ph, X = PF_6; M = Fe, R = Me, X = ClO_4; M = Mn, R = Me, X = ClO_4, PF_6)[236] which are structurally analogous to the Tp-supported metalloenzyme model complexes pioneered by Lippard *et al.* Notwithstanding the fact that the presence of imidazolyl donors gives rise to more accurate model compounds, the properties of the $^2Tip^x$-supported complexes were found to be otherwise very similar to those of their Tp analogues, though it should be noted that no dimeric manganese(III) complexes could be obtained when ^2Tip was employed as the capping ligand. This behaviour was attributed by the researchers as an effect of the reduced steric bulk of the ^2Tip ligand in comparison to $^2Tip^{N\text{-}Me}$.[236] Treatment of $[\{(^2Tip^{N\text{-}Me})Fe\}_2(\mu\text{-}O)(\mu\text{-}OAc)_2)][ClO_4]_2$ with $HBF_4.OEt_2$ furnished the corresponding hydroxo-bridged complex $[\{(^2Tip^{N\text{-}Me})Fe\}_2(\mu\text{-}OH)(\mu\text{-}OAc)_2][ClO_4]_2[BF_4]$ (**210**),[236] in concurrence with the previously observed reactivity of $[\{(Tp)Fe\}_2(\mu\text{-}O)(\mu\text{-}OAc)_2]$.

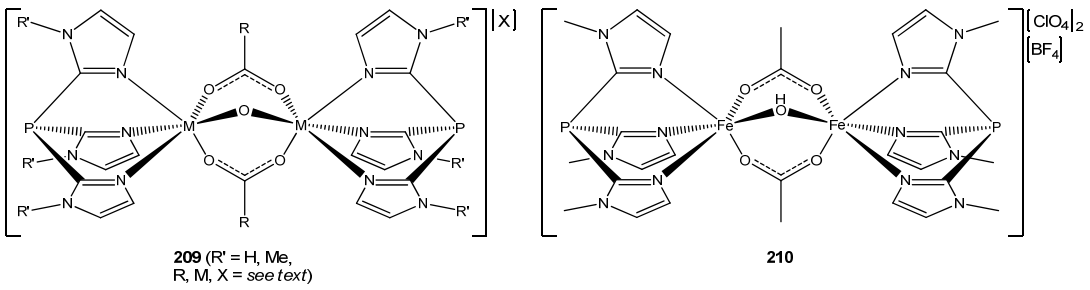

Figure 1.60 Structures of $[\{(^2Tip^x)M\}_2(\mu\text{-}O)(\mu\text{-}O_2CR)_2][X]_2$ (209) and $[\{(^2Tip^{N\text{-}Me})Fe\}_2(\mu\text{-}OH)(\mu\text{-}OAc)_2][ClO_4]_2[BF_4]$ (210)

It was subsequently shown that when the bulkier tris(*N*,4-dimethylimidazol-2-yl)phosphine ($^2Tip^{Me,N\text{-}Me}$) is employed as the capping ligand, the trinuclear complex $[(^2Tip^{Me,N\text{-}Me})Fe(\mu\text{-}OH)(\mu\text{-}OAc)_2Fe(\mu\text{-}OH)(\mu\text{-}OAc)_2Fe(^2Tip^{Me,N\text{-}Me})][PF_6]_3$ (**211a**) is obtained instead, although single crystals suitable for X-ray diffraction could not be isolated.[237] Reaction of the acetate-bridged complex with benzoic acid in acetonitrile did however give access to the corresponding benzoate-bridged species $[(^2Tip^{Me,N\text{-}Me})Fe(\mu\text{-}OH)(\mu\text{-}O_2CPh)_2Fe(\mu\text{-}OH)(\mu\text{-}O_2CPh)_2Fe(^2Tip^{Me,N\text{-}Me})][PF_6]_3$ (**211b**)[237] the molecular structure of which shows a

symmetrical trinuclear arrangement, with Fe-O_{OH} bond lengths that are on average 0.4 Å longer than the Fe-$O_{O(H)}$ distances observed in the aforementioned crystallographically disordered $(Tp^{iPr2})Fe(\mu\text{-}O)(\mu\text{-}OAc)_2Fe(\mu\text{-}OH)(\mu\text{-}OAc)_2Fe(Tp^{iPr2})$ (**section 1.4.6**). This observation is concurrent with the ascribed asymmetric nature of the latter complex, as the disorder of the μ-oxo and μ-hydroxo ligands gives rise to Fe-O bond distances intermediate between those normally seen for bridging oxides (shorter) and hydroxides (longer).

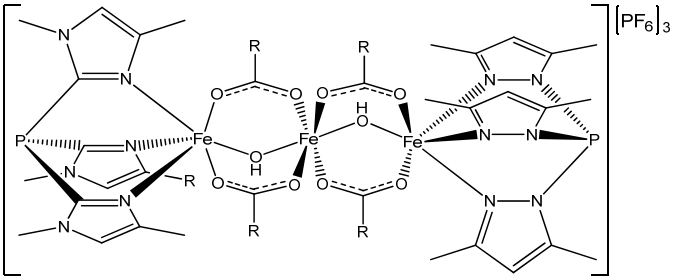

211a (R = Me)
211b (R = Ph)

Figure 1.61 Structure of $[(^2Tip^{Me,N\text{-}Me})Fe(\mu\text{-}OH)(\mu\text{-}O_2CR)_2Fe(\mu\text{-}OH)(\mu\text{-}O_2CR)_2Fe(^2Tip^{Me,N\text{-}Me})][PF_6]_3$ (211)

The same researchers also used tris(*N*-ethyl-4-methylimidazol-2-yl)phosphine ($^2Tip^{Me,N\text{-}Et}$) and tris(*N*-ethyl-4-isopropylimidazol-2-yl)phosphine ($^2Tim^{iPr,N\text{-}Et}$) to prepare the copper(I) adducts $[(^2Tip^x)Cu(NCMe)][X]$ (X = ClO_4, PF_6, OTf) and $(^2Tip^x)CuCl$, all of which react quantitatively with O_2 at low temperature to give the corresponding $[\{(^2Tip^x)Cu\}_2(\mu\text{-}\eta^2\text{:}\eta^2\text{-}O_2)][X]_2$ (**212**, X = ClO_4, PF_6, OTf, Cl) as isolable, purple-coloured solids. The dioxygen adducts supported by the $^2Tip^{Me,N\text{-}Et}$ ligand are indefinitely stable in the solid-state up to -20°C, and show stability on the order of days or hours even at room temperature under an argon atmosphere, while in solution decomposition starts to occur above -30°, eventually yielding the corresponding copper(II) sandwich complexes $[(^2Tip^{Me,N\text{-}Et})_2Cu][X]_2$ (X = ClO_4, PF_6, OTf, Cl) as the ultimate products of oxidation. Conversely, the peroxo-bridged complexes containing the more sterically bulky $^2Tip^{iPr,N\text{-}Et}$ ligand were found to be much less stable, with rapid decomposition occurring above -20°C even in the solid state. However, when solutions of $[\{(^2Tip^{iPr,N\text{-}Et})Cu\}_2(\mu\text{-}\eta^2\text{:}\eta^2\text{-}O_2)][X]_2$ (X = ClO_4, PF_6, OTf, Cl) in methanol were cycled rapidly between -78°C and approximately -20°C, reversible dissociation and subsequent re-uptake of O_2 was observed and could be maintained for at least ten cycles. This is in contrast to the behaviour of the $[\{(^2Tip^{Me,N\text{-}Et})Cu\}_2(\mu\text{-}\eta^2\text{:}\eta^2\text{-}O_2)][X]_2$ adducts, as well as that of the prototypical peroxo-dicopper adduct $\{(Tp^{iPr2})Cu\}_2(\mu\text{-}\eta^2\text{:}\eta^2\text{-}O_2)$, both of which undergo irreversible loss of O_2 above -20°C and -10°C respectively.[238]

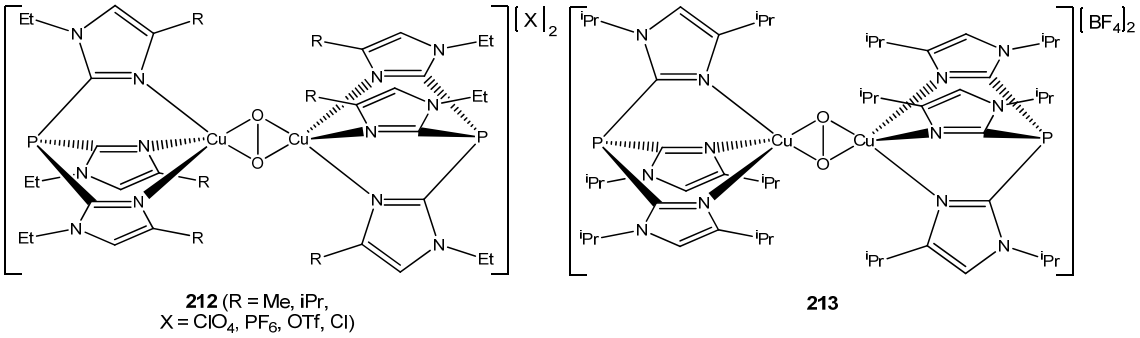

Figure 1.62 Structures of $[\{(^2Tip^x)Cu\}_2(\mu\text{-}\eta^2\text{:}\eta^2\text{-}O_2)][X]_2$ (212) and $[\{(^2Tip^{iPr,N\text{-}iPr})Cu\}_2(\mu\text{-}\eta^2\text{:}\eta^2\text{-}O_2)][BF_4]_2$ (213)

Similar work was undertaken by the group of Sorrell *et al.*, who investigated the dioxygen reactivity of the more sterically encumbered complex $[(^2Tim^{iPr,N\text{-}iPr})Cu(NCMe)][BF_4]$ ($^2Tim^{iPr,N\text{-}iPr}$ = tris(*N*,4-diisopropylimidazol-2-yl)phosphine). Crystals of $[\{(^2Tip^{iPr,N\text{-}iPr})Cu\}_2(\mu\text{-}\eta^2\text{:}\eta^2\text{-}O_2)][BF_4]_2$ (**213**) were obtained from an oxygenated methanol solution of $[(^2Tim^{iPr,N\text{-}iPr})Cu(NCMe)][BF_4]$ at -78°C, though these were insufficiently large to allow for characterisation by X-ray crystallography.[239] As observed for the analogous $^2Tip^{iPr,N\text{-}Et}$ complexes,[238] the reaction with O_2 was again shown to be reversible, although by measurement of the amount of O_2 uptake it could be seen that the reaction never went to more than approximately 50% of completion.[239] This observed reduction in reactivity is likely due to the increased steric bulk of the $^2Tip^{iPr,N\text{-}iPr}$ ligand in comparison to $^2Tip^{iPr,N\text{-}Et}$. In an attempt to effect the oxidation of triphenylphosphine, a solution of $[\{(^2Tip^{iPr,N\text{-}iPr})Cu\}_2(\mu\text{-}\eta^2\text{:}\eta^2\text{-}O_2)][BF_4]_2$ was treated with PPh_3 at -78°C and allowed to warm to room temperature. However, no formation of triphenylphosphine oxide was observed, and the only product that could be isolated was $[(^2Tip^{iPr,N\text{-}iPr})Cu(PPh_3)][BF_4]$. Similar treatment with H_2O followed by subsequent warming yielded $[\{(^2Tip^{iPr,N\text{-}iPr})Cu(\mu\text{-}OH)\}_2][BF_4]_2$, which reacted readily with atmospheric CO_2 upon exposure to air to give $[\{(^2Tip^{iPr,N\text{-}iPr})Cu\}_2(\mu\text{-}\eta^2\text{:}\eta^{2'}\text{-}CO_3)][BF_4]_2$ (**214**).[239]

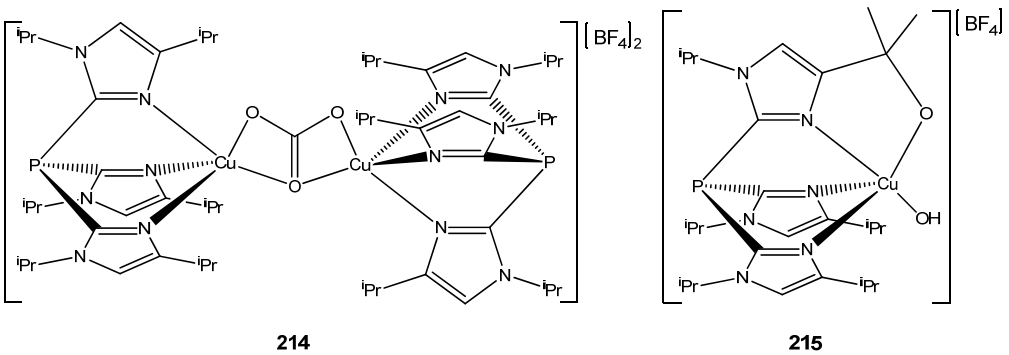

Figure 1.63 Structures of $[\{(^2Tip^{iPr,N\text{-}iPr})Cu\}_2(\mu\text{-}\eta^2\text{:}\eta^{2'}\text{-}CO_3)][BF_4]_2$ (214) and 215

The molecular structure of the latter complex shows the carbonate anion bridging the two copper centres in a symmetrical bis-bidentate fashion, which is analogous to the aforementioned Tp^{iPr2} complex described in **section 1.4.6**. $[\{(^2Tip^{iPr,N\text{-}iPr})Cu(\mu\text{-}OH)\}_2][BF_4]_2$ and $[\{(^2Tip^{iPr,N\text{-}iPr})Cu\}_2(\mu\text{-}\eta^2\text{:}\eta^{2'}\text{-}CO_3)][BF_4]_2$ could also be prepared by the direct reaction of $Cu(BF_4)_2$ with NaOH and $NaHCO_3$ respectively, whilst the reaction of $Cu(BF_4)_2$ with Na(OAc) gave the five-coordinate monomeric $[(^2Tip^{iPr,N\text{-}iPr})Cu(\eta^2\text{-}OAc)][BF_4]$.[239] Unsurprisingly, the related $[(^2Tim^{tBu,N\text{-}iPr})Cu(NCMe)][BF_4]$ ($^2Tim^{tBu,N\text{-}iPr}$ = tris(*N*-isopropyl-4-*tert*-butylimidazol-2-yl)methane) was completely unreactive towards O_2, and although formation of a monomeric side-on superoxo adduct in analogy with $(Tp^{tBu,iPr})Cu(\eta^2\text{-}O_2)$ (**section 1.4.3**) may have seemed feasible, no such species was observed.[239] This is most likely a consequence of the reduced electron donating ability of the neutral $^2Tim^{tBu,N\text{-}iPr}$ in comparison to the anionic $Tp^{tBu,iPr}$, as the latter ligand will give rise to a more electron-rich copper centre, thus increasing the strength of its interaction with the superoxide anion. Indeed, the carbonyl stretching frequency observed for $[(^2Tim^{tBu,N\text{-}iPr})Cu(CO)][BF_4]$[239] was found to be 32 cm^{-1} higher than that of $(Tp^{tBu,iPr})Cu(CO)$.[223] The end product arising from the oxidative decomposition of $[\{(^2Tip^{iPr,N\text{-}iPr})\}_2Cu(\mu\text{-}\eta^2\text{:}\eta^2\text{-}O_2)][BF_4]_2$ was subsequently shown to be a cationic five-coordinate hydroxo-copper(II) complex (**215**), in which one of the ligand isopropyl moieties has been hydroxylated and the alcohol group is coordinated to the copper centre. This complex was structurally characterised as its triflate salt, and it was shown that by treatment with concentrated ammonium hydroxide solution, the free mono-hydroxylated ligand could be extracted in up to 45% yield. The fact that this was always accompanied by unchanged $^2Tip^{iPr,N\text{-}iPr}$ in up to 50% yield led the researchers to posit a radical mechanism for the asymmetric decomposition reaction.[240]

The $^2Tip^{tBu,N\text{-}iPr}$ ligand was also employed by Parkin and colleagues to prepare the cobalt(II) complexes $[(^2Tip^{tBu,N\text{-}iPr})CoI][I]$ (**216**) and $[(^2Tip^{tBu,N\text{-}iPr})Co(\eta^2\text{-}NO_3)][NO_3]$ (**217**, M = Co) which show the expected four- and five-coordinate geometries respectively in the solid-state.[241] The bonding mode of the coordinated nitrate ion in the latter complex is essentially symmetric bidentate, which is in contrast to the situation in $(Tp^{tBu})Co(\eta^2\text{-}NO_3)$ where the nitrate is bound in a highly asymmetric bidentate fashion.[58(b)] The adoption of the symmetric binding mode in $[(^2Tip^{tBu,N\text{-}iPr})Co(\eta^2\text{-}NO_3)][NO_3]$ is likely due to the cobalt centre being less electron-rich in comparison to that in $(Tp^{tBu})Co(\eta^2\text{-}NO_3)$, which allows for a stronger interaction between the metal and the two oxygen donors of the nitrate

ligand. The investigation into the structural properties of nitrate complexes was then extended to a whole series of d-block metal ions with the preparation of [(^{2}Tip$^{tBu,N-iPr}$)M(NO$_3$)][NO$_3$] (M = Co, Cu, (**217**) Zn (**218**)) and [(^{2}Tip$^{tBu,N-iPr}$)M(NO$_3$)][M(NO$_3$)$_4$]$_{½}$ (M = Cu, Cd (**217**), Hg (**218**)). The bonding mode of the nitrate ion in all of these complexes was found to be roughly symmetric bidentate, except in the case of the zinc(II) and mercury(II) adducts where the nitrate was bound in essentially a unidentate fashion.[242]

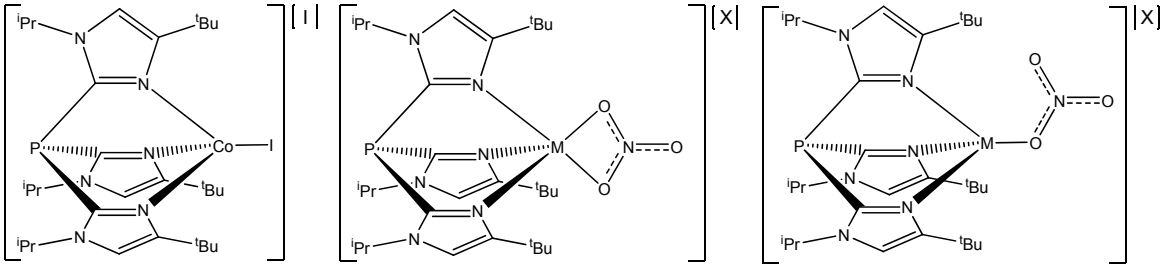

216 **217** (M = Co, X = NO_3; M = Cd, X = ½Cd(NO_3)$_4$; M = Cu, X = NO_3, ½Cu(NO_3)$_4$) **218** (M = Zn, X = NO_3; M = Hg, X = ½Hg(NO_3)$_4$)

Figure 1.64 Structures of [(^{2}Tip$^{tBu,N-iPr}$)CoI][I] (216) and [(^{2}Tip$^{tBu,N-iPr}$)M(NO$_3$)][NO$_3$] (217, 218)

Through the reaction of ^{2}Tip$^{iPr,N-iPr}$ with Co(ClO$_4$)$_2$.6H$_2$O in methanol, the same researchers synthesised the octahedral complex [(^{2}Tip$^{iPr,N-iPr}$)Co(OH$_2$)(HOMe)(η^1-ClO$_4$)][ClO$_4$] (**219**). Interestingly, the aqua and methanol ligands are labile under vacuum (**scheme 1.33**), giving [(^{2}Tip$^{iPr,N-iPr}$)Co(ClO$_4$)][ClO$_4$] (**220**) which was also structurally characterised. The bonding mode of the perchlorate ion in this complex is highly asymmetric, and could reasonably be described as monodentate, although close examination of the molecular structure reveals the presence of a very weak interaction between the cobalt centre and a second perchlorate oxygen atom.[243]

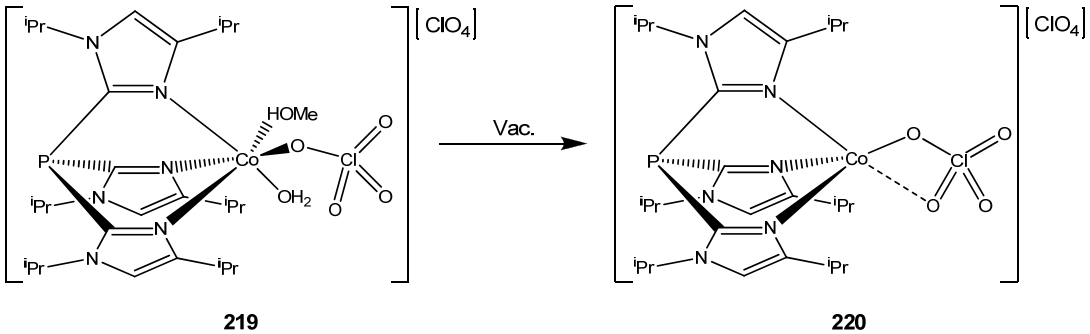

219 **220**

Scheme 1.33 Structures of [(^{2}Tip$^{iPr,N-iPr}$)Co(OH$_2$)(HOMe)(η^1-ClO$_4$)][ClO$_4$] (219) and [(^{2}Tip$^{iPr,N-iPr}$)Co(ClO$_4$)][ClO$_4$] (220)

Cavell and colleagues demonstrated that (^{2}Tip$^{tBu,N\text{-}iPr}$)$CrCl_3$ is active as a precatalyst for the polymerisation of ethylene, though the activity was very low.[244] In contrast to the similar but much less sterically encumbered (MeO^{2}Tim)$CrCl_3$, which gives mainly ethylene oligomers and only a very small amount of polymer (3.4% of the total mass of products),[230] (^{2}Tip$^{tBu,N\text{-}iPr}$)$CrCl_3$ produces polyethylene as 70% of the overall mass of products.[244] The related ligand tris(*N*-methyl-4-(*p*-tolyl)imidazol-2-yl)phosphine (^{2}Tip$^{Tol,N\text{-}Me}$) was synthesised by Kläui and co-workers and used to prepare the four-coordinate adducts [(^{2}Tip$^{Tol,N\text{-}Me}$)ZnCl][$ZnCl_4$]$_{½}$ (**221**), [(^{2}Tip$^{Tol,N\text{-}Me}$)ZnX][X] (**222**, X = Br, I) and [(^{2}Tip$^{Tol,N\text{-}Me}$)Zn(η^1-NO_3)][NO_3] (**223**). The binding mode of NO_3^- in the nitrate complex is strictly monodentate, which is somewhat surprising in view of the relatively low steric demand of the ^{2}Tip$^{Tol,N\text{-}Me}$ ligand.[245]

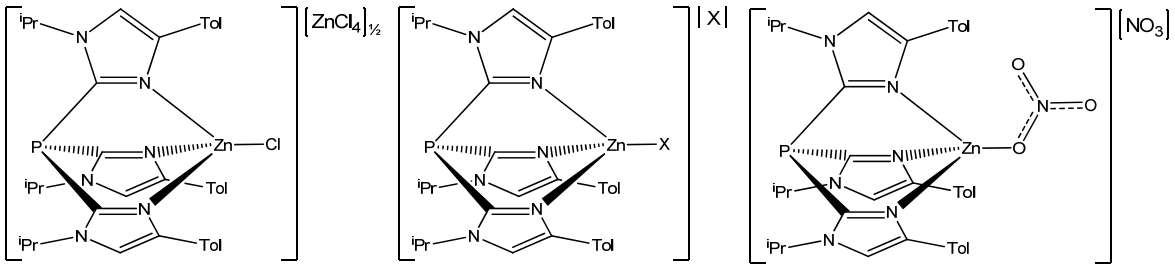

Figure 1.65 Structures of [(^{2}Tip$^{Tol,N\text{-}Me}$)ZnCl][$ZnCl_4$]$_{½}$ (221), [(^{2}Tip$^{Tol,N\text{-}Me}$)ZnX][X] (222) and [(^{2}Tip$^{Tol,N\text{-}Me}$)Zn(η^1-NO_3)][NO_3] (223).

More recently, it has been shown by Severin *et al.* that tris(*N*-vinylimidazol-2-yl)phosphine (**224**) can be homopolymerised (or alternatively co-polymerised with ethylene glycol dimethacrylate), to give a polymer-supported network of tripodal ligand sites (**scheme 1.34**). Incorporation of $CuCl_2$ into these network polymers gave adducts which were shown to efficiently catalyse the hydrolysis of activated phosphate esters.[246]

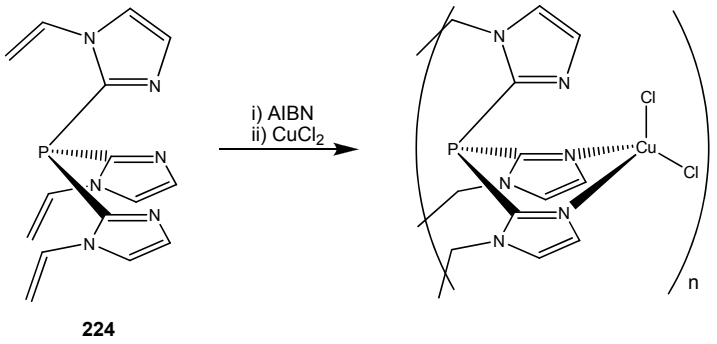

Scheme 1.34 Formation of polymer-supported network of ^{2}Pim ligands and impregnation with $CuCl_2$

Tris(2-isopropylimidazol-4-yl)phosphine (^{4}Tip^{iPr}) has been employed by the group of Klaüi and Kunz to generate the octahedral nitrate complexes [(^{4}Tip^{iPr})M(η^2-NO$_3$)(HOMe)][NO$_3$] (**225**, M = Co, Ni), as well as the tetrahedral [(^{4}Tip^{iPr})MCl][Cl] (**226**, M = Co, Zn). As the exodentate imidazole nitrogen atoms in ^{4}Tip^{iPr} are unsubstituted, they are able to engage in hydrogen bonding interactions, which imparts an increased level of aqueous solubility to the derived complexes. The solid-state structures of [(^{4}Tip^{iPr})MCl][Cl] (M = Co, Zn) show that the imidazole NH atoms form hydrogen bonds with the chloride counter ions, giving rise to an extended network structure.[247]

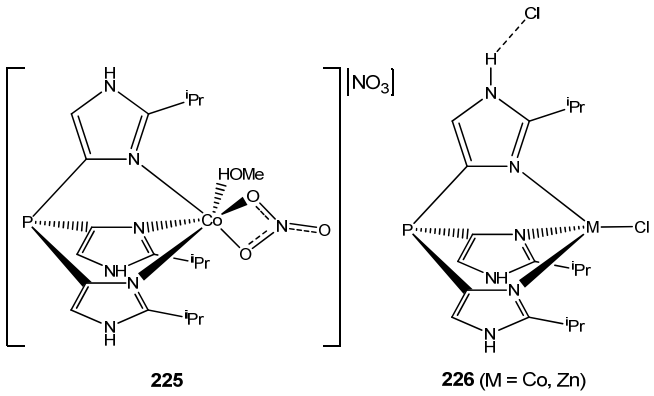

Figure 1.66 Structures of [(^{4}Tip^{iPr})M(η^2-NO$_3$)(HOMe)][NO$_3$] (225) and [(^{4}Tip^{iPr})MCl][Cl] (226) with simplified depiction of hydrogen-bonding interaction

Coordination of ^{4}Tip^{iPr} to a gold(I) chloride fragment furnished the dimeric [{(μ-η^{1}:$\eta^{1'}$-*N,P*-^{4}Tip^{iPr})Au}$_2$][Cl]$_2$ (**227**), in which each linear two-coordinate gold atom is bound by one phosphorus and one imidazole donor from different ligands. Reaction of [{(μ-η^{1}:$\eta^{1'}$-*N,P*-^{4}Tip^{iPr})Au}$_2$][Cl]$_2$ with ZnCl$_2$ (**scheme 1.35**) gave access to the bimetallic complex [ClAu(^{4}Tip^{iPr})ZnCl][Cl] (**228**), where the gold atom is coordinated by the central phosphorus donor of ^{4}Tip^{iPr}, and the zinc centre is bound in a regular tripodal η^3-fashion by the three imidazole moieties.[248]

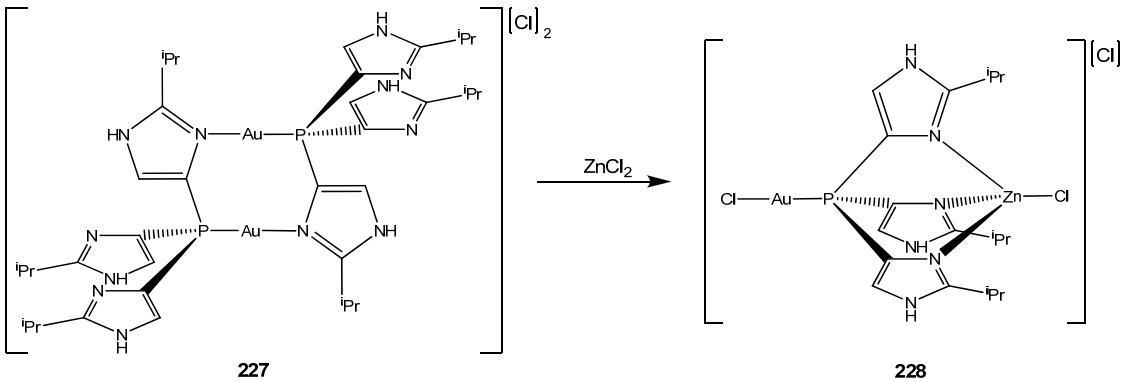

Scheme 1.35 Reaction of [{(μ-η^{1}:$\eta^{1'}$-*N,P*-^{4}Tip^{iPr})Au}$_2$][Cl]$_2$ (227) with ZnCl$_2$

The phosphine oxide derivative of $^{4}Tip^{iPr}$ ($^{4}Tipo^{iPr}$) has also been used to prepare the six-coordinate $[(^{4}Tipo^{iPr})M(\eta^{2}\text{-}NO_3)(OH_2)][NO_3]$ (**229**, M = Co, Zn), as well as the square-pyramidal $(^{4}Tipo^{iPr})Cu(\eta^{1}\text{-}SO_4)(OH_2)$ (**230**), all of which show high solubility in water.[249]

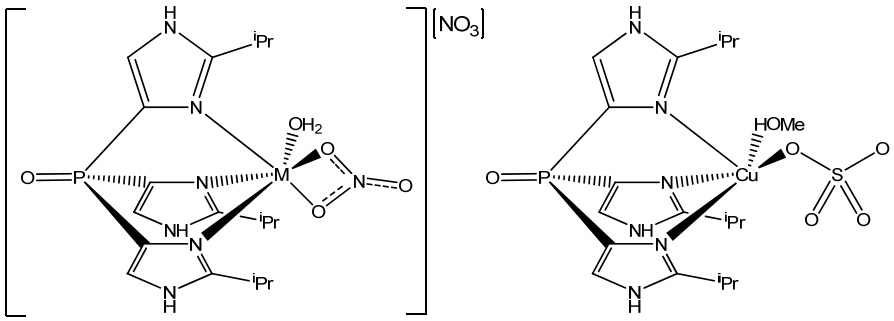

Figure 1.67 Structures of $[(^{4}Tipo^{iPr})M(\eta^{2}\text{-}NO_3)(OH_2)][NO_3]$ (229) and $(^{4}Tipo^{iPr})Cu(\eta^{1}\text{-}SO_4)(OH_2)$ (230)

Upon reaction of $^{4}Tipo^{iPr}$ with the dichlorides of cobalt and zinc, the ligand binds in a bidentate fashion to the metal centres giving the four coordinate $(\eta^{2}\text{-}N,N'\text{-}^{4}Tipo^{iPr})MCl_2$ (**231**, M = Co, Zn). Bidentate coordination is also observed upon reaction with $NiCl_2$, however in this case the $^{4}Tipo^{iPr}$ ligand binds through the oxygen atom in addition to a single imidazole donor, and two bidentate ligands are accommodated by the nickel centre giving the six coordinate $(\eta^{2}\text{-}N,O\text{-}^{4}Tipo^{iPr})_2NiCl_2$ (**232**).[250] The markedly different coordination behaviour of $^{4}Tip^{iPr}$ and $^{4}Tipo^{iPr}$ is very likely due a reduction in electron donating ability of the phosphine oxide, as the difference in steric demand between the two ligands is negligible.

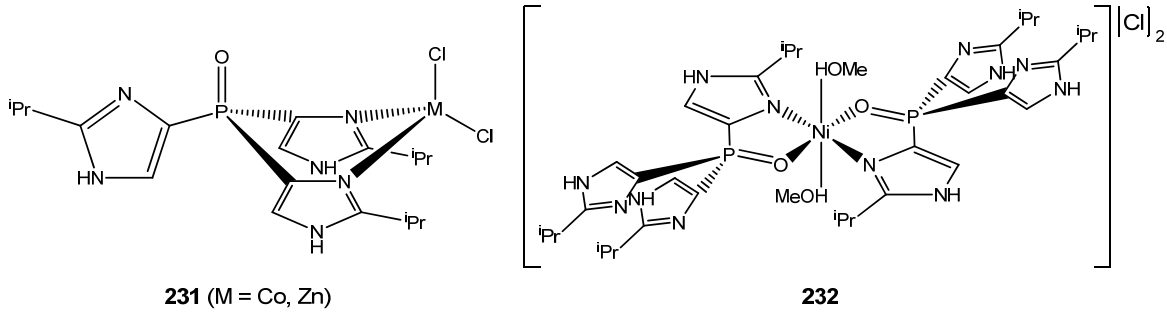

Figure 1.68 Structures of $(\eta^{2}\text{-}N,N'\text{-}^{4}Tipo^{iPr})MCl_2$ (231) and $(\eta^{2}\text{-}N,O\text{-}^{4}Tipo^{iPr})_2NiCl_2$ (232)

1.10 Tris(oxazolinyl) Ligands

Due to the partially saturated nature of the oxazoline heterocycle, mono-substitution at the 4-position gives rise to a chiral centre. If an enantiomerically pure oxazoline is then included as the donor moiety in a tripodal ligand, the resultant ligand will contain three identical chiral centres, and will impart its inherent molecular asymmetry to any derived metal complexes. Such complexes are highly sought after, as they have potential application in the asymmetric catalysis of a variety of synthetic transformations.

1.10.1 Tris(oxazolinyl)methanes

Tris(oxazolin-2-yl)methanes (Tom^x) were first reported in 2002 by Gade and Bellemin-Laponnaz, who synthesised as a proof-of-concept the achiral ligand 1,1,1-tris(4,4-dimethyloxazolin-2-yl)ethane ($MeTom^{Me2}$). Reaction with one equivalent of $[Cu(NCMe)_4][BF_4]$ gave the tetrameric $[\{(MeTom^{Me2})Cu\}_4][BF_4]_4$, where each ligand bridges two trigonal-planar copper centres in a μ-$\{\eta^2$-*N,N′*:$\eta^{1'}$-*N″*$\}$ fashion.[251] The first chiral Tom^x ligands to be prepared were 1,1,1-tris(4-(*S*)-isopropyloxazolin-2-yl)ethane ((*S*)- $MeTom^{iPr}$) and 1,1,1-tris(4-(*S*)-*tert*-butyloxazolin-2-yl)ethane ((*S*)-$MeTom^{tBu}$), and their ability to act as regular tripodal donor ligands was demonstrated with the preparation of the octahedral ((*S*)-$MeTom^{iPr}$)$RhCl_3$ (**233**).[252] To fully establish the efficacy of bulky Tom^x ligands as tripodal chelators, a large number of transition metal derivatives were prepared as part of an in-depth structural study. When (*S*)-$MeTom^{iPr}$ and its reduced symmetry variant 1,1-bis(4-(*S*)-phenyloxazolin-2-yl)-1-(4-(*R*)-phenyloxazolin-2-yl)ethane ((*S,S,R*)-$MeTom^{iPr}$) were reacted with $Mo(CO)_6$, the corresponding (Tom^x)$Mo(CO)_3$ (**234**, (*S*)-$MeTom^{iPr}$; **235**, (*S,S,R*)-$MeTom^{iPr}$) adducts were obtained. The structural parameters of both complexes were found to be very similar, and differ only in the orientation of a single isopropyl substituent, which is inherent to the chirality of the ligands. However, as a result of the reduction in molecular symmetry in (*S,S,R*)-$MeTom^{iPr}$, the ^1H and ^{13}C NMR spectra of ((*S,S,R*)-$MeTom^{iPr}$)$Mo(CO)_3$ in CD_2Cl_2 are more complicated when compared to those of ((*S*)-$MeTom^{iPr}$)$Mo(CO)_3$.[253]

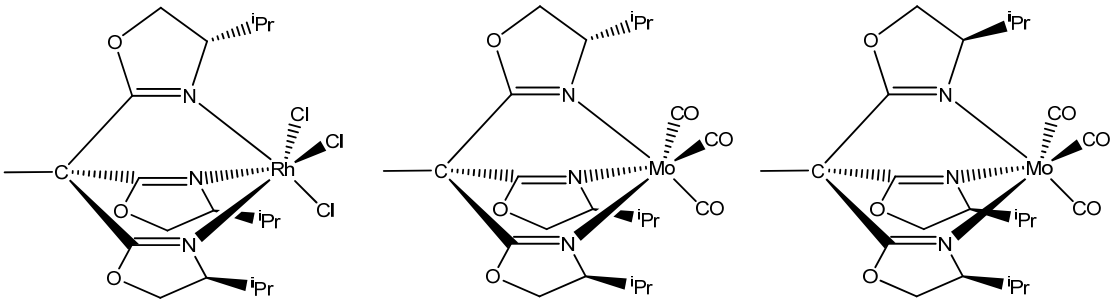

233 **234** **235**

Figure 1.69 Structures of ((*S*)-MeTom^{iPr})RhCl$_3$ (233) and (Tom^{x})Mo(CO)$_3$ (234, 235)

Comparison of the carbonyl stretching frequencies observed for (Tom^{x})Mo(CO)$_3$[253] with the structural analogue [NEt$_4$][(Tp^{iPr})Mo(CO)$_3$][254] implies that the Tom^{x} ligands are very weak electron-donors, comparable to Tppo*. Reaction of racemic MeTom^{iPr} (i.e. 50:50 (*S*)-MeTom^{iPr}/(*R*)-MeTom^{iPr}) with Co(ClO$_4$)$_2$ in acetonitrile furnished the octahedral [(*rac*-MeTom^{iPr})Co(NCMe)$_3$][ClO$_4$]$_2$ (**236**), the molecular structure of which shows that both stereoisomers occur with equal propensity in the solid state.[253] The same reaction carried out in DCM solvent gave the sandwich complex [((*S*)-MeTom^{iPr})((*R*)-MeTom^{iPr})Co][ClO$_4$]$_2$ (**237**), where each cobalt centre is coordinated tridentately by one of each ligand stereoisomer. Due to the opposing orientation of isopropyl substituents in the two stereoisomers, this heterochiral arrangement serves so as to minimise unfavourable steric interactions between the two ligand molecules. To illustrate this effect, when enantiomerically pure (*S*)-MeTom^{iPr} was used in place of the racemate, no products could be isolated from the reaction with Co(ClO$_4$)$_2$ in DCM, showing that a homochiral sandwich complex is strongly disfavoured due to the close spatial arrangement of the ligand substituent groups that would result.[253] Rather remarkably, reaction of (*S*)-MeTom^{tBu} with FeCl$_2$ and NaBF$_4$ in acetonitrile gave the six-coordinate tris-acetonitrile adduct [((*S*)-MeTom^{tBu})Fe(NCMe)$_3$][BF$_4$]$_2$ (**238**),[253] a structural arrangement which is unprecedented for transition metal complexes of similar 3-*tert*-butyl substituted ligands, except where one of the ancillary ligands is both very small and bidentate, such as the peroxide dianion in [(Tp^{tBu,Me})Cr(η^2-O$_2$)(Hpz^{tBu,Me})][BAr$^{F}_4$].

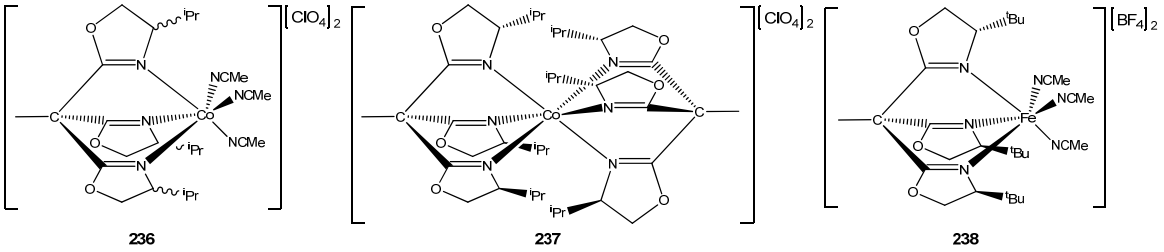

236 237 238

Figure 1.70 Structures of [(*rac*-MeTom^{iPr})Co(NCMe)$_3$][ClO$_4$]$_2$ (236), [((*S*)-MeTom^{iPr})((*R*)-MeTom^{iPr})Co][ClO$_4$]$_2$ (237) and [((*S*)-MeTom^{tBu})Fe(NCMe)$_3$][BF$_4$]$_2$ (238)

The face-sharing bioctahedral species [{((*S*)-MeTom^{iPr})M}$_2$(μ-Cl)$_3$][PF$_6$] (**239**, M = Fe, Co, Ni) were prepared by reaction of (*S*)-MeTom^{iPr} with the appropriate MCl$_2$ salt in the presence of KPF$_6$. The only compound that could be isolated following the reaction of CuCl$_2$ with (*S*)-MeTom^{iPr} was the highly distorted tetrahedral (η^2-(*S*)-MeTom^{iPr})CuCl$_2$ (**240**), both in the presence or absence of KPF$_6$, which seems to indicate a reluctance of the Tom^x ligands to adopt a tridentate binding mode upon coordination to copper(II) centres.[253]

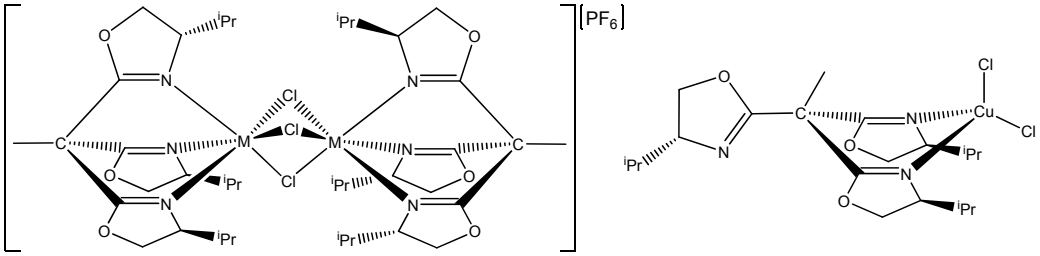

239 (M = Fe, Co, Ni) **240**

Figure 1.71 Structures of [{((*S*)-MeTom^{iPr})M}$_2$(μ-Cl)$_3$][PF$_6$] (239) and (η^2-(*S*)-MeTom^{iPr})CuCl$_2$ (240)

1.10.2 Tris(oxazolinyl)borates

Anionic tris(oxazolinyl)borates have recently been introduced by Sadow and colleagues, who described the synthesis of phenyltris(4,4-dimethyloxazolin-2-yl)borate (PhTob^{Me2}) and its subsequent use in the preparation of the zirconium (IV) derivatives (PhTob^{Me2})ZrX$_3$ (X = Cl, NMe$_2$). Treatment of (PhTob^{Me2})ZrCl$_3$ with KO^{t}Bu furnished (PhTob^{Me2})ZrCl$_2$(O^{t}Bu), for which the molecular structure was determined by X-ray diffraction.[255] PhTob^{Me2} was also used to prepare (PhTob^{Me2})Y(CH$_2$SiMe$_3$)$_2$(THF), which reacts with a variety of amines to give the six-coordinate (PhTob^{Me2})Y(NHR)$_2$(THF) (R = ^{t}Bu, 4-MeC$_6$H$_4$) complexes, as well as the five-coordinate (PhTob^{Me2})Y(NHC$_6$H$_3$-2,6-^{i}Pr$_2$)$_2$. (PhTob^{Me2})Y(CH$_2$SiMe$_3$)$_2$(THF) is an effective precatalyst for the intramolecular hydroamination of aminoalkenes.[256] (PhTob^{Me2})ZnCl (**241**) has been shown to be a synthetic precursor for the zinc-hydride complex (PhTob^{Me2})ZnH (**242**), which is

accessible through a variety of synthetic transformations (**scheme 1.36**). It is notable that one reaction pathway occurs through a formal β-hydrogen elimination reaction, a very rare method of decomposition for zinc complexes, and also that the synthesis of (PhTob^{Me2})ZnH can be effected in the absence of any traditional hydride transfer reagent such as a hydrosilane.[257]

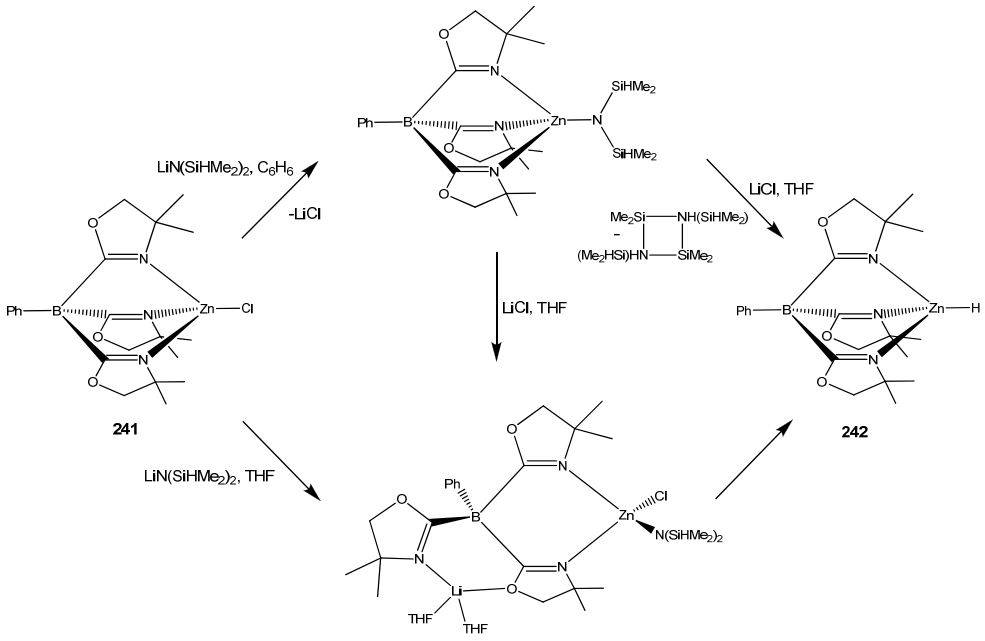

Scheme 1.36 Various routes for the conversion of (PhTob^{Me2})ZnCl (241) to (PhTob^{Me2})ZnH (242)

The same researchers have also synthesised the chiral phenyltris(4-(*S*)-isopropyloxazolin-2-yl)borate ((*S*)-PhTob^{iPr}), and applied it to the preparation of (η^2-(*S*)-PhTob^{iPr})Ir(η^4-cod) and (η^3-(*S*)-PhTob^{iPr})Ir(CO)$_2$.[258] Additionally, the dimethylaluminium derivatives of PhTob^{Me2} and (*S*)-PhTob^{iPr}, (η^2-PhTob^{x})AlMe$_2$, as well as the alkoxide (η^2-PhTob^{Me2})Al(O^{i}Pr)$_2$, have been shown to be active as catalysts for the ring-opening polymerisation of lactide, with (η^2- PhTob^{Me2})AlMe$_2$ displaying the highest level of activity.[259]

1.11 Ligands Based on 1,3,5-Triaminocyclohexane

Trinitrogen ligands in which the donor atoms are part of a macrocyclic system, such as 1,4,7-triazacyclononane (Tacn) and 1,5,9-triazacyclododecane (Tacdd), also coordinate to metal centres in an exclusively *fac* manner, and are therefore often considered under the umbrella term 'tripodal ligands'. However, such macrocyclic ligands do not conform to a strict definition of 'tripodal'; that is, a central scaffold with three protruding donor functionalities or 'legs', and as such shall not be considered further. Conversely, the related *cis,cis*-1,3,5-triaminocyclohexane (Tach) and its N-substituted derivatives can be included under the definition of 'tripodal', if one considers the central cyclohexane moiety as being supported by three amine 'legs'.

1.11.1 Complexes of Saturated Tach Ligands

The ability of unsubstituted Tach to act as a tripodal donor ligand has been known since 1962[260] and, excluding bis-Tach sandwich complexes, examples of crystallographically characterised derivatives include $[(Tach)Ni(OH_2)_3][NO_3]_2$,[261] $[\{(Tach)Co\}_2(\mu\text{-}OH)_2(\mu\text{-}NO_3)][NO_3]_3$,[262] $[\{(Tach)Cu(\mu\text{-}OH)\}_2][ClO_4]_2$,[263] $(Tach)M(CN)_3$ (M = Cr, Fe, Co)[264] and $[Na][(Tach)Fe(CN)_3]$.[264] In addition to the preparation of $[(Tach)_2Zn][X]_2$ (X = OTf, ClO_4) and [(Tach)ZnX][X] (X = Cl, Br, I, NO_3), Vahrenkamp and Brand also reported the use of *cis,cis*-1,3,5-tris(methylamino)cyclohexane ($Tach^{Me}$) in preparing the corresponding $[(Tach^{Me})ZnX][X]$ (**243**, X = Cl, NO_3) complexes. No sandwich complexes of $Tach^{Me}$ could be isolated, which is likely an effect of the increased steric bulk of $Tach^{Me}$ in comparison to Tach.[265]

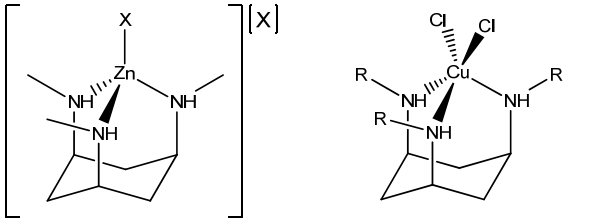

243 (X = Cl, NO_3) **244** (R = Me, Et, ^nPr, CH_2Th, CH_2Fr)

Figure 1.72 Structures of $[(Tach^{Me})ZnX][X]$ (243) and $(Tach^{R})CuCl_2$ (244)

Planalp and co-workers have also employed the $Tach^{Me}$ ligand, in addition to *cis,cis*-1,3,5-tris(ethylamino)cyclohexane ($Tach^{Et}$), *cis,cis*-1,3,5-tris(*n*-propylamino)cyclohexane ($Tach^{nPr}$), *cis,cis*-1,3,5-tris(2-thienylmethylamino)cyclohexane ($Tach^{CH2Th}$) and *cis,cis*-1,3,5-tris(2-furanylmethylamino)cyclohexane ($Tach^{CH2Fr}$), to prepare the corresponding

square-pyramidal ($Tach^{R}$)$CuCl_2$ derivatives (**244**). Reaction of the very sterically encumbered ligand *cis,cis*-1,3,5-tris(neopentylamino)cyclohexane ($Tach^{Np}$) with $CuCl_2$ however gave a highly insoluble material of unidentified composition, which is likely a coordination polymer arising from the inability of all three N-donors of one $Tach^{Np}$ molecule to coordinate to the same copper(II) centre. In aqueous solution at pH 7.2, ($Tach^{Me3}$)$CuCl_2$ has been shown to selectively catalyse the hydrolysis of activated phosphate diesters, the rate of decomposition of the associated monoesters being 1000 times slower when employing the same catalyst system.[266]

Masuda *et al.* reported the synthesis of *cis,cis*-1,3,5-tris(benzylamino)cyclohexane ($Tach^{Bn}$) and *cis,cis*-1,3,5-tris(isobutylamino)cyclohexane ($Tach^{iBu}$), and used these ligands, in addition to $Tach^{Et3}$, to prepare the corresponding [($Tach^{R}$)Cu(L)][SbF_6] (L = NCMe, CO) adducts. Like many of the aforementioned copper(I) species, the [($Tach^{R}$)Cu(NCMe)][SbF_6] complexes react with O_2 at low temperature, though rather than a side-on peroxo bridged dimer, the obtained products are in fact the bis μ-oxo dicopper(III) complexes [{($Tach^{R}$)Cu(μ-O)}$_2$][SbF_6]$_2$ (**245**).[267]

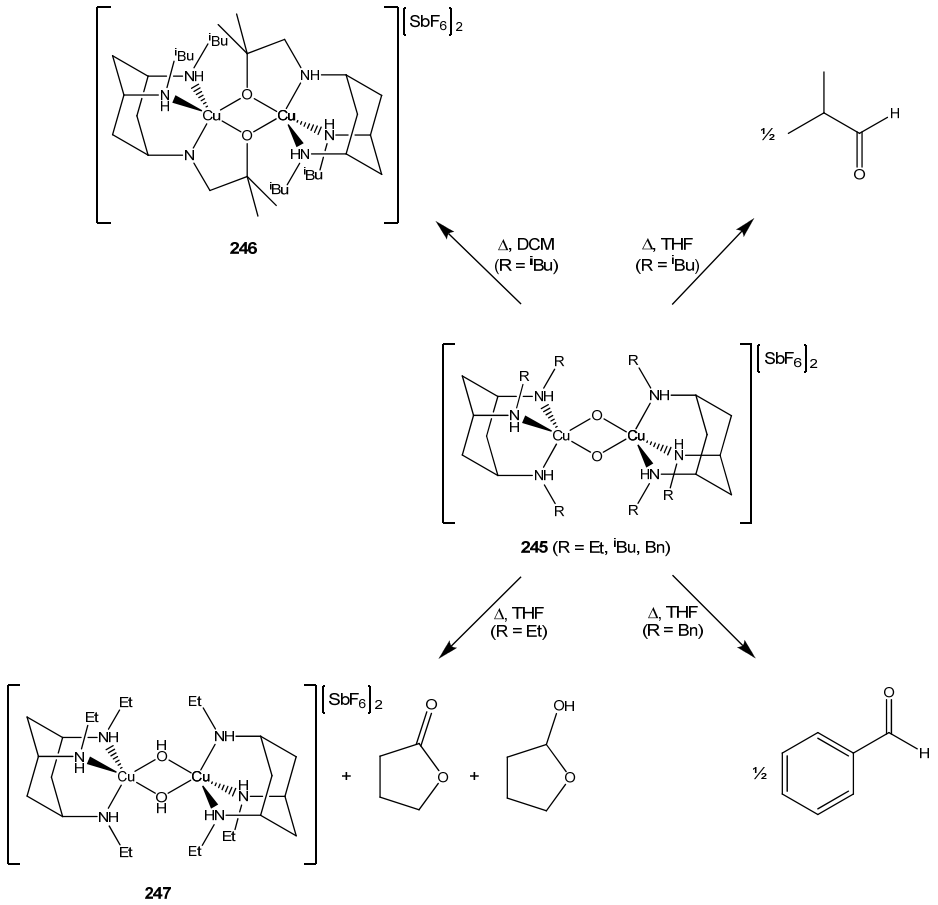

Scheme 1.37 Decomposition pathways of [{($Tach^{R}$)Cu(μ-O)}$_2$][SbF_6]$_2$ (245)

Due to the fact that the carbonyl stretching vibrations of $[(Tach^{R})Cu(CO)][SbF_6]$ imply that the $Tach^{R}$ ligands are stronger electron donors even than Tp^{x},[267] it is tempting to attribute this difference in oxygen reactivity to solely electronic factors. However, it has been shown that the bis(μ-oxo) dicopper(III) and μ-peroxo dicopper(II) adducts are energetically very similar, and that in addition to electronic considerations both steric and solvent effects are equally important in dictating which of the two isomeric species is formed. Indeed, equilibrium mixtures of both structural types have been shown to occur in solution.[268] The decomposition pathways of $[\{(Tach^{R})Cu(\mu\text{-}O)\}_2][SbF_6]_2$ have also been shown to be solvent dependent (**scheme 1.37**); for example, warming of a DCM solution of $[\{(Tach^{iBu})Cu(\mu\text{-}O)\}_2][SbF_6]_2$ to room temperature furnished crystals of a dimeric complex (**246**) in which one of the isobutyl groups from each the of $Tach^{iBu}$ ligands have been oxygenated at the β-position, and form alkoxide bridges between the two copper(II) centres.[267] Conversely, the same process carried out in THF results in mono-N-dealkylation of one of the $Tach^{iBu}$ ligands, producing a half equivalent of isobutyraldehyde. $[\{(Tach^{Bn})Cu(\mu\text{-}O)\}_2][SbF_6]_2$ decomposes by an identical process in THF with concomitant formation of benzaldehyde, whereas in the case of $[\{(Tach^{Et})Cu(\mu\text{-}O)\}_2][SbF_6]_2$ the THF solvent is oxidised, yielding 2-hydroxytetrahydrofuran and γ-butyrolactone in addition to $[\{(Tach^{Et})Cu(\mu\text{-}OH)\}_2][SbF_6]_2$ (**247**).[267]

1.11.2 Tris(benzylideneamine)cyclohexanes

In 1996 Walton and colleagues described the reaction of *cis,cis*-1,3,5-tris((*E*)-benzylideneamino)cyclohexane (Bzd-Tach, **248**), an unsaturated imino variant of $Tach^{Bn}$, with $ZnCl_2$ in the presence of $NaBPh_4$. The Bzd-Tach ligand was found to undergo an unusual partial hydrolysis reaction (**scheme 1.38**), yielding a cationic four-coordinate zinc chloride complex (**249**). The molecular structure of this complex revealed the presence of a new unsymmetrical tripodal ligand in which two of the benzylidene moieties of Bzd-Tach have been cleaved to give unsubstituted amines, both of which are co-ordinated to the zinc atom in addition to the sole remaining imino group.[269]

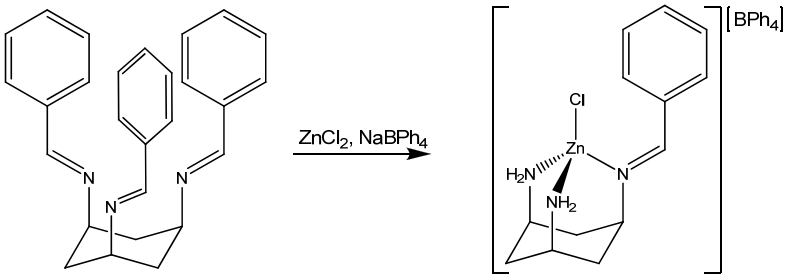

Scheme 1.38 Partial hydrolysis of Bzd-Tach (248) upon reaction with $ZnCl_2$/$NaBPh_4$

Identical reactivity of Bzd-Tach has also been observed in combination with the transition metal salts $M(NO_3)_2$ (M = Ni, Cu) and $Cu(OAc)_2$, furnishing the corresponding five- (Cu, **250**) and six-coordinate (Ni, **251**) complexes. The more heavily substituted *cis,cis*-1,3,5-tris((*E*)-3-hydroxybenzylideneamino)cyclohexane (Bzd-Tach^{OH}), *cis,cis*-1,3,5-tris((*E*)-3,5-dimethoxybenzylideneamino)cyclohexane (Bzd-Tach$^{(OMe)2}$) and *cis,cis*-1,3,5-tris((*E*)-4-acetamidobenzylideneamino)cyclohexane (Bzd-Tach^{Am}) also undergo the same double hydrolysis reaction in the presence of $Cu(OAc)_2$, $CuCl_2$ and $ZnCl_2$/$NaBPh_4$ respectively, yielding the corresponding five-coordinate copper (**252**) and four-coordinate zinc (**253**) complexes.[270]

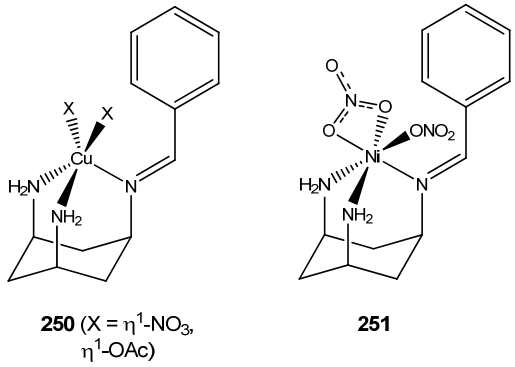

Figure 1.73 Structures of 250 and 251

Conversely, *cis,cis*-1,3,5-tris((*E*)-mesitylideneamino)cyclohexane (Bzd-Tach^{Me3}), synthesised by Wass *et al.*, is stable upon coordination to copper(I) and has been used to prepare [(Bzd-Tach^{Me3})Cu(L)][PF_6] (**254**, L= NCMe, CO).[271] The carbonyl stretching vibration observed for [(Bzd-Tach^{Me3})Cu(CO)][PF_6][271] is shifted to higher energy by 18 cm^{-1} in comparison to [(Tach^{Bn})Cu(CO)][SbF_6],[267] which illustrates the reduced electron donating ability of imine nitrogen atoms when compared to secondary amines.

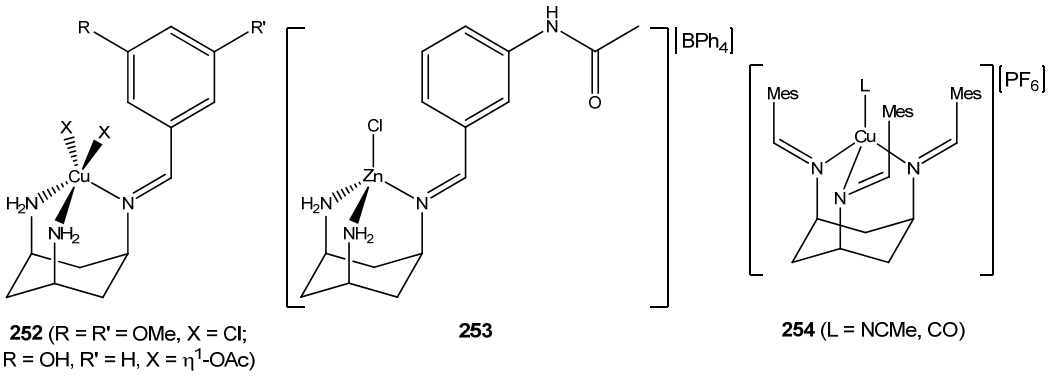

Figure 1.74 Structures of 252, 253 and [(Bzd-Tach^{Me3})Cu(L)][PF_6] (254)

1.11.3 Pro-Tach Ligands

The original report by Walton *et al.* on the reactivity of Bzd-Tach also included the synthesis of a further new ligand based on the Tach skeleton, namely *cis,cis*-1,3,5-tris((*E,E*)-phenylpropenylideneamino)cyclohexane (Pro-Tach^{Ph}). In contrast to the behaviour of the Bzd-Tach^{x} compounds, Pro-Tach^{Ph} remains unchanged upon reaction with $ZnSO_4$, giving the four co-ordinate complex (Pro-Tach^{Ph})Zn(η^1-SO_4) (**255**).[269] Positioning the bulky phenyl groups more remotely from the zinc centre appears to eliminate the propensity for hydrolysis, and gives a ligand architecture that provides a hydrophobic pocket which extends to a relatively large distance from the coordinated metal atom in comparison to the other aforementioned tripodal ligands. This hydrophobic pocket is large enough to accommodate several solvent molecules, both free and coordinated, as evidenced by the solid state structures of [(Pro-Tach^{Ph})Ni(η^1-OAc)$(HOMe)_2$][BPh_4] (**256**) and [(Pro-Tach^{Fr})Co$(HOMe)_3$][BPh_4]$_2$ (**257**, Pro-Tach^{Fr} = *cis,cis*-1,3,5-tris((*E,E*)-2-furanylpropenylideneamino)cyclohexane) which, in addition to the coordinated solvent molecules, show the presence of two and three extra hydrogen-bonded methanol molecules respectively.[272]

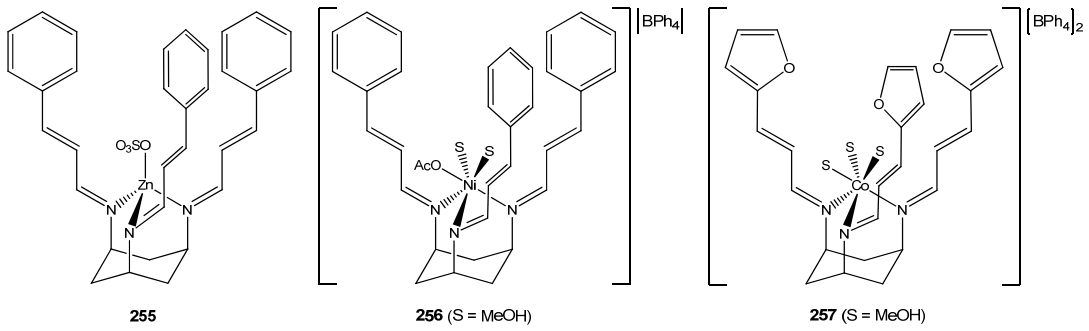

Figure 1.75 Structures of (Pro-Tach^{Ph})Zn(η^1-SO_4) (255), [(Pro-Tach^{Ph})Ni(η^1-OAc)$(HOMe)_2$][BPh_4] (256) and [(Pro-Tach^{Fr})Co$(HOMe)_3$][BPh_4]$_2$ (257)

Analogous inclusion of anions in an even more extensive hydrophobic pocket was also demonstrated with the preparation of [(Pro-Tach^{tBuPh})Co(HOMe)$_3$][NO$_3$]$_2$ (**258**, Pro-Tach^{tBuPh} = *cis,cis*-1,3,5-tris((*E,E*)-(4-*tert*-butylphenyl)propenylideneamino)cyclohexane), the molecular structure of which shows the presence of a single nitrate ion, hydrogen-bonded to each of the two co-ordinated methanol molecules, with a further two free methanol molecules also present in the pocket. [(Pro-Tach^{tBuPh})Co(HOMe)$_3$][NO$_3$]$_2$ was crystallised from a 90:10 methanol/DCM solvent mixture; when this ratio was changed to 70:30, crystals of [(Pro-Tach^{tBuPh})Co(η^2-NO$_3$)(HOMe)][NO$_3$] (**259**) were obtained in which no additional solvent molecules are incorporated in the pocket, though the coordinated methanol is hydrogen-bonded to an exterior chain of three further hydrogen-bonded methanol molecules.[273]

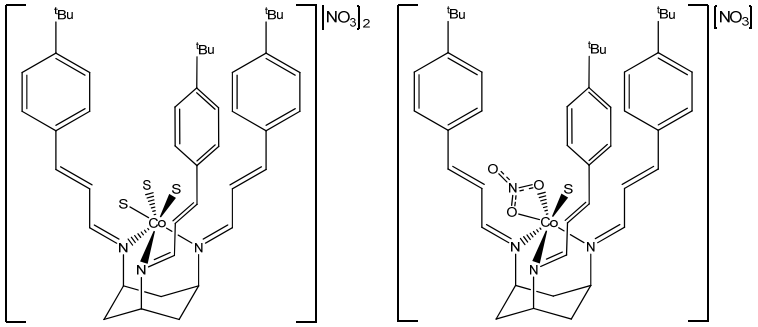

Figure 1.76 Structures of [(Pro-Tach^{tBuPh})Co(HOMe)$_3$][NO$_3$]$_2$ (258) and [(Pro-Tach^{tBuPh})Co(η^2-NO$_3$)(HOMe)][NO$_3$] (259)

Pro-Tach^{Ph} was also used to prepare the cobalt(II) complexes [(Pro-Tach^{Ph})Co(η^1-X)(OH$_2$)$_2$][BPh$_4$] (**260** X = NO$_3$, ClO$_4$) and [(Pro-Tach^{Ph})CoX][BPh$_4$] (X = Cl, Br, I). The former nitrate and perchlorate complexes react with NaOH followed by either dimethyl dicarbonate or diethyl dicarbonate (**scheme 1.39**) to give the cobalt(II) alkoxide species [(Pro-Tach^{Ph})Co(OR)][BPh$_4$] (**261**, R = Me, Et) *in situ*, which then catalyse the decomposition of the dialkyl dicarbonates to their corresponding dialkyl carbonates and CO$_2$. The formation of the alkoxide compounds results from the reaction of the dialkyl dicarbonates with a putative [(Pro-Tach^{Ph})CoOH][BPh$_4$] (**262**) species (**scheme 1.39**), itself arising due to the reaction of HO$^-$ with the precursor complexes. Although this hydroxo-complex could not be isolated, exposure to CO$_2$ produced the carbonate-bridged dimer [{(Pro-Tach^{Ph})Co}$_2$(μ-η^2:$\eta^{2'}$-CO$_3$)][BPh$_4$]$_2$ (**263**).[274]

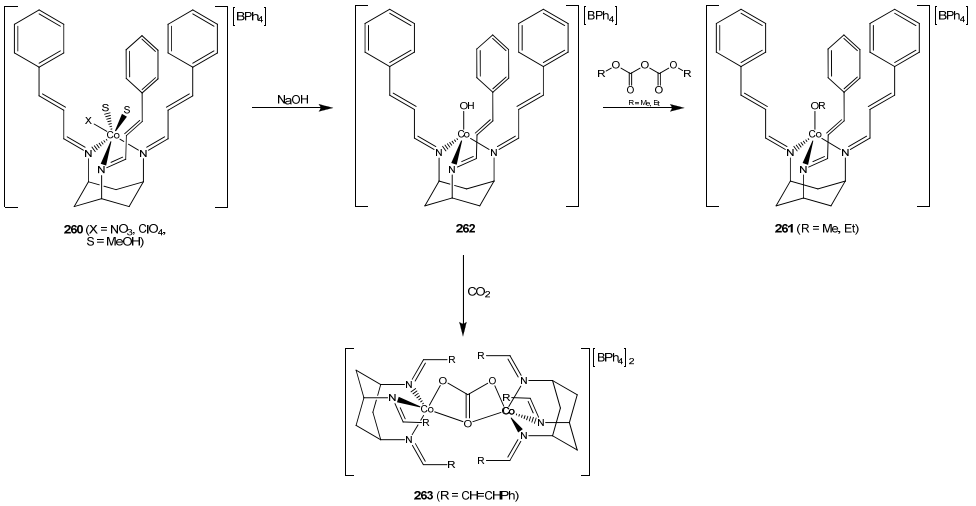

Scheme 1.39 Formation of [(Pro-Tach^{Ph})Co(OR)][BPh$_4$] (261) and [{(Pro-Tach^{Ph})Co}$_2$(μ-η^2:η$^{2'}$-CO$_3$)][BPh$_4$]$_2$ (263)

It was subsequently shown that [(Pro-Tach^{Ph})Co(OEt)][BPh$_4$] and [(Pro-Tach^{Ph})Co(OPh)][BPh$_4$], in this instance prepared by reaction of the corresponding sodium alkoxide with [(Pro-Tach^{Ph})CoCl][BPh$_4$] and [(Pro-Tach^{Ph})Co(NO$_3$)][BPh$_4$] respectively, could be isolated as pure compounds and both were structurally characterised. Additionally, these complexes could also be synthesised by addition of either ethanol or phenol to a solution of [(Pro-Tach^{Ph})CoOH][BPh$_4$]. [(Pro-Tach^{Ph})Co(OR)][BPh$_4$] (**264**, R = Et, Ph) were shown to react with CO_2 in methanol solution to give the corresponding six-coordinate alkylcarbonate complexes [(Pro-Tach^{Ph})Co(η^2-O$_2$COR)(HOMe)][BPh$_4$] (**265**, R = Et, Ph), and if the CO_2 atmosphere is replaced with one of N_2 or Ar, the starting alkoxides are regenerated with concomitant loss of CO_2 (**scheme 1.40**).[275] The trinuclear copper(II) methoxide complex [(Pro-Tach^{Fr})Cu(μ-OMe)$_2$Cu(μ-OMe)$_2$Cu(Pro-Tach^{Fr})][BF$_4$]$_2$ was obtained by direct reaction of Pro-Tach^{Fr} with Cu(OAc)$_2$/NaBF$_4$ in methanol,[276] and is a dicationic structural analogue of the neutral (Tp^{Cum,Me})Cu(μ-OMe)$_2$Cu(μ-OMe)$_2$Cu(Tp^{Cum,Me}) (**section 1.4.9**).

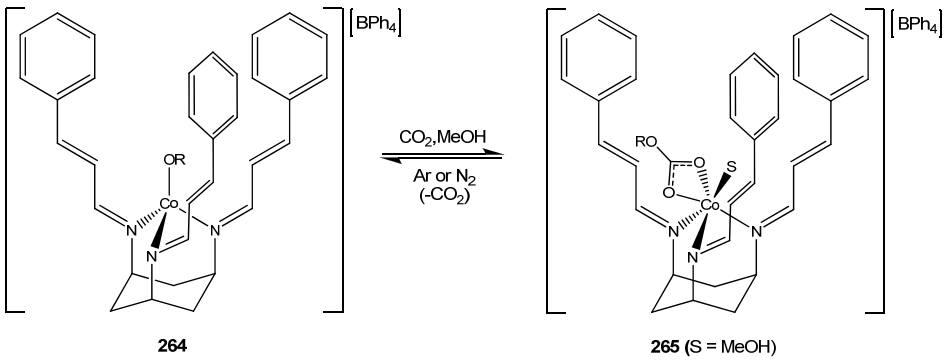

Scheme 1.40 Reversible reaction of [(Pro-Tach^{Ph})Co(OR)][BPh$_4$] (264) with CO_2

The ability of the Pro-Tach^{Ph} ligand to support metal complexes of varying coordination number was further demonstrated with the preparation of the four-coordinate [(Pro-Tach^{Ph})MX][BPh$_4$] (**266**, M = Zn, X = Cl, Br; M = Ni, X = Cl; M = Cd, X = Br), the five-coordinate [(Pro-Tach^{Ph})CdCl(HOMe)][BPh$_4$] (**267**) and the six-coordinate [(Pro-Tach^{Ph})Cd(η^2-NO$_3$)(HOMe)][BPh$_4$] (**268**). The molecular structure of [(Pro-Tach^{Ph})ZnCl][BPh$_4$] shows that two DCM solvent molecules are included within the hydrophobic pocket while one is situated just outside, whereas [(Pro-Tach^{Ph})Cd(η^2-NO$_3$)(HOMe)][BPh$_4$] incorporates one additional molecule of methanol, which is hydrogen-bonded to the metal-bound methanol.[277]

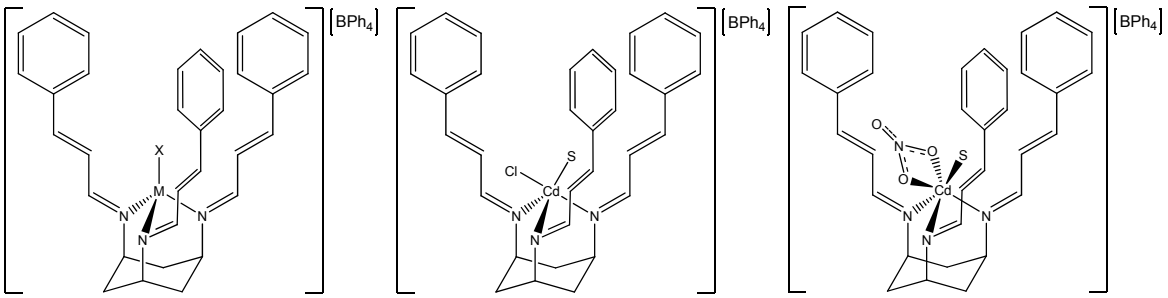

266 (M, X = *see text*) **267** (S = MeOH) **268** (S = MeOH)

Figure 1.77 Structures of [(Pro-Tach^{Ph})MX][BPh$_4$] (266), [(Pro-Tach^{Ph})CdCl(HOMe)][BPh$_4$] (267) and [(Pro-Tach^{Ph})Cd(η^2-NO$_3$)(HOMe)][BPh$_4$] (268)

Interestingly, the solid-state structure of the crystalline product arising from coordination of Pro-Tach^{Ph} to CuSO$_4$ in methanol revealed the presence of two discrete five-coordinate copper(II) complexes, (Pro-Tach^{Ph})Cu(η^2-SO$_4$) (**269**) and (Pro-Tach^{Ph})Cu(η^1-SO$_4$)(HOMe) (**270**).

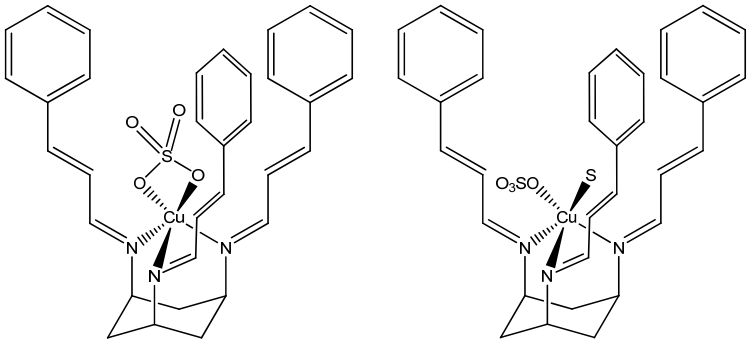

269 **270** (S = MeOH)

Figure 1.78 Structures of (Pro-Tach^{Ph})Cu(η^2-SO$_4$) (269) and (Pro-Tach^{Ph})Cu(η^1-SO$_4$)(HOMe) (270)

Similarly, Pro-Tach^{Fr} has also been used to prepare the six-coordinate [(Pro-Tach^{Fr})M(η^2-NO_3)(HOMe)][BPh_4] (**271**, M = Co, Zn) and [(Pro-Tach^{Fr})Co(η^2-OAc)(HOMe)][BPh_4] (**272**), as well as the four-coordinate [(Pro-Tach^{Fr})Zn(η^1-OAc)][BPh_4] (**273**). The acetate complexes have been postulated as active site structural models for the bicarbonate adducts of both endogenous carbonic anhydrase, and its cobalt-substituted variant.[278]

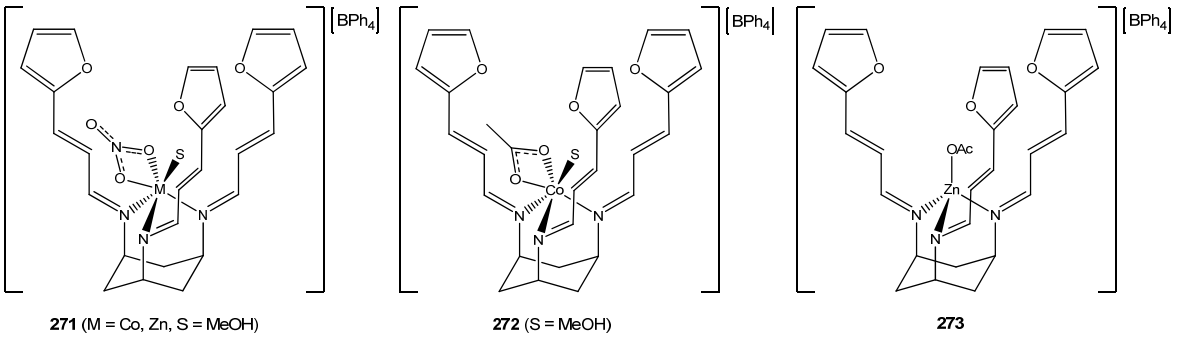

Figure 1.79 Structures of [(Pro-Tach^{Fr})M(η^2-NO_3)(HOMe)][BPh_4] (271), [(Pro-Tach^{Fr})Co(η^2-OAc)(HOMe)][BPh_4] (272) and [(Pro-Tach^{Fr})Zn(η^1-OAc)][BPh_4] (273)

Most recently, Pro-Tach^{Ph} was used to prepare the copper(I) complex [(Pro-Tach^{Ph})Cu(NCMe)][BF_4], which was then shown to undergo a number of ligand metathesis reactions, yielding (Pro-Tach^{Ph})Cu(X) (X = Cl, Br, SPh, η^1-*N*-NO_2). (Pro-Tach^{Ph})CuCl could also be prepared by means of the direct reaction between Pro-Tach^{Ph} and CuCl in DCM.[279]

1.12 Concluding Remarks

In summary, it has been shown that a large variety of tripodal nitrogen donor ligands are available to the coordination chemist, and the coordination numbers of obtained complexes are highly dependent on the steric demand imparted by the ligand substituents. However, the nature of the metal ions, and the identity of the ancillary ligands, is also very important in dictating the coordination number of a metal centre bound by a tripodal ligand. Different ligand systems can give rise to subtle differences in the properties of otherwise very similar complexes, which can in turn give rise to differences in reactivity. Therefore, the development of new tripodal nitrogen ligands is likely to lead to the formation of metal complexes with distinct structural characteristics, and potentially novel or enhanced modes of reactivity.

The following chapters describe the synthesis and characterisation of a series of new tripodal nitrogen ligands, the β-triketimines. These ligands form isolable complexes with a variety of metals, and a number of their complexes with nickel(II) are shown to be active as precatalysts for the polymerisation of ethylene.

2. The Synthesis and Characterisation of β-Triketimines and Their Group 6 Metal Carbonyl Derivatives

2.1 Introduction

2.1.1 β-Diketiminates and Their Application in Coordination Chemistry

β-diketiminate complexes have been the subject of an extensive review article, though it is some considerable time since this was published.[280] This short review shall again report the key achievements in β-diketiminate chemistry, with an emphasis on complexes with low coordination numbers. The second part of the review (**section 2.1.2**) shall then focus on modification of the β-diketiminate ligand architecture, most commonly through the reaction of their derived metal complexes.

As described briefly in **section 1.2** the β-diketiminates, in particular BDK^{iPr2}, have been applied extensively to the preparation of a wide variety of novel, low-coordinate metal complexes. For instance, the complexes $(BDK^{iPr2})M$ (**274**, M = Al,[281] Ga,[282] In[283]) are examples of two-coordinate, six electron 'carbene-analogues' in which the metal atoms are in the +1 oxidation state. Also, BDK^{iPr2} has been shown to be extremely effective in stabilising first-row transition metal complexes where the metal centre has a three-coordinate planar geometry, the first such examples of which were $(BDK^{iPr2})CuX$ (**275**, X = Cl, $SCPh_3$).[284]

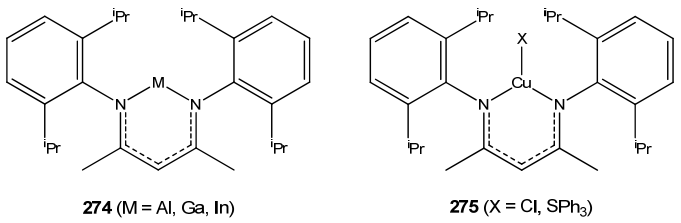

Figure 2.1 Structures of $(BDK^{iPr2})M$ (274) and $(BDK^{iPr2})CuX$ (275)

The related, even more bulky $^{t}Bu_2BDK^{iPr2}$ ($H^{t}Bu_2BDK^{iPr2}$ = 2,2,6,6-tetramethyl-bis(2,4-(2,6-diisopropyl)phenylimino)pentane) was subsequently employed to prepare the analogous $(^{t}Bu_2BDK^{iPr2})MCl$ (**276**, M = Fe, Co, Ni) which, in the case of M = Fe, Co, gave access to the very electronically unsaturated $(^{t}Bu_2BDK^{iPr2})MMe$ (**277**, M = Fe, Co) upon reaction with methyllithium in THF (**scheme 2.1**). Conversely, identical treatment of $(^{t}Bu_2BDK^{iPr2})NiCl$ with methyllithium gave the nickel(I) complex $(^{t}Bu_2BDK^{iPr2})Ni(THF)$ (**278**).[285]

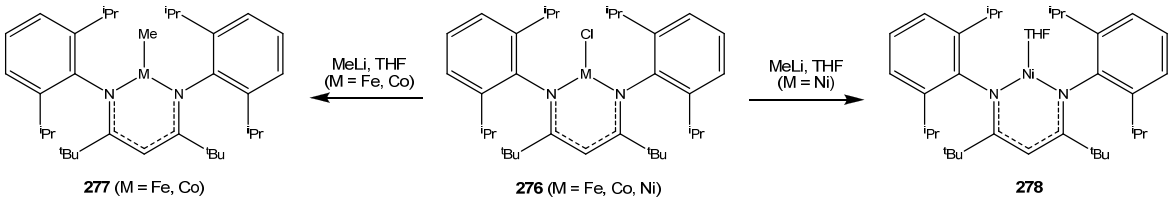

Scheme 2.1 Reaction of ($^{t}Bu_2BDK^{iPr2}$)MCl (276) with methyllithium

Reduction of ($^{t}Bu_2BDK^{iPr2}$)FeCl with sodium naphthalenide or KC_8 under an atmosphere of N_2 furnished the dinuclear three-coordinate iron(I) dinitrogen adduct {($^{t}Bu_2BDK^{iPr2}$)Fe}$_2$(μ-η^1:η$^{1'}$-N_2) (**279a**) which, upon further treatment with potassium metal undergoes a reduction in the N-N bond order to give [K]$_2$[{($^{t}Bu_2BDK^{iPr2}$)Fe}$_2$(μ-η^1:η$^{1'}$-N_2)], which contains a formally zerovalent [FeNNFe] core.[286] The related nickel(I) complex {($^{t}Bu_2BDK^{iPr2}$)Ni}$_2$(μ-η^1:η$^{1'}$-N_2) (**279b**) has been described recently, and was shown to undergo stepwise one-electron reductions to [K][{($^{t}Bu_2BDK^{iPr2}$)Ni}$_2$(μ-η^1:η$^{1'}$-N_2)], and finally [K]$_2$[{($^{t}Bu_2BDK^{iPr2}$)Ni}$_2$(μ-η^1:η$^{1'}$-N_2)].[287] BDK^{iPr2} has also been employed to prepare the metal-metal bonded dinuclear species {(BDK^{iPr2})M}$_2$ (**280**, M = Mn,[288] Zn,[289] Mg[290]). In the case of M = Zn, Mg, these are extremely rare examples of complexes where the metal atoms are in the formal +1 oxidation state.

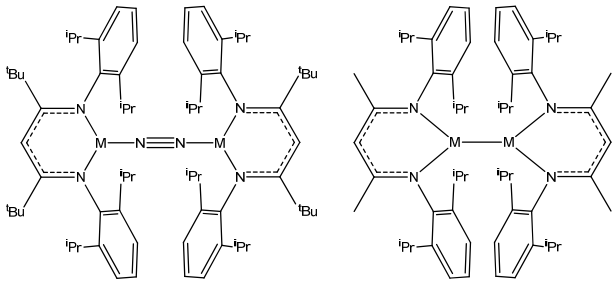

Figure 2.2 Structures of {($^{t}Bu_2BDK^{iPr2}$)M}$_2$(μ-η^1:η$^{1'}$-N_2) (279) and {(BDK^{iPr2})M}$_2$ (280)

The related metal-metal bonded compounds {(BDK^{Me2})Ni}$_2$(μ-NAd) (**281**, $HBDK^{Me2}$ = 2-(2,6-dimethyl)phenylamino-4-(2,6-dimethyl)phenyliminopent-2-ene, Ad = 1-adamantyl)[291] and {(BDK^{Me3})Cu}$_2$(μ-NC_6H_3-3,5-Me_2) (**282**, $HBDK^{Me3}$ = 2-(2,4,6-trimethyl)phenylamino-4-(2,4,6-trimethyl)phenyliminopent-2-ene)[292] were prepared by the reaction of the corresponding azides with β-diketiminate supported metal(I) precursors. Lastly, in contrast to the tridentate ligands discussed in **section 1**, BDK^{iPr2} was found to be effective in stabilising the square-planar superoxo-nickel(II) complex (BDK^{iPr2})Ni(η^2-O_2) (**283**), which was the first such superoxo-compound to be structurally characterised.[293]

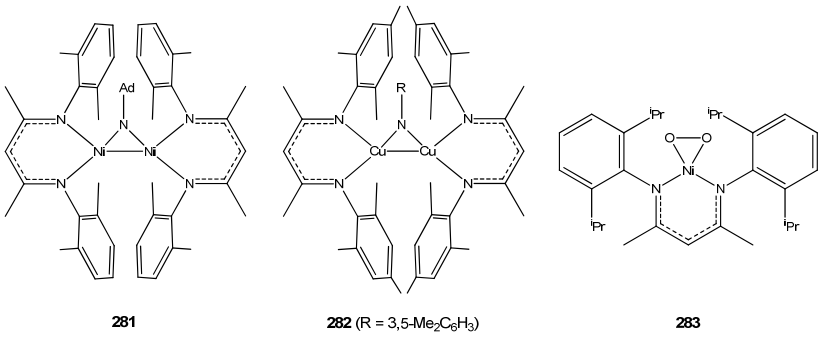

281 **282** (R = 3,5-$Me_2C_6H_3$) **283**

Figure 2.3 Structures of {(BDK^{Me2})Ni}$_2$(μ-NAd) (281), {(BDK^{Me3})Cu}$_2$(μ-NC_6H_3-3,5-Me_2) (282) and (BDK^{iPr2})Ni(η^2-O_2) (283)

2.1.2 Elaboration of β-Diketiminates and Related Species to Compounds with a More Complicated Ligand Architecture

Although there is a vast amount of literature concerning β-diketiminate ligands, relatively little has been reported regarding their further synthetic elaboration to new ligands with a modified framework, either through direct reaction of their derived metal complexes, or alternatively by modification of the free β-iminoenamines. Mair *et al.* have demonstrated that the lithium β-diketiminates (BDK^{iPr2})Li (**283a**) and (BDK^{iPr})Li (**283b**, HBDK^{iPr} = 2-(2-isopropyl)phenylamino-4-(2-isopropyl)phenyliminopent-2-ene) undergo reaction with alkyl chlorides (**scheme 2.2**) to give the corresponding α,α-dialkylated β-diimines (**284**),[294] which are devoid of imino-azaenol tautomerism and have been applied as neutral ligands.[295]

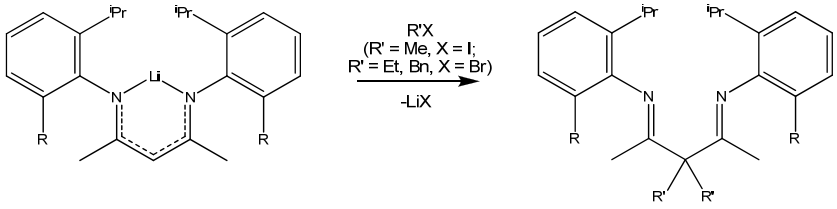

283a (R = ^{i}Pr)
283b (R = H)

284 (R' = Me, Et, Bn)

Scheme 2.2 Reaction of lithium β-diketiminates (283) with alkyl halides

It has also been described in two associated patents that the reaction (**scheme 2.3**) of a variety of lithium β-diketiminates (**285**) with 2-(bromomethyl)pyridine gives access to a series of tridentate 2-pyridylmethyl-β-iminoenamine ligands (**286**).[296] Although the authors reported the preparation of a number of metal complexes derived from these ligands, in both their neutral and monoanionic forms, very little supporting data was provided, and some of the ascribed structures seem rather unlikely.

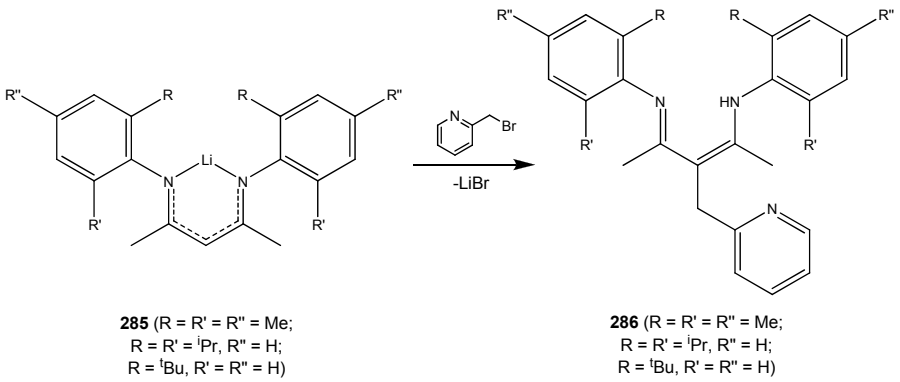

285 (R = R' = R'' = Me;
R = R' = ^{i}Pr, R'' = H;
R = ^{t}Bu, R' = R'' = H)

286 (R = R' = R'' = Me;
R = R' = ^{i}Pr, R'' = H;
R = ^{t}Bu, R' = R'' = H)

Scheme 2.3 Preparation of 2-pyridylmethyl-β-iminoenamines (286)

The reaction of (BDK^{iPr2})K (**287**) with trimethylacetyl chloride (**scheme 2.4**) was reported recently by Lappert and colleagues, and produces a neutral α-trimethylacetyl β-diimine (**288**).[297] This compound has the potential to act as a tridentate N,N,O ligand, though no further discussion of its coordination chemistry was provided.

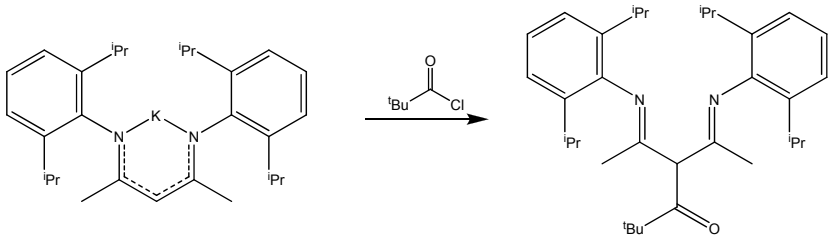

287 **288**

Scheme 2.4 Preparation of α-trimethylacetyl β-diimine (288)

The reaction of (BDK^{iPr2})Li (**283a**) with chlorophosphines has been shown to occur exclusively at the α-carbon of (BDK^{iPr2})Li, giving α-phosphino-β-iminoenamines (**289**) (**scheme 2.5**). Following metallation, these mixed hard/soft ligands have been shown to coordinate through either the phosphorus atom, or the β-diketiminate moiety, dependent on the identity of the metal.[298] Despite the obvious potential of these ligands for the generation of heterobimetallic complexes, no such species have been reported.

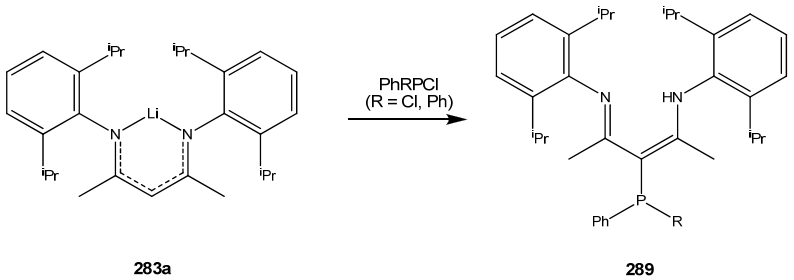

283a **289**

Scheme 2.5 Preparation of α-phosphino β-iminoenamines (289)

In an attempt to prepare a silver(I) β-diketiminate complex, HBDK^{iPr2} (**290**) was treated with trimethylamine and $AgPF_6$. However, one-electron oxidation of [BDK^{iPr2}]$^-$ was found to occur, concomitant with the formation of silver(0), producing a dimer (**291**) of HBDK^{iPr2} which is coupled at the α-carbon atoms (**scheme 2.6**).[299] It has also been shown that **291** is formed as a side-product in the reaction of (BDK^{iPr2})Li with $TiCl_4$, in addition to the desired (BDK^{iPr2})$TiCl_3$.[300] Once again, the likely ability of this coupled ligand to produce bimetallic species remains unutilised.

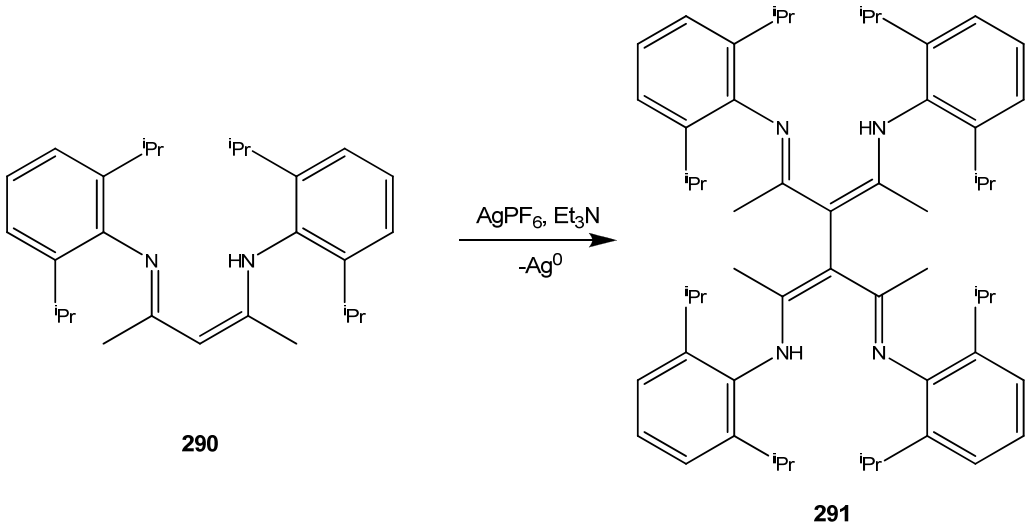

290 **291**

Scheme 2.6 Formation of coupled β-iminoenamine (291)

Itoh and co-workers have described the preparation of a novel α-keto-β-diimine ligand (**293**), formed via aerobic oxidation of the copper(II) acetate derivative (**292**) of HBDK^{Me3} (**scheme 2.7**).[301] The α-keto derivative of HBDK^{iPr2} was prepared in an analogous fashion, and its nickel dibromide derivative has been shown to be highly active as a precatalyst for the polymerisation of α-olefins.[302]

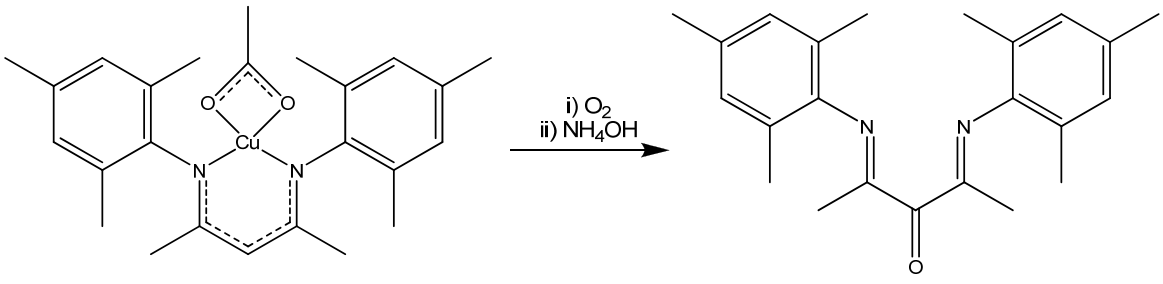

292 **293**

Scheme 2.7 Synthesis of α-keto-β-diimine ligand (293)

The cationic three-coordinate iron complex [(^{t}Bu$_2$BDK^{iPr2})Fe(OEt$_2$)][BAr$^{F}_4$] (**294**) was shown by Holland and co-workers to react with ethyl diazoacetate (**scheme 2.8**) to furnish a five-coordinate iron(II) complex (**295**), which features a novel tetradentate ligand.[303] However, no report was made of any attempts to isolate this new ligand in its free, protonated form.

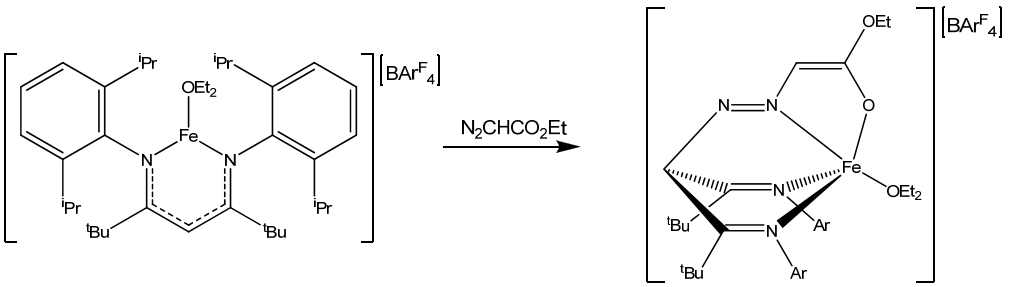

294 **295** (Ar = 2,6-^{i}Pr$_2$C$_6$H$_3$)

Scheme 2.8 Reaction of [(^{t}Bu$_2$BDK^{iPr2})Fe(OEt$_2$)][BAr$^{F}_4$] (294) with ethyl diazoacetate

A number of other β-diketiminate complexes have also been shown to undergo similar reactions with other small, highly reactive molecules to give species featuring modified β-diimine ligands. For example, the imido-titanium(IV) complex (BDK^{iPr2})Ti(NC$_6$H$_3$-2,6-^{i}Pr$_2$)(η^1-OTf) (**296**) was shown to react with diphenylketene, affording a five-coordinate complex (**297**) of a tridentate N,N,O alkoxo-β-diimine ligand (**scheme 2.9**).[304] Similar reactivity of analogous titanium alkylidene complexes has also been reported, giving dimeric complexes with identical tripodal ligand architectures.[305]

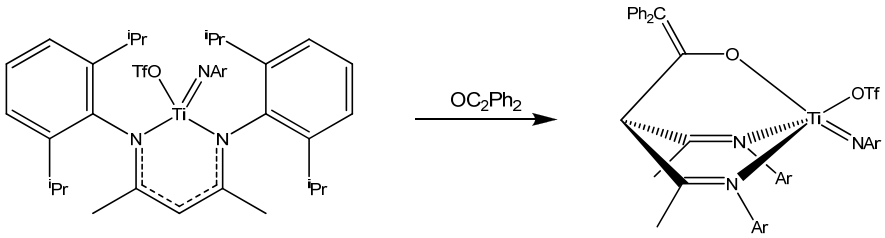

296 **297** (Ar = 2,6-^{i}Pr$_2$C$_6$H$_3$)

Scheme 2.9 Reaction of (BDK^{iPr2})Ti(NC$_6$H$_3$-2,6-^{i}Pr$_2$)(η^1-OTf) (296) with diphenylketene

Nixon *et al.* have demonstrated that the platinum(IV) complex (BDK^{Cl})PtH$_2$(SiPh$_3$) (**298**, HBDK^{Cl} = 2-(4-chloro)phenylamino-4-(4-chloro)phenyliminopent-2-ene) undergoes reaction with phosphaalkynes to give the corresponding six-coordinate complexes (**299**), which contain phosphaalkenyl-β-diimine ligands (**scheme 2.10**). The phosphorus atoms in **299** are nucleophilic and can be protonated or methylated to give the related cationic complexes.[306]

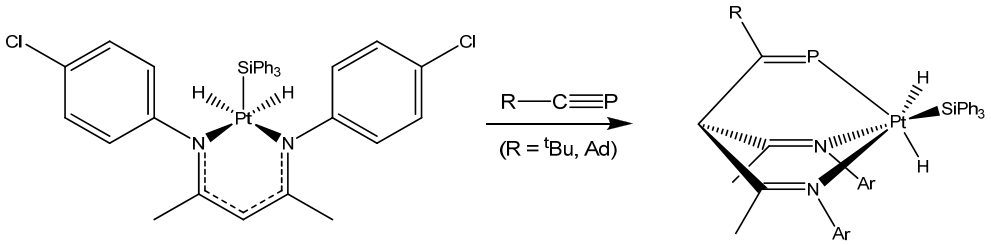

298 **299** (Ar = 4-ClC$_6$H$_4$; R = ^{t}Bu, Ad)

Scheme 2.10 Reaction of (BDK^{Cl})PtH$_2$(SiPh$_3$) (298) with phosphaalkynes

In a similar fashion, the complex [(BDK^{Me2})Ru(η^6-C$_6$H$_6$)][OTf] (**300**) has been shown to react with ethylene and acetylene to give the corresponding alkyl (**301**) and alkenyl (**302**) complexes respectively (**scheme 2.11**). Although in both cases the products were sufficiently stable to be crystallographically characterised, the insertion reactions were found to be reversible. In the case of **301**, the starting materials are regenerated at temperatures above 50°C, whereas **302** loses acetylene over a period of one day at room temperature under an N_2 atmosphere.[307] Similar insertion of ethylene has been observed for an aluminium β-diketiminate complex, though the products were characterised in solution only.[308]

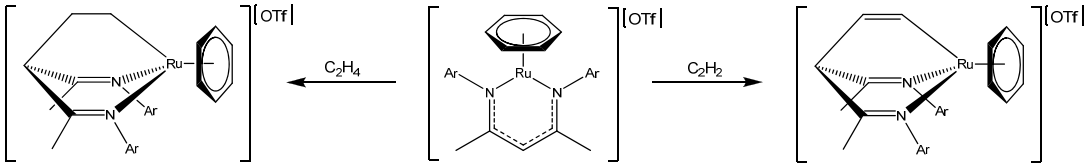

301 (Ar = 2,6-Me$_2$C$_6$H$_3$) **300** (R = 2,6-Me$_2$C$_6$H$_3$) **302** (Ar = 2,6-Me$_2$C$_6$H$_3$)

Scheme 2.11 Reaction of [(BDK^{Me2})Ru(η^6-C$_6$H$_6$)][OTf] (300) with ethylene and acetylene

Goto and colleagues have reported that an iron(II) complex (**303**) of the neutral 2,4-bis(2-pyridylmethylimino)pentane ligand undergoes an insertion reaction of acetonitrile upon treatment with triethylamine (**scheme 2.12**). The product of this reaction was found to be an octahedral iron(II) complex (**304**) which contains a novel ligand based on a β-triimine framework. By employing nitrile solvents other than acetonitrile, it has also been shown that this reaction allows for the incorporation of substituents other than methyl on the imino-carbon arising from insertion of the solvent molecule.[309]

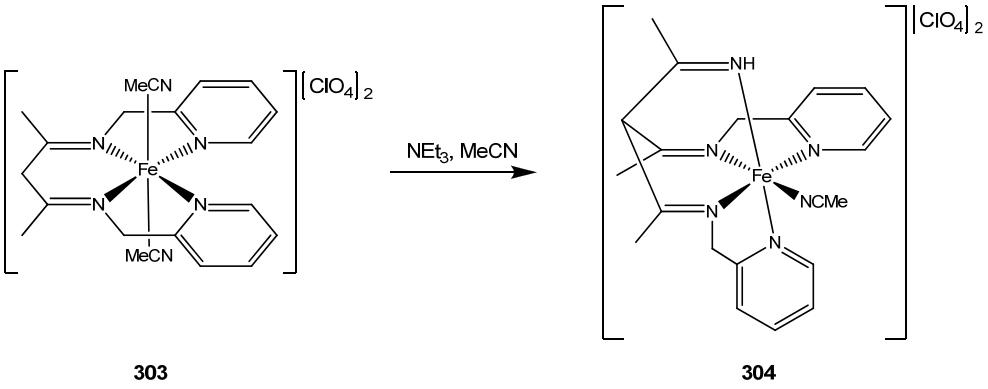

Scheme 2.12 Formation of complex 304

2.1.3 Other Ligands Based on a β-Triimine Framework

In relation to the work of Goto *et al.*, it had already been shown a number of years previously by Busch and colleagues that iron complexes of macrocyclic ligands which contain two β-iminoenamine moieties, such as **305**, undergo an analogous double insertion reaction with acetonitrile (**scheme 2.13**). In this case, the products are 'clathrochelate' complexes (**306**), based on a bis(β-triimine) ligand architecture.[310] Mono-insertion of acetonitrile has also been observed for cobalt(II) complexes of related dianionic ligands,[311] as well as with organometallic group 6 complexes of neutral macrocycles.[312]

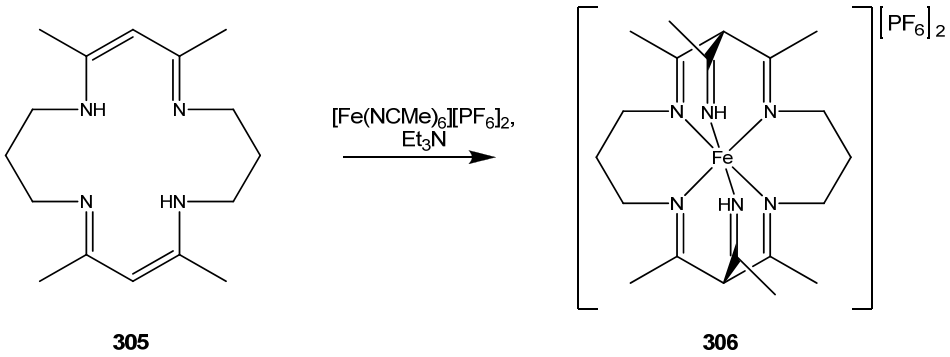

Scheme 2.13 Formation of clathrochelate complex 306

The trialdimines (or 'vinamidines'), prepared by Knorr *et al.*,[313] could also be expected to display a β-triimine structural motif upon coordination to a metal centre. However, such tridentate coordination has never been reported, and the only known complexes of these ligands are tetrahedral, homoleptic nickel(II) complexes such as **307**. In these complexes, the trialdimine ligands are bound bidentately in their anionic, β-dialdiminate form, with an additional pendant, uncoordinated imine group. If, unlike in **307**, the arylimino substituents are not all equivalent, the fluxional coordinating behaviour of these ligands can be observed by ^{1}H NMR spectroscopy.[314]

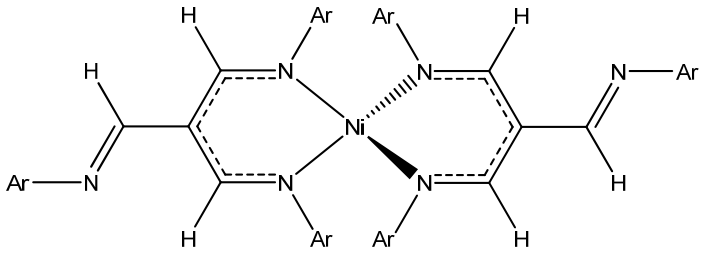

307 (Ar = 4-MeC$_6$H$_4$)

Figure 2.4 Structure of nickel(II) derivative of β-trialdimine ligand (307)

The β-trialdimines are the closest literature precedent to the subject of this current work, the β-triketimines. However, unlike the β-trialdimines, the new ligands presented here coordinate reliably in the neutral, tridentate form to a variety of metal centres, which shall now be discussed in this and the following chapters.

2.2 Results and Discussion

2.2.1 Synthesis and Characterisation of β-Triketimines

The β-triketimine ligands were synthesised in a modular fashion, through the addition of imidoyl chlorides to lithium β-diketiminates. The precursor β-iminoenamines (**HBDK^{x}**) were prepared by means of acid-catalysed condensation of ring-substituted anilines, according to a literature procedure.[13] The reagents were heated to reflux in toluene in the presence of a catalytic amount of *p*-toluenesulfonic acid, and the water of condensation was removed by azeotropic distillation using a Dean-Stark apparatus (**scheme 2.14**). This process gave the products in low to moderate yields after recrystallisation from a methanol/DCM solvent mixture. The low cost of the precursor chemicals, the ease with which this reaction can be scaled up to >50 g quantities and the short reaction times make the moderate yields obtained with this method acceptable.

Table 2.1 Key to β-iminoenamines (HBDK^{x})

	R^1	R^2	R^3
HBDK^{iPr}	^{i}Pr	H	H
HBDK^{iPr2}	^{i}Pr	^{i}Pr	H
HBDK^{tBu}	^{t}Bu	H	H
HBDK^{Me3}	Me	Me	Me

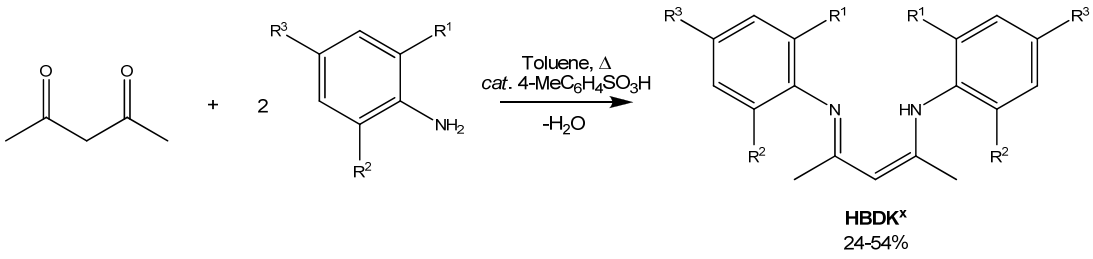

Scheme 2.14 Synthesis of β-iminoenamines (HBDK^{x})

The asymmetric β-iminoenamine **HBDK$^{iPr2/OMe}$** was prepared in moderate yield by means of a two-step literature procedure (**scheme 2.15**).[315]

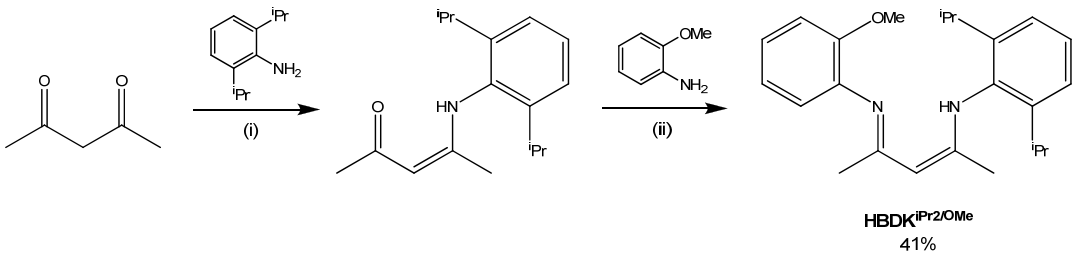

Scheme 2.15 Synthesis of HBDK$^{iPr2/OMe}$, conditions: (i) Toluene, Δ, *cat.* 4-MeC$_6$H$_4$SO$_3$H, -H$_2$O; (ii) Benzene, Δ, 1 equiv. 4-MeC$_6$H$_4$SO$_3$H, -H$_2$O

Imidoyl chlorides (**IMC$^{1-9}$**) were synthesised through the reaction of the corresponding amides (themselves obtained via the reaction of anilines with acid chlorides) with the appropriate chlorinating agent, either triphosgene or thionyl chloride (**scheme 2.16**). Where R^7 = ^{t}Bu or Ph, simply refluxing the amide in neat thionyl chloride produces the corresponding imidoyl chloride, whereas if R^7 = Me then the milder reaction conditions of refluxing in DCM with triphosgene are essential to inhibit self-condensation of the formed imidoyl chlorides. This side-reaction is due to the presence of aza-enolisable protons for imidoyl chlorides where R^7 = Me, and is inhibited somewhat by the presence of bulky, weakly electron-donating aryl *ortho*-substituents.[316] Therefore, whilst the introduction of strongly electron-releasing substituents such as OMe is possible where R^7 = ^{t}Bu or Ph, in the case of imidoyl chlorides derived from N-acetylanilines the chlorination conditions do not tolerate such substitution and dimerised products are obtained exclusively. All the imidoyl chlorides produced here were purified by vacuum distillation, and were isolated as viscous liquids, except in the case of **IMC^7** which is a solid.

Table 2.2 Key to imidoyl chlorides (IMC$^{1-9}$)

	R^4	R^5	R^6	R^7
IMC^1	^{i}Pr	H	H	Me
IMC^2	^{i}Pr	^{i}Pr	H	Me
IMC^3	^{t}Bu	H	H	Me
IMC^4	Me	Me	Me	Me
IMC^5	^{i}Pr	H	H	^{t}Bu
IMC^6	^{i}Pr	^{i}Pr	H	^{t}Bu
IMC^7	Me	Me	Me	^{t}Bu
IMC^8	OMe	H	H	^{t}Bu
IMC^9	^{i}Pr	H	H	Ph

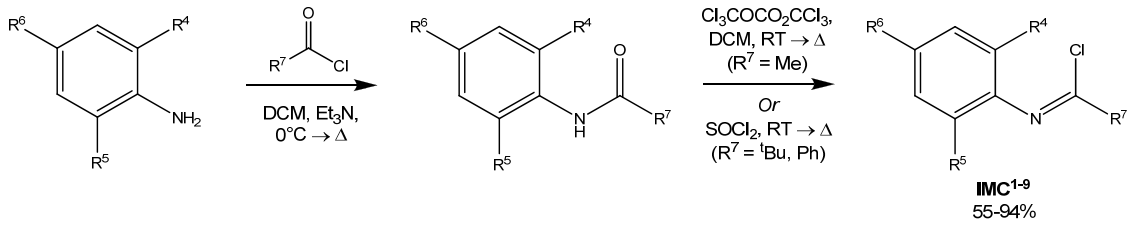

Scheme 2.16 Synthesis of imidoyl chlorides (IMC$^{1-9}$)

The β-triketimines **L$^{1-14}$** were then synthesised by the reaction of imidoyl chlorides with lithium β-diketiminates, formed *in situ* by the addition of *n*-butyllithium to a solution of the appropriate β-iminoenamine (**scheme 2.17**), giving the products in low to high yields after recrystallisation from methanol or methanol/DCM mixtures. The reaction proceeds with apparent high selectivity for C-C bond formation, as has been demonstrated previously for other electrophiles (see **section 2.1.2**), and does not appear to be affected by competing N-

imidoylation as observed by Knorr *et al.* in the synthesis of β-trialdimines.[313] This enhanced selectivity can very likely be attributed to the presence of bulky aryl *ortho*-substituents in the precursor β-diketiminates, and as such the formation of an amidine derivative arising from attack of the electrophile at one of the β-diketiminate nitrogen atoms is strongly disfavoured due to steric hindrance.

Table 2.3 Key to β-triketimines (L^{1-14})

	R^1	R^2	R^3	R^4	R^5	R^6	R^7
L^1	^{i}Pr	H	H	^{i}Pr	H	H	Me
L^2	^{i}Pr	^{i}Pr	H	^{i}Pr	^{i}Pr	H	Me
L^3	^{i}Pr	H	H	^{t}Bu	H	H	Me
L^4	^{t}Bu	H	H	^{i}Pr	^{i}Pr	H	Me
L^5	^{i}Pr	H	H	^{i}Pr	^{i}Pr	H	Me
L^6	^{i}Pr	^{i}Pr	H	^{i}Pr	H	H	Me
L^7	Me	Me	Me	Me	Me	Me	Me
L^8	^{i}Pr	H	H	OMe	H	H	^{t}Bu
L^9	^{t}Bu	H	H	OMe	H	H	^{t}Bu
L^{10}	^{i}Pr	H	H	^{i}Pr	H	H	^{t}Bu
L^{11}	^{i}Pr	H	H	^{i}Pr	^{i}Pr	H	^{t}Bu
L^{12}	^{i}Pr	H	H	Me	Me	Me	^{t}Bu
L^{13}	^{i}Pr	H	H	^{i}Pr	H	H	Ph
L^{14}	^{t}Bu	H	H	^{i}Pr	H	H	Ph

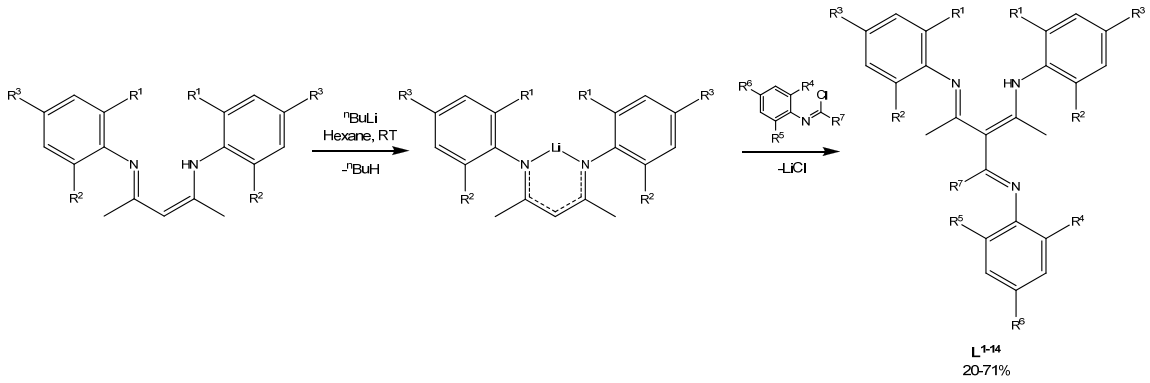

Scheme 2.17 Synthesis of β-triketimines L^{1-14}

β-triketimines **L^{15}** and **L^{16}** were prepared in an analogous fashion, through the reaction of the asymmetric lithium β-diketiminate derived from **HBDK$^{iPr2/OMe}$** with **IMC^2** and **IMC^8** respectively (**scheme 2.18**).

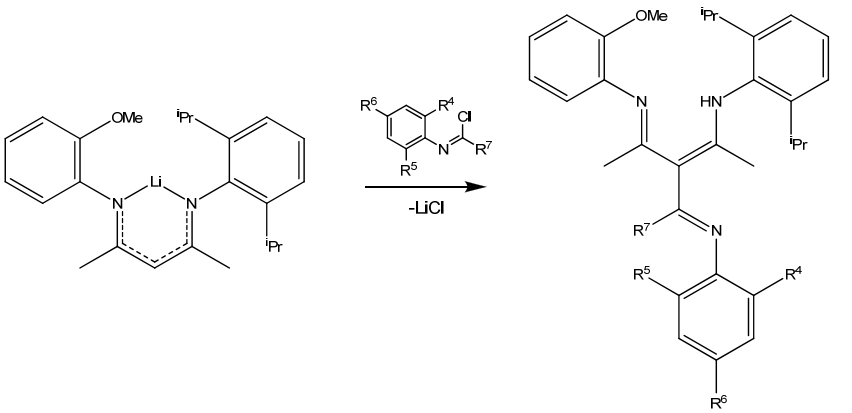

Scheme 2.18 Synthesis of L^{15} and L^{16}

In **schemes 2.17** and **2.18**, the β-triketimines are depicted structurally as their enamine-diimine tautomers, which are stabilised by the presence of a planar, N-H-N hydrogen-bonded six-membered ring, in analogous fashion to their precursor β-iminoenamines. However, the actual identity of the isomers present in both solution and the solid state is highly dependent on the nature of the R substituents. For $\mathbf{L^{1\text{-}7}}$ and $\mathbf{L^{15}}$ (R^7 = Me), a number of isomeric species are observed in solution, representing the interconversion between the enamine-diimine and β-triketimine tautomers. This situation is complicated further due to the potential for *E*/*Z* isomerism at the C=N bond of the pendant arylimino moiety, as well as the fact that in cases where the aryl substituents are not all identical, two different isomeric arrangements in the enamine-diimine tautomer are also possible. This gives rise to a total of five possible isomeric species in solution: the β-triketimine tautomer (**A**); and the four possible forms of the enamine-diimine tautomer (**B-D**) (**figure 2.5**). For simplicity not all interconversion pathways between one isomer and another are shown, in theory any of **A**-**E** may potentially isomerise to any of the other forms. In the case of $\mathbf{L^1}$, $\mathbf{L^2}$ and $\mathbf{L^7}$, only three possible isomers exist, as **B**/**D** and **C**/**E** are identical due to the symmetrical nature of the aryl substituents. This is illustrated by the ^{1}H NMR spectrum of $\mathbf{L^1}$ (**figure 2.6**), which shows evidence for the presence of one major and two minor isomeric species in solution. The major component is the *E*-isomer of the enamine-diimine tautomer (**B**), while the minor components are the corresponding *Z*-isomer (**C**) and the β-triketimine tautomer (**A**). Although the β-triketimine is only a minor isomer in solution, its presence in the spectrum is conspicuous due to a pair of isopropyl CH_3 doublets at 0.93 and 0.96 ppm, which are related to the methyl singlet (1.69 ppm), isopropyl CH septet (2.70 ppm) and α-CH singlet (4.59 ppm) resonances in a ratio of 18:9:3:1 respectively.

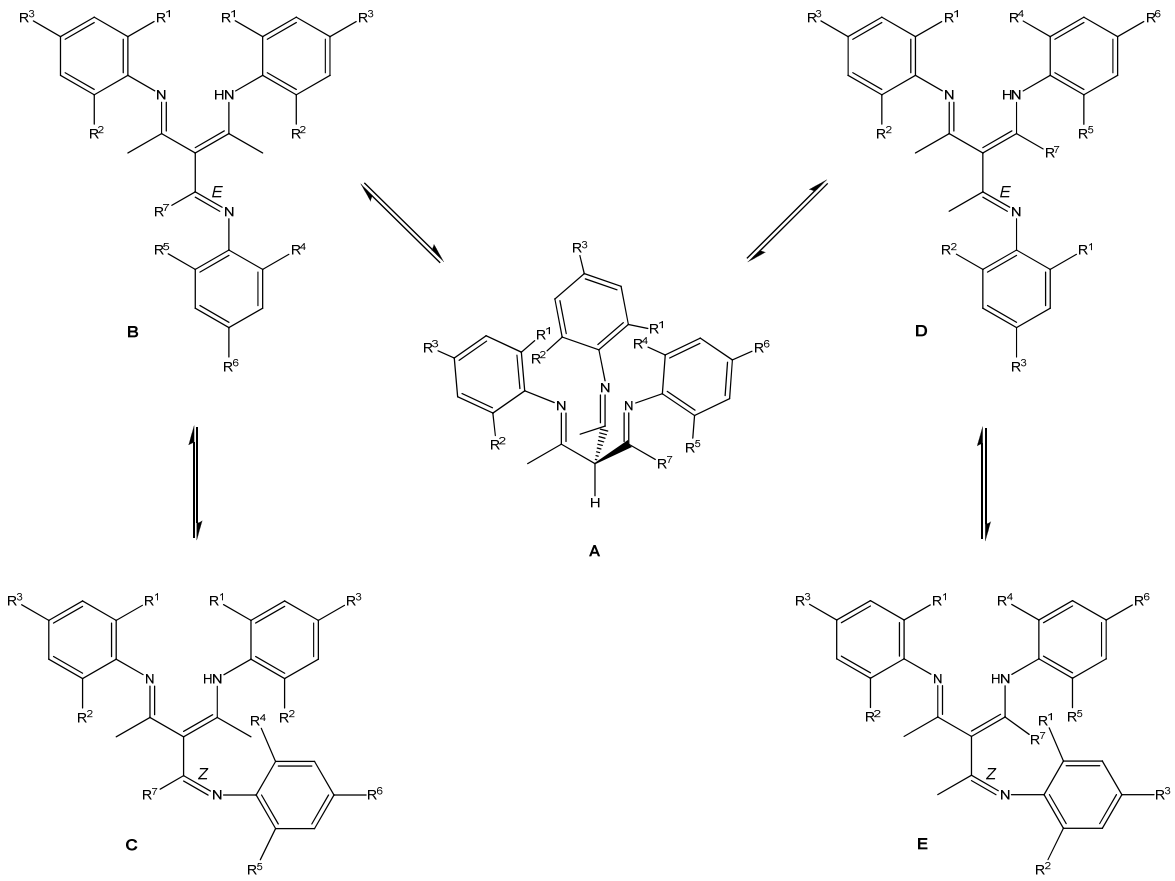

Figure 2.5 Solution-phase isomerism of L^{1-7} and L^{15}

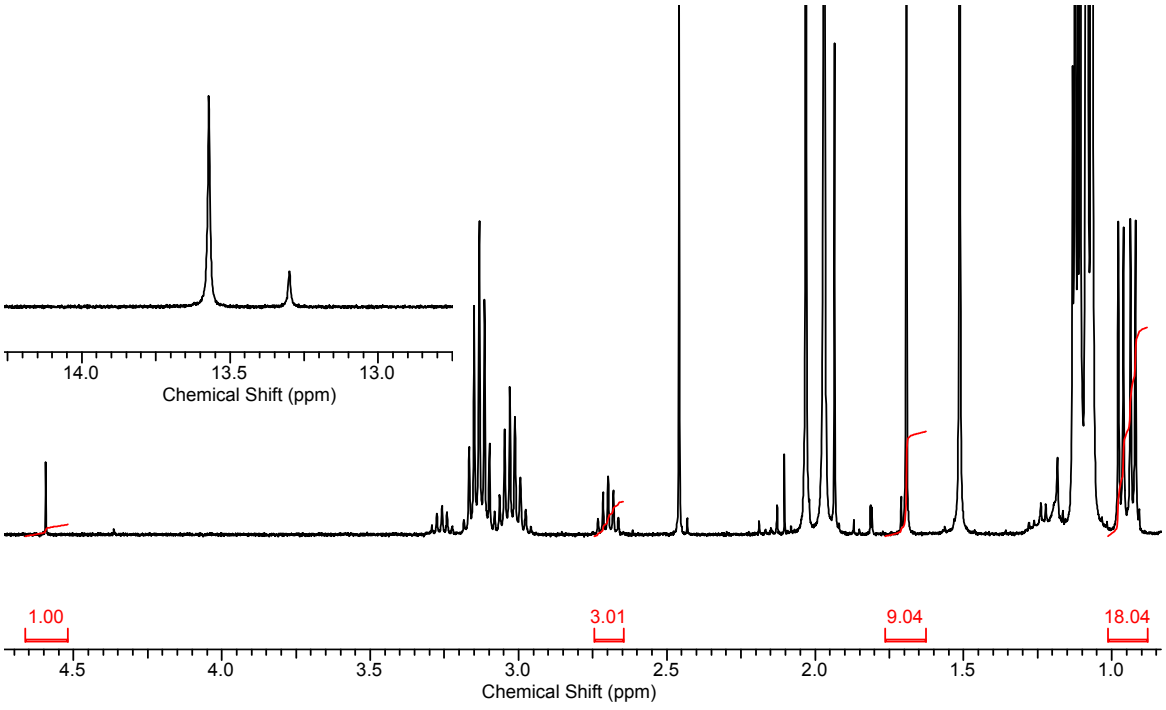

Figure 2.6 ^{1}H NMR spectrum of L^{1} in $CDCl_3$, aryl region not shown; illustrated integrals are for peaks due to β-triketimine tautomer, peak at 1.51 ppm (H_2O) is due to solvent contaminant

The α-CH resonance at 4.59 ppm is unequivocally attributable to the β-triketimine tautomer, its deshielded nature being typical of a methine proton adjacent to three strongly electron-withdrawing groups. Additionally, its chemical shift is rather close to the value of 5.24 ppm, which was reported for the α-CH proton in the α-trimethylacetyl β-diimine prepared by Lappert *et al.* (**section 2.1.2**). The splitting of the isopropyl CH_3 resonances into a pair of doublets, where normally only a single doublet would be expected to be observed, is due to the fact that in the β-triketimine tautomer, the two isopropyl methyl groups are stereochemically distinct. Despite the seemingly C_{3v} symmetric nature of this tautomer, there is an absence of molecular planes of symmetry in any accessible conformation able to bisect the two methyl groups, and as a result they are anisochronous. The peaks in the aryl region are heavily overlapped, and it is not possible to identify all the resonances attributable each of the tautomers, therefore this part of the spectrum shall not be discussed further. The remainder of the peaks can be assigned to the *E*- and *Z*-isomers (**B** and **C**) of the enamine-diimine tautomer, with the presence of two characteristic hydrogen-bonded NH resonances appearing at 13.30 ppm and 13.57 ppm being indicative of the existence of these two isomers. The major component (~70%) in solution is identified as the *E*-isomer, due to the energetic unfavourability of the *Z*-isomer which would render adjacent the two most bulky substituents about the C=N bond. This assumption is supported by the crystal structure of $\mathbf{L^1}$ (**figure 2.7**), which indeed does show that isomer **B** is present exclusively, and it is highly likely that the isomeric form adopted in the solid state will be representative of the predominant isomer in solution.

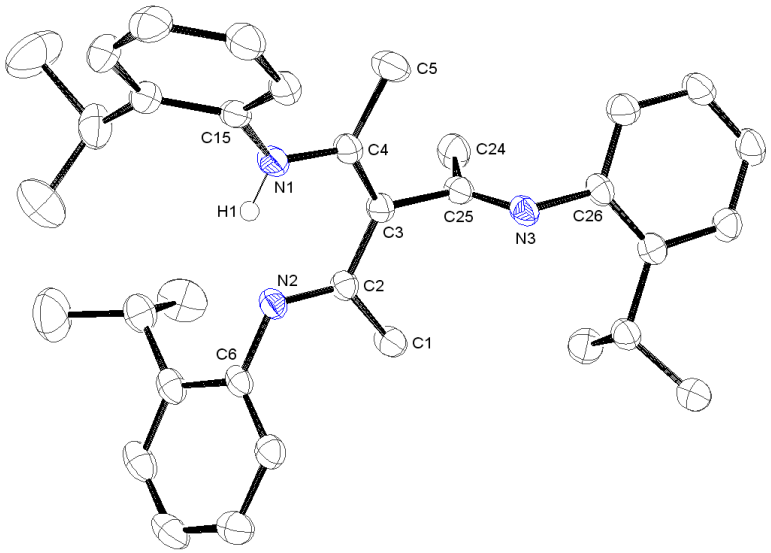

Figure 2.7 ORTEP representation of the molecular structure of L^1 with thermal ellipsoids set at the 50% probability level; enamine hydrogen shown, all others omitted for clarity

Table 2.4 Selected bond lengths (Å), angles (°) and interplanar torsion angles (°) for L^1, L^{10} and L^{11}

L^1	L^{10}	L^{11}
N(1)-C(4) 1.358(2)	N(1)-C(2) 1.326(2)	N(1)-C(10) 1.272(3)
N(2)-C(2) 1.3047(19)	N(2)-C(4) 1.326(2)	N(2)-C(25) 1.276(4)
N(3)-C(25) 1.277(2)	N(3)-C(25) 1.286(2)	N(3)-C(39) 1.274(4)
N(1)-C(13) 1.417(2)	N(1)-C(15) 1.429(3)	N(1)-C(1) 1.432(4)
N(2)-C(6) 1.4156(19)	N(2)-C(6) 1.426(2)	N(2)-C(13) 1.425(4)
N(3)-C(26) 1.4270(19)	N(3)-C(26) 1.417(2)	N(3)-C(30) 1.427(4)
C(1)-C(2) 1.507(2)	C(1)-C(2) 1.506(3)	C(10)-C(11) 1.504(4)
C(2)-C(3) 1.450(2)	C(2)-C(3) 1.416(3)	C(10)-C(12) 1.526(4)
C(3)-C(4) 1.379(2)	C(3)-C(4) 1.425(3)	C(12)-C(39) 1.520(4)
C(4)-C(5) 1.509 (2)	C(4)-C(5) 1.503(3)	C(12)-C(25) 1.536(4)
C(3)-C(25) 1.512(2)	C(3)-C(25) 1.509(3)	C(25)-C(26) 1.557(4)
C(24)-C(25) 1.508(2)	C(24)-C(25) 1.551(3)	C(39)-C(40) 1.506(4)
C(2)-N(2)-C(6) 121.34(13)	C(2)-N(1)-C(15) 123.89(17)	C(1)-N(1)-C(10) 119.8(2)
C(4)-N(1)-C(15) 127.59(14)	C(4)-N(2)-C(6) 122.92(17)	C(13)-N(2)-C(25) 129.2(2)
C(25)-N(3)-C(26) 121.95(13)	C(25)-N(3)-C(26) 123.04(16)	C(30)-N(3)-C(39) 120.5(2)
C(1)-C(2)-N(2) 122.36(13)	C(1)-C(2)-N(1) 117.97(17)	N(1)-C(10)-C(11) 126.6(2)
C(5)-C(4)-N(1) 118.27(14)	C(5)-C(4)-N(2) 119.16(16)	N(2)-C(25)-C(26) 128.3(2)
C(24)-C(25)-N(3) 125.35(14)	C(24)-C(25)-N(3) 114.24(16)	N(3)-C(39)-C(40) 126.5(3)
N(2)-C(2)-C(3) 120.24(14)	N(1)-C(2)-C(3) 121.40(17)	N(1)-C(10)-C(12) 117.7(2)
N(1)-C(4)-C(3) 120.57(14)	N(2)-C(4)-C(3) 120.56(16)	N(2)-C(25)-C(12) 114.4(2)
N(3)-C(25)-C(3) 117.44(14)	N(3)-C(25)-C(3) 123.89(16)	N(3)-C(39)-C(12) 118.6(2)
C(1)-C(2)-C(3) 117.39(13)	C(1)-C(2)-C(3) 120.55(16)	C(11)-C(10)-C(12) 115.6(2)
C(3)-C(4)-C(5) 121.13(14)	C(3)-C(4)-C(5) 120.28(16)	C(12)-C(25)-C(26) 117.2(2)
C(3)-C(25)-C(24) 117.21(14)	C(3)-C(25)-C(24) 121.78(16)	C(12)-C(39)-C(40) 114.8(2)
C(2)-C(3)-C(4) 123.90(14)	C(2)-C(3)-C(4) 122.71(16)	C(10)-C(12)-C(25) 111.2(2)
C(2)-C(3)-C(25) 118.09(13)	C(2)-C(3)-C(25) 118.54(16)	C(10)-C(12)-C(39) 109.0(2)
C(4)-C(3)-C(25) 117.92(13)	C(4)-C(3)-C(25) 118.54(16)	C(25)-C(12)-C(39) 112.7(2)
θ_T (C(1)-C(2)-N(2)-C(3)/C(6)$_{Ar}$) = 69.09(13)	θ_T (C(1)-C(2)-N(2)-C(3)/C(15)$_{Ar}$) = 76.78(17)	θ_T (C(10)-C(11)-N(1)-C(12)/C(1)$_{Ar}$) = 71.2(2)
θ_T (C(3)-C(4)-N(1)-C(5)/C(15)$_{Ar}$) = 53.15(14)	θ_T (C(3)-C(4)-N(1)-C(5)/C(6)$_{Ar}$) = 76.59(17)	θ_T (C(12)-C(25)-N(2)-C(26)/C(13)$_{Ar}$) = 89.8(2)
θ_T (C(24)-C(25)-N(3)-C(3)/C(26)$_{Ar}$) = 69.32(13)	θ_T (C(24)-C(25)-N(3)-C(3)/C(26)$_{Ar}$) = 53.11(16)	θ_T (C(12)-C(39)-N(3)-C(40)/C(30)$_{Ar}$) = 75.3(3)

The *Z*-isomer and the β-triketimine tautomer are present in solution in approximately equal quantities, ca. 15% each. Through inspection of the molecular structure of **L^1** it is obvious that the *E*-isomer is preferred in order to avoid a steric clash of the 2-isopropylphenyl group of the pendant imine arm with the atoms of the central, planar enamine-imine moiety, namely C(2), C(3) and C(4). Additionally, the 2-isopropylphenyl groups of the enamine-imine component are arranged in a *syn*-conformation, and are also oriented in the opposite direction to the pendant arylimino function, so as to further minimise unfavourable steric interactions. The bond lengths (**table 2.4**) within the hydrogen-bonded enamine-imine ring are characteristic of the alternating single and double bonds of a conjugated system, a situation which is analogous with that observed for the precursor β-iminoenamine.[294] The pendant imine is approximately orthogonal to the plane defined by the enamine-imine moiety, and the C=N bond distance (1.277(2) Å) is indicative of minimal conjugation. It is also useful here to define a further structural parameter, the torsion angle (θ_T) between the plane defined by a particular C=N bond and the plane of its aryl substituent (**table 2.4**), as this can give an indication of the magnitude of steric

encumbrance imparted by the substituent groups in both the free ligands, and their derived complexes. For example, the torsion angle between the pendant imine plane C(24)-C(25)-N(3)-C(3) and the C(26) aryl plane is 69.32(13)°, showing that a substantial degree of deviation from co-planarity is necessary in order to minimise steric repulsion.

In all cases where R^7 = Me, and at least one of the aryl substituents is not 2,6-disubstituted (i.e. $\mathbf{L^1}$, $\mathbf{L^{3\text{-}6}}$ and $\mathbf{L^{15}}$), equilibration in solution is seemingly very rapid and no change in the nature of the observed spectra occurs over time. However, in the case of $\mathbf{L^2}$, where each imine moiety bears a 2,6-diisopropylphenyl substituent, this process is very slow. A ^{1}H NMR spectrum of $\mathbf{L^2}$ recorded immediately after dissolution (**figure 2.8**) shows that the β-triketimine tautomer is overwhelmingly dominant, inferred by the appearance of the characteristic α-CH resonance at 4.74 ppm. The amount of enamine-diimine tautomer present is negligible, though the NH resonance and the signal due to one of the isopropyl CH protons related to this isomer are clearly visible at 13.51 and 3.08 ppm respectively.

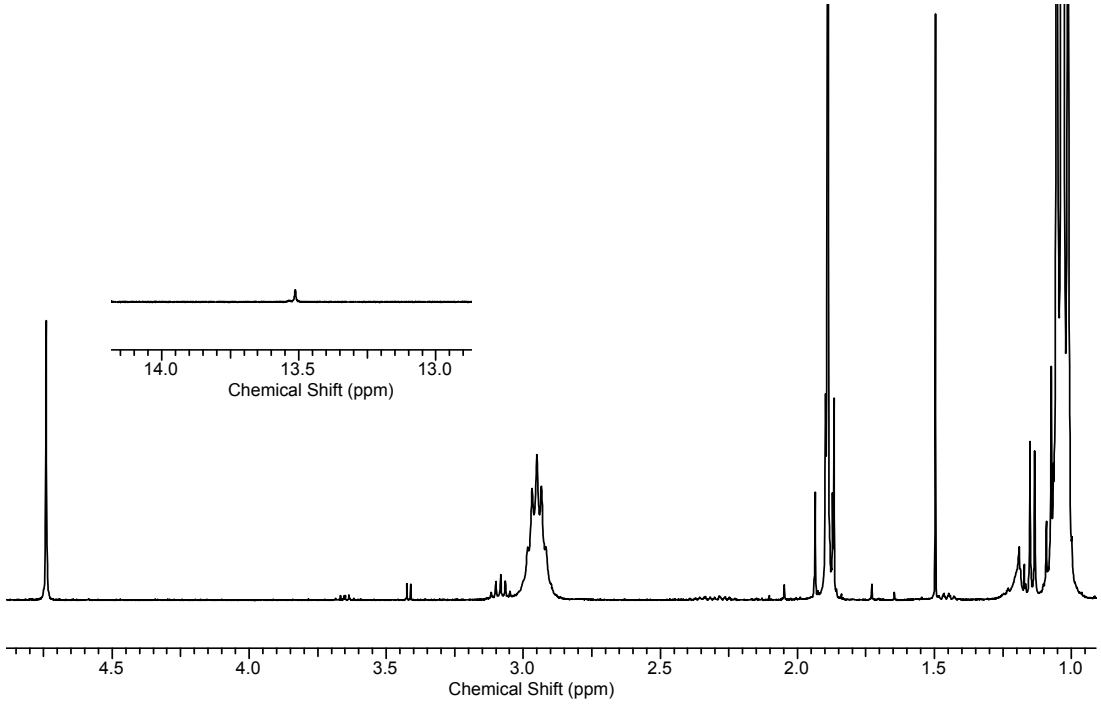

Figure 2.8 ^{1}H NMR spectrum of L^2 in $CDCl_3$ recorded immediately after dissolution, aryl region not shown; peaks at 1.49 ppm (H_2O) and 3.42 ppm (MeOH) are due to solvent contaminants

The sample was then allowed to stand at room temperature for a period of approximately 72 hours, after which time the ^{1}H NMR spectrum was recorded again (**figure 2.9**). The relative intensities of the peaks due to the enamine-diimine tautomer were found to have increased, showing that the sample was now composed of an approximately 1:1 mixture of this isomer and the β-triketimine tautomer. Subsequent re-recording of the spectrum after

an additional period of 24 hours showed that no further changes occurred. This behaviour is likely a consequence of the rate-determining step of the mechanism of 1,3-sigmatropic rearrangement requiring at least one of the aryl groups to be co-planar with its attached imine moiety. This arrangement will be extremely disfavoured sterically, and as such the process is very slow. Even in cases where not all of the aryl groups are 2,6-disubstituted, such an arrangement is still likely to be energetically unfavourable, though somewhat more feasible. Similar considerations also explain why in the case of $\mathbf{L^2}$ only the *E*-isomer of the enamine-diimine is observed in solution; the *Z*-isomer is very unlikely to occur due to the steric repulsion which would result between the 2,6-diisopropylphenyl group and the rest of the molecule. The solution-phase behaviour of the all-mesityl substituted $\mathbf{L^7}$ is similar, though in contrast to $\mathbf{L^2}$ the major component in solution immediately after dissolution was found to be the enamine-diimine tautomer, with the relative amount of the β-triketimine increasing over time. This reversal of equilibration is likely due to the reduced steric bulk of $\mathbf{L^7}$ in comparison to $\mathbf{L^2}$.

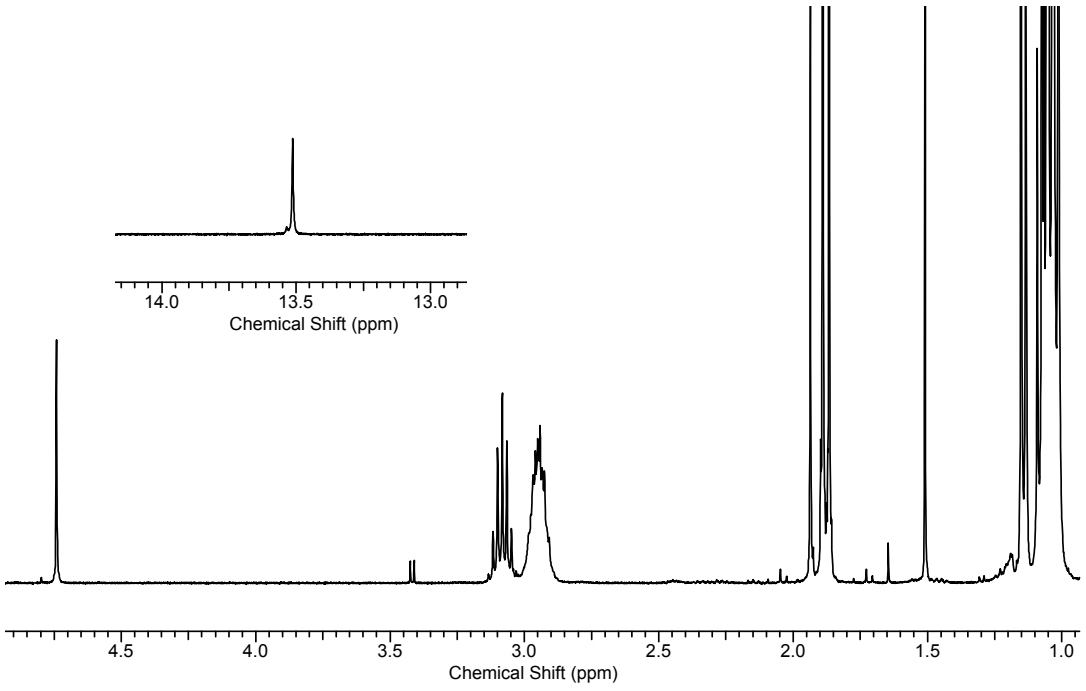

Figure 2.9 ^{1}H NMR spectrum of L^2 in $CDCl_3$ recorded 72 hours after dissolution, aryl region not shown; peaks at 1.49 ppm (H_2O) and 3.42 ppm (MeOH) are due to solvent contaminants

For $\mathbf{L^{3\text{-}6}}$ and $\mathbf{L^{15}}$, all five isomeric forms may be present in solution, due to the fact that the aryl substituents are no longer identical. However, some of these may be present in very small quantities, or absent completely. For example, in the case of $\mathbf{L^3}$ isomer **D** is the dominant form in solution (~70%), while the remainder is composed of approximately equal quantities of isomers **A**, **D** and **E**; isomer **C** is not observed. In all cases the most

abundant isomer in solution is that in which the imine group bearing the least bulky aryl substituent occupies the pendant position, while the more heavily substituted aryl groups are part of the planar conjugated system. This is illustrated by the situation observed for $\mathbf{L}^{15}$, where only isomers **D** and **E** are present, due to the sterically favourable nature of having the small 2-methoxyphenyl substituent occupy the pendant position.

In those examples where R^7 = ^{t}Bu or Ph ($\mathbf{L}^{8\text{-}14}$ and $\mathbf{L}^{16}$), a single isomer is observed in solution. Where the arylimino moiety derived from the imidoyl chloride is 2-substituted only (i.e. R^5 = H), isomer **C** is adopted exclusively in solution. For example, the ^{1}H NMR spectrum of $\mathbf{L}^{10}$ (**figure 2.10**) has only one NH signal 13.49 ppm, and shows no evidence of an α-CH resonance characteristic to the β-triketimine tautomer in the region of 4.50-5.00 ppm. Additionally, all of the peaks can easily be assigned to a single isomer.

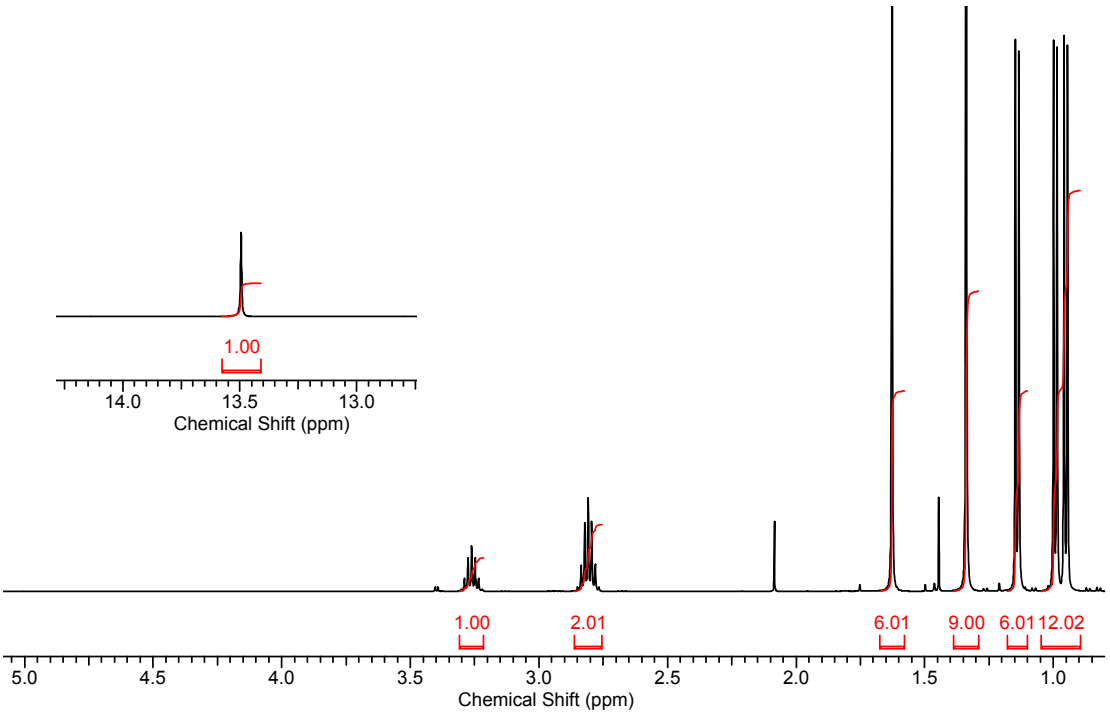

Figure 2.10 ^{1}H NMR spectrum of L^{10} in $CDCl_3$, aryl region not shown; peaks at 1.45 ppm (H_2O) and 2.09 ppm (acetone) are due to solvent contaminants

The *Z*-geometry about the pendant imine bond is now favoured so as to minimise unfavourable steric interactions between the aryl group and the backbone R^7 substituent. This preference for the *Z*-isomer is inferred through inspection of the solid-state structure of $\mathbf{L}^{10}$ (**figure 2.11**), and it can be seen that if the molecule were to adopt the *E*-geometry, the *tert*-butyl group would be forced into a severe steric clash with the planar enamine-imine moiety. Interestingly, the steric influence of the *tert*-butyl group is so great that the

2-isopropylphenyl substituents of the enamine-imine component are forced to point in the same direction as that of the pendant imine arm, rather than the opposite arrangement as observed in the molecular structure of $\mathbf{L}^1$. Likewise, in contrast to $\mathbf{L}^1$ where the conjugated nature of the enamine-imine moiety is evident from the bond distances, the C(2)-C(3) and C(3)-C(4) bond lengths (**table 2.4**) are both close to 1.42 Å, which is the arithmetic mean of the corresponding distances in $\mathbf{L}^1$. Additionally, the N(1)-C(2) and N(2)-C(4) bond lengths are indistinguishable, and as such this situation was modelled as a two-site disorder in the NH hydrogen position, with an implicit disorder in the positioning of the single and double bonds across the enamine-imine. Through examination of the values of θ_T for $\mathbf{L}^{10}$ (**table 2.4**), it can be seen that the 2-isopropylphenyl substituents of the enamine-imine moiety are forced further towards orthogonality than is the case in $\mathbf{L}^1$, while the pendant aryl group has actually moved further towards co-planarity with the imine. This latter effect is likely a consequence of the need to minimise steric interactions between the pendant aryl and both the *tert*-butyl substituent, and the other 2-isopropylphenyl groups.

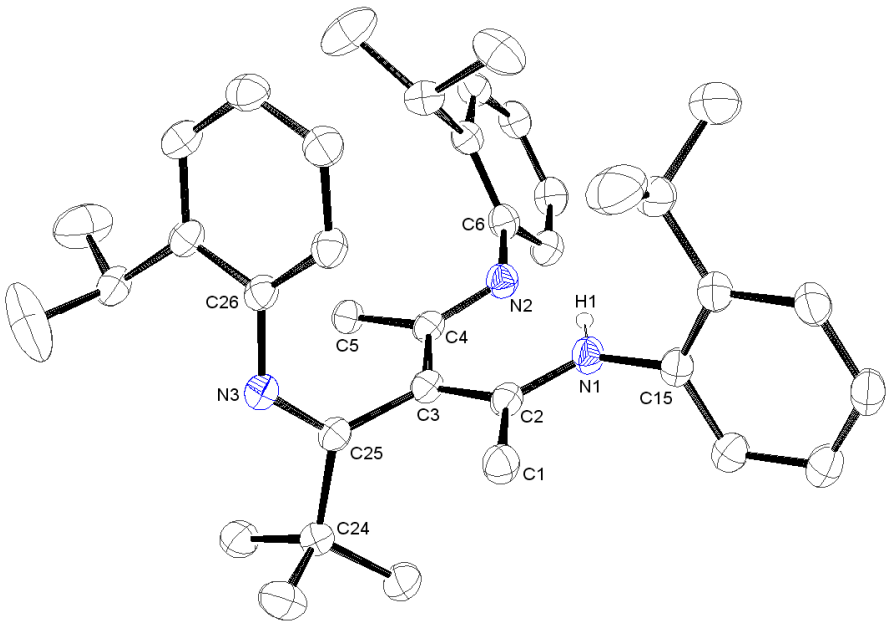

Figure 2.11 ORTEP representation of the molecular structure of L^{10} with thermal ellipsoids set at the 30% probability level; enamine hydrogen shown, all others omitted for clarity

In the case of $\mathbf{L^{11}}$ and $\mathbf{L^{12}}$ ($R^7 = {}^tBu$, $R^4 = R^5 \neq H$), the true β-triketimine tautomer is observed exclusively in solution, as evidenced by the appearance of the α-CH singlet at 4.80-4.90 ppm, and the absence of any NH peak across the range 13.00-15.00 ppm (**figure 2.12**). The adoption of the β-triketimine tautomer in solution is analogous to the previously observed behaviour of similarly bulky β-diimines.[317]

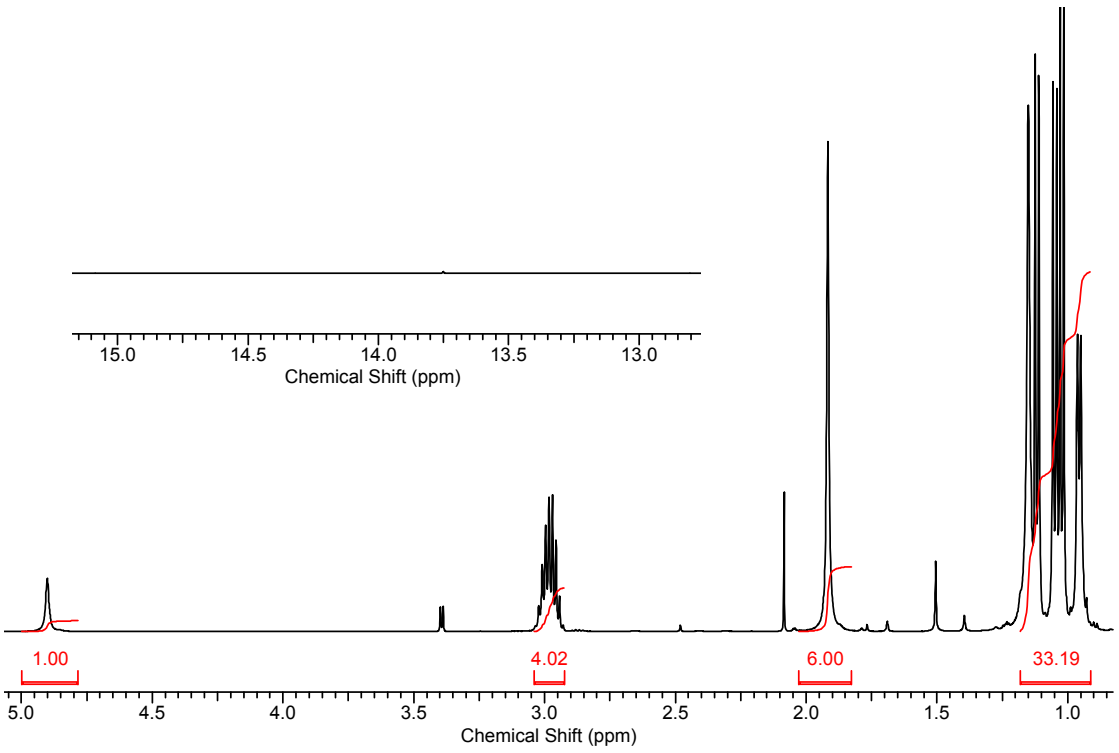

Figure 2.12 ^{1}H NMR spectrum of L^{11} in $CDCl_3$, aryl region not shown; peaks at 1.51 ppm (H_2O), 2.08 ppm (acetone) and 3.39 ppm (MeOH) are due to solvent contaminants

The solid-state structure of $\mathbf{L^{11}}$ (**figure 2.13**) shows that the 2,6-diisopropylphenyl substituted imine group adopts the *Z*-geometry, though it should be noted that due to the alternate position of the tautomerising hydrogen in the true β-triketimine, the priorities for assignment of stereochemistry at the imine bond are reversed in comparison to $\mathbf{L^1}$ and $\mathbf{L^{10}}$. As such, the arrangement is actually the same as that observed for the pendant arylimino moiety in $\mathbf{L^1}$. However, in this case the enforced orthogonality of the 2,6-diisopropylphenyl group with respect to the imine plane (θ_T = 89.8(2)°) precludes the formation of the enamine-diimine tautomer, due to the unfavourable steric repulsion which would result from its interaction with the central carbon atom C(12). Additionally, the steric clash of the 2,6-diisopropyphenyl moiety with the *tert*-butyl group forces it towards C(12) also, and the adoption of the β-triketimine tautomer serves so as to minimise all of the aforementioned unfavourable steric interactions. The presence of one less isopropyl

group on the pendant arylimino arm in $\mathbf{L}^{10}$ means that it is able to twist away from orthogonality, moving the 2-isopropyl substituent away from the central carbon atom and thus allowing the molecule to adopt the enamine-diimine tautomer. This is not possible in the case of $\mathbf{L}^{11}$, as the combination of *tert*-butyl and 2,6-diisopropylphenyl substitution at the same imine group forces strict orthogonality of the aryl group. The C=N bond lengths for $\mathbf{L}^{11}$ all lie in the range 1.272-1.276 Å (**table 2.4**), as would be expected when there is minimal conjugation, and the 2-isopropylphenyl substituted imines adopt the more energetically favourable *E*-geometry.

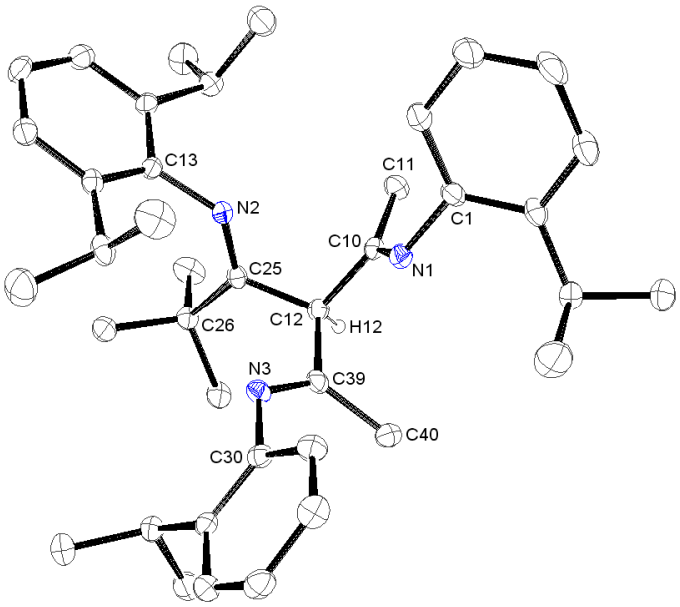

Figure 2.13 ORTEP representation of the molecular structure of L^{11} with thermal ellipsoids set at the 30% probability level; hydrogen atom of α-carbon shown, all others omitted for clarity

2.2.2 Synthesis and Characterisation of β-Triketimine Group 6 Metal Carbonyl Complexes

Reaction of β-triketimines with $M(CO)_6$ (M = Cr, Mo, W) in refluxing dibutyl ether with a catalytic amount of THF gave the corresponding octahedral **(L)M(CO)$_3$** adducts (**scheme 2.19**). The relative abundance of the different tautomers in solution appears to have little effect on the speed of the reaction, and in concurrence with previous observations the reactions proceeded most rapidly in the case of molybdenum (Cr < Mo >> W).[318] For **(L^1)W(CO)$_3$**, yields in excess of 30% could not be achieved, even when trimethylamine *N*-oxide was employed as a CO scavenger. Therefore, the preparation of $W(CO)_3$ derivatives of β-triketimines other than **L^1** was not attempted. The **(L)M(CO)$_3$** complexes are bright red or crimson (Cr), orange or bright-red (Mo) and dark-crimson (W) in colour, except in the case of **(L^{13})Cr(CO)$_3$** and **(L^{13})Mo(CO)$_3$** which appear black and very dark purple respectively. The UV/Vis spectra of **(L)M(CO)$_3$** all feature two MLCT absorptions in the visible region, usually at around 470 and 550 nm (Cr), or 450 and 510 nm (Mo). However when the R^7 phenyl substituent of **L^{13}** is present, the two MLCT absorptions are both red-shifted, most markedly so for the longer wavelength absorption, and hence the colour of the complexes is drastically altered from red/orange to black or near-black.

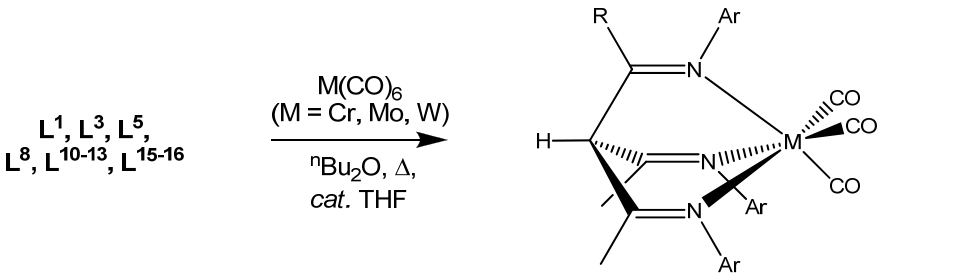

Scheme 2.19 Synthesis of β-triketimine metal carbonyl complexes

Reaction of the very bulky **L^4** and **L^6** with $Mo(CO)_6$ furnished similarly-coloured products in very low yields, yet these were too unstable to characterise in solution, and both were seen to lose their colouration even in the solid state over a period of days (**L^6**) or weeks (**L^4**). Conversely, all the **(L)M(CO)$_3$** complexes depicted in **scheme 2.19** are indefinitely stable in the solid state (if protected from light), and decompose slowly over a period of days in solution. In the case of **L^2**, where each aryl group is 2,6-diisopropyl substituted, the

reaction with $M(CO)_6$ (M = Cr, Mo) failed to proceed at all. These observations suggest that $\mathbf{L^4}$ and $\mathbf{L^6}$ represent the limit of β-triketimine steric bulk which can be can be accommodated at an octahedral metal, and for the compounds to be sufficiently stable in order to characterise them effectively not more than one of the aryl groups may have other substituents in addition to those at the 2-position. An exception to this rule is $\mathbf{L^{15}}$, in which the presence of a small 2-methoxy substituent on one of the aryl groups allows for the other two 2,6-diisopropylphenyl moieties to be comfortably accommodated at an octahedral metal centre without any detriment to stability. All of the **(L)M(CO)$_3$** compounds display rather low solubility, though they are sufficiently soluble in polar solvents such as DMSO to allow for characterisation by ^{1}H NMR spectroscopy. The observed spectra are uncomplicated by isomerism (except in the case of $\mathbf{(L^{16})M(CO)_3}$, which exist as two unique isomeric forms in solution), and the presence of the α-CH resonances (now shifted to higher frequency by ~1 ppm in comparison to uncoordinated **L**) indicate that the ligands are coordinated tridentately in the β-triketimine form. The ^{1}H NMR spectrum of $\mathbf{(L^1)Cr(CO)_3}$ (**figure 2.14**) once again displays a pair of doublets at 1.07 and 1.43 ppm arising due to the stereochemical inequivalence of the isopropyl methyl groups, in analogy with the situation observed for the free β-triketimine in solution. However, the remainder of the peaks are consistent with effective C_3-symmetry, providing further support to the ascribed tridentate coordination in solution. The ^{1}H NMR spectra of $\mathbf{(L^1)Mo(CO)_3}$ and $\mathbf{(L^1)W(CO)_3}$ are essentially identical to that of $\mathbf{(L^1)Cr(CO)_3}$.

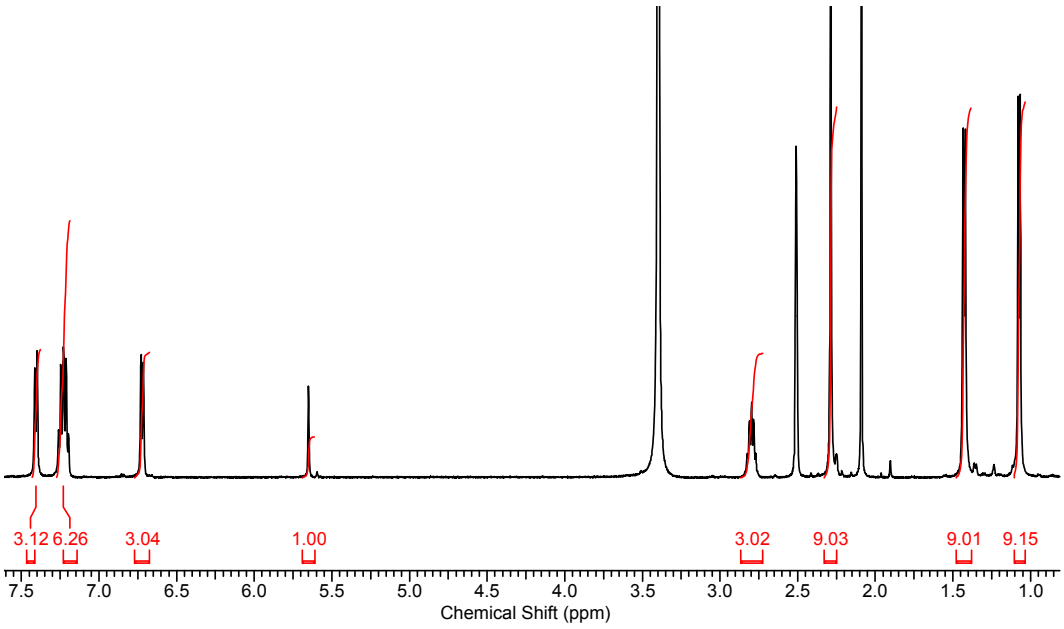

Figure 2.14 ^{1}H NMR spectrum of $(L^1)Cr(CO)_3$ in d_6-DMSO; peaks at 2.09 ppm (acetone), 2.51 ppm (DMSO) and 3.40 ppm (H_2O) are due to solvent contaminants

In all the other examples of **(L)M(CO)$_3$** complexes, there is effectively a lack of any molecular symmetry, and as a result of this individual, distinct resonances are observed in the ^{1}H NMR spectra for substituent groups which may have been expected to be in an identical chemical environment. For example, the ^{1}H NMR spectrum of **(L^{10})Mo(CO)$_3$** (**figure 2.15**) displays six unique doublets in the region of 1.00-1.50 ppm, one for each of the isopropyl methyl groups, as well as two distinct singlets at 2.27 and 2.28 ppm due to the methyl groups of the ligand backbone. As such, the observation of three individual signals corresponding to the isopropyl CH protons may also have been expected; however, only two such signals are observed, at 2.83 and 2.91 ppm in a ratio of 2:1 respectively. Even so, the splitting of all the other aforementioned signals is consistent with the molecule being of very low symmetry.

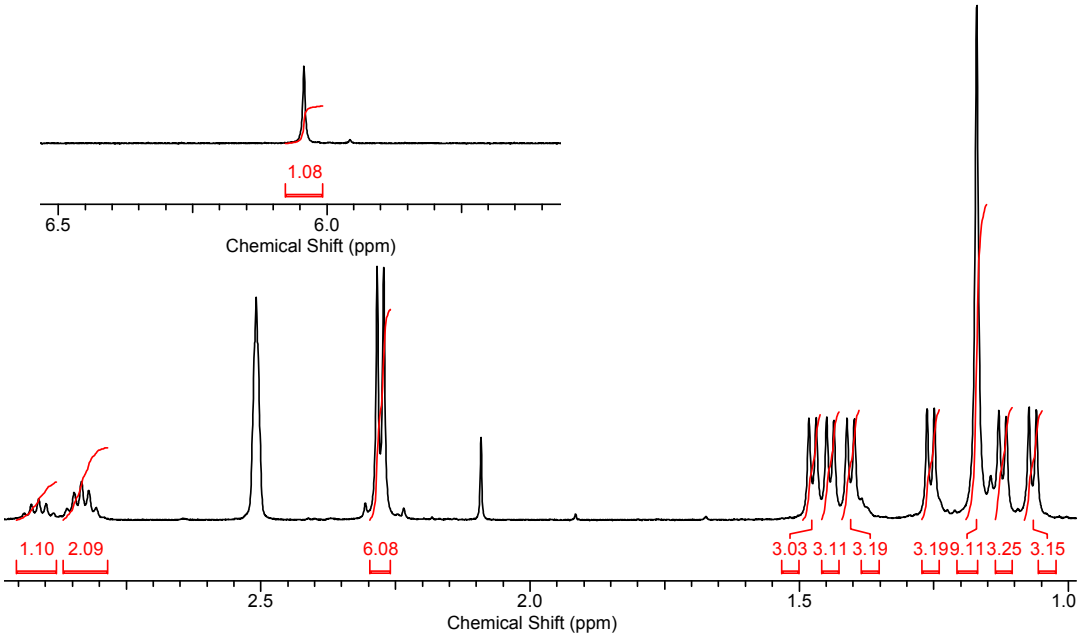

Figure 2.15 ^{1}H NMR spectrum of (L^{10})Mo(CO)$_3$ in d$_6$-DMSO, aryl region not shown; peaks at 2.09 ppm (acetone) and 2.51 ppm (DMSO) are due to solvent contaminants

Infra-red spectroscopy is also a useful tool when investigating metal carbonyl adducts, due to the characteristic carbonyl stretching vibrations that are observed in the region 1700-2150 cm^{-1}. For a C_{3v}-symmetric, *fac*-N$_3$M(CO)$_3$ complex, two absorption bands (A$_1$ and E) are expected due to the molecular symmetry. However, for all of the **(L)M(CO)$_3$** complexes *three* absorption bands are observed, even in the most symmetrical examples, which is indicative of only C_s-symmetry. It is possible that very rapid exchange in the ligand coordination mode between tridentate and bidentate may give rise to a transient C_s-

symmetric arrangement which is observable on the IR timescale. Conversely, due the much longer timescale of the NMR experiment, a C_3-symmetric arrangement is observed in the ^{1}H NMR spectra of the most symmetrical examples (i.e. **$(L^1)M(CO)_3$**). Comparison of the mean carbonyl stretching frequencies observed for **$(L)M(CO)_3$** with the corresponding complexes of a variety of other tripodal nitrogen ligands (**table 2.5**) shows that the β-triketimines are rather weak electron donors, even more so than other similar weakly-donating neutral ligands such as Tpm^x, though their electron-donating ability is somewhat greater than Tom^x and Tppo*.

Table 2.5 Mean CO stretching frequencies for $(L)M(CO)_3$ and related complexes of other tripodal nitrogen ligands

	Mean $\nu_{C\equiv O}$ (cm^{-1})	Ref.
$(L^1)Cr(CO)_3$	1821	This work
$(L^1)Mo(CO)_3$	1822	This work
$(L^1)W(CO)_3$	1816	This work
$(L^3)Cr(CO)_3$	1820	This work
$(L^3)Mo(CO)_3$	1821	This work
$(L^5)Cr(CO)_3$	1818	This work
$(L^5)Mo(CO)_3$	1820	This work
$(L^8)Cr(CO)_3$	1821	This work
$(L^8)Mo(CO)_3$	1820	This work
$(L^{10})Cr(CO)_3$	1823	This work
$(L^{10})Mo(CO)_3$	1825	This work
$(L^{11})Cr(CO)_3$	1820	This work
$(L^{11})Mo(CO)_3$	1823	This work
$(L^{12})Cr(CO)_3$	1821	This work
$(L^{12})Mo(CO)_3$	1823	This work
$(L^{13})Cr(CO)_3$	1825	This work
$(L^{13})Mo(CO)_3$	1826	This work
$(L^{15})Cr(CO)_3$	1814	This work
$(L^{15})Mo(CO)_3$	1822	This work
$(L^{16})Cr(CO)_3$	1817	This work
$(L^{16})Mo(CO)_3$	1818	This work
$NEt_4[(Tp^*)Cr(CO)_3]$	1795	319
$NEt_4[(Tp^*)Mo(CO)_3]$	1797	319
$NEt_4[(Tp^*)W(CO)_3]$	1789	319
$NEt_4[(Tp^{iPr})Mo(CO)_3]$	1801	254
Na[(MeTpg)Mo(CO)$_3$]	1797	320
Na[(MeTpg*)Mo(CO)$_3$]	1788	320
$NEt_4[(Ttz)Mo(CO)_3]$	1810	219
$(Tpm)Cr(CO)_3$	1804	145
$(Tpm)Mo(CO)_3$	1804	145
$(Tpm)W(CO)_3$	1801	145
$(Tpm^*)Mo(CO)_3$	1806	145
$(MeTps^*)Cr(CO)_3$	1803	206
$(MeTps^*)Mo(CO)_3$	1802	206
$(MeTps^*)W(CO)_3$	1794	206
$(Tpp^*)Mo(CO)_3$	1815	197
$(Tppo^*)Mo(CO)_3$	1883	198
$((S)\text{-}MeTom^{iPr})Mo(CO)_3$	1864	253
$(Tach)Cr(CO)_3$	1759	264

It is known that the coordinating ability of isolated imines is rather weak, and indeed *N*-aryl monoketimines and *N*-aryl monoaldimines have been shown to coordinate to $M(CO)_3$ fragments exclusively via η^6-coordination of the aryl group.[321] However, in the case of the β-triketimines, the tris(chelating) nature of the ligands ensures that stable, facially N_3-coordinated complexes are obtained. It can also be seen that the presence of different substituent groups on the various β-triketimine ligands has little effect on their electron-donating ability, as the mean CO stretching frequencies for **(L)M(CO)$_3$** vary over a range of only 12 cm^{-1} across the whole series (**table 2.5**).

The solid-state structures of **(L^1)Cr(CO)$_3$** (**figure 2.16**) and **(L^1)Mo(CO)$_3$** (**figure 2.17**) confirm unequivocally that the β-triketimine ligand is tridentately coordinated in these complexes. The two compounds are essentially isomorphous, save for the small increases in certain parameters on going from Cr to Mo. This is an effect of the increased atomic radius of Mo relative to Cr, and is manifested in the larger cell constants (**appendix**) and longer M(1)-C(13) and M(1)-N(1) bond distances (**table 2.6**) observed for the Mo complex. The larger atomic radius of Mo is accommodated by an expansion of the ligand pocket, as evidenced by the N-N distance of 2.927(2) Å in **(L^1)Mo(CO)$_3$** versus 2.834(2) Å in **(L^1)Cr(CO)$_3$**. This expansion allows the C=N-M angle to remain close to the idealised value of 120°, and also accounts to some extent for the increase in M(1)-C(13) and M(1)-N(1) distances. The molecules are C_3-symmetric, and the asymmetric unit consists of a single arylimino moiety and a carbonyl group, with a crystallographic axis passing through C(1) and M(1).

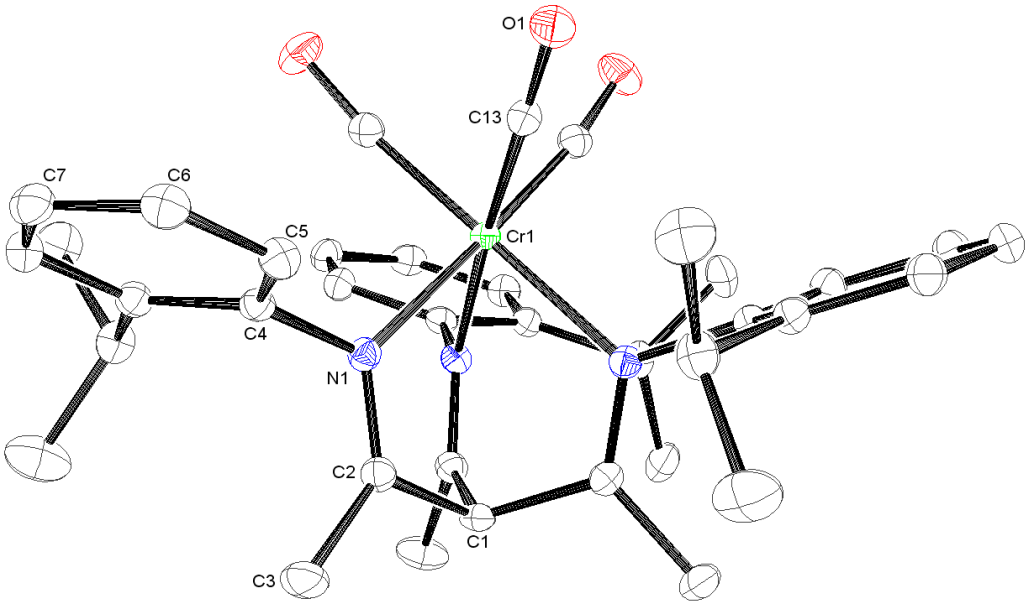

Figure 2.16 ORTEP representation of the molecular structure of $(L^1)Cr(CO)_3$ with thermal ellipsoids set at the 50% probability level, hydrogen atoms omitted for clarity

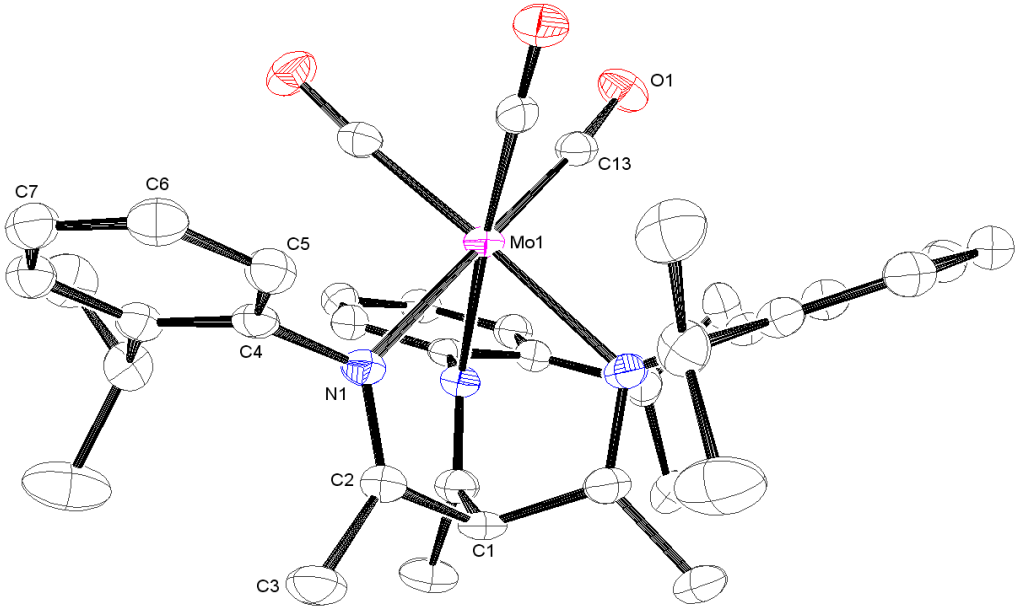

Figure 2.17 ORTEP representation of the molecular structure of $(L^1)Mo(CO)_3$ with thermal ellipsoids set at the 30% probability level, hydrogen atoms omitted for clarity

Table 2.6 Selected bond lengths (Å), angles (°) and interplanar torsion angles (°) for $(L^1)Cr(CO)_3$ and $(L^1)Mo(CO)_3$

$(L^1)Cr(CO)_3$	$(L^1)Mo(CO)_3$
O(1)-C(13) 1.1673(15)	O(1)-C(13) 1.170(2)
Cr(1)-C(13) 1.8336(12)	Mo(1)-C(13) 1.9434(19)
Cr(1)-N(1) 2.1217(10)	Mo(1)-N(1) 2.2599(16)
N(1)-C(2) 1.2805(15)	N(1)-C(2) 1.287(2)
N(1)-C(4) 1.4460(15)	N(1)-C(4) 1.448(2)
C(1)-C(2) 1.5211(14)	C(1)-C(2) 1.521(2)
C(2)-C(3) 1.4949(18)	C(2)-C(3) 1.494(3)
O(1)-C(13)-Cr(1) 172.11(10)	O(1)-C(13)-Mo(1) 175.07(16)
N(1)-Cr(1)-C(13) 98.87(6)	N(1)-Mo(1)-C(13) 176.11(8)
N(1)-Cr(1)-C(13)′ 176.36(6)	N(1)-Mo(1)-C(13)′ 95.51(8)
N(1)-Cr(1)-C(13)″ 93.99(5)	N(1)-Mo(1)-C(13)″ 99.68(8)
C(13)-Cr(1)-C(13)′ 83.46(6)	C(13)-Mo(1)-C(13)′ 84.19(9)
N(1)-Cr(1)-N(1)′ 83.81(4)	N(1)-Mo(1)-N(1)′ 80.71(6)
Cr(1)-N(1)-C(2) 120.73(8)	Mo(1)-N(1)-C(2) 120.81(13)
Cr(1)-N(1)-C(4) 121.43(7)	Mo(1)-N(1)-C(4) 120.85(11)
C(2)-N(1)-C(4) 117.83(10)	C(2)-N(1)-C(4) 118.34(16)
θ_T (C(1)-C(2)-N(1)-C(3)/C(4)$_{Ar}$) = 84.94(10)	θ_T (C(1)-C(2)-N(1)-C(3)/C(4)$_{Ar}$) = 86.75(16)

The aryl groups are effectively orthogonal to the imine planes (**table 2.6**), which results in inefficient packing of the molecules in the crystal. This, coupled with the C_3-symmetry, results in the generation of significant hexagonal pores along the *c*-axis (**figure 2.18**). In the case of **$(L^1)Mo(CO)_3$**, where the single crystal was obtained directly from the mother liquor, the pores are occupied by disordered diethyl ether molecules (1 per complex unit). In contrast, the single crystal of **$(L^1)Cr(CO)_3$** was air dried for a number of days before the data collection was performed, and as a result the pores are free of solvent. This implies that the presence of solvent is not essential to the formation of the porous network structures of **$(L^1)Cr(CO)_3$** and **$(L^1)Mo(CO)_3$**. The pore volumes of 219 Å^3 (**$(L^1)Cr(CO)_3$**) and 311 Å^3 (**$(L^1)Mo(CO)_3$**, after removal of solvent) per unit cell (6.5% and 8.8% of the unit cell respectively) are modest in comparison to those seen in a trinuclear osmium carbonyl complex reported by Wong *et al.*, though in this case the crystal lattice does not survive desolvation.[322]

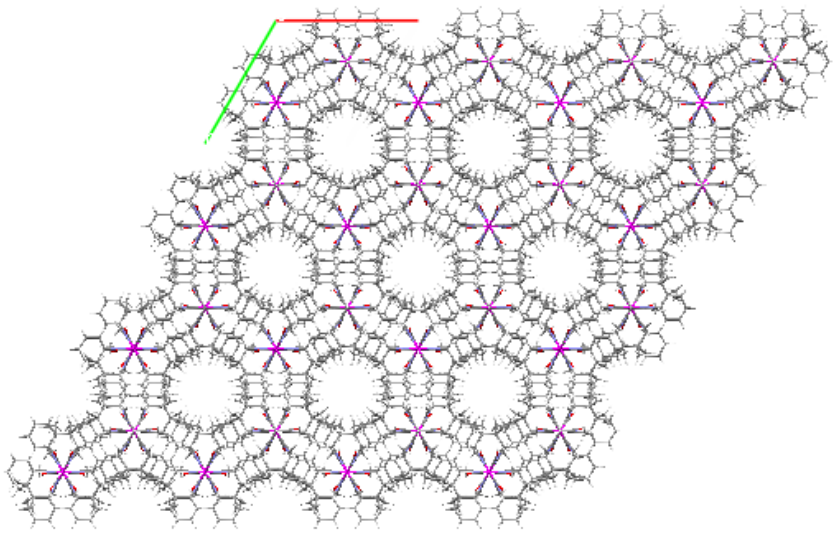

Figure 2.18 MERCURY representation of the extended crystal structure of $(L^1)Cr(CO)_3$, viewed along the *c*-axis

The lack of an observable melting point for **$(L^1)Cr(CO)_3$** and **$(L^2)Mo(CO)_3$** (both compounds decompose at elevated temperatures), coupled with their low solubility, suggests that the supramolecular structural frameworks are rather robust. Investigation of close contacts revealed that two distinct intermolecular interactions may be responsible: CO---H-C hydrogen bonds between the carbonyl ligands and one of the aryl hydrogen atoms; and aryl-aryl interactions. In the case of **$(L^1)Cr(CO)_3$**, the C---O distance (3.408 Å) and C-H---O angle (148.11°) both lie comfortably within the ranges described as being indicative of such interactions. However, the CO---H angle (93.61°) deviates significantly from the mean value of 127.1° previously observed for H-bonding interactions of terminal carbonyl groups.[323] As such, the aryl-aryl interactions may be of greater importance in directing the crystal packing. These contacts are relatively short (C(6)-C(6)′ = 3.365 Å, C(7)-C(7)′ = 3.382 Å), which signifies that the interactions are rather strong.[324] The two phenyl rings are co-planar, yet the degree of slippage indicates that this is primarily a σ-π interaction, as opposed to a true π-π interaction.[324,325] The combination of these distinct intermolecular interactions between the two asymmetric units of different molecules is outlined in **figure 2.19**. In **$(L^1)Mo(CO)_3$**, the larger atomic radius of Mo causes a noticeable increase in the aryl-aryl distances (C(6)-C(6)′ = 3.419 Å, C(7)-C(7)′ = 3.434 Å), which are less indicative of an obvious structure-directing influence. Additionally, the C---O distance of 3.471 Å in **$(L^1)Mo(CO)_3$** is more than 0.06 Å longer than that in **$(L^1)Cr(CO)_3$**, and as such both interactions must be deemed weaker.

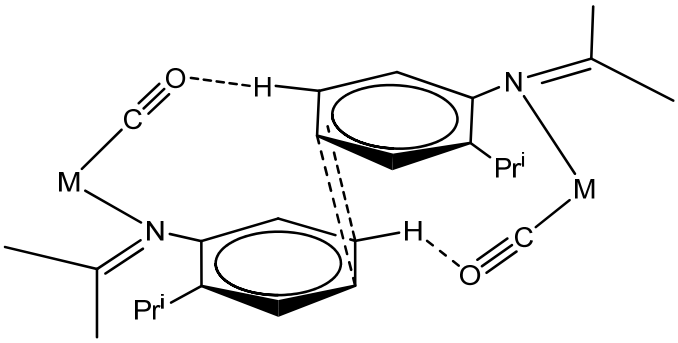

Figure 2.19 Schematic representation of supramolecular interactions between two asymmetric units of $(L^1)M(CO)_3$ (M = Cr, Mo)

2.3 Concluding Remarks

The reaction of lithium β-diketiminates with imidoyl chlorides has been shown to reliably give access to a series of novel β-triketimine ligands with varying degrees of substitution, on both the aryl groups and the R^7 substituent derived from the imidoyl chloride. In the case of β-triketimines where R^7 = Me, multiple isomeric species are observed in solution due to tautomerism between the true β-triketimine tautomer and a number of possible enamine-diimine isomers. Equilibration in solution is rapid unless all of the aryl groups are 2,6-disubstituted; in these cases the process is slow and occurs over a period of days. In contrast, β-triketimines where R^7 = Ph or ^{t}Bu exist as single isomers both in solution and in the solid state. In those cases where the aryl substituent of the R^7 imine is 2,6-disubstituted the β-triketimine tautomer is observed exclusively, whereas all other examples exist solely as the enamine-diimine tautomer.

The majority of the β-triketimines have been shown to act as *fac*-coordinating tridentate ligands towards group 6 metal carbonyl fragments, though there is a limit to the amount of ligand steric bulk which can be accommodated at such metal centres. The complexes are indefinitely stable in the solid state, provided not more than one of the ligand aryl groups is 2,6-disubstitued. Comparison of the carbonyl stretching frequencies observed for the β-triketimine complexes with those of related compounds shows that the β-triketimines are rather weak σ-donors relative to other previously reported tripodal nitrogen ligands. Crystalline derivatives were obtained only in the case of the most symmetrical β-triketimine ligand, and these have been found to feature porous infinite network structures generated by relatively weak hydrogen-bonding and aryl-aryl interactions.

The preparation of metal carbonyl complexes provides a useful 'proving ground' in order to establish the donor ability of a new ligand system. However, such compounds are functionally very limited, and in order to gauge the usefulness of the β-triketimines in areas such as biomimetic chemistry and catalysis it is necessary to investigate their coordination chemistry with oxidised transition metal ions. The results of this research are presented in the following chapters.

3. Complexes of β-Triketimines with Zinc(II) and Thallium(I)

3.1 Introduction

As discussed briefly in **chapter 1**, tripodal nitrogen ligands, in particular the tris(pyrazolyl)borates, have been extensively applied to the preparation of zinc complexes which replicate the structure and function of metalloenzymes in which the zinc centre is coordinated by three histidine residues, for example carbonic anhydrase. The ability of ($Tp^{tBu,Me}$)ZnOH to react reversibly with CO_2, producing a dinuclear carbonate complex by means of an unstable bicarbonate intermediate and thereby mimicking accurately the catalytic cycle of carbonic anhydrase (**section 1.4.2**), stands as one of the key achievements in small-molecule biomimetic chemistry. However, the preparation of ($Tp^{tBu,Me}$)ZnOH was predated by over a decade by the synthesis and structural characterisation of [($^2Tip^{iPr2}$)ZnCl][Cl] (**308**, $^2Tip^{iPr2}$ = tris(4,5-diisopropylimidazol-2-yl)phosphine).[326] It may at first seem that a chloride complex is a poor structural mimic for the enzymatic system, where the terminal coordination site is occupied by either a water molecule or hydroxide ligand. However, the tris(imidazole) coordination sphere provided by $^2Tip^{iPr2}$ reproduces very closely that seen in the metalloenzyme, and indeed [($^2Tip^{iPr2}$)ZnCl][Cl] was the first structurally characterised complex to feature such ligation. No attempts to prepare and isolate the corresponding hydroxo-complex were reported, though solutions of $^2Tip^{iPr2}$ and $Zn(ClO_4)_2$ at neutral or slightly basic pH were shown to catalyse the hydration of CO_2 to bicarbonate.[327]

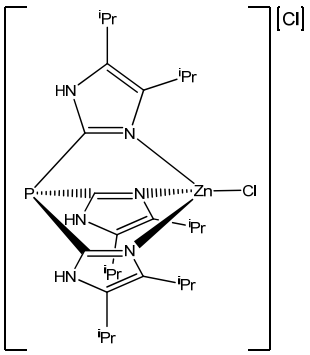

308

Figure 3.1 Structure of [($^2Tip^{iPr2}$)ZnCl][Cl] (308)

Although $Tp^{tBu,Me}$ was the first tris(pyrazolyl)borate ligand to be applied effectively to the preparation of biomimetic zinc complexes, the majority of the subsequent work in this area has employed other Tp^x ligands, most commonly $Tp^{Ph,Me}$ and $Tp^{Cum,Me}$. Despite its status as one of the most widely used Tp^x ligands, Tp^{iPr2} has rarely been utilised in this respect, save for single report in addition to those already discussed in **section 1.4.6**. This

described the ability of (Tp^{iPr2})ZnOH (prepared by reaction of (Tp^{iPr2})Zn(OAc) with NaOH) to cleave activated phosphate esters, thereby mimicking the function of zinc enzymes such as alkaline phosphatase. When (Tp^{iPr2})ZnOH (**309**) was treated with an excess of sodium bis(*p*-nitrophenyl)phosphate, a mixture of products comprising (Tp^{iPr2})Zn(OC_6H_4-4-NO_2) (**310**) and the novel dinuclear phosphate-bridged complex {(Tp^{iPr2})Zn}$_2$(μ-η^1:$\eta^{1'}$-*O,O'*-$O_3POC_6H_4$-4-NO_2) (**311**) was obtained (**scheme 3.1**). However, the effectiveness of this system as a functional enzyme model is limited due to the fact that the observed reactivity is strictly stoichiometric, rather than catalytic.[328]

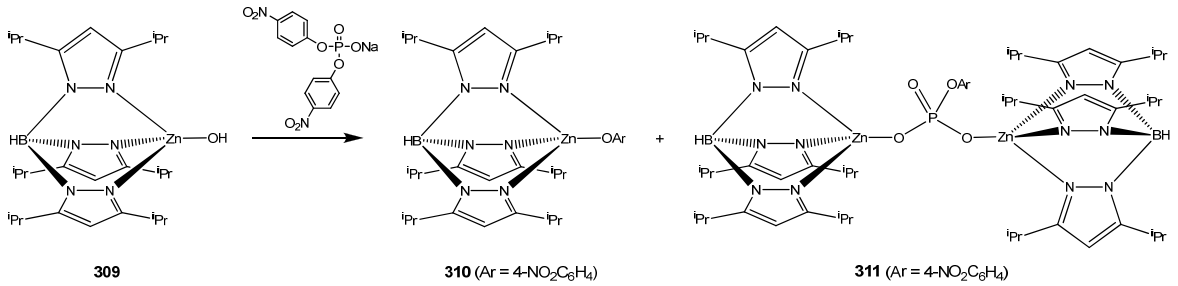

Scheme 3.1 Reaction of (Tp^{iPr2})ZnOH (309) with sodium bis(*p*-nitrophenyl)phosphate

Similar reactivity was also demonstrated for ($Tp^{Cum,Me}$)ZnOH, though this system was also shown to be capable of cleaving unactivated phosphate esters, as well as activated amides and esters. This increased level of reactivity in comparison to (Tp^{iPr2})ZnOH can be ascribed to an increase in nucleophilicty of the bound hydroxide ion, which is a result of the more extensive hydrophobic pocket provided by the *p*-cumenyl groups around the Zn-OH unit.[329,330] Accordingly, although ($Tp^{tBu,Me}$)ZnOH and ($Tp^{Ph,Me}$)ZnOH have also been shown to undergo similar reactions with activated phosphates and diphosphates, neither is capable of cleaving esters or amides.[330] It should be noted here that the zinc hydroxide derivatives of $Tp^{tBu,Me}$, $Tp^{Cum,Me}$ and $Tp^{Ph,Me}$ were all prepared in an analogous fashion, by means of the direct reaction between the appropriate Tp^x ligand, $Zn(ClO_4)_2.6H_2O$ and KOH in a 1:1:1 ratio.[57,329(a),331] If, in the case of $Tp^{Cum,Me}$, this ratio is altered to 3:3:1 respectively, a different crystalline product is obtained. This was found to be the dinuclear complex [{($Tp^{Cum,Me}$)Zn}$_2$(μ-H_3O_2)][ClO_4] (**312**), in which the two zinc centres are bridged by a $[H_3O_2]^-$ (hydrated hydroxide) ion. This structural motif has been postulated to exist in trinuclear zinc enzymes such as phospholipase C, though this has not been proven crystallographically. Additionally, [{($Tp^{Cum,Me}$)Zn}$_2$(μ-H_3O_2)][ClO_4] may also reasonably be considered a hydrogen-bonded zinc-aqua / zinc-hydroxo complex, with a structure similar to the aforementioned [($Tp^{tBu,Me}$)Zn(OH_2)][$HOB(C_6F_5)_3$] (**section 1.4.2**). However,

the asymmetric nature of the $[H_3O_2]^-$ unit in the latter complex is more consistent with a true zinc-aqua complex, whereas $[\{(Tp^{Cum,Me})Zn\}_2(\mu\text{-}H_3O_2)][ClO_4]$ has a centre of symmetry midway between the two oxygen atoms (i.e. the likely location of the bridging hydrogen atom), though this may be due to crystallographic disorder.[332] The fact that the related $[\{(Tp^{Ph,Me})Zn\}_2(\mu\text{-}H_3O_2)][ClO_4]$ was also found to show a symmetrical structure in the solid state, makes the latter argument seem somewhat less feasible.[333]

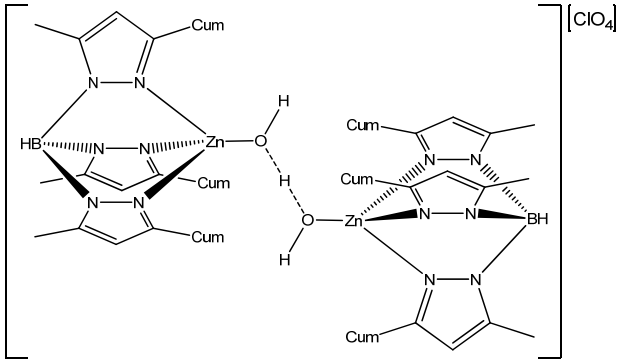

312

Figure 3.2 Structure of $[\{(Tp^{Cum,Me})Zn\}_2(\mu\text{-}H_3O_2)][ClO_4]$ (312)

Liver alcohol dehydrogenase is a mononuclear zinc enzyme, responsible for the catalytic oxidation of alcohols to aldehydes (or ketones) with concomitant reduction of NAD^+ to NADH. Terminal zinc alkoxides are widely accepted as intermediates in this process, and indeed the crystal structure of the metalloenzyme featuring zinc-bound non-productive alkoxides such as pentafluorobenzyloxide has been reported.[334] However, small-molecule terminal zinc alkoxide complexes remain to date extremely rare, and as such their synthesis is an on-going goal of biomimetic coordination chemistry. $(Tp^{Cum,Me})Zn(OR)$ (**314**, R = $CH_2C_6H_4$-4-NO_2, $CH_2C_6F_5$, CH_2CF_3, CH_2CCl_3), the first terminal zinc alkoxide complexes of tripodal nitrogen ligands, were prepared by Vahrenkamp and colleagues by means of the reaction of $(Tp^{Cum,Me})ZnOH$ (**313**) with the corresponding highly acidic alcohols (**scheme 3.2**). However, when the same reaction was attempted with less acidic alcohols such as methanol and ethanol, the formed alkoxides were rapidly hydrolysed back to the starting materials as a result of their highly reactive nature.[335] Their fleeting existence is however inferred by the fact that when alcoholic solutions of $(Tp^{Cum,Me})ZnOH$ are exposed to CO_2, the corresponding alkylcarbonate complexes $(Tp^{Cum,Me})Zn(OCO_2R)$ (R = Me, Et) could be isolated.[336]

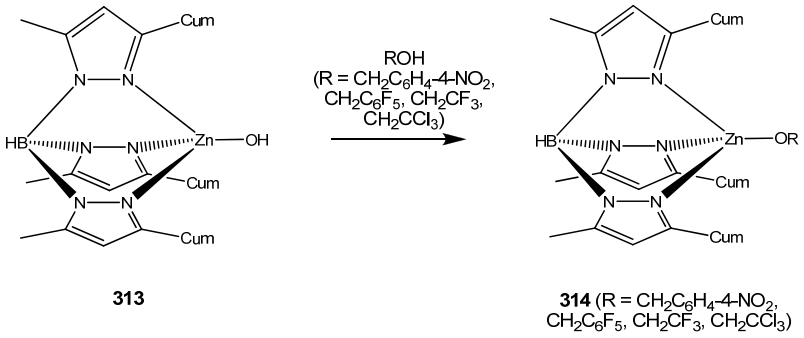

313 **314** (R = $CH_2C_6H_4$-4-NO_2, $CH_2C_6F_5$, CH_2CF_3, CH_2CCl_3)

Scheme 3.2 Preparation of $(Tp^{Cum,Me})Zn(OR)$ (314)

It was subsequently shown by Parkin and co-workers that reaction of $(Tp^{tBu,Me})ZnH$ (**315**) with the appropriate alcohol (**scheme 3.3**) gives access to the terminal alkoxides $(Tp^{tBu,Me})Zn(OR)$ (**316**, R = Me, Et, ^{i}Pr), and a structure determination was performed for R = Et.[337] By employing the same synthetic method, Vahrenkamp *et al.* then described the preparation of the series of alkoxides $(Tp^{Ph,Me})Zn(OR)$ (R = Me, Et, ^{i}Pr) and $(Tp^{Cum,Me})Zn(OR)$ (R = Me, ^{i}Pr), and their reactivity towards an extremely wide variety of substrates was investigated in detail.[338]

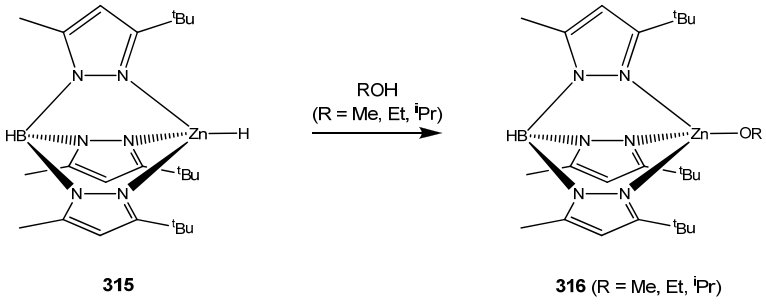

315 **316** (R = Me, Et, ^{i}Pr)

Scheme 3.3 Preparation of $(Tp^{tBu,Me})Zn(OR)$ (316)

The group of Lippard and colleagues also reported the serendipitous preparation and structural characterisation of $(Tp^{Ph,Me})Zn(OMe)$ (**318**), which was isolated as a minor by-product in the synthesis of $(Tp^{Ph,Me})ZnOH$ (**317**) following recrystallisation from methanol at -30°C (**scheme 3.4**).[339]

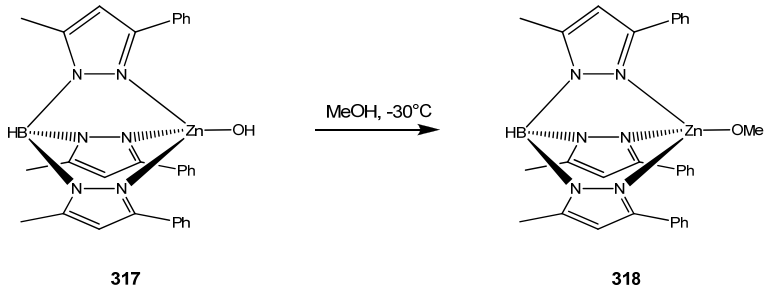

317 **318**

Scheme 3.4 Preparation of $(Tp^{Ph,Me})Zn(OMe)$ (318)

In contrast to the anionic tris(pyrazolyl)borates, similar neutral tripodal nitrogen ligands have been used much less extensively for the synthesis of biomimetic four-coordinate zinc complexes, despite the increased biological relevance inherent to the use of neutral ligating systems. The cationic hydroxo-complex [(^{2}Tip$^{tBu,N\text{-}iPr}$)ZnOH][ClO_4] (**319**) was reported by Parkin *et al.* in 1995, and was synthesised simply by the direct reaction of ^{2}Tip$^{tBu,N\text{-}Me}$ with $Zn(ClO_4)_2.6H_2O$ in the absence of any alkali metal hydroxide, the hydroxide ligand presumably arising from the hydrated perchlorate salt.[340] However, no further information regarding the reactivity of this complex has ever been reported. In contrast, the complex [(Tach)Zn(η^1-OAc)][ClO_4] (**320**) in basic solution has been shown to promote efficiently the hydrolysis of 2,4-dinitrophenyl diethyl phosphate.[341]

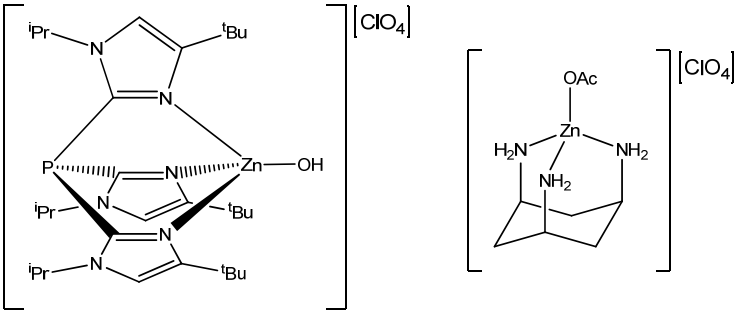

319 **320**

Figure 3.3 Structures of [(^{2}Tip$^{tBu,N\text{-}iPr}$)ZnOH][ClO_4] (319) and [(Tach)Zn(η^1-OAc)][ClO_4] (320)

Walton *et al.* have described the synthesis of [(Pro-Tach^{Fr})ZnOH][BPh_4], which was formed by the direct reaction of Pro-Tach^{Fr} with $Zn(ClO_4)_2$ and KOH followed by metathesis of the intermediate complex with $NaBPh_4$. Recrystallisation of [(Pro-Tach^{Fr})ZnOH][BPh_4] (**321**) from methanol/DCM at 4°C gave a novel complex which was found by analysis of the solid-state structure to have the composition [(Pro-Tach^{Fr})Zn(OMe)][(Pro-Tach^{Fr})ZnOH][BPh_4]$_2$ (**322**), arising from partial reaction of [(Pro-Tach^{Fr})ZnOH][BPh_4] with the methanol solvent (**scheme 3.5**). This mixed cationic complex is, to date, the only known example of a four-coordinate alkoxide complex where the zinc atom is bound by a neutral tripodal ligand. The methoxide ligand is hydrogen-bonded to a single methanol solvent molecule trapped inside the large hydrophobic pocket of the Pro-Tach^{Fr} ligand (see **section 1.11.3**), which is similar to the situation observed in liver alcohol dehydrogenase, where the bound alkoxide engages in a hydrogen-bonding interaction with an amino acid side chain. An analogous interaction is also observed in the [(Pro-Tach^{Fr})ZnOH] cation.[342]

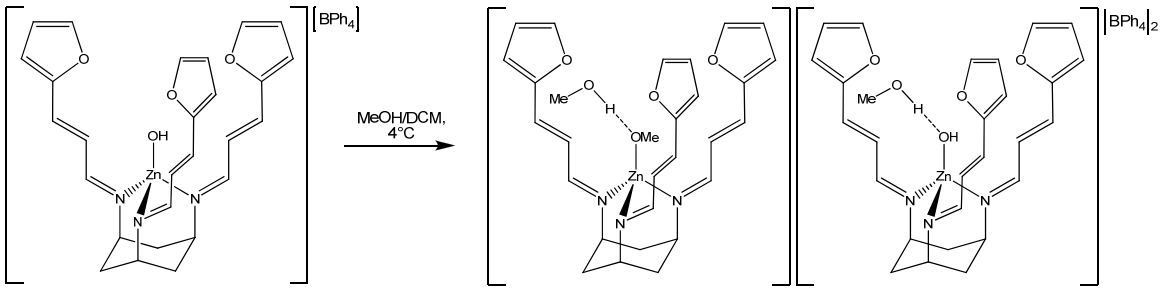

321 322

Scheme 3.5 Preparation of [(Pro-Tach^{Fr})Zn(OMe)][(Pro-Tach^{Fr})ZnOH][BPh_4]$_2$ (322)

The dinuclear zinc complex [{((*S*)-MeTom^{iPr})Zn}$_2$(μ-η^1:η$^{1'}$-*O,O'*-OTf)$_3$][OTf] (**323**) has been postulated as a functional model for zinc hydrolase enzymes such as carboxypeptidase, and indeed this chiral system has been shown to display catalytic activity for the transesterification of a variety of phenyl esters with moderate levels of enantioselectivity.[343]

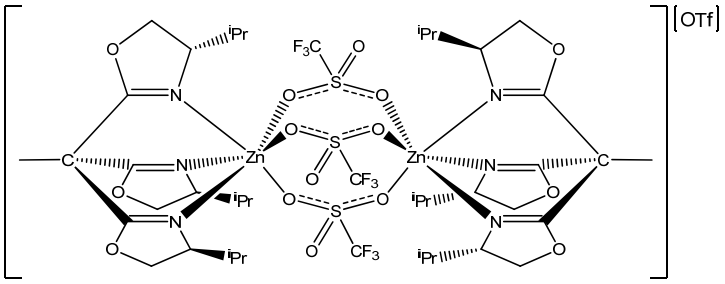

323

Figure 3.4 Structure of [{((*S*)-MeTom^{iPr})Zn}$_2$(μ-η^1:η$^{1'}$-*O,O'*-OTf)$_3$][OTf] (323)

Given the wide range of novel coordination chemistry accessible with tripodal nitrogen ligands in combination with zinc, this metal ion therefore seemed a most appropriate testing ground in order to probe the coordination chemistry of β-triketimines with oxidised metal ions. Additionally, the use of the diamagnetic zinc(II) ion will also facilitate detailed study of the behaviour of the complexes in solution, by means of NMR spectroscopy. The remainder of this chapter shall be concerned with the results of these investigations.

3.2 Results and Discussion

3.2.1 Synthesis and Characterisation of Cationic Zinc Chloride Complexes of β-Triketimine Ligands

3.2.1.1 $[(L^1)ZnCl][Cl]$ and $[(L)ZnCl]_2[Zn_2Cl_6]$ Complexes

The reaction of $\mathbf{L^1}$ with anhydrous zinc chloride in DCM or Et_2O produces a colourless precipitate which is insoluble in most common solvents, except for THF and DMSO, and thus has proven difficult to characterise effectively. Nonetheless, the ^{1}H NMR spectrum of this product (**figure 3.5**) shows only a single set of resonances for each proton environment, related to each other in the correct ratio, which is consistent with a tetrahedral complex where the β-triketimine ligand is tridentately coordinated. Microanalytical data are consistent with a 1:1 adduct, and MALDI mass spectrometry shows the existence of a $[(L^1)ZnCl]^+$ molecular ion. Therefore, in analogy with $[(^2Tip^{iPr2})ZnCl][Cl]$,[326] this complex can be tentatively formulated as **$[(L^1)ZnCl][Cl]$**. However, none of these data provide any indication as to the nature of the coordination mode of the ligand in the solid state, and despite all efforts it has not been possible to produce single crystals of this compound. Its insolubility, even in polar solvents such as acetonitrile, coupled with a marked reluctance to crystallise, suggest that **$[(L^1)ZnCl][Cl]$** may form a coordination polymer in the solid state, which would likely arise due to asymmetric coordination of the imine donors of one molecule of $\mathbf{L^1}$ to two or three different zinc centres.

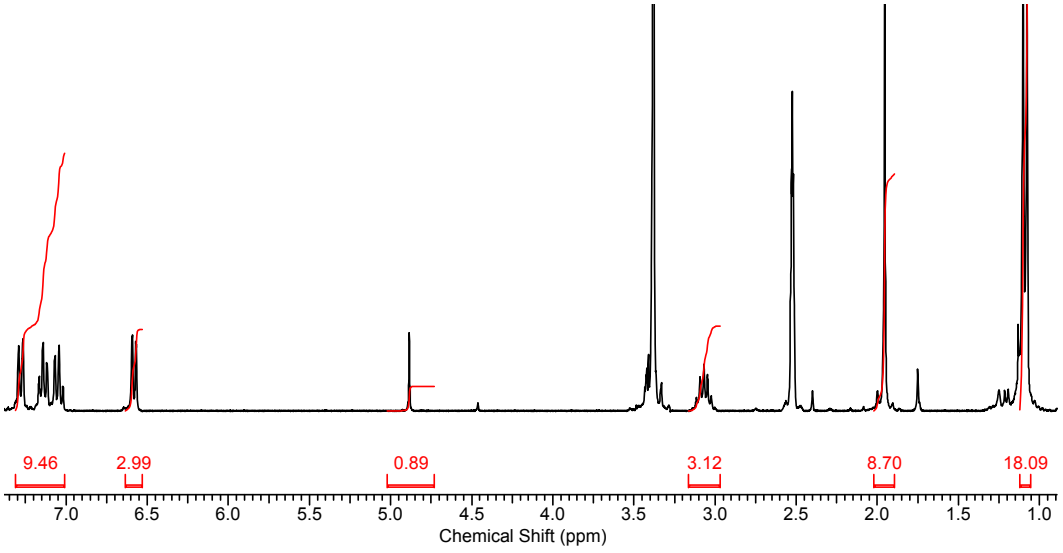

Figure 3.5 ^{1}H NMR spectrum of $[(L^1)ZnCl][Cl]$ in d_6-DMSO; peaks at 2.51 ppm (DMSO) and 3.40 ppm (H_2O) are due to solvent contaminants

In light of the highly insoluble nature of **[(L^1)ZnCl][Cl]**, it was assumed that the direct reaction of β-triketimines in which R^7 = ^{t}Bu with zinc chloride may give access to products which are more soluble, and therefore easier to crystallise. Indeed, **L^8**, **L$^{10\text{-}12}$** and **L^{16}** were all found to react with zinc chloride in DCM to give complexes of the general formula **[(L)ZnCl]$_2$[Zn$_2$Cl$_6$]** (**scheme 3.6**), which were precipitated as colourless solids by addition of either Et_2O or hexane.

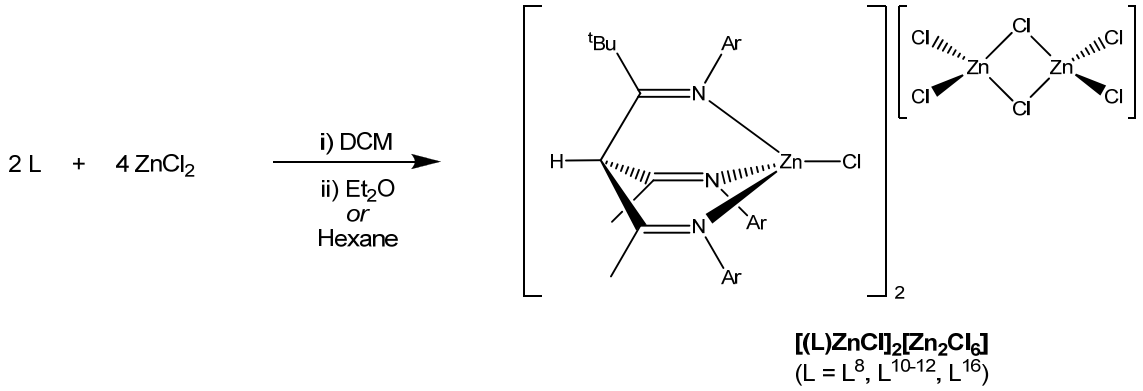

[(L)ZnCl]$_2$[Zn$_2$Cl$_6$]
(L = L^8, L$^{10\text{-}12}$, L^{16})

Scheme 3.6 Synthesis of [(L)ZnCl]$_2$[Zn$_2$Cl$_6$] complexes

The zinc:ligand ratio in these complexes is 2:1 respectively, which implies that the aforementioned 1:1 complex of **L^1** cannot be assigned to this structural formula. The autoionisation of zinc chloride to a cationic complex upon coordination of a neutral tridentate nitrogen ligand is relatively uncommon; in many of the cases described in **chapter 1** metathesis with a weakly coordinating anion has been necessary for the formation of isolable complexes. However, this process has been previously seen to occur with the generation of [(^{2}Tip^{iPr2})ZnCl][Cl],[326] [(^{4}Tip^{iPr})ZnCl][Cl][247] and [(^{2}Tip$^{Tol,N\text{-}Me}$)ZnCl][ZnCl$_4$].[245] In comparison to the latter complex, which features a tetrachlorozincate dianion, the fact that the β-triketimines induce the formation of the larger hexachlorodizincate species is likely due to cation-anion size-matching considerations. The [(L)ZnCl]$^+$ ions reported here are considerably larger than [(^{2}Tip$^{Tol,N\text{-}Me}$)ZnCl]$^+$, and it is well known that in order to promote maximum efficiency in packing of molecules in the solid state, it is favourable for cations and anions to be of approximately equal size.[344]

In contrast to the behaviour of **[(L^1)ZnCl][Cl]**, all of the **[(L)ZnCl]$_2$[Zn$_2$Cl$_6$]** complexes are soluble in polar solvents such as acetonitrile and alcohols, as well as DCM where **L** = **L$^{11\text{-}12}$** and **L^{16}**. This increase in solubility in DCM is most likely a result of the greater number of aryl substituent groups present in these ligands relative to **L^8** and **L^{10}**, which in turn imparts an enhanced degree of hydrophobicity to the resultant complexes. Single

crystals of **[(L)ZnCl]$_2$[Zn$_2$Cl$_6$]** suitable for X-ray diffraction were therefore obtained by slow diffusion of Et_2O into a solution of the appropriate zinc complex in either acetonitrile (**L** = **L^8**) or DCM (**L** = **L^{12}**, **L^{16}**). The solid-state structure of **[(L^8)ZnCl]$_2$[Zn$_2$Cl$_6$]** features two independent cationic units in the unit cell, though as their structural parameters are very similar only one of these is included here (**figure 3.6**); pertinent bond lengths and angles for both molecules are listed in **table 3.1**. The zinc atoms are in a highly distorted tetrahedral geometry, the Cl-Zn-N and N-Zn-N angles deviating significantly from the idealised value of 109.5°. The Zn-N distances vary little throughout the two unique molecules, and it can also be seen that the presence of the backbone *tert*-butyl substituent has negligible influence on the Zn(1)-N(1)/Zn(2)-N(4) distances. However, in comparison to the C=N-C_{Ar} angles of the methyl-substituted imine moieties (119.0(10)-121.7(9)°), which are close to the sp^2 ideal of 120°, the corresponding angles of the *tert*-butyl substituted imines are somewhat wider, at 127.3(10)° and 125.6(11)°. The steric repulsion between the *tert*-butyl group and the aryl moiety causes the latter to be pushed closer in towards the metal atom, and thus increases the overall steric demand of the ligand. The oxygen atom of the methoxy-substituted aryl group is oriented in the direction of the zinc atom, though the Zn-O distances (3.462(11) and 3.587(11) Å) lie well outside the range of which could be termed even a very weak bonding interaction.

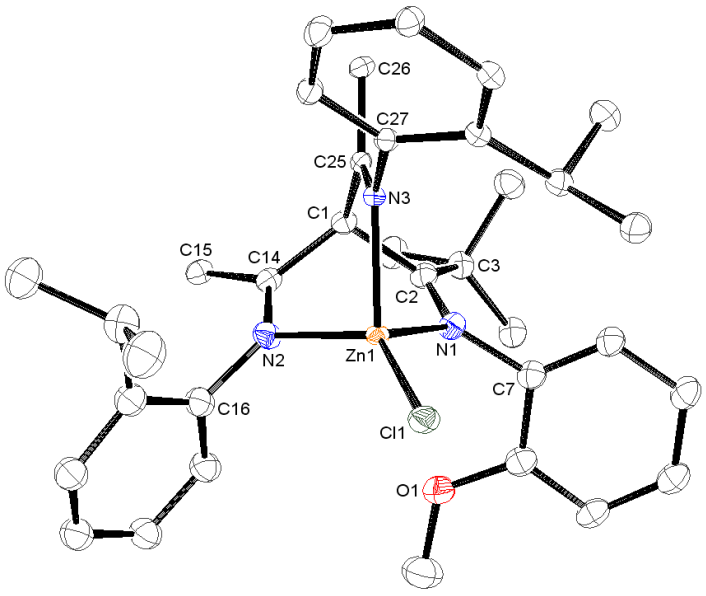

Figure 3.6 ORTEP representation of one of the cationic units in [(L^8)ZnCl]$_2$[Zn$_2$Cl$_6$] with thermal ellipsoids set at the 50% probability level; hydrogen atoms omitted for clarity

Table 3.1 Selected bond lengths (Å), angles (°) and interplanar torsion angles (°) for the two unique cations in $[(L^8)ZnCl][Zn_2Cl_6]$

$[(L^8)ZnCl]^+$ molecule 1	$[(L^8)ZnCl]^+$ molecule 2
Cl(1)-Zn(1) 2.150(4)	Cl(2)-Zn(2) 2.157(4)
Zn(1)-N(1) 2.082(10)	Zn(2)-N(4) 2.053(10)
Zn(1)-N(2) 2.008(11)	Zn(2)-N(5) 2.044(9)
Zn(1)-N(3) 2.049(9)	Zn(2)-N(6) 2.006(11)
N(1)-C(2) 1.276(16)	N(4)-C(37) 1.263(15)
N(2)-C(14) 1.289(16)	N(5)-C(49) 1.279(16)
N(3)-C(25) 1.283(15)	N(6)-C(60) 1.311(16)
N(1)-C(7) 1.449(15)	N(4)-C(42) 1.469(18)
N(2)-C(16) 1.445(16)	N(5)-C(51) 1.442(14)
N(3)-C(27) 1.413(14)	N(6)-C(62) 1.487(16)
C(1)-C(2) 1.565(16)	C(36)-C(37) 1.570(16)
C(1)-C(14) 1.499(17)	C(36)-C(49) 1.563(17)
C(1)-C(25) 1.541(16)	C(36)-C(60) 1.537(17)
Cl(1)-Zn(1)-N(1) 120.4(3)	Cl(2)-Zn(2)-N(4) 120.8(3)
Cl(1)-Zn(1)-N(2) 132.6(3)	Cl(2)-Zn(2)-N(5) 122.3(3)
Cl(1)-Zn(1)-N(3) 120.2(3)	Cl(2)-Zn(2)-N(6) 129.4(3)
N(1)-Zn(1)-N(2) 90.8(4)	N(4)-Zn(2)-N(5) 89.5(4)
N(1)-Zn(1)-N(3) 90.4(4)	N(4)-Zn(2)-N(6) 93.3(4)
N(2)-Zn(1)-N(3) 91.5(4)	N(5)-Zn(2)-N(6) 91.2(4)
Zn(1)-N(1)-C(7) 116.6(8)	Zn(2)-N(4)-C(42) 115.7(8)
Zn(1)-N(2)-C(16) 124.0(8)	Zn(2)-N(5)-C(51) 124.6(8)
Zn(1)-N(3)-C(27) 125.1(8)	Zn(2)-N(6)-C(62) 127.2(8)
Zn(1)-N(1)-C(2) 116.0(8)	Zn(2)-N(4)-C(37) 118.6(9)
Zn(1)-N(2)-C(14) 114.6(8)	Zn(2)-N(5)-C(49) 114.5(8)
Zn(1)-N(3)-C(25) 113.2(7)	Zn(2)-N(6)-C(60) 113.8(8)
C(2)-N(1)-C(7) 127.3(10)	C(37)-N(4)-C(42) 125.6(11)
C(14)-N(2)-C(16) 120.7(10)	C(49)-N(5)-C(51) 120.9(10)
C(25)-N(3)-C(27) 121.7(9)	C(60)-N(6)-C(62) 119.0(10)
C(1)-C(2)-N(1) 115.2(11)	C(36)-C(37)-N(4) 112.5(11)
C(1)-C(14)-N(2) 118.8(10)	C(36)-C(49)-N(5) 116.5(10)
C(1)-C(25)-N(3) 119.1(9)	C(36)-C(60)-N(6) 117.5(10)
N(1)-C(2)-C(3) 125.6(10)	N(4)-C(37)-C(38) 131.7(11)
N(2)-C(14)-C(15) 123.5(11)	N(5)-C(49)-C(50) 126.4(11)
N(3)-C(25)-C(26) 124.4(10)	N(6)-C(60)-C(61) 125.6(11)
θ_T (C(1)-C(2)-N(1)-C(3)/$C(7)_{Ar}$) = 81.7(11)	θ_T (C(36)-C(37)-N(4)-C(38)/$C(42)_{Ar}$) = 87.4(11)
θ_T (C(1)-C(14)-N(2)-C(15)/$C(16)_{Ar}$) = 75.2(10)	θ_T (C(36)-C(49)-N(5)-C(50)/$C(51)_{Ar}$) = 70.9(11)
θ_T (C(1)-C(25)-N(3)-C(26)/$C(27)_{Ar}$) = 73.710)	θ_T (C(36)-C(60)-N(6)-C(61)/$C(62)_{Ar}$) = 64.3(11)

Rotation of the 2-methoxyphenyl substituent could potentially allow for closer interaction of the oxygen atom with the zinc centre, though this is prohibited by the steric influence of the *tert*-butyl group, which causes the aryl group to be fixed approximately orthogonal to the imine plane (**table 3.1**). Conversely, the aryl groups of the methyl-substituted imines are able to move further towards coplanarity, thus minimising unfavourable interactions between the three aryl moieties present in the molecule. The mean N-N distances (2.917(16) and 2.909(18) Å) are comparable to the value of 2.927(2) Å observed in **$(L^1)Mo(CO)_3$**, which may at first seem surprising when considering the much larger size of Mo^0 relative to Zn^{2+}. However, in a four-coordinate complex the inter- and intra-ligand repulsion is reduced in comparison to that which exists in a related six-coordinate complex. For a given metal-ligand distance, intra-ligand distances are larger in a tetrahedral complex than in a corresponding octahedral one, and as such the nitrogen atoms are able to move

further apart. It is also possible that this effect may be attributable to the presence of the *tert*-butyl substituent in $\mathbf{L^8}$, which is responsible for an increase in ligand steric bulk in comparison to $\mathbf{L^1}$, where the ligand backbone is entirely methyl-substituted.

The aforementioned steric effects are even more pronounced in the molecular structure of **$[(L^{12})ZnCl]_2[Zn_2Cl_6]$** (**figure 3.7**), where both of the 2-isopropylphenyl moieties move closer to coplanarity with the imines relative to the situation observed in **$[(L^8)ZnCl]_2[Zn_2Cl_6]$**, in order to accommodate the near-orthogonal mesityl group (**table 3.2**). The Zn-N distances differ very little from those in **$[(L^8)ZnCl]_2[Zn_2Cl_6]$**, whilst the mean N-N distance is slightly larger at 2.926(6) Å. Once again, the C(2)-N(1)-C(7) angle of 126.3(4)° is somewhat wider than the corresponding angles in the methyl-substituted imine groups (**table 3.2**). Additionally, the 2-isopropylphenyl substituents are oriented in opposite directions relative to each other, which implies that the steric demand of the mesityl group is not so great as to cause them to point in the same direction. The molecular structure of **$[(L^{16})ZnCl]_2[Zn_2Cl_6]$** (**figure 3.8**) does not deviate to any noticeable extent from the precedent set by **$[(L^8)ZnCl]_2[Zn_2Cl_6]$** and **$[(L^{12})ZnCl]_2[Zn_2Cl_6]$**, though in this case both of the 2-methoxyphenyl substituents, as well as N(1), are disordered over two sites, which is reflected in the rather low quality of the data (R = 10.51%). The mean N-N separation of 2.93(2) Å is very close to that observed in **$[(L^{12})ZnCl]_2[Zn_2Cl_6]$**. As seen previously in **$[(L^8)ZnCl]_2[Zn_2Cl_6]$**, the oxygen atoms from both of the methoxy groups point in the direction of the zinc atom, and due to the increased propensity of the N(2) aryl substituent to move towards coplanarity with the imine (**table 3.2**), the Zn(1)-O(2) distance (3.065(18) Å) is considerably shorter than Zn(1)-O(1) (3.40(3) Å). However, the former distance is still somewhat larger than the sum of the van der Waals' radii of oxygen and zinc (2.91 Å), which shows that there is an absence of any appreciable bonding interaction between the two atoms. The N(1) aryl substituent is also further from orthogonality than is the case for the analogous group in **$[(L^8)ZnCl]_2[Zn_2Cl_6]$**; the increased steric clash that this causes with the *tert*-butyl group is a direct effect of the need to minimise unfavourable interactions with the very bulky 2,6-diisopropylphenyl moiety. This is also manifested in the fact the both 2-methoxyphenyl groups point in the same direction, away from the 2,6-diisopropylphenyl group. However, the minor component of the disordered structure (not shown) has both 2-methoxyphenyl groups oriented towards the 2,6-diisopropylphenyl group, which suggest that such an arrangement is possible when the *ortho*-aryl substituents are small in size. Interestingly, the rearrangement of $\mathbf{L^{16}}$ to the β-triketimine tautomer

upon coordination to zinc generates a chiral centre at C(1), due to the fact that in this case none of the three imine moieties are identical.

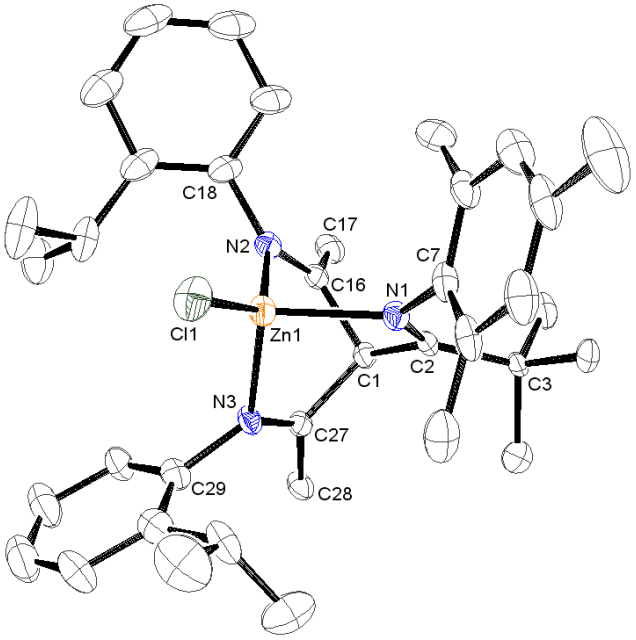

Figure 3.7 ORTEP representation of the cationic unit in $[(L^{12})ZnCl]_2[Zn_2Cl_6]$ with thermal ellipsoids set at the 50% probability level; hydrogen atoms omitted for clarity

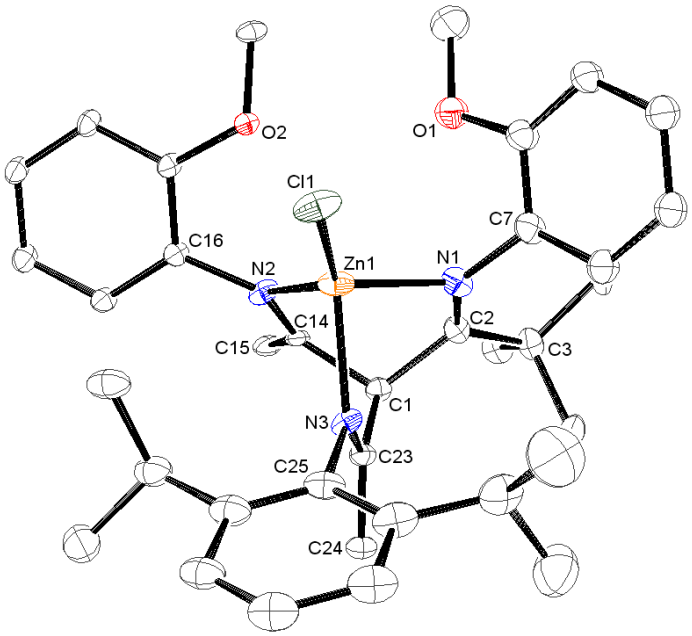

Figure 3.8 ORTEP representation of the cationic unit in $[(L^{16})ZnCl]_2[Zn_2Cl_6]$ with thermal ellipsoids set at the 30% probability level; hydrogen atoms omitted for clarity

Table 3.2 Selected bond lengths (Å), angles (°) and interplanar torsion angles (°) for the cationic units in $[(L^{12})ZnCl][Zn_2Cl_6]$ and $[(L^{16})ZnCl][Zn_2Cl_6]$

$[(L^{12})ZnCl]^+$	$[(L^{16})ZnCl]^+$
Cl(1)-Zn(1) 2.1444(16)	Cl(1)-Zn(1) 2.153(4)
Zn(1)-N(1) 2.054(4)	Zn(1)-N(1) 2.084(18)
Zn(1)-N(2) 2.028(4)	Zn(1)-N(2) 2.049(10)
Zn(1)-N(3) 2.045(3)	Zn(1)-N(3) 2.041(8)
N(1)-C(2) 1.266(6)	N(1)-C(2) 1.28(2)
N(2)-C(16) 1.269(6)	N(2)-C(14) 1.263(14)
N(3)-C(27) 1.262(6)	N(3)-C(23) 1.282(14)
N(1)-C(7) 1.457(6)	N(1)-C(7) 1.44(2)
N(2)-C(18) 1.440(6)	N(2)-C(16) 1.489(15)
N(3)-C(29) 1.449(6)	N(3)-C(25) 1.444(10)
C(1)-C(2) 1.546(6)	C(1)-C(2) 1.551(16)
C(1)-C(16) 1.549(7)	C(1)-C(14) 1.542(16)
C(1)-C(27) 1.540(6)	C(1)-C(23) 1.534(15)
Cl(1)-Zn(1)-N(1) 117.05(11)	Cl(1)-Zn(1)-N(1) 120.9(5)
Cl(1)-Zn(1)-N(2) 136.59(11)	Cl(1)-Zn(1)-N(2) 133.0(3)
Cl(1)-Zn(1)-N(3) 118.61(12)	Cl(1)-Zn(1)-N(3) 119.1(3)
N(1)-Zn(1)-N(2) 89.88(15)	N(1)-Zn(1)-N(2) 94.3(6)
N(1)-Zn(1)-N(3) 94.68(14)	N(1)-Zn(1)-N(3) 87.6(5)
N(2)-Zn(1)-N(3) 89.93(15)	N(2)-Zn(1)-N(3) 90.1(4)
Zn(1)-N(1)-C(7) 118.2(3)	Zn(1)-N(1)-C(7) 117.3(12)
Zn(1)-N(2)-C(18) 123.5(3)	Zn(1)-N(2)-C(16) 125.2(7)
Zn(1)-N(3)-C(29) 122.7(3)	Zn(1)-N(3)-C(25) 125.4(6)
Zn(1)-N(1)-C(2) 115.5(3)	Zn(1)-N(1)-C(2) 114.8(12)
Zn(1)-N(2)-C(16) 113.7(3)	Zn(1)-N(2)-C(14) 114.8(8)
Zn(1)-N(3)-C(27) 113.7(3)	Zn(1)-N(3)-C(23) 114.9(7)
C(2)-N(1)-C(7) 126.3(4)	C(2)-N(1)-C(7) 127.9(15)
C(16)-N(2)-C(18) 122.7(4)	C(14)-N(2)-C(16) 119.8(10)
C(27)-N(3)-C(29) 121.7(4)	C(23)-N(3)-C(25) 119.1(8)
C(1)-C(2)-N(1) 115.0(4)	C(1)-C(2)-N(1) 115.6(12)
C(1)-C(16)-N(2) 117.9(4)	C(1)-C(14)-N(2) 117.2(10)
C(1)-C(27)-N(3) 117.8(4)	C(1)-C(23)-N(3) 116.7(9)
N(1)-C(2)-C(3) 130.6(4)	N(1)-C(2)-C(3) 126.3(13)
N(2)-C(16)-C(17) 127.2(5)	N(2)-C(14)-C(15) 126.3(10)
N(3)-C(27)-C(28) 126.5(4)	N(3)-C(23)-C(24) 126.3(10)
θ_T (C(1)-C(2)-N(1)-C(3)/C(7)$_{Ar}$) = 85.7(4)	θ_T (C(1)-C(2)-N(1)-C(3)/C(7)$_{Ar}$) = 75.0(15)
θ_T (C(1)-C(16)-N(2)-C(17)/C(18)$_{Ar}$) = 57.8(5)	θ_T (C(1)-C(14)-N(2)-C(15)/C(16)$_{Ar}$) = 57.4(10)
θ_T (C(1)-C(27)-N(3)-C(28)/C(29)$_{Ar}$) = 64.7(4)	θ_T (C(1)-C(23)-N(3)-C(24)/C(25)$_{Ar}$) = 87.9(10)

Frustratingly, the ^{1}H NMR spectra of **$[(L)ZnCl]_2[Zn_2Cl_6]$** were found to be of little use for the characterisation of these complexes in solution, as in all cases more peaks than would be expected are observed, and all the peaks appear rather broadened. Additionally, the peaks lack any fine structure, and as such the ^{1}H NMR spectra do not warrant inclusion here. This effect may be due to an exchange process between the cationic zinc chloride unit and the hexachlorodizincate anion, and the inherent change in geometry and coordination number that this involves. However, all of the **$[(L)ZnCl]_2[Zn_2Cl_6]$** compounds gave satisfactory elemental analyses, and in all cases mass spectrometry showed the presence of $[(L)ZnCl]^+$ ions. These data provide strong supporting evidence that the crystal structures are representative of the bulk solid material, and that the complexes remain unchanged even following recrystallisation from coordinating solvents such as acetonitrile.

3.2.1.2 [(L)ZnCl][BAr$^F_4$] Complexes

Due to the difficulties in characterisation associated with the putative **[(L^1)ZnCl][Cl]** complex, it was deemed that *in situ* metathesis of this with NaBAr$^F_4$ would likely give access to a crystalline derivative. The weakly-coordinating BAr$^F_4$ anion is renowned for its ability to stabilise cationic metal complexes, and its relativley high degree of soubility in organic solvents aids efficient crystallisation.[345] Indeed, the reaction of equimolar amounts of **L^1**, $ZnCl_2$ and NaBAr$^F_4$ in THF, followed by replacement of the solvent with DCM and overlayering of this with hexane produced crystalline **[(L^1)ZnCl][BAr$^F_4$]** (**scheme 3.7**). The analogous reactions employing **L^5**, **L^8** and **L$^{10\text{-}12}$** were also found to give access to the corresponding **[(L)ZnCl][BAr$^F_4$]** complexes (**scheme 3.7**).

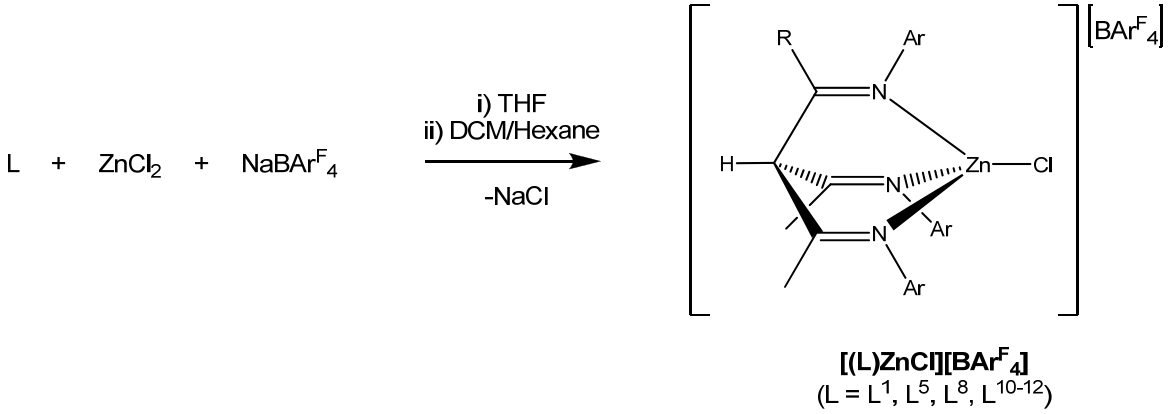

Scheme 3.7 Synthesis of [(L)ZnCl][BAr$^F_4$] complexes

[(L^1)ZnCl][BAr$^F_4$] crystallises as a DCM solvate, with two unique cationic units in the unit cell; the molecular structure of one of these is presented in **figure 3.9**. The Zn-N distances (**table 3.3**) and mean N-N separations (2.95(2) and 2.91(3) Å) do not differ by any significant degree from those seen in **[(L)ZnCl]$_2$[Zn$_2$Cl$_6$]**, though the sizeable difference in the latter parameters observed between the two unique cations may be a result of the rather low quality of the data (R = 9.69%). In contrast to the situation in **[(L)ZnCl]$_2$[Zn$_2$Cl$_6$]**, the absence of a bulky backbone *tert*-butyl substituent in this case causes all the C=N-C$_{Ar}$ angles to be roughly equivalent (**table 3.3**). All but one of the aryl groups are twisted away from orthogonality with the imines by up to 28°, which suggests that the rotation about the N-C$_{Ar}$ bonds occurs more freely than in **(L^1)M(CO)$_3$**, where all the aryl moieties lie approximately orthogonal to the imines. This is concurrent with the aforementioned notion that intraligand repulsion in a tetrahedral complex is reduced in comparison to that in an octahedral complex of the same ligand.

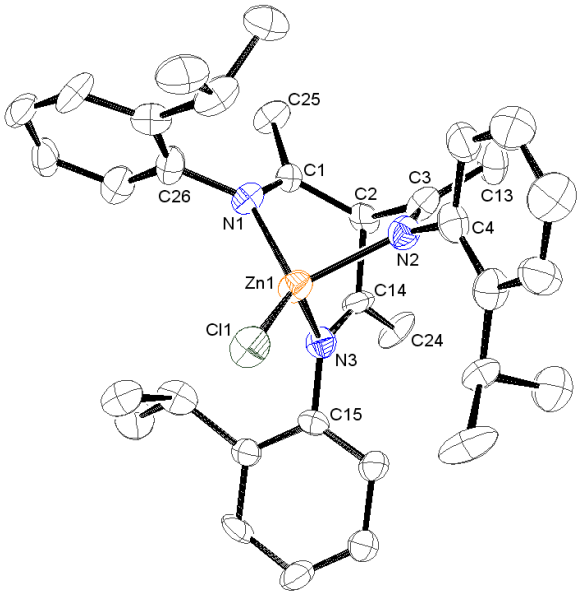

Figure 3.9 ORTEP representation of one of the cationic units in $[(L^1)ZnCl][BAr^F{}_4].½CH_2Cl_2$ with thermal ellipsoids set at the 30% probability level; hydrogen atoms omitted for clarity

Table 3.3 Selected bond lengths (Å), angles (°) and interplanar torsion angles (°) for the two unique cations in $[(L^1)ZnCl][BAr^F{}_4].½CH_2Cl_2$

$[(L^1)ZnCl]^+$ molecule 1	$[(L^1)ZnCl]^+$ molecule 2
Zn(1)-Cl(1) 2.143(3)	Zn(2)-Cl(2) 2.136(3)
Zn(1)-N(1) 2.032(10)	Zn(2)-N(4) 1.986(10)
Zn(1)-N(2) 2.054(10)	Zn(2)-N(5) 2.032(13)
Zn(1)-N(3) 2.070(11)	Zn(2)-N(6) 2.049(11)
N(1)-C(1) 1.278(17)	N(4)-C(35) 1.275(18)
N(2)-C(3) 1.282(18)	N(5)-C(37) 1.26(2)
N(3)-C(14) 1.268(17)	N(6)-C(48) 1.268(18)
N(1)-C(26) 1.475(15)	N(4)-C(60) 1.459(17)
N(2)-C(4) 1.411(18)	N(5)-C(38) 1.44(3)
N(3)-C(15) 1.44(2)	N(6)-C(49) 1.448(19)
C(1)-C(2) 1.541(17)	C(35)-C(36) 1.497(17)
C(2)-C(3) 1.567(9)	C(36)-C(37) 1.54(2)
C(2)-C(14) 1.54(2)	C(36)-C(48) 1.577(19)
Cl(1)-Zn(1)-N(1) 128.7(3)	Cl(2)-Zn(2)-N(4) 126.2(3)
Cl(1)-Zn(1)-N(2) 119.2(3)	Cl(2)-Zn(2)-N(5) 128.2(5)
Cl(1)-Zn(1)-N(3) 123.6(4)	Cl(2)-Zn(2)-N(6) 117.0(3)
N(1)-Zn(1)-N(2) 92.7(4)	N(4)-Zn(2)-N(5) 91.6(5)
N(1)-Zn(1)-N(3) 90.8(4)	N(4)-Zn(2)-N(6) 91.2(4)
N(2)-Zn(1)-N(3) 92.2(4)	N(5)-Zn(2)-N(6) 92.8(5)
Zn(1)-N(1)-C(26) 123.8(8)	Zn(2)-N(4)-C(60) 122.9(9)
Zn(1)-N(2)-C(4) 123.1(9)	Zn(2)-N(5)-C(38) 124.1(9)
Zn(1)-N(3)-C(15) 122.4(7)	Zn(2)-N(6)-C(49) 123.6(9)
Zn(1)-N(1)-C(1) 113.9(8)	Zn(2)-N(4)-C(35) 115.2(8)
Zn(1)-N(2)-C(3) 115.0(9)	Zn(2)-N(5)-C(37) 112.9(11)
Zn(1)-N(3)-C(14) 112.9(11)	Zn(2)-N(6)-C(48) 114.3(9)
C(1)-N(1)-C(26) 122.3(10)	C(35)-N(4)-C(60) 121.9(11)
C(3)-N(2)-C(4) 121.8(12)	C(37)-N(5)-C(38) 122.3(13)
C(14)-N(3)-C(15) 122.9(11)	C(48)-N(6)-C(49) 122.0(12)
N(1)-C(1)-C(2) 116.9(11)	N(4)-C(35)-C(36) 117.2(11)
N(2)-C(3)-C(2) 114.7(11)	N(5)-C(37)-C(36) 118.0(13)
N(3)-C(14)-C(2) 116.7(12)	N(6)-C(48)-C(36) 116.2(12)
N(1)-C(1)-C(25) 126.1(10)	N(4)-C(35)-C(59) 127.7(11)
N(2)-C(3)-C(13) 127.4(12)	N(5)-C(37)-C(47) 126.4(14)
N(3)-C(14)-C(24) 125.1(13)	N(6)-C(48)-C(58) 125.1(12)
θ_T (C(2)-C(1)-N(1)-C(25)/C(26)$_{Ar}$) = 70.2(11)	θ_T (C(36)-C(35)-N(4)-C(59)/C(60)$_{Ar}$) = 85.7(11)
θ_T (C(2)-C(3)-N(2)-C(13)/C(4)$_{Ar}$) = 66.6(12)	θ_T (C(36)-C(37)-N(5)-C(47)/C(38)$_{Ar}$) = 62.5(14)
θ_T (C(2)-C(14)-N(3)-C(24)/C(15)$_{Ar}$) = 72.6(13)	θ_T (C(36)-C(48)-N(6)-C(58)/C(49)$_{Ar}$) = 67.7(12)

An increased propensity for rotation about the N-C_{Ar} bonds in four-coordinate β-triketimine complexes is also supported by the ^{1}H NMR spectrum of **[(L^1)ZnCl][BAr^F_4]** (**figure 3.10**), which does not feature a conspicuous pair of doublets arising due to the inequivalence of the isopropyl methyl protons, as seen in both free $\mathbf{L^1}$ and **(L^1)M(CO)$_3$**. Instead, a broadened pair of resonances at 1.05 and 1.11 ppm are observed, which appear to be in the process of coalescing to a single doublet. This gives good indication that, in four-coordinate complexes of $\mathbf{L^1}$, rotation of the aryl groups about the N-C_{Ar} bonds is faster than in the related six-coordinate complexes, and occurs at a rate that is comparable to the NMR timescale. In contrast to the complicated spectra observed for **[(L)ZnCl]$_2$[Zn_2Cl_6]**, the ^{1}H NMR spectrum of **[(L^1)ZnCl][BAr^F_4]** is consistent with there being no structural change upon dissolution in chlorinated solvents. Additionally, the spectrum is very similar to that observed for **[(L^1)ZnCl][Cl]**, which adds credence to the assumption that the latter complex forms a monomeric, four-coordinate complex in DMSO solution, in which the β-triketimine ligand is tridentately coordinated.

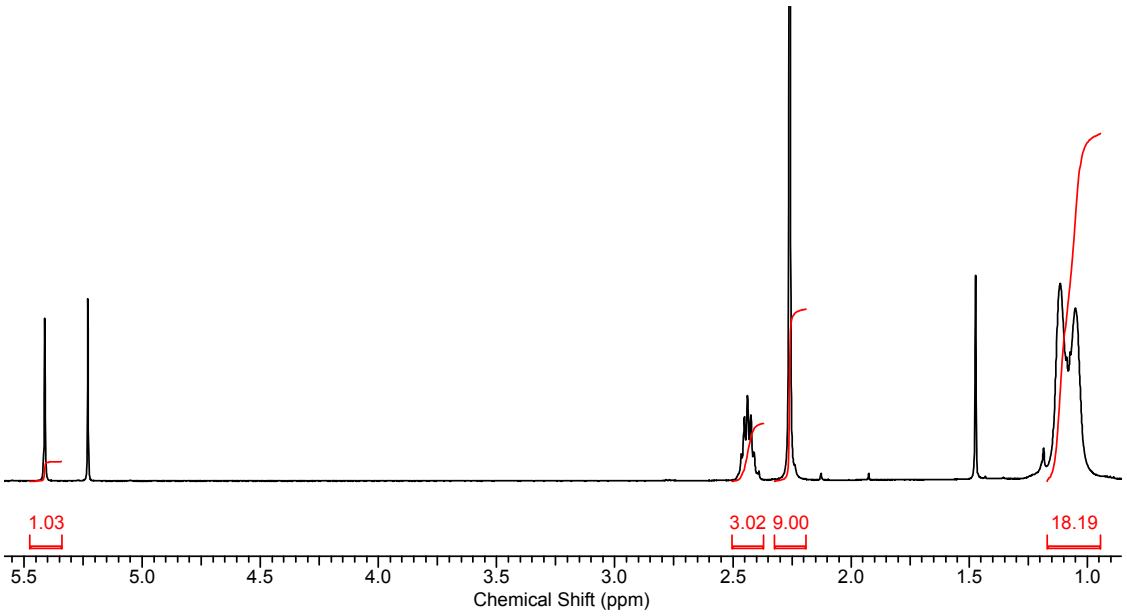

Figure 3.10 ^{1}H NMR spectrum of [(L^1)ZnCl][BAr^F_4] in $CDCl_3$, aryl region not shown; peaks at 1.19 ppm (hexane, CH_2), 1.47 ppm (H_2O) and 5.23 ppm (DCM) are due to solvent contaminants

In contrast to **[(L^1)ZnCl][BAr^F_4]**, the ^{1}H NMR spectrum of **[(L^5)ZnCl][BAr^F_4]**, which features a single additional aryl isopropyl substituent with respect to the former compound, shows three sharp isopropyl methyl resonances in a ratio of 12:6:6 (**experimental**). The larger resonance is due to the methyl protons of the 2-isopropylphenyl groups, while the two smaller resonances are due to the inequivalent methyl protons of the 2,6-diisopropylphenyl group. Considering the aforementioned solution-phase behaviour of

[(L^1)ZnCl][BAr$^F_4$], it may have been expected that if rotation about the N-C_{Ar} bonds of the 2-isopropylphenyl groups in **[(L^5)ZnCl][BAr$^F_4$]** was similarly rapid, then only two isopropyl methyl resonances would be observed. However, the introduction of a single additional isopropyl group in **[(L^5)ZnCl][BAr$^F_4$]** removes the availability of any accessible conformation in which a molecular plane of symmetry bisects the methyls of the 2,6-diisopropylphenyl group, and as such three resonances are observed even if rotation of the 2-isopropylphenyl groups is relatively fast (**figure 3.11**). In the case of **[(L^1)ZnCl][BAr$^F_4$]**, a plane of symmetry able to bisect the methyls of the 2-isopropylphenyl groups does exist, and a single doublet may be observed provided rotation about the N-C_{Ar} bonds is fast (**figure 3.11**). A pair of resonances is actually observed, though these appear to be in the process of coalescing into a single doublet at room temperature. The fact that they are not completely coalesced suggests that the rotation of the 2-isopropylphenyl groups in **[(L^1)ZnCl][BAr$^F_4$]** may occur more slowly than in **[(L^5)ZnCl][BAr$^F_4$]**, where rapid N-C_{Ar} rotation results in only a single resonance being observed for the methyls of both 2-isopropylphenyl groups (**figure 3.11**). Due to the fact that the ^{1}H NMR spectrum of **[(L^{11})ZnCl][BAr$^F_4$]** (where the R^7 methyl substituent of **L^5** is replaced by a *tert*-butyl group) displays four unique methyl resonances (**experimental**), it is likely that one less resonance is observed for **[(L^5)ZnCl][BAr$^F_4$]** as a result of increased freedom of rotation about the N-C_{Ar} bonds as a result of the reduced steric bulk of **L^5** in comparison to **L^{11}**. By forcing the 2,6-diisopropylphenyl moiety further towards the other aryl substituents, the *tert*-butyl group is effectively acting as a 'brake' to rotation about the N-C_{Ar} bonds (**figure 3.11**).

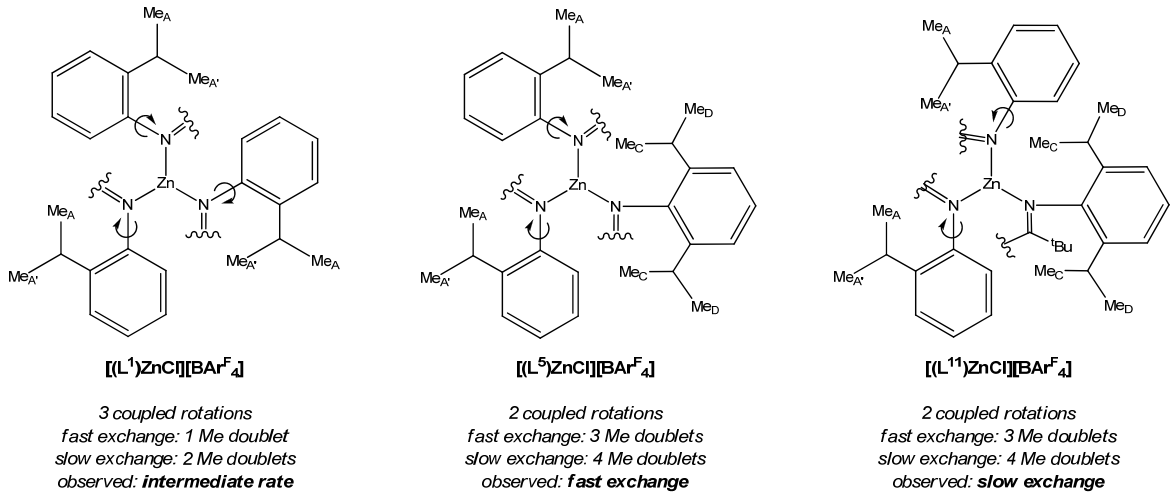

Figure 3.11 Effect of rate of N-C_{Ar} rotation on ^{1}H NMR spectra of β-triketimine zinc complexes

The molecular structure of the cation in **[(L^8)ZnCl][BAr$^F_4$].1½CH$_2$Cl$_2$** (**figure 3.12**) is similar to those in **[(L^8)ZnCl]$_2$[Zn$_2$Cl$_6$]**, though there are some small yet significant differences. The mean N-N separation (2.888(5) Å) is slightly less than those seen in the two independent cations of **[(L^8)ZnCl]$_2$[Zn$_2$Cl$_6$]**, while the Zn-O distance (3.045(5) Å) is much shorter, which signifies an increased degree of interaction between the oxygen atom and the zinc centre, though this distance is still well outside what could reasonably be termed a bonding interaction. The reduced Zn-O separation causes the 2-methoxyphenyl group to move much further towards coplanarity with the imine (**table 3.4**) in comparison to the situation in **[(L^8)ZnCl]$_2$[Zn$_2$Cl$_6$]**, and to accommodate this arrangement both of the 2-isopropylphenyl group lie approximately orthogonal to the planes defined by their respective imine substituents. The increased propensity for interaction of the oxygen atom with the zinc centre in this instance is likely due to a combination of crystal-packing effects, and a reduced level of interaction between the cation and the very weakly coordinating BAr$^F_4$ anion. In contrast to the subtle differences observed between **[(L^8)ZnCl][BAr$^F_4$]** and **[(L^8)ZnCl]$_2$[Zn$_2$Cl$_6$]**, the molecular structure of the cation in **[(L^{12})ZnCl][BAr$^F_4$]** (**figure 3.13**) was found to be essentially identical to its $Zn_2Cl_6^{2-}$ analogue, with none of the structural parameters (**table 3.4**) differing by any noteworthy degree. The mean N-N distance (2.922(5) Å) is essentially identical to that observed in **[(L^{12})ZnCl]$_2$[Zn$_2$Cl$_6$]**.

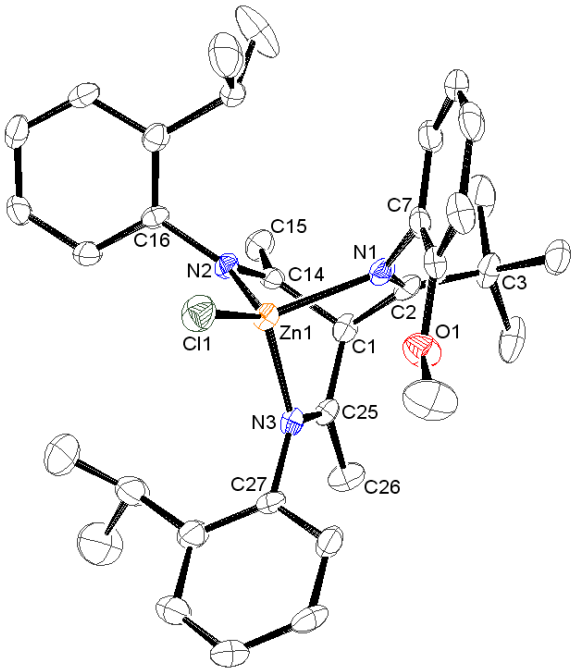

Figure 3.12 ORTEP representation of the cationic unit in [(L^8)ZnCl][BAr$^F_4$].1½CH$_2$Cl$_2$ with thermal ellipsoids set at the 50% probability level; hydrogen atoms omitted for clarity

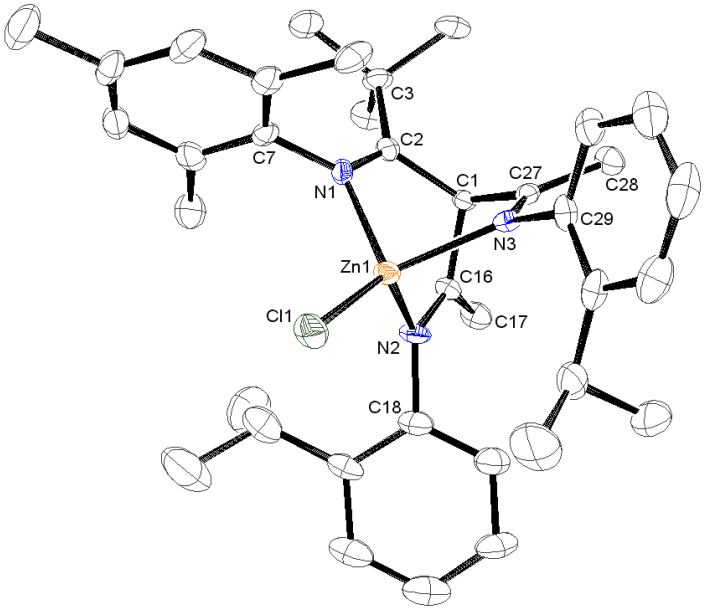

Figure 3.13 ORTEP representation of the cationic unit in $[(L^{12})ZnCl][BAr^{F}_{4}]$ with thermal ellipsoids set at the 50% probability level; hydrogen atoms omitted for clarity

Table 3.4 Selected bond lengths (Å), angles (°) and interplanar torsion angles (°) for the cationic units in $[(L^{8})ZnCl][BAr^{F}_{4}].1½CH_2Cl_2$ and $[(L^{12})ZnCl][BAr^{F}_{4}]$

$[(L^{8})ZnCl]^{+}$	$[(L^{12})ZnCl]^{+}$
Cl(1)-Zn(1) 2.1439(11)	Cl(1)-Zn(1) 2.1478(13)
Zn(1)-N(1) 2.070(3)	Zn(1)-N(1) 2.043(3)
Zn(1)-N(2) 2.050(3)	Zn(1)-N(2) 2.035(3)
Zn(1)-N(3) 2.025(3)	Zn(1)-N(3) 2.050(3)
N(1)-C(2) 1.280(5)	N(1)-C(2) 1.293(5)
N(2)-C(14) 1.282(5)	N(2)-C(16) 1.277(5)
N(3)-C(25) 1.280(5)	N(3)-C(27) 1.270(5)
N(1)-C(7) 1.434(5)	N(1)-C(7) 1.441(5)
N(2)-C(16) 1.457(5)	N(2)-C(18) 1.470(5)
N(3)-C(27) 1.452(5)	N(3)-C(29) 1.455(5)
C(1)-C(2) 1.549(6)	C(1)-C(2) 1.537(5)
C(1)-C(14) 1.531(6)	C(1)-C(16) 1.533(5)
C(1)-C(25) 1.527(6)	C(1)-C(27) 1.540(5)
Cl(1)-Zn(1)-N(1) 128.31(9)	Cl(1)-Zn(1)-N(1) 120.33(10)
Cl(1)-Zn(1)-N(2) 125.53(9)	Cl(1)-Zn(1)-N(2) 123.16(10)
Cl(1)-Zn(1)-N(3) 122.69(9)	Cl(1)-Zn(1)-N(3) 129.39(9)
N(1)-Zn(1)-N(2) 87.70(12)	N(1)-Zn(1)-N(2) 93.07(13)
N(1)-Zn(1)-N(3) 90.37(11)	N(1)-Zn(1)-N(3) 90.89(12)
N(2)-Zn(1)-N(3) 90.93(11)	N(2)-Zn(1)-N(3) 90.09(12)
Zn(1)-N(1)-C(7) 112.2(2)	Zn(1)-N(1)-C(7) 116.3(2)
Zn(1)-N(2)-C(16) 124.0(2)	Zn(1)-N(2)-C(18) 122.1(3)
Zn(1)-N(3)-C(27) 120.7(2)	Zn(1)-N(3)-C(29) 123.9(2)
Zn(1)-N(1)-C(2) 117.9(3)	Zn(1)-N(1)-C(2) 115.6(3)
Zn(1)-N(2)-C(14) 114.9(3)	Zn(1)-N(2)-C(16) 113.7(3)
Zn(1)-N(3)-C(25) 116.1(2)	Zn(1)-N(3)-C(27) 114.0(2)
C(2)-N(1)-C(7) 129.9(3)	C(2)-N(1)-C(7) 128.1(3)
C(14)-N(2)-C(16) 121.0(3)	C(16)-N(2)-C(18) 122.3(3)
C(25)-N(3)-C(27) 123.2(3)	C(27)-N(3)-C(29) 122.0(3)
C(1)-C(2)-N(1) 113.9(3)	C(1)-C(2)-N(1) 115.1(3)
C(1)-C(14)-N(2) 118.1(4)	C(1)-C(16)-N(2) 118.1(3)
C(1)-C(25)-N(3) 117.5(3)	C(1)-C(27)-N(3) 117.6(3)
N(1)-C(2)-C(3) 128.9(4)	N(1)-C(2)-C(3) 129.7(3)
N(2)-C(14)-C(15) 124.9(4)	N(2)-C(16)-C(17) 125.6(3)
N(3)-C(25)-C(26) 124.4(3)	N(3)-C(27)-C(28) 125.8(3)
θ_T (C(1)-C(2)-N(1)-C(3)/$C(7)_{Ar}$) = 68.8(4)	θ_T (C(1)-C(2)-N(1)-C(3)/$C(7)_{Ar}$) = 82.3(3)
θ_T (C(1)-C(14)-N(2)-C(15)/$C(16)_{Ar}$) = 83.6(4)	θ_T (C(1)-C(16)-N(2)-C(17)/$C(18)_{Ar}$) = 67.9(3)
θ_T (C(1)-C(25)-N(3)-C(26)/$C(27)_{Ar}$) = 90.0(3)	θ_T (C(1)-C(27)-N(3)-C(28)/$C(29)_{Ar}$) = 63.9(3)

As already discussed briefly with regard to **[(L^{11})ZnCl][BAr$^{F}_{4}$]**, the ^{1}H NMR spectra of **[(L)ZnCl][BAr$^{F}_{4}$]** (**L** = **L^{8}**, **L$^{10\text{-}12}$**) are consistent with the complexes being of very low symmetry, in analogy with the ^{1}H NMR spectra observed for **(L)M(CO)$_3$** complexes where the β-triketimine ligand has an R^{7} *tert*-butyl substituent (**chapter 2**). To illustrate this, the ^{1}H NMR spectrum of **[(L^{10})ZnCl][BAr$^{F}_{4}$]** is presented in **figure 3.14**, and shows three individual septet resonances at 2.48, 2.54 and 2.63 ppm, which correspond to the three unique isopropyl methine protons. These resonances are all slightly overlapped, and in turn also overlap with the two backbone methyl singlet resonances, which appear at 2.39 and 2.43 ppm. Six overlapping isopropyl methyl doublets are observed over the range 1.10-1.30 ppm, though one of these is obscured by the *tert*-butyl singlet resonance at 1.23 ppm.

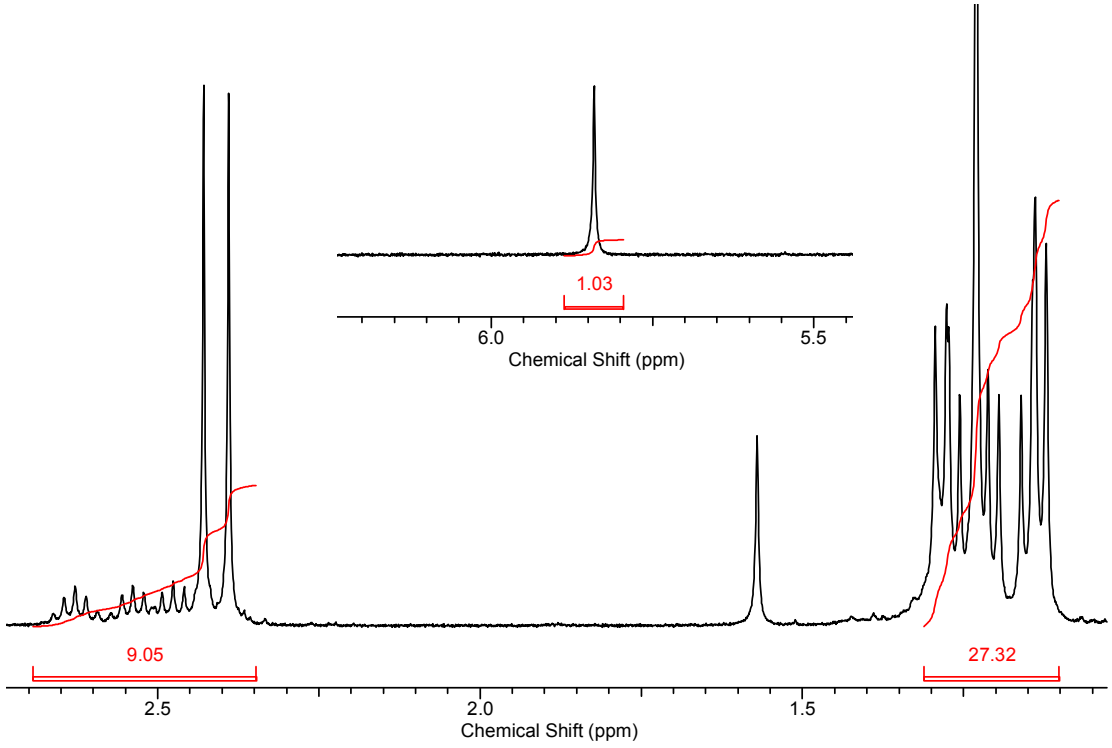

Figure 3.14 ^{1}H NMR spectrum of [(L^{10})ZnCl][BAr$^{F}_{4}$] in $CDCl_3$, aryl region not shown; peak at 1.57 ppm (H_2O) is due to solvent contaminant

To further illustrate the degree of asymmetry in these complexes, the ^{1}H NMR spectrum of **[(L^{12})ZnCl][BAr$^{F}_{4}$]** (**experimental**) displays a unique resonance for each of the three methyl groups of the mesityl substituent, and the two aryl protons of this moiety also appear as two distinct singlets. As before, the four isopropyl methyl groups, the two isopropyl methine protons and two backbone methyl groups also all appear as distinct

resonances. These observations confirm that the backbone *tert*-butyl substituent acts as an effective brake towards rotation about the N-C_{Ar} bonds of 2-isopropylphenyl groups.

3.2.1.3 $[(\eta^4\text{-}L^{16})ZnCl][BAr^F{}_4]$

The product arising from the reaction of equimolar amounts of $\mathbf{L^{16}}$, $ZnCl_2$ and $NaBAr^F{}_4$ was assumed to be a tetrahedral complex, in analogy with $\mathbf{[(L^{16})ZnCl]_2[Zn_2Cl_6]}$. However, X-ray crystallography revealed that in $\mathbf{[(\eta^4\text{-}L^{16})ZnCl][BAr^F{}_4]}$, the oxygen donor of the N(2) 2-methoxyphenyl moiety is also coordinated to the zinc centre, giving a five-coordinate complex that displays a very distorted ($\tau = 0.27$)[346] square-pyramidal geometry (**figure 3.15**). This behaviour is consistent with that observed in $\mathbf{[(L^8)ZnCl][BAr^F{}_4]}$, where the Zn-O distance, though outside the range of a bonding interaction, is much shorter than in the corresponding $Zn_2Cl_6^{2-}$ salt. Relatively free rotation about the N(2)-C(7) bond due to the absence of any bulky substituents allows O(2) to approach the zinc centre much more closely than is permitted for O(1) (O(1)-Zn(1) = 3.368(4) Å). This, coupled with the likely reduced propensity for interaction of the $BAr^F{}_4$ anion with the cationic complex relative to the $Zn_2Cl_6^{2-}$ ion, enables $\mathbf{L^{16}}$ to act as a tetradentate *N,N′,N″,O*-donor ligand.

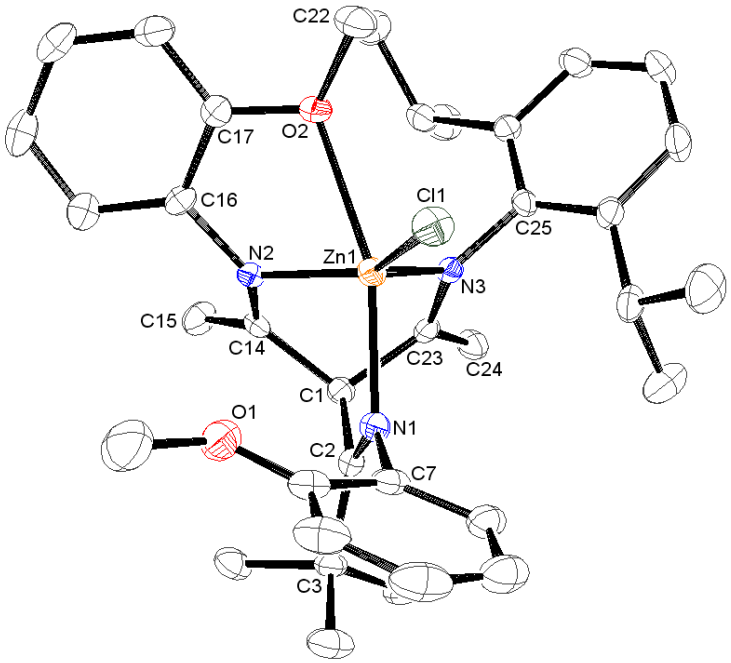

Figure 3.15 ORTEP representation of the cationic unit in $[(\eta^4\text{-}L^{16})ZnCl][BAr^F{}_4]$ with thermal ellipsoids set at the 50% probability level; hydrogen atoms omitted for clarity

Table 3.5 Selected bond lengths (Å), angles (°) and interplanar torsion angles (°) for the cationic unit in $[(\eta^4\text{-}L^{16})ZnCl][BAr^F{}_4]$

Zn(1)-Cl(1) 2.1936(6)	N(1)-Zn(1)-O(2) 159.68(5)
Zn(1)-O(1) 2.3891(14)	N(2)-Zn(1)-O(2) 70.92(5)
Zn(1)-N(1) 2.1134(16)	N(3)-Zn(1)-O(2) 92.56(5)
Zn(1)-N(2) 2.0580(16)	Zn(1)-O(2)-C(17) 109.24(11)
Zn(1)-N(3) 2.0642(16)	Zn(1)-O(2)-C(22) 122.55(13)
N(1)-C(2) 1.278(3)	Zn(1)-N(1)-C(7) 115.34(13)
N(2)-C(14) 1.279(2)	Zn(1)-N(2)-C(16) 117.37(12)
N(3)-C(23) 1.281(3)	Zn(1)-N(3)-C(25) 120.89(12)
N(1)-C(7) 1.439(3)	Zn(1)-N(1)-C(2) 117.03(13)
N(2)-C(16) 1.444(2)	Zn(1)-N(2)-C(14) 116.69(13)
N(3)-C(25) 1.455(2)	Zn(1)-N(3)-C(23) 115.83(13)
C(1)-C(2) 1.539(3)	C(2)-N(1)-C(7) 126.93(16)
C(1)-C(14) 1.547(3)	C(14)-N(2)-C(16) 123.45(16)
C(1)-C(23) 1.543(3)	C(23)-N(3)-C(25) 123.28(16)
O(2)-C(17) 1.379(2)	C(1)-C(2)-N(1) 115.24(16)
O(2)-C(22) 1.451(3)	C(1)-C(14)-N(2) 116.66(17)
	C(1)-C(23)-N(3) 117.86(17)
Cl(1)-Zn(1)-N(1) 106.50(5)	N(1)-C(2)-C(3) 130.25(17)
Cl(1)-Zn(1)-N(2) 143.61(5)	N(2)-C(14)-C(15) 126.98(18)
Cl(1)-Zn(1)-N(3) 123.76(5)	N(3)-C(23)-C(24) 125.93(18)
Cl(1)-Zn(1)-O(2) 89.47(4)	
N(1)-Zn(1)-N(2) 88.88(6)	θ_T (C(1)-C(2)-N(1)-C(3)/C(7)$_{Ar}$) = 85.56(17)
N(1)-Zn(1)-N(3) 88.90(6)	θ_T (C(1)-C(14)-N(2)-C(15)/C(16)$_{Ar}$) = 49.39(18)
N(2)-Zn(1)-N(3) 88.44(6)	θ_T (C(1)-C(23)-N(3)-C(24)/C(25)$_{Ar}$) = 76.12(18)

In order to accommodate the additional coordination of the methoxy group, the 2,6-diisopropylphenyl substituent is forced to move much further away from orthogonality (**table 3.5**) with the imine plane than was observed in **$[(L^{16})ZnCl]_2[Zn_2Cl_6]$**. The Zn(1)-N(1) distance of 2.1134(16) is noticeably longer (~0.06 Å) than the Zn(1)-N(2) and Zn(1)-N(3) distances, which is a result of the *trans*-influence of the coordinated methoxy group.[347] Structurally characterised cationic N_3OZnCl complexes are rare,[348] and none of these feature a coordinated 2-methoxyphenyl moiety. The structural parameters of **$[(\eta^4\text{-}L^{16})ZnCl][BAr^F{}_4]$** compare most closely to a cationic zinc chloride complex of a tridentate 'tethered nucleobase' ligand, which also features one coordinated water molecule.[349] However, the Zn-O distance in this complex is much shorter than that in **$[(\eta^4\text{-}L^{16})ZnCl][BAr^F{}_4]$**, which is likely due to a combination of increased steric hindrance in the latter compound, and the increased electron-donating ability of H_2O relative to the very weakly-donating aryl ether functionality. This also accounts for the fact that the Zn-Cl distance in the former complex is much longer than in **$[(\eta^4\text{-}L^{16})ZnCl][BAr^F{}_4]$**, the increased strength of the Zn-Cl interaction compensating for a considerably weakened Zn-O bond. There are only nine structurally characterised five-coordinate complexes of zinc which feature a coordinated methoxyphenyl group known in the literature, and the Zn(1)-O(2) distance (2.3891(14) Å) in **$[(\eta^4\text{-}L^{16})ZnCl][BAr^F{}_4]$** lies very close to the mean (2.361 Å) of previously reported values for such Zn-O bond lengths (range: 2.275-2.557 Å).[350]

Additionally, the Zn(1)-O(2) bond length is very similar to the values of 2.391(2) and 2.406(3) Å seen in a dinuclear methylzinc complex of a bis(methoxy)-substituted calixarene ligand.[351]

The ^{1}H NMR spectrum of **[(L^{16})ZnCl][BAr$^{F}_{4}$]** displays two sets of peaks, which are representative of major and minor components in solution. A number of the resonances appear rather broadened, which is indicative of a relatively slow change in coordination number at the zinc centre in solution. In particular, the chemical shifts (3.53 and 3.63 ppm) of the two singlets which correspond to the methoxy groups of the major component are essentially unchanged from those observed for the free ligand (3.54 and 3.65 ppm), which suggests that the major component in solution is a tetrahedral complex in which the degree of interaction of either methoxy group with the zinc centre is negligible. Conversely, the two methoxy resonances of the minor component in solution are separated by 0.57 ppm, with one resonance (3.91 ppm) shifted to higher frequency relative to the major component, whilst the other (3.34 ppm) is shifted to lower frequency. This effect could possibly be due to the methoxy group being coordinated to the zinc centre in the minor component, as observed in the solid state structure, which causes the OMe resonance to be shifted to higher frequency relative to that observed in the free ligand. A simple difference in conformation of the aryl groups in the four- and five-coordinate complexes is likely responsible for the fact that signal due to the non-coordinated methoxy group is shifted to lower frequency. Alternatively, both components in solution may be four-coordinate complexes, and their differing chemical shifts maybe due to the presence of diastereoisomers, arising from a combination of the chiral centre in **L^{16}** with the inherent axial chirality that results from the restricted rotation of the aryl groups in the coordinated ligand. The fact that **[(L^{16})M(CO)$_3$]** (M = Cr, Mo) also exist as pairs of isomers in solution suggests that the latter hypothesis is true, as additional coordination of the methoxy group to give seven-coordinate complexes is very unlikely due to steric considerations, and all the experimental data are consistent with the carbonyl adducts being six-coordinate. As such, it can reasonably be assumed that coordination of the methoxy group in **[(L^{16})ZnCl][BAr$^{F}_{4}$]** does not occur in solution, or occurs only transiently.

3.2.1.4 [(L)ZnCl][OTf] Complexes

In order to investigate further the effect of the anion on the properties of cationic β-triketimine zinc chloride complexes, it was decided to prepare a series of β-triketimine zinc chloride complexes where the BAr^F_4 anion is replaced by the smaller and less weakly-coordinating triflate ion. The synthetic procedure utilised for the preparation of **[(L)ZnCl][OTf]** (**scheme 3.8**) is essentially identical to that employed for the synthesis of **[(L)ZnCl][BAr^F_4]**, though the products may be precipitated by the addition of Et_2O, which is not possible for the latter complexes due to their appreciable solubility in Et_2O.

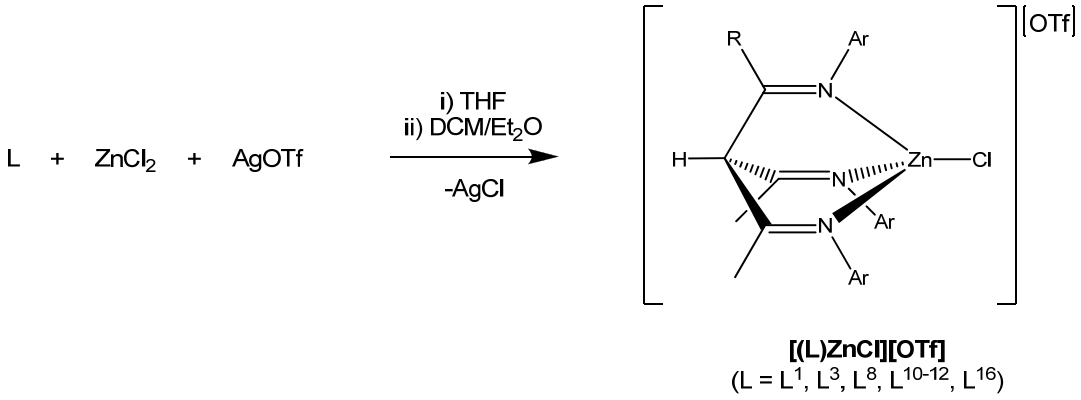

[(L)ZnCl][OTf]
(L = L^1, L^3, L^8, L^{10-12}, L^{16})

Scheme 3.8 Synthesis of [(L)ZnCl][OTf] complexes

Single crystals of all the **[(L)ZnCl][OTf]** complexes were easily obtained by diffusion of Et_2O into concentrated DCM solutions, though not all of these were suitable for X-ray diffraction. **[(L^8)ZnCl][OTf]** was found to crystallise as an Et_2O solvate, though the solvent molecule was highly disordered and was therefore removed from the model using the SQUEEZE function in PLATON.[352] The cationic unit is displayed in **figure 3.16**, and the structural parameters (**table 3.6**) are very similar to those of the two unique cations in **[(L^8)ZnCl]$_2$[Zn_2Cl_6]**. The mean N-N separation (2.886(3) Å) is slightly shorter than in the latter complex, yet is almost identical to the analogous distance in **[(L^8)ZnCl][BAr^F_4]**. However, the Zn(1)-O(1) distance (3.480(3) Å) in **[(L^8)ZnCl][OTf]** is much greater than in the corresponding $BAr^F_4{}^-$ compound, this likely being a result of an increased level of cation-anion interaction in the triflate salt relative to the $BAr^F_4{}^-$ salt. The molecular structure of the cation in **[(L^{12})ZnCl][OTf]** (**figure 3.17**) is essentially identical to those of the aforementioned $BAr^F_4{}^-$ and $Zn_2Cl_6{}^{2-}$ derivatives, save for slight differences in the orientation of the 2-isopropylphenyl groups (**table 3.6**), and a very small increase in the mean N-N distance of 2.932(2) Å, as compared to 2.922(5) and 2.926(6) Å in the latter compounds respectively.

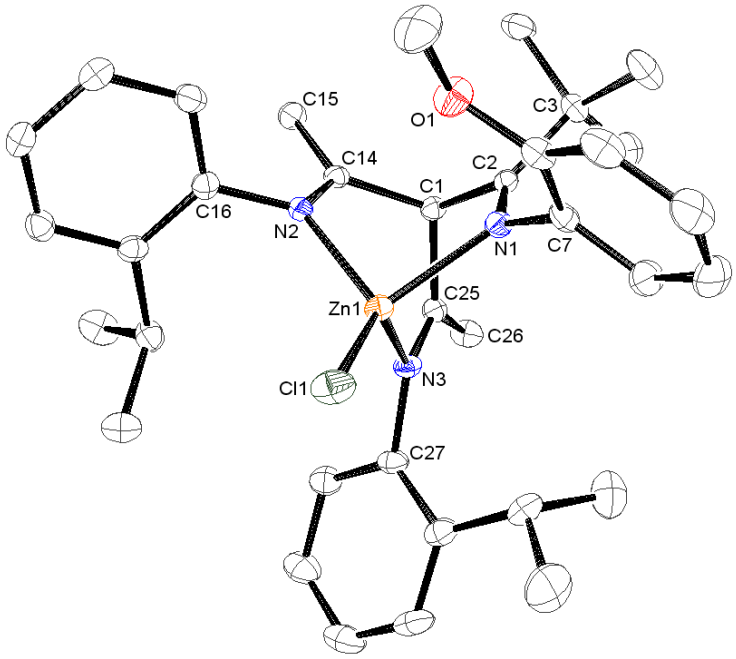

Figure 3.16 ORTEP representation of the cationic unit in [(L^{8})ZnCl][OTf] with thermal ellipsoids set at the 50% probability level; hydrogen atoms omitted for clarity

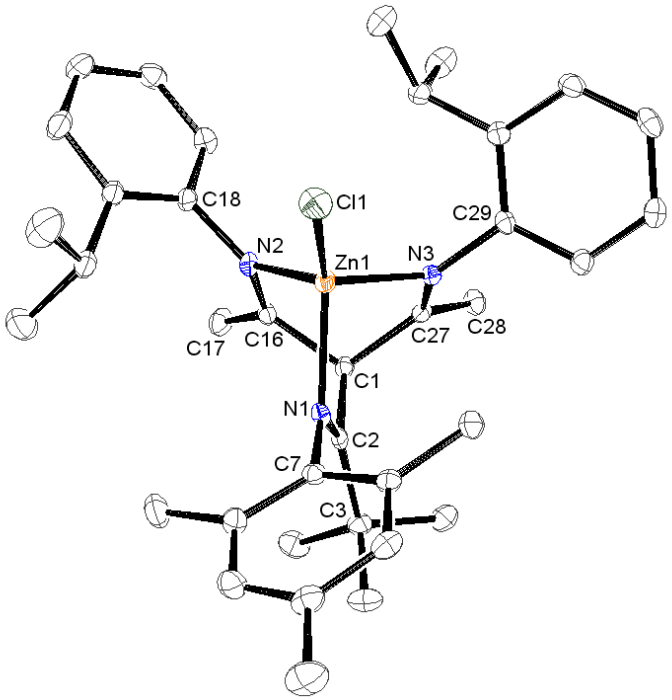

Figure 3.17 ORTEP representation of the cationic unit in [(L^{12})ZnCl][OTf] with thermal ellipsoids set at the 50% probability level; hydrogen atoms omitted for clarity

Table 3.6 Selected bond lengths (Å), angles (°) and interplanar torsion angles (°) for the cationic units in $[(L^{8})ZnCl][OTf]$ and $[(L^{12})ZnCl][OTf]$

$[(L^{8})ZnCl]^{+}$	$[(L^{12})ZnCl]^{+}$
Cl(1)-Zn(1) 2.1408(6)	Cl(1)-Zn(1) 2.1525(5)
Zn(1)-N(1) 2.0478(17)	Zn(1)-N(1) 2.0653(15)
Zn(1)-N(2) 2.0191(16)	Zn(1)-N(2) 2.0469(15)
Zn(1)-N(3) 2.0356(17)	Zn(1)-N(3) 2.0489(14)
N(1)-C(2) 1.275(3)	N(1)-C(2) 1.286(2)
N(2)-C(14) 1.273(3)	N(2)-C(16) 1.280(2)
N(3)-C(25) 1.278(3)	N(3)-C(27) 1.278(2)
N(1)-C(7) 1.439(3)	N(1)-C(7) 1.446(2)
N(2)-C(16) 1.444(3)	N(2)-C(18) 1.444(2)
N(3)-C(27) 1.449(3)	N(3)-C(29) 1.447(2)
C(1)-C(2) 1.552(3)	C(1)-C(2) 1.546(2)
C(1)-C(14) 1.546(3)	C(1)-C(16) 1.532(2)
C(1)-C(25) 1.539(3)	C(1)-C(27) 1.542(2)
Cl(1)-Zn(1)-N(1) 125.08(5)	Cl(1)-Zn(1)-N(1) 127.87(4)
Cl(1)-Zn(1)-N(2) 123.81(5)	Cl(1)-Zn(1)-N(2) 124.33(4)
Cl(1)-Zn(1)-N(3) 126.17(5)	Cl(1)-Zn(1)-N(3) 121.06(5)
N(1)-Zn(1)-N(2) 90.92(6)	N(1)-Zn(1)-N(2) 91.69(6)
N(1)-Zn(1)-N(3) 89.89(7)	N(1)-Zn(1)-N(3) 90.61(6)
N(2)-Zn(1)-N(3) 90.23(6)	N(2)-Zn(1)-N(3) 91.01(6)
Zn(1)-N(1)-C(7) 115.50(12)	Zn(1)-N(1)-C(7) 119.24(11)
Zn(1)-N(2)-C(16) 120.43(12)	Zn(1)-N(2)-C(18) 126.03(12)
Zn(1)-N(3)-C(27) 122.41(13)	Zn(1)-N(3)-C(29) 122.94(11)
Zn(1)-N(1)-C(2) 117.35(14)	Zn(1)-N(1)-C(2) 114.87(12)
Zn(1)-N(2)-C(14) 116.15(13)	Zn(1)-N(2)-C(16) 113.20(12)
Zn(1)-N(3)-C(25) 115.00(13)	Zn(1)-N(3)-C(27) 114.29(11)
C(2)-N(1)-C(7) 127.03(17)	C(2)-N(1)-C(7) 124.76(15)
C(14)-N(2)-C(16) 123.28(16)	C(16)-N(2)-C(18) 120.59(15)
C(25)-N(3)-C(27) 122.52(17)	C(27)-N(3)-C(29) 122.28(14)
C(1)-C(2)-N(1) 114.40(17)	C(1)-C(2)-N(1) 115.50(15)
C(1)-C(14)-N(2) 116.79(17)	C(1)-C(16)-N(2) 118.38(16)
C(1)-C(25)-N(3) 117.45(17)	C(1)-C(27)-N(3) 116.91(14)
N(1)-C(2)-C(3) 130.30(19)	N(1)-C(2)-C(3) 130.48(16)
N(2)-C(14)-C(15) 126.16(19)	N(2)-C(16)-C(17) 125.55(16)
N(3)-C(25)-C(26) 126.29(18)	N(3)-C(27)-C(28) 125.69(16)
θ_T (C(1)-C(2)-N(1)-C(3)/$C(7)_{Ar}$) = 87.29(19)	θ_T (C(1)-C(2)-N(1)-C(3)/$C(7)_{Ar}$) = 83.25(16)
θ_T (C(1)-C(14)-N(2)-C(15)/$C(16)_{Ar}$) = 81.21(19)	θ_T (C(1)-C(16)-N(2)-C(17)/$C(18)_{Ar}$) = 68.69(16)
θ_T (C(1)-C(25)-N(3)-C(26)/$C(27)_{Ar}$) = 69.25(18)	θ_T (C(1)-C(27)-N(3)-C(28)/$C(29)_{Ar}$) = 84.17(16)

The molecular structure of the cation in **$[(L^{10})ZnCl][OTf]$** (**figure 3.18**) shows little difference to that of its R^7 methyl-substituted analogue **$[(L^{1})ZnCl][BAr^{F}_{4}]$**, aside from the enlarged C=N-C_{Ar} angles (**table 3.6**) and slightly reduced mean N-N distance of 2.882(3) Å, though it should be noted that in the case of **$[(L^{10})ZnCl][OTf]$** the structure solution was obtained from a much higher quality dataset (R = 3.30%). All of the 2-isopropylphenyl groups are moved away from orthogonality with the imine planes by a considerable degree, though this is more pronounced for the aryl groups of the methyl-substituted imine moieties. The introduction of a single additional isopropyl substituent in **$[(L^{11})ZnCl][OTf]$** causes significant changes to the molecular structure of the cationic unit (**figure 3.19**), as the steric influence of the 2,6-diisopropylphenyl group causes the two 2-isopropylphenyl moieties to be oriented in the same direction, an analogy with the situation observed in the bis(2-methoxyphenyl)-substituted **$[(L^{16})ZnCl]_2[Zn_2Cl_6]$**. The increased

steric bulk of $\mathbf{L^{11}}$ also causes an increase in the N-N separation to 2.956(2) Å, which is over 0.05 Å longer than that seen in **[($\mathbf{L^{10}}$)ZnCl][OTf]**. The combination of 2,6-diisopropylphenyl and *tert*-butyl substitution at the same imine moiety also causes the C(2)-N(1)-C(7) angle to be a full 10° wider than the corresponding C=N-C_{Ar} angles of the methyl-substituted imines (**table 3.7**), a steric effect the magnitude of which is unprecedented in any of the other aforementioned β-triketimine complexes.

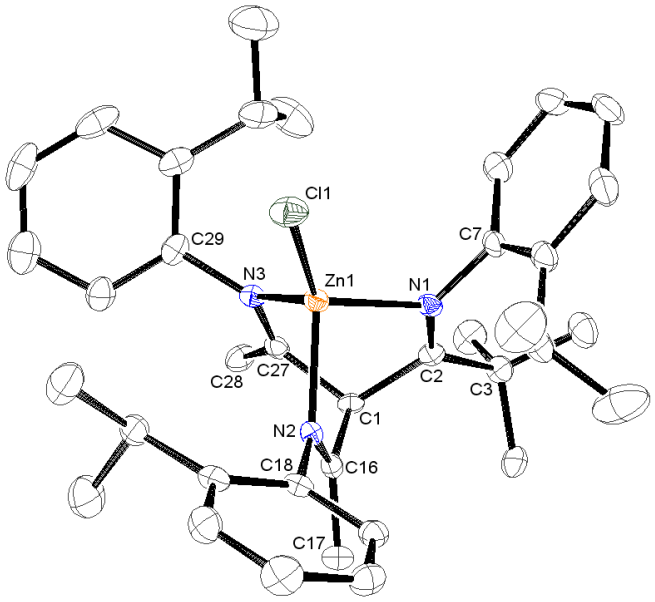

Figure 3.18 ORTEP representation of the cationic unit in [($\mathbf{L^{10}}$)ZnCl][OTf] with thermal ellipsoids set at the 50% probability level; hydrogen atoms omitted for clarity

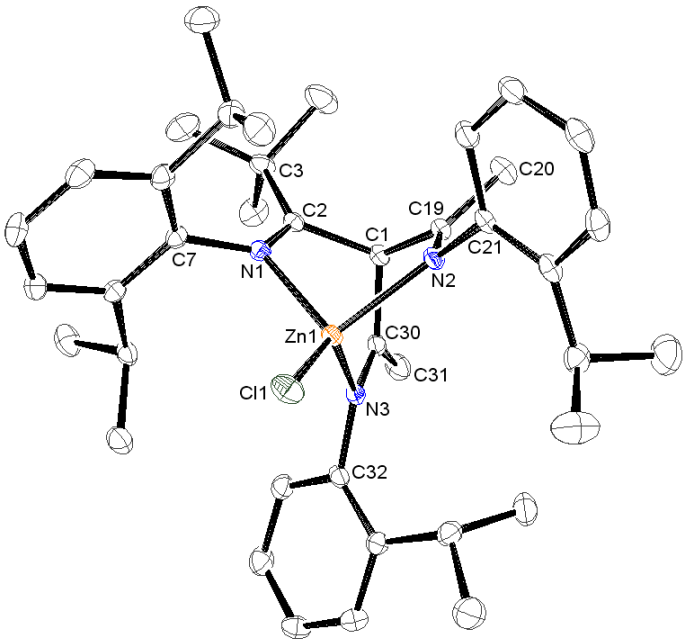

Figure 3.19 ORTEP representation of the cationic unit in [($\mathbf{L^{11}}$)ZnCl][OTf] with thermal ellipsoids set at the 50% probability level; hydrogen atoms omitted for clarity

Table 3.7 Selected bond lengths (Å), angles (°) and interplanar torsion angles (°) for the cationic units in $[(L^{10})ZnCl][OTf]$ and $[(L^{11})ZnCl][OTf]$

$[(L^{10})ZnCl]^+$	$[(L^{11})ZnCl]^+$
Cl(1)-Zn(1) 2.1344(6)	Cl(1)-Zn(1) 2.1485(5)
Zn(1)-N(1) 2.0370(16)	Zn(1)-N(1) 2.0676(14)
Zn(1)-N(2) 2.0242(16)	Zn(1)-N(2) 2.0367(14)
Zn(1)-N(3) 2.0191(16)	Zn(1)-N(3) 2.0429(14)
N(1)-C(2) 1.276(3)	N(1)-C(2) 1.282(2)
N(2)-C(16) 1.274(3)	N(2)-C(19) 1.282(2)
N(3)-C(27) 1.270(3)	N(3)-C(30) 1.284(2)
N(1)-C(7) 1.444(2)	N(1)-C(7) 1.455(2)
N(2)-C(18) 1.436(3)	N(2)-C(21) 1.456(2)
N(3)-C(29) 1.447(3)	N(3)-C(32) 1.453(2)
C(1)-C(2) 1.549(3)	C(1)-C(2) 1.567(3)
C(1)-C(16) 1.540(3)	C(1)-C(19) 1.534(3)
C(1)-C(27) 1.540(3)	C(1)-C(30) 1.536(3)
Cl(1)-Zn(1)-N(1) 124.38(5)	Cl(1)-Zn(1)-N(1) 119.66(4)
Cl(1)-Zn(1)-N(2) 126.43(5)	Cl(1)-Zn(1)-N(2) 121.21(4)
Cl(1)-Zn(1)-N(3) 123.59(5)	Cl(1)-Zn(1)-N(3) 129.28(4)
N(1)-Zn(1)-N(2) 89.82(6)	N(1)-Zn(1)-N(2) 91.47(6)
N(1)-Zn(1)-N(3) 91.05(6)	N(1)-Zn(1)-N(3) 90.37(6)
N(2)-Zn(1)-N(3) 91.09(6)	N(2)-Zn(1)-N(3) 95.23(6)
Zn(1)-N(1)-C(7) 113.44(13)	Zn(1)-N(1)-C(7) 114.77(11)
Zn(1)-N(2)-C(18) 119.17(13)	Zn(1)-N(2)-C(21) 126.94(11)
Zn(1)-N(3)-C(29) 119.54(13)	Zn(1)-N(3)-C(32) 128.31(11)
Zn(1)-N(1)-C(2) 117.34(13)	Zn(1)-N(1)-C(2) 115.23(12)
Zn(1)-N(2)-C(16) 115.53(13)	Zn(1)-N(2)-C(19) 112.51(12)
Zn(1)-N(3)-C(27) 115.22(13)	Zn(1)-N(3)-C(30) 112.19(12)
C(2)-N(1)-C(7) 128.99(17)	C(2)-N(1)-C(7) 129.94 (15)
C(16)-N(2)-C(18) 124.54(17)	C(19)-N(2)-C(21) 119.08(15)
C(27)-N(3)-C(29) 123.87(17)	C(30)-N(3)-C(32) 118.79(15)
C(1)-C(2)-N(1) 114.49(17)	C(1)-C(2)-N(1) 114.34(15)
C(1)-C(16)-N(2) 116.97(17)	C(1)-C(19)-N(2) 118.46(16)
C(1)-C(27)-N(3) 117.58(17)	C(1)-C(30)-N(3) 118.60(16)
N(1)-C(2)-C(3) 129.99(17)	N(1)-C(2)-C(3) 130.54(16)
N(2)-C(16)-C(17) 125.17(19)	N(2)-C(19)-C(20) 125.14(17)
N(3)-C(27)-C(28) 125.59(19)	N(3)-C(30)-C(31) 125.52(17)
θ_T (C(1)-C(2)-N(1)-C(3)/$C(7)_{Ar}$) = 78.03(17)	θ_T (C(1)-C(2)-N(1)-C(3)/$C(7)_{Ar}$) = 88.01(16)
θ_T (C(1)-C(16)-N(2)-C(17)/$C(18)_{Ar}$) = 64.57(19)	θ_T (C(1)-C(19)-N(2)-C(20)/$C(21)_{Ar}$) = 70.87(17)
θ_T (C(1)-C(27)-N(3)-C(28)/$C(29)_{Ar}$) = 66.71(19)	θ_T (C(1)-C(30)-N(3)-C(31)/$C(32)_{Ar}$) = 62.26(17)

The solid-state structures of the aforementioned **[(L)ZnCl][OTf]** compounds all feature extensive intermolecular hydrogen-bonding interactions between the triflate anions and various alkyl and aryl hydrogen atoms in the cationic complexes. For example, examination of close contacts in **$[(L^{10})ZnCl][OTf]$** reveals that two cationic units interact with two triflate ions, which in turn form bridges between the two cations. This generates a symmetrical dimeric arrangement, in which one oxygen atom of each triflate ion acts as a tetrafurcated acceptor, and interacts with three hydrogen atoms from one cation and one hydrogen atom from another. Additionally, a separate oxygen atom from each triflate ion is also hydrogen-bonded to the α-CH of each cationic unit. The combination of these intermolecular interactions is depicted in **figure 3.20**.

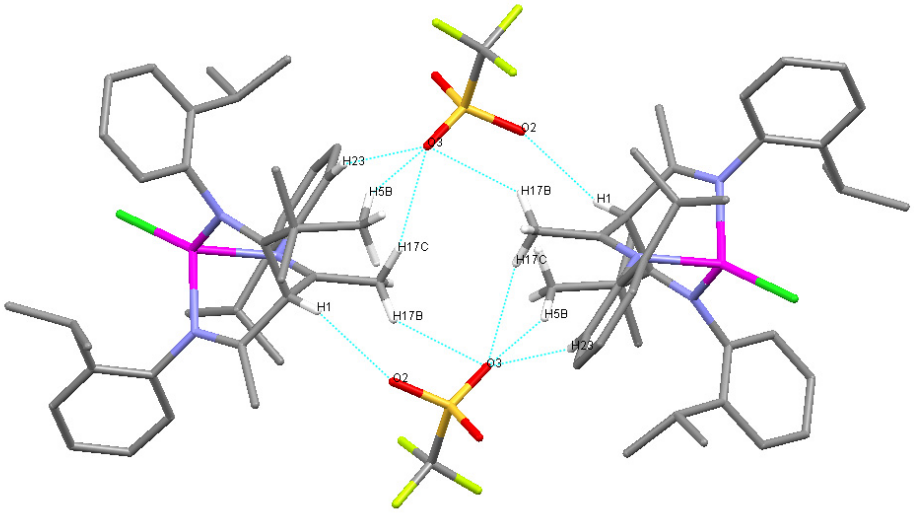

Figure 3.20 MERCURY representation of intermolecular hydrogen-bonding interactions in [(L^{10})ZnCl][OTf]; hydrogen atoms of H-bonded groups shown, all others omitted

The structure-directing influence of 'weak' hydrogen bonds has been codified, and the observed CH---O distances of 2.34-2.71 Å in the **[(L)ZnCl][OTf]** complexes indicate that some are at the stronger end of the spectrum of C-H---O hydrogen bonds.[353] The α-CH---O(2) distance of 2.44 Å in **[(L^{10})ZnCl][OTf]** is among the shorter distances found; however, in all of the other structurally characterised **[(L)ZnCl][OTf]** complexes the hydrogen-bonding interactions generate an extensive 3D network arrangement in the solid state, lacking the α-CH---O interaction. It therefore seems that in these cases the α-CH---O hydrogen bond is sacrificed in favour of a more extended 3D network.

The ^{1}H NMR spectra of all the **[(L)ZnCl][OTf]** compounds provide compelling evidence that the hydrogen-bonding interactions are maintained in solution, as a number of the aliphatic resonances are shifted to higher frequency relative to those observed in the ^{1}H NMR spectra of the corresponding **[(L)ZnCl][BAr^{F}_{4}]** complexes. The magnitude of this effect is greatest for the α-CH resonances, which are shifted by up to 1.30 ppm, well into the aryl region. The resonances corresponding to the ligand backbone methyl and *tert*-butyl groups are also affected, albeit to a lesser degree. For example, the ^{1}H NMR spectrum of **[(L^{10})ZnCl][OTf]** (**figure 3.21**) displays the α-CH resonance at 6.85 ppm, which is shifted to higher frequency by 1.01 ppm relative to the analogous resonance observed for **[(L^{10})ZnCl][BAr^{F}_{4}]**, whilst the backbone methyl (two overlapping singlets at 2.69 ppm) and *tert*-butyl resonances (1.34 ppm) are shifted by 0.28 and 0.11 ppm respectively. In contrast, no significant change in the resonances due to the aryl protons, or

the isopropyl substituents occurs, which suggests that hydrogen-bonding interactions with these groups are not maintained in solution. These observations imply that the compounds exist as contact ion-pairs in solution, and that the cation-anion interactions in solution are similar to those depicted in **figure 3.20**, with the strongest interaction being that between the triflate anion and the α-CH hydrogen atom. One half of the dimer shown in **figure 3.20** may approximate to the solution structure.

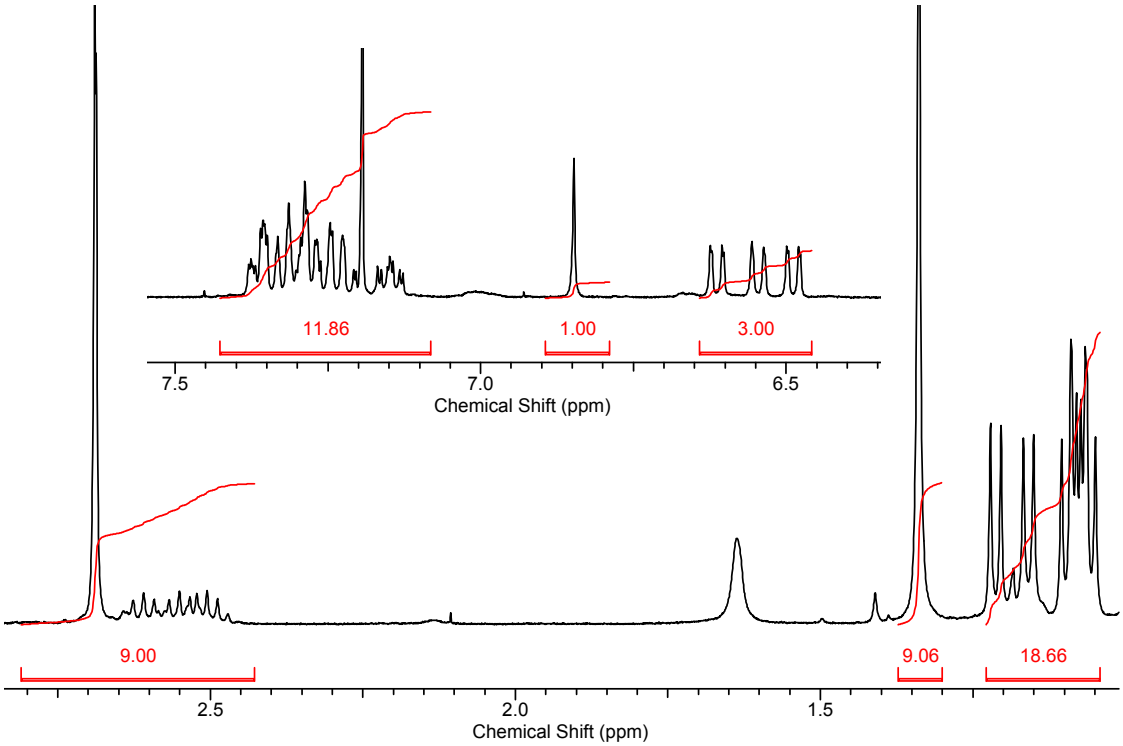

Figure 3.21 ^{1}H NMR spectrum of [(L^{10})ZnCl][OTf] in $CDCl_3$; peaks at 1.57 ppm (H_2O) and 7.29 ppm ($CHCl_3$) are due to solvent contaminants

Unfortunately, single crystals of **[(L^{16})ZnCl][OTf]** suitable for X-ray diffraction could not be obtained, and therefore it is not possible to determine conclusively if this compound features a five-coordinate cationic complex, as in **[(L^{16})ZnCl][BAr^{F}_{4}]**, or a four-coordinate one as in **[(L^{16}ZnCl][Zn_2Cl_6]**. The ^{1}H NMR spectrum of **[(L^{16})ZnCl][OTf]** is very similar to that of **[(L^{16})ZnCl][BAr^{F}_{4}]**, save for the shift in resonances due to the presence of hydrogen-bonding interactions in the former complex. However, in contrast to the latter complex, the ^{1}H NMR spectrum of **[(L^{16})ZnCl][OTf]** shows no broadening of the peaks. It is hard to envisage how this broadening in **[(L^{16})ZnCl][BAr^{F}_{4}]** could be due to an approach to coalescence in a process involving conformational fluxionality, since no hypothesis is formable to explain why the process should be faster for the $BAr^{F}_{4}^{-}$ salt than it is for the triflate salt. If however, the $BAr^{F}_{4}^{-}$ salt was also contact ion-paired in solution,

an explanation of general broadening exists, as the larger **[(L^{16})ZnCl][BAr$^{F}_4$]** contact ion-pair would tumble more slowly in solution.

3.2.1.5 Structural Features of Four-Coordinate Zinc Chloride Complexes

All of the four-coordinate β-triketimine zinc chloride complexes described here show very little variation in structural parameters; for example, the Zn-Cl bond distances vary by only 0.023 Å, over the range 2.1344(6)-2.157(4) Å. The Zn-N distances show a greater variation of 1.986(10)-2.084(18) Å, though it should be noted that the minimum and maximum values of this range are both taken from low-quality datasets (**[(L^{1})ZnCl][BAr$^{F}_4$].½CH$_2$Cl$_2$** and **[(L^{16})ZnCl]$_2$[Zn$_2$Cl$_6$]**). Considering only examples for which R = <8, the range of Zn-N bond lengths is much narrower, at 2.0191(16)-2.070(3) Å. Additionally, the Zn-Cl and Zn-N distances are essentially indistinguishable to those reported for zinc chloride complexes of other tripodal nitrogen ligands, such as (Tp^{tBu})ZnCl (Zn-Cl = 2.183(2) Å; Zn-N = 2 × 2.054(3) Å, 2.045(4) Å),[354] (Tp^{iPr2})ZnCl (Zn-Cl = 2.172(2) Å; Zn-N = 3 × 2.019(5) Å),[355] [(^{2}Tip^{iPr2})ZnCl][Cl] (Zn-Cl = 2.170(2) Å; Zn-N = 3 × 2.057(2) Å),[326] [(^{2}Tip^{Tol,Me})ZnCl]$_2$[ZnCl$_4$] (Zn-Cl = 2.1725(10) Å; Zn-N = 2.061(3) Å, 2.074(3) Å, 2.057(3) Å),[245] and [(Pro-Tach^{Ph})ZnCl][BPh$_4$] (Zn-Cl = 2.188(2) Å; Zn-N = 2.028(5) Å, 2.038(5) Å, 2.041(5) Å).[277] The lack of variation in these parameters suggests that the Zn-N and Zn-Cl bonds have a sizeable degree of covalency, as purely electrostatic interactions would be expected to show a much greater degree of variation. The mean N-N separations in the β-triketimine complexes also differ over a very small range (2.882(3)-2.956(2) Å), though the variation does show a correlation with ligand steric bulk. For example, the mean N-N distances in **[(L^{8})ZnCl][BAr$^{F}_4$]** and **[(L^{8})ZnCl][OTf]** are 2.888(5) and 2.886(3) Å respectively, while in the much more sterically hindered **[(L^{12})ZnCl][BAr$^{F}_4$]** and **[(L^{12})ZnCl][OTf]** they are 2.922(5) and 2.932(2) Å respectively. A relationship between N-N distance and ligand steric bulk is also supported by the fact that the most sterically encumbered complex, **[(L^{11})ZnCl][OTf]**, also displays the greatest mean N-N separation (2.956(2) Å). Previously reported complexes are also found to follow this trend; for example, the mean N-N distance in (Tp^{tBu})ZnCl (3.010(3) Å)[354] is larger than those in (Tp^{iPr2})ZnCl (2.925(2) Å)[355] and (Tp^{Mes})ZnCl (2.932(3) Å, Tp^{Mes} = hydrotris(3-mesitylpyrazolyl)borate).[356] The mean N-N separations in the β-triketimine complexes are noticeably shorter than those in related complexes of other neutral tripodal ligands, such as [(^{2}Tip^{iPr2})ZnCl][Cl] (mean N-N = 3.050(2) Å),[326] [(^{2}Tip^{Tol,Me})ZnCl]$_2$[ZnCl$_4$] (mean N-N = 3.049(3) Å)[245] and [(Pro-Tach^{Ph})ZnCl][BPh$_4$]

(mean N-N = 2.988(5) Å).[277] However, both the $^{2}Tip^{x}$ and Pro-Tach^{Ph} ligands are based on larger molecular scaffolds than the β-triketimines, and as such the mean N-N distances are accordingly greater. In the former case this is due to the larger size of the central phosphorus atom relative to carbon, whilst in the latter it is a simply as a result of the inherently larger cyclohexane ligand backbone.

3.2.2 Attempts to Synthesise Hydroxo- and Alkoxo-Zinc(II) Complexes of β-Triketimines, and the Serendipitous Preparation of β-Triketimine Thallium(I) Complexes

The use of tripodal nitrogen ligands in the preparation of biomimetic hydroxo- and alkoxo-zinc complexes was outlined in **section 3.1**, and due to the relatively small number of such complexes, and their differing modes of reactivity towards various substrates, it was decided that the preparation of analogous β-triketimine-supported complexes would be a worthwhile area of research. However, it has not been possible to effectively characterise any such compounds, though some of the reactions carried out have led to the isolation of novel complexes of thallium(I).

In an attempt to prepare the corresponding **[(L^{1})ZnOH][ClO$_4$]** complex, **L^{1}** was combined directly with Zn(ClO$_4$).6H$_2$O in methanol (**scheme 3.9**), in analogy with the method used by Parkin *et al.* for the preparation of [($^{2}Tip^{tBu,N\text{-}iPr}$)ZnOH][ClO$_4$].[340] Removal of the solvent gave a yellow oil, which was redissolved in DCM. However, addition of either hexane or Et$_2$O to this solution caused no precipitation, and additionally no solid product was formed when a concentrated DCM/hexane solution was cooled to -20°C for an extended period. An identical procedure was also performed using **L^{8}**, though once again no solid product could be isolated from the reaction mixture.

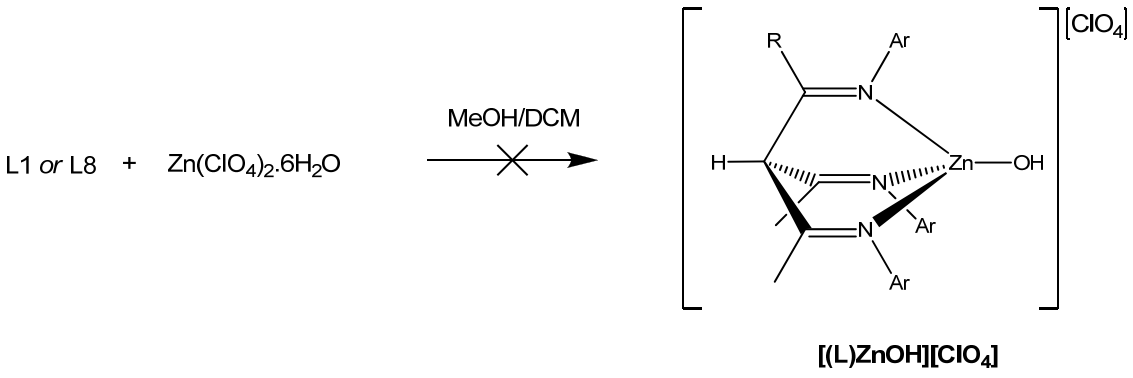

Scheme 3.9 Attempted preparation of [(L)Zn(OH)][ClO$_4$]

An alternative synthetic strategy was aimed at the preparation of **[(L^1)ZnOH][BAr$^F_4$]**, and involved the reaction of **[(L^1)ZnCl][BAr$^F_4$]** with powdered KOH in DCM (**scheme 3.10**). Addition of hexane to the filtered reaction mixture gave a small amount of solid product, though this was determined by elemental analysis to be K[BAr$^F_4$]. No other products could be isolated from this reaction, and an analogous procedure employing **[(L^{16})ZnCl][BAr$^F_4$]** as starting material gave an identical result.

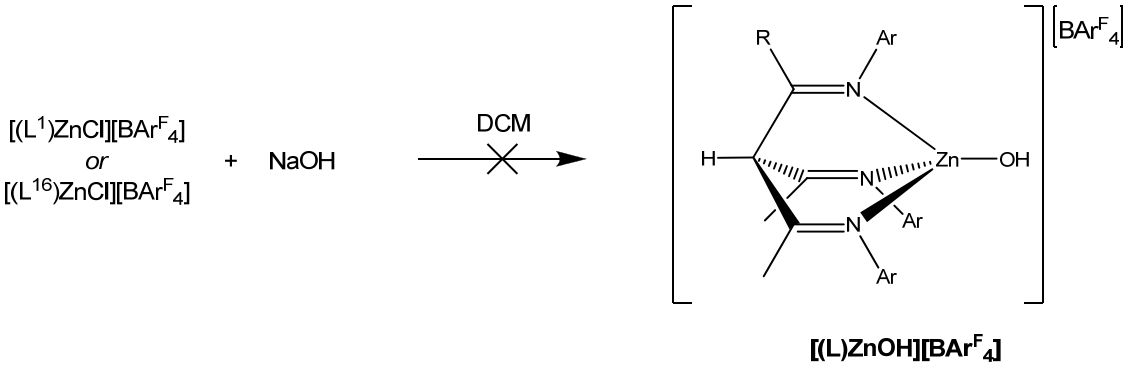

Scheme 3.10 Attempted preparation of [(L)ZnOH][BAr$^F_4$]

As described in **section 3.1**, it has been shown that the stability of zinc alkoxide derivatives of Tp^x are relatively high when the alkoxide is derived from a relatively acidic alcohol, i.e. one that bears strongly electron withdrawing substituents. Indeed, Tp^{Ph,Me}Zn{OCH(CF$_3$)$_2$} was described as being stable to atmospheric conditions.[338] As such, **[(L^1)ZnCl][BAr$^F_4$]** was reacted with the sodium salt of hexafluoroisopropanol in DCM, and produced a microcrystalline product following filtration and overlayering with hexane (**scheme 3.11**).

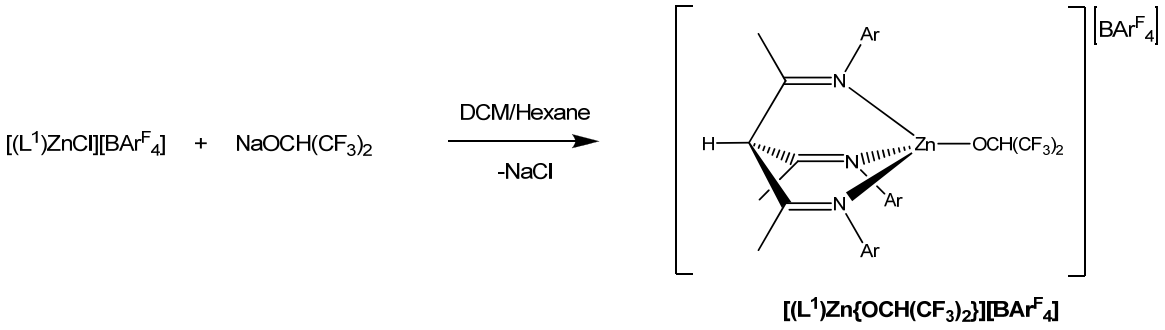

Scheme 3.11 Synthesis of [(L^1)Zn{OCH(CF$_3$)$_2$}][BAr$^F_4$]

Microanalytical data for this product are in very strong agreement with the formulation **[(L^1)Zn{OCH(CF$_3$)$_2$}][BAr$^F_4$]**, and, most tellingly, show a complete absence of any chlorine, which offers conclusive proof that the reaction has gone to completion and none of the starting complex remains. MALDI mass spectrometry also shows a major set of peaks with maximum intensity at *m/z* = 784, which is indicative of a [(L^1)Zn{OCH(CF$_3$)$_2$}]

cation plus adventitious KF, and the isotope distribution pattern is in complete agreement with that predicted for such a species. However, the behaviour of this complex in solution was found by NMR spectroscopy to be very complicated, with a number of different species being observed. For example, peaks corresponding to at least three different β-triketimine compounds are observed in the ^{1}H NMR spectrum, and no evidence for the alkoxide ligand can be found in either the ^{1}H or ^{19}F NMR spectra. Additionally, one set of resonances corresponds very closely to those observed for the starting chloro-complex, which may possibly be regenerated in solution by reaction of the alkoxide adduct with HCl impurity present in the CD_2Cl_2 solvent, or alternatively via attack on the solvent. This hypothesis is supported by the fact that the MALDI mass spectrum of **[(L^{1})Zn{OCH(CF$_3$)$_2$}][BAr$^{F}_{4}$]** in DCM also displays a small set of peaks which are indicative of the presence of starting material. The major component in solution has all the β-triketimine resonances shifted to lower frequency relative to the chloro-complex, which is in contrast to the situation which would be expected due to the influence of a strongly electron-withdrawing alkoxide moiety. As such, it is not possible to draw any effective conclusion from NMR spectroscopy as to the behaviour of this complex in solution. Despite repeated efforts, it has also not been possible to grow single crystals of **[(L^{1})Zn{OCH(CF$_3$)$_2$}][BAr$^{F}_{4}$]** suitable for X-ray diffraction. Analogous treatment of the more heavily substituted **[(L^{8})ZnCl][BAr$^{F}_{4}$]** and **[(L^{10})ZnCl][BAr$^{F}_{4}$]** with $NaOCH(CF_3)_2$ gave a sizeable recovery of unreacted chloro-complex in both cases, which suggests that the increased steric bulk of **L^{8}** and **L^{10}** relative to **L^{1}** is inhibitive towards further metathesis reactions of their respective zinc chloride derivatives. Failure of these reactions may also be attributed to protection of the reaction site by contact ion-pairing in solution, as was alluded to in **section 3.2.1.4**.

Solan and co-workers have reported that when a Zn_2Cl_3 adduct of a dinucleating phenoxide-bridged ligand was treated with thallium(I) ethoxide, the corresponding hydroxo-complex was obtained, which presumably arises from hydrolysis of a highly reactive zinc ethoxide intermediate.[357] Therefore, it was assumed that the analogous reaction of β-triketimine zinc chloride complexes may give access to either hydroxo- or alkoxo-zinc derivatives, and accordingly **[(L^{1})ZnCl][BAr$^{F}_{4}$]** and **[(L^{8})ZnCl][BAr$^{F}_{4}$]** were reacted with Tl(OEt) in DCM (**scheme 3.12**). The rapid formation of a dense precipitate, originally assumed to be TlCl, suggested that the desired reaction had occurred. In both cases, subsequent filtration and overlayering with hexane produced large colourless

crystals. However, X-ray crystallography revealed that, rather than β-triketimine-supported zinc complexes, the products were in fact the respective thallium(I) derivatives **[(L)Tl][BAr$^F_4$]** (**L** = **L^1**, **L^8**). The intended metathesis reactions failed to occur, and instead the bound zinc chloride unit has been substituted by a thallium(I) ion, with apparent precipitation of a putative ZnCl(OEt) compound. Both **[(L)Tl][BAr$^F_4$]** compounds show weakly associated dimeric structures in the solid state, which are generated by a combination of thallium-thallium interactions and intermolecular aryl-thallium interactions. The molecular structure of the dimeric dicationic unit in **[(L^1)Tl][BAr$^F_4$].½C$_6$H$_{14}$** is presented in **figure 3.22**, and relevant bond lengths are listed in **table 3.8**. The η^6 aryl-Tl interaction has a significant *trans*-influence on the N(1)-Tl(1) bond distance, this being over 0.1 Å longer than the N(2)-Tl(1) and N(3)-Tl(1) distances. In order to accommodate the increased size of thallium(I) relative to zinc(II), there is considerable rotation about the ligand C(1)-$C_{C=N}$ bonds, giving a splayed arrangement of the imine groups which is reminiscent of that observed in the solid-state structure of free **L^{11}** (**section 2.2.1**). The Tl(1)-Tl(1)′ distance (3.649(3) Å) is considerably longer than the shortest Tl(I)-Tl(I) distance (3.0936(8) Å) described to date in a terphenyl-ligated dimer,[358] though the former can still be considered as being indicative of a significant thallophilic interaction.[359]

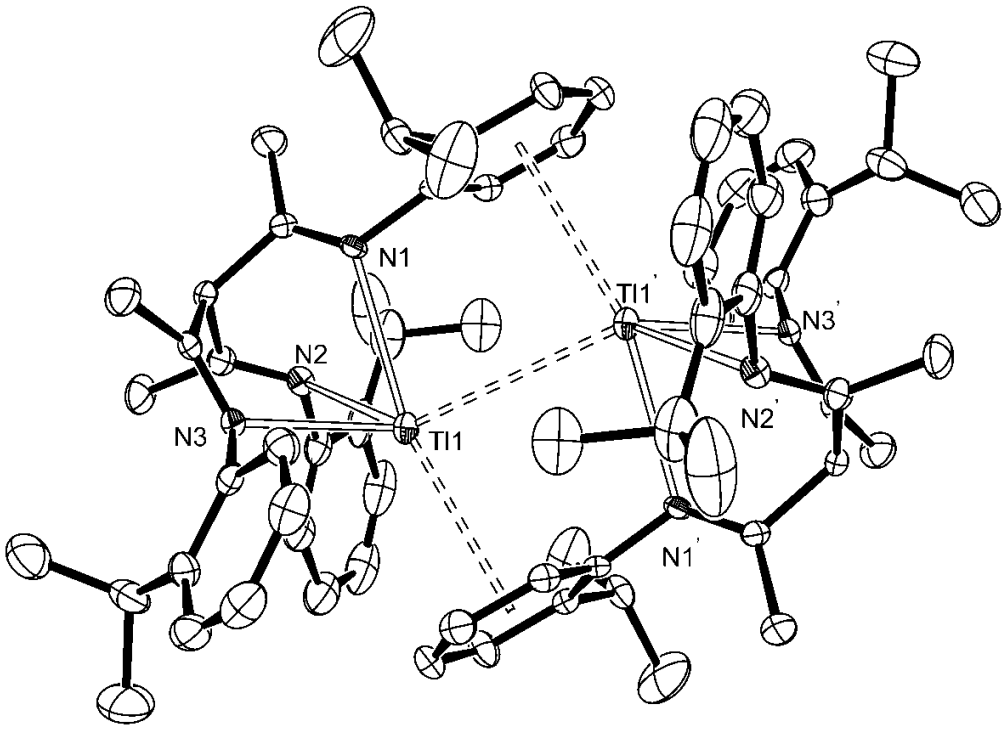

Figure 3.22 ORTEP representation of the dimeric unit of [(L^1)Tl][BAr$^F_4$].½C$_6$H$_{14}$ with thermal ellipsoids set at the 50% probability level; hydrogen atoms omitted for clarity

The Tl(1)-Tl(1)′ distance in **[(L^1)Tl][BAr$^F_4$].½C$_6$H$_{14}$** compares very closely to the value of 3.6468(4) Å as seen in the tetrameric (Tp^{Cpr})Tl (Tp^{Cpr} = hydrotris(3-cyclopropylpyrazolyl)borate), though the anionic nature of the Tp^{Cpr} ligand renders the Tl-N distances (2.532(3) Å) considerably shorter.[360] In comparison to {(Tp^{Cpr})Tl}$_4$, the propensity for further clustering in **[(L^1)Tl][BAr$^F_4$].½C$_6$H$_{14}$** is reduced due to the presence of the additional inter-monomer η^6 aryl-Tl interactions. For a dimeric complex of the general form LTlTlL (L = monodentate ligand), an L-Tl-Tl′ angle of 120° has been described as indicating a maximisation of Tl-Tl overlap.[359(g)] Indeed, the {N(1)-N(2)-N(3)}centroid-Tl(1)-Tl(1)′ angle (119.82°) is effectively identical to this idealised value, which further supports the description of the Tl-Tl interaction in **[(L^1)Tl][BAr$^F_4$].½C$_6$H$_{14}$** as being relatively strong.

Table 3.8 Selected bond lengths (Å) for the dimeric units of [(L^1)Tl][BAr$^F_4$] and [(L^8)Tl][BAr$^F_4$]

[(L^1)Tl]$^+$	[(L^8)Tl]$^+$
N(1)-Tl(1) 2.746(3)	N(1)-Tl(1) 2.667(2)
N(2)-Tl(1) 2.630(3)	N(2)-Tl(1) 2.579(3)
N(3)-Tl(1) 2.642(3)	N(3)-Tl(1) 2.947(2)
Tl(1)-Tl(1)′ 3.649(3)	Tl(1)-Tl(1)′ 3.887(2)
Ar(η^6 centroid)-Tl(1) 3.154(5)	Ar(η^3 centroid)-Tl(1) 3.369(4)
	O(1)-Tl(1) 2.982(2)

The molecular structure of **[(L^8)Tl][BAr$^F_4$]** (**figure 3.23**) shows a considerably lengthened Tl(1)-Tl(1)′ distance (3.887(2) Å) relative to that seen in **[(L^1)Tl][BAr$^F_4$].½C$_6$H$_{14}$**, though this is still within the sum of the van der Waals' radii of two thallium atoms (3.92 Å). It has previously been shown that a simple increase in ligand steric bulk results in a weakening of the Tl-Tl interaction; for example the Tl-Tl distance of 3.8636(4) Å in the dimeric (Tp$^{p\text{-Tol}}$)Tl (Tp$^{p\text{-Tol}}$ = hydrotris(3-*p*-tolylpyrazolyl)borate)[361] is considerably longer than that observed in the aforementioned tetrameric (Tp^{Cpr})Tl, and indeed the shortest Tl(I)-Tl(I) interactions are promoted by very strongly donating monodentate ligands.[357] However, the lengthening of the Tl-Tl distance in **[(L^8)Tl][BAr$^F_4$]** cannot be solely attributed to steric factors, as the methoxy substituent of **L^8** also engages in a weak bonding interaction with the thallium centre. This increase in coordination number results in an overall lengthening of both the Tl(1)-Tl(1)′ and Tl(l)-N(3) distances, and in this case the latter distance is on average over 0.35 Å longer than the other N-Tl(1) distances (**table 3.8**). The variation between the N(1)-Tl(1) and N(2)-Tl(1) distances also gives good indication that the bonding is primarily electrostatic. The O(1)-Tl(1) distance of 2.982(2) Å is close to one of the O-Tl distances (3.017 Å) found in the five-coordinate (Tp$^{o\text{-Anis}}$)Tl, where the

additional coordination of two methoxy groups form the Tp$^{o\text{-Anis}}$ ligand inhibits any intermolecular Tl-Tl interaction.[362] A further effect inherent to the increased coordination number and lengthened Tl(1)-Tl(1)′ distance in **[(L^{8})Tl][BAr$^{F}_{4}$]** is a reduction in the hapticity of the coordinated aryl to η^3, as well as a significantly increased Ar-Tl(1) distance (**table 3.8**). The two thallium(I) complexes described here represent the first reported examples of the association of $[(L)Tl^{I}]^{+}$ cationic moieties. Whilst there are a considerable number of neutral L_2Tl_2 species known, these are the first $[(L)_2Tl_2]^{2+}$ dications.

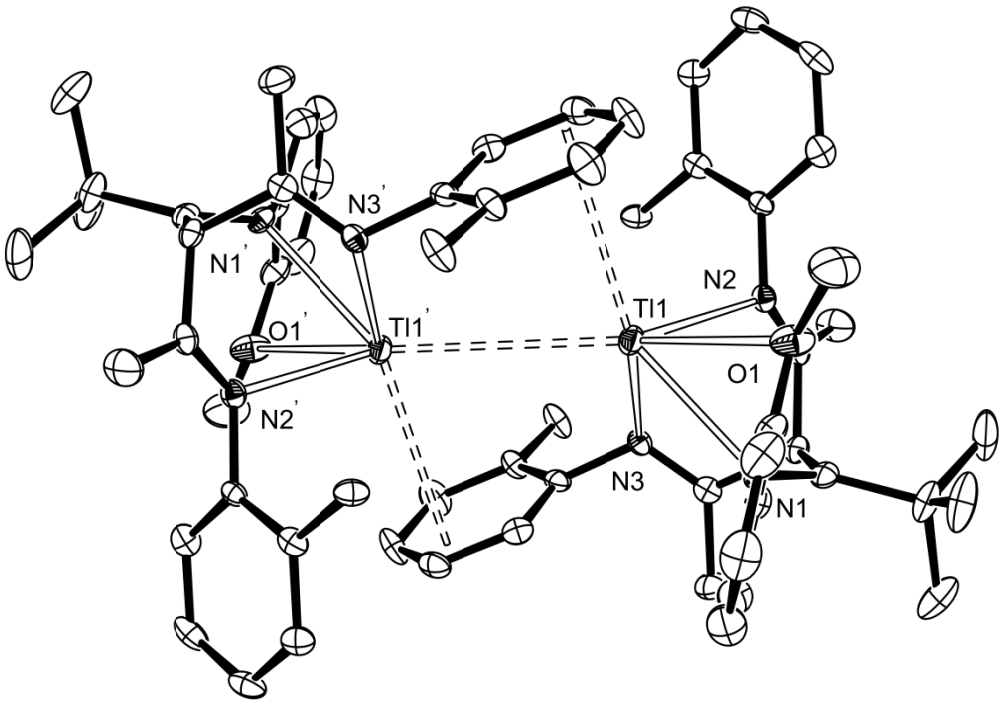

Figure 3.23 ORTEP representation of the dimeric unit of [(L^{8})Tl][BAr$^{F}_{4}$] with thermal ellipsoids set at the 50% probability level; hydrogen atoms and isopropyl methyl groups omitted for clarity

3.3 Concluding Remarks

It has been shown that a number of β-triketimine ligands form stable, four-coordinate cationic zinc chloride complexes, both with and without the use of weakly-coordinating anions. In the vast majority of cases the complexes are easily characterised by a variety of different methods, though X-ray crystallographic studies on a number of the complexes has shown them to display little structural variation in the solid-state with respect to differences in both the ligand steric bulk, and the nature of the anion. However, when triflate is employed as the anion, the solid-state structures show extensive intermolecular hydrogen-bonding interactions, some of which are maintained in solution as evidenced by ^{1}H NMR

spectroscopy. Additionally, NMR studies have shown how subtle steric variation can affect the rate of conformational fluxion. When 2-methoxyphenyl groups are present in the β-triketimine ligand, and rotation of these aryl groups is not prohibited by steric factors, the ligand may act as a tetradentate donor, forming a five-coordinate zinc complex, though the propensity to do so is also strongly dependent on the nature of the anion.

The ability of β-triketimine zinc chloride complexes to undergo further metathesis with a number of reagents in order to generate more biologically relevant species has been shown to be severely limited, and none of the reactions attempted have produced zinc-containing products which can be effectively characterised.

The following chapter details the synthesis and characterisation of β-triketimine complexes of nickel(II), which are found to show much greater structural variation than the zinc compounds described in this chapter, and a number of these are also shown to have significant catalytic properties.

4. Complexes of β-Triketimines with Nickel(II) and Their Application as Precatalysts for the Polymerisation of Ethylene

4.1 Introduction

4.1.1 Transition Metal-Catalysed Ethylene Polymerisation

Polyethylene is the most widely produced synthetic polymer, with an annual production of over 65 million tonnes, and is the major component of a multi-billion dollar per year polyolefin industry.[363] Polyethylene has numerous applications, though the most common of these are as packaging and insulating materials. The properties of polyethylene can be tailored specifically to a particular application by precise control of the polymer microstructure, achieved through modification of the various catalytic processes employed in its production. As such, polyethylene is classified into three broad classes which are defined by the microstructure of the polymer, specifically the degree of branching present in the polyethylene molecules. Low density polyethylene (LDPE) is highly branched, and features large numbers of long-chain branches, as a result of the high-temperature and high-pressure free radical process employed in its production.[364] High density polyethylene (HDPE) is a linear polymer with a very low degree of branching, and is traditionally produced by Ziegler-Natta (titanium)[365] and chromium-based catalysts.[366] These catalyst systems are heterogeneous, with multiple different active catalytic sites, and as such the resultant polymers show broad molecular weight distributions. The introduction of well-defined, homogeneous group 4 metallocene catalysts in the 1980s has allowed for the production of HDPE with much narrower molecular weight distribution, and therefore superior physical properties to that produced with Ziegler-Natta and related catalysts.[363,367] Linear low density polyethylene (LLDPE) is a short-chain branched copolymer of ethylene with other α-olefins such as 1-hexene or 1-octene, and is produced by both Ziegler-Natta and metallocene catalysts. However, due to the heterogeneous nature of Ziegler-Natta catalysts, incorporation of the comonomer occurs in a random fashion, giving irregular distributions of short branches along the polymer chain.[365] Conversely, metallocene catalysts incorporate comonomers in a much more uniform manner, giving rise to regular sequences of branches and therefore a vastly improved level of control over the polymer characteristics.[363,367]

A common feature of all the processes used to prepare HDPE and LLDPE is the use of catalysts based on highly oxophilic, early transition metals such as titanium, zirconium and chromium. Consequently, the copolymerisation of ethylene with polar monomers such as methyl methacrylate is not possible due to strong coordination of the polar monomer to the

oxophilic metal centre, which inactivates the catalyst. Such copolymers are therefore produced exclusively by free-radical processes, in a manner analogous to that employed for the production of LDPE.[368] The low tolerance of early transition metal catalysts for polar comonomers has motivated substantial research into the preparation of polymerisation catalysts based on much less oxophilic late transition metals such as nickel and palladium. Usually, complexes of such metals show very low activities towards the polymerisation of olefins, due to the fact that the rate of chain propagation is normally much slower in comparison to that of the early transition metals. Additionally, for late transition metal complexes, the rate of β-hydrogen elimination is comparable to the rate of chain propagation, and as such dimers and short-chain oligomers rather than polymers are normally obtained.[369] However, the discovery by Brookhart and co-workers that complexes of very bulky α-diimines such as (BIAN^{iPr2})NiBr$_2$ (**section 1.2**) show extremely high activities (>10^4 kgmol^{-1}h^{-1}) towards the polymerisation of ethylene and other α-olefins has revolutionised the field of transition-metal catalysed olefin polymerisation.[10,370] Additionally, the development of related complexes of palladium has allowed for the copolymerisation of ethylene with a variety of polar comonomers.[370,371]

Polyethylene produced by sterically encumbered late metal catalysts can have very high molecular weight, and the degree of branching can be controlled through variation of a number of parameters such as ligand steric bulk, reaction conditions and the nature of the cocatalyst. Brookhart *et al.* have postulated a mechanism for the polymerisation of ethylene by α-diimine nickel complexes, and this is outlined in **Scheme 4.1**. The active catalytic species in these systems is assumed to be a square-planar, cationic 14-electron methylnickel complex (**A**), derived from the dihalide precursor by treatment with an activator such as methylaluminoxane (MAO). Exposure of this species to ethylene gives a methyl ethylene complex (**B**), which undergoes a rapid migratory insertion reaction yielding a cationic β-agostic alkylnickel complex (**C**); subsequent trapping and migratory insertion of further ethylene molecules thus results in linear chain propagation. However, the cationic β-agostic complexes (**C**, **C′**) can also undergo a series of β-hydrogen transfer and readdition reactions, causing the metal to migrate along the polymer chain ('Chain-Walking'). Trapping and insertion of ethylene by complex **E**, and by the complexes produced by more extensive chain-walking, results in the formation of a branches on the polymer chain.[10,370(b),372] This process is unique to nickel and palladium catalysts; for the early transition metals the relative rate of propagation is vastly greater than the rate of β-

hydrogen transfer, and as such only a very low degree of branching is observed in polyethylene produced by metallocene and Ziegler-Natta catalysis. For the group 10 metals, the increased covalency of the M-R bonds gives rise to slower rates of propagation in comparison to the early transition metal systems. However, the concentration of active species is much greater, so the overall productivity of late transition metal catalysts can be comparable with that of the early transition metals. This notwithstanding, the inherently slower propagation rate per active centre means that the rate of β-hydrogen transfer is therefore increased relative to the rate of propagation, and as such there is a much higher occurrence of chain-walking. If the rate of chain-walking is comparable to the rate of propagation, then highly branched polymers are obtained.[370(b),372,373] Nickel catalysts ligated by α-diimines typically produce polyethylene with a moderate degree of branching, usually in the region of 10-100 branches per 1000 carbons. The precise degree of branching is dictated by a number of factors such as reaction temperature, ethylene pressure and nature of the cocatalyst, while a reduction in ligand steric bulk gives rise to a reduced degree of branching.[370(b)]

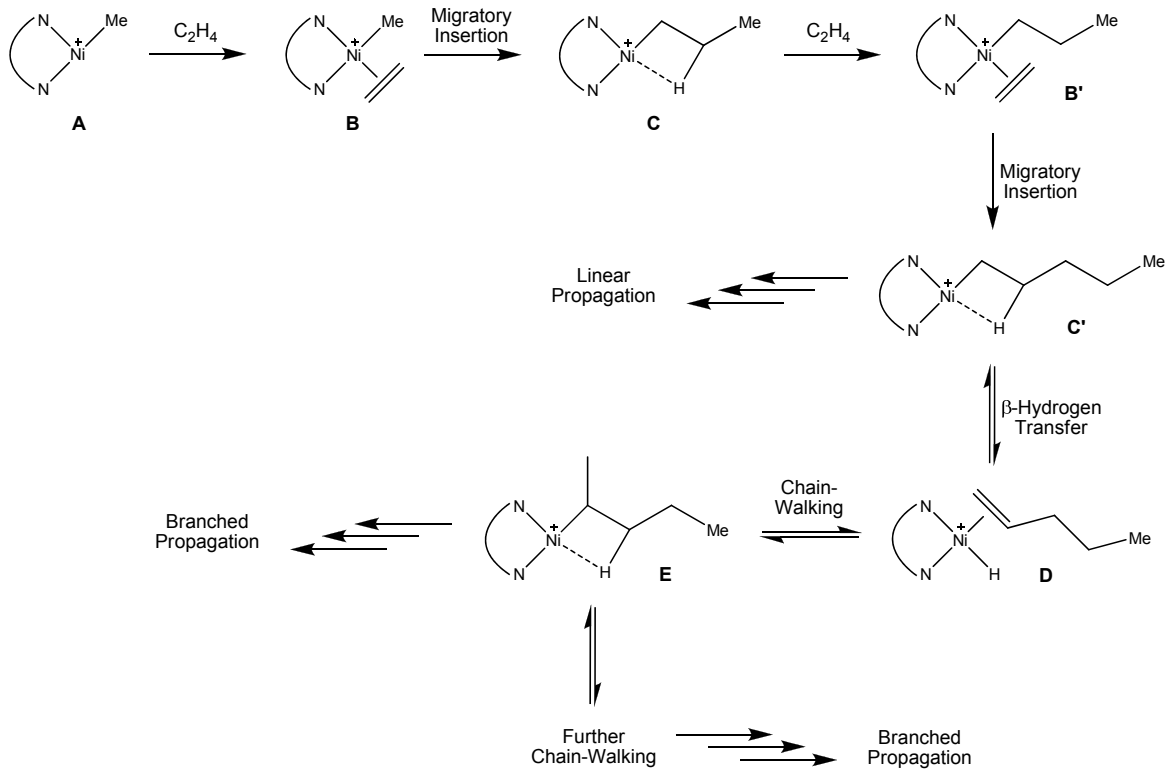

Scheme 4.1 Mechanism of ethylene polymerisation by α-diimine nickel complexes[10,370(b),372]

4.1.2 Living Polymerisation of Ethylene

The term 'Living Polymerisation' can be use to define a polymerisation process in which chain-transfer and chain-termination are absent, and the rate of chain-initiation is much greater than the rate of chain-propagation. The polymer chains therefore all grow at a constant rate, giving rise to very narrow molecular weight distributions. Provided that the catalyst has long-term stability to the reaction conditions, polymerisation will continue to occur as long as monomer is present. Despite the very high activities of nickel α-diimine complexes, the catalysts are usually very short-lived, with rapid deactivation most likely occurring due to reduction of the ligands under the harsh polymerisation conditions. Chain transfer to monomer is inhibited by the steric bulk of the α-diimine ligands, and although the molecular weight distributions observed with these catalysts are generally rather narrow, relatively facile chain transfer to aluminium likely also accounts for the lack of living behaviour. Polymerisation of ethylene in a living manner is rather uncommon, particularly with late transition metal catalysts, and the achievements in this area have been summarised in a comprehensive review article.[374] More recently, Bazan and colleagues have shown that a nickel dibromide complex supported by the α-keto derivative of HBDK^{iPr2} (**324**) has a very high catalytic activity, and is able to polymerise ethylene in a living manner. Upon activation with either MAO or MMAO, this compound produces very high molecular weight polyethylene, and is stable over reaction times of up to 30 minutes, even at a temperature of 75°C.[302,375]

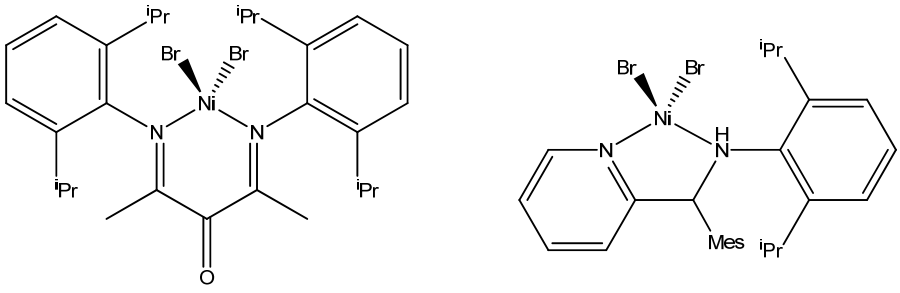

324 **325**

Figure 4.1 Nickel(II) precatalysts for the living polymerisation of ethylene

True living behaviour is only observed at a reaction temperature of -10°C, as evidenced by the very low molecular weight distribution of the obtained polyethylene, as well as the fact that there is an approximately linear increase in polymer yield with increasing reaction time. Additionally, when the polymerization is performed under identical reaction conditions, doubling of the reaction time causes the molecular weight of the obtained

polymer to increase by approximately a factor of two.[375] Notably, the optimum catalytic activity of **324** is two orders of magnitude greater than that of the related ($HBDK^{iPr2}$)$NiBr_2$ (**section 1.2**).[12] This observation can be attributed to the presence of the exocyclic ketone moiety in **324**, which under the conditions of polymerisation will very likely be coordinated to the strongly Lewis acidic alkylaluminium cocatalyst. This has a strong electron-withdrawing effect on the metal centre, which enhances its electrophilicy and is therefore likely to be responsible for the markedly increased activity.[375] Additionally, in contrast to α-diimines, β-diimines do not undergo facile reduction, which may account for the increased catalyst lifetime.

Wu and colleagues have reported that the nickel dibromide complex of a 2-pyridinemethanamine ligand (**325**) also catalyses the living polymerisation of ethylene at -10°C, though the catalytic activities are significantly lower than those observed with complex **324**, and polymers with slightly broader molecular weight distributions are obtained. However, **325** gives rise to a very long-lived catalytic species, as shown by the observation that an increase in reaction time from three to six hours gives an approximate doubling of both molecular weight and polymer yield. Additionally, even when the polymerisation reaction is terminated after one hour by purging with N_2, reintroduction of monomer after ten hours results in continued living polymerisation.[376]

Given the highly fruitful application of imine-ligated nickel complexes in the polymerisation of ethylene, the preparation of β-triketimine derivatives of nickel was therefore deemed to merit extensive investigation. Indeed, certain such compounds have been found to be catalytically active, and show evidence for long catalyst lifetimes. The remainder of this chapter shall be concerned with the synthesis and characterisation of these complexes, and their subsequent testing as precatalysts for the polymerisation of ethylene.

4.2 Results and Discussion

4.2.1 Synthesis and Characterisation of Nickel(II) Complexes of β-Triketimine Ligands

The direct reaction of either $\mathbf{L^1}$ or $\mathbf{L^5}$ with $NiBr_2(DME)$ in DCM followed by filtration and overlayering with hexane gives a microcrystalline pale-green solid in both instances. In analogy with the product arising from the direct reaction of $\mathbf{L^1}$ with $ZnCl_2$, it has not been possible to effectively characterise these two nickel complexes, due to the fact that single crystals suitable for X-ray diffraction could not be obtained in either case. MALDI mass spectrometry experiments show the presence of $[(L)NiBr]^+$ ions, and the pale-green colouration is indicative of five- or six-coordinate nickel centres (*vide infra*). Potential structures for these complexes therefore include the five-coordinate **(L)NiBr$_2$** and **[{(L)Ni(μ-Br)}$_2$][Br]$_2$**, as well as the six-coordinate **{(L)NiBr(μ-Br)}$_2$** (**figure 4.2**), all of which have identical elemental formulae. However, the microanalytical data are not consistent with this formulation, and it has not been possible to conclusively assign the elemental analyses to any other feasible structural type. In contrast to **[(L^1)ZnCl][Cl]**, the nickel dibromide derivatives of $\mathbf{L^1}$ and $\mathbf{L^5}$ display moderate solubility in a number of solvents, which suggests that these compounds do not form coordination polymers in the solid state.

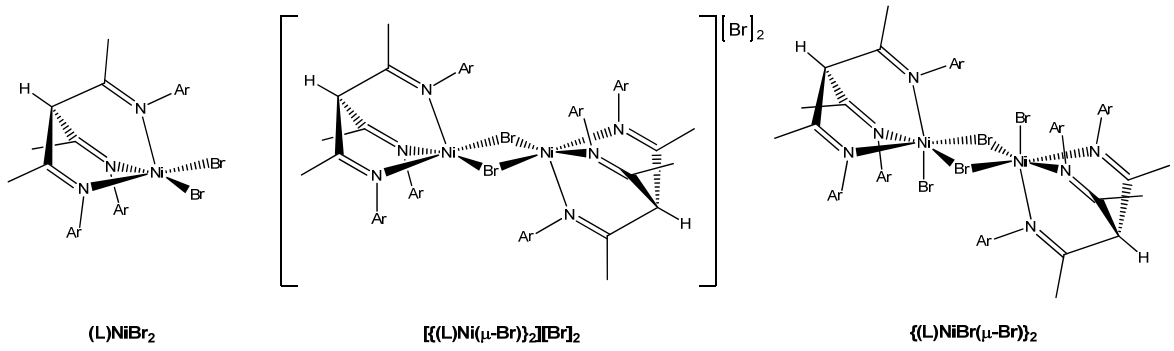

Figure 4.2 Possible structures for the products arising from the reaction of L^1/L^5 with $NiBr_2(DME)$

4.2.1.1 [(L)NiBr]$_2$[NiBr$_4$] Complexes

As was previously observed in their reactions with $ZnCl_2$, β-triketimines where R^7 = ^{t}Bu have also been found to give much more easily characterised products upon reaction with $NiBr_2(DME)$ in DCM, yielding complexes of the general formula **[(L)NiBr]$_2$[NiBr$_4$]** (**L** = $\mathbf{L^8}$, $\mathbf{L^{10\text{-}12}}$) as yellow-brown coloured powders upon addition of hexane or Et_2O (**scheme**

4.2). Once again, the increased steric bulk of the β-triketimines with backbone *tert*-butyl substitution causes facile autoionisation of the metal halide to yield cationic four-coordinate complexes, which in this case are charge-balanced by a tetrabromonickellate dianion.

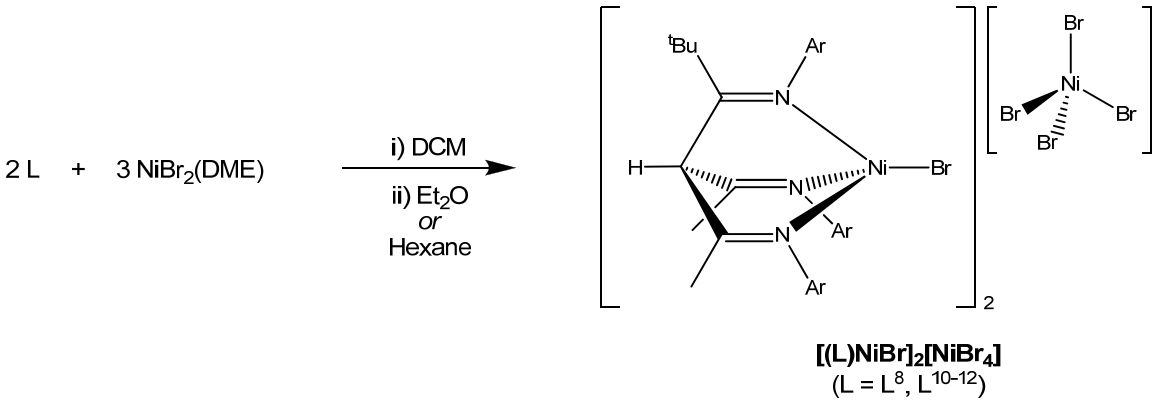

[(L)NiBr]$_2$[NiBr$_4$]
(L = L^8, L$^{10\text{-}12}$)

Scheme 4.2 Synthesis of [(L)NiBr][NiBr$_4$] complexes

Red-brown coloured single crystals of **[(L^8)NiBr]$_2$[NiBr$_4$]** and **[(L^{10})NiBr]$_2$[NiBr$_4$]** suitable for X-ray diffraction were obtained by overlayering of DCM solutions with hexane, whilst it has not been possible to obtain crystalline samples of either **[(L^{11})NiBr]$_2$[NiBr$_4$]** or **[(L^{12})NiBr]$_2$[NiBr$_4$]**. **[(L^8)NiBr]$_2$[NiBr$_4$]** crystallises with two molecules of DCM and one of hexane in the unit cell, though the hexane molecule was found to be highly disordered and was therefore removed using SQUEEZE. The N(1) and N(3) aryl substituents are also disordered over two sites due to librational movement about the C-N$_{Ar}$ bonds; the structure depicted in **figure 4.3** represents the most feasible arrangement, i.e. the one in which the C=N and C-N$_{Ar}$ bonds are closest to coplanarity. The molecular structure of the cationic unit is similar to the four-coordinate zinc complexes described in **chapter 3**, the nickel atom being in a highly distorted tetrahedral geometry (**table 4.1**). The Ni-N distances are slightly shorter than those observed in the aforementioned zinc chloride derivatives of **L^8**, while the mean N-N separation is considerably smaller at 2.802(9) Å. Both of these effects are very likely a result of the slightly smaller ionic radius of four-coordinate Ni^{2+} (0.55 Å) in comparison to four-coordinate Zn^{2+} (0.60 Å).[377] The O(7a)-Ni(1) distance of 3.007(6) Å, though still outside the range of even a weak bonding interaction, is comparable to the shorter non-bonded O-Zn distances such as that seen in **[(L^8)ZnCl][BAr$^F{}_4$]** (**section 3.2.1.2**). However, the disordered nature of the N(1) aryl substituent means that the actual precision of this distance is questionable, and this effect is also likely responsible for the unfeasibly wide

C(2)-N(1)-C(7a) angle of 134.4(9)°. Additionally, the disorder in the positions of the two aryl groups means that direct comparison of the interplanar torsion angles with those seen in the zinc chloride derivatives of $\mathbf{L^8}$ is not possible, though the observed values for this parameter in $\mathbf{[(L^8)NiBr]_2[NiBr_4]}$ are unremarkable.

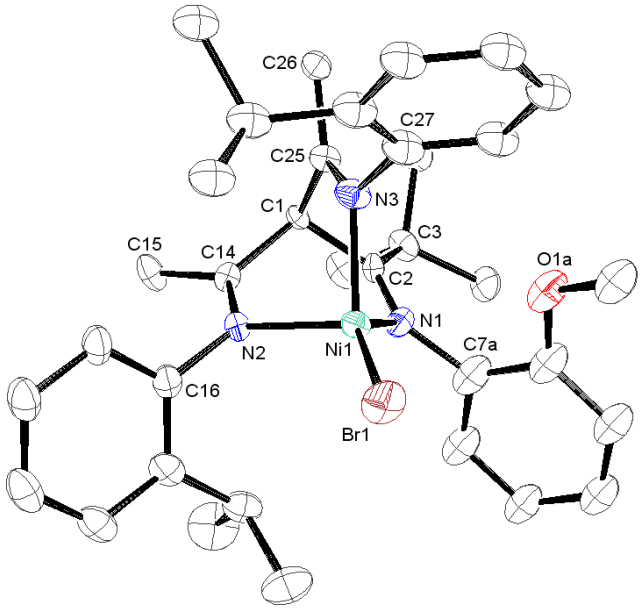

Figure 4.3 ORTEP representation of the cationic unit in $[(L^8)NiBr]_2[NiBr_4]$ with thermal ellipsoids set at the 30 % probability level; hydrogen atoms omitted for clarity

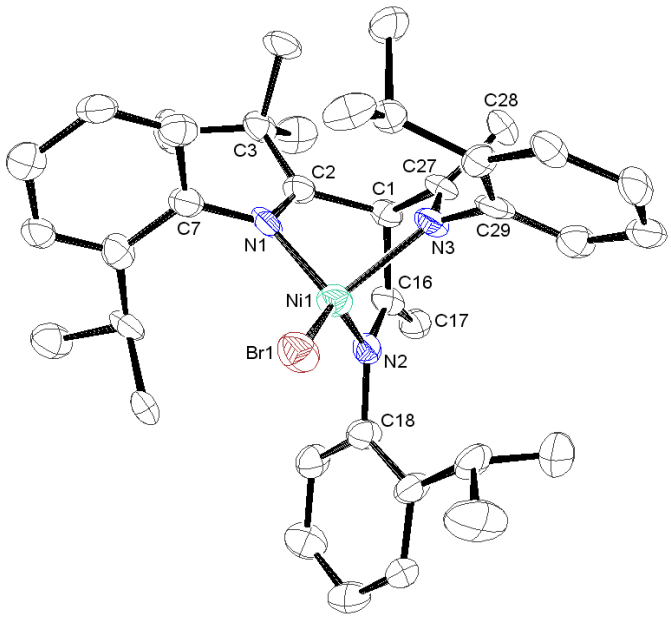

Figure 4.4 ORTEP representation of one of the cationic units in $[(L^{10})NiBr]_2[NiBr_4]$ with thermal ellipsoids set at the 30 % probability level; hydrogen atoms omitted for clarity

Table 4.1 Selected bond lengths (Å), angles (°) and interplanar torsion angles (°) for the cationic units in $[(L^8)NiBr]_2[NiBr_4].2CH_2Cl_2.C_6H_{14}$ and $[(L^{10})NiBr]_2[NiBr_4]$

$[(L^8)NiBr]^+$	$[(L^{10})NiBr]^+$ molecule 1	$[(L^{10})NiBr]^+$ molecule 2
Br(1)-Ni(1) 2.2727(12)	Br(1)-Ni(1) 2.301(4)	Br(2)-Ni(2) 2.299(4)
Ni(1)-N(1) 2.014(6)	Ni(1)-N(1) 1.979(16)	Ni(2)-N(4) 2.027(14)
Ni(1)-N(2) 1.988(6)	Ni(1)-N(2) 1.964(18)	Ni(2)-N(5) 2.011(15)
Ni(1)-N(3) 1.976(6)	Ni(1)-N(3) 1.986(18)	Ni(2)-N(6) 1.998(15)
N(1)-C(2) 1.261(9)	N(1)-C(2) 1.29(3)	N(4)-C(39) 1.29(3)
N(2)-C(14) 1.284(9)	N(2)-C(16) 1.29(2)	N(5)-C(53) 1.24(2)
N(3)-C(25) 1.274(9)	N(3)-C(27) 1.28(2)	N(6)-C(64) 1.27(3)
N(1)-C(7a) 1.429(19)	N(1)-C(7) 1.46(2)	N(4)-C(44) 1.41(2)
N(2)-C(16) 1.431(6)	N(2)-C(18) 1.45(2)	N(5)-C(55) 1.44(2)
N(3)-C(27) 1.444(9)	N(3)-C(29) 1.46(2)	N(6)-C(66) 1.444(19)
C(1)-C(2) 1.546(9)	C(1)-C(2) 1.56(3)	C(38)-C(39) 1.58(3)
C(1)-C(14) 1.532(9)	C(1)-C(16) 1.50(3)	C(38)-C(53) 1.55(3)
C(1)-C(25) 1.515(9)	C(1)-C(27) 1.51(3)	C(38)-C(64) 1.52(3)
Br(1)-Ni(1)-N(1) 138.20(19)	Br(1)-Ni(1)-N(1) 123.9(5)	Br(2)-Ni(2)-N(4) 122.8(5)
Br(1)-Ni(1)-N(2) 118.79(13)	Br(1)-Ni(1)-N(2) 136.3(5)	Br(2)-Ni(2)-N(5) 133.1(4)
Br(1)-Ni(1)-N(3) 119.03(18)	Br(1)-Ni(1)-N(3) 116.0(5)	Br(2)-Ni(2)-N(6) 118.7(5)
N(1)-Ni(1)-N(2) 88.0(2)	N(1)-Ni(1)-N(2) 87.9(7)	N(4)-Ni(2)-N(5) 90.6(7)
N(1)-Ni(1)-N(3) 90.1(2)	N(1)-Ni(1)-N(3) 90.5(7)	N(4)-Ni(2)-N(6) 91.3(6)
N(2)-Ni(1)-N(3) 90.0(2)	N(2)-Ni(1)-N(3) 90.0(7)	N(5)-Ni(2)-N(6) 89.1(7)
Ni(1)-N(1)-C(7a) 104.2(7)	Ni(1)-N(1)-C(7) 113.7(11)	Ni(2)-N(4)-C(44) 115.7(10)
Ni(1)-N(2)-C(16) 123.8(4)	Ni(1)-N(2)-C(18) 121.1(12)	Ni(2)-N(5)-C(55) 119.7(11)
Ni(1)-N(3)-C(27) 115.6(5)	Ni(1)-N(3)-C(29) 123.3(11)	Ni(2)-N(6)-C(66) 120.7(11)
Ni(1)-N(1)-C(2) 119.1(5)	Ni(1)-N(1)-C(2) 118.9(15)	Ni(2)-N(4)-C(39) 116.7(14)
Ni(1)-N(2)-C(14) 116.0(4)	Ni(1)-N(2)-C(16) 117.8(14)	Ni(2)-N(5)-C(53) 117.4(14)
Ni(1)-N(3)-C(25) 118.7(5)	Ni(1)-N(3)-C(27) 118.1(15)	Ni(2)-N(6)-C(64) 117.7(14)
C(2)-N(1)-C(7a) 134.4(9)	C(2)-N(1)-C(7) 126.8(16)	C(39)-N(4)-C(44) 127.4(14)
C(14)-N(2)-C(16) 120.2(6)	C(16)-N(2)-C(18) 121.2(17)	C(53)-N(5)-C(55) 122.8(16)
C(25)-N(3)-C(27) 124.2(6)	C(27)-N(3)-C(29) 118.6(17)	C(64)-N(6)-C(66) 121.3(16)
C(1)-C(2)-N(1) 114.3(5)	C(1)-C(2)-N(1) 114.9(17)	C(38)-C(39)-N(4) 114.5(16)
C(1)-C(14)-N(2) 118.1(6)	C(1)-C(16)-N(2) 116.9(19)	C(38)-C(53)-N(5) 116.1(19)
C(1)-C(25)-N(3) 116.1(5)	C(1)-C(27)-N(3) 116.4(19)	C(38)-C(64)-N(6) 115.3(19)
N(1)-C(2)-C(3) 130.1(6)	N(1)-C(2)-C(3) 126.3(19)	N(4)-C(39)-C(40) 128.9(19)
N(2)-C(14)-C(15) 125.2(6)	N(2)-C(16)-C(17) 126.0(18)	N(5)-C(53)-C(54) 128.1(18)
N(3)-C(25)-C(26) 124.6(6)	N(3)-C(27)-C(28) 128(2)	N(6)-C(64)-C(65) 128(2)
θ_T (C(1)-C(2)-N(1)-C(3)/C(7a)$_{Ar}$) = 76.3(9)	θ_T (C(1)-C(2)-N(1)-C(3)/C(7)$_{Ar}$) = 82.6(19)	θ_T (C(38)-C(39)-N(4)-C(40)/C(44)$_{Ar}$) = 88.5(19)
θ_T (C(1)-C(14)-N(2)-C(15)/C(16)$_{Ar}$) = 78.4(6)	θ_T (C(1)-C(16)-N(2)-C(17)/C(18)$_{Ar}$) = 63.3(19)	θ_T (C(38)-C(53)-N(5)-C(54)/C(55)$_{Ar}$) = 62.0(19)
θ_T (C(1)-C(25)-N(3)-C(26)/C(27)$_{Ar}$) = 82.8(6)	θ_T (C(1)-C(27)-N(3)-C(28)/C(29)$_{Ar}$) = 71(2)	θ_T (C(38)-C(64)-N(6)-C(65)/C(66)$_{Ar}$) = 62(2)

The solid-state structure of **$[(L^{10})NiBr]_2[NiBr_4]$** features two independent cations in the asymmetric unit, though for simplicity only one of these is displayed in **figure 4.4**. The structural parameters of the two independent cations are very similar, though the Ni-N distances in molecule 2 are on average slightly longer than in molecule 1 (**table 4.1**), which is likely a result of the rather poor quality of the data (R = 9.81 %). This may also account for the inconsistency in the mean N-N separations in the two independent cations, which are 2.78(3) and 2.85(3) Å for molecules 1 and 2 respectively. The interplanar torsion angles do not differ by any significant degree from those seen in **$[(L^{10})ZnCl][OTf]$**.

In contrast to the **$[(L)NiBr]_2[NiBr_4]$** complexes, which are yellow-brown in colour, the product arising from the reaction of **L^{16}** and $NiBr_2$(DME) in DCM is bright-green. As the

microanalytical data are consistent with the identical formulation **[(L^{16})NiBr]$_2$[NiBr$_4$]**, it can be assumed that the difference in colouration is due to the presence of a five-coordinate cationic nickel complex, in which **L^{16}** is tetradentately coordinated, in analogy with the five-coordinate **[(L^{16})ZnCl][BAr$^F_4$]**. However, the microanalytical data are also consistent with the complex **[{(L^{16})Ni(μ-Br)}$_2$][NiBr$_4$]**, in which **L^{16}** may act as a tridentate or tetradentate donor, as either of the resultant five- or six-coordinate dimeric species would also be expected to show a similar green colouration. Although single crystals of this complex could be obtained by a number of different methods, they were consistently of insufficient quality for X-ray diffraction, and it is therefore not possible to unequivocally assign this complex to a particular structural type. However, due to the fact that **L^{16}** has been found to form other monomeric five-coordinate complexes with nickel which display a similar green colouration (*vide infra*), the monomeric five-coordinate **[(η^4-L^{16})NiBr]$_2$[NiBr$_4$]** (**scheme 4.3**) seems by far the most likely structure.

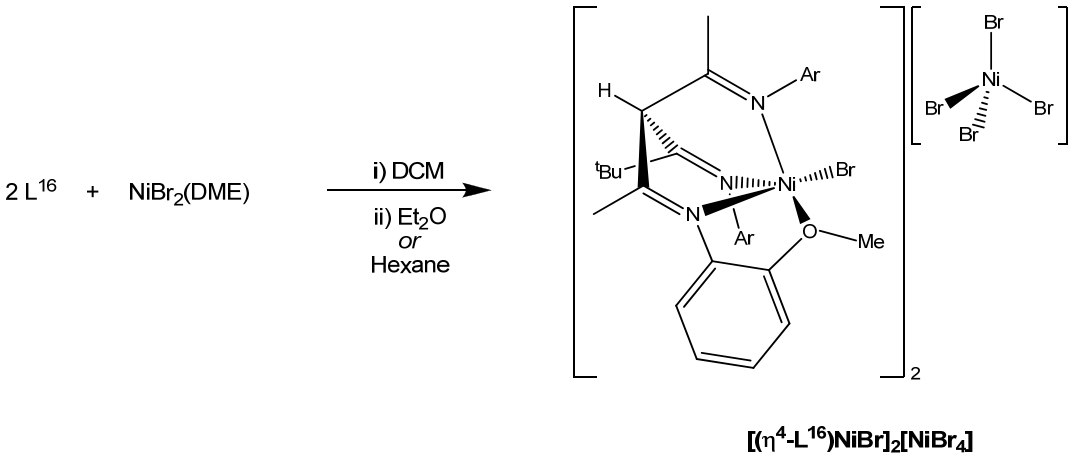

Scheme 4.3 Synthesis and likely structure of [(L^{16})NiBr]$_2$[NiBr$_4$]

4.2.1.2 [{(L)Ni(μ-Br)}$_2$][BAr$^F_4$]$_2$ complexes

Given the highly effective application of the BAr$^F_4^-$ ion in generating zinc complexes of β-triketimines which do not otherwise give access to easily characterised products, coupled with the fact that when screening for ethylene polymerisation reactivity the presence of the $NiBr_4^{2-}$ ion may complicate the potential catalytic reactivity, it was deemed desirable to carry out the reactions of a number of β-triketimine ligands with $NiBr_2$(DME) in the presence of NaBAr$^F_4$. In all cases the reactants were combined in THF, which was then removed after a short period and replaced with DCM. After filtration of the DCM solution the crude products were obtained by addition of excess hexane. It was originally assumed

that the products of these reactions would be four-coordinate cationic complexes of the form **[(L)NiBr][BAr$^F_4$]**, in analogy with the zinc complexes described in **chapter 3**. However, the actual nature of the products has been found to be dependent on the steric bulk of the β-triketimine ligands. In the case of **L^1**, **L^3**, **L^5**, **L^7**, **L^8** and **L^{12}**, the pale-green five-coordinate dimeric bromide-bridged species **[{(L)Ni(μ-Br)}$_2$][BAr$^F_4$]$_2$** were formed exclusively (**scheme 4.4**).

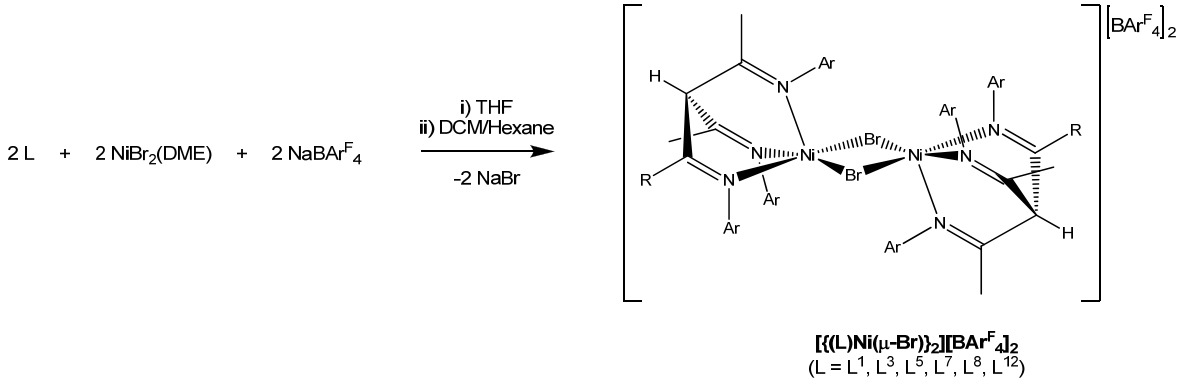

Scheme 4.4 Synthesis of [{(L)Ni(μ-Br)}$_2$][BAr$^F_4$]$_2$ complexes

Though the BAr$^F_4$ ion is relatively large, this preference for the formation of a dimeric dication cannot be solely attributed to cation-anion size-matching, as it would therefore be equally feasible for the monomeric **[(L)ZnCl][BAr$^F_4$]** complexes to form dimeric species in the solid state. The fact that the latter complexes exist solely as four-coordinate monomers indicates that the preference for nickel to form dimeric complexes is due to a combination of size-matching and crystal field stabilisation energy (CFSE) considerations. By adopting a five-coordinate geometry, the Ni^{2+} ion (d^8) increases its CFSE in comparison that which would result from the adoption of a four-coordinate geometry, whilst Zn^{2+} (d^{10}) is not subject to CFSE effects. The fact that all of the **[(L)ZnCl][BAr$^F_4$]** complexes are monomeric whilst the majority of the nickel analogues are dimeric indicates that CFSE effects are more important than size-matching in determining the nuclearity of the β-triketimine complexes, as in the absence of CFSE effects the formation of monomeric complexes appears to be strongly favoured.

Single crystals of **[{(L^1)Ni(μ-Br)}$_2$][BAr$^F_4$]$_2$** suitable for X-ray diffraction were obtained directly from the reaction mixture (i.e. under anhydrous conditions), by careful layering of hexane onto the DCM solution. However, the structure was found to be highly disordered and as such an acceptable refinement could not be obtained. Single crystals of this compound could also be obtained by recrystallisation from hot fluorobenzene, though these

were also found to be similarly disordered. Fortunately, the same problems were not encountered in the case of **[{(L^7)Ni(μ-Br)}$_2$][BAr$^F{}_4$]$_2$**, single crystals of which were obtained by vapour diffusion of hexane into a DCM solution under non-anhydrous conditions. The molecular structure of **[{(L^7)Ni(μ-Br)}$_2$][BAr$^F{}_4$]$_2$** (**figure 4.5**) features a centrosymmetric dimeric dication, in which the nickel centres are in a slightly distorted square-pyramidal geometry ($\tau = 0.12$).

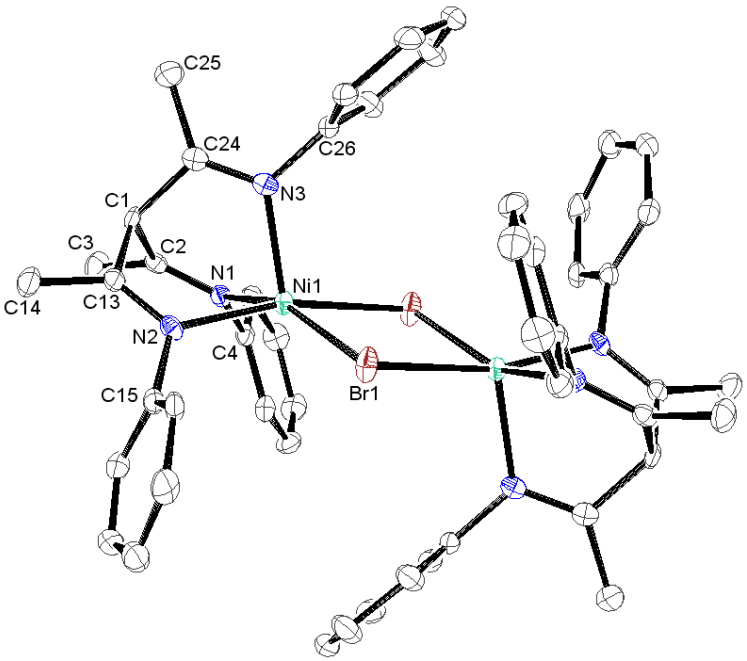

Figure 4.5 ORTEP representation of the dicationic unit in [{(L^7)Ni(μ-Br)}$_2$][BAr$^F{}_4$]$_2$ with thermal ellipsoids set at the 50 % probability level; all hydrogen atoms and methyl groups of mesityls omitted for clarity

The Ni-N bond distances (**table 4.2**) are noticeably longer than in the aforementioned four-coordinate complexes, which is simply as a result of the increased coordination number at nickel. The increase in coordination number is also responsible for the fact that the N-N separation of 2.887(4) Å is somewhat larger than the corresponding distances seen in the **[(L)NiBr]$_2$[NiBr$_4$]** complexes. The basal Ni(1)-N(1) and Ni(1)-N(2) distances of 2.083(3) Å and 2.126(3) Å respectively are somewhat longer than the axial Ni(1)-N(3) distance (2.038(3) Å), which is likely due to the *trans*-influence of the two bridging bromide ligands. The fact that there is a significant difference between the two longer distances may be due to the fact that the N(1) mesityl substituent is twisted away from orthogonality with the imine plane to a much greater degree than the other two mesityl groups, both of which lie approximately orthogonal to their respective imine planes. As such, N(1) is able to approach the nickel centre more closely than N(2), resulting in a slightly shortened bond

distance. The notion that the difference between the Ni(1)-N(1) and Ni(1)-N(2) distances is due purely to steric effects is also supported by the fact that there is no similar discrepancy in the Br(1)-Ni(1) and Br(1)′-Ni(1) distances, which are very similar at 2.4969(6) Å and 2.5072(5) Å respectively. The bridging nature of the bromide ligands accounts for the fact that the Ni-Br distances are much longer than those observed in the four-coordinate derivatives. Additionally, The C=N-C_{Ar} bond angles all lie close to the sp^2 ideal of 120° (**table 4.2**), as would be expected for an all-methyl backbone substituted ligand.

Table 4.2 Selected bond lengths (Å), angles (°) and interplanar angles (°) for the dicationic units in $[\{(L^7)Ni(\mu\text{-}Br)\}_2][BAr^F{}_4]_2$ and $[\{(L^8)Ni(\mu\text{-}Br)\}_2][BAr^F{}_4]_2.2CH_2Cl_2$

$[\{(L^7)Ni(\mu\text{-}Br)\}_2]^{2+}$	$[\{(L^8)Ni(\mu\text{-}Br)\}_2]^{2+}$
Br(1)-Ni(1) 2.4969(6)	Br(1)-Ni(1) 2.4691(8)
Br(1)′-Ni(1) 2.5072(5)	Br(1)′-Ni(1) 2.4929(8)
Ni(1)-N(1) 2.083(3)	Ni(1)-N(1) 2.088(4)
Ni(1)-N(2) 2.126(3)	Ni(1)-N(2) 2.085(4)
Ni(1)-N(3) 2.038(3)	Ni(1)-N(3) 2.027(4)
N(1)-C(2) 1.283(4)	N(1)-C(2) 1.283(6)
N(2)-C(13) 1.276(4)	N(2)-C(14) 1.279(6)
N(3)-C(24) 1.282(4)	N(3)-C(25) 1.271(6)
N(1)-C(4) 1.455(4)	N(1)-C(7) 1.434(7)
N(2)-C(15) 1.454(4)	N(2)-C(16) 1.445(7)
N(3)-C(26) 1.451(4)	N(3)-C(27) 1.445(6)
C(1)-C(2) 1.536(4)	C(1)-C(2) 1.547(7)
C(1)-C(13) 1.516(4)	C(1)-C(14) 1.514(8)
C(1)-C(24) 1.523(4)	C(1)-C(25) 1.533(7)
Ni(1)-Br(1)-Ni(1)′ 98.70(2)	Ni(1)-Br(1)-Ni(1)′ 96.38(3)
Br(1)-Ni(1)-Br(1)′ 81.30(2)	Br(1)-Ni(1)-Br(1)′ 83.62(3)
Br(1)-Ni(1)-N(1) 159.16(7)	Br(1)-Ni(1)-N(1) 163.69(12)
Br(1)-Ni(1)-N(2) 93.69(8)	Br(1)-Ni(1)-N(2) 91.89(11)
Br(1)-Ni(1)-N(3) 113.59(8)	Br(1)-Ni(1)-N(3) 107.02(12)
Br(1)′-Ni(1)-N(1) 94.64(7)	Br(1)′-Ni(1)-N(1) 95.91(12)
Br(1)′-Ni(1)-N(2) 166.39(7)	Br(1)′-Ni(1)-N(2) 171.08(12)
Br(1)′-Ni(1)-N(3) 103.00(7)	Br(1)′-Ni(1)-N(3) 98.45(12)
N(1)-Ni(1)-N(2) 85.55(10)	N(1)-Ni(1)-N(2) 86.23(16)
N(1)-Ni(1)-N(3) 87.25(11)	N(1)-Ni(1)-N(3) 89.21(16)
N(2)-Ni(1)-N(3) 90.61(10)	N(2)-Ni(1)-N(3) 90.22(17)
Ni(1)-N(1)-C(4) 121.70(19)	Ni(1)-N(1)-C(7) 117.6(3)
Ni(1)-N(2)-C(15) 123.90(19)	Ni(1)-N(2)-C(16) 123.7(3)
Ni(1)-N(3)-C(26) 123.69(19)	Ni(1)-N(3)-C(27) 123.0(3)
Ni(1)-N(1)-C(2) 116.7(2)	Ni(1)-N(1)-C(2) 117.8(4)
Ni(1)-N(2)-C(13) 116.5(2)	Ni(1)-N(2)-C(14) 115.8(4)
Ni(1)-N(3)-C(24) 117.3(2)	Ni(1)-N(3)-C(25) 117.1(3)
C(2)-N(1)-C(4) 121.1(3)	C(2)-N(1)-C(7) 124.5(4)
C(13)-N(2)-C(15) 119.3(3)	C(14)-N(2)-C(16) 120.4(5)
C(24)-N(3)-C(26) 118.8(3)	C(25)-N(3)-C(27) 119.6(4)
C(1)-C(2)-N(1) 117.2(3)	C(1)-C(2)-N(1) 115.2(5)
C(1)-C(13)-N(2) 117.1(3)	C(1)-C(14)-N(2) 117.9(5)
C(1)-C(24)-N(3) 118.3(3)	C(1)-C(25)-N(3) 117.9(5)
N(1)-C(2)-C(3) 127.0(3)	N(1)-C(2)-C(3) 130.1(5)
N(2)-C(13)-C(14) 125.5(3)	N(2)-C(14)-C(15) 126.3(5)
N(3)-C(24)-C(25) 125.9(3)	N(3)-C(25)-C(26) 126.7(5)
θ_T (C(1)-C(2)-N(1)-C(3)/$C(4)_{Ar}$) = 61.3(3)	θ_T (C(1)-C(2)-N(1)-C(3)/$C(7)_{Ar}$) = 85.2(5)
θ_T (C(1)-C(13)-N(2)-C(14)/$C(15)_{Ar}$) = 83.9(3)	θ_T (C(1)-C(14)-N(2)-C(15)/$C(16)_{Ar}$) = 71.1(5)
θ_T (C(1)-C(24)-N(3)-C(25)/$C(26)_{Ar}$) = 85.5(3)	θ_T (C(1)-C(25)-N(3)-C(26)/$C(27)_{Ar}$) = 83.4(5)

[{(L^8)Ni(μ-Br)}$_2$][BAr$^F_4$]$_2$ was crystallised directly from the reaction mixture, through layering of hexane onto the DCM solution, and was found to contain two molecules of DCM in the unit cell. The molecular structure of the dicationic unit (**figure 4.6**) again shows the nickel centres to be in a slightly distorted square planar geometry; the τ value of 0.12 is identical to that observed in **[{(L^7)Ni(μ-Br)}$_2$][BAr$^F_4$]$_2$**, though the Br-Ni-N$_{basal}$ angles (**table 4.2**) are on average closer to 180°. The majority of the structural parameters are very similar to those of the latter complex, except for the fact that the C(2)-N(1)-C(7) angle is slightly widened at 124.5(4)° as a result of the presence of the bulky *tert*-butyl substituent. The Ni(1)-N(1) and Ni(1)-N(2) distances are practically identical at 2.088(4) and 2.085(4) Å respectively; the lack of discrepancy between the two distances in this case is likely a result of the reduced steric hindrance of the 2-isopropylphenyl and 2-methoxyphenyl substituents relative to the bulkier mesityl groups present in **[{(L^7)Ni(μ-Br)}$_2$][BAr$^F_4$]$_2$**. Additionally, the mean N-N separation of 2.885(7) Å is essentially no different to that seen in **[{(L^7)Ni(μ-Br)}$_2$][BAr$^F_4$]$_2$**.

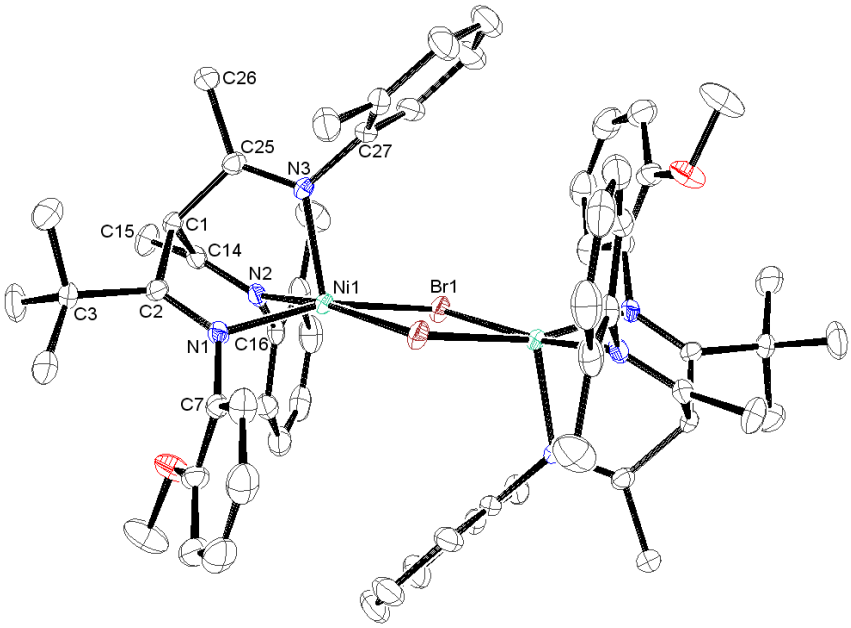

Figure 4.6 ORTEP representation of the dicationic unit in [{(L^8)Ni(μ-Br)}$_2$][BAr$^F_4$]$_2$.2CH$_2$Cl$_2$ with thermal ellipsoids set at the 30 % probability level; all hydrogen atoms and methyl groups of isopropyls omitted for clarity

The five-coordinate dimeric species described in this work represent the first structurally characterised dicationic [{LNi(μ-X)}$_2$]$^{2+}$ complexes (L = tridentate ligand). The closest literature precedent is the neutral complex {(Tp^{Mes**})Ni(μ-Cl)}$_2$,[378] (Tp^{Mes**} = hydrobis(5-mesitylpyrazolyl)(3-mesitylpyrazolyl)borate) though as this is a chloride-bridged species no close comparator for the Ni-Br bond distances exists. However, the Ni-Br distances in

[{(L^7)Ni(μ-Br)}$_2$][BAr$^F_4$]$_2$ and **[{(L^8)Ni(μ-Br)}$_2$][BAr$^F_4$]$_2$** are on average shorter than the corresponding distances of 2.5192(4) and 2.5648(4) Å as seen in the five-coordinate dimeric {(Tm^{Me})Ni(μ-Br)}$_2$ (Tm^{Me} = hydrotris(1-methyl-2-thioimidazol-3-yl)borate), which may be as a result of the increased electron-donating ability of the anionic trisulfur-ligating Tm^{Me} ligand relative to the β-triketimines.[379] The Ni-N distances in both **[{(L^7)Ni(μ-Br)}$_2$][BAr$^F_4$]$_2$** and **[{(L^8)Ni(μ-Br)}$_2$][BAr$^F_4$]$_2$** are on average longer than the corresponding distances in {(Tp^{Mes*})Ni(μ-Cl)}$_2$ (Ni-N$_{basal}$ = 2.029(2) Å, 2.0390(18) Å; Ni-N$_{axial}$ = 2.0355(17) Å), which is likely due to both the reduced electron-donating ability, and greatly increased steric bulk, of **L^7** and **L^8** relative to Tp^{Mes**}. Such considerations are also likely responsible for the fact that {(Tp^{Mes**})Ni(μ-Cl)}$_2$ shows no discrepancy between the Ni-N$_{basal}$ and Ni-N$_{axial}$ bond lengths, whereas the β-triketimine complexes display noticeably lengthened Ni-N$_{basal}$ distances. Accordingly, the mean N-N separation of 2.857(3) Å in {(Tp^{Mes**})Ni(μ-Cl)}$_2$ is also slightly smaller than that measured in either of the β-triketimine complexes.[378]

In the case of **[{(L^5)Ni(μ-Br)}$_2$][BAr$^F_4$]$_2$** and **[{(L^3)Ni(μ-Br)}$_2$][BAr$^F_4$]$_2$**, vapour diffusion of hexane into 1,2-difluorobenzene solutions of the appropriate complex under non-anhydrous conditions furnished crystals suitable for X-ray diffraction. However, in both cases the complexes were found to have crystallised as six-coordinate dimeric species, containing one molecule of adventitious water bound to each of the nickel centres. Similarly, recrystallisation of **[{(L^{12})Ni(μ-Br)}$_2$][BAr$^F_4$]$_2$** by vapour diffusion of hexane into a DCM solution under non-anhydrous conditions gave an analogous crystalline species. It is not clear why the aforementioned **[{(L^7)Ni(μ-Br)}$_2$][BAr$^F_4$]$_2$** did not also crystallise with adventitious coordinated water, though this may possibly be due to the combined steric hindrance of the three mesityl groups, or alternatively to simple crystal packing effects. **[{(L^5)Ni(μ-Br)(OH$_2$)}$_2$][BAr$^F_4$]$_2$** crystallises as a 1,2-difluorobenzene solvate, and the molecular structure of the dicationic unit is presented in **figure 4.7**. The location of one of the isopropyl groups is disordered over two sites, such that the 2,6-diisopropylphenyl moiety may be bound to either N(1) or N(3), giving two possible arrangements in which the two 2-isopropylphenyl substituents either point in the same direction (i.e. away from the 2,6-diisopropylphenyl group), or in opposite directions. This offers further support to the hypothesis outlined in **chapter 3** that rotation of the 2-isopropylphenyl substituents in complexes of **L^5** occurs more freely than in the related *tert*-butyl backbone substituted **L^{11}**, complexes of which invariably feature the two 2-

isopropylphenyl substituents oriented in the same direction, away from the 2,6-diisopropylphenyl group. The nickel centres are in a slightly distorted octahedral geometry, though the Br-Ni-N angles (**table 4.3**) are on average closer to 180° than the Br-Ni-N_{basal} angles in the aforementioned five-coordinate dimeric complexes. The increase in coordination number is also manifested as a relative increase in the Br(1)-Ni(1) and Br(1)′-Ni(1) distances, which at 2.5279(5) Å and 2.5497(6) Å respectively are somewhat longer than the corresponding distances in the five-coordinate complexes. Similarly, the Ni-N distances are on average increased slightly, as is the mean N-N separation (2.929(4) Å). The Ni(1)-N(3) distance (2.132(3) Å) is slightly longer than Ni(1)-N(1) (2.103(3) Å) and Ni(1)-N(2) (2.105(3) Å), which may be as a result of the placement of the Ni(1)-N(3) bond *trans* to the shorter of the Ni-Br bonds. A further effect of the increased coordination number is an increase in inter- and intra-ligand repulsion, which is manifested in the fact that all of the aryl groups are oriented essentially orthogonal to the planes defined by their respective imine moieties (**table 4.3**), in contrast to the situation observed in the related five-coordinate complexes where at least one of the aryl groups is twisted away from orthogonality by a substantial amount (i.e. >15°, **table 4.2**).

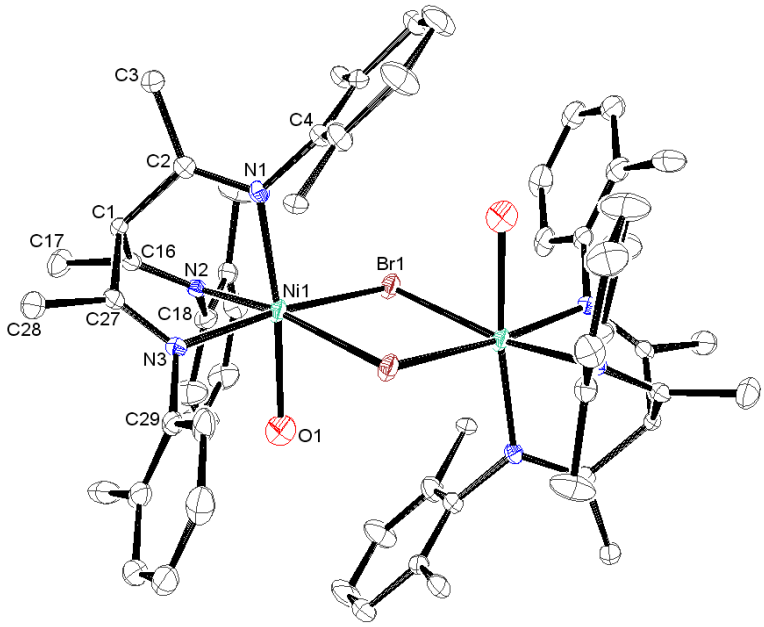

Figure 4.7 ORTEP representation of the dicationic unit in $[\{(L^5)Ni(\mu\text{-}Br)(OH_2)\}_2][BAr^F{}_4]_2.C_6H_4F_2$ with thermal ellipsoids set at the 40% probability level; all hydrogen atoms and methyl groups of isopropyls omitted for clarity

Table 4.3 Selected bond lengths (Å), angles (°) and interplanar torsion angles (°) for the dicationic units in $[\{(L^5)Ni(\mu\text{-}Br)(OH_2)\}_2][BAr^F{}_4]_2.C_6H_4F_2$, $[\{(L^3)Ni(\mu\text{-}Br)(OH_2)\}_2][BAr^F{}_4]_2$ and $[\{(L^{12})Ni(\mu\text{-}Br)(OH_2)\}_2][BAr^F{}_4]_2.CH_2Cl_2$

$[\{(L^5)Ni(\mu\text{-}Br)(OH_2)\}_2]^{2+}$	$[\{(L^3)Ni(\mu\text{-}Br)(OH_2)\}_2]^{2+}$	$[\{(L^{12})Ni(\mu\text{-}Br)(OH_2)\}_2]^{2+}$
Br(1)-Ni(1) 2.5279(5)	Br(1)-Ni(1) 2.5538(15)	Br(1)-Ni(1) 2.5171(10)
Br(1)′-Ni(1) 2.5497(6)	Br(1)′-Ni(1) 2.5508(15)	Br(1)′-Ni(1) 2.5590(11)
Ni(1)-O(1) 2.162(3)	Ni(1)-O(1) 2.091(6)	Ni(1)-O(1) 2.138(7)
Ni(1)-N(1) 2.103(3)	Ni(1)-N(1) 2.128(8)	Ni(1)-N(1) 2.123(5)
Ni(1)-N(2) 2.105(3)	Ni(1)-N(2) 2.095(8)	Ni(1)-N(2) 2.103(5)
Ni(1)-N(3) 2.132(3)	Ni(1)-N(3) 2.118(8)	Ni(1)-N(3) 2.064(5)
N(1)-C(2) 1.283(4)	N(1)-C(2) 1.250(13)	N(1)-C(2) 1.265(8)
N(2)-C(16) 1.275(4)	N(2)-C(14) 1.279(13)	N(2)-C(16) 1.259(9)
N(3)-C(27) 1.270(4)	N(3)-C(25) 1.247(13)	N(3)-C(27) 1.278(9)
N(1)-C(4) 1.452(3)	N(1)-C(4) 1.469(14)	N(1)-C(7) 1.443(8)
N(2)-C(18) 1.451(4)	N(2)-C(16) 1.469(13)	N(2)-C(18) 1.465(9)
N(3)-C(29) 1.437(3)	N(3)-C(27) 1.445(13)	N(3)-C(29) 1.455(9)
C(1)-C(2) 1.522(5)	C(1)-C(2) 1.524(14)	C(1)-C(2) 1.532(9)
C(1)-C(16) 1.523(4)	C(1)-C(14) 1.509(15)	C(1)-C(16) 1.542(9)
C(1)-C(27) 1.529(5)	C(1)-C(25) 1.536(14)	C(1)-C(27) 1.526(9)
Ni(1)-Br(1)-Ni(1)′ 95.55(2)	Ni(1)-Br(1)-Ni(1)′ 97.10(5)	Ni(1)-Br(1)-Ni(1)′ 97.14(3)
Br(1)-Ni(1)-Br(1)′ 84.45(2)	Br(1)-Ni(1)-Br(1)′ 82.91(5)	Br(1)-Ni(1)-Br(1)′ 82.86(3)
Br(1)-Ni(1)-O(1) 86.06(7)	Br(1)-Ni(1)-O(1) 87.80(18)	Br(1)-Ni(1)-O(1) 86.74(19)
Br(1)′-Ni(1)-O(1) 82.24(7)	Br(1)′-Ni(1)-O(1) 86.47(17)	Br(1)′-Ni(1)-O(1) 81.43(19)
Br(1)-Ni(1)-N(1) 99.64(7)	Br(1)-Ni(1)-N(1) 98.4(2)	Br(1)-Ni(1)-N(1) 95.64(14)
Br(1)-Ni(1)-N(2) 92.45(7)	Br(1)-Ni(1)-N(2) 175.5(2)	Br(1)-Ni(1)-N(2) 173.08(15)
Br(1)-Ni(1)-N(3) 173.72(8)	Br(1)-Ni(1)-N(3) 95.4(2)	Br(1)-Ni(1)-N(3) 99.40(15)
Br(1)′-Ni(1)-N(1) 102.35(7)	Br(1)′-Ni(1)-N(1) 100.5(2)	Br(1)′-Ni(1)-N(1) 168.08(15)
Br(1)′-Ni(1)-N(2) 168.58(8)	Br(1)′-Ni(1)-N(2) 94.7(2)	Br(1)′-Ni(1)-N(2) 92.16(14)
Br(1)′-Ni(1)-N(3) 94.28(7)	Br(1)′-Ni(1)-N(3) 171.8(2)	Br(1)′-Ni(1)-N(3) 104.11(15)
O(1)-Ni(1)-N(1) 172.95(10)	O(1)-Ni(1)-N(1) 171.1(3)	O(1)-Ni(1)-N(1) 86.7(2)
O(1)-Ni(1)-N(2) 86.60(11)	O(1)-Ni(1)-N(2) 88.3(3)	O(1)-Ni(1)-N(2) 87.8(2)
O(1)-Ni(1)-N(3) 87.67(10)	O(1)-Ni(1)-N(3) 85.4(3)	O(1)-Ni(1)-N(3) 172.1(2)
N(1)-Ni(1)-N(2) 89.00(10)	N(1)-Ni(1)-N(2) 85.8(3)	N(1)-Ni(1)-N(2) 88.2(2)
N(1)-Ni(1)-N(3) 86.64(10)	N(1)-Ni(1)-N(3) 87.7(3)	N(1)-Ni(1)-N(3) 87.8(2)
N(2)-Ni(1)-N(3) 87.61(10)	N(2)-Ni(1)-N(3) 86.5(3)	N(2)-Ni(1)-N(3) 86.5(2)
Ni(1)-N(1)-C(4) 127.11(17)	Ni(1)-N(1)-C(4) 123.8(6)	Ni(1)-N(1)-C(7) 116.9(4)
Ni(1)-N(2)-C(18) 123.45(19)	Ni(1)-N(2)-C(16) 122.5(6)	Ni(1)-N(2)-C(18) 122.4(4)
Ni(1)-N(3)-C(29) 124.37(17)	Ni(1)-N(3)-C(27) 122.7(6)	Ni(1)-N(3)-C(29) 124.1(4)
Ni(1)-N(1)-C(2) 115.3(2)	Ni(1)-N(1)-C(2) 115.9(7)	Ni(1)-N(1)-C(2)118.5(4)
Ni(1)-N(2)-C(16) 115.1(2)	Ni(1)-N(2)-C(14) 117.0(7)	Ni(1)-N(2)-C(16) 116.8(4)
Ni(1)-N(3)-C(27) 116.8(2)	Ni(1)-N(3)-C(25) 117.0(7)	Ni(1)-N(3)-C(27) 116.3(4)
C(2)-N(1)-C(4) 117.6(3)	C(2)-N(1)-C(4) 119.5(8)	C(2)-N(1)-C(7) 124.4(5)
C(16)-N(2)-C(18) 119.5(3)	C(14)-N(2)-C(16) 119.3(8)	C(16)-N(2)-C(18) 120.5(6)
C(27)-N(3)-C(29) 118.9(3)	C(25)-N(3)-C(27) 120.3(9)	C(27)-N(3)-C(29) 119.0(5)
C(1)-C(2)-N(1) 119.0(3)	C(1)-C(2)-N(1) 119.5(9)	C(1)-C(2)-N(1) 115.5(5)
C(1)-C(16)-N(2) 118.5(3)	C(1)-C(14)-N(2) 117.7(8)	C(1)-C(16)-N(2) 117.6(6)
C(1)-C(27)-N(3) 117.0(3)	C(1)-C(25)-N(3) 118.5(9)	C(1)-C(27)-N(3) 118.8(6)
N(1)-C(2)-C(3) 126.7(3)	N(1)-C(2)-C(3) 126.8(9)	N(1)-C(2)-C(3) 130.3(6)
N(2)-C(16)-C(17) 125.7(3)	N(2)-C(14)-C(15) 126.0(9)	N(2)-C(16)-C(17) 125.2(6)
N(3)-C(27)-C(28) 126.9(3)	N(3)-C(25)-C(26) 126.7(10)	N(3)-C(27)-C(28) 125.6(6)
θ_T (C(1)-C(2)-N(1)-C(3)/C(4)$_{Ar}$) = 85.6(3)	θ_T (C(1)-C(2)-N(1)-C(3)/C(4)$_{Ar}$) = 88.3(9)	θ_T (C(1)-C(2)-N(1)-C(3)/C(7)$_{Ar}$) = 88.0(6)
θ_T (C(1)-C(16)-N(2)-C(17)/C(18)$_{Ar}$) = 87.1(3)	θ_T (C(1)-C(14)-N(2)-C(15)/C(16)$_{Ar}$) = 82.7(9)	θ_T (C(1)-C(16)-N(2)-C(17)/C(18)$_{Ar}$) = 88.8(6)
θ_T (C(1)-C(27)-N(3)-C(28)/C(29)$_{Ar}$) = 89.2(3)	θ_T (C(1)-C(25)-N(3)-C(26)/C(27)$_{Ar}$) = 85.2(10)	θ_T (C(1)-C(27)-N(3)-C(28)/C(29)$_{Ar}$) = 82.1(6)

The solid-state structure of **$[\{(L^3)Ni(\mu\text{-}Br)(OH_2)\}_2][BAr^F{}_4]_2$** features a highly disordered $BAr^F{}_4^-$ ion, where all but one of the 3,5-bis(trifluoromethyl)phenyl groups are disordered over two sites. As a result of this, the data are of low quality (R = 10.71%), though the dicationic unit (**figure 4.8**) is not similarly affected by disorder. The structural parameters

of this complex (**table 4.3**) are very similar to those of **[{(L^5)Ni(μ-Br)(OH$_2$)}$_2$][BAr$^F{}_4$]$_2$**, though in this case there is less of a difference between the Br(1)-Ni(1) and Br(1)-Ni(1)′ distances, and the Br-Ni-N angles are on average slightly closer to 180°. The mean N-N separation of 2.899(14) Å is also slightly smaller than that in **[{(L^5)Ni(μ-Br)(OH$_2$)}$_2$][BAr$^F{}_4$]$_2$**, as a result of the reduced steric bulk of **L^3** relative to **L^5**. Additionally, the Ni(1)-O(1) distance of 2.091(6) Å is somewhat shorter than the related distance of 2.162(3) Å as observed in the latter complex. Of course, the precision of all these parameters must be treated with caution when considering such a low-quality dataset; for example, any differences between the Ni-N distances are within experimental error.

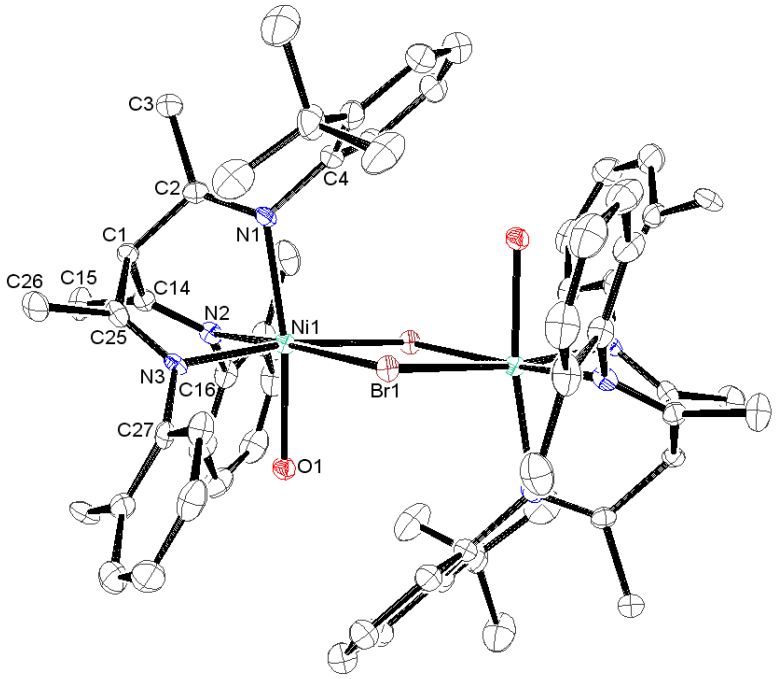

Figure 4.8 ORTEP representation of the dicationic unit in [{(L^3)Ni(μ-Br)(OH$_2$)}$_2$][BAr$^F{}_4$]$_2$ with thermal ellipsoids set at the 30% probability level; all hydrogen atoms and methyl groups of isopropyls omitted for clarity

Owing to the fact that **L^{12}** features both *tert*-butyl and mesityl substitution at the same imine moiety, a degree of steric bulk which is sufficient to cause the free ligand to exist solely as the β-triketimine tautomer (**chapter 2**), it is surprising not only that a dimeric complex is obtained, but also that single crystals of the six-coordinate complex **[{(L^{12})Ni(μ-Br)(OH$_2$)}$_2$][BAr$^F{}_4$]$_2$.CH$_2$Cl$_2$** were obtained upon recrystallisation from DCM and hexane under non-anhydrous conditions. The molecular structure of the dicationic unit (**figure 4.9**) does not differ to any significant degree from the precedent set by the two aforementioned six-coordinate dimers, though there is a slight difference between the Br(1)-Ni(1) and Br(1)′-Ni(1) distances of 2.5171(10) and 2.5590(11) Å respectively. In

concurrence with previous observations, the shorter of these lies *trans* to the longest of the Ni-N bonds, namely N(1)-Ni(1) (**table 4.3**). Additionally, whilst the Ni(1)-N(1) and Ni(1)-N(2) distances (2.123(5) and 2.103(5) Å) are of a similar size to the corresponding distances in **[{(L^5)Ni(μ-Br)(OH$_2$)}$_2$][BAr$^F{}_4$]$_2$** and **[{(L^3)Ni(μ-Br)(OH$_2$)}$_2$][BAr$^F{}_4$]$_2$**, the Ni(1)-N(3) distance of 2.064(5) Å is relatively shorter. This may be due to the fact that in this case, the bulkiest imine substituent of **L^{12}** does not occupy the coordination site *trans* to the aqua ligand, in contrast to the situation observed in both **[{(L^5)Ni(μ-Br)(OH$_2$)}$_2$][BAr$^F{}_4$]$_2$** and **[{(L^3)Ni(μ-Br)(OH$_2$)}$_2$][BAr$^F{}_4$]$_2$**. The mean N-N separation of 2.901(9) Å is of a similar size to those measured in the other six-coordinate dimeric complexes.

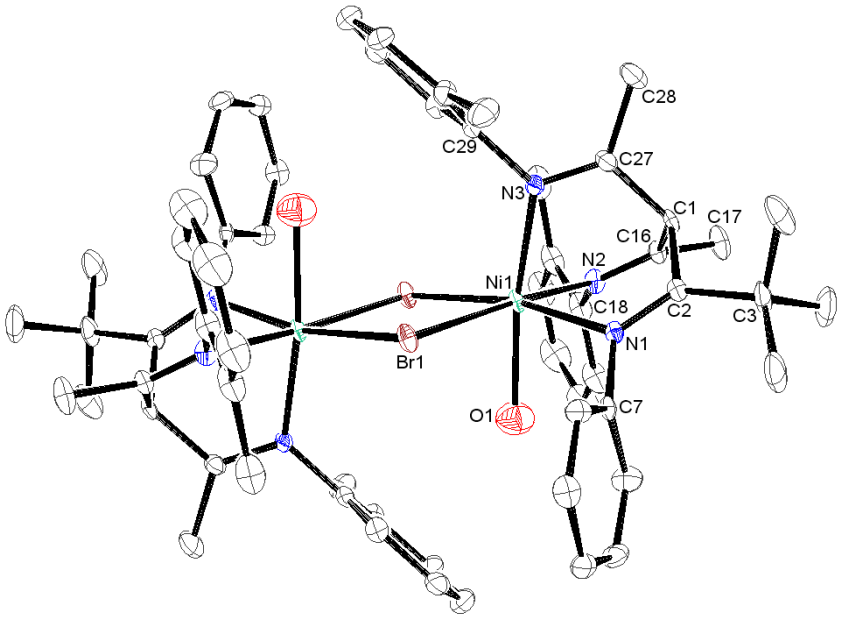

Figure 4.9 ORTEP representation of the dicationic unit in [{(L^{12})Ni(μ-Br)(OH$_2$)}$_2$][BAr$^F{}_4$]$_2$.CH$_2$Cl$_2$ with thermal ellipsoids set at the 30 % probability level; all hydrogen atoms and methyl groups of mesityls and isopropyls omitted for clarity

The closest literature precedent to the dimeric six-coordinate aqua complexes described herein is the dicationic [{(*fac*-dien)Ni(μ-Br)(OH$_2$)}$_2$][Cl]$_2$. The Ni-O distance (2.0674(18) Å) and Ni-N distances (2.0733(17) Å, 2.0774(17) Å, 2.0797 (18) Å) in this complex are all shorter than the majority of the corresponding distances in the three aforementioned β-triketimine complexes, which is likely due to the negligible steric demand and increased electron-donating ability of the dien ligand in comparison to **L^3**, **L^5** and **L^8**.[380] The Br-Ni distances in the β-triketimine complexes are similar on average to the corresponding distances (2.5157(17) and 2.5884(16) Å) in the complex [{(*mer*-L)Ni(μ-Br)(OH$_2$)}$_2$][Br]$_2$

(L = *N,N′,N″*-(5-bromo-imidazol-4-yl-methylene)(2-pyridylmethyl)amine). The rather large discrepancy between the two Br-Ni distances in the literature compound is probably due to the fact that one of the bromine atoms lies *trans* to the aqua ligand, while the other bromine is *trans* to an imine donor.[381] In contrast, all of the six-coordinate β-triketimine complexes feature the bromine atoms exclusively *cis* to the aqua ligand, and as such any discrepancies in the Br-Ni bond lengths are less pronounced.

4.2.1.3 [(L)NiBr][BAr$^F_4$] complexes

When the very bulky **L^{11}** was reacted with $NiBr_2$(DME) and $NaBAr^F_4$ and the product crystallised directly from the reaction mixture, bright-red crystals of the monomeric four-coordinate complex **[(L^{11})NiBr][BAr$^F_4$]** were obtained exclusively (**scheme 4.5**). The presence of the *tert*-butyl group in **L^{11}** obviously has a great effect towards the inhibition of dimerisation, as the related **L^5** yielded only a dimeric complex.

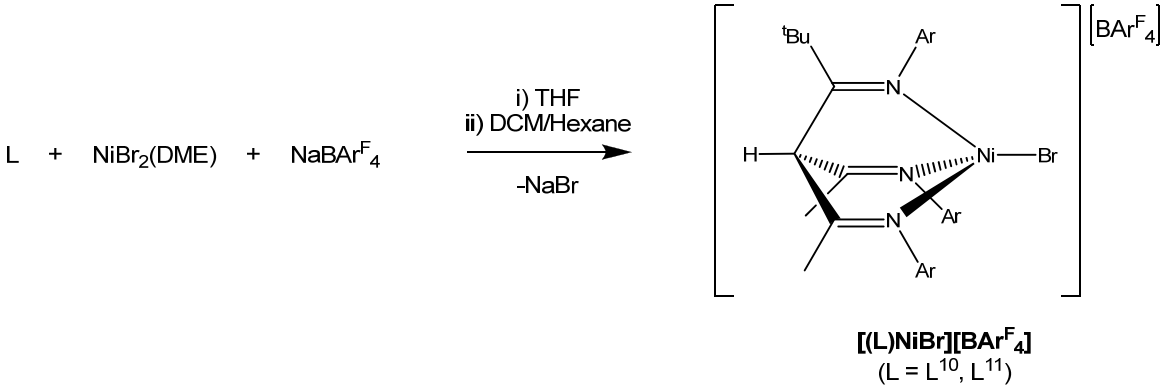

Scheme 4.5 Synthesis of [(L)NiBr][BAr$^F_4$] complexes

[(L^{11})NiBr][BAr$^F_4$] crystallises with a molecule each of DCM and hexane in the unit cell, though both of these were found to be highly disordered and were thus removed using SQUEEZE.[352] Additionally the two 2-isopropylphenyl groups are disordered over two sites by slight rotation about their respective N-C_{Ar} bonds; **figure 4.10** shows the major contributor to this disordered structure. In all possible arrangements of the disordered components the 2-isopropylphenyl groups are oriented in the same direction, away from the 2,6-diisopropylphenyl moiety. This again gives support to the hypothesis that rotation about the N-C_{Ar} bonds of the 2-isopropylphenyl substituted imines in **L^{11}** is severely restricted by the presence of the *tert*-butyl group, whereas in **L^5** (which is identical to **L^{11}** except for the fact that the R^7 *tert*-butyl substituent is replaced by methyl) rotation of the corresponding aryl groups occurs relatively freely.

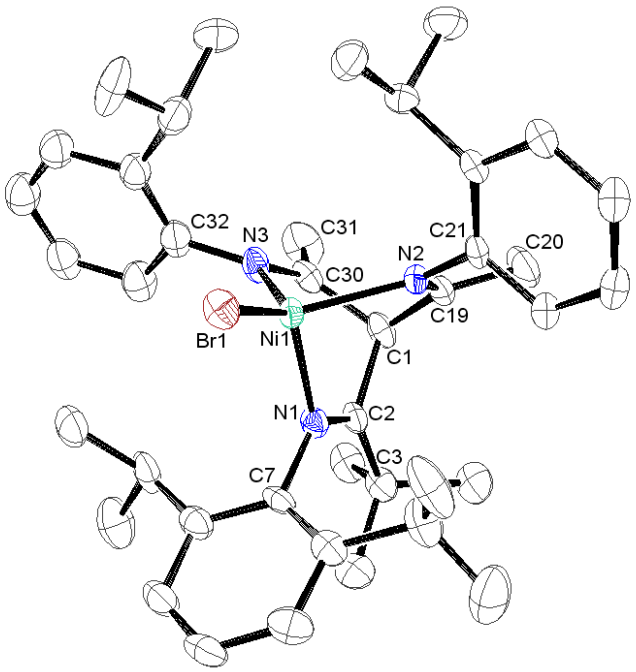

Figure 4.10 ORTEP representation of the cationic unit in $[(L^{11})NiBr][BAr^{F}_{4}].½CH_2Cl_2.½C_6H_{14}$ with thermal ellipsoids set at the 40 % probability level; hydrogen atoms omitted for clarity

As expected, the C(2)-N(1)-C(7) angle of 126.2(5)° is wider than the corresponding angles of the methyl substituted imines (**table 4.4**), as well as being wider than all the C=N-C_{Ar} angles in **$[\{(L^5)Ni(\mu\text{-}Br)(OH_2)\}_2][BAr^{F}_{4}]_2$**, which offers further explanation as to why **$[(L^{11})NiBr][BAr^{F}_{4}]$** exists solely as a monomer, whereas the reduced steric bulk of $\mathbf{L^5}$ allows for dimerisation. The *tert*-butyl group effectively 'pushes' the 2,6-diisopropylphenyl moiety further in towards the metal centre, and thus increases the steric repulsion that would result upon dimerisation to such a degree that a monomeric species is obtained exclusively. The Ni-N distances in **$[(L^{11})NiBr][BAr^{F}_{4}]$** (**table 4.4**) are essentially no different to those seen in the aforementioned **$[(L)NiBr]_2[NiBr_4]$** compounds, whilst the mean N-N separation of 2.864(8) Å is considerably larger, as a result of the increased steric bulk of $\mathbf{L^{11}}$ relative to $\mathbf{L^8}$ and $\mathbf{L^{10}}$. In fact, the mean N-N separation in **$[(L^{11})NiBr][BAr^{F}_{4}]$** is only slightly smaller than those observed in the five-coordinate dimeric complexes.

Table 4.4 Selected bond lengths (Å), angles (°) and interplanar torsion angles (°) for the cationic units in $[(L^{11})NiBr][BAr^F_4].½CH_2Cl_2.½C_6H_{14}$ and $[(L^{10})NiBr][BAr^F_4]$

$[(L^{11})NiBr]^+$	$[(L^{10})NiBr]^+$
Br(1)-Ni(1) 2.321(6)	Br(1)-Ni(1) 2.314(17)
Ni(1)-N(1) 1.992(5)	Ni(1)-N(1) 2.032(18)
Ni(1)-N(2) 2.022(4)	Ni(1)-N(2) 2.007(17)
Ni(1)-N(3) 2.035(4)	Ni(1)-N(3) 2.016(17)
N(1)-C(2) 1.264(7)	N(1)-C(2) 1.29(2)
N(2)-C(19) 1.258(7)	N(2)-C(16) 1.25(2)
N(3)-C(30) 1.267(7)	N(3)-C(27) 1.274(17)
N(1)-C(7) 1.451(7)	N(1)-C(7) 1.497(11)
N(2)-C(21) 1.473(8)	N(2)-C(18) 1.479(11)
N(3)-C(32) 1.407(8)	N(3)-C(29) 1.448(10)
C(1)-C(2) 1.553(9)	C(1)-C(2) 1.544(14)
C(1)-C(19) 1.522(10)	C(1)-C(16) 1.524(15)
C(1)-C(30) 1.525(9)	C(1)-C(27) 1.507(15)
Br(1)-Ni(1)-N(1) 121.3(2)	Br(1)-Ni(1)-N(1) 116.6(9)
Br(1)-Ni(1)-N(2) 121.4(3)	Br(1)-Ni(1)-N(2) 120.5(10)
Br(1)-Ni(1)-N(3) 131.3(3)	Br(1)-Ni(1)-N(3) 139.6(11)
N(1)-Ni(1)-N(2) 89.6(2)	N(1)-Ni(1)-N(2) 90.7(9)
N(1)-Ni(1)-N(3) 88.40(19)	N(1)-Ni(1)-N(3) 87.3(8)
N(2)-Ni(1)-N(3) 93.64(17)	N(2)-Ni(1)-N(3) 89.0(8)
Ni(1)-N(1)-C(7) 115.4(3)	Ni(1)-N(1)-C(7) 119.6(11)
Ni(1)-N(2)-C(21) 122.4(4)	Ni(1)-N(2)-C(18) 119.4(12)
Ni(1)-N(3)-C(32) 124.7(4)	Ni(1)-N(3)-C(29) 119.5(9)
Ni(1)-N(1)-C(2) 118.4(4)	Ni(1)-N(1)-C(2) 118.5(10)
Ni(1)-N(2)-C(19) 115.2(4)	Ni(1)-N(2)-C(16) 115.5(11)
Ni(1)-N(3)-C(30) 114.3(4)	Ni(1)-N(3)-C(27) 118.3(10)
C(2)-N(1)-C(7) 126.2(5)	C(2)-N(1)-C(7) 121.7(12)
C(19)-N(2)-C(21) 122.2(5)	C(16)-N(2)-C(18) 125.1(14)
C(30)-N(3)-C(32) 119.6(5)	C(27)-N(3)-C(29) 121.6(10)
C(1)-C(2)-N(1) 114.0(5)	C(1)-C(2)-N(1) 114.7(13)
C(1)-C(19)-N(2) 117.4(6)	C(1)-C(16)-N(2) 120.4(15)
C(1)-C(30)-N(3) 117.6(5)	C(1)-C(27)-N(3) 116.2(13)
N(1)-C(2)-C(3) 130.4(5)	N(1)-C(2)-C(3) 129.2(13)
N(2)-C(19)-C(20) 126.1(7)	N(2)-C(16)-C(17) 123.1(16)
N(3)-C(30)-C(31) 126.6(6)	N(3)-C(27)-C(28) 125.7(14)
θ_T (C(1)-C(2)-N(1)-C(3)/$C(7)_{Ar}$) = 89.7(5)	θ_T (C(1)-C(2)-N(1)-C(3)/$C(7)_{Ar}$) = 85.7(13)
θ_T (C(1)-C(19)-N(2)-C(20)/$C(21)_{Ar}$) = 71.7(7)	θ_T (C(1)-C(16)-N(2)-C(17)/$C(18)_{Ar}$) = 62.0(16)
θ_T (C(1)-C(30)-N(3)-C(31)/$C(32)_{Ar}$) = 56.0(6)	θ_T (C(1)-C(27)-N(3)-C(28)/$C(29)_{Ar}$) = 61.4(14)

The analogous reaction employing the less sterically encumbered **L^{10}** yielded **$[(L^{10})NiBr][BAr^F_4]$** as a yellow-orange powder upon precipitation with hexane (**scheme 4.5**). However, upon recrystallisation from DCM and hexane under anhydrous conditions, a mixture of crystalline species was obtained, consisting of the red monomeric **$[(L^{10})NiBr][BAr^F_4]$**, as well as a small quantity of a green-coloured compound, which is most likely the corresponding five-coordinate dimer **$[\{(L^{10})Ni(\mu\text{-}Br)\}_2][BAr^F_4]_2$**. Unfortunately, only the crystals of the red **$[(L^{10})NiBr][BAr^F_4]$** were found to be suitable for X-ray diffraction, though the entire cationic unit was found to be disordered over two sites. For the sake of completeness the molecular structure of the major contributor to the disordered structure is shown in **figure 4.11**, though the precision of the bond lengths and angles (**table 4.4**) must be treated with a considerable degree of caution due to the large number of restraints that were applied in order to obtain a satisfactory refinement. Most

tellingly, the C(2)-N(1)-C(7) angle is not the widest of the C=N-C_{Ar} angles, which contradicts the established precedent set by all other complexes of tridentately coordinated R^7 *tert*-butyl substituted β-triketimine ligands.

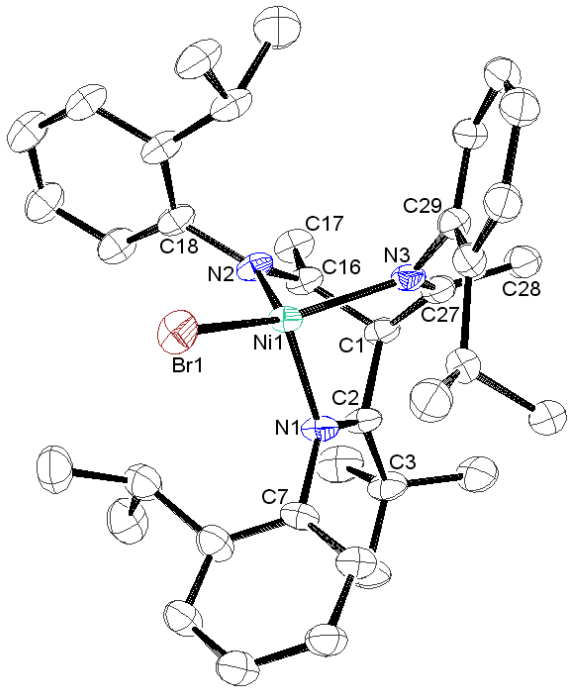

Figure 4.11 ORTEP representation of the cationic unit in [(L^{10})NiBr][BAr^F_4] with thermal ellipsoids set at the 30 % probability level; hydrogen atoms omitted for clarity

4.2.1.4 [(η^4-L)NiBr][BAr^F_4] complexes

In analogy with the aforementioned **[(η^4-L^{16})ZnCl][BAr^F_4] (chapter 3)**, **L^{16}** was found to react with $NiBr_2$(DME) and $NaBAr^F_4$ to furnish the five-coordinate complex **[(η^4-L^{16})NiBr][BAr^F_4] (scheme 4.6)**.

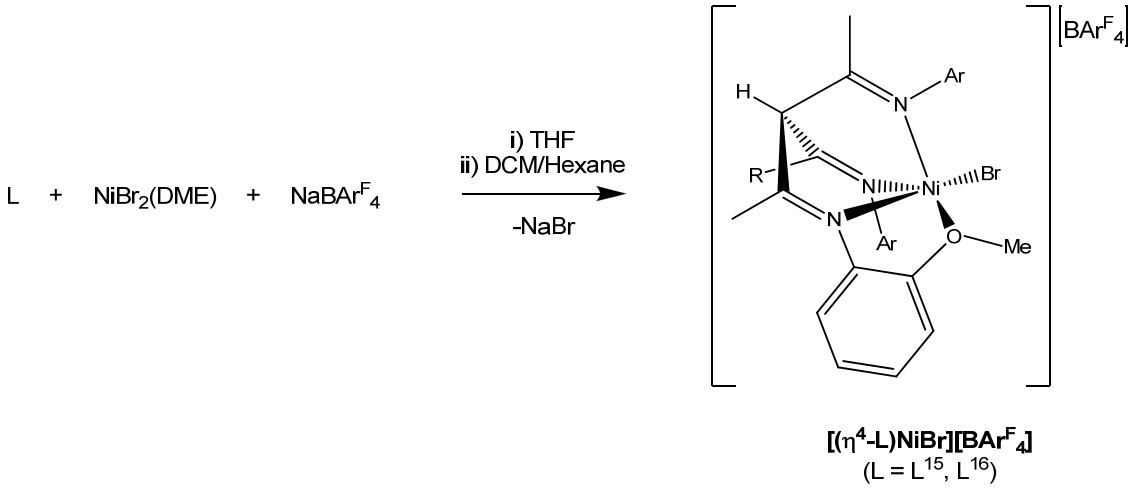

Scheme 4.6 Synthesis of [(η^4-L)NiBr][BAr^F_4] complexes

Additionally, the related, yet considerably bulkier bis(2,6-diisopropylphenyl)-substituted **L^{15}** was also found to give the analogous *N,N′,N″,O*-coordinated **[(η^4-L^{15})NiBr][BAr$^F_4$]** upon reaction with $NiBr_2$(DME) and $NaBAr^F_4$ (**scheme 4.6**). The molecular structure of the cationic unit in **[(η^4-L^{16})NiBr][BAr$^F_4$]** (**figure 4.12**) shows a very distorted square-pyramidal nickel centre; the τ value of 0.27 is identical to that seen in **[(η^4-L^{16})ZnCl][BAr$^F_4$]**, though the Br(1)-Ni(1)-N(2) and N(1)-Ni(1)-O(2) angles (**table 4.5**) are on average closer to 180° than in the latter complex.

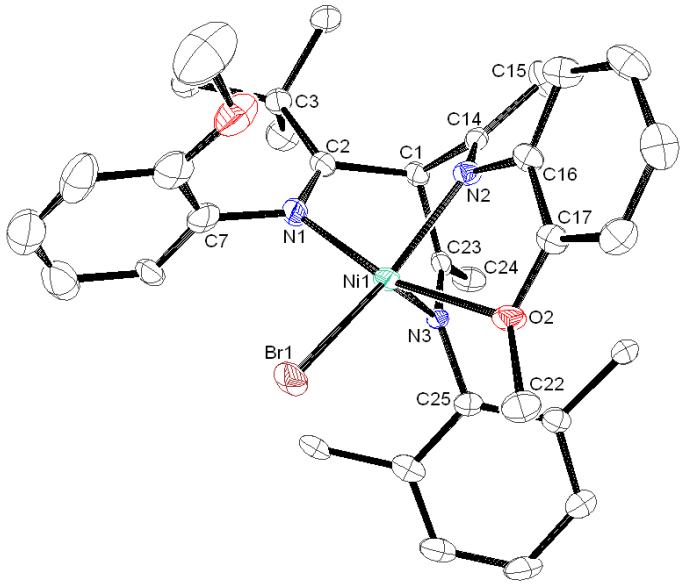

Figure 4.12 ORTEP representation of the cationic unit in [(η^4-L^{16})NiBr][BAr$^F_4$] with thermal ellipsoids set at the 50 % probability level; hydrogen atoms and isopropyl methyl groups omitted for clarity

The coordination of the O(2) methoxy group causes the C(14)-N(2)-C(16) angle (125.0(2)°) to be wider than would normally be expected for a methyl substituted imine moiety, and in this case is actually very slightly broader than C(2)-N(1)-C(7) (124.1(2)°), the corresponding angle of the *tert*-butyl substituted imine group. The Ni(1)-O(2) distance of 2.2063(16) Å is considerably shorter than the corresponding metal-oxygen distance in **[(η^4-L^{16})ZnCl][BAr$^F_4$]**, which may simply be a reflection of the increased preference of nickel for the adoption of a five-coordinate geometry in comparison to zinc. As expected, the mean N-N separation (2.829(4) Å) is smaller than that seen in **[(η^4-L^{16})ZnCl][BAr$^F_4$]**, and is also somewhat smaller than the corresponding distances in the five-coordinate dimeric nickel complexes, though effective comparison of this parameter between complexes of the tetradentate **L^{16}** and those of other tridentate β-triketimines is not possible due to the influence of the additional coordinated methoxy group on the overall complex geometry. The Ni(1)-N(2) and Ni(1)-N(3) distances of 1.994(2) and 2.006(2) Å

respectively are essentially no different to those seen in the four-coordinate complexes, whilst the Ni(1)-N(1) distance is somewhat longer at 2.057(2) Å, due to the *trans*-influence of the coordinated methoxy group.

Table 4.5 Selected bond lengths (Å), angles (°) and interplanar torsion angles (°) for the cationic units in $[(\eta^4\text{-}L^{16})NiBr][BAr^F{}_4]$ and $[(\eta^4\text{-}L^{15})NiBr][BAr^F{}_4].¼CH_2Cl_2$

$[(\eta^4\text{-}L^{16})NiBr]^+$	$[(\eta^4\text{-}L^{15})NiBr]^+$
Br(1)-Ni(1) 2.3540(4)	Br(1)-Ni(1) 2.3357(7)
Ni(1)-O(2) 2.2063(16)	Ni(1)-O(1) 2.252(3)
Ni(1)-N(1) 2.057(2)	Ni(1)-N(1) 1.997(3)
Ni(1)-N(2) 1.994(2)	Ni(1)-N(2) 2.065(3)
Ni(1)-N(3) 2.006(2)	Ni(1)-N(3) 2.006(3)
N(1)-C(2) 1.277(3)	N(1)-C(2) 1.270(5)
N(2)-C(14) 1.271(3)	N(2)-C(11) 1.282(5)
N(3)-C(23) 1.278(3)	N(3)-C(25) 1.283(5)
N(1)-C(7) 1.444(3)	N(1)-C(4) 1.428(5)
N(2)-C(16) 1.432(3)	N(2)-C(13) 1.463(5)
N(3)-C(25) 1.443(4)	N(3)-C(27) 1.453(6)
C(1)-C(2) 1.535(4)	C(1)-C(2) 1.533(6)
C(1)-C(14) 1.527(3)	C(1)-C(11) 1.521(5)
C(1)-C(23) 1.516(4)	C(1)-C(25) 1.538(6)
O(2)-C(17) 1.380(3)	O(1)-C(5) 1.389(5)
O(2)-C(22) 1.446(3)	O(1)-C(10) 1.446(5)
Br(1)-Ni(1)-N(1) 100.65(6)	Br(1)-Ni(1)-N(1) 141.63(9)
Br(1)-Ni(1)-N(2) 148.87(6)	Br(1)-Ni(1)-N(2) 99.95(9)
Br(1)-Ni(1)-N(3) 120.80(6)	Br(1)-Ni(1)-N(3) 129.43(10)
Br(1)-Ni(1)-O(2) 90.78(4)	Br(1)-Ni(1)-O(1) 91.79(7)
N(1)-Ni(1)-N(2) 89.73(8)	N(1)-Ni(1)-N(2) 86.55(13)
N(1)-Ni(1)-N(3) 88.70(8)	N(1)-Ni(1)-N(3) 87.41(13)
N(2)-Ni(1)-N(3) 88.39(8)	N(2)-Ni(1)-N(3) 92.92(13)
N(1)-Ni(1)-O(2) 164.39(7)	N(1)-Ni(1)-O(1) 74.19(11)
N(2)-Ni(1)-O(2) 75.14(7)	N(2)-Ni(1)-O(1) 159.83(12)
N(3)-Ni(1)-O(2) 94.58(7)	N(3)-Ni(1)-O(1) 92.16(12)
Ni(1)-O(2)-C(17) 109.93(15)	Ni(1)-O(1)-C(5) 105.7(2)
Ni(1)-O(2)-C(22) 125.05(14)	Ni(1)-O(1)-C(10) 125.4(2)
Ni(1)-N(1)-C(7) 117.81(16)	Ni(1)-N(1)-C(4) 112.3(2)
Ni(1)-N(2)-C(16) 114.39(15)	Ni(1)-N(2)-C(13) 123.3(2)
Ni(1)-N(3)-C(25) 120.97(14)	Ni(1)-N(3)-C(27) 120.4(2)
Ni(1)-N(1)-C(2) 117.77(17)	Ni(1)-N(1)-C(2) 119.5(3)
Ni(1)-N(2)-C(14) 118.56(17)	Ni(1)-N(2)-C(11) 116.6(3)
Ni(1)-N(3)-C(23) 116.44(19)	Ni(1)-N(3)-C(25) 117.2(3)
C(2)-N(1)-C(7) 124.1(2)	C(2)-N(1)-C(4) 128.0(3)
C(14)-N(2)-C(16) 125.0(2)	C(11)-N(2)-C(13) 119.7(3)
C(23)-N(3)-C(25) 122.6(2)	C(25)-N(3)-C(27) 121.9(3)
C(1)-C(2)-N(1) 114.2(2)	C(1)-C(2)-N(1) 115.1(4)
C(1)-C(14)-N(2) 115.4(2)	C(1)-C(11)-N(2) 116.3(3)
C(1)-C(23)-N(3) 117.6(2)	C(1)-C(25)-N(3) 116.7(4)
N(1)-C(2)-C(3) 130.9(2)	N(1)-C(2)-C(3) 126.9(4)
N(2)-C(14)-C(15) 126.8(2)	N(2)-C(11)-C(12) 126.8(4)
N(3)-C(23)-C(24) 125.4(3)	N(3)-C(25)-C(26) 127.2(4)
θ_T (C(1)-C(2)-N(1)-C(3)/C(7)$_{Ar}$) = 84.9(2)	θ_T (C(1)-C(2)-N(1)-C(3)/C(4)$_{Ar}$) = 40.1(4)
θ_T (C(1)-C(14)-N(2)-C(15)/C(16)$_{Ar}$) = 44.1(2)	θ_T (C(1)-C(11)-N(2)-C(12)/C(13)$_{Ar}$) = 79.6(4)
θ_T (C(1)-C(23)-N(3)-C(24)/C(25)$_{Ar}$) = 77.9(3)	θ_T (C(1)-C(25)-N(3)-C(26)/C(27)$_{Ar}$) = 73.0(4)

$[(\eta^4\text{-}L^{15})NiBr][BAr^F{}_4]$ crystallises with a single molecule of DCM and four unique cations in the asymmetric unit, though for the sake of simplicity only one of these is displayed in **figure 4.13**, and structural parameters (**table 4.5**) are included for this molecule only. Like the aforementioned **$[(\eta^4\text{-}L^{16})NiBr][BAr^F{}_4]$**, this complex displays a highly distorted

square-pyramidal geometry, though the degree of distortion is even higher as evidenced by the increased τ value of 0.30, and the fact that the Br(1)-Ni(1)-N(1) and N(2)-Ni(1)-O(1) angles are on average further from 180° (**table 4.5**). A similar *trans*-influence of the coordinated methoxy group is observed, as the Ni(1)-N(2) distance of 2.065(3) Å is over 0.05 Å longer than the other Ni-N distances. There is very little difference between the Ni-N distances and the corresponding distances in **[(η^4-L^{16})NiBr][BAr$^F_4$]**, though the Ni(1)-O(1) distance of 2.252(3) is somewhat longer than the Ni(1)-O(2) distance of 2.2063(16) Å in the latter complex. The cause of this is not directly apparent, as both the widening of the C(2)-N(1)-C(4) angle relative to the corresponding angle in **[(η^4-L^{16})NiBr][BAr$^F_4$]**, as well as the reduced value of θ_T for the N(1) aryl moiety (**table 4.5**), would be expected to facilitate closer approach of the methoxy donor to the nickel centre. The fact that the opposite is observed may possibly be due to the steric repulsion imparted on the 2-methoxyphenyl moiety by the two bulky 2,6-diisopropylphenyl groups. Accordingly, the mean N-N separation of 2.845(6) Å in **[(η^4-L^{15})NiBr][BAr$^F_4$]** is slightly larger than that observed in **[(η^4-L^{16})NiBr][BAr$^F_4$]**.

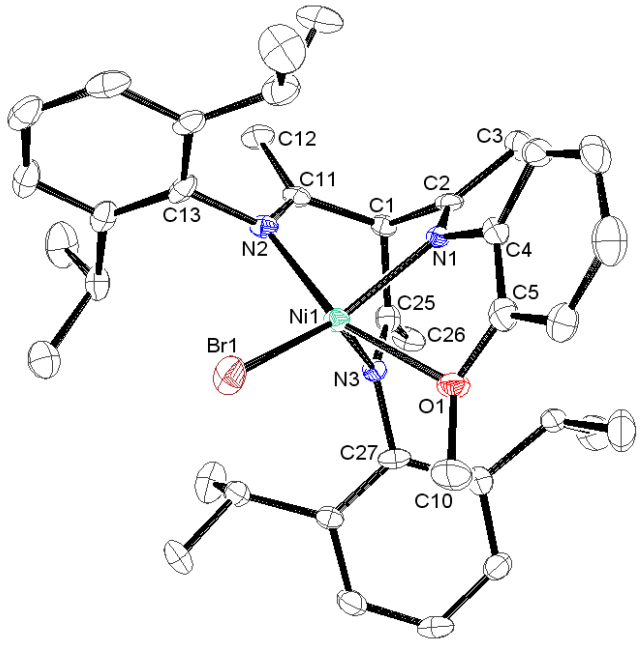

Figure 4.13 ORTEP representation one of the cationic units in [(η^4-L^{15})NiBr][BAr$^F_4$].¼CH_2Cl_2 with thermal ellipsoids set at the 50 % probability level; hydrogen atoms omitted for clarity

4.2.1.5 [(η²-L⁶)NiBr(THF)][BAr$^F_4$]

Given that the very bulky **L⁶** was found to give products that were too unstable to characterise upon reaction with $Mo(CO)_6$ (**chapter 2**), it was assumed that this ligand would be of little use with respect to the coordination chemistry of other metal centres. However, when **L⁶** was reacted with $NiBr_2$(DME) and $NaBAr^F_4$ in THF and the product crystallised from DCM and hexane, olive-green coloured crystals of the novel complex **[(η²-L⁶)NiBr(THF)][BAr$^F_4$]** were obtained (**scheme 4.7**).

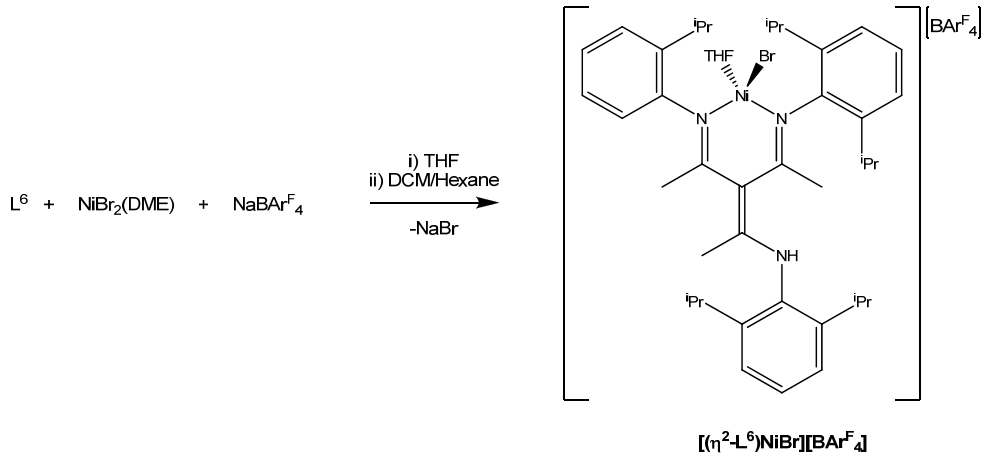

Scheme 4.7 Synthesis of [(η²-L⁶)NiBr(THF)][BAr$^F_4$]

The molecular structure of the cationic unit in this compound (**figure 4.14**) shows that, due to its large steric bulk, **L⁶** exists as the enamine-diimine tautomer, and is coordinated via the two imine donors in a bidentate mode to the nickel centre. By adopting this coordination mode, the ligand is able to position one of the 2,6-diisopropylphenyl groups as far as possible from the metal centre, due to the planar nature of the enamine moiety. The coordination sphere at nickel is completed by a bromide ligand and a molecule of THF, giving a complex with a distorted tetrahedral geometry. The THF ligand appears to be rather tightly bound, as it was not removed by pumping of the crude product under vacuum for ~3 hours with moderate heating prior to recrystallisation. To further minimise unfavourable steric interactions, all of the aryl groups lie approximately orthogonal to the planes defined by their respective imine groups (**table 4.6**). The Ni(1)-Br(1) and Ni-N distances are similar to the corresponding distances seen in other four-coordinate nickel complexes of tridentate β-triketimines, whereas the C(1)-C(2) and C(1)-C(13) distances of 1.472(6) and 1.466(6) Å respectively are somewhat shorter, as would be expected when comparing a sp^2-sp^3 carbon-carbon single bond to a sp^2-sp^2 single bond. Additionally, the C(1)-C(27) and N(3)-C(27) bond lengths of 1.382(6) and 1.347(7) Å are very similar to the

corresponding distances in the conjugated enamine moiety of free **L**[1] (**chapter 2**), while the N-N separation of 2.784(6) Å is similar to the distances seen in the four-coordinate nickel complexes of less bulky β-triketimines such as **L**[8].

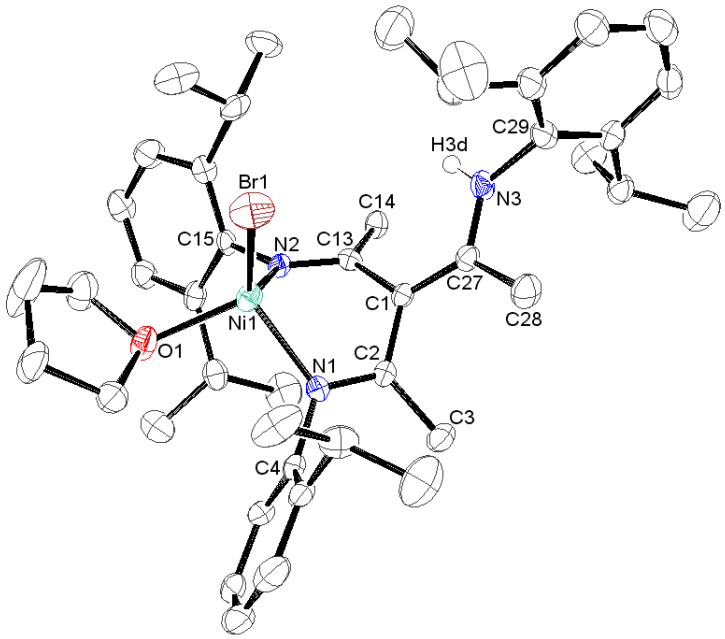

Figure 4.14 ORTEP representation of the cationic unit in [(η²-L⁶)NiBr(THF)][BAr$^F_4$] with thermal ellipsoids set at the 50 % probability level; enamine hydrogen shown, all others omitted for clarity

Table 4.6 Selected bond lengths (Å), angles (°) and interplanar torsion angles (°) for the cationic unit in [(η²-L⁶)NiBr(THF)][BAr$^F_4$]

Br(1)-Ni(1) 2.3030(13)	Ni(1)-N(1)-C(2) 115.1(3)
Ni(1)-O(1) 2.010(3)	Ni(1)-N(2)-C(13) 115.7(3)
Ni(1)-N(1) 1.974(4)	C(2)-N(1)-C(4) 122.3(4)
Ni(1)-N(2) 1.962(3)	C(13)-N(2)-C(15) 122.2(3)
N(1)-C(2) 1.293(6)	C(1)-C(2)-N(1) 119.4(4)
N(2)-C(13) 1.290(6)	C(1)-C(13)-N(2) 118.0(4)
N(1)-C(4) 1.441(6)	N(1)-C(2)-C(3) 120.2(4)
N(2)-C(15) 1.435(5)	N(2)-C(13)-C(14) 121.1(3)
C(1)-C(2) 1.472(6)	C(1)-C(2)-C(3) 120.3(4)
C(1)-C(13) 1.466(6)	C(1)-C(13)-C(14) 120.7(4)
C(1)-C(27) 1.382(6)	C(2)-C(1)-C(13) 117.3(4)
N(3)-C(27) 1.347(7)	C(2)-C(1)-C(27) 120.7(4)
N(3)-C(29) 1.456(7)	C(13)-C(1)-C(27) 121.9(4)
	C(1)-C(27)-C(28) 124.0(4)
Br(1)-Ni(1)-N(1) 122.24(11)	C(1)-C(27)-N(3) 122.5(4)
Br(1)-Ni(1)-N(2) 122.52(11)	N(3)-C(27)-C(28) 113.3(4)
Br(1)-Ni(1)-O(1) 113.17(11)	C(27)-N(3)-C(29) 128.1(4)
N(1)-Ni(1)-O(1) 102.38(14)	
N(2)-Ni(1)-O(1) 102.27(13)	θ_T (C(1)-C(2)-N(1)-C(3)/C(4)$_{Ar}$) = 85.5(4)
N(1)-Ni(1)-N(2) 90.03(15)	θ_T (C(1)-C(13)-N(2)-C(14)/C(15)$_{Ar}$) = 80.8(4)
Ni(1)-N(1)-C(4) 122.6(3)	θ_T (C(1)-C(27)-N(3)-C(28)/C(29)$_{Ar}$) = 88.2(4)
Ni(1)-N(2)-C(15) 121.6(3)	

Remarkably, there are only three examples of structurally characterised four-coordinate N_2ONiBr complexes reported in the literature, and none of these are cationic.[382] The closest precedent to **[(η²-L⁶)NiBr(THF)][BAr$^F_4$]** is a neutral LNiBr(THF) complex, where

L is a bidentate, monoanionic sufonamido-imine ligand.[383] However, in the latter complex there is also an additional weak yet non-insignificant interaction between one of the sulfonamide oxygen atoms and the nickel centre, and thus the geometry may be better described as square-pyramidal rather than highly distorted tetrahedral as ascribed by the authors. As the THF molecule occupies the nominally axial site in the literature compound, the O_{THF}-Ni distance of 2.026(2) Å is very similar to the Ni(1)-O(1) distance of 2.010(3) Å in **[(η^2-L^6)NiBr(THF)][BAr$^F_4$]**. In contrast, the Br(1)-Ni(1) distance of 2.3030(13) Å and Ni-N distances (1.962(3) and 1.974(4) Å) in **[(η^2-L^6)NiBr(THF)][BAr$^F_4$]** are shorter than the corresponding Br-Ni distance of 2.363(1) Å and Ni-N_{imine} distance of 2.029(3) Å in the sulfonamido-imine complex. This is likely due both to the fact that the latter is a neutral complex whilst **[(η^2-L^6)NiBr(THF)][BAr$^F_4$]** is cationic, as well as to the respective *trans*-influences of the sulfonamide nitrogen and the weakly coordinated sulfonamide oxygen.[383] The C(1)-C(2) and C(1)-C(13) distances in **[(η^2-L^6)NiBr(THF)][BAr$^F_4$]** are also slightly shorter than the corresponding distances in both (HBDK^{iPr2})$NiBr_2$ (1.513(9) and 1.500(9) Å)[12] and the α-keto-β-diimine complex **324** (1.518(12) and 1.511(12) Å).[302] In the former case this is simply due to the fact that in (HBDK^{iPr2})$NiBr_2$ the sp^2 imine carbons are bonded to a sp^3 carbon, whilst in the latter example the presence of the very electronegative oxygen atom gives rise to a partial positive charge at the central carbon atom, and thus the C-C bonds are slightly longer than would be expected for a sp^2-sp^2 single bond.

4.2.1.6 [{(L)Ni(μ-Br)}$_2$][OTf]$_2$ and [(L)NiBr][OTf] complexes

As the use of the large $BAr^F_4^-$ ion had been found to strongly favour the formation of dimeric nickel complexes with all but the most sterically encumbered β-triketimine ligands, it was anticipated that the substitution of $BAr^F_4^-$ for the much smaller triflate anion may promote the generation of monomeric complexes. Indeed, when the R^7 *tert*-butyl substituted ligands **L^8** and **L$^{10\text{-}12}$** were reacted with $NiBr_2$(DME) and AgOTf in THF and the crude products crystallised from DCM and Et_2O, bright-red crystals of the monomeric four-coordinate complexes **[(L)NiBr][OTf]** were obtained exclusively (**scheme 4.8**). It should be noted here that, in the case of the less bulky ligand **L^8**, use of Et_2O in crystallisation is essential to the isolation of the monomeric complex, as the use of hexane gave only a green-coloured compound, presumably the corresponding dimeric species **[{(L^8)Ni(μ-Br)}$_2$][OTf]$_2$**, though single crystals suitable for X-ray diffraction could not be obtained. It seems that the very weakly donating Et_2O acts so as to inhibit dimer

formation, presumably by transient coordination to the nickel centre. In contrast to the behaviour of $\mathbf{L^8}$, the bulkier $\mathbf{L^{10\text{-}12}}$ produced only monomeric complexes regardless of which solvent is employed in crystallisation. Similarly, the analogous reaction of $\mathbf{L^1}$ (R^7 = Me) gave exclusively a red-coloured compound when Et_2O was used in crystallisation (**scheme 4.8**), though the crystals obtained were unsuitable for X-ray diffraction.

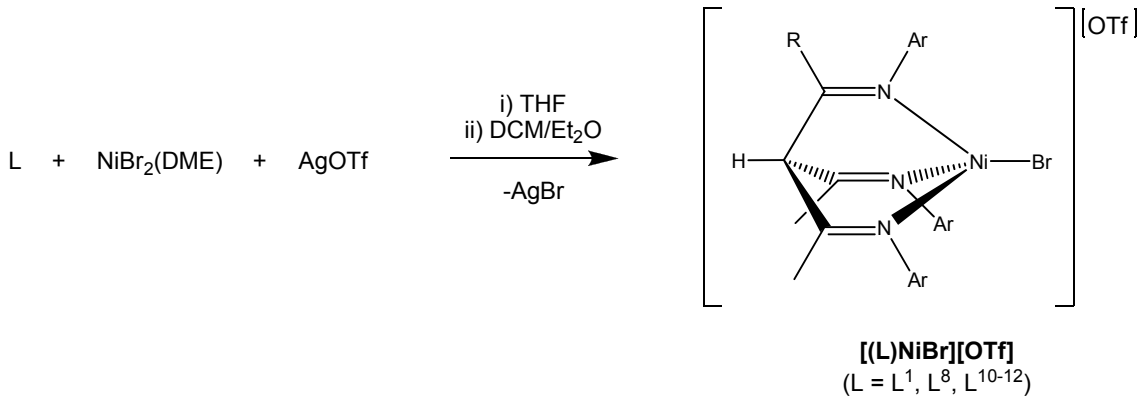

Scheme 4.8 Synthesis of [(L)NiBr][OTf] complexes

In marked contrast to the behaviour of $\mathbf{L^1}$, the very similar yet slightly bulkier $\mathbf{L^3}$ and $\mathbf{L^5}$ (R^7 = Me) gave only the green dimeric complexes $\mathbf{[\{(L)Ni(\mu\text{-}Br)\}_2][OTf]_2}$ ($\mathbf{L}$ = $\mathbf{L^3}$, $\mathbf{L^8}$), even when Et_2O was used as the precipitating solvent (**scheme 4.9**). Again, single crystals suitable for X-ray diffraction could not be obtained for either complex, though the green colouration and microanalytical data are in agreement with the ascribed formulae. As $\mathbf{[\{(L^5)Ni(\mu\text{-}Br)\}_2][OTf]_2}$ was seen to precipitate from a DCM solution upon reduction in volume and without the addition of any precipitating solvent, it appears that reduced solubility of $\mathbf{[\{(L)Ni(\mu\text{-}Br)\}_2][OTf]_2}$ ($\mathbf{L}$ = $\mathbf{L^3}$, $\mathbf{L^8}$) relative to their corresponding monomers is likely responsible for the fact that they are obtained exclusively from the reaction mixtures.

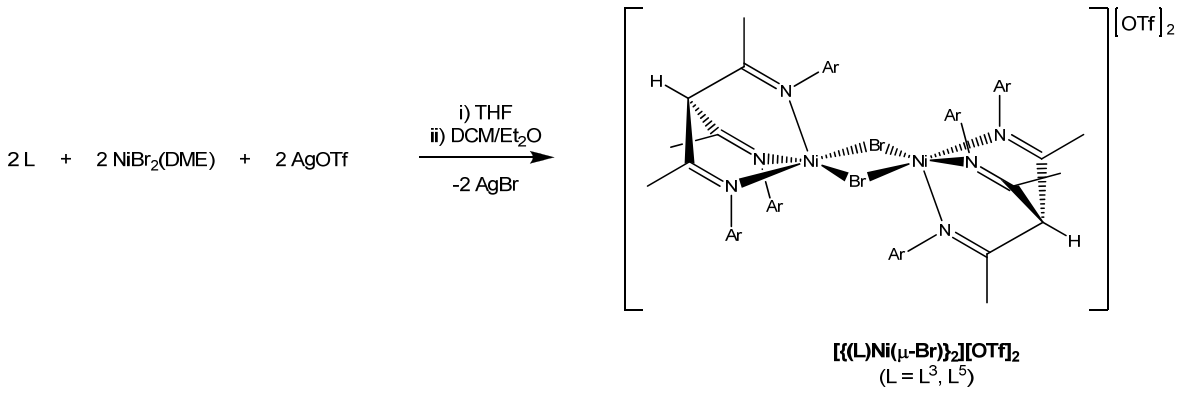

Scheme 4.9 Synthesis of $[\{(L)Ni(\mu\text{-}Br)\}_2][OTf]_2$ complexes

The molecular structure of **[(L^8)NiBr][OTf]** features a cationic unit in which each of the aryl groups are disordered over two sites by librational movement about the N-C_{Ar} bonds. The structure depicted in **figure 4.15** is the one in which C=N and N-C_{Ar} bonds are closest to coplanarity, and for the sake of simplicity structural parameters are included for this component only (**table 4.7**). None of the structural parameters, including the mean N-N separation of 2.784(9) Å, deviate to any significant degree from those observed in **[(L^8)NiBr]$_2$[NiBr$_4$]**.

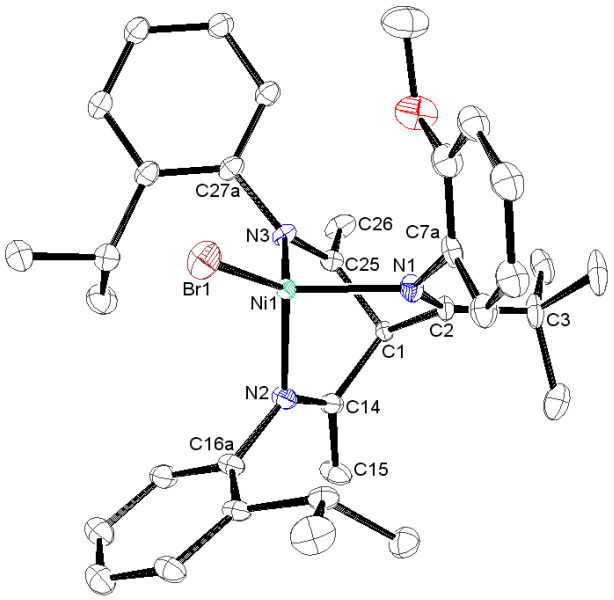

Figure 4.15 ORTEP representation of the cationic unit in [(L^8)NiBr][OTf] with thermal ellipsoids set at the 40 % probability level; hydrogen atoms omitted for clarity

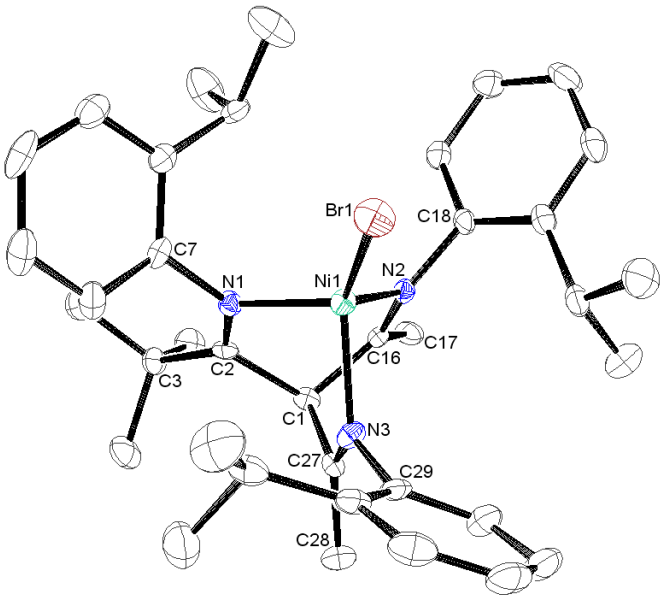

Figure 4.16 ORTEP representation of the cationic unit in [(L^{10})NiBr][OTf] with thermal ellipsoids set at the 50 % probability level; hydrogen atoms omitted for clarity

Table 4.7 Selected bond lengths (Å), angles (°) and interplanar torsion angles (°) for the cationic units in [(L^8)NiBr][OTf] and [(L^{10})NiBr][OTf]

$[(L^8)NiBr]^+$	$[(L^{10})NiBr]^+$
Br(1)-Ni(1) 2.2626(10)	Br(1)-Ni(1) 2.2701(4)
Ni(1)-N(1) 1.979(5)	Ni(1)-N(1) 1.979(2)
Ni(1)-N(2) 1.969(5)	Ni(1)-N(2) 1.9702(19)
Ni(1)-N(3) 1.966(5)	Ni(1)-N(3) 1.9750(19)
N(1)-C(2) 1.281(7)	N(1)-C(2) 1.276(3)
N(2)-C(14) 1.288(9)	N(2)-C(16) 1.277(3)
N(3)-C(25) 1.282(7)	N(3)-C(27) 1.270(3)
N(1)-C(7a) 1.451(11)	N(1)-C(7) 1.445(3)
N(2)-C(16a) 1.432(10)	N(2)-C(18) 1.443(3)
N(3)-C(27a) 1.429(13)	N(3)-C(29) 1.447(3)
C(1)-C(2) 1.536(8)	C(1)-C(2) 1.539(4)
C(1)-C(14) 1.535(8)	C(1)-C(16) 1.533(3)
C(1)-C(25) 1.526(8)	C(1)-C(27) 1.532(3)
Br(1)-Ni(1)-N(1) 123.90(16)	Br(1)-Ni(1)-N(1) 125.60(6)
Br(1)-Ni(1)-N(2) 122.39(15)	Br(1)-Ni(1)-N(2) 126.42(6)
Br(1)-Ni(1)-N(3) 129.72(15)	Br(1)-Ni(1)-N(3) 123.66(6)
N(1)-Ni(1)-N(2) 90.3(2)	N(1)-Ni(1)-N(2) 89.47(8)
N(1)-Ni(1)-N(3) 89.3(2)	N(1)-Ni(1)-N(3) 90.52(8)
N(2)-Ni(1)-N(3) 90.0(2)	N(2)-Ni(1)-N(3) 90.17(8)
Ni(1)-N(1)-C(7a) 111.0(5)	Ni(1)-N(1)-C(7) 111.88(14)
Ni(1)-N(2)-C(16a) 119.6(5)	Ni(1)-N(2)-C(18) 117.29(15)
Ni(1)-N(3)-C(27a) 118.4(7)	Ni(1)-N(3)-C(29) 117.83(16)
Ni(1)-N(1)-C(2) 119.6(4)	Ni(1)-N(1)-C(2) 119.48(18)
Ni(1)-N(2)-C(14) 117.0(4)	Ni(1)-N(2)-C(16) 118.13(16)
Ni(1)-N(3)-C(25) 118.6(4)	Ni(1)-N(3)-C(27) 117.13(16)
C(2)-N(1)-C(7a) 129.0(7)	C(2)-N(1)-C(7) 128.3(2)
C(14)-N(2)-C(16a) 123.4(6)	C(16)-N(2)-C(18) 123.8(2)
C(25)-N(3)-C(27a) 123.0(8)	C(27)-N(3)-C(29) 123.8(2)
C(1)-C(2)-N(1) 114.1(5)	C(1)-C(2)-N(1) 113.5(2)
C(1)-C(14)-N(2) 117.4(5)	C(1)-C(16)-N(2) 115.2(2)
C(1)-C(25)-N(3) 115.6(5)	C(1)-C(27)-N(3) 116.5(2)
N(1)-C(2)-C(3) 130.0(5)	N(1)-C(2)-C(3) 130.5(2)
N(2)-C(14)-C(15) 125.7(6)	N(2)-C(16)-C(17) 125.8(2)
N(3)-C(25)-C(26) 125.9(6)	N(3)-C(27)-C(28) 125.6(2)
θ_T (C(1)-C(2)-N(1)-C(3)/$C(7a)_{Ar}$) = 80.3(7)	θ_T (C(1)-C(2)-N(1)-C(3)/$C(7)_{Ar}$) = 76.0(2)
θ_T (C(1)-C(14)-N(2)-C(15)/$C(16a)_{Ar}$) = 68.5(6)	θ_T (C(1)-C(16)-N(2)-C(17)/$C(18)_{Ar}$) = 65.3(2)
θ_T (C(1)-C(25)-N(3)-C(260/$C(27a)_{Ar}$) = 63.3(8)	θ_T (C(1)-C(27)-N(3)-C(28)/$C(29)_{Ar}$) = 67.9(2)

The molecular structure of the cationic unit in **[(L^{10})NiBr][OTf]** is shown in **figure 4.16**, and any sizeable differences in the structural parameters (**table 4.7**) in comparison to **[(L^{10})NiBr]$_2$[$NiBr_4$]** (R = 9.81 %) and **[(L^{10})NiBr][BAr^F_4]** (R = 7.68 %) can be attributed to the fact that in this case the data are of much greater quality (R = 3.45 %). **[(L^{10})NiBr][OTf]** is isomorphous with **[(L^{10})ZnCl][OTf]**, as evidenced by the very similar unit cell parameters (**appendix**). Additionally, there is little difference in the structural parameters of the cationic units in **[(L^{10})NiBr][OTf]** and **[(L^{10})ZnCl][OTf]**, aside from the shorter metal-nitrogen distances and mean N-N separation (2.794(3) Å) in the nickel complex. In analogy with the **[(L)ZnCl][OTf]** complexes, both **[(L^8)NiBr][OTf]** and **[(L^{10})NiBr][OTf]** display multiple hydrogen-bonding interactions between the triflate ion and numerous alkyl and aryl hydrogen atoms of the cationic units, and in the case of

[(L^{10})NiBr][OTf] these are essentially identical to those seen in **[(L^{10})ZnCl][OTf]** save for very small differences in O-H distances.

Single crystals of **[(L^{11})NiBr][OTf]** suitable for X-ray diffraction were obtained by vapour diffusion of Et_2O into a concentrated $CHCl_3$ solution, and the complex was found to crystallise with a single molecule of $CHCl_3$ in the asymmetric unit. The solvent molecule is disordered over two sites, and engages in a hydrogen bonding interaction with the triflate anion (CH---O = 2.173 Å) which is towards the stronger end of the range of such previously reported interactions (1.640-2.716 Å).[384] Interaction with the $CHCl_3$ solvent molecule does not preclude hydrogen-bonding of the triflate anion with the cationic complex, and numerous such interactions are indeed observed. The N(3) 2-isopropylphenyl substituent is disordered over two sites, by librational movement and rotation about the N-C_{Ar} bond; only the major contributor to this disordered structure is shown in **figure 4.17**. The structural parameters of this complex (**table 4.8**) do not differ to any substantial degree from those of **[(L^{11})NiBr][BAr$^{F}_4$]**, and the mean N-N separation of 2.841(7) Å is similar to yet slightly smaller than that seen in the latter compound.

In analogy with the aforementioned **[(L^{10})NiBr][OTf]**, **[(L^{12})NiBr][OTf]** is also isomorphous with its zinc chloride analogue, and displays approximately identical cation-anion hydrogen-bonding interactions in the solid state. The molecular structure of the cationic unit in **[(L^{12})NiBr][OTf]** is presented in **figure 4.18**, and again the structural parameters (**table 4.8**) are very similar to those of **[(L^{12})ZnCl][OTf]**, except for the shorter metal-nitrogen distances in the nickel complex. The mean N-N separation of 2.840(3) Å is essentially identical to that seen in the more sterically encumbered **[(L^{11})NiBr][OTf]**, which does not corroborate with the established trend in average N-N distances being related to overall ligand steric bulk. However, as the structure of **[(L^{12})ZnCl][OTf]** is of higher quality (R = 3.88%) than both **[(L^{11})NiBr][OTf]** (R = 6.22%) and **[(L^{11})NiBr][BAr$^{F}_4$]** (R = 6.70%), the mean N-N separation in **[(L^{12})ZnCl][OTf]** must be regarded as being of higher accuracy. Therefore it seems reasonable that the observed mean N-N separations in the nickel bromide derivatives of **L^{12}** may appear artificially smaller than expected due to the relatively lower quality of the data and greater number of restraints employed in order to obtain a satisfactory refinement.

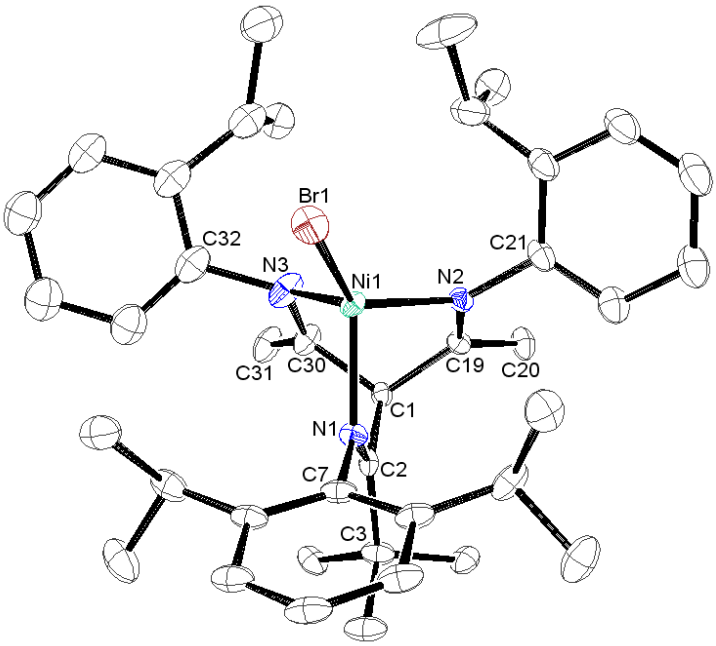

Figure 4.17 ORTEP representation of the cationic unit in [(L^{11})NiBr][OTf].$CHCl_3$ with thermal ellipsoids set at the 30 % probability level; hydrogen atoms omitted for clarity

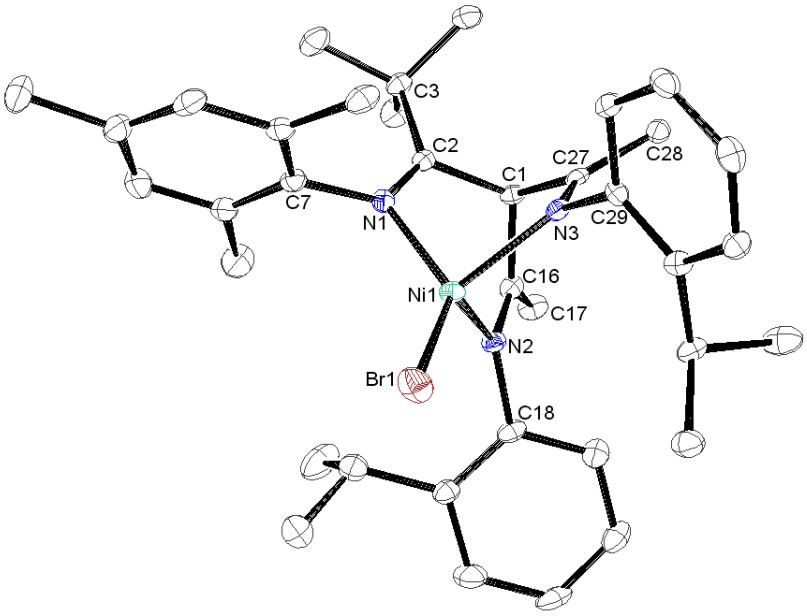

Figure 4.18 ORTEP representation of the cationic unit in [(L^{12})NiBr][OTf] with thermal ellipsoids set at the 50 % probability level; hydrogen atoms omitted for clarity

Table 4.8 Selected bond lengths (Å), angles (°) and interplanar torsion angles (°) for the cationic units in $[(L^{I1})NiBr][OTf].CHCl_3$ and $[(L^{I2})NiBr][OTf]$

$[(L^{I1})NiBr]^+$	$[(L^{I2})NiBr]^+$
Br(1)-Ni(1) 2.2742(12)	Br(1)-Ni(1) 2.2962(4)
Ni(1)-N(1) 2.001(4)	Ni(1)-N(1) 2.015(2)
Ni(1)-N(2) 1.982(5)	Ni(1)-N(2) 1.999(2)
Ni(1)-N(3) 2.001(5)	Ni(1)-N(3) 1.9905(19)
N(1)-C(2) 1.273(6)	N(1)-C(2) 1.275(3)
N(2)-C(19) 1.281(6)	N(2)-C(16) 1.281(3)
N(3)-C(30) 1.287(7)	N(3)-C(27) 1.277(3)
N(1)-C(7) 1.459(6)	N(1)-C(7) 1.455(3)
N(2)-C(21) 1.470(8)	N(2)-C(18) 1.452(3)
N(3)-C(32) 1.495(10)	N(3)-C(29) 1.458(3)
C(1)-C(2) 1.533(6)	C(1)-C(2) 1.539(3)
C(1)-C(19) 1.529(7)	C(1)-C(16) 1.521(3)
C(1)-C(30) 1.517(8)	C(1)-C(27) 1.540(4)
Br(1)-Ni(1)-N(1) 124.77(11)	Br(1)-Ni(1)-N(1) 131.94(6)
Br(1)-Ni(1)-N(2) 130.08(11)	Br(1)-Ni(1)-N(2) 122.00(6)
Br(1)-Ni(1)-N(3) 119.19(15)	Br(1)-Ni(1)-N(3) 120.52(6)
N(1)-Ni(1)-N(2) 89.34(17)	N(1)-Ni(1)-N(2) 90.87(8)
N(1)-Ni(1)-N(3) 92.39(19)	N(1)-Ni(1)-N(3) 90.07(8)
N(2)-Ni(1)-N(3) 90.59(19)	N(2)-Ni(1)-N(3) 90.29(8)
Ni(1)-N(1)-C(7) 116.9(3)	Ni(1)-N(1)-C(7) 117.02(16)
Ni(1)-N(2)-C(21) 123.4(3)	Ni(1)-N(2)-C(18) 124.29(16)
Ni(1)-N(3)-C(32) 120.9(6)	Ni(1)-N(3)-C(29) 121.79(15)
Ni(1)-N(1)-C(2) 117.8(3)	Ni(1)-N(1)-C(2) 117.55(17)
Ni(1)-N(2)-C(19) 115.8(4)	Ni(1)-N(2)-C(16) 115.14(17)
Ni(1)-N(3)-C(30) 114.9(4)	Ni(1)-N(3)-C(27) 116.90(16)
C(2)-N(1)-C(7) 125.3(4)	C(2)-N(1)-C(7) 124.8(2)
C(19)-N(2)-C(21) 120.5(5)	C(16)-N(2)-C(18) 120.2(2)
C(30)-N(3)-C(32) 115.9(7)	C(27)-N(3)-C(29) 121.1(2)
C(1)-C(2)-N(1) 114.9(4)	C(1)-C(2)-N(1) 114.3(2)
C(1)-C(19)-N(2) 117.1(5)	C(1)-C(16)-N(2) 117.6(2)
C(1)-C(30)-N(3) 117.5(5)	C(1)-C(27)-N(3) 115.7(2)
N(1)-C(2)-C(3) 130.3(4)	N(1)-C(2)-C(3) 131.1(2)
N(2)-C(19)-C(20) 125.7(5)	N(2)-C(16)-C(17) 125.5(2)
N(3)-C(30)-C(31) 125.8(6)	N(3)-C(27)-C(28) 126.7(2)
θ_T (C(1)-C(2)-N(1)-C(3)/$C(7)_{Ar}$) = 89.3(4)	θ_T (C(1)-C(2)-N(1)-C(3)/$C(7)_{Ar}$) = 82.2(2)
θ_T (C(1)-C(19)-N(2)-C(20)/$C(21)_{Ar}$) = 69.6(5)	θ_T (C(1)-C(16)-N(2)-C(17)/$C(18)_{Ar}$) = 68.2(2)
θ_T (C(1)-C(30)-N(3)-C(31)/$C(32)_{Ar}$) = 67.1(7)	θ_T (C(1)-C(27)-N(3)-C(28)/$C(29)_{Ar}$) = 82.3(2)

The Ni-Br distances in the four-coordinate **$[(L)NiBr]^+$** complexes reported here vary over the relatively small range of 2.2626(10)-2.321(6) Å, though it should be noted that all of the Ni-Br distances above 2.30 Å are taken from highly disordered structures or low-quality datasets. Similarly, the Ni-N distances vary over the range 1.964(18)-2.035(18) Å, though when low-quality structures are excluded the range is narrower at 1.9702(19)-2.015(2) Å. There are only two other examples of structurally characterised (L)NiBr (L = tripodal nitrogen ligand) complexes known in the literature, namely (Tp*)NiBr[385] and (Tp^{Ph2})NiBr;[386] neither of these are cationic. The Ni-Br bond distance of 2.293(1) Å in the former compares closely to those seen in the β-triketimine complexes, whilst the latter features a somewhat longer Ni-Br bond distance of 2.3523(6) Å. Additionally, the Ni-N distances in the β-triketimine complexes do not differ to any substantial degree from those found in (Tp*)NiBr (2 × 1.968(4) Å, 1.957(6) Å),[385] (Tp^{Ph2})NiBr (3 × 2.042(2) Å),[386]

(Tp^{Mes})NiCl (2.004(3) Å, 1.993(3) Å, 1.990(3) Å),[378] (Tp^{iPr2})NiCl (1.975(3) Å, 1.965(4) Å, 1.978(4) Å),[111] (Tp^{tBu})NiCl (2.033(3) Å, 2.023(4) Å, 2.006(4) Å)[387] and [(Pro-Tach^{Ph})NiBr][BPh_4] (2 × 1.989(4) Å, 1.995(4) Å).[277] Again, the literature examples display a similar correlation between ligand steric bulk and average N-N distance; (Tp^{Ph2})NiBr and (Tp^{tBu})NiCl have the largest mean N-N separations of 2.963(2) and 2.926(4) Å respectively, whilst the mean N-N separation in (Tp*)NiBr (2.834(6) Å) is much smaller. As expected, the mean N-N separation in [(Pro-Tach^{Ph})NiBr][BPh_4] (2.901(4) Å) is larger than in any of the four-coordinate β-triketimine complexes, due to the inherently larger backbone of the Pro-Tach ligands.

4.2.1.7 [(η^4-L)NiBr][OTf] complexes

In analogy with their previously observed behaviour, the tetradentate **L^{15}** and **L^{16}** were both found to react with $NiBr_2$(DME) and AgOTf to give the corresponding five-coordinate complexes **[(η^4-L)NiBr][OTf]** (**scheme 4.10**). This behaviour implies that the choice of anion has little effect on the coordination number adopted by nickel when presented with tetradentate ligands such as **L^{15}** and **L^{16}**, and adds further credence to the assumption that the aforementioned **[(L^{16})NiBr]$_2$[$NiBr_4$]** does indeed contain a five coordinate cationic complex.

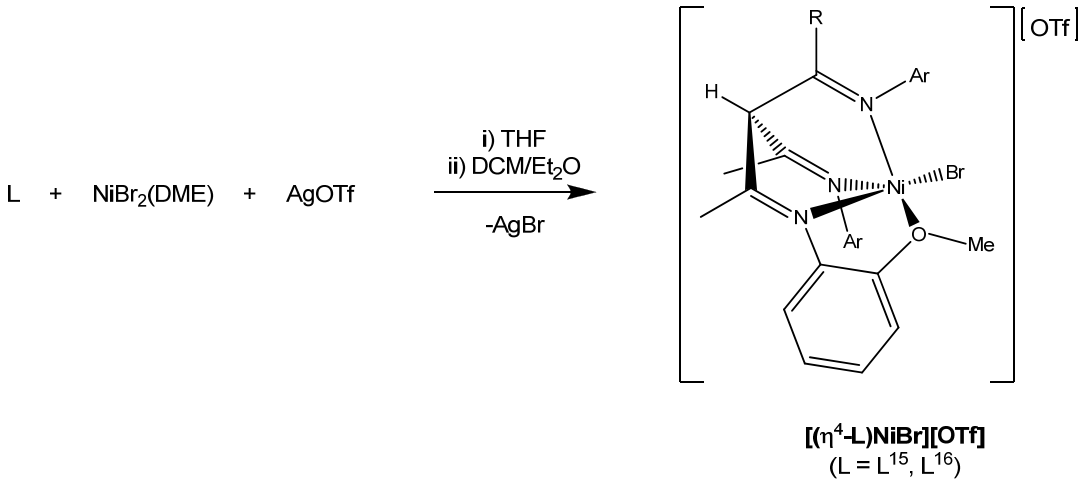

Scheme 4.10 Synthesis of [(η^4-L)NiBr][OTf] complexes

The molecular structure of **[(η^4-L^{16})NiBr][OTf]** features two independent cationic units in the asymmetric unit, both of which display distorted square-pyramidal nickel centres. However, the degree of distortion differs between the two independent units, as evidenced by the τ values of 0.21 and 0.45, though for simplicity the structure of the less distorted unit only is presented in **figure 4.19**. Other than this, there is very little difference between

the structural parameters (**table 4.9**) of the two independent units. However, in comparison to **[(η^4-L^{16})NiBr][BAr^F_4]** there are some significant structural differences, most notably the fact that in **[(η^4-L^{16})NiBr][OTf]** both cationic units feature the *tert*-butyl substituted imine in the axial position, rather than in a basal position as observed in the $BAr^F_4{}^-$ salt. The coordinated methoxy groups in **[(η^4-L^{16})NiBr][OTf]** are also much less strongly bound, as evidenced by the Ni(1)-O(2) and Ni(2)-O(4) bond distances, which at 2.316(4) and 2.320(4) Å are considerably longer than the corresponding distance of 2.2063(16) Å seen in **[(η^4-L^{16})NiBr][BAr^F_4]**. This effect is likely due to a combination of increased steric repulsion caused by placement of the *tert*-butyl substituted imine in the axial position, and an increased level of interaction between the cationic complex and the less weakly-coordinating triflate anion. The reduced interaction of the coordinated methoxy group with the nickel centre means that, in contrast **[(η-L^{16})NiBr][BAr^F_4]**, there is no notable *trans*-influence on the Ni(1)-N(3) and Ni(2)-N(6) bond distances, which are very similar to the other Ni-N distances. Additionally, the Ni-N bond distances in **[(η^4-L^{16})NiBr][OTf]** are all very similar to the shorter Ni-N distances in **[(η-L^{16})NiBr][BAr^F_4]**. The mean N-N separations of 2.801(8) and 2.817(8) Å in the two independent cationic units are also similar to that seen in the $BAr^F_4{}^-$ salt.

[(η^4-L^{15})NiBr][OTf] crystallises with a single molecule of DCM in the asymmetric unit, though one of the chlorine atoms is disordered over two sites. The cationic unit (**figure 4.20**) displays a very slightly distorted square-pyramidal geometry (τ = 0.04), though the Br(1)-Ni(1)-N(1) and O(1)-Ni(1)-N(3) angles both deviate considerably from 180° (**table 4.9**). The Ni(1)-O(1) distance of 2.320(2) is longer than the corresponding distance in **[(η^4-L^{15})NiBr][BAr^F_4]**, and the *trans*-influence of the coordinated methoxy group on the Ni(1)-N(3) bond distance is negligible. The Ni-N distances are on average slightly longer than the shorter distances in **[(η^4-L^{15})NiBr][BAr^F_4]**, though the difference is very small (~0.03 Å). Again, these differences are likely due to an increased level of interaction between the cationic complex and the triflate anion relative to the very weakly-coordinating BAr^F_4 anion. Indeed, as expected the solid-state structures of both **[(η^4-L^{15})NiBr][OTf]** and **[(η^4-L^{16})NiBr][OTf]** display numerous cation-anion hydrogen-bonding interactions. Additionally, the mean N-N separation of 2.855(4) Å in**[(η^4-L^{15})NiBr][OTf]** is very similar to that seen in **[(η^4-L^{15})NiBr][BAr^F_4]**.

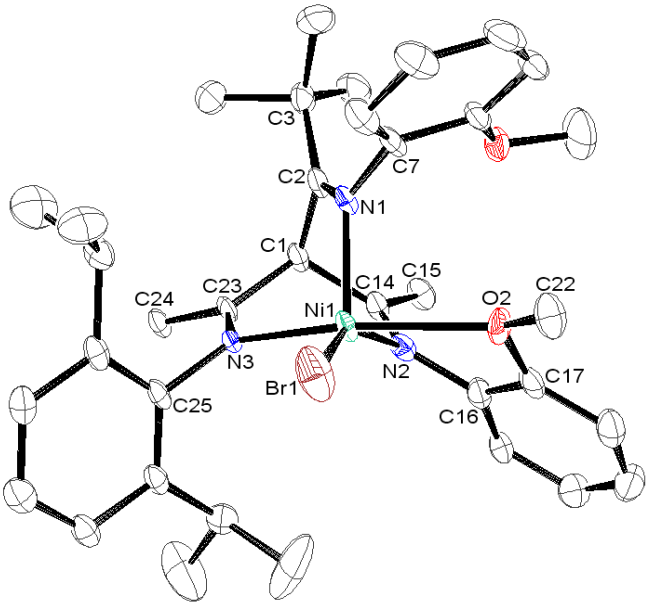

Figure 4.19 ORTEP representation one of the cationic units in [(η^4-L^{16})NiBr][OTf] with thermal ellipsoids set at the 50 % probability level; hydrogen atoms omitted for clarity

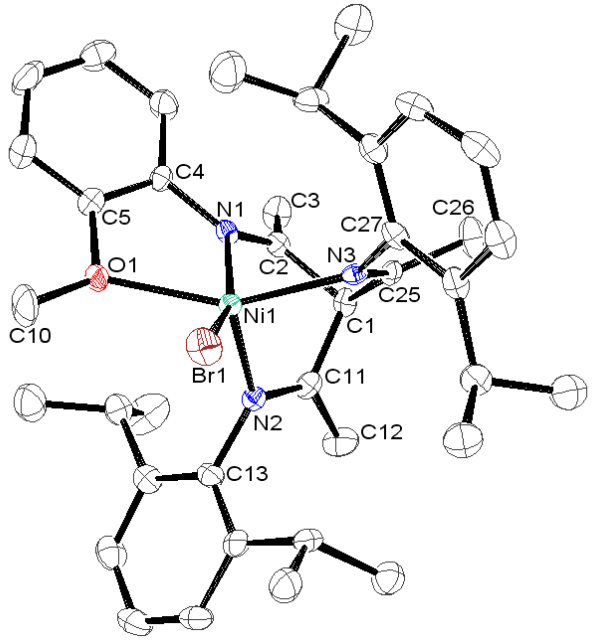

Figure 4.20 ORTEP representation of the cationic unit in [(η^4-L^{15})NiBr][OTf].CH_2Cl_2 with thermal ellipsoids set at the 50 % probability level; hydrogen atoms omitted for clarity

Table 4.9 Selected bond lengths (Å), angles (°) and interplanar torsion angles (°) for the cationic units in $[(\eta^4\text{-}L^{16})NiBr][OTf]$ and $[(\eta^4\text{-}L^{15})NiBr][OTf].CH_2Cl_2$

$[(\eta^4\text{-}L^{16})NiBr]^+$ molecule 1	$[(\eta^4\text{-}L^{16})NiBr]^+$ molecule 2	$[(\eta^4\text{-}L^{15})NiBr]^+$
Br(1)-Ni(1) 2.3273(12)	Br(2)-Ni(2) 2.3254(12)	Br(1)-Ni(1) 2.3477(7)
Ni(1)-O(2) 2.316(4)	Ni(2)-O(4) 2.320(4)	Ni(1)-O(1) 2.320(2)
Ni(1)-N(1) 2.005(5)	Ni(2)-N(4) 2.034(5)	Ni(1)-N(1) 2.029(2)
Ni(1)-N(2) 1.979(5)	Ni(2)-N(5) 1.993(5)	Ni(1)-N(2) 2.024(3)
Ni(1)-N(3) 2.015(4)	Ni(2)-N(6) 2.033(4)	Ni(1)-N(3) 2.051(2)
N(1)-C(2) 1.295(8)	N(4)-C(38) 1.266(7)	N(1)-C(2) 1.276(4)
N(2)-C(14) 1.292(7)	N(5)-C(50) 1.266(8)	N(2)-C(11) 1.273(4)
N(3)-C(23) 1.271(7)	N(6)-C(59) 1.253(8)	N(3)-C(25) 1.271(4)
N(1)-C(7) 1.425(8)	N(4)-C(43) 1.432(8)	N(1)-C(4) 1.423(4)
N(2)-C(16) 1.418(8)	N(5)-C(52) 1.411(8)	N(2)-C(13) 1.458(4)
N(3)-C(25) 1.478(7)	N(6)-C(61) 1.455(8)	N(3)-C(27) 1.443(4)
C(1)-C(2) 1.532(8)	C(37)-C(38) 1.538(8)	C(1)-C(2) 1.544(4)
C(1)-C(14) 1.533(8)	C(37)-C(50) 1.509(8)	C(1)-C(11) 1.530(4)
C(1)-C(23) 1.518(8)	C(37)-C(59) 1.547(8)	C(1)-C(25) 1.521(5)
O(2)-C(17) 1.359(8)	O(4)-C(53) 1.370(8)	O(1)-C(5) 1.389(4)
O(2)-C(22) 1.441(8)	O(4)-C(58) 1.455(8)	O(1)-C(10) 1.433(5)
Br(1)-Ni(1)-N(1) 120.77(15)	Br(2)-Ni(2)-N(4) 135.37(15)	Br(1)-Ni(1)-N(1) 156.55(7)
Br(1)-Ni(1)-N(2) 148.98(14)	Br(2)-Ni(2)-N(5) 135.36(15)	Br(1)-Ni(1)-N(2) 113.98(9)
Br(1)-Ni(1)-N(3) 102.33(13)	Br(2)-Ni(2)-N(6) 102.20(14)	Br(1)-Ni(1)-N(3) 98.92(7)
Br(1)-Ni(1)-O(2) 92.08(11)	Br(2)-Ni(2)-O(4) 90.06(11)	Br(1)-Ni(1)-O(1) 93.92(6)
N(1)-Ni(1)-N(2) 87.4(2)	N(4)-Ni(2)-N(5) 87.1(2)	N(1)-Ni(1)-N(2) 88.33(11)
N(1)-Ni(1)-N(3) 89.95(18)	N(4)-Ni(2)-N(6) 88.69(19)	N(1)-Ni(1)-N(3) 86.70(10)
N(2)-Ni(1)-N(3) 89.42(18)	N(5)-Ni(2)-N(6) 89.46(19)	N(2)-Ni(1)-N(3) 92.32(10)
N(1)-Ni(1)-O(2) 92.63(16)	N(4)-Ni(2)-O(4) 91.51(16)	N(1)-Ni(1)-O(1) 73.64(9)
N(2)-Ni(1)-O(2) 72.40(16)	N(5)-Ni(2)-O(4) 72.86(16)	N(2)-Ni(1)-O(1) 103.24(10)
N(3)-Ni(1)-O(2) 161.48(16)	N(6)-Ni(2)-O(4) 162.27(18)	N(3)-Ni(1)-O(1) 154.31(8)
Ni(1)-O(2)-C(17) 107.4(3)	Ni(2)-O(4)-C(53) 106.4(3)	Ni(1)-O(1)-C(5) 109.60(16)
Ni(1)-O(2)-C(22) 125.7(4)	Ni(2)-O(4)-C(58) 123.8(4)	Ni(1)-O(1)-C(10) 124.6(3)
Ni(1)-N(1)-C(7) 113.6(4)	Ni(2)-N(4)-C(43) 112.6(3)	Ni(1)-N(1)-C(4) 115.17(19)
Ni(1)-N(2)-C(16) 116.4(4)	Ni(2)-N(5)-C(52) 114.0(4)	Ni(1)-N(2)-C(13) 125.3(2)
Ni(1)-N(3)-C(25) 122.0(4)	Ni(2)-N(6)-C(61) 122.0(4)	Ni(1)-N(3)-C(27) 122.39(18)
Ni(1)-N(1)-C(2) 118.9(4)	Ni(2)-N(4)-C(38) 119.8(4)	Ni(1)-N(1)-C(2) 118.6(2)
Ni(1)-N(2)-C(14) 118.6(4)	Ni(2)-N(5)-C(50) 118.4(4)	Ni(1)-N(2)-C(11) 115.6(2)
Ni(1)-N(3)-C(23) 117.1(4)	Ni(2)-N(6)-C(59) 116.5(4)	Ni(1)-N(3)-C(25) 116.1(2)
C(2)-N(1)-C(7) 126.7(5)	C(38)-N(4)-C(43) 126.6(5)	C(2)-N(1)-C(4) 125.9(3)
C(14)-N(2)-C(16) 123.5(5)	C(50)-N(5)-C(52) 125.8(5)	C(11)-N(2)-C(13) 119.1(3)
C(23)-N(3)-C(25) 120.8(5)	C(59)-N(6)-C(61) 121.3(5)	C(25)-N(3)-C(27) 119.9(2)
C(1)-C(2)-N(1) 114.9(5)	C(37)-C(38)-N(4) 114.1(5)	C(1)-C(2)-N(1) 114.8(3)
C(1)-C(14)-N(2) 115.6(5)	C(37)-C(50)-N(5) 116.5(5)	C(1)-C(11)-N(2) 118.9(3)
C(1)-C(23)-N(3) 117.9(5)	C(37)-C(59)-N(6) 118.1(5)	C(1)-C(25)-N(3) 117.9(2)
N(1)-C(2)-C(3) 129.1(6)	N(4)-C(38)-C(39) 129.3(5)	N(1)-C(2)-C(3) 127.9(3)
N(2)-C(14)-C(15) 127.0(6)	N(5)-C(50)-C(51) 126.5(5)	N(2)-C(11)-C(12) 126.5(3)
N(3)-C(23)-C(24) 125.3(5)	N(6)-C(59)-C(60) 126.1(5)	N(3)-C(25)-C(26) 126.5(3)
θ_T (C(1)-C(2)-N(1)-C(3)/C(7)$_{Ar}$) = 77.6(6)	θ_T (C(37)-C(38)-N(4)-C(39)/C(43)$_{Ar}$) = 75.8(5)	θ_T (C(1)-C(2)-N(1)-C(3)/C(4)$_{Ar}$) = 38.7(3)
θ_T (C(1)-C(14)-N(2)-C(15)/C(16)$_{Ar}$) = 50.1(6)	θ_T (C(37)-C(50)-N(5)-C(51)/C(52)$_{Ar}$) = 48.4(5)	θ_T (C(1)-C(11)-N(2)-C(12)/C(13)$_{Ar}$) = 88.9(3)
θ_T (C(1)-C(23)-N(3)-C(24)/C(25)$_{Ar}$) = 81.8(5)	θ_T (C(37)-C(59)-N(6)-C(60)/C(61)$_{Ar}$) = 77.5(5)	θ_T (C(1)-C(25)-N(3)-C(26)/C(27)$_{Ar}$) = 84.5(3)

There are only six structurally characterised N_3ONiX complexes reported in the literature, and none of these represents an appropriate comparator to the **$[(\eta^4\text{-L})NiBr][BAr^F{}_4]$** and **$[(\eta^4\text{-L})NiBr][OTf]$** compounds, as there are no examples where X = Br.[388] The nickel chloride derivative of a tetradentate (bis(2-pyridylmethyl)aminomethyl)phenolate ligand displays a similarly distorted square-pyramidal geometry, though the Ni-N distances (2.046(5) Å, 2.125(4) Å, 2.134(5) Å) are on average much longer than those seen in the

complexes of $\mathbf{L^{15}}$ and $\mathbf{L^{16}}$.[389] The Ni-O_{OMe} distances in the **[(η^4-L)NiBr][BAr^F_4]** compounds lie very close to the mean (2.222 Å) of previously reported values for such interactions.[390] The shorter Ni-O_{OMe} distance in **[(η^4-L^{16})NiBr][BAr^F_4]** compares most closely to the two corresponding unique distances (2.211(2) and 2.218(2) Å) in a six-coordinate complex bearing two bidentate bis(2-methoxyphenyl)formamidine ligands.[391] The much longer Ni-O_{OMe} distances seen in the **[(η^4-L)NiBr][OTf]** compounds are similar to the longer of two such distances (2.279(4) and 2.301(4) Å) as found in a tetranuclear nickel cubane cluster supported by two doubly-deprotonated tetradentate *N*-(2-hydroxyethyl)-3-methoxysalicylaldimine ligands.[392]

4.2.1.8 (η^2-L^6)$NiBr_2$

As the very bulky $\mathbf{L^6}$ was found to give access to the novel cationic complex **[(η^2-L^6)NiBr(THF)][BAr^F_4]**, it was assumed that the substitution of $BAr^F_4^-$ for triflate may give access to the analogous triflate salt. However, when $\mathbf{L^6}$ was reacted with $NiBr_2$(DME) and AgOTf in THF, the only product which could be isolated upon crystallisation from DCM and hexane was a small number of intensely violet-coloured crystals. Rather than a cationic complex, these were shown by X-ray crystallography to be the neutral **(η^2-L^6)$NiBr_2$**, in which $\mathbf{L^6}$ is coordinated in an identical fashion to that observed in **[(η^2-L^6)NiBr(THF)][BAr^F_4]**, though the intended metathesis reaction with AgOTf has failed to occur. This is presumably due to the fact that the triflate ion is much less weakly-coordinating than $BAr^F_4^-$, and is thus unable to abstract a bromide ion from $NiBr_2$(DME) and support an analogous electrophilic, four-coordinate cationic THF complex. Repeating the reaction in the absence of AgOTf using only DCM solvent gave exclusively **(η^2-L^6)$NiBr_2$** in a greatly improved yield (**scheme 4.11**).

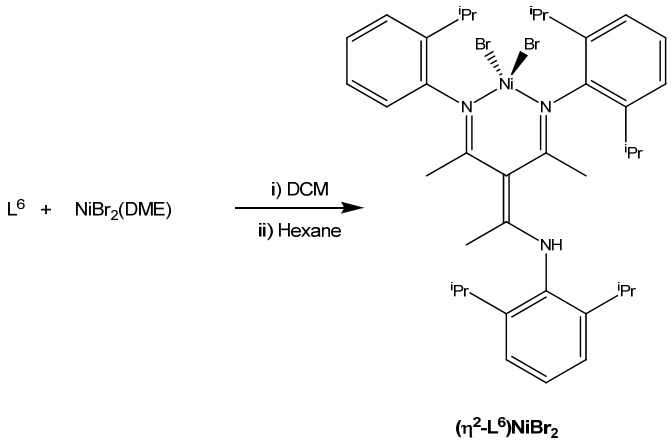

Scheme 4.11 Synthesis of (η^2-L^6)$NiBr_2$

The molecular structure of **(η^2-L^6)$NiBr_2$** (**figure 4.21**) is similar to that of **[(η^2-L^6)NiBr(THF)][BAr^F_4]**, though Br(1) and Br(2) are oriented further towards the enamine moiety than the bromine and oxygen atoms in the latter complex, as evidenced by the fact that the Br(1)-Ni(1)-Br(2), Br(1)-Ni(1)-N(1) and Br(1)-Ni(1)-N(2) angles (**table 4.10**) are respectively wider than the corresponding Br(1)-Ni(1)-O(1), N(1)-Ni(1)-O(1) and N(2)-Ni(1)-O(1) angles in **[(η^2-L^6)NiBr(THF)][BAr^F_4]**.

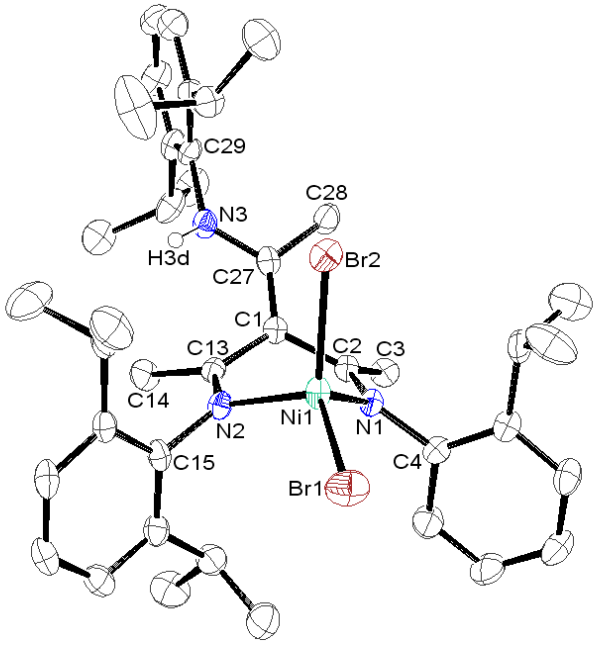

Figure 4.21 ORTEP representation of (η^2-L^6)$NiBr_2$ with thermal ellipsoids set at the 40 % probability level; enamine hydrogen shown, all others omitted for clarity

The steric repulsion between Br(2) and the isopropyl groups is therefore increased, and as such the Br(2)-Ni(1) distance of 2.3886(6) Å is noticeably longer than both the Br(1)-Ni(1) distance of 2.3228(6) Å, and the Br-Ni distance of 2.3030(16) Å in **[(η^2-L^6)NiBr(THF)][BAr^F_4]**. In contrast, the Ni-N distances (**table 4.10**) and N-N separation of 2.779(5) Å are very similar to the corresponding parameters as observed in the cationic complex. Additionally, aside from the comparatively shorter C(1)-C(2) and C(1)-C(13) bond lengths, **(η^2-L^6)$NiBr_2$** shows very little structural difference to either ($HBDK^{iPr2}$)$NiBr_2$,[12] or complex **324**.[302] However, the N-N separations in both **(η^2-L^6)$NiBr_2$** and **[(η^2-L^6)NiBr(THF)][BAr^F_4]** are much shorter than those found in ($HBDK^{iPr2}$)$NiBr_2$ (2.941(8) Å) and **324** (2.918(11) Å). This is likely due to steric factors, as in the β-diimine complexes two 2,6-diisopropylphenyl substituents are accommodated at the nickel centre, whereas in the **L^6** adducts one of these groups is formally replaced by a much less bulky 2-isopropylphenyl moiety.

Table 4.10 Selected bond lengths (Å), angles (°) and interplanar torsion angles (°) for (η^2-L^6)$NiBr_2$

Br(1)-Ni(1) 2.3228(6)	Ni(1)-N(1)-C(2) 120.1(2)
Br(2)-Ni(1) 2.3886(6)	Ni(1)-N(2)-C(13) 118.9(2)
Ni(1)-N(1) 1.984(3)	C(2)-N(1)-C(4) 120.6(3)
Ni(1)-N(2) 1.990(3)	C(13)-N(2)-C(15) 120.5(3)
N(1)-C(2) 1.290(4)	C(1)-C(2)-N(1) 118.8(3)
N(2)-C(13) 1.279(4)	C(1)-C(13)-N(2) 120.8(3)
N(1)-C(4) 1.448(4)	N(1)-C(2)-C(3) 121.5(3)
N(2)-C(15) 1.447(5)	N(2)-C(13)-C(14) 121.0(3)
C(1)-C(2) 1.486(4)	C(1)-C(2)-C(3) 119.5(3)
C(1)-C(13) 1.468(5)	C(1)-C(13)-C(14) 118.1(3)
C(1)-C(27) 1.363(5)	C(2)-C(1)-C(13) 116.5(3)
N(3)-C(27) 1.362(5)	C(2)-C(1)-C(27) 121.5(3)
N(3)-C(29) 1.454(4)	C(13)-C(1)-C(27) 122.0(3)
	C(1)-C(27)-C(28) 125.3(3)
Br(1)-Ni(1)-Br(2) 120.08(2)	C(1)-C(27)-N(3) 120.5(3)
Br(1)-Ni(1)-N(1) 117.25(8)	N(3)-C(27)-C(28) 114.0(3)
Br(1)-Ni(1)-N(2) 117.05(8)	C(27)-N(3)-C(29) 127.4(3)
Br(2)-Ni(1)-N(1) 103.71(8)	
Br(2)-Ni(1)-N(2) 104.94(8)	θ_T (C(1)-C(2)-N(1)-C(3)/$C(4)_{Ar}$) = 81.8(3)
N(1)-Ni(1)-N(2) 88.74(11)	θ_T (C(1)-C(13)-N(2)-C(14)/$C(15)_{Ar}$) = 86.0(3)
Ni(1)-N(1)-C(4) 119.3(2)	θ_T (C(1)-C(27)-N(3)-C(28)/$C(29)_{Ar}$) = 82.1(3)
Ni(1)-N(2)-C(15) 120.7(2)	

4.2.2 Ethylene Polymerisation

4.2.2.1 Screening of β-Triketimine Nickel(II) Complexes for Catalytic Activity

A number of the nickel complexes described in this work have been investigated as precatalysts for the polymerisation of ethylene in toluene at room temperature and 1 atm ethylene pressure. MAO was employed as a cocatalyst for all polymerisation experiments, the results of which are presented in **table 4.11**. Complexes of β-triketimines in which R^7 = Me (**L^3**, **L^5**, **L^7** and **L^8**) display varying degrees of catalytic activity, though all derivatives of both the least bulky **L^1**, and the tetradentate **L^{15}** were found to be completely inactive. Additionally, all of the complexes of β-triketimines where R^7 = ^{t}Bu tested were also found to be inactive, regardless of overall ligand steric bulk. It should be noted here that, whilst no polymer was obtained from these reactions, the catalysts may produce ethylene oligomers, as has previously been shown for the related (Tp^{Mes})NiCl.[378] However, in this work no attempts were made to analyse the reaction mixtures for the presence of any oligomeric species. The activities of the catalysts range from 5.3-64.9 $kgmol^{-1}h^{-1}$, which can be described as 'low' to 'moderate' according to the criteria described by Gibson and Spitzmesser.[370(a)] However, many of the previously reported activities for α-diimine supported catalysts are derived from very short reaction times, most commonly ten minutes, as a result of the very short catalyst lifetimes. In contrast, the activities reported here are representative of significantly longer reaction times, generally of 1-2 hours but also even longer. At first the polymerisations were performed with very small solvent volumes (10-20 cm^3), though the reaction mixtures rapidly became too viscous to allow for adequate stirring due to the presence of dissolved polyethylene. Increasing the solvent volume by a factor of ten eliminated this problem, but did not give rise to any increase in the overall catalyst activities as was anticipated. Similarly, variation of the [Al]/[Ni] ratio does not appear to have any consistent effect on the catalytic activities, though in certain cases the lowest activity observed for a particular catalyst were for those reactions in which the [Al]/[Ni] ratio was lowest (**table 4.11**, **entries 14** and **20**). These results provide good evidence that the catalysts have extended lifetimes, as in many cases optimum activities are observed for reaction times greater than one hour. For example, the highest activity seen for **[(η^2-L^6)NiBr(THF)][BAr^F_4]** was for a reaction time of 150 minutes (**table 4.11**, **entry 24**), whilst all of the other catalysts show activities for reaction times greater than one hour which are comparable to their optimum values.

Table 4.11 Results of ethylene polymerisation experiments; [a] Turnover Frequency, [b] ethylene addition stopped after 1h, reaction not quenched for further ~3h

Entry	Catalyst	Toluene (cm^3)	Ni (µmol)	[Al]/[Ni]	Time (min)	Yield (g)	Activity ($kg\ mol^{-1}\ Ni\ h^{-1}$)	TOF[a] (h^{-1})
1	$[\{(L^1)Ni(\mu\text{-}Br)\}_2][BAr^F{}_4]_2$	10	3.34	4970	60	0	0	0
2	$[(L^1)NiBr][OTf]$	10	6.40	2593	60	0	0	0
3	$[\{(L^3)Ni(\mu\text{-}Br)\}_2][BAr^F{}_4]_2$	10	3.31	5013	60	0.123	37.2	1327
4	$[\{(L^3)Ni(\mu\text{-}Br)\}_2][BAr^F{}_4]_2$	15	5.83	518	120	0.178	15.3	545
5	$[\{(L^3)Ni(\mu\text{-}Br)\}_2][OTf]_2$	10	6.29	2639	60	0.046	7.3	261
6	$[\{(L^3)Ni(\mu\text{-}Br)\}_2][OTf]_2$	20	5.66	534	120	0.064	5.7	199
7	$[\{(L^5)Ni(\mu\text{-}Br)\}_2][BAr^F{}_4]_2$	10	3.25	5107	60	0.211	64.9	2318
8	$[\{(L^5)Ni(\mu\text{-}Br)\}_2][BAr^F{}_4]_2$	15	6.12	493	120	0.499	40.8	1456
9	$[\{(L^5)Ni(\mu\text{-}Br)\}_2][BAr^F{}_4]_2$	200	6.05	997	107	0.660	61.1	2185
10	$[\{(L^5)Ni(\mu\text{-}Br)\}_2][BAr^F{}_4]_2$	200	5.98	1008	60[b]	0.657	109.9	3924
11	$[\{(L^5)Ni(\mu\text{-}Br)\}_2][BAr^F{}_4]_2$	200	6.18	976	60	0.238	38.5	1375
12	$[\{(L^5)Ni(\mu\text{-}Br)\}_2][OTf]_2$	10	6.07	2735	60	0.366	60.3	2153
13	$[\{(L^5)Ni(\mu\text{-}Br)\}_2][OTf]_2$	10	8.50	1952	120	0.441	25.9	926
14	$[\{(L^5)Ni(\mu\text{-}Br)\}_2][OTf]_2$	15	6.07	498	120	0.233	19.2	685
15	$[\{(L^5)Ni(\mu\text{-}Br)\}_2][OTf]_2$	200	6.31	956	135	0.762	53.7	1917
16	$[\{(L^5)Ni(\mu\text{-}Br)\}_2][OTf]_2$	200	6.19	974	60	0.167	27.0	966
17	$[\{(L^5)Ni(\mu\text{-}Br)\}_2][OTf]_2$	150	5.83	1034	60	0.133	24.7	814
18	$(\eta^2\text{-}L^6)NiBr_2$	10	6.28	2642	60	0.234	37.3	1330
19	$(\eta^2\text{-}L^6)NiBr_2$	10	7.53	2204	120	0.412	27.4	977
20	$(\eta^2\text{-}L^6)NiBr_2$	15	7.03	430	136	0.085	5.3	191
21	$(\eta^2\text{-}L^6)NiBr_2$	200	6.78	889	120	0.368	27.1	969
22	$(\eta^2\text{-}L^6)NiBr_2$	200	6.15	980	60	0.224	36.4	1300
23	$[(\eta^2\text{-}L^6)NiBr(THF)][BAr^F{}_4]$	10	3.03	5476	60	0.132	43.6	1556
24	$[(\eta^2\text{-}L^6)NiBr(THF)][BAr^F{}_4]$	10	3.63	4573	150	0.576	63.5	2267
25	$[(\eta^2\text{-}L^6)NiBr(THF)][BAr^F{}_4]$	15	6.17	489	126	0.619	47.8	1706
26	$[(\eta^2\text{-}L^6)NiBr(THF)][BAr^F{}_4]$	200	5.75	1049	135	0.561	43.4	1549
27	$[(\eta^2\text{-}L^6)NiBr(THF)][BAr^F{}_4]$	200	6.11	987	245	0.459	18.4	657
28	$[(\eta^2\text{-}L^6)NiBr(THF)][BAr^F{}_4]$	200	5.93	1017	63	0.202	32.4	1159
29	$[\{(L^7)Ni(\mu\text{-}Br)\}_2][BAr^F{}_4]_2$	75	59.5	101	120	1.870	15.7	561
30	$[\{(L^8)Ni(\mu\text{-}Br)\}_2][BAr^F{}_4]_2$	10	3.28	5061	60	0	0	0
31	$[(L^{10})NiBr][BAr^F{}_4]$	10	3.25	5107	120	0	0	0
32	$[(L^{11})NiBr][BAr^F{}_4]$	10	3.80	4368	120	0	0	0
33	$[\{(L^{12})Ni(\mu\text{-}Br)\}_2][BAr^F{}_4]_2$	10	3.90	4256	120	0	0	0
34	$[(L^{11})NiBr][OTf]$	10	6.93	2395	120	0	0	0
35	$[(\eta^4\text{-}L^{15})NiBr][BAr^F{}_4]$	10	3.82	4345	120	0	0	0
36	$[(\eta^4\text{-}L^{15})NiBr][OTf]$	10	7.03	2361	120	0	0	0

However, when the polymerisation reaction catalysed by **[(η^2-L^6)NiBr(THF)][BAr^F_4]** was performed over 245 minutes, the overall activity was considerably lower at 18.4 $kgmol^{-1}h^{-1}$. This suggests that the catalyst lifetimes are not as great as those claimed for complex **325**, though in this case the polymerisation reactions were carried out at the much lower temperature of -10°C. [376] The highest catalytic activities are observed for **[{(L^5)Ni(μ-Br)}$_2$][BAr^F_4]$_2$** (64.9 $kgmol^{-1}h^{-1}$), **[{(L^5)Ni(μ-Br)}$_2$][OTf]$_2$** (60.3 $kgmol^{-1}h^{-1}$) and **[(η^2-L^6)NiBr(THF)][BAr^F_4]** (63.5 $kgmol^{-1}h^{-1}$); whilst it might have been anticipated that the triflate complexes may show lower activities due to an increased level of cation-anion interaction, no such discrepancy was observed. The anomalously high activity of 109.9 $kgmol^{-1}h^{-1}$ observed in a single experiment where **[{(L^5)Ni(μ-Br)}$_2$][BAr^F_4]$_2$** was employed as the catalyst (**table 4.11**, **entry 10**) is likely due to the fact that, although the addition of ethylene was ceased after 60 minutes, the reaction was not terminated for a further ~3 hours. As such, a relatively high concentration of dissolved ethylene in the reaction medium may have allowed the reaction to continue, even though the addition of ethylene had been stopped. The neutral **(η^2-L^6)NiBr$_2$** (maximum activity 37.3 $kgmol^{-1}h^{-1}$) is considerably less active than its cationic analogue **[(η^2-L^6)NiBr(THF)][BAr^F_4]**, which implies that the use of a precatalyst which is a cationic complex rather than a neutral one has a beneficial effect on catalytic activity (*vide infra*). Complexes of the least bulky ligands (**L^3** and **L^7**) represent the least active catalysts, which is likely due to the fact that the relative stability of the intermediate nickel methyl ethylene complex (**scheme 4.1**) is actually increased when the steric bulk of the ligand decreases, due to less crowding at the metal centre, and thus the rate of migratory insertion decreases. Decreasing the steric bulk yet further as in the case of **L^1** gives rise to complexes which show no catalytic activity for polymerisation whatsoever. As such, it is somewhat surprising that the formal addition of a single methyl group upon going from **L^1** to **L^3** is a sufficient increase in steric bulk so as to allow for polymerisation to occur.

Although the maximum catalytic activities observed for the β-triketimine complexes fall well short of the α-diimine catalysts,[370] they are higher than the optimum activities seen for related compounds such as ($Tp^{tBu,Me}$)NiBr (10.5 $kgmol^{-1}h^{-1}$),[393] ($Tp^{Cum,Me}$)NiBr($Hpz^{Cum,Me}$) (12.0 $kgmol^{-1}h^{-1}$)[393] and ($HBDK^{iPr2}$)$NiBr_2$ (14.5 and 54.6 $kgmol^{-1}h^{-1}$).[11,394] However, in the case of the latter complex the activity values are derived from reactions performed at high ethylene pressures (280 and 150 psig respectively). When these values are adjusted to 1 atm ethylene pressure the rather more modest activities of 0.8 and 5.3 $kgmol^{-1}h^{-1}$ are

obtained. As such, it is clear that the β-triketimine complexes display optimum activities that are on average a single order of magnitude greater than those observed for $(HBDK^{iPr2})NiBr_2$. The β-diketiminate complexes $\{(BDK^{iPr2})NiBr\}_2$ and $(BDK^{iPr2})NiBr(PPh_3)$ have been reported to display optimum activities of 16.0 and 20.1 $kgmol^{-1}h^{-1}$ respectively when adjusted to 1 atm ethylene pressure,[394] whilst the activity of the heavily fluorinated $\{(^{F}BDK^{iPr2})NiBr\}_2$ ($H^{F}BDK^{iPr2}$ = 1,1,1,3,3,3-hexafluoro-2-(2,6-diisopropyl)phenylamino-4-(2,6-diisopropyl)phenyliminopent-2-ene) was somewhat higher at 38.5 $kgmol^{-1}$. However, in the case of $\{(^{F}BDK^{iPr2})NiBr\}_2$, the optimum activity was achieved at -10°C; at a polymerisation temperature of 30°C, the activity was reduced almost ten-fold, which is indicative of low thermal stability of the catalyst. [395]

An extremely high activity of 27764 $kgmol^{-1}h^{-1}$ has been reported for the α-keto-β-diketimine complex **324**, though this was derived from a ten minute run at 50°C and an ethylene pressure of 450 psig.[302] Adjusting this value to 1 atm ethylene pressure gives an activity of 895.6 $kgmol^{-1}h^{-1}$, though this is still comparable to many of the α-diimine catalysts. However, when the polymerisation was carried out at 20°C with an ethylene pressure of 300 psig, the activity was found to be 71.5 $kgmol^{-1}h^{-1}$ when adjusted to 1 atm ethylene, which is very similar to the optimum activities seen for a number of the β-triketimine complexes.[375] As such, it can reasonably be anticipated that if ethylene polymerisation catalysed by complex **324** was performed under identical conditions to those described in this work, it is likely the catalytic activities would be found to be very similar.

4.2.2.2 Polymer Properties

The polymers produced by the nickel complexes of $\mathbf{L^5}$ and $\mathbf{L^6}$ have a considerable degree of elasticity, yet are relatively hard to pull apart, though they tear rapidly when stretched beyond a certain point. The polymers are soluble at 140°C in solvents such as 1,2-dichlorobenzene and xylenes, though the dissolution of even small amounts of polymer causes a very large increase in viscosity. All of these observations are indicative of high molecular weight polyethylene, though actual determination of molecular weight values by GPC was not possible due to the limitations of the instruments in the School of Chemistry. In contrast, the polymers produced by complexes of $\mathbf{L^3}$ and $\mathbf{L^7}$ are noticeably more soluble, even at temperatures well below 140°C, and are also much more easily stretched and torn apart. This suggests that these polymers are of much lower molecular weight, which is a

result of the reduced steric bulk of $\mathbf{L^3}$ and $\mathbf{L^7}$ relative to $\mathbf{L^5}$ and $\mathbf{L^6}$. As a result of the reduced steric encumbrance, chain transfer to both aluminium and monomer becomes more energetically favourable, and as such polymers of lower molecular weight are obtained. The elastomeric nature of all the polymers prepared in this work indicates a relatively high degree of branching, and this is reflected in the very low T_m values (**table 4.12**). These were determined by differential scanning calorimetry (DSC), and for all of the polymers the traces invariably show very small, broad endothermic events, which correspond to a very low degree of crystallinity (X_c). Additionally, when any of the polymers are stretched or cast into films they display a high degree of transparency, which is consistent with the polymers being of low crystallinity, and also indicates that any crystallites which are present must be very small in size (i.e. smaller than the wavelength of visible light).

Table 4.12 Physical properties of polyethylene produced by β-triketimine nickel complexes

Entry	Catalyst	T_m (°C)[a]	X_c (%)[b]	Branches per 1000 C[c]
4	$[\{(L^3)Ni(\mu\text{-}Br)\}_2][BAr^F{}_4]_2$	42.6	2.30	84
6	$[\{(L^3)Ni(\mu\text{-}Br)\}_2][OTf]_2$	44.6	5.29	66
11	$[\{(L^5)Ni(\mu\text{-}Br)\}_2][BAr^F{}_4]_2$	41.3	2.98	48
16	$[\{(L^5)Ni(\mu\text{-}Br)\}_2][OTf]_2$	38.9	2.44	46
21	$(L^6)NiBr_2$	42.0	0.54	43
26	$[(L^6)NiBr(THF)][BAr^F{}_4]$	37.9	1.88	65
27	$[(L^6)NiBr(THF)][BAr^F{}_4]$	-	-	55
29	$[\{(L^7)Ni(\mu\text{-}Br)\}_2][BAr^F{}_4]_2$	33.6	0.84	-

[a] Determined by DSC; [b] determined by DSC (ΔH_m = 293 Jg^{-1} for 100% crystalline polyethylene); [c] determined by ^{13}C NMR

The degree of branching (**table 4.12**) in the polymers varies between 43 and 84 branches per 1000 carbons, though there is no discernible trend in the branching rates dependent on the identity of the catalyst. Additionally, there appears to be little correlation between the branching rates and the T_m values, which vary over the rather narrow range of 33.6-44.6°C. The T_m values, as well as the higher of the branching rates, are similar to those seen for polymer produced by $(BIAN^{iPr2})NiBr_2$ at 1 atm ethylene pressure (T_m = 39.0°C, 71 branches per 1000 C),[10] whilst the branching rates are also similar to those achieved with complex **325** (57-93 branches per 1000 C).[376] Direct comparison of the T_m values and branching rates with those seen for all of the aforementioned β-diketimine/β-diketiminate complexes is not possible due to the fact that the reactions were performed with high ethylene pressures, which causes a relative decrease in the degree of branching, and thus an increase in T_m.

The branching rates of the polymers were determined by ^{13}C NMR spectroscopy; a fully assigned spectrum of the polyethylene produced by $\mathbf{[\{(L^5)Ni(\mu\text{-}Br)\}_2][BAr^F{}_4]_2}$ is presented

in **figure 4.22**. The polymers produced by each of the different catalysts display very similar ^{13}C NMR spectra, and all are predominantly methyl-branched, as indicated by the relatively large resonance at 20.1 ppm. However, the spectra also indicate the presence of longer branches (ethyl to hexyl and longer), as well as 1,4-dimethyl, 1,5-dimethyl and 1,6-dimethyl branches, which are identified by the characteristic peaks at 34.9 ppm (1,4-α), 25.8 ppm (1,5-β) and 27.8 ppm (1,6-β) respectively. Additionally, the small yet distinct peak at 31.7 ppm is indicative of the presence of 1,4 pairs of branches longer than methyl. The spectra of the polymers produced by the β-triketimine complexes are all very similar to those of polyethylene produced by α-diimine supported nickel catalysts.[396,397]

4.2.2.3 Mechanism of Catalyst Activation

The molecular structures of **[(η^2-L^6)NiBr(THF)][BAr$^F_4$]** and **(η^2-L^6)NiBr$_2$**, both of which feature the ligand coordinated in a bidentate mode, give good indication as to the mechanism by which the precursor complexes undergo activation upon stepwise treatment with MAO and ethylene. By adopting this coordination mode, it is very likely that the ligand is equally able to support either a tetrahedral or square-planar geometry at nickel. Owing to the fact that a square-planar nickel methyl ethylene complex is assumed to be a key intermediate in the catalytic cycle of polymerisation, and that square-planar geometry is strongly favoured for nickel with strongly σ-donating alkyl ligands, it can easily be envisioned how such a species may be formed upon sequential treatment of the cationic **[(η^2-L^6)NiBr(THF)][BAr$^F_4$]** with MAO and ethylene (**scheme 4.12**).

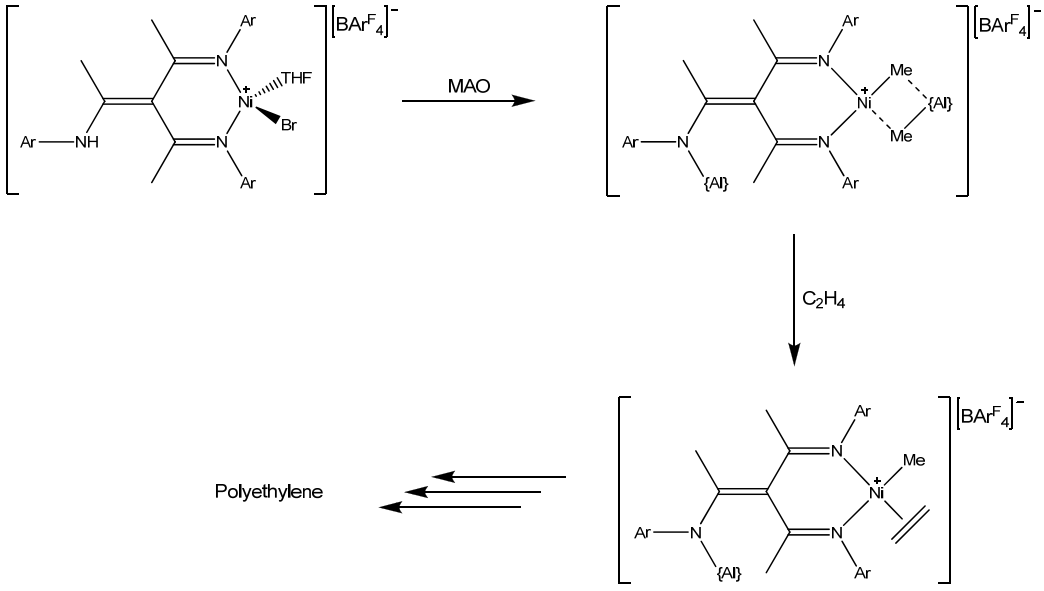

Scheme 4.12 Proposed mechanism for activation of [(η^2-L^6)NiBr(THF)][BAr$^F_4$] by MAO

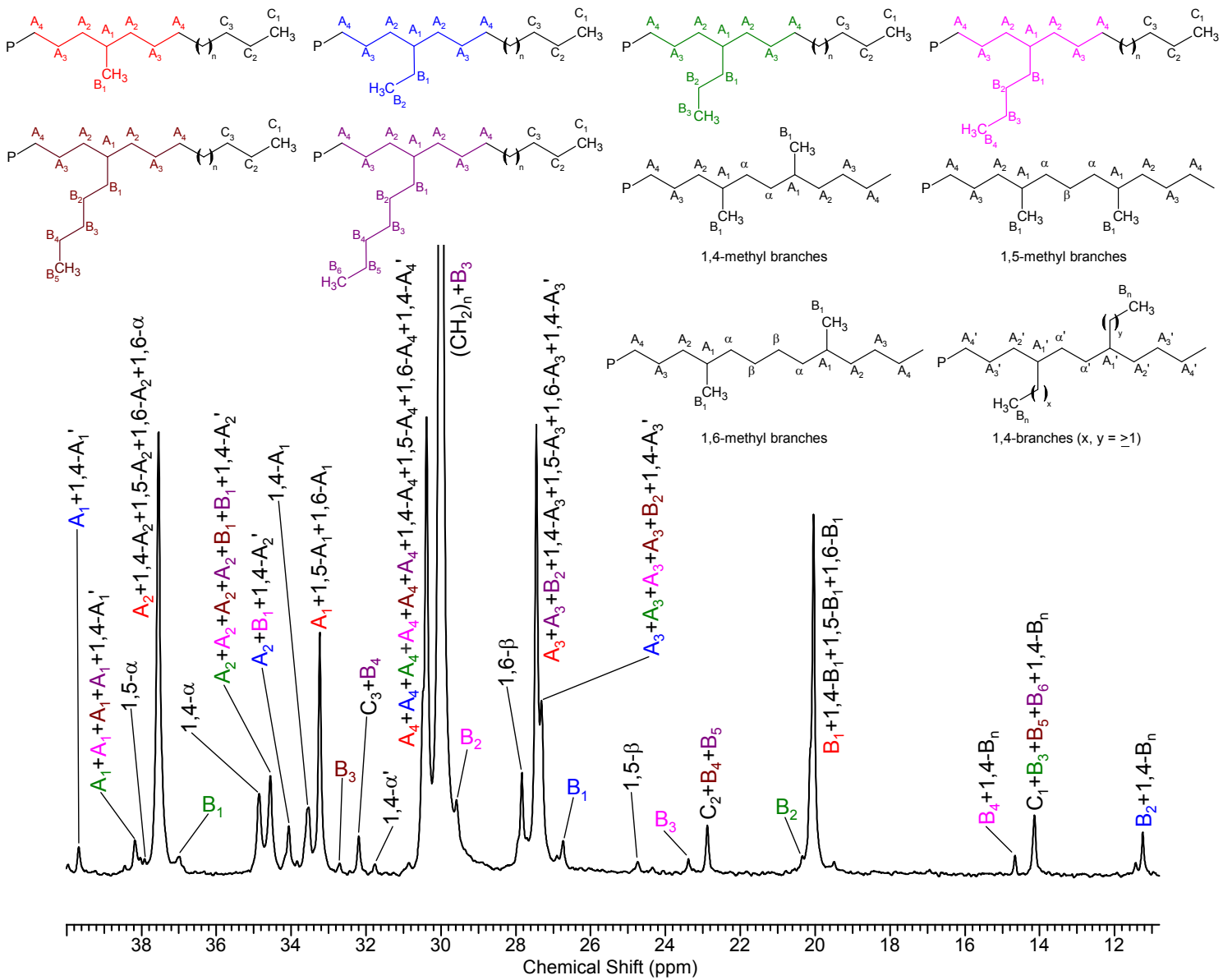

Figure 4.22 ^{13}C NMR spectrum of polyethylene produced by [{(L^5)Ni(μ-Br)}$_2$][BAr$^F{}_4$]$_2$; assignments according to refs. 396-398

The mechanism of activation in the case of **$(\eta^2\text{-}L^6)NiBr_2$** may differ slightly, and likely involves the formation of a contact ion-pair composed of a cationic nickel complex and an anionic MAO-based species (**scheme 4.13**). A reduced degree of interaction between the cation and the $BAr^F{}_4$ anion may account for the increased activity of **$[(\eta^2\text{-}L^6)NiBr(THF)][BAr^F{}_4]$** relative to **$(\eta^2\text{-}L^6)NiBr_2$**, as the cationic nickel methyl ethylene species generated from both precursors are very likely identical. Following treatment with MAO, it is very likely that the enamine NH of the bidentately coordinated ligands is deprotonated, and the resulting amide is bound by an aluminium centre of some MAO-derived species (denoted {Al}). The strongly Lewis acidic aluminium may act as a 'sink' for electron density from the ligand due to conjugation of the deprotonated enamine moiety with the imine donors, thus causing a reduction in their electron donating ability relative to analogous β-diketiminate ligands. This has the effect of causing a reduction in the electron density at the nickel centre, and thus an increase in its electrophilicity. This may account for the fact that the β-triketimine catalysts are more active than any of the related β-diketimine/β-diketiminate complexes, and show similar activity to complex **324** when accounting for the different reaction conditions. Indeed, the increased activity of **324** has been postulated to be as a result of the coordination of the exodentate ketone moiety to a strongly Lewis acidic aluminium species upon treatment with MAO.[302]

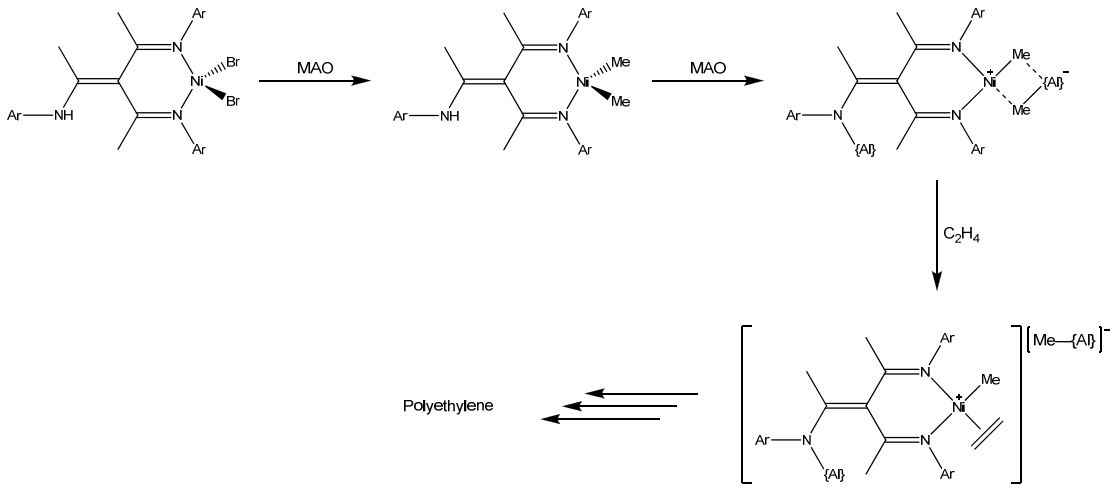

Scheme 4.13 Proposed mechanism for activation of $(\eta^2\text{-}L^6)NiBr_2$ by MAO

In contrast to **L^6**, it is impossible for the tridentately coordinating ligands **L^3**, **L^5** and **L^7** to support a square-planar geometry at nickel. However, it is likely that upon treatment of **$[\{(L)Ni(\mu\text{-}Br)\}_2][X]_2$** (**X = $BAr^F{}_4$, OTf**) with MAO and ethylene, the formation of a nickel methyl complex provides a strong driving force for the dissociation of one imine group, which in turn allows for the formation of a square-planar complex (**scheme 4.14**). As

such, the catalytically active species are likely to be very similar to that obtained from **[(η^2-L^6)NiBr(THF)][BAr$^F_4$]**. If it is assumed that in the case of bidentately coordinated square-planar complexes of **L^5**, the 2,6-diisopropylphenyl substituted imine is bound to the nickel centre, then this implies that the steric shielding of the metal is essentially identical to that seen in complexes of **L^6**, as the two ligands differ only in the nature of the exodentate enamine moiety (**figure 4.23**). As such, this may account for the fact that **[(η^2-L^6)NiBr(THF)][BAr$^F_4$]**, **[{(L^5)Ni(μ-Br)}$_2$][BAr$^F_4$]$_2$** and **[{(L^5)Ni(μ-Br)}$_2$][OTf]$_2$** are all found to display similar optimum catalytic activities.

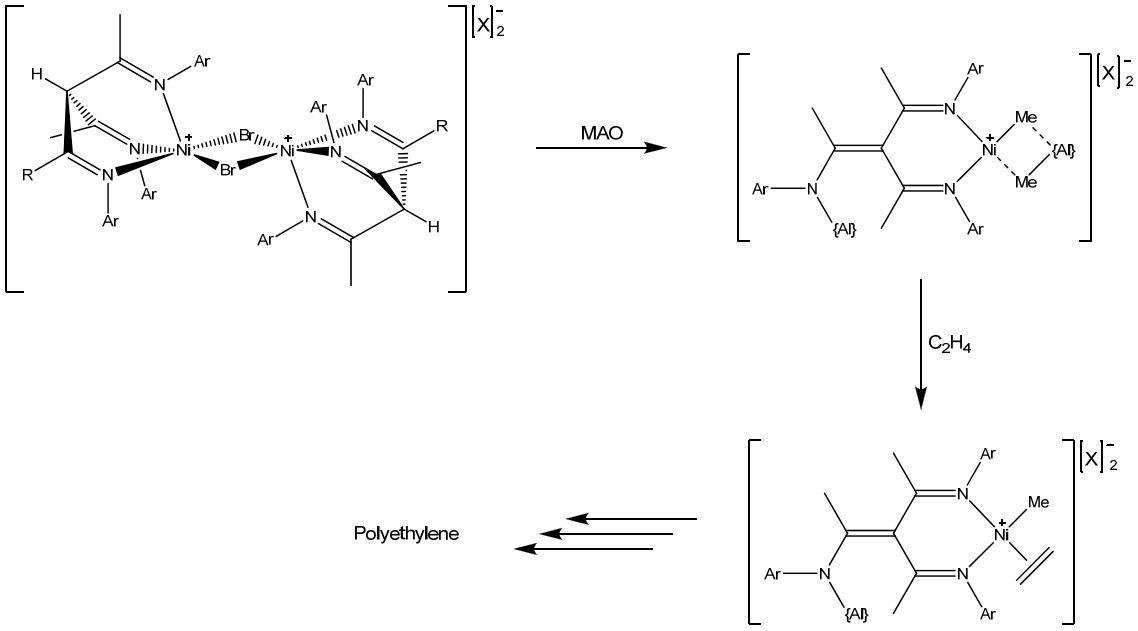

Scheme 4.14 Proposed mechanism for activation of [{(L)Ni(μ-Br)}$_2$][X]$_2$ (X = BAr$^F_4$, OTf)

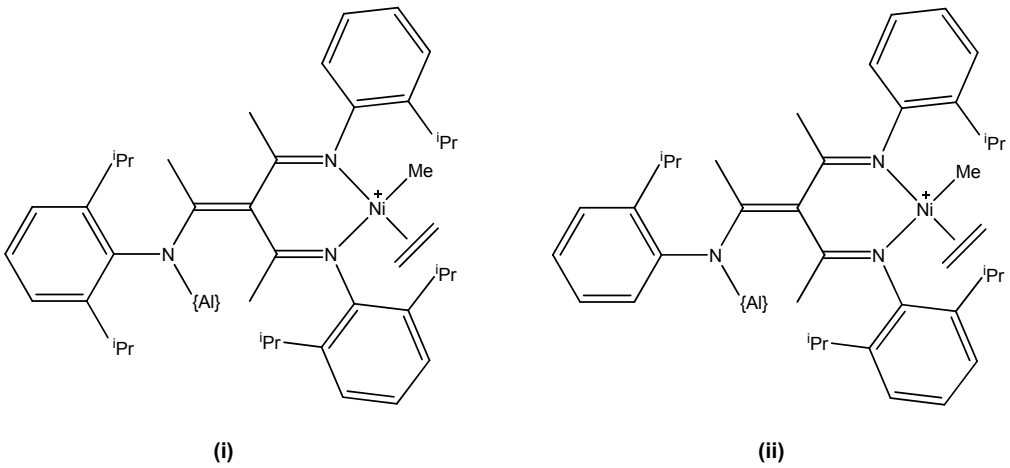

Figure 4.23 Structures of putative nickel methyl ethylene complexes of (i) L^6 and (ii) L^5 showing similar steric environments at nickel

The notion that the ability of the R^7 Me-substituted β-triketimine ligands to adopt a bidentate coordination mode is essential to the catalytic activity of their nickel derivatives also provides good suggestion as to why all the complexes of R^7 *tert*-butyl substituted ligands tested were found to be completely inactive. Placement of the *tert*-butyl group in any of the positions depicted in **scheme 4.15** would result in numerous severe steric clashes; consequently, none of these ligands are able to adopt the bidentate coordination mode necessary for the formation of a square-planar nickel methyl ethylene complex. This hypothesis is also supported by the fact that free $\mathbf{L^{11}}$ and $\mathbf{L^{12}}$ exist exclusively as the β-triketimine tautomer both in solution and in the solid state, and also that the molecular structure of $\mathbf{L^{10}}$ features the *tert*-butyl group orthogonal to the enamine-imine moiety. As such, the feasibility of accommodating the *tert*-butyl group, either as part of the planar enamine moiety or at either of the coordinated imines is extremely low. It is certainly possible that the treatment of $\mathbf{[\{(L)Ni(\mu\text{-}Br)\}_2][BAr^F{}_4]_2}$ ($\mathbf{L = L^8}$, $\mathbf{L^{12}}$) / $\mathbf{[(L)NiBr][BAr^F{}_4]}$ ($\mathbf{L = L^{10}}$, $\mathbf{L^{11}}$) with MAO may furnish a tridentately coordinated cationic methyl complex (**scheme 4.15**), though as the dissociation of a single imine group is not possible, binding of ethylene cannot occur and the complex is not catalytically active.

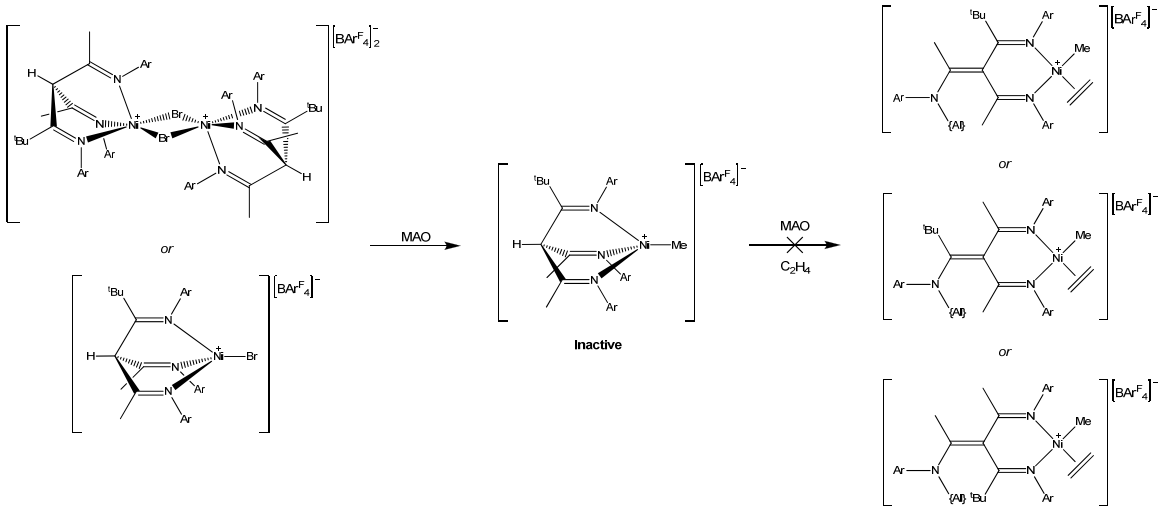

Scheme 4.15 Inactivity of R^7 *tert*-butyl substituted β-triketimine complexes

5. Conclusions

The reaction of lithium β-diketiminates with imidoyl chlorides has been shown to provide a reliable synthetic route to a series of novel β-triketimine ligands. The modular nature of the synthetic procedure allows for the preparation of β-triketimines with a variety of substitution patterns, which is achieved through variation of the substituent groups on the component β-diketiminates and imidoyl chlorides. This in turn allows for 'fine tuning' of the overall steric demand of the β-triketimines, as seemingly subtle changes in substitution can have a drastic effect on the properties of the ligands. All of the β-triketimines in which R^7 = Me (**L**$^{1\text{-}7}$, **L**^{15}) show solution-phase behaviour which is complicated by the presence of numerous isomeric species, as a result of tautomerism between the true β-triketimine and enamine-diimine forms, as well as *E/Z*-isomerism in the pendant imine of the enamine-diimine tautomer. If the three aryl groups are not all identical, then the situation is complicated further by the fact that two potential geometric isomers exist for the enamine-diimine tautomer, giving a total of five possible isomeric species in solution. However, not all of these are always observed, or are present in negligible quantities. The process of equilibration in solution is rapid, unless all of the aryl groups are at least 2,6-disubstituted. In these cases (**L**^{2}, **L**^{7}) equilibration occurs slowly over a period of days, ultimately yielding an approximately equal solution mixture of the β-triketimine and *E*-isomer of the enamine-diimine. The seeming preference of the enamine-diimine tautomers for the *E*-isomer is inferred through inspection of the solid-state structure of **L**^{1}. For all those β-triketimines in which R^7 = Ph or ^{t}Bu (**L**$^{8\text{-}14}$, **L**^{16}), a single isomer is observed both in solution and the solid state. If the aryl group of the R^7 imine is 2,6-disubstituted, the β-triketimine tautomer is favoured exclusively, whilst if the aryl group is 2-substituted only then the *Z*-isomer of the enamine-diimine is the sole form observed. Although the prochiral **L**^{16} features a different substitution pattern at each imine moiety, two of the aryl groups are identical; no β-triketimine bearing three different aryl groups has been prepared in this work. However, such a species is likely to be easily accessible by combination of **Li(BDK**$^{iPr2/OMe}$**)** with a number of the imidoyl chlorides described herein.

The widely differing solution-phase behaviour of the β-triketimines apparently has little effect on their ability to acts as ligands, as in the majority of cases stable *fac*-coordinated complexes are obtained upon reaction with group 6 metal carbonyls. However, if more than one of the aryl groups is 2,6-disubstituted, or if more than one aryl *tert*-butyl substituent is present, the stability of the $M(CO)_3$ derivatives is decreased drastically. A single exception to this rule is found in **L**^{15}, where the presence of a single relatively small

2-methoxyphenyl group allows for accommodation of two 2,6-diisopropylphenyl groups at the group 6 metal centres without any detriment to complex stability. Comparison of the mean carbonyl stretching frequencies observed for the β-triketimine complexes with those of analogous complexes of related neutral tripodal nitrogen ligands suggests that the β-triketimines are relatively weak σ-donors. Their electron donating ability appears to be slightly less than the tris(pyrazolyl)methanes, and is comparable to that of the tris(pyrazolyl)phosphines. However, these data also suggest that the β-triketimines are significantly stronger donors than both the tris(pyrazolyl)phosphine oxides and the tris(oxazolinyl)methanes. In contrast to some of the free β-triketimines, the group 6 carbonyl derivatives show no evidence of isomerism in solution, except in the case of **$(L^{16})M(CO)_3$** where major and minor isomers are observed due to the diasteroisomeric relationship between the chiral centre of **L^{16}** and the axial chirality arising due to restricted rotation of the aryl groups in the coordinated ligand. Crystalline metal carbonyl complexes are obtained only in the case of the most symmetrical ligand (**L^1**), and feature porous infinite network structures generated by a combination of relatively weak CH---OC hydrogen bonds and aryl-aryl interactions. Both of these supramolecular interactions are considerably weaker in the molybdenum complex than they are in the chromium complex.

The reaction of the majority of β-triketimines with $ZnCl_2$ either in the presence or absence of weakly-coordinating anions produces complexes which invariably feature four-coordinate, cationic zinc centres. The structural features of these complexes vary little, regardless of the nature of the ligand or anion, and are very similar to previously reported zinc complexes of related tripodal nitrogen ligands. It has been shown that **L^{16}** may act as a tetradentate ligand towards zinc by means of additional coordination of a single 2-methoxyphenyl group, which is permitted by relatively free rotation about the N-C_{Ar} bond when the imine is also backbone methyl-substituted. However, the propensity of **L^{16}** to act as a tetradentate donor towards zinc is strongly dependent on the nature of the anion; when $BAr^F{}_4^-$ is used a five-coordinate complex is obtained, whereas in the case of the $Zn_2Cl_6^{2-}$ salt the methoxy group remains uncoordinated. All of the triflate salts prepared in this work display numerous weak hydrogen-bonding interactions in the solid state, which are formed between the triflate oxygens and various ligand hydrogen atoms. ^{1}H NMR studies provide good evidence that some of these interactions are maintained in solution. The β-triketimine zinc complexes do not display complicated solution-phase behaviour, except in the case of complexes of **L^{16}** where major and minor isomers are observed in analogy with

the corresponding metal carbonyl derivatives. However, an effect of ligand structure on the complexity of the solution spectra has been observed, and has been ascribed to the relative propensity for rotation about the N-C_{Ar} bonds. An increase in ligand steric bulk (i.e. substitution of R^7 Me with ^{t}Bu) causes a reduction in the freedom for rotation of the aryl groups, and as such greater numbers of unique chemical environments are present. Attempts to form more biorelevant zinc complexes by metathesis of the β-triketimine zinc chloride derivatives with a variety of reagents have been unsuccessful, as no zinc-containing complexes which could be fully characterised were obtained. However, the reaction with TlOEt has yielded two novel cationic β-triketimine thallium complexes, the solid-state structures of which show the existence of thallophilic interactions. In the case of **[(L^8)Tl][BAr^F_4]** these interactions are very weak, whereas in **[(L^1)Tl][BAr^F_4]** they are considerably stronger, due both to a reduction in coordination number, and in ligand steric bulk.

When β-triketimines are coordinated to nickel, the nuclearity of the obtained complexes is dependent to some degree on the steric demand of the ligands, but much more so on the size of the anion. The very large $BAr^F_4{}^-$ ion overwhelmingly favours the formation of dimeric bromide-bridge species for all but the most bulky ligands, except in cases where the ligands are able to coordinate in a bidentate or tetradentate manner. The overall steric demand of the ligands appears to be much more strongly affected by the R^7 substituent than by the aryl groups, as no β-triketimines where R^7 = Me give monomeric complexes with $BAr^F_4{}^-$. For the much smaller triflate and $NiBr_4{}^{2-}$ ions, monomeric species are strongly favoured except in the case of two dimeric triflate complexes. The reason for this anomalous behaviour is not clear, though it may be due to the reduced solubility of these compounds relative to their respective monomers. In contrast to the behaviour observed with zinc, **L^{15}** and **L^{16}** display exclusively tetradentate coordination towards nickel, yielding cationic five-coordinate complexes irrespective of the nature of the anion. All of the five-coordinate complexes prepared in this work display geometries which are closer to square-pyramidal than trigonal-bipyramidal. This is due to the fact that for all the β-triketimines the inherent ligand geometry enforces rigid N-M-N bite angles that deviate by very little from 90°, and this is not conducive to the formation of trigonal-bipyramidal complexes. The very bulky **L^6** has been found to coordinate in a bidentate fashion via the two imine donors of its enamine-diimine tautomer, yielding both cationic and neutral four-coordinate nickel complexes. The six-coordinate dimers and N_2ONiBr complex described

in this work represent very rare structural types, whereas the dicationic five-coordinate dimers are the first of their kind to be structurally characterised.

Analysis of average N-N distances in all of the structurally characterised β-triketimine complexes show the expected correlation with both the size of the metal ion, as well as with its coordination number. However, a relationship between the ligand bulk and mean N-N separation has also been observed, in that the most sterically demanding ligands give rise to complexes with the largest mean N-N distances. The variation in this parameter between the individual ligands is comparatively small, though in definite correlation with a trend dependent on ligand steric bulk.

A number of the β-triketimine nickel complexes have been tested for activity as precatalysts for the polymerisation of ethylene, and some have been found to show moderate activity. However, only certain examples of complexes with ligands where R^7 = Me are active, whilst all those in which $R^7 = {}^tBu$ are invariably inactive. A mechanism for the activation of the precatalysts upon treatment with MAO has been proposed, and the ability of the β-triketimines to adopt a bidentate coordination mode analogous to that seen for $\mathbf{L^6}$ is assumed to be essential for the formation of a catalytically active square-planar nickel methyl ethylene complex. Due to steric considerations, such bidentate coordination is likely impossible for β-triketimines where $R^7 = {}^tBu$, and as such their complexes are inactive. The optimum catalytic activities of the β-triketimine nickel catalysts are comparable to those reported for the α-keto-β-diimine complex **324**, and are also somewhat greater than those of a number of related β-diketimine and β-diketiminate complexes. The polymers produced in this work are elastomeric and of very low crystallinity, and show branching rates in the range 43-84 branches per 1000 carbon atoms. ^{13}C NMR spectroscopy reveals the presence of all common short-chain branches from methyl to hexyl, as well as longer chain branches and pairs of branches. In these respects the polymers are very similar to those produced by α-diimine nickel catalysts. Preliminary investigations show that the polyethylene produced with the more sterically encumbered β-triketimine complexes has high molecular weight, due to its relative toughness and low solubility. In contrast the polyethylene produced by complexes of less bulky ligands has greatly increased solubility, and is easier to tear apart. Both of these observations are indicative of a much lower molecular weight polymer.

6. Experimental

6.1 Materials and Methods

All procedures requiring inert conditions were performed under an atmosphere of either N_2 or argon using standard high vacuum and Schlenk line techniques, or in an N_2-filled recirculating glovebox equipped with internal moisture- and oxygen-scrubbing columns. All gases were pre-dried by passage through a column of phosphorus pentoxide supported on vermiculite. Hexane and Et_2O were distilled from Na/K alloy, toluene from molten Na and THF from sodium/benzophenone ketyl. Anilines, amines and chlorinated solvents were distilled from calcium hydride; anilines and amines were stored over 4 Å molecular sieves, which were activated by heating under vacuum at 120°C. $SOCl_2$ was distilled under N_2 immediately prior to use. d_6-DMSO was stored over freshly activated 4 Å molecular sieves. $Mo(CO)_6$ was purified by vacuum sublimation. $NaBAr^F{}_4$[345(a)] and $NaOCH(CF_3)_2$[399] were prepared according to literature procedures. All other materials were purchased from commercial vendors and used as received. Anhydrous metal salts and TlOEt were stored and dispensed in the glovebox.

^1H NMR spectra were recorded on a Varian Inova 300 MHz, Bruker Avance 300 MHz, Bruker Avance III 400 MHz or Bruker Avance II+ 500 MHz spectrometer; ^{13}C NMR spectra on a Bruker Avance III 400 MHz or Bruker Avance II+ 500 MHz spectrometer; ^{19}F NMR spectra on a Bruker Avance III 400 MHz spectrometer. IR spectra were recorded on a Perkin-Elmer Spectrum RX1 FT-IR spectrometer using Nujol mulls between KBr plates, or on a Perkin-Elmer Spectrum BX FT-IR spectrometer using neat solids. UV/Vis spectra were recorded on a Varian Cary 5000 spectrometer using DCM solutions in 10×10 mm quartz cuvettes. ESI-MS experiments were performed on a Micromass Platform II spectrometer; MALDI-MS experiments were performed on a Micromass ToF Spec 2E spectrometer. Elemental analyses and DSC measurements were carried out by the Microanalytical Service in the School of Chemistry at the University of Manchester.

6.2 X-Ray Crystallography

In all examples single crystals were mounted in perfluoropolyether oil into an Oxford Instruments Cryostream 700. For all crystals except those of $\mathbf{(L^1)M(CO)_3}$, $\mathbf{[(L^1)ZnCl][BAr^F{}_4]}$ and $\mathbf{[(L^{10})NiBr]_2[NiBr_4]}$ diffraction measurements were performed on a Oxford Diffraction X-Calibur 2 diffractometer using graphite-monochromated Mo-K_α

radiation, and the data were collected and processed by the programs CrysAlis PRO and CrysAlis RED.[400] For **$(L^1)Mo(CO)_3$**, **$[(L^1)ZnCl][BAr^F_4]$** and **$[(L^{10})NiBr]_2[NiBr_4]$**, diffraction measurements were performed on a Bruker-Nonius Kappa CCD diffractometer using graphite-monochromated Mo-K_α radiation, whilst in the case of **$(L^1)Cr(CO)_3$** a Bruker APEX II diffractometer fitted to Station 9.8 of the Daresbury Synchrotron using Si-monochromated Zr-edge radiation was employed. In these cases the data were collected by the COLLECT[401] program, and processed using DENZO-SMN.[402] Absorption correction was performed with MULTISCAN.[403] All structures were solved using either SHELXS[404] or SIR-92,[405] and refined with SHELXL.[404] In certain cases where highly disordered solvent molecules were encountered the SQUEEZE function in PLATON[352] was employed to generate a modified solvent-free *hkl* file. Structures were displayed graphically using ORTEP[406] and MERCURY.[407]

6.3 Synthesis of β-Iminoenamines

$HBDK^{iPr}$: In a typical procedure, a mixture of 2-isopropylaniline (78.5 cm^3, 0.556 mol), acetylacetone (28.5 cm^3, 0.278 mol) and a catalytic amount of *p*-toluenesulfonic acid was heated to reflux in toluene (150 cm^3). Heating was continued for approximately 5 hours, and the water produced (~7 cm^3) was removed using a Dean-Stark apparatus. The majority of the toluene was then removed by distillation through the Dean-Stark arm, and the dark brown oil remaining in the reaction flask was allowed to cool to room temperature. Trituration with a small amount of methanol rapidly caused the crystallisation of a large amount of cream-coloured solid, which was collected by filtration and washed with methanol. Recrystallisation from a mixture of methanol and DCM gave **$HBDK^{iPr}$** as long, needle-like yellow crystals (50 g, 54%); mp: 102-104°C. ^{1}H NMR (500 MHz, $CDCl_3$): δ 1.08 (12H, d, $^3J_{HH}$ = 6.9 Hz, $CH(CH_3)_2$), 1.81 (6H, s, CH_3), 3.11 (2H, septet, $^3J_{HH}$ = 6.9 Hz, $CH(CH_3)_2$), 4.83 (1H, s, alkenyl C*H*), 6.70-7.20 (8H, non-first-order m, aromatic C*H*), 12.38 (1H, br s, N*H*).

$HBDK^{iPr2}$: 2,6-diisopropylaniline (50 cm^3, 0.266 mol), acetylacetone (13.5 cm^3, 0.132 mol) and toluene (150 cm^3) were used. Pale brown needles (26.9 g, 48%); mp: 137-140°C. ^{1}H NMR (300 MHz, $CDCl_3$): δ 1.16 (12H, d, $^3J_{HH}$ = 6.9 Hz, $CH(CH_3)_2$), 1.26 (12H, d, $^3J_{HH}$

= 6.9 Hz, CH(CH_3)$_2$), 1.63 (6H, s, CH_3), 3.15 (4H, septet, $^3J_{HH}$ = 6.9 Hz, CH(CH$_3$)$_2$), 4.91 (1H, s, alkenyl CH), 7.05-7.35 (6H, non-first-order m, aromatic CH), 12.16 (1H, br s, NH).

HBDK^{tBu}: 2-tert-butylaniline (13.5 cm^3, 0.088 mol), acetylacetone (4.4 cm^3, 0.043 mol) and toluene (80 cm^3) were used. Yellow crystals (6.43 g, 44%); mp: 98-100°C. ^{1}H NMR (300 MHz, $CDCl_3$): δ 1.30 (18H, s, C(CH_3)$_3$), 1.85 (6H, s, CH_3), 4.93 (1H, s, alkenyl CH), 6.75-7.40 (8H, non-first-order m, aromatic CH), 12.50 (1H, br s, NH).

HBDK^{Me3}: 2,4,6-trimethylaniline (30 cm^3, 0.213 mol, acetylacetone (10 cm^3, 0.0973 mol) and toluene (100 cm^3) were used. Pale-brown crystals (16.89 g, 52%); mp: 59-60°C. ^{1}H NMR (300 MHz, $CDCl_3$): δ 1.61 (6H, s, CH_3C=N), 2.04 (12H, s, Mes *o*-CH_3), 2.18 (6H, s, Mes *p*-CH_3), 4.77 (1H, alkenyl CH), 6.77 (4H, Mes-CH), 12.08 (1H, br s, NH).

HBDK$^{iPr2/OMe}$: 2,6-diisopropylaniline (75 cm^3, 0.398 mol) and acetylacetone (41 cm^3, 0.398 mol) were refluxed in toluene (160 cm^3) for 3 hours, and the water produced in the reaction (6.6 cm^3) was removed by the aid of a Dean-Stark trap. The majority of the toluene was removed by distillation, and the red-coloured oil residue was distilled under vacuum, yielding a yellow oil at 120-125°C which slowly set to a pale yellow mass. This was 4-(2,6-diisopropylphenyl)amino-2-penten-2-one, which was used in the following step without further purification. ^{1}H NMR (500 MHz, $CDCl_3$): δ 1.08 (6H, d, $^3J_{HH}$ = 7.0 Hz, CH(CH_3)$_2$), 1.14 (6H, d, $^3J_{HH}$ = 7.0 Hz, CH(CH_3)$_2$), 1.56 (3H, s, CH_3), 2.05 (3H, s, CH_3), 2.96 (2H, septet, $^3J_{HH}$ = 7.0 Hz, CH(CH$_3$)$_2$), 5.14 (1H, s, alkenyl CH), 6.95-7.25 (3H, non-first-order m, aromatic CH), 11.99 (1H, br s, NH).

4-(2,6-diisopropylphenyl)amino-2-pentene-2-one (25 g, 0.0965 mol), *o*-anisidine (11 cm^3, 0.0965 mol) and *p*-toluenesulfonic acid monohydrate (18.36 g, 0.0965 mol) were heated to reflux in benzene (100 cm^3) for 3 hours, the water of condensation being collected in a Dean-Stark trap. The majority of the benzene was removed through distillation, and the solid black mass that remained was treated with diethyl ether (150 cm^3) and saturated sodium carbonate solution (150 cm^3). The aqueous layer was separated and extracted with diethyl ether (3 x 50 cm^3). The combined organic fractions were washed with water (100 cm^3), dried with $MgSO_4$, filtered and stripped of solvent under vacuum giving a yellow solid. This was recrystallised from methanol/DCM to give **HBDK$^{iPr2/OMe}$** as pale-yellow needles (14.49 g, 41%); mp: 121-122°C. ^{1}H NMR (500 MHz, $CDCl_3$): δ 1.05 (6H, d, $^3J_{HH}$ = 7.0 Hz, CH(CH_3)$_2$), 1.12 (6H, d, $^3J_{HH}$ = 7.0 Hz, CH(CH_3)$_2$), 1.63 (3H, s, CH_3), 1.99 (3H,

s, CH_3), 2.93 (2H, septet, $^3J_{HH}$ = 7.0 Hz, CH(CH$_3$)$_2$), 3.63 (3H, s, OCH_3), 4.82 (1H, s, alkenyl CH), 6.75-7.07 (7H, non-first-order m, aromatic CH), 12.50 (1H, br s, NH).

6.4 Synthesis of Aryl Amides

MeCONH-2-^{i}PrC$_6$H$_4$: In a typical procedure, a solution of 2-isopropylaniline (50 cm^3, 0.354 mol) and triethylamine (49.2 cm^3, 0.354 mol) in DCM (80 cm^3) was prepared and cooled to 0°C with the aid of an external ice-bath. To this a solution of acetyl chloride (25.1 cm^3, 0.354 mol) in DCM (20 cm^3) was then added dropwise, complete addition taking around one hour. The mixture was heated to reflux for two hours, and then stirred at room temperature overnight. The triethylammonium chloride formed was removed by filtration and washed with DCM (100 cm^3). The filtrate was washed with dilute HCl (100 cm^3) and then with water (100 cm^3). The organic phase was dried with $MgSO_4$, filtered and stripped of solvent under vacuum. The crude product was treated with petroleum ether (200 cm^3) and filtered, in order to remove its red colouration. Recrystallisation from petroleum ether/DCM gave **MeCONH-2-^{i}PrC$_6$H$_4$** as white plates (51 g, 80%); mp: 84-86°C. ^{1}H NMR (500 MHz, $CDCl_3$): δ 1.17 (6H, d, $^3J_{HH}$ = 7.0 Hz, CH(CH_3)$_2$), 2.14 (3H, s, CH_3), 2.97 (1H, septet, $^3J_{HH}$ = 7.0 Hz, CH(CH$_3$)$_2$), 6.98 (1H, br s, NH), 7.03-7.60 (4H, non-first-order m, aromatic CH).

MeCONH-2,6-^{i}Pr$_2$C$_6$H$_3$: 2,6-diisopropylaniline (50 cm^3, 0.266 mol), triethylamine (37 cm^3, 0.266 mol) and acetyl chloride (19 cm^3, 0.266 mol) were used. Small white needles (31.65 g, 55%); mp: 180-181°C. ^{1}H NMR (300 MHz, $CDCl_3$): δ 1.19-1.25 (12H, overlapping d, $^3J_{HH}$ = 6.9 Hz, CH(CH_3)$_2$), 2.28 (3H, s, tautomeric CH_3), 3.12, 3.23 (2H, overlapping septets, $^3J_{HH}$ = 6.9 Hz, CH(CH$_3$)$_2$), 6.70 (1H, br s, NH), 7.18-7.44 (3H, non-first-order m, aromatic CH).

MeCONH-2-^{t}BuC$_6$H$_4$: 2-tert-butylaniline (12.5 cm^3, 0.08 mol), triethylamine (11.1 cm^3, 0.08 mol) and acetyl chloride (5.7 cm^3, 0.08 mol) were used. Off-white crystals (14.37 g, 94%); mp: 163-164°C. ^{1}H NMR (400 MHz, $CDCl_3$): δ 1.40 (9H, s, C(CH_3)$_3$), 2.25 (3H, s, CH_3), 7.10 (1H, br s, NH), 7.15-7.60 (4H, non-first-order m, aromatic CH).

MeCONH-2,4,6-Me$_3$C$_6$H$_2$: 2,4,6-trimethylaniline (22.5 cm^3, 0.173 mol), triethylamine (24.5 cm^3, 0.176 mol) and acetyl chloride (12.5 cm^3, 0.176 mol) were used; off-white

crystals (24.60 g, 80%). ^{1}H NMR (400 MHz, $CDCl_3$): δ 2.17 (6H, s, Mes *o*-C*H*$_3$), 2.22 (3H, s, Mes *p*-C*H*$_3$), 2.40 (3H, s, C*H*$_3$), 6.80 (2H, s, Mes-C*H*).

^{t}BuCONH-2-^{i}PrC$_6$H$_4$: 2-isopropylaniline (40 cm^3, 0.286 mol), triethylamine (40 cm^3, 0.288 mol), trimethylacetyl chloride (32 cm^3, 0.260 mol) and DCM (40 cm^3) were used; pale-pink crystals (56.90 g, 99%). ^{1}H NMR (400 MHz, $CDCl_3$): δ 1.20 (6H, d, $^3J_{HH}$ = 7.0 Hz, CH(C*H*$_3$)$_2$), 1.27 (9H, s, C(C*H*$_3$)$_3$), 2.90 (1H, septet, $^3J_{HH}$ = 7.0 Hz, C*H*(CH$_3$)$_2$), 4.61 (1H, s, N*H*), 7.05-7.22 (3H, non-first-order m, aromatic protons), 7.71 (1H, d, $^3J_{HH}$ = 7.5 Hz).

^{t}BuCONH-2,6-^{i}Pr$_2$C$_6$H$_3$: 2,6-diisopropylaniline (21.5 cm^3, 0.114 mol), triethylamine (16 cm^3, 0.115 mol), trimethylacetyl chloride (14 cm^3, 0.114 mol) and DCM (35 cm^3) were used; white needles (22.65 g, 77%). ^{1}H NMR (500 MHz, $CDCl_3$): δ 1.13 (12H, d, $^3J_{HH}$ = 7.0 Hz, CH(C*H*$_3$)$_2$), 1.29 (9H, s, C(C*H*$_3$)$_3$), 2.94 (2H, $^3J_{HH}$ = 7.0 Hz, C*H*(CH$_3$)$_2$), 6.75 (1H, br s, N*H*), 7.07-7.22 (3H, non-first-order m, aromatic C*H*).

^{t}BuCONH-2,4,6-Me$_3$C$_6$H$_2$: 2,4,6-trimethylaniline (21 cm^3, 0.150 mol), triethylamine (21 cm^3, 0.151 mol), trimethylacetyl chloride (18.5 cm^3, 0.150 mol) and DCM (100 cm^3) were used; white needles (19.38 g, 60%). ^{1}H NMR (500 MHz, $CDCl_3$): δ 1.28 (9H, s, C(C*H*$_3$)$_3$), 2.08 (6H, s, Mes *o*-C*H*$_3$), 2.19 (3H, s, Mes *p*-C*H*$_3$), 6.74 (1H, br s, N*H*); 6.80 (2H, s, Mes C*H*).

^{t}BuCONH-2-MeOC$_6$H$_4$: *o*-anisidine (18.3 cm^3, 0.163 mol), triethylamine (22.7 cm^3, 0.163 mol) and trimethylacetyl chloride (20 cm^3, 0.163 mol) were used. This compound is too soluble in all organic solvents to allow for efficient recrystallisation, and as such the crude product was used without further purification. White crystals (26.67 g, 79%); mp: 35-37°C. ^{1}H NMR (300 MHz, $CDCl_3$): δ 1.25 (9H, s, C(C*H*$_3$)$_3$), 3.83 (3H, s, OC*H*$_3$), 6.80 (1H, dd, $^3J_{HH}$ = 8.0 Hz, $^4J_{HH}$ = 1.2 Hz, *m'*-C*H*), 6.89 (1H, td, $^3J_{HH}$ = 7.8 Hz, $^4J_{HH}$ = 1.3 Hz, *m*-C*H*), 6.96 (1H, td, $^3J_{HH}$ = 7.9 Hz, $^4J_{HH}$ = 1.5 Hz, *p*-C*H*), 8.15 (1H, br s, N*H*), 8.34 (1H, dd, $^3J_{HH}$ = 8.0 Hz, $^4J_{HH}$ = 1.6 Hz, *o*-C*H*).

PhCONH-2-^{i}PrC$_6$H$_4$: 2-isopropylaniline (32.7 ml, 0.231 mol), triethylamine (35ml, 0.231 mol), benzoyl chloride (26.8 ml, 0.231 mol) and DCM (100 ml) were used; white solid (53.83 g, 98%). ^{1}H NMR (400 MHz, $CDCl_3$): δ 1.08 (6H, d, $^3J_{HH}$ = 7.0 Hz, CH(C*H*$_3$)$_2$), 1.82 (6H, s, C*H*$_3$), 3.11 (2H, septet, $^3J_{HH}$ = 7.0 Hz, C*H*(CH$_3$)$_2$), 6.81 (1H, br s, N*H*), 6.90-7.20 (9H, non-first-order m, aromatic C*H*).

6.5 Synthesis of Imidoyl Chlorides

IMC[1]: In a typical procedure, a solution of **MeCONH-2-^{i}PrC$_6$H$_4$** (29 g, 0.164 mol) in DCM (100 cm^3) was treated with triphosgene (16.51 g, 0.0556 mol) portionwise by means of a solids addition tube. The colourless solution was then heated to reflux for 4 hours, and left to stir at room temperature overnight. Distillation under vacuum gave **IMC[1]** as a colourless liquid at 72-76°C (23.3 g, 73%). ^{1}H NMR (300 MHz, $CDCl_3$): δ 1.24 (6H, d, $^3J_{HH}$ = 7.0 Hz, CH(C*H*$_3$)$_2$), 2.68 (3H, s, C*H*$_3$), 2.98 (1H, septet, $^3J_{HH}$ = 7.0 Hz, C*H*(CH$_3$)$_2$), 6.75-7.38 (4H, non-first-order m, aromatic C*H*).

IMC[2]: **MeCONH-2,6-^{i}Pr$_2$C$_6$H$_3$** (10 g, 0.046 mol) and triphosgene (4.5 g, 0.015 mol) were used. Colourless liquid obtained at 110-120°C (6.01 g, 55%). ^{1}H NMR (300 MHz, $CDCl_3$): δ 1.20 (12H, d, $^3J_{HH}$ = 6.9 Hz, CH(C*H*$_3$)$_2$), 2.20 (3H, s, C*H*$_3$), 2.80 (2H, septet, $^3J_{HH}$ = 6.9 Hz, C*H*(CH$_3$)$_2$), 7.10-7.50 (3H, non-first-order m, aromatic C*H*).

IMC[3]: **MeCONH-2-^{t}BuC$_6$H$_4$** (6.5 g, 0.034 mol) and triphosgene (3.37 g, 0.011 mol) were used. Colourless liquid obtained at 84-92°C (4.97 g, 70%). ^{1}H NMR (400 MHz, $CDCl_3$): δ 1.40 (9H, s, C(C*H*$_3$)$_3$), 2.25 (3H, s, C*H*$_3$), 7.20-7.65 (4H, non-first-order m, aromatic C*H*).

IMC[4]: **MeCONH-2,4,6-Me$_3$C$_6$H$_2$** (16.52 g, 0.0933 mol) and triphosgene (11.67 g, 0.0393 mol) were used. Colourless liquid obtained at 70-80°C (12.70 g, 70%). ^{1}H NMR (400 MHz, $CDCl_3$): δ 2.09 (6H, s, Mes *o*-C*H*$_3$), 2.17 (3H, s, Mes *p*-C*H*$_3$), 2.93 (3H, s, C*H*$_3$), 6.76 (2H, s, Mes-C*H*).

IMC[5]: **^{t}BuCONH-2-^{i}PrC$_6$H$_4$** (28.5 g, 0.130 mol) was dissolved in $SOCl_2$ (100 cm^3, 1.371 mol) producing an orange solution. This was heated to reflux for two hours, and the excess thionyl chloride was removed by distillation under argon. Vacuum distillation gave **IMC[5]** as a yellow oil at 130ºC (24.90 g, 84 %). ^{1}H NMR (400 MHz, $CDCl_3$): δ 1.12 (6H, d, $^3J_{HH}$ = 7.0 Hz, CH(C*H*$_3$)$_2$), 1.33 (9H, s, C(C*H*$_3$)$_3$), 2.83 (1H, septet, $^3J_{HH}$ = 7.0 Hz, C*H*(CH$_3$)$_2$), 6.60-7.30 (4H, non-first-order m, aromatic C*H*).

IMC[6]: **^{t}BuCONH-2,6-^{i}Pr$_2$C$_6$H$_3$** (22.53 g, 0.0863 mol) and $SOCl_2$ (55 cm^3, 0.753 mol) were used. Yellow oil obtained at 82-85ºC (22.52 g, 93 %). ^{1}H NMR (500 MHz, $CDCl_3$): δ 1.10 (12H, br d, CH(C*H*$_3$)$_2$), 1.35 (9H, s, C(C*H*$_3$)$_3$), 2.67 (2H, septet, $^3J_{HH}$ = 6.8 Hz, C*H*(CH$_3$)$_2$), 7.02-7.10 (3H, non-first-order m, aromatic C*H*).

IMC[7]: **^{t}BuCONH-2,4,6-Me$_3$C$_6$H$_2$** (19.22 g, 0.0878 mol) and $SOCl_2$ (35 cm^3, 0.480 mol) were used. Colourless oil obtained at 80-82 ºC, which set to an off-white solid mass upon cooling (19.60 g, 94 %). ^{1}H NMR (500 MHz, $CDCl_3$): δ 1.33 (9H, s, C(C*H*$_3$)$_3$), 1.93 (6H, s, Mes *o*-C*H*$_3$), 2.19 (3H, s, Mes *p*-C*H*$_3$), 6.77 (2H, s, Mes C*H*).

IMC[8]: **^{t}BuCONH-2-MeOC$_6$H$_4$** (26 g, 0.126 mol) and $SOCl_2$ (36 cm^3, 0.493 mol) were used. Bright-yellow oil obtained at 80-84°C (26.82 g, 94%). ^{1}H NMR (400 MHz, $CDCl_3$): δ 1.40 (9H, s, C(C*H*$_3$)$_3$), 3.85 (3H, s, OC*H*$_3$), 6.75-7.15 (4H, non-first-order m, aromatic C*H*).

IMC[9]: **PhCONH-2-^{i}PrC$_6$H$_4$** (20.02 g, 0.084 mol) and $SOCl_2$ (91.70 cm^3, 1.257 mol) were used. Yellow oil obtained at 122°C (15.10 g, 70 %). ^{1}H NMR (400 MHz, $CDCl_3$): δ 1.14 (6H, d, $^3J_{HH}$ = 7.0 Hz, CH(C*H*$_3$)$_2$), 2.96 (1H, septet, $^3J_{HH}$ = 7.0 Hz, C*H*(CH$_3$)$_2$), 6.70-7.50 (8H, non-first-order m, aromatic C*H*), 8.12 (1H, d, $^3J_{HH}$ = 7.6 Hz, *o*-C*H*).

6.6 Synthesis of β-Triketimines

L[1]: In a typical procedure, a suspension of **HBDK^{iPr}** (17.10 g, 0.0512 mol) in hexane (100 cm^3) was treated with n-butyllithium (32 cm^3 of a 1.6 M solution in hexanes, 0.0512 mol) at 0°C, forming a dark-yellow solution. This was stirred at 0°C for 30 minutes, after which time **IMC[1]** (10 cm^3, 0.0512 mol) was added, immediately causing the formation of a heavy yellow precipitate. The mixture was allowed to warm to room temperature and stirred overnight. The thick yellow mixture was poured into water (200 cm^3), and diethyl ether was added until two distinct phases formed. The organic phase was separated and the aqueous phase was extracted with diethyl ether (3 x 200 cm^3). The combined organic layers were washed with water (200 cm^3), dried over $MgSO_4$, filtered and stripped of solvent under vacuum. The crude product was treated with a small amount of methanol, filtered and washed with cold methanol. Recrystallisation from methanol gave **L[1]** as a pale yellow crystalline material (16.63 g, 66%); mp: 130-132°C. ^{1}H NMR (500 MHz, $CDCl_3$), β-triketimine tautomer (~15%, reported integrals normalised): δ 0.93, 0.96 (18H, 2 × d, $^3J_{HH}$ = 6.9 Hz, CH(C*H*$_3$)$_2$), 1.69 (9H, s, C*H*$_3$C=N), 2.70 (3H, septet, $^3J_{HH}$ = 6.9 Hz, C*H*(CH$_3$)$_2$), 4.59 (1H, s, α-C*H*), 6.69 (3H, dd, $^3J_{HH}$ = 7.0 Hz, $^4J_{HH}$ = 1.8 Hz, *o*-C*H*); enamine-diimine tautomer (*E*-isomer ~70%, reported integrals normalised): δ 1.07 (12H, d, $^3J_{HH}$ = 6.9 Hz, CH(C*H*$_3$)$_2$), 1.11 (6H, d, $^3J_{HH}$ = 7.0 Hz, CH(C*H*$_3$)$_2$), 1.97 (6H, s, C*H*$_3$C=N),

2.02 (3H, s, C*H*$_3$C=N), 3.03 (1H, septet, $^3J_{HH}$ = 7.0 Hz, C*H*(CH$_3$)$_2$), 3.13 (2H, septet $^3J_{HH}$ = 6.9 Hz, C*H*(CH$_3$)$_2$), 6.54 (1H, dd, $^3J_{HH}$ = 7.4 Hz, $^4J_{HH}$ = 1.5 Hz, unique *o*-C*H*), 6.83 (2H, dd, $^3J_{HH}$ = 7.5 Hz, $^4J_{HH}$ = 1.6 Hz, *o*-C*H*), 7.0-7.1 (6H, complex multiplet, 4 × t overlapped, *m*- and *p*-C*H*), 7.20 (2H, dd, $^3J_{HH}$ = 7.4 Hz, $^4J_{HH}$ = 1.0 Hz, *m*'-C*H*), 7.25 (1H, dd, $^3J_{HH}$ = 7.7 Hz, $^4J_{HH}$ = 1.0 Hz, unique *m*'-C*H*), 13.57 (1H, br s, N*H*); enamine-diimine tautomer (*Z*-isomer ~15%, reported integrals normalised): δ 1.07, 1.11 (18H, 2 × d overlapped with peaks due to major isomer, CH(C*H*$_3$)$_2$), 1.93 (3H, s, C*H*$_3$C=N), 2.45 (6H, s, C*H*$_3$C=N), 3.02 (2H, septet, $^3J_{HH}$ = 6.9 Hz, C*H*(CH$_3$)$_2$), 3.26 (1H, septet $^3J_{HH}$ = 6.9 Hz, C*H*(CH$_3$)$_2$), 6.56 (2H, dd , $^3J_{HH}$ = 7.7 Hz, $^4J_{HH}$ = 1.4 Hz, *o*-C*H*), 6.52, (1H, dd, $^3J_{HH}$ = 7.8 Hz, $^4J_{HH}$ = 1.1 Hz, unique *o*-C*H*), 6.68-6.69 (non-first-order m), 6.83 (dd, $^3J_{HH}$ = 7.5 Hz, $^4J_{HH}$ = 1 Hz), 6.94-7.09 (non-first-order m), 7.12-7.15 (non-first-order m), 7.18-7.25 (non-first-order m); 13.30 (1H, br s, N*H*). Other minor isomer/tautomer aryl CH peaks overlapped with major isomer, in range 6.94-7.24. $^{13}C\{^1H\}$ NMR (125 MHz, $CDCl_3$), β-triketimine tautomer: δ 19.03 (*C*H$_3$C=N), 23.15, 23.19 (CH(*C*H$_3$)$_2$), 27.88 (*C*H(CH$_3$)$_2$); enamine-diimine tautomer (*E*-isomer): δ 18.68 (2 *C*H$_3$C=N), 24.51 (1 *C*H$_3$C=N), 23.34, 23.62 (CH(*C*H$_3$)$_2$), 27.81 (1 *C*H(CH$_3$)$_2$), 28.11 (2 *C*H(CH$_3$)$_2$), 110.44 (alkenyl α –*C*); enamine-diimine tautomer (*Z*-isomer): δ 20.41 (1 *C*H$_3$C=N), 31.28 (2 *C*H$_3$C=N), 23.06, 23.46 (CH(*C*H$_3$)$_2$), 27.44, 27.92 (*C*H(CH$_3$)$_2$), 105.58 (alkenyl α –*C*); peaks due to aromatic *C*H for all isomeric species: 118.29, 118.58, 119.68, 123.84, 123.98, 124.14. 124.20, 124.57, 124.61, 124.80, 125.02, 125.45, 125.56, 125.70, 125.74, 125.81, 125.91, 125.95, 126.13, 126.23; peaks due to aromatic *ipso*-*C*N and -*C*^{i}Pr for all isomeric species: 138.47, 141.29, 141.80, 141.84, 142.47, 142.65, 146.58, 148.74; peaks due to conjugated *C*=N for all species: 157.81, 158.17; peaks due to isolated *C*=N/β-triketimine *C*=N for all species: 169.95, 171.96. Elemental analysis, calculated for $C_{34}H_{43}N_3$ (%): C, 82.71; H, 8.78; N, 8.51. Found: C, 82.75; H, 9.01; N, 8.46. MS (ESI+) *m/z*: 494.4 $[MH]^+$. IR: 1643, 1610, 1593, 1573, 1537 cm^{-1} ($\nu_{C=N}$, $\nu_{C=C(Ar)}$).

L^2: **HBDK^{iPr2}** (4.2g, 0.01 mol), ^{n}BuLi (6.3 cm^3, 0.01 mol), **IMC^2** (2.5 cm^3, 0.01 mol) and hexane (40 cm^3) were used. Pale-green crystals from methanol/DCM (2.90 g, 47%); mp: 166-168°C. ^{1}H NMR (500 MHz, $CDCl_3$), solution composition immediately after dissolution: β-triketimine tautomer, 93%, enamine-diimine tautomer (*E*-isomer), 7%; solution composition ~72 hours after dissolution: β-triketimine tautomer, 48%, enamine-diimine tautomer (*E*-isomer), 52%; peaks due to β-triketimine tautomer: δ 1.02 (18H, d, $^3J_{HH}$ = 6.8 Hz, CH(C*H*$_3$)$_2$), 1.04 (18H, d, $^3J_{HH}$ = 6.8 Hz, CH(C*H*$_3$)$_2$), 1.89 (9H, s, C*H*$_3$C=N),

2.95 (6H, septet, overlapped with one septet due to enamine-diimine tautomer, C*H*(CH_3)$_2$), 4.74 (1H, s, α-C*H*); peaks due to enamine-diimine tautomer: δ 1.00-1.10 (24H, multiple d, overlapped with peaks due to β-triketimine, CH(C*H*$_3$)$_2$), 1.14 (12H, d, $^3J_{HH}$ = 6.9 Hz, CH(C*H*$_3$)$_2$), 1.87 (6H, s, C*H*$_3$C=N), 1.94 (3H, s, C*H*$_3$C=N), 2.95 (2H, septet, overlapped with peaks due to β-triketimine, C*H*(CH_3)$_2$), 3.08 (4H, septet, $^3J_{HH}$ = 6.8 Hz, C*H*(CH_3)$_2$), 13.50 (1H, br s, N*H*); peaks due to both isomeric species: δ 6.97-7.07 (2 × 9H, non-first-order m, aromatic C*H*). $^{13}C\{^1H\}$ NMR (125 MHz, $CDCl_3$), peaks due to both isomeric species (unless otherwise specified): δ 19.03 (2 *C*H_3C=N, enamine-diimine tautomer), 21.59 (*C*H_3C=N, β-triketimine tautomer), 23.26, 23.34, 23.74, 23.83, 23.96, 24.36 (CH(*C*H_3)$_2$), 25.27 (1 *C*H_3C=N, enamine-diimine tautomer), 27.75, 27.84, 28.31 ((*C*H(CH_3)$_2$), 72.06 (α-*C*H, β-triketimine tautomer), 108.68 (alkenyl α-*C*, enamine-diimine tautomer), 122.96, 123.26, 123.34, 123.59, 123.79, 123.35 (aromatic *C*H), 136.55, 136.87, 140.22, 142.47, 145.91, 146.12 (aromatic *ipso*-*C*N and -*C*^{i}Pr), 160.15 (conjugated *C*=N, enamine-diimine tautomer), 169.01, 171.97 (isolated *C*=N of enamine-diimine/*C*=N of β-triketimine tautomer). Elemental analysis, calculated for $C_{43}H_{61}N_3$ (%): C, 83.31; H, 9.92; N, 6.78. Found: C, 82.87; H, 9.98; N, 6.74. MS (ESI+) *m/z*: 620.5 $[MH]^+$. IR: 1631, 1599, 1585, 1537 cm^{-1} ($\nu_{C=N}$, $\nu_{C=C(Ar)}$).

L^3: **HBDK^{iPr}** (4.45 g, 0.013 mol), ^{n}BuLi (8.2 cm^3, 0.013 mol), **IMC^3** (3.0 cm^3, 0.013 mol) and hexane (40 cm^3) were used. Pale-yellow crystals from methanol/DCM (3.27 g, 50%); mp: 130-133°C. ^{1}H NMR (500 MHz, $CDCl_3$), enamine-diimine isomer **D** (**section 2.2.1**) dominant (~70%); peaks reported refer to this, unless otherwise stated: δ 1.04, (6H, d, $^3J_{HH}$ = 6.9 Hz, CH(C*H*$_3$)$_2$), 1.11 (6H, d, $^3J_{HH}$ = 6.9 Hz, CH(C*H*$_3$)$_2$), 0.90, 0.94, (2 × d, β-triketimine tautomer), 1.07 (2 overlapping doublets, *Z*-isomer of major tautomer), 1.28 (9H, s, C(C*H*$_3$)$_3$), 1.13, 1.29, 1.31, 1.38 (4 × s, C(C*H*$_3$)$_3$, other isomers), 1.92, 1.96, 2.00, (3 × 3H, C*H*$_3$C=N), 1.63, 1.64, 1.74, 1.97, 1.98, 2.09, 2.44 (7× s, C*H*$_3$C=N, other isomers), 3.02 (1H, septet, $^3J_{HH}$ = 6.9 Hz, C*H*(CH_3)$_2$), 3.13 (1H, septet, $^3J_{HH}$ = 6.9 Hz, C*H*(CH_3)$_2$), 2.67, 2.88, 2.97, 3.12, 3.26 (5 × septet, C*H*(CH_3)$_2$, other isomers), 4.60 (s, α-C*H*, β-triketimine tautomer), 6.53 (1H, dd, $^3J_{HH}$ = 7.4 Hz, $^4J_{HH}$ = 1.2 Hz, Ar$^{i Pr}$ *o*-C*H* of unique imine), 6.73, (1H, dd, $^3J_{HH}$ = 7.8 Hz, $^4J_{HH}$ = 1.2 Hz, Ar$^{t Bu}$ *o*-C*H*); 6.82-6.87 (1H + overlap from other isomers, non-first-order m, enamine-imine Ar$^{i Pr}$ *o*-CH), 6.93-7.12 (6H + overlap from other isomers, non-first-order m, Ar$^{t Bu}$ and Ar$^{i Pr}$ *m*- and *p*-C*H*), 7.18 (1H, dd, Ar$^{t Bu}$ *m'*-C*H*), 7.24 (1H, dd, $^3J_{HH}$ = 7.7 Hz, $^4J_{HH}$ = 1.3 Hz, Ar$^{i Pr}$ *m'*-C*H*), 7.30 (1H, dd, $^3J_{HH}$ = 7.8 Hz, $^4J_{HH}$ = 1.3 Hz, Ar$^{i Pr}$ *m'*-C*H*), 6.45, 6.47, 6.55, 6.60, 6.62, 6.68, 6.83, 7.15, 7.21, 7.25,

7.29, 7.33 (non-first-order m, aromatic protons of other isomers), 13.38 (1H, br s, N*H*), 13.20, 13.39, 13.65 (3 × br s, N*H*, other isomers). $^{13}C\{^{1}H\}$ NMR (125 Hz, $CDCl_3$), peaks due to all isomeric species (unless otherwise specified): δ 18.42, 19.00 19.35 19.59, 19.76, 20.72, 21.12, 24.61, 25.08, 31.38 (*C*H_3C=N), 23.06, 23.11, 23.24, 23.28, 23.34, 23.42, 23.59, 29.63, 29.97, 30.36, 30.46 (CH(*C*H_3)$_2$ and C(*C*H_3)$_3$), 27.42, 27.64, 27.82, 27.88, 28.15 (*C*H(CH$_3$)$_2$), 35.05, 35.18, 35.29 (*C*(CH$_3$)$_3$), 72.46 (α-*C*H, β-triketimine tautomer), 106.41, 111.09 (alkenyl α-*C*, enamine-diimine isomers), 118.30, 118.57, 119.52, 119.83, 120.61, 123.42, 123.53, 123.89, 123.95, 124.15, 124.19, 124.37, 124.43, 124.55, 124.62, 124.87, 125.18, 125.43, 125.55, 125.71, 125.79, 125.81, 125.86, 125.89, 126.15, 126.21, 126.23, 126.32, 126.50, 126.52, 126.56, 126.63 (aromatic *C*H), 138.06, 138.45, 139.64, 140.17, 141.21, 141.81, 141.87, 142.19, 142.35, 142.51, 142.74, 143.17, 143.83, 144.78, 146.56, 148.44, 148.80, 149.67, 149.94 (aromatic *ipso*-*C*N, -*C*^{i}Pr and -*C*^{t}Bu), 156.88, 157.17, 157.50, 158.87, 158.97 (conjugated *C*=N, enamine-diimine isomers), 167.63, 168.63, 168.72, 169.88, 171.90 (isolated *C*=N, enamine-diimine isomers/*C*=N, β-triketimine tautomer). Elemental analysis, calculated for $C_{35}H_{45}N_3$ (%): C, 82.79; H, 8.93; N, 8.28. Found: C, 82.80; H, 9.02; N, 8.26. MS (ESI+) *m/z*: 508.4 $[MH]^+$. IR: 1643, 1608, 1593, 1571, 1537 cm^{-1} ($\nu_{C=N}$, $\nu_{C=C(Ar)}$).

L^4: **HBDK^{tBu}** (2.0 g, 0.0055 mol), ^{n}BuLi (3.5 cm^3, 0.0055 mol), **IMC^2** (1.3 cm^3, 0.0055 mol) and toluene (40 cm^3) were used. Pale-yellow powder from methanol (0.60 g, 20%); mp: 116-118°C. ^{1}H NMR (500 MHz, $CDCl_3$), peaks due to enamine-diimine isomer **D** (~57%; reported integrals normalised): δ 1.29 (9H, s, C(C*H*$_3$)$_3$), 1.30 (9H, s, C(C*H*$_3$)$_3$), 1.00 (6H, $^3J_{HH}$ = 6.7 Hz, CH(C*H*$_3$)$_2$), 1.14 (6H, $^3J_{HH}$ = 6.9 Hz, CH(C*H*$_3$)$_2$), 1.79, 1.94, 2.09 (3 × 3H, s, C*H*$_3$C=N), 3.06 (2H, 2 × septet, $^3J_{HH}$ = 6.7 Hz, C*H*(CH$_3$)$_2$), 6.47 (1H, dd, $^3J_{HH}$ = 7.7 Hz, $^4J_{HH}$ = 1.3 Hz, isolated Ar^{tBu} *o*-C*H*), 6.68 (1H, dd, $^3J_{HH}$ = 7.7 Hz, $^4J_{HH}$ = 1.3 Hz, enamine Ar^{tBu} *o*-C*H*), 6.92-7.10 (7H, non-first-order m, Ar^{tBu} and Ar^{iPr2} *m*- and *p*-C*H*), 7.29 (1H, d, overlapped with minor isomer peaks, isolated Ar^{tBu} *m'*-C*H*), 7.32 (1H, d, $^3J_{HH}$ = 7.9 Hz, $^4J_{HH}$ = 1.2 Hz, enamine-imine Ar^{tBu} *m'*-C*H*), 13.30 (1H, br s, N*H*); peaks due to other isomers: 0.85, 0.90, 0.94, 1.02, 1.04, 1.06, 1.09, 1.10 (8 × d, CH(C*H*$_3$)$_2$), 1.24, 1.28, 1.37, 1.43 (4 × s, C(C*H*$_3$)$_3$), 1.75, 1.90, 1.93, 1.98, 2.03, 2.08, 2.42 (7 × s, C*H*$_3$C=N), 2.53 (septet, $^3J_{HH}$ = 6.5 Hz, C*H*(CH$_3$)$_2$, β-triketimine tautomer), 2.88, 2.95 (2 × septet, C*H*(*C*H$_3$)$_2$, other isomers), 4.69 (s, α-C*H*, β-triketimine tautomer), 6.42 (dd, $^3J_{HH}$ = 7.5 Hz, $^4J_{HH}$ = 1.2 Hz, β-triketimine Ar^{tBu} *o*-CH); 6.54 (br d, Ar^{tBu} *o*-C*H*, isomer **B**), 6.77, 7.26 (2 × dd, *m'*-C*H*), 13.25 (br s, N*H*, isomer **E**), 13.89 (v br s, N*H*, isomer **B**). $^{13}C\{^{1}H\}$ NMR (125

MHz, $CDCl_3$), peaks due to all isomeric species (unless otherwise specified): δ 18.95, 19.03, 19.78, 20.28, 21.54, 21.95, 22.89, 23.00, 23.11, 23.73, 23.85, 23.99, 24.19, 24.41, 24.55, 25.05, 25.44, 30.96, 32.13 ($CH(\mathit{C}H_3)_2$/$\mathit{C}H_3C$=N), 27.78, 28.26, 28.47 ($\mathit{C}H(CH_3)_2$), 29.58, 29.85, 30.44, 30.55, 31.27 ($C(\mathit{C}H_3)_3$), 35.14, 35.19, 35.29, 36.08 ($\mathit{C}(CH_3)_3$), 72.84 (α-*C*H, triketimine tautomer), 105.97, 111.10 (alkenyl α-*C*, enamine-diimine isomers), 119.42, 120.51, 121.26, 123.01, 123.21, 123.24, 123.34, 123.57, 123.61, 123.94, 124.16, 124.35, 124.81, 125.15, 125.42, 125.54, 125.70, 125.95, 126.26, 126.31, 126.33, 126.35, 126.45, 126.47, 126.53, 126.59, 126.61 (aromatic *C*H), 136.29, 136.83, 139.20, 139.43, 139.57, 140.23, 142.69, 142.77, 142.98, 143.29, 143.41, 143.48, 143.60, 144.09, 144.34, 144.99, 145.78, 146.93, 149.77, 149.85 (aromatic *ipso*-*C*N, -C^{i}Pr and -C^{t}Bu), 158.07, 158.43, 158.86, 159.61 (conjugated *C*=N, enamine-diimine isomers), 164.98, 166.16, 167.91, 169.22 (isolated *C*=N, enamine-diimine isomers/*C*=N, β-triketimine tautomer). Elemental analysis, calculated for $C_{39}H_{53}N_3$ (%): C, 83.07; H, 9.47; N, 7.45. Found: C, 83.20; H, 9.40; N, 7.45. MS (ESI+) *m/z*: 564.4 $[MH]^+$. IR: 1638, 1602, 1586, 1534 cm^{-1} ($\nu_{C=N}$, $\nu_{C=C(Ar)}$).

L^5: **HBDK^{iPr}** (3.55 g, 0.0106 mol), ^{n}BuLi (6.6 cm^3, 0.0106 mol), **IMC^2** (2.6 cm^3, 0.0106 mol) and hexane (50 cm^3) were used. Off-white powder from methanol/DCM (3.39 g, 60%); mp: 111-114°C. ^{1}H NMR (500 MHz, $CDCl_3$), peaks due to enamine-diimine isomer **D** (~64%, reported integrals normalised): 1.03, 1.07, 1.11, 1.14 (4 × 6H, 4 × d, $^3J_{HH}$ = 6.9 Hz, $CH(C\mathit{H}_3)_2$), 1.79, 1.99, 2.01 (3 × 3H, 3 × s, $C\mathit{H}_3C$=N); 3.02 (2H, septet, $^3J_{HH}$ = 6.9 Hz, $C\mathit{H}(CH_3)_2$), 3.03 (1H, septet, $^3J_{HH}$ = 6.9 Hz, $C\mathit{H}(CH_3)_2$), 3.14 (1H, septet, $^3J_{HH}$ = 6.9 Hz, $C\mathit{H}(CH_3)_2$), 6.53 (1H, dd, $^3J_{HH}$ = 7.6 Hz, isolated Ar^{iPr} *o*-C*H*), 6.82 (1H, dd, $^3J_{HH}$ = 7.6 Hz, enamine-imine Ar^{iPr} *o*-C*H*), 6.94-7.10 (7H, non-first order m, Ar^{iPr} and Ar^{iPr2} *m*- and *p*-C*H*), 7.19 (1H, dd, $^3J_{HH}$ = 7.4 Hz, isolated Ar^{iPr} *m'*-C*H*); 7.24 (1H, dd, $^3J_{HH}$ = 7.7 Hz, enamine-imine Ar^{iPr} *m'*-C*H*), 13.47 (1H, br s, N*H*); peaks due to β-triketimine tautomer (9%) and enamine-diimine isomer **B** (27%): 0.84, 0.90, 0.98, 0.99, 1.01 (5 × d, $CH(C\mathit{H}_3)_2$), 1.49, 1.76, 1.83, 1.95, 2.45 (5 × s, $C\mathit{H}_3C$=N), 4.65 (1H, s, α-C*H*, β-triketimine tautomer), 2.34, 2.81, 2.90, 2.94, 3.25 (5 × septet, $C\mathit{H}(CH_3)_2$), 6.49, 6.59, 6.66, 7.14, 7.21 (5 × dd, Ar^{iPr} *o*- and *m'*-C*H*), 13.34 (br s, N*H*). $^{13}C\{^1H\}$ NMR (125 MHz, $CDCl_3$), peaks due to all isomeric species (unless otherwise specified): δ 18.52, 18.53, 18.55, 19.19, 19.22, 20.53, 20.63, 24.60, 24.25, 31.35 ($\mathit{C}H_3C$=N), 22.64, 22.84, 22.94, 22.99, 23.02, 23.13, 23.15, 23.24, 23.31, 23.54, 23.67, 23.72, 24.18, 24.28 ($CH(\mathit{C}H_3)_2$), 27.45, 27.83, 27.88, 28.08, 28.36, 28.56 ($\mathit{C}H(CH_3)_2$), 72.32 (α-*C*H, β-triketimine tautomer), 104.64, 109.66 (alkenyl α-

C, enamine-diimine isomers), 118.31, 118.46, 119.81, 122.94, 123.02, 123.13, 123.16, 123.36, 123.54, 123.83, 123.86, 123.94, 124.22, 124.54, 124.59, 124.60, 124.90, 125.22, 125.48, 125.53, 125.68, 125.71, 125.74, 125.79, 125.93, 125.99, 126.14, 126.23 (aromatic *C*H), 136.36, 138.04, 138.35, 139.37, 140.50, 141.27, 141.64, 141.95, 142.12, 142.34, 142.37, 142.55, 143.09, 146.65, 148.53, 148.84 (aromatic *ipso*-*C*N and -*C*^{i}Pr), 157.64, 157.80, 158.64, 158.86, 159.80 (conjugated *C*=N, enamine-diimine isomers), 168.62, 170.10, 171.84 (isolated *C*=N, enamine-diimine isomers/*C*=N, β-triketimine tautomer). Elemental analysis, calculated for $C_{37}H_{49}N_3$ (%): C, 82.94; H, 9.22; N, 7.84. Found: C, 82.69; H, 9.27; N, 7.78. MS (ESI+) *m/z*: 536.4 $[MH]^+$. IR: 1593 (br), 1537 cm^{-1} ($\nu_{C=N}$, $\nu_{C=C(Ar)}$).

L^{6}: **HBDK^{iPr2}** (3.68 g, 0.0088 mol), ^{n}BuLi (5.5 cm^3, 0.0088 mol), **IMC^{1}** (1.8 cm^3, 0.0088 mol) and hexane (40 cm^3) were used. Large yellow crystals from methanol / DCM (2.82 g, 56%); mp: 139-141°C. ^{1}H NMR (500 MHz, $CDCl_3$), peaks due to β-triketimine tautomer (9%) and enamine-diimine isomers **B** (45%), **C** (39%) and **D** (7%): δ 0.89, 0.94, 1.02-1.15 (30H, multiple overlapping d, CH(CH_3)$_2$), 1.56, 1.57, 1.81, 1.83, 1.85, 1.94, 1.99, 2.05, 2.43 (9H, s, CH_3C=N), 2.55, 2.86-3.19, 3.26 (5H, multiple overlapping septets, CH(CH$_3$)$_2$), 6.47, 6.51, 6.64, 6.82 (1H, 4 × dd, Ar^{iPr} *o*-CH), 6.97-7.09, 7.15-7.24 (9H, 2 × non-first-order m, Ar^{iPr} and Ar^{iPr2} *m*-, *m'*- and *p*-C*H*), 4.71, 13.08, 13.10, 13.83 (1H, β-triketimine α-C*H* and enamine-diimine N*H*). ^{13}C{^{1}H} NMR (125 MHz, $CDCl_3$), peaks due to all isomeric species (unless otherwise specified): δ 18.45, 18.96, 20.89, 24.38, 24.68, 31.49 (*C*H$_3$C=N), 22.93, 23.08, 23.10, 23.18, 23.20, 23.35, 23.37, 23.41, 23.50, 23.71, 23.81, 23.86, 23.99, 24.15, 24.32 (CH(*C*H$_3$)$_2$), 27.46, 27.85, 27.90, 28.31 28.37, 28.40 (*C*H(CH$_3$)$_2$), 103.88, 108.55 (alkenyl α-*C*, enamine-diimine isomers), 118.31, 119.73, 122.96, 123.00, 123.14, 123.18, 123.23, 123.27, 123.37, 123.61, 123.91, 124.62, 124.72, 124.76, 125.34, 125.36, 125.61, 125.76, 125.25 (aromatic *C*H), 136.36, 136.49, 136.85, 138.24, 139.89, 140.19, 141.40, 142.14, 142.23, 142.52, 146.01, 146.62, 148.61, 148.96 (aromatic *ipso*-*C*N and -*C*^{i}Pr), 158.83, 159.44 (conjugated *C*=N, enamine-diimine isomers), 169.05, 169.46, 169.65, 170.04, 171.72 (isolated *C*=N, enamine-diimine isomers/*C*=N, β-triketimine tautomer). Elemental analysis, calculated for $C_{40}H_{55}N_3$ (%): C, 83.14; H, 9.59; N, 7.27. Found: C, 83.36; H, 9.69; N, 7.26. MS (ESI+) *m/z*: 578.3 $[MH]^+$. IR: 1617, 1589, 1602, 1537 cm^{-1} ($\nu_{C=N}$, $\nu_{C=C(Ar)}$).

L[7]: **HBDK^{Me3}** (4.40 g, 0.0132 mol), ^{n}BuLi (8.3 cm^3, 0.0133 mol), **IMC[4]** (2.6 cm^3, 0.0133 mol) and hexane (20 cm^3) were used. Pale-yellow crystals from methanol/DCM (2.17 g, 34%); mp: 132-134°C. ^{1}H NMR (400 MHz, $CDCl_3$), solution composition immediately after dissolution: enamine-diimine tautomer (*E*-isomer), 87%, β-triketimine tautomer, 13%; solution composition ~24 hours after dissolution: enamine-diimine tautomer (*E*-isomer), 66%, β-triketimine tautomer, 34%; peaks due to both isomers (unless otherwise specified): δ 1.84, 1.88, 1.96, 2.03, 2.06, 2.19 (36H, 6 × s, Mes-CH_3 and CH_3C=N), 6.77, 6.79 (6H, 2 × s, Mes-C*H*), 4.68, 13.56 (1H, 2 × s, α-C*H* of β-triketimine tautomer, N*H* of enamine-diimine tautomer). ^{13}C{^{1}H} NMR (100 MHz, $CDCl_3$), peaks due to both isomers (unless otherwise specified): δ 18.47, 18.51, 20.72, 20.81, 20.87, 24.91 (*C*H_3C=N and Mes-*C*H_3), 72.18 (α-*C*H, β-triketimine tautomer), 108.42 (alkenyl α-*C*, enamine-diimine tautomer), 125.63, 128.56, 128.66, 129.12, 131.78, 132.10, 146.17 (aromatic *C*), 159.74 (conjugated *C*=N, enamine-diimine tautomer), 169.20 (*C*=N, β-triketimine tautomer), 172.19 (isolated *C*=N, enamine-diimine tautomer). Elemental analysis, calculated for $C_{34}H_{43}N_3$ (%): C, 82.33; H, 8.94; N, 8.73. Found: C, 82.41; H, 8.80; N, 8.38. MS (ESI+) *m/z*: 494.4 $[MH]^+$. IR: 1662, 1644 cm^{-1} ($\nu_{C=N}$).

L[8]: **HBDK^{iPr}** (14.0 g, 0.0419 mol), ^{n}BuLi (26.2 cm^3, 0.0419 mol), **IMC[8]** (9.5 cm^3, 0.0419 mol) and hexane (100 cm^3) were used. Large pale-yellow blocks from methanol (10.15 g, 46%); mp: 107-109°C. ^{1}H NMR (500 MHz, $CDCl_3$): δ 0.91 (6H, d, $^3J_{HH}$ = 6.8 Hz), 0.94 (6H, d, $^3J_{HH}$ = 7.0 Hz) (CH(CH_3)$_2$), 1.68 (6H, s, CH_3C=N), 2.71 (2H, septet, $^3J_{HH}$ = 6.8 Hz, C*H*(CH$_3$)$_2$), 3.61 (3H, s, OCH_3), 6.46 (1H, dd, $^3J_{HH}$ = 7.6 Hz, $^4J_{HH}$ = 1.3 Hz, Ar^{OMe} *o*-C*H*), 6.61 (2H, dd, $^3J_{HH}$ = 7.1 Hz, $^4J_{HH}$ = 1.1 Hz , Ar^{iPr} *o*-C*H*), 6.70 (1H, d, $^3J_{HH}$ = 8.0 Hz, Ar^{OMe} *m'*-C*H*), 6.74 (1H, td, $^3J_{HH}$ = 7.6 Hz, $^4J_{HH}$ = 1.0 Hz, Ar^{OMe} *p*-C*H*), 6.90 (1H, td, $^3J_{HH}$ = 7.9 Hz, $^4J_{HH}$ = 1.6 Hz, Ar^{OMe} *m*-C*H*), 6.94-6.99 (4H, non-first-order m, Ar^{iPr} *m*- and *p*-C*H*), 7.10 (2H, dd, $^3J_{HH}$ = 6.9 Hz, $^4J_{HH}$ = 2.4 Hz, Ar^{iPr} *m'*-*C*H), 13.48 (1H, br s, N*H*). ^{13}C NMR (125 MHz, $CDCl_3$): δ 20.65 (*C*H_3C=N), 23.16 (CH(*C*H_3)$_2$), 27.93 (*C*H(CH$_3$)$_2$), 30.73 (C(*C*H_3)$_3$), 42.16 (*C*(CH$_3$)$_3$), 55.21 (OCH_3), 104.53 (alkenyl α-*C*), 111.12 (Ar^{OMe} *m'*-*C*H), 119.32 (Ar^{OMe} *o*-*C*H), 120.17 (Ar^{OMe} *p*-*C*H), 124.04 (Ar^{OMe} *m*-*C*H), 124.41 (Ar^{iPr} *o*-*C*H), 125.65 (Ar^{iPr} *p*-*C*H), 125.69 (Ar^{iPr} *m'*-*C*H), 125.90 (Ar^{iPr} *m*-*C*H), 140.85 (Ar^{iPr} *ipso*-*C*^{i}Pr), 141.83, 142.84 (aromatic *ipso*-*C*N), 150.34 (Ar^{OMe} *ipso*-*C*OCH$_3$), 158.61 (conjugated *C*=N), 182.36 (isolated *C*=N). Elemental analysis, calculated for $C_{35}H_{45}N_3O$ (%): C, 80.26; H, 8.66; N, 8.02. Found: C, 80.79; H, 8.57; N, 8.08. MS (ESI+) *m/z*: 524.4 $[MH]^+$. IR: 1604, 1589, 1531 cm^{-1} ($\nu_{C=N}$, $\nu_{C=C(Ar)}$).

L[9]: **HBDK^{tBu}** (2.03 g, 0.00561 mol), ^{n}BuLi (4 cm^3, 0.00640 mol), **IMC[8]** (1.4 cm^3, 0.00621 mol) and hexane (100 cm^3) were used. Yellow solid from methanol (1.89 g, 61%); mp: 117-119°C. ^{1}H NMR (500 MHz. $CDCl_3$): δ 1.07 (18H, v br s, Ar^{tBu} C(CH_3)$_3$), 1.35 (9H, s, (CH_3)$_3$CC=N), 1.73 (6H, s, CH_3C=N), 3.63 (3H, s, OCH_3), 1 extremely broad resonance in aryl region (2H, Ar^{tBu} *o*-C*H*), 6.54 (1H, d, $^3J_{HH}$ = 7.2 Hz, Ar^{OMe} o-C*H*), 6.71 (1H, d, $^3J_{HH}$ = 7.9 Hz, Ar^{OMe} *m'*-C*H*), 6.77 (1H, t, $^3J_{HH}$ = 7.5 Hz, Ar^{OMe} *p*-C*H*), 6.91 (1H, t, $^3J_{HH}$ = 7.5 Hz, Ar^{OMe} *m*-C*H*), 6.94 (2H, t, $^3J_{HH}$ = 7.0 Hz, Ar^{tBu} *p*-C*H*), 7.02 (2H, t, $^3J_{HH}$ = 7.3 Hz, Ar^{tBu} *m*-C*H*), 7.23 (2H, d, $^3J_{HH}$ = 8.0 Hz, Ar^{tBu} *m'*-C*H*), 14.00 (1H, br s, N*H*). ^{13}C{^{1}H} NMR (125 MHz, $CDCl_3$): δ 20.03 (*C*H$_3$C=N), 29.32 (Ar^{tBu} C(*C*H$_3$)$_3$), 29.79 ((*C*H$_3$)$_3$CC=N), 33.93 (Ar^{tBu} *C*(CH$_3$)$_3$), 40.87 ((CH$_3$)$_3$*C*C=N), 54.10 (O*C*H$_3$), 104.50 (alkenyl α-*C*), 109.96 (Ar^{OMe} *m'*-*C*H), 118.25 (Ar^{OMe} *o*-*C*H), 119.25 (Ar^{OMe} *p*-*C*H), 123.01 (Ar^{OMe} *m*-*C*H), 123.13 (Ar^{tBu} *p*-*C*H), 125.14 (Ar^{tBu} *m*-*C*H), 125.36 (Ar^{tBu} *m'*-*C*H), 125.47 (br, Ar^{tBu} *o*-*C*H), 139.80 (Ar^{tBu} *ipso*-*C*^{t}Bu), 142.21, 143.01 (aromatic *ipso*-*C*N), 149.12 (Ar^{OMe} *ipso*-*C*OCH$_3$), 157.07 (br, conjugated *C*=N), 181.38 (isolated *C*=N). Elemental analysis, calculated for $C_{37}H_{49}N_3O$ (%): C, 80.54; H, 8.95; N, 7.61. Found: C, 80.30; H, 8.99; N, 7.54. MS (ESI+) *m/z*: 552.6 [MH]$^+$. IR: 1622, 1604, 1586, 1529 cm^{-1} ($\nu_{C=N}$, $\nu_{C=C(Ar)}$).

L[10]: **HBDK^{iPr}** (10.15 g, 0.0304 mol), ^{n}BuLi (19.25 cm^3, 0.0308 mol), **IMC[5]** (7.10 cm^3, 0.0300 mol) and hexane (80 cm^3) were used. Yellow crystals from methanol (9.41 g, 59%); mp: 128-130°C. ^{1}H NMR (500 MHz. $CDCl_3$): δ 0.95 (6H, d, $^3J_{HH}$ = 6.9 Hz, CH(CH_3)$_2$), 0.99 (6H, d, $^3J_{HH}$ = 6.9 Hz, CH(CH_3)$_2$), 1.14 (6H, d, $^3J_{HH}$ = 6.8 Hz, CH(CH_3)$_2$), 1.34 (9H, s, C(CH_3)$_3$), 1.63 (6H, s, CH_3C=N), 2.81 (2H, septet, $^3J_{HH}$ = 6.9 Hz, C*H*(CH$_3$)$_2$), 3.26 (1H, septet, $^3J_{HH}$ = 6.8 Hz, C*H*(CH$_3$)$_2$), 6.58-6.62 (1H, non-first-order m, unique Ar^{iPr} *o*-C*H*), 6.65 (2H, dd, $^3J_{HH}$ = 7.0 Hz, $^4J_{HH}$ = 2.3 Hz, enamine-imine Ar^{iPr} *o*-C*H*), 6.95-7.02 (6H, non-first-order m, Ar^{iPr} *m*- and *p*-C*H*), 7.11-7.17 (3H, non-first-order m, Ar^{iPr} *m'*-C*H*), 13.49 (1H, br s, N*H*). ^{13}C{^{1}H} NMR (125 MHz, $CDCl_3$): δ 20.60 (*C*H$_3$C=N)), 22.98, 23.12, 23.30 (CH(*C*H$_3$)$_2$), 27.79 (1 *C*H(CH$_3$)$_2$), 27.96 (2 *C*H(CH$_3$)$_2$), 30.57 (C(*C*H$_3$)$_3$), 43.00 (*C*(CH$_3$)$_3$), 103.79 (alkenyl α-*C*), 118.64, 124.38, 124.72, 125.07, 125.20, 125.76, 125.94 (aromatic *C*H), 141.51, 141.83, 142.77, 146.91 (aromatic *ipso*-*C*N and -*C*^{i}Pr), 158.57 (conjugated *C*=N), 179.34 (isolated *C*=N). Elemental analysis, calculated for $C_{37}H_{49}N_3$ (%): C, 82.94; H, 9.22; N, 7.84. Found: C, 83.89; H, 9.18; N, 7.93. MS (ESI+) *m/z*: 536.4 [MH]$^+$. IR: 1604, 1589, 1558, 1527 cm^{-1} ($\nu_{C=N}$, $\nu_{C=C(Ar)}$).

L[11]: **HBDK[iPr]** (10g, 0.0299 mol), ^{n}BuLi (19.5 cm^3, 0.0312 mol), **IMC[6]** (8.6 cm^3, 0.0308 mol) and hexane (70 cm^3) were used. Large colourless crystals from methanol/DCM (11.96g, 70%); mp: 123-126°C. ^{1}H NMR (500 MHz. $CDCl_3$): δ 0.96 (6H, d, $^3J_{HH}$ = 6.5 Hz, CH(CH_3)$_2$), 1.02 (6H, d, $^3J_{HH}$ = 6.9 Hz, CH(CH_3)$_2$), 1.05 (6H, d, $^3J_{HH}$ = 7.1 Hz, CH(CH_3)$_2$), 1.12 (6H, d, $^3J_{HH}$ = 6.9 Hz, CH(CH_3)$_2$), 1.15 (9H, s, C(CH_3)$_3$), 1.92 (6H, s, CH_3C=N), 2.97-2.98 (4H, 2 × overlapping septets, $^3J_{HH}$ = 6.5 and 6.9 Hz, CH(CH$_3$)$_2$), 4.90 (1H, br s, α-CH), 6.48 (2H, dd, $^3J_{HH}$ = 7.6 Hz, $^4J_{HH}$ = 1.3 Hz, Ar^{iPr} *o*-CH), 6.87 (1H, t, $^3J_{HH}$ = 7.6 Hz, Ar^{iPr2} *p*-CH), 6.96 (2H, d, $^3J_{HH}$ = 7.6 Hz, Ar^{iPr2} *m*-CH), 6.98 (2H, td, $^3J_{HH}$ = 7.6 Hz, $^4J_{HH}$ = 1.2 Hz, Ar^{iPr} *p*-CH), 7.03 (2H, td, $^3J_{HH}$ = 7.5 Hz, $^4J_{HH}$ = 1.5 Hz, Ar^{iPr} *m*-CH), 7.19 (2H, dd, $^3J_{HH}$ = 7.7 Hz, $^4J_{HH}$ = 1.3 Hz, Ar^{iPr} *m'*-CH). ^{13}C{^{1}H} NMR (125 MHz, $CDCl_3$): δ 20.61 (*C*H$_3$C=N), 22.04, 23.26, 24.44 (CH(*C*H$_3$)$_2$), 27.68, 28.11 (*C*H(CH$_3$)$_2$), 29.04 (C(*C*H$_3$)$_3$), 44.20 (*C*(CH$_3$)$_3$), 68.11 (α-*C*H), 118.38 (Ar^{iPr} *o*-*C*H), 122.21 (Ar^{iPr2} *p*-*C*H); 122.38 (Ar^{iPr2} *m*-*C*H), 123.60 (Ar^{iPr} *p*-*C*H), 125.50 (Ar^{iPr} *m'*-*C*H), 126.05 (Ar^{iPr} *m*-*C*H), 134.04, 138.00 (aromatic *ipso*-*C*^{i}Pr), 146.23, 148.71 (aromatic *ipso*-*C*N), 169.58 (*C*=N). Elemental analysis, calculated for $C_{40}H_{55}N_3$ (%): C, 83.14; H, 9.59; N, 7.27. Found: C, 83.55; H, 9.87; N, 7.26. MS (ESI+) *m/z*: 578.3 [MH]$^+$. IR: 1663, 1656, 1591, 1574 cm^{-1} ($\nu_{C=N}$, $\nu_{C=C(Ar)}$).

L[12]: **HBDK[iPr]** (10.11 g, 0.0302 mol), ^{n}BuLi (19.5 cm^3, 0.0312 mol), **IMC[7]** (7.20 g, 0.0303 mol) and hexane (70 cm^3) were used. Colourless crystals from methanol/DCM (11.36 g, 71%); mp: 144-146°C. ^{1}H NMR (500 MHz. $CDCl_3$): δ 0.99-1.10 (12H, overlapping d, $^3J_{HH}$ = 7.0 Hz, CH(CH_3)$_2$), 1.17 (9H, br s, C(CH_3)$_3$), 1.88 (6H, br s, CH_3C=N), 2.02 (6H, s, Mes *o*-CH_3); 2.16 (3H, s, Mes *p*-CH_3), 3.02 (2H, septet, $^3J_{HH}$ = 7.0 Hz, CH(CH$_3$)$_2$), 4.83 (1H, br s, α-CH), 6.47 (2H, dd, $^3J_{HH}$ = 7.7 Hz, $^4J_{HH}$ = 1.3 Hz, Ar^{iPr} *o*-CH), 6.69 (2H, br s, Mes CH), 6.96 (2H, td, $^3J_{HH}$ = 7.6 Hz, $^4J_{HH}$ = 1.3 Hz, Ar^{iPr} *p*-CH), 7.02 (2H, td, $^3J_{HH}$ = 7.6. Hz, $^4J_{HH}$ = 1.3 Hz, Ar^{iPr} *m*-CH), 7.18 (2H, dd, $^3J_{HH}$ = 7.8 Hz, $^4J_{HH}$ = 1.3 Hz, Ar^{iPr} *m'*-CH). ^{13}C{^{1}H} NMR (125 MHz, $CDCl_3$): δ 19.32 (Mes *o*-*C*H$_3$), 20.62 (Mes *p*-*C*H$_3$), 21.01 (*C*H$_3$C=N), 23.20, 23.31 (CH(*C*H$_3$)$_2$), 27.51 (*C*H(CH$_3$)$_2$), 28.91 (C(*C*H$_3$)$_3$), 43.49 (*C*(CH$_3$)$_3$), 67.86 (α-*C*H), 118.21 (Ar^{iPr} *o*-*C*H), 123.56 (Ar^{iPr} *p*-*C*H), 125.61 (Ar^{iPr} *m'*-*C*H), 126.03 (Ar^{iPr} *m*-*C*H), 128.37 (Mes *C*H), 130.71 (br, Mes *ipso*-*C*CH$_3$), 138.17 (Ar^{iPr} *ipso*-*C*^{i}Pr), 146.46, 148.65 (aromatic *ipso*-*C*N), 169.58 (*C*=N). Elemental analysis, calculated for $C_{37}H_{49}N_6$ (%): C, 82.94; H, 9.22; N, 7.84. Found: C, 83.46; H, 9.61; N, 7.81. MS (ESI+) *m/z*: 536.5 [MH]$^+$. IR: 1683, 1659, 1595, 1571 cm^{-1} ($\nu_{C=N}$, $\nu_{C=C(Ar)}$).

L[13]: **HBDK^{iPr}** (3.34 g, 0.0100 mol), ^{n}BuLi (6.3 cm^3, 0.0101 mol), **IMC[9]** (2.70 cm^3, 0.0105 mol) and diethyl ether (20 cm^3) were used. Large yellow crystals from methanol/DCM (3.63 g, 65%); mp: 121-124°C. ^{1}H NMR (500 MHz. $CDCl_3$): δ 0.98 (6H, d, $^3J_{HH}$ = 6.9 Hz, CH(CH_3)$_2$), 1.01 (6H, d, $^3J_{HH}$ = 6.9 Hz, CH(CH_3)$_2$), 1.16 (6H, d, $^3J_{HH}$ = 6.9 Hz, CH(CH_3)$_2$), 1.56 (6H, s, CH_3C=N), 2.82 (2H, septet, $^3J_{HH}$ = 6.9 Hz, C*H*(CH$_3$)$_2$), 3.31 (1H, septet, $^3J_{HH}$ = 6.9 Hz, C*H*(CH$_3$)$_2$), 6.66-6.70 (2H, non-first-order m, enamine-imine Ar^{iPr} *o*-C*H*), 6.73-6.77 (1H, non-first-order m, unique Ar^{iPr} *o*-C*H*), 6.97-7.02 (4H, non-first-order m, enamine-imine Ar^{iPr} *m*- and *p*-C*H*), 7.03-7.07 (2H, non-first-order m, unique Ar^{iPr} *m*- and *p*-C*H*), 7.12-7.14 (2H, non-first-order m, enamine-imine Ar^{iPr} *m'*-C*H*), 7.20-7.24 (1H, non-first-order m, unique Ar^{iPr} *m'*-C*H*), 7.37-7.43 (3H, non-first-order m, Ph *m*- and *p*-C*H*), 8.09-8.13 (2H, dd, $^3J_{HH}$ = 7.6 Hz, Ph *o*-C*H*), 13.56 (1H, br s, N*H*). ^{13}C{^{1}H} NMR (125 MHz, $CDCl_3$): δ 18.19 (*C*H$_3$C=N), 22.05, 22.11, 22.20 (CH(*C*H$_3$)$_2$), 26.99 (*C*H(CH$_3$)$_2$), 101.15 (alkenyl α-*C*), 118.05, 123.27, 123.73, 123.88, 124.08, 124.49, 124.69, 124.86, 127.37, 127.52, 129.25 (aromatic *C*H), 140.64, 140.80, 141.40, 141.47,146.00 (aromatic *ipso*-*C*N and -*C*^{i}Pr), 158.44 (conjugated *C*=N), 165.34 (isolated *C*=N). Elemental analysis, calculated for $C_{39}H_{45}N_3$ (%): C, 84.28; H, 8.16; N, 7.56. Found: C, 84.08; H, 8.05; N, 7.53. MS (ESI+) *m/z*: 556.4 [MH]$^+$. IR: 1607, 1589, 1569, 1543 cm^{-1} ($\nu_{C=N}$, $\nu_{C=C(Ar)}$).

L[14]: **HBDK^{tBu}** (1.91 g, 0.00528 mol), ^{n}BuLi (3.3 cm^3, 0.00530 mol), **IMC[9]** (1.4 cm^3, 0.00540 mol) and hexane (20 cm^3) were used. Pale-yellow powder from methanol (2.14 g, 69%); mp: 176-178°C. ^{1}H NMR (500 MHz. $CDCl_3$): δ 1.15-1.16 (24H, overlapping s and d, C(CH_3)$_3$ and CH(CH_3)$_2$), 1.52 (6H, s, CH_3C=N), 3.31 (1H, septet, $^3J_{HH}$ = 7.0 Hz, C*H*(CH$_3$)$_2$), 6.51 (2H, br s, Ar^{tBu} *o*-C*H*), 6.82-6.86 (1H, non-first-order m, Ar^{iPr} *o*-C*H*), 6.94 (2H, td, $^3J_{HH}$ = 7.5 Hz, $^4J_{HH}$ = 1.3 Hz, Ar^{tBu} *p*-C*H*), 6.98-7.07 (4H, non-first-order m, Ar^{tBu} *m*-C*H*, Ar^{iPr} *m*- and *p*-C*H*) 7.19-7.22 (1H, non-first-order m, Ar^{iPr} *m'*-C*H*), 7.24 (2H, dd, $^3J_{HH}$ = 7.9 Hz, $^4J_{HH}$ = 1.2 Hz, Ar^{tBu} *m'*-C*H*), 7.37-7.43 (3H, non-first-order m, Ph *m*- and *p*-C*H*), 8.10-8.11 (2H, non-first-order m, Ph *o*-C*H*), 13.89 (1H, br s, N*H*). ^{13}C{^{1}H} NMR (125 MHz, $CDCl_3$): δ 19.84 (*C*H$_3$C=N), 23.15 (CH(*C*H$_3$)$_2$), 28.02 (*C*H(CH$_3$)$_2$), 30.46 (C(*C*H$_3$)$_3$), 35.05 (*C*(CH$_3$)$_3$), 103.11 (alkenyl α-*C*), 119.22, 124.38, 124.92, 125.31, 125.45, 126.27, 126.46, 126.60, 128.35, 128.53, 130.24 (aromatic *C*H), 141.72, 142.28, 143.26, 143.82, 147.04 (aromatic *ipso*-*C*N, -*C*^{t}Bu and -*C*^{i}Pr), 159.02 (conjugated *C*=N), 166.31 (isolated *C*=N). Elemental analysis, calculated for $C_{41}H_{49}N_3$ (%): C, 84.34; H, 8.46; N,

7.20. Found: C, 83.87; H, 8.17; N, 7.16. MS (ESI+) *m/z*: 584.2 $[MH]^+$. IR: 1607, 1594, 1586, 1569, 1537 cm^{-1} ($\nu_{C=N}$, $\nu_{C=C(Ar)}$).

L^{15}: **$HBDK^{iPr2/OMe}$** (1.98 g, 0.00554 mol), ^{n}BuLi (3.4 cm^3, 0.00554 mol), **IMC^2** (1.3 cm^3, 0.00554 mol) and hexane (40 cm^3) were used. Long yellow needles from methanol (1.23 g, 40%); mp: 105-108°C. ^{1}H NMR (500 MHz, $CDCl_3$), peaks due to enamine-diimine isomer **E** (56%): δ 0.85 (6H, d, $^3J_{HH}$ = 6.8 Hz, CH(CH_3)$_2$), 0.99 (6H, d, $^3J_{HH}$ = 6.9 Hz, CH(CH_3)$_2$), 1.05 (6H, d, overlapped with peak due to other isomer, CH(CH_3)$_2$), 1.13 (6H, d, overlapped with peak due to other isomer, $^3J_{HH}$ = 6.9 Hz, CH(CH_3)$_2$), 1.64 (6H, s, CH_3C=N), 2.46 (3H, s, CH_3C=N), 2.51 (2H, septet, $^3J_{HH}$ = 6.8 Hz, CH(CH$_3$)$_2$), 2.97 (2H, septet, $^3J_{HH}$ = 6.8 Hz, CH(CH$_3$)$_2$), 3.67 (3H, s, OCH_3), 6.58 (1H, dd, $^3J_{HH}$ = 7.8 Hz, $^4J_{HH}$ = 1.5 Hz, Ar^{OMe} *o*-C*H*), 13.05 (1H, br s, N*H*); peaks due to enamine-diimine isomer **D** (44%): 1.05 (12H, d, overlapped with peak due to other isomer, CH(CH_3)$_2$), 1.13 (12H, d, $^3J_{HH}$ = 6.8 Hz, CH(CH_3)$_2$), 1.83 (6H, s, CH_3C=N), 1.93 (3H, s, CH_3C=N), 3.08 (4H, septet, $^3J_{HH}$ = 6.8 Hz, CH(CH$_3$)$_2$), 3.68 (3H, s, OCH_3), 6.70 (1H, dd, $^3J_{HH}$ = 7.6 Hz, $^4J_{HH}$ = 1.6 Hz, Ar^{OMe} *o*-C*H*), 13.07 (1H, br s, N*H*); peaks due to both isomers: 6.77-6.90 (non-first-order m, Ar^{OMe} *m*- and *p*-C*H*), 6.96-7.10 (non-first-order m, Ar^{iPr2} *m*- and *p*-C*H*, Ar^{iPr} *m'*-C*H*). ^{13}C{^{1}H} NMR (125 MHz, $CDCl_3$), peaks due to both isomers: δ 18.40, 18.87, 24.61, 31.06 (*C*H$_3$C=N), 23.16, 23.36, 23.51, 24.23, 24.25, 24.31 (CH(*C*H$_3$)$_2$), 27.82, 28.25, 28.36 (*C*H(CH$_3$)$_2$), 55.14, 55.38 (O*C*H$_3$), 104.14, 108.72 (alkenyl α-*C*); 110.95, 111.50 (Ar^{OMe} *m'*-*C*H), 119.86, 119.94, 120.39, 120.96, 123.16, 124.11, 124.59, 125.23, 125.30 (all other aromatic *C*H), 139.85, 139.95, 140.34, 140.61, 142.15, 142.52, 148.85, 150.93 (aromatic *ipso*-*C*N, -*C*^{i}Pr and -*C*OCH$_3$), 158.99, 159.79 (conjugated *C*=N), 172.11, 173.46 (isolated *C*=N). Elemental analysis, calculated for $C_{38}H_{51}N_3O$ (%): C, 80.66; H, 9.08; N, 7.43. Found: C, 79.70; H, 9.02; N, 7.28. MS (ESI+) *m/z*: 566.4 $[MH]^+$. IR: 1630, 1603, 1586, 1560, 1536 cm^{-1} ($\nu_{C=N}$, $\nu_{C=C(Ar)}$).

L^{16}: **$HBDK^{iPr2/OMe}$** (5.10 g, 0.0140 mol), ^{n}BuLi (9 cm^3, 0.0144 mol), **IMC^8** (3.2 cm^3, 0.0142 mol) and hexane (50 cm^3) were used. Yellow crystals from methanol (6.35, 84%); mp: 94-96°C. ^{1}H NMR (500 MHz, $CDCl_3$): δ 0.75 (3H, d, $^3J_{HH}$ = 6.9 Hz, CH(CH_3)$_2$), 0.92 (3H, d, $^3J_{HH}$ = 6.9 Hz, CH(CH_3)$_2$), 1.02 (3H, d, $^3J_{HH}$ = 6.9 Hz, CH(CH_3)$_2$), 1.11 (3H, d, $^3J_{HH}$ = 6.9 Hz, CH(CH_3)$_2$), 1.35 (9H, s, C(CH_3)$_3$), 1.51 (3H, s, CH_3C=N), 1.88 (3H, s, CH_3C=N), 2.17 (1H, septet, $^3J_{HH}$ = 6.9 Hz), 2.91 (1H, septet, $^3J_{HH}$ = 6.9 Hz) (CH(CH$_3$)$_2$), 3.54 (3H, s, OCH_3), 3.65 (3H, s, OCH_3), 6.53 (1H, dd, $^3J_{HH}$ = 7.6 Hz, $^4J_{HH}$ = 1.3 Hz,

isolated Ar^{OMe} *o*-C*H*), 6.73-6.80 (5H, non-first-order m), 6.91-7.01 (5H, non-first-order m), 13.76 (1H, br s, N*H*). $^{13}C\{^1H\}$ NMR (125 MHz, $CDCl_3$): δ 20.18, 20.80 (*C*H_3C=N); 22.32, 22.81, 23.90, 23.93 (CH(*C*H_3)$_2$), 27.83, 28.48 (*C*H(CH$_3$)$_2$), 30.68 (C(*C*H_3)$_3$), 42.25 (*C*(CH$_3$)$_3$), 55.19, 55.77 (O*C*H$_3$), 104.31 (alkenyl α-*C*), 110.92, 112.13 (Ar^{OMe} (-OMe) ortho-*C*H), 119.64, 120.10, 120.78, 122.89, 122.91, 124.07, 124.21, 124.26, 124.43 (all other aromatic *C*H), 133.98, 140.63, 140.73, 140.94, 141.61 (aromatic *ipso*-*C*N and -*C*^{i}Pr), 150.5, 152.5 (aromatic *ipso*-*C*OCH$_3$), 157.16, 160.22 (conjugated *C*=N); 182.24 (isolated *C*=N). Elemental analysis, calculated for $C_{36}H_{47}N_3O_2$ (%): C, 78.08; H, 8.55; N, 7.59. Found: C, 78.33; H, 8.69; N, 7.64. MS (ESI+) *m/z*: 554.5 $[MH]^+$. IR: 1622, 1607, 1589, 1546 cm^{-1} ($\nu_{C=N}$, $\nu_{C=C(Ar)}$).

6.7 Synthesis of β-Triketimine Group 6 Metal Carbonyl Complexes

None of the compounds described below has an observable melting point. However, all of the chromium complexes darken slowly above ~250°C, and all of the molybdenum complexes darken slowly above ~300°C.

(L^1)Cr(CO)$_3$: In a typical procedure, a mixture of **L^1** (0.493 g, 0.001 mol) and $Cr(CO)_6$ (0.220 g, 0.001 mol) in di-*n*-butyl ether (20 cm^3) and THF (1 cm^3) were heated to reflux. A red precipitate became visible after approximately 20 minutes, and heating was continued for a further 2 hours and 10 minutes. The mixture was allowed to cool to room temperature and the red precipitate was collected by filtration and washed with hexane (3 x 10 cm^3). Yield: 0.220 g, 35%. Single crystals suitable for X-ray diffraction were obtained by vapour diffusion of hexane into a saturated $CHCl_3$ solution of **(L^1)Cr(CO)$_3$**. ^1H NMR (500 MHz, d$_6$-DMSO): δ 1.07 (9H, d, $^3J_{HH}$ = 6.8 Hz, CH(C*H*$_3$)$_2$), 1.43 (9H, d, $^3J_{HH}$ = 6.8 Hz, CH(C*H*$_3$)$_2$), 2.29 (9H, s, C*H*$_3$C=N), 2.80 (3H, septet, $^3J_{HH}$ = 6.8 Hz, C*H*(CH$_3$)$_2$), 5.65 (1H, s, α-C*H*), 6.72 (3H, d, $^3J_{HH}$ = 7.5 Hz, *o*-C*H*), 7.21, 7.25 (2 × 3H, overlapping t, $^3J_{HH}$ = 7.2 Hz, *m*- and *p*-C*H*), 7.41 (3H, d $^3J_{HH}$ = 7.3 Hz, *m'*-C*H*). Elemental analysis, calculated for $C_{37}H_{43}N_3O_3Cr$ (%): C, 70.57; H, 6.88; N, 6.67. Found: C, 69.73; H, 6.93; N, 6.53. IR: 1893, 1796, 1775 cm^{-1} ($\nu_{C=O}$); 1619, 1598, 1574 cm^{-1} ($\nu_{C=N}$, $\nu_{C=C(Ar)}$). UV/Vis (DCM): λ_{max} = 330 nm (n-π*), 469, 550 (MLCT).

(L^1)Mo(CO)$_3$: **L^1** (0.990 g, 0.002 mol), $Mo(CO)_6$ (0.53 g, 0.002 mol), $^nBu_2O$ (40 cm^3) and THF (2 cm^3) were heated to reflux for 1 hour and 45 minutes; orange powder (0.80 g,

60%). Single crystals suitable for X-ray diffraction were obtained by vapour diffusion of Et_2O into a saturated DCM solution of **$(L^1)Mo(CO)_3$**. ^{1}H NMR (500 MHz, d_6-DMSO): δ 1.10 (9H, d, $^3J_{HH}$ = 6.7 Hz, CH(CH_3)$_2$) 1.41 (9H, d, $^3J_{HH}$ = 6.7 Hz, CH(CH_3)$_2$), 2.31 (9H, s, CH_3C=N), 2.91 (3H, septet, $^3J_{HH}$ = 6.7 Hz, CH(CH$_3$)$_2$), 5.66 (1H, br s, α-CH), 6.69 (3H, d, $^3J_{HH}$ = 7.5 Hz, *o*-CH), 7.22, 7.27 (2 × 3H, overlapping t, $^3J_{HH}$ = 7.3 Hz, *m*- and *p*-CH), 7.41 (3H, d, $^3J_{HH}$ = 7.5 Hz, *m'*-CH). Elemental analysis, calculated for $C_{37}H_{43}N_3O_3Mo$ (%): C, 65.96; H, 6.43; N, 6.24. Found: C, 66.05; H, 6.50; N, 6.24. IR: 1897, 1787, 1776 cm^{-1} ($\nu_{C=O}$); 1618, 1599, 1574 cm^{-1} ($\nu_{C=N}$, $\nu_{C=C(Ar)}$). UV/Vis (DCM): λ_{max} = 290 nm (n-π*), 444, 510 nm (MLCT).

$(L^1)W(CO)_3$: **L^1** (0.250 g, 0.0005 mol), $W(CO)_6$ (0.180 g, 0.0005 mol), ^{n}Bu$_2$O (10 cm^3), THF (1.2 cm^3) and trimethylamine-*N*-oxide (0.170 g, 0.0015 mol) were stirred for 30 min, then heated to 100 °C for 2 h, then allowed to stir overnight; dark crimson powder (0.11g, 29%). ^{1}H NMR (500 MHz, d_6-DMSO): δ 1.10 (9H, d, $^3J_{HH}$ = 6.7 Hz, (CH(CH_3)$_2$) 1.39 (9H, d, $^3J_{HH}$ = 6.7 Hz, (CH(CH_3)$_2$), 2.31 (9H, s, CH_3C=N), 2.82 (3H, septet, $^3J_{HH}$ = 6.7 Hz, CH(CH$_3$)$_2$), 5.62 (1H, br s, α-CH), 6.69 (3H, d, $^3J_{HH}$ = 7.2 Hz, *o*-CH), 7.22, 7.25 (2 × 3H, overlapping t, $^3J_{HH}$ = 7.2 Hz, *m*- and *p*-CH), 7.39 (3H, d, $^3J_{HH}$ = 7.2 Hz, *m'*-CH). IR: 1889, 1785, 1775 cm^{-1} ($\nu_{C\equiv O}$); 1620, 1599, 1575 cm^{-1} ($\nu_{C=N}$, $\nu_{C=N(Ar)}$). UV/Vis (DCM): λmax = 325 nm (n-π*); 450, 530 nm (MLCT).

$(L^3)Cr(CO)_3$: **L^3** (0.507 g, 0.001 mol), $Cr(CO)_6$ (0.220 g, 0.001 mol), ^{n}Bu$_2$O (20 cm^3) and THF (1 cm^3) were heated to reflux for 5 hours; bright-red powder (0.580 g, 90%). ^{1}H NMR (500 MHz, d_6-DMSO): δ 1.08 (3H, d, $^3J_{HH}$ = 6.7 Hz, CH(CH_3)$_2$), 1.12 (3H, d, $^3J_{HH}$ = 6.7 Hz, CH(CH_3)$_2$), 1.43, 1.44 (2 × 3H, overlapping d, $^3J_{HH}$ = 6.7 Hz, CH(CH_3)$_2$), 1.38 (9H, s, C(CH_3)$_3$), 2.24 (3H, s, CH_3C=N), 2.29 (6H, s, CH_3C=N), 2.67 (1H, septet, $^3J_{HH}$ = 6.7 Hz, CH(CH$_3$)$_2$), 2.70 (1H, septet, $^3J_{HH}$ = 6.7 Hz, CH(CH$_3$)$_2$), 5.63 (1H, br s, α-CH), 6.75, 6.84 (2 × 1H, non-first-order m, *o*-CH), 7.09 (1H, d, $^3J_{HH}$ = 7.5 Hz, *o*-CH); 7.14-7.27 (6H, non-first-order m, *m*- and *p*-CH); 7.40-7.45 (2H, non-first-order m, *m'*-CH), 7.52-7.56 (1H, non-first-order m, *m'*-CH). Elemental analysis, calculated for $C_{38}H_{45}N_3O_3Cr$ (%): C, 70.90; H, 7.05; N, 6.53; Cr, 8.08. Found: C, 70.90; H, 7.27; N, 6.42; Cr, 8.04. IR: 1894, 1796, 1772 cm^{-1} ($\nu_{C=O}$); 1617, 1598, 1573 cm^{-1} ($\nu_{C=N}$, $\nu_{C=C(Ar)}$). UV/Vis (DCM): λ_{max} = 330 nm (n-π*), 471, 540 nm (MLCT).

$(L^3)Mo(CO)_3$: **L^3** (0.260 g, 0.000513 mol), $Mo(CO)_6$ (0.133 g, 0.000504 mol), ^{n}Bu$_2$O (15 cm^3) and THF (1 cm^3) were heated to reflux for 7 hours; orange powder (0.240 g, 69%).

^{1}H NMR (500 MHz, d_6-DMSO): δ 0.98 (3H, d, $^3J_{HH}$ = 6.5 Hz, CH(CH_3)$_2$), 1.01 (3H, d, $^3J_{HH}$ = 6.5 Hz, CH(CH_3)$_2$), 1.31 (6H, non-first-order m, CH(CH_3)$_2$), 1.29 (9H, s, ^{t}Bu C(CH_3)$_3$), 2.16 (3H, s, CH_3C=N), 2.19 (6H, s, CH_3C=N), 2.73 (1H, septet, $^3J_{HH}$ = 6.5 Hz, CH(CH$_3$)$_2$), 2.74 (1H, septet, $^3J_{HH}$ = 6.5 Hz, CH(CH$_3$)$_2$), 5.54 (1H, s, α-CH), 6.60 (1H, d, $^3J_{HH}$ = 6.8 Hz, *o*-CH), 6.67 (1H, d, $^3J_{HH}$ = 7.1 Hz, *o*-CH), 6.86 (1H, d, $^3J_{HH}$ = 7.5 Hz, *o*-CH), 7.03-7.21 (6H, non-first-order m, *m*- and *p*-CH), 7.31, 7.32 (2 × 1H, overlapping d, *m'*-CH), 7.43 (1H, d, $^3J_{HH}$ = 6.9 Hz, *m'*-CH). Elemental analysis, calculated for $C_{38}H_{45}N_3O_3Mo$ (%): C, 66.37; H, 6.59; N, 6.11; Mo, 13.96. Found: C, 64.34; H, 6.60; N, 5.79; Mo, 13.34. IR: 1898, 1792, 1773 cm^{-1} ($\nu_{C=O}$); 1617, 1597, 1578, 1571 cm^{-1} ($\nu_{C=N}$, $\nu_{C=C(Ar)}$). UV/Vis (DCM): λ_{max} = 290 nm (n-π*), 444, 510 nm (MLCT).

(L^5)Cr(CO)$_3$: **L^5** (0.500 g, 0.000930 mol), Cr(CO)$_6$ (0.20 g, 0.000930 mol), ^{n}Bu$_2$O (30 cm^3) and THF (1 cm^3) were heated to reflux for 5 hours; dark-red powder (0.38 g, 60%). ^{1}H NMR (500 MHz, d_6-DMSO): δ 0.99, 1.13 (2 × 6H, overlapping d, CH(CH_3)$_2$), 1.27-1.58 (12H, non-first-order m, CH(CH_3)$_2$), 2.26 (3H, s, CH_3C=N), 2.29 (6H, s, CH_3C=N); 2.87-3.16 (4H, multiple poorly-defined septets, CH(CH$_3$)$_2$), 5.64 (1H, br s, α-CH), 6.71-7.51 (11H, poorly defined m, aromatic CH). Elemental analysis, calculated for $C_{40}H_{49}N_3O_3Cr$ (%): C, 71.51; H, 7.35; N, 6.25; Cr, 7.74. Found: C, 70.76; H, 7.49; N, 6.08; Cr, 7.87. IR: 1893, 1792, 1770 cm^{-1} ($\nu_{C=O}$); 1612, 1599, 1578 cm^{-1} ($\nu_{C=N}$, $\nu_{C=C(Ar)}$). UV/Vis (DCM): λ_{max} = 340 nm (n-π*), 471, 550 nm (MLCT).

(L^5)Mo(CO)$_3$: **L^5** (0.500 g, 0.000930 mol), Mo(CO)$_6$ (0.247 g, 0.000930 mol), ^{n}Bu$_2$O (30 cm^3) and THF (1 cm^3) were heated to reflux for 3.5 hours; bright-red powder (0.62 g, 93%). ^{1}H NMR (400 MHz, d_6-DMSO): δ 0.93-1.49 (24H, multiple d, CH(CH_3)$_2$), 2.28-2.36 (9H, multiple s, CH_3C=N), 2.80-3.17 (4H, multiple septets, CH(CH$_3$)$_2$), 5.66 (1H, br s, α-CH), 6.50-7.48 (11H, non-first-order m, aromatic CH). Elemental analysis, calculated for $C_{40}H_{49}N_3O_3Mo$ (%): C, 67.12; H, 6.90; N, 5.87; Mo, 13.40. Found: C, 65.70; H, 7.21; N, 5.70; Mo, 12.08. IR: 1897, 1790, 1774 cm^{-1} ($\nu_{C=O}$); 1612, 1597, 1578, 1571 cm^{-1} ($\nu_{C=N}$, $\nu_{C=C(Ar)}$). UV/Vis (DCM): λ_{max} = 293 nm (n-π*), 446, 525 nm (MLCT).

(L^8)Cr(CO)$_3$: **L^8** (0.525 g, 0.001 mol), Cr(CO)$_6$ (0.221 g, 0.001 mol), ^{n}Bu$_2$O (20 cm^3) and THF (1 cm^3) were heated to reflux for 5.5 hours; red powder (0.481 g, 73%). ^{1}H NMR (500 MHz, d_6-DMSO): δ 1.05, 1.08, 1.41, 1.45 (4 × 3H, poorly defined d, CH(CH_3)$_2$), 1.12 (9H, s, C(CH_3)$_3$), 2.21 (3H, s, CH_3C=N), 2.23 (3H, s, CH_3C=N), 2.72-2.87 (2H, poorly defined overlapping septets, CH(CH$_3$)$_2$), 3.88 (3H, s, OCH_3), 5.97 (1H, s, α-CH), 6.70 (1H,

poorly defined d, aromatic C*H*), 6.78-6.92 (3H, non-first-order m, aromatic C*H*), 6.95-7.01 (1H, non-first-order m, aromatic C*H*), 7.02-7.10 (1H, non-first-order m, aromatic C*H*), 7.13-7.29 (4H, non-first-order m, aromatic C*H*), 7.36 (1H, poorly defined d, aromatic C*H*), 7.40 (1H, poorly defined d, aromatic C*H*). Elemental analysis, calculated for $C_{38}H_{45}N_3O_4Cr$ (%): C, 69.18; H, 6.87; N, 6.37; Cr, 7.88. Found: C, 66.48; H, 6.76; N, 6.02; Cr, 7.62. IR: 1897, 1802, 1766 cm^{-1} ($\nu_{C=O}$); 1620, 1597, 1573 cm^{-1} ($\nu_{C=N}$, $\nu_{C=C(Ar)}$). UV/Vis (DCM): λ_{max} = 340 nm (n-π*), 469, 540 nm (MLCT).

(L^8)Mo(CO)$_3$: L^8 (0.529 g, 0.00101 mol), $Mo(CO)_6$ (0.260 g, 0.000985 mol), $^nBu_2O$ (20 cm^3) and THF (1 cm^3) were heated to reflux for 5 hours; orange powder (0.531 g, 77%). ^{1}H NMR (500 MHz, d_6-DMSO): δ 1.08 (3H, d, $^3J_{HH}$ = 6.8 Hz, CH(CH_3)$_2$), 1.11 (3H, d, $^3J_{HH}$ = 6.8 Hz, CH(CH_3)$_2$), 1.39 (3H, d, $^3J_{HH}$ = 6.8 Hz, CH(CH_3)$_2$), 1.43 (3H, d, $^3J_{HH}$ = 6.8 Hz, CH(CH_3)$_2$), 1.15 (9H, s, C(CH_3)$_3$), 2.24 (3H, s, CH_3C=N), 2.26 (3H, s, CH_3C=N), 2.86 (1H, septet, $^3J_{HH}$ = 6.8 Hz, C*H*(CH$_3$)$_2$), 2.91 (1H, septet, $^3J_{HH}$ = 6.8 Hz, C*H*(CH$_3$)$_2$), 3.89 (3H, s, OCH_3), 5.97 (1H, s, α-C*H*), 6.68 (1H, d, $^3J_{HH}$ = 7.6 Hz, Ar^{OMe} *o*-C*H*), 6.82 (2H, d, $^3J_{HH}$ = 7.7 Hz, Ar^{iPr} *o*-C*H*), 6.87 (1H, t, $^3J_{HH}$ = 7.5 Hz, Ar^{OMe} *p*-C*H*), 6.99 (1H , d, $^3J_{HH}$ = 8.3 Hz, Ar^{OMe} *m'*-C*H*), 7.06 (1H, t, $^3J_{HH}$ = 7.7 Hz, Ar^{OMe} *m*-C*H*), 7.19, 7.24 (2 × 2H, overlapping t, Ar^{iPr} *m*- and *p*-C*H*), 7.37, 7.41 (2 × 1H, d, $^3J_{HH}$ = 7.7 Hz, Ar^{iPr} *m'*-C*H*). Elemental analysis, calculated for $C_{38}H_{45}N_3O_4Mo$ (%): C, 64.86; H, 6.45; N, 5.97; Mo, 13.63. Found: C, 64.07; H, 6.60; N, 5.77; Mo, 13.35. IR: 1895, 1790, 1776 cm^{-1} ($\nu_{C=O}$); 1615, 1597, 1576 cm^{-1} ($\nu_{C=N}$, $\nu_{C=C(Ar)}$). UV/Vis (DCM): λ_{max} = 293 (n-π*), 444, 505 nm (MLCT).

(L^{10})Cr(CO)$_3$: L^{10} (0.538 g, 0.00101 mol), $Cr(CO)_6$ (0.217 g, 0.000986 mol), $^nBu_2O$ (15 cm^3) and THF (1 cm^3) were heated to reflux for 5 hours; bright-red powder (0.310 g, 47%). ^{1}H NMR (500 MHz, d_6-DMSO): δ 1.06 (3H, d, $^3J_{HH}$ = 6.8 Hz, CH(CH_3)$_2$), 1.10 (3H, d, $^3J_{HH}$ = 6.8 Hz, CH(CH_3)$_2$), 1.24 (3H, d, $^3J_{HH}$ = 6.8 Hz, CH(CH_3)$_2$), 1.43 (3H, d, $^3J_{HH}$ = 6.8 Hz, CH(CH_3)$_2$), 1.47 (3H, d, $^3J_{HH}$ = 6.8 Hz, CH(CH_3)$_2$), 1.51 (3H, d, $^3J_{HH}$ = 6.8 Hz, CH(CH_3)$_2$), 1.14 (9H, s, C(CH_3)$_3$), 2.25 (3H, s, CH_3C=N), 2.27 (3H, s, CH_3C=N), 2.73-2.83 (3H, overlapping septets, $^3J_{HH}$ = 6.8 Hz, C*H*(CH$_3$)$_2$), 6.06 (1H, s, α-C*H*), 6.75 (1H, dd, $^3J_{HH}$ = 7.6 Hz, *o*-C*H*), 6.79 (1H, dd, $^3J_{HH}$ = 7.5 Hz, *o*-C*H*), 6.82 (1H, dd, $^3J_{HH}$ = 7.6 Hz, *o*-C*H*), 7.07-7.13 (2H, non-first-order m, *p*-C*H*), 7.20-7.26 (5H, non-first-order m, *m*-, *p*- and *m'*-C*H*), 7.42 (2 × 1H, overlapping d, *m'*-C*H*). Elemental analysis, calculated for $C_{40}H_{49}N_3O_3Cr$ (%): C, 71.51; H, 7.35; N, 6.25; Cr, 7.74. Found: C, 69.79; H, 7.08; N,

5.95; Cr, 7.64. IR: 1898, 1802, 1770 cm^{-1} ($\nu_{C=O}$); 1620, 1597, 1578 cm^{-1} ($\nu_{C=N}$, $\nu_{C=C(Ar)}$). UV/Vis (DCM): λ_{max} = 330 nm (n-π*), 471, 550 nm (MLCT).

(L^{10})Mo(CO)$_3$: **L^{10}** (0.540 g, 0.00101 mol), $Mo(CO)_6$ (0.268 g, 0.00102 mol), $^{n}Bu_2O$ (15 cm^3) and THF (1 cm^3) were heated to reflux for 6 hours; red powder (0.448 g, 63%). ^{1}H NMR (500 MHz, d_6-DMSO): δ 1.07 (3H, d, $^3J_{HH}$ = 6.8 Hz, CH(CH_3)$_2$), 1.12 (3H, d, $^3J_{HH}$ = 6.8 Hz, CH(CH_3)$_2$), 1.26 (3H, d, $^3J_{HH}$ = 6.8 Hz, CH(CH_3)$_2$), 1.40 (3H, d, $^3J_{HH}$ = 6.8 Hz, CH(CH_3)$_2$), 1.44 (3H, d, $^3J_{HH}$ = 6.8 Hz, CH(CH_3)$_2$), 1.47 (3H, d, $^3J_{HH}$ = 6.8 Hz, CH(CH_3)$_2$); 1.17 (9H, s, C(CH_3)$_3$); 2.27 (3H, s, CH_3C=N), 2.28 (3H, s, CH_3C=N), 2.83 (2H, septet, $^3J_{HH}$ = 6.8 Hz, CH(CH$_3$)$_2$), 2.91 (1H, septet, $^3J_{HH}$ = 6.8 Hz, CH(CH$_3$)$_2$), 6.04 (1H, s, α-CH), 6.72, 6.74 (2 × 1H, overlapping d, *o*-CH), 6.81 (1H, dd, $^3J_{HH}$ = 7.0 Hz, $^4J_{HH}$ = 2 Hz, *o*-CH), 7.07-7.13 (2H, non-first-order m, *p*-CH), 7.20-7.29 (5H, non-first-order m, *m*-, *p*- and *m'*-CH), 7.41, 7.43 (2 × 1H, overlapping d, *m'*-CH). Elemental analysis, calculated for $C_{40}H_{49}N_3O_3Mo$ (%): C, 67.12; H, 6.90; N, 5.87; Mo, 13.40. Found: C, 65.40; H, 6.84; N, 5.63; Mo, 13.11. IR: 1904, 1803, 1769 cm^{-1} ($\nu_{C=O}$); 1617, 1597, 1586, 1576 cm^{-1} ($\nu_{C=N}$, $\nu_{C=C(Ar)}$). UV/Vis (DCM): λ_{max} = 289 nm (n-π*), 445, 505 nm (MLCT).

(L^{11})Cr(CO)$_3$: **L^{11}** (0.570 g, 0.000988 mol), $Cr(CO)_6$ (0.222 g, 0.00101 mol), $^{n}Bu_2O$ (15 cm^3) and THF (1 cm^3) were heated to reflux for 6.5 hours; red powder (0.478 g, 68%). ^{1}H NMR (500 MHz, d_6-DMSO): δ 1.09 (3H, d, $^3J_{HH}$ = 6.7 Hz, CH(CH_3)$_2$), 1.16 (3H, d, $^3J_{HH}$ = 6.7 Hz, CH(CH_3)$_2$), 1.20 (3H, d, $^3J_{HH}$ = 6.7 Hz, CH(CH_3)$_2$), 1.28 (3H, d, $^3J_{HH}$ = 6.7 Hz, CH(CH_3)$_2$), 1.38-1.41 (2 × 3H, overlapping d, CH(CH_3)$_2$), 1.44 (3H, d, $^3J_{HH}$ = 6.7 Hz, CH(CH_3)$_2$), 1.54 (3H, d, $^3J_{HH}$ = 6.7 Hz, CH(CH_3)$_2$), 1.12 (9H, s, C(CH_3)$_3$), 2.25 (3H, s, CH_3C=N), 2.28 (3H, s, CH_3C=N), 2.63 (1H, septet, $^3J_{HH}$ = 6.7 Hz, CH(CH$_3$)$_2$), 2.72 (1H, septet, $^3J_{HH}$ = 6.7 Hz, CH(CH$_3$)$_2$), 2.93 (1H, septet, $^3J_{HH}$ = 6.7 Hz, CH(CH$_3$)$_2$), 3.33 (1H, septet, $^3J_{HH}$ = 6.7 Hz, CH(CH$_3$)$_2$), 6.06 (1H, s, α-CH), 6.84-6.87 (1H, non-first-order m, Ar^{iPr} *o*-CH), 7.09-7.11 (1H, non-first-order m, Ar^{iPr} *o*-CH), 7.16-7.30 (7H, non-first-order m, Ar^{iPr} *m*- and *p*-CH, Ar^{iPr2} *m*- and *p*-CH), 7.44-7.48 (2H, non-first-order m, Ar^{iPr} *m'*-CH). Elemental analysis, calculated for $C_{43}H_{55}N_3O_3Cr$ (%): C, 72.34; H, 7.76; N, 5.89, Cr, 7.28. Found: C, 72.31; H, 8.02; N, 5.81; Cr, 7.18. IR: 1894, 1796, 1770 cm^{-1} ($\nu_{C=O}$); 1617, 1599, 1572 cm^{-1} ($\nu_{C=N}$, $\nu_{C=C(Ar)}$). UV/Vis (DCM): λ_{max} = 345 nm (n-π*), 475, 550 nm (MLCT).

(L^{11})Mo(CO)$_3$: **L^{11}** (0.571 g, 0.000990 mol), $Mo(CO)_6$ (0.260 g, 0.000985 mol), $^{n}Bu_2O$ (15 cm^3) and THF (3 cm^3) were heated to reflux for 6 hours; red powder (0.640 g, 86%). ^{1}H NMR (500 MHz, d_6-DMSO): δ 1.08-1.50 (24H, multiple d, CH(CH_3)$_2$), 1.15 (9H, s,

C(CH_3)$_3$), 2.27 (3H, s, CH_3C=N), 2.30 (3H, s, CH_3C=N), 2.82 (1H, septet, $^3J_{HH}$ = 6.7 Hz, CH(CH$_3$)$_2$), 3.00 (1H, septet, $^3J_{HH}$ = 6.7 Hz, CH(CH$_3$)$_2$), 3.09 (1H, septet, $^3J_{HH}$ = 6.7 Hz, CH(CH$_3$)$_2$), 3.29 (1H, septet, $^3J_{HH}$ = 6.7 Hz, CH(CH$_3$)$_2$), 6.05 (1H, s, α-CH), 6.74-6.78 (1H, non-first-order m, Ar^{iPr} *o*-CH), 6.95 (1H, br d, Ar^{iPr} *o*-CH), 7.15-7.21 (3H, non-first-order m, Ar^{iPr} *p*-CH, Ar^{iPr2} *p*-CH), 7.23-7.31 (4H, non-first-order m, Ar^{iPr} *m*-CH, Ar^{iPr2} *m*-CH), 7.44-7.48 (2H, non-first-order m, Ar^{iPr} *m'*-CH). Elemental analysis, calculated for $C_{43}H_{55}N_3O_3Mo$ (%): C, 68.15; H, 7.31; N, 5.54; Mo, 12.66. Found: C, 67.49; H, 7.42; N, 5.40; Mo, 11.84. IR: 1900, 1799, 1769 cm^{-1} ($\nu_{C=O}$); 1617, 1597, 1572 cm^{-1} ($\nu_{C=N}$, $\nu_{C=C(Ar)}$). UV/Vis (DCM): λ_{max} = 290 nm (n-π*), 447, 515 nm (MLCT).

(L^{12})Cr(CO)$_3$: **L^{12}** (0.533 g, 0.000997 mol), Cr(CO)$_6$ (0.218 g, 0.00991 mol), ^{n}Bu$_2$O (15 cm^3) and THF (1 cm^3) were heated to reflux for 7 hours; deep-red powder (0.520 g, 78%). ^{1}H NMR (500 MHz, d$_6$-DMSO): δ 1.08-1.09 (6H, m, CH(CH_3)$_2$), 1.27 (3H, d, $^3J_{HH}$ = 6.7 Hz, CH(CH_3)$_2$), 1.42 (3H, d, $^3J_{HH}$ = 6.7 Hz, CH(CH_3)$_2$), 1.11 (9H, s, C(CH_3)$_3$), 2.13, 2.22, 2.24, 2.25, 2.28 (15H, s, CH_3C=N and Mes-CH_3), 2.67 (1H, septet, $^3J_{HH}$ = 6.7 Hz CH(CH$_3$)$_2$), 2.83 (1H, septet, $^3J_{HH}$ = 6.7 Hz, CH(CH$_3$)$_2$), 6.06 (1H, s, α-CH), 6.78, 6.81 (2H, s, Mes-CH), 6.87-6.91 (1H, non-first-order m, *o*-CH), 7.07-7.11 (1H, non-first-order m, *o*-CH), 7.20-7.28 (4H, non-first-order m, *m*- and *p*-CH), 7.40-7.46 (2H, non-first-order m, *m'*-CH). Elemental analysis, calculated for $C_{40}H_{49}N_3O_3Cr$ (%): C, 71.51; H, 7.35; N, 6.25; Cr, 7.74. Found: C, 71.50; H, 7.69; N, 6.19; Cr, 7.62. IR: 1894, 1796, 1773 cm^{-1} ($\nu_{C=O}$); 1612, 1598, 1578 cm^{-1} ($\nu_{C=N}$, $\nu_{C=C(Ar)}$). UV/Vis (DCM): λ_{max} = 355 (n-π*), 470, 550 nm (MLCT).

(L^{12})Mo(CO)$_3$: **L^{12}** (0.535 g, 0.001 mol), Mo(CO)$_6$ (0.266 g, 0.00101 mol), ^{n}Bu$_2$O (15 cm^3) and THF (3 cm^3) were heated to reflux for 7 hours; bright-red powder (0.588 g, 82%). ^{1}H NMR (500 MHz, d$_6$-DMSO): δ 1.08 (3H, d, $^3J_{HH}$ = 6.8 Hz, CH(CH_3)$_2$), 1.10 (3H, d, $^3J_{HH}$ = 6.8 Hz, CH(CH_3)$_2$), 1.25 (3H, d, $^3J_{HH}$ = 6.8 Hz, CH(CH_3)$_2$), 1.41 (3H, d, $^3J_{HH}$ = 6.8 Hz, CH(CH_3)$_2$), 1.13 (9H, s, C(CH_3)$_3$), 2.18, 2.23, 2.25, 2.29 (15H, s, CH_3C=N and Mes-CH_3), 2.87 (1H, septet, $^3J_{HH}$ = 6.8 Hz, CH(CH$_3$)$_2$), 2.88 (1H, septet, $^3J_{HH}$ = 6.8 Hz, CH(CH$_3$)$_2$), 6.05 (1H, s, α-CH), 6.78, 6.80 (2H, s, Mes-CH), 6.81-6.85 (1H, non-first-order m, *o*-CH), 6.96 (1H , d, $^3J_{HH}$ = 7.5 Hz, *o*-CH), 7.20-7.29 (4H, non-first-order m, *m*- and *p*-CH), 7.40-7.46 (2H, non-first-order m, *m'*-CH). Elemental analysis, calculated for $C_{40}H_{49}N_3O_3Mo$ (%): C, 67.12; H, 6.90; N, 5.87; Mo, 13.40. Found: C, 66.43; H, 6.97; N,

5.75; Mo, 12.60. IR: 1899, 1799, 1772 cm^{-1} ($\nu_{C=O}$); 1612, 1598, 1576 cm^{-1} ($\nu_{C=N}$, $\nu_{C=C(Ar)}$). UV/Vis (DCM): λ_{max} = 290 nm (n-π*), 445, 508 (MLCT).

(L^{13})Cr(CO)$_3$: **L^{13}** (0.205 g, 0.000369 mol), $Cr(CO)_6$ (0.081 g, 0.000368 mol) and $^nBu_2O$ (10 cm^3) containing a few drops of THF were heated to reflux for 2.5 hours; black powder (0.129 g, 51%). ^{1}H NMR (500 MHz, d_6-DMSO): δ 0.44 (3H, d, $^3J_{HH}$ = 7.5 Hz, CH(CH_3)$_2$), 1.03 (3H, d, $^3J_{HH}$ = 6.7 Hz, CH(CH_3)$_2$), 1.10 (3H, d, $^3J_{HH}$ = 6.7 Hz, CH(CH_3)$_2$), 1.30 (3H, d, $^3J_{HH}$ = 6.7 Hz, CH(CH_3)$_2$), 1.45 (3H, d, $^3J_{HH}$ = 6.7 Hz, CH(CH_3)$_2$), 1.56 (3H, d, $^3J_{HH}$ = 6.7 Hz, CH(CH_3)$_2$), 2.14 (3H, s, CH_3C=N) 2.52 (3H, s, CH_3C=N), 2.30 (1H, septet, $^3J_{HH}$ = 6.7 Hz, C*H*(CH$_3$)$_2$), 2.83 (1H, septet, $^3J_{HH}$ = 6.7 Hz, C*H*(CH$_3$)$_2$), 2.98 (1H, septet, $^3J_{HH}$ = 6.7 Hz, C*H*(CH$_3$)$_2$), 6.05 (1H, s, α-C*H*), 6.72-6.76 (2H, non-first-order m, aromatic C*H*), 7.05-7.10 (2H, non-first-order m, aromatic C*H*), 7.18-7.30 (7H, non-first-order m, aromatic C*H*), 7.33-7.39 (4H, non-first-order m, aromatic C*H*), 7.42-7.47 (2H, non-first-order m, aromatic C*H*). Elemental analysis, calculated for $C_{42}H_{45}N_3O_3Cr$ (%): C, 72.92; H, 6.56; N, 6.07; Cr, 7.52. Found: C, 72.62; H, 6.67; N, 6.00; Cr, 7.30. IR: 1893, 1804, 1780 cm^{-1} ($\nu_{C=O}$); 1620, 1597, 1579, 1557 cm^{-1} ($\nu_{C=N}$, $\nu_{C=C(Ar)}$). UV/Vis (DCM): λ_{max} = 360 (n-π*), 489, 610 nm (MLCT).

(L^{13})Mo(CO)$_3$: **L^{13}** (0.201 g, 0.000362 mol), $Mo(CO)_6$ (0.095 g, 0.000360 mol) and $^nBu_2O$ (10 cm^3) containing a few drops of THF were heated to reflux for 5 hours; very dark purple powder (0.196 g, 74%). ^{1}H NMR (500 MHz, d_6-DMSO): δ 0.30 (3H, d, $^3J_{HH}$ = 6.9 Hz, CH(CH_3)$_2$), 0.83 (3H, d, $^3J_{HH}$ = 6.9 Hz, CH(CH_3)$_2$), 0.88 (3H, d, $^3J_{HH}$ = 6.9 Hz, CH(CH_3)$_2$), 1.05 (3H, d, $^3J_{HH}$ = 6.9 Hz, CH(CH_3)$_2$), 1.20 (3H, d, $^3J_{HH}$ = 6.9 Hz, CH(CH_3)$_2$), 1.31 (3H, d, $^3J_{HH}$ = 6.9 Hz, CH(CH_3)$_2$), 1.91 (3H, s, CH_3C=N), 2.30 (3H, s, CH_3C=N), 2.18 (1H, septet, $^3J_{HH}$ = 6.9 Hz, C*H*(CH$_3$)$_2$), 2.72 (1H, septet, $^3J_{HH}$ = 6.9 Hz, C*H*(CH$_3$)$_2$), 2.84 (1H, septet, $^3J_{HH}$ = 6.9 Hz, C*H*(CH$_3$)$_2$), 5.82 (1H, s, α-C*H*), 6.46-6.51 (2H, non-first-order m, aromatic C*H*), 6.80-6.87 (2H, non-first order m, aromatic C*H*), 6.94-7.24 (13H, non-first-order m, aromatic C*H*). Elemental analysis, calculated for $C_{42}H_{45}N_3O_3Mo$ (%): C, 68.56; H, 6.16; N, 5.71; Mo, 13.04. Found: C, 67.87; H, 6.25; N, 5.59; Mo, 13.01. IR: 1898, 1802, 1779 cm^{-1} ($\nu_{C=O}$); 1621, 1597, 1581, 1562 cm^{-1} ($\nu_{C=N}$, $\nu_{C=C(Ar)}$). UV/Vis (DCM): λ_{max} = 289 nm (n-π*), 462, 575 nm (MLCT).

(L^{15})Cr(CO)$_3$: **L^{15}** (0.196 g, 0.000347 mol), $Cr(CO)_6$ (0.081 g, 0.000368 mol) and $^nBu_2O$ (10 cm^3) containing a few drops of THF were heated to reflux for 6.5 hours; very dark-red powder (0.112 g, 46%). ^{1}H NMR (500 MHz, d_6-DMSO): δ 0.81 (3H, d, $^3J_{HH}$ = 5.7 Hz,

CH(CH_3)$_2$), 0.95 (3H, d, $^3J_{HH}$ = 5.7 Hz, CH(CH_3)$_2$), 1.02 (2 × 3H, overlapping d, CH(CH_3)$_2$), 1.08 (3H, d, $^3J_{HH}$ = 5.7 Hz, CH(CH_3)$_2$), 1.35-1.48 (9H, non-first-order m, CH(CH_3)$_2$), 2.24 (3H, s, CH_3C=N), 2.31 (6H, s, CH_3C=N), 2.55, 2.70, 3.10, 3.21 (4 × 1H, poorly defined septets, CH(CH$_3$)$_2$), 3.87 (3H, s, OCH_3), 5.61 (1H, s, α-CH), 7.00-7.06 (1H, non-first-order m, aromatic CH), 7.09-7.34 (8H, non-first-order m, aromatic CH), 8.00 (1H, d, $^3J_{HH}$ = 7.5 Hz, aromatic CH). Elemental analysis, calculated for $C_{41}H_{51}N_3O_4Cr$ (%): C, 70.16; H, 7.32; N, 5.99; Cr, 7.41. Found: C, 68.90; H, 7.44; N, 5.80; Cr, 7.40. IR: 1890, 1782, 1770 cm^{-1} ($\nu_{C=O}$); 1617, 1604, 1595 cm^{-1} ($\nu_{C=N}$, $\nu_{C=C(Ar)}$). UV/Vis (DCM): λ_{max} = 340 nm (n-π*), 473, 550 nm (MLCT).

(L^{15})Mo(CO)$_3$: **L^{15}** (0.198 g, 0.000350 mol), Mo(CO)$_6$ (0.097 g, 0.000367 mol) and ^{n}Bu$_2$O (10 cm^3) containing a few drops of THF were heated to reflux for 6.5 hours; red powder (0.176 g, 67%). ^{1}H NMR (300 MHz, d$_6$-DMSO): δ 0.83 (3H, d, $^3J_{HH}$ = 6.8 Hz, CH(CH_3)$_2$), 0.98-1.06 (3 × 3H, overlapping d, CH(CH_3)$_2$), 1.10 (3H, d, $^3J_{HH}$ = 6.7 Hz, CH(CH_3)$_2$), 1.36-1.45 (3 × 3H, overlapping d, CH(CH_3)$_2$), 2.28 (3H, s, CH_3C=N), 2.33 (6H, s, CH_3C=N), 2.58 (1H, septet, $^3J_{HH}$ = 6.5 Hz, CH(CH$_3$)$_2$), 2.81 (1H, septet, $^3J_{HH}$ = 6.8 Hz, CH(CH$_3$)$_2$), 3.13 (1H, septet, $^3J_{HH}$ = 6.7 Hz, CH(CH$_3$)$_2$), 3.16 (1H, septet, $^3J_{HH}$ = 6.6 Hz, CH(CH$_3$)$_2$), 3.89 (3H, s, OCH_3), 5.64 (1H, s, α-CH), 6.99-7.33 (9H, non-first-order m, aromatic CH), 7.84 (1H, dd, $^3J_{HH}$ = 7.9 Hz, $^4J_{HH}$ = 1.3 Hz, aromatic CH). Elemental analysis, calculated for $C_{41}H_{51}N_3O_4Mo$ (%): C, 66.03; H, 6.89; N, 5.63; Mo, 12.86. Found: C, 64.09; H, 6.72; N, 5.37; Mo, 12.88. IR: 1899, 1794, 1775 cm^{-1} ($\nu_{C=O}$); 1604, 1591 cm^{-1} ($\nu_{C=N}$, $\nu_{C=C(Ar)}$). UV/Vis (DCM): λ_{max} = 290 nm (n-π*), 445, 520 nm (MLCT).

(L^{16})Cr(CO)$_3$: **L^{16}** (0.555 g, 0.001 mol), Cr(CO)$_6$ (0.218 g, 0.000991 mol), ^{n}Bu$_2$O (20 cm^3) and THF (1 cm^3) were heated to reflux for 6 hours; red powder (0.480 g, 70%). ^{1}H NMR (500 MHz, d$_6$-DMSO), peaks due to major isomeric component: δ 0.93 (3H, d, $^3J_{HH}$ = 6.7 Hz, CH(CH_3)$_2$), 1.04 (3H, d, $^3J_{HH}$ = 6.7 Hz, CH(CH_3)$_2$), 1.35 (3H, d, $^3J_{HH}$ = 6.7 Hz, CH(CH_3)$_2$), 1.45 (3H, d, $^3J_{HH}$ = 6.7 Hz, CH(CH_3)$_2$), 1.12 (9H, s, C(CH_3)$_3$), 2.17 (3H, s, CH_3C=N), 2.25 (3H, s, CH_3C=N), 2.88 (1H, septet, $^3J_{HH}$ = 6.7 Hz, CH(CH$_3$)$_2$), 3.30 (1H, septet, $^3J_{HH}$ = 6.7 Hz, CH(CH$_3$)$_2$), 3.83 (3H, s, OCH_3), 3.87 (3H, s, OCH_3), 5.93 (1H, s, α-CH), 6.64-7.27 (11H, non-first-order m, aromatic CH); peaks due to minor isomeric component: δ 1.01, 1.14, 1.28, 1.49 (4 × 3H, d, CH(CH_3)$_2$), 1.11 (9H, s, C(CH_3)$_3$), 2.20 (3H, s, CH_3C=N), 2.23 (3H, s, CH_3C=N), 2.94 (1H, septet, CH(CH$_3$)$_2$), 3.05 (1H, septet, CH(CH$_3$)$_2$), 3.70 (3H, s, OCH_3), 3.85 (3H, s, OCH_3), 5.89 (1H, br s, α-CH). Elemental

analysis, calculated for $C_{39}H_{47}N_3O_5Cr$ (%): C, 67.91; H, 6.87; N, 6.09; Cr, 7.54. Found: C, 63.71; H, 6.56; N, 5.60; Cr, 7.27. IR: 1892, 1792, 1768 cm^{-1} ($\nu_{C=O}$); 1609, 1594, 1578, 1570 cm^{-1} ($\nu_{C=N}$, $\nu_{C=C(Ar)}$). UV/Vis (DCM): λ_{max} = 350 nm (n-π*), 468, 540 nm (MLCT).

(L^{16})Mo(CO)$_3$: **L^{16}** (0.558 g, 0.00101 mol), $Mo(CO)_6$ (0.263 g, 0.000996 mol), $^nBu_2O$ (20 cm^3) and THF (1 cm^3) were heated to reflux for 6 hours; orange-red powder (0.497 g, 68%). ^{1}H NMR (500 MHz, d_6-DMSO), peaks due to major isomeric component: δ 0.96 (3H, d, $^3J_{HH}$ = 6.8 Hz, CH(CH_3)$_2$), 1.06 (3H, d, $^3J_{HH}$ = 6.8 Hz, CH(CH_3)$_2$), 1.34 (3H, d, $^3J_{HH}$ = 6.8 Hz, CH(CH_3)$_2$), 1.43 (3H, d, $^3J_{HH}$ = 6.8 Hz, CH(CH_3)$_2$), 1.15 (9H, s, C(CH_3)$_3$), 2.19 (3H, s, CH_3C=N), 2.27 (3H, s, CH_3C=N), 2.99 (1H, septet, $^3J_{HH}$ = 6.8 Hz, CH(CH$_3$)$_2$), 3.27 (1H, septet, $^3J_{HH}$ = 6.8 Hz, CH(CH$_3$)$_2$), 3.84 (3H, s, OCH_3), 3.89 (3H, s, OCH_3), 5.93 (1H, s, α-CH), 6.62-7.26 (11H, non-first-order m, aromatic CH). Peaks due to minor isomeric components: δ 0.73-1.49 (12H, multiple overlapping d, CH(CH_3)$_2$), 1.17 (9H, s, C(CH_3)$_3$), 2.21 (3H, s, CH_3C=N), 2.25 (3H, s, CH_3C=N), 3.04 (1H, septet, CH(CH$_3$)$_2$), 3.09 (1H, septet, CH(CH$_3$)$_2$), 3.72 (3H, s, OCH_3), 3.86 (3H, s, OCH_3), 5.90 (1H, br s, α-CH). Elemental analysis, calculated for $C_{39}H_{47}N_3O_5Mo$ (%): C, 63.84; H, 6.46; N, 5.73; Mo, 13.08. Found: C, 60.29; H, 6.37; N, 5.33; Mo, 12.97. IR: 1893, 1788, 1774 cm^{-1} ($\nu_{C=O}$); 1612, 1593 cm^{-1} ($\nu_{C=N}$, $\nu_{C=C(Ar)}$). UV/Vis (DCM): λ_{max} = 290 nm (n-π*), 444, 505 nm (MLCT).

6.8 Synthesis of β-Triketimine Zinc Complexes

[(L^1)ZnCl][Cl]: DCM (7 cm^3) was added to a mixture of $ZnCl_2$ (0.136 g, 0.001 mol) and **L^1** (0.493 g, 0.001 mol), forming a yellow solution with undissolved $ZnCl_2$. This was stirred at room temperature for 3 days, after which time a white precipitate had formed. This was collected by filtration and washed with diethyl ether (2 x 20 cm^3), giving **8** as a white powder. Yield 0.267 g, 42%; mp: 228-231°C. ^{1}H NMR (500 MHz, d_6-DMSO): δ 1.09 (18H, d, $^3J_{HH}$ = 6.8 Hz, CH(CH_3)$_2$), 1.96 (9H, s, CH_3), 3.07 (3H, septet, $^3J_{HH}$ = 6.8 Hz, CH(CH$_3$)$_2$), 4.89 (1H, s, α-CH), 6.58-7.28 (12H, aromatic CH). Elemental analysis, calculated for $C_{34}H_{43}N_3ZnCl_2$ (%): C, 64.82; H, 6.88; N, 6.67; Cl, 11.25. Found: C, 62.48; H, 6.62; N, 6.45; Cl, 11.86. MS (MALDI) *m*/*z*: 592-599 [(L^1)ZnCl]$^+$. IR: 1680, 1662, 1651, 1636, 1595, 1575 cm^{-1} ($\nu_{C=N}$, $\nu_{C=C(Ar)}$).

$[(L^8)ZnCl]_2[Zn_2Cl_6]$: In a typical procedure, DCM (15 cm^3) was added to a solid mixture of $ZnCl_2$ (0.280 g, 0.00205 mol) and ligand $\mathbf{L^8}$ (0.519 g, 0.000992 mol), producing a red solution with undissolved $ZnCl_2$. This was stirred at room temperature for 7 days, after which time the solution had become pale-orange in colour. The volume of the solution was reduced under vacuum to approximately 25%, causing the precipitation of a small amount of white solid. Addition of diethyl ether (20 cm^3) gave more white precipitate, and this was collected by filtration in air and washed with diethyl ether (3 x 20 cm^3). Yield: 0.576 g, 73%; mp: 238-242°C. Crystals suitable for X-ray crystallographic analysis were obtained by vapour diffusion of Et_2O into an acetonitrile solution of **$[(L^8)ZnCl]_2[Zn_2Cl_6]$**. Elemental analysis, calculated for $C_{70}H_{90}N_6O_2Zn_4Cl_8$ (%): C, 52.79; H, 5.70; N, 5.28; Zn, 16.42; Cl, 17.80. Found: C, 52.14; H, 5.70; N, 5.11; Zn, 16.53; Cl, 17.65. MS (MALDI) *m/z*: 623-630 $[(L^8)ZnCl]^+$. IR: 1651, 1622, 1594, 1577 cm^{-1} ($\nu_{C=N}$, $\nu_{C=C(Ar)}$).

$[(L^{10})ZnCl]_2[Zn_2Cl_6]$: $\mathbf{L^{10}}$ (0.540 g, 0.00101 mol) and $ZnCl_2$ (0.264 g, 0.00194 mol) were used; white solid (0.476 g, 61%). Elemental analysis, calculated for $C_{74}H_{98}N_6Cl_8Zn_4$ (%): C, 54.97; H, 6.11; N, 5.20; Zn, 16.18; Cl, 17.54. Found: C, 53.70; H, 6.09; N, 5.04; Zn, 15.72; Cl, 17.87. MS (MALDI) *m/z*: 635-642 $[(L^{10})ZnCl]^+$. IR: 1648, 1626, 1611, 1597, 1577 cm^{-1} ($\nu_{C=N}$, $\nu_{C=C(Ar)}$).

$[(L^{11})ZnCl]_2[Zn_2Cl_6]$: $\mathbf{L^{11}}$ (0.576 g, 0.000998 mol) and $ZnCl_2$ (0.273 g, 0.00201 mol) were used; white solid (0.601 g, 71%). Elemental analysis, calculated for $C_{80}H_{110}N_6Cl_8Zn_4$ (%): C, 56.49; H, 6.52; N, 4.94; Zn, 15.38; Cl, 16.67. Found: C, 54.95; H, 6.58; N, 4.91; Zn, 14.67; Cl, 18.35. MS (MALDI) *m/z*: 676-683 $[(L^{11})ZnCl]^+$. IR: 1642, 1618, 1604, 1580, 1551, 1519 cm^{-1} ($\nu_{C=N}$, $\nu_{C=C(Ar)}$).

$[(L^{12})ZnCl]_2[Zn_2Cl_6]$: $\mathbf{L^{12}}$ (0.500 g, 0.000935 mol) and $ZnCl_2$ (0.258 g, 0.00190 mol) were used: off-white solid precipitated from solution by addition of a 1:1 mixture of diethyl ether and hexane (0.578 g, 77%). Crystals suitable for X-ray diffraction were obtained by vapour diffusion of Et_2O into a DCM solution of **$[(L^{12})ZnCl]_2[Zn_2Cl_6]$**. Elemental analysis, calculated for $C_{74}H_{98}N_6Cl_8Zn_4$ (%): C, 54.97; H, 6.11; N, 5.20; Zn, 16.18; Cl, 17.54. Found: C, 53.98; H, 6.06; N, 5.05; Zn, 15.83; Cl, 17.39. MS (MALDI) *m/z*: 634-641 $[(L^{12})ZnCl]^+$. IR: 1644, 1621, 1614, 1596, 1580 cm^{-1} ($\nu_{C=N}$, $\nu_{C=C(Ar)}$).

$[(L^{16})ZnCl]_2[Zn_2Cl_6]$: $\mathbf{L^{16}}$ (0.554 g, 0.00100 mol) and $ZnCl_2$ (0.275 g, 0.00202 mol) were used; off-white solid (0.505 g, 61%). Crystals suitable for X-ray diffraction were obtained

by vapour diffusion into a saturated DCM solution of **[(L^{16})ZnCl]$_2$[Zn_2Cl_6]**. Elemental analysis, calculated for $C_{72}H_{94}N_6O_4Cl_8Zn_4$ (%): C, 52.33; H, 5.73; N, 5.08; Zn, 15.82; Cl, 17.16. Found: C, 51.79; H, 5.65; N, 4.93; Zn, 15.85; Cl, 17.16. MS (MALDI) *m/z*: 650-657 [(L^{16})ZnCl]$^+$. IR: 1656, 1628, 1593 cm^{-1} ($\nu_{C=N}$, $\nu_{C=C(Ar)}$).

[(L^1)ZnCl][BAr^F_4]: In a typical procedure, THF (20 cm^3) was added to a solid mixture of **L^1** (0.247 g, 0.000501 mol), $ZnCl_2$ (0.069 g, 0.000507 mol) and $NaBAr^F_4$ (0.443 g, 0.000500 mol), forming a yellow solution. This was stirred at room temperature for approximately 1 hour, after which time the THF was removed under vacuum. The orange coloured residue was digested with DCM (15 cm^3), and the resultant bright-yellow solution was filtered through celite under N_2. The celite pad was washed with DCM (2 × 15 cm^3) and the filtrate was reduced in volume under vacuum to ~4 cm^3. Layering of this solution with hexane (10 cm^3) caused the rapid formation of colourless crystals which were collected by filtration in air and washed with a large amount of hexane. Yield: 0.382 g, 52%; mp: 179-182°C. ^{1}H NMR (500 MHz, $CDCl_3$): δ 1.08 (18H, br d, CH(C*H*$_3$)$_2$), 2.26 (9H, s, C*H*$_3$C=N), 2.44 (3H, septet, $^3J_{HH}$ = 6.6 Hz, C*H*(CH$_3$)$_2$), 5.41 (1H, s, α-C*H*), 6.44 (3H, d, $^3J_{HH}$ = 7.9 Hz, *o*-C*H*), 7.27 (3H, t, $^3J_{HH}$ = 7.0 Hz, *p*-C*H*), 7.36-7.43 (6H, non-first-order m, *m*- and *m'*-C*H*), 7.44 (4H, s, BAr^F_4 *p*-C*H*), 7.61 (8H, s, BAr^F_4 *o*-C*H*). ^{19}F NMR (376 MHz, $CDCl_3$): δ -62.15 (s, BAr^F_4 C*F*$_3$). Elemental analysis, calculated for $C_{66}H_{55}N_3ClF_{24}ZnB$ (%): C, 54.38; H, 3.80; N, 2.88; Zn, 4.48; Cl, 2.43. Found: C, 53.33; H, 3.74; N, 2.74; Zn, 4.29; Cl, 4.18. MS (MALDI) *m/z*: 592-599 [(L^1)ZnCl]$^+$. IR: 1659, 1629, 1609, 1577 cm^{-1} ($\nu_{C=N}$, $\nu_{C=C(Ar)}$).

[(L^5)ZnCl][BAr^F_4]: **L^5** (0.268 g, 0.000501 mol), $ZnCl_2$ (0.072 g, 0.000529 mol) and $NaBAr^F_4$ (0.447 g, 0.000505 mol) were used; colourless crystals (0.486 g, 65%). ^{1}H NMR (400 MHz, $CDCl_3$): δ 1.02 (6H, d, $^3J_{HH}$ = 6.9 Hz, Ar^{iPr} CH(C*H*$_3$)$_2$), 1.10 (12H, d, $^3J_{HH}$ = 6.9 Hz, Ar^{iPr2} CH(C*H*$_3$)$_2$), 1.13 (6h, d, $^3J_{HH}$ = 6.9 Hz, Ar^{iPr} CH(C*H*$_3$)$_2$), 2.05 (3H, s, C*H*$_3$C=N), 2.28 (6H, s, C*H*$_3$C=N), 2.62 (2H, septet, $^3J_{HH}$ = 6.9 Hz, Ar^{iPr} C*H*(CH$_3$)$_2$), 2.79 (2H, septet, $^3J_{HH}$ = 6.9 Hz, Ar^{iPr2} C*H*(CH$_3$)$_2$), 5.23 (1H, s, α-C*H*), 6.76 (2H, br d, Ar^{iPr} *o*-C*H*), 7.13-7.41 (9H, non-first-order m, other aromatic C*H*), 7.44 (4H, s, BAr^F_4 *p*-C*H*), 7.62 (8H, s, BAr^F_4 *o*-C*H*). ^{19}F NMR (376 MHz, $CDCl_3$): δ -62.24 (s, BAr^F_4 C*F*$_3$). Elemental analysis, calculated for $C_{69}H_{61}N_3ZnClF_{24}B$ (%): C, 55.26; H, 4.10; N, 2.80; Zn, 4.36; Cl, 2.36. Found: C, 54.10; H, 3.90; N, 2.67; Zn, 4.02; Cl, 4.04. MS (MALDI) *m/z*: 634-641 [(L^5)ZnCl]$^+$. IR: 1663, 1636, 1610, 1559, 1514 cm^{-1} ($\nu_{C=N}$, $\nu_{C=C(Ar)}$).

[(L^8)ZnCl][BAr^F_4]: **L^8** (0.265 g, 0.000507 mol), $ZnCl_2$ (0.069 g, 0.000507 mol) and $NaBAr^F_4$ (0.446 g, 0.000503 mol) were used; colourless crystals (0.394 g, 53%). ^{1}H NMR (400 MHz, $CDCl_3$): δ 1.09 (3H, d, $^3J_{HH}$ = 7.0 Hz, CH(C*H*$_3$)$_2$), 1.13 (3H, br d, CH(C*H*$_3$)$_2$), 1.16 (3H, d, $^3J_{HH}$ = 6.8 Hz, CH(C*H*$_3$)$_2$), 1.22 (3H, d, $^3J_{HH}$ = 6.8 Hz, CH(C*H*$_3$)$_2$), 1.26 (9H, s, C(C*H*$_3$)$_3$), 2.35 (6H, s, C*H*$_3$C=N), 2.44 (1H, poorly defined septet, C*H*(CH$_3$)$_2$), 2.55 (1H, septet, $^3J_{HH}$ = 6.8 Hz, C*H*(CH$_3$)$_2$), 3.71 (3H, s, OC*H*$_3$), 5.77 (1H, s, α-C*H*), 6.53, 6.65 (2H, 2 × br d, *o*-C*H*), 6.73 (1H, dd, $^3J_{HH}$ = 7.8 Hz, $^4J_{HH}$ = 1.4 Hz, *o*-C*H*), 7.03 (1H, br d, Ar^{OMe} *m'*-C*H*), 7.09 (1H, td, $^3J_{HH}$ = 7.7 Hz, Ar^{OMe} *p*-C*H*), 7.30-7.52 (7H, non-first-order m, other aromatic C*H*), 7.54 (4H, s, BAr^F_4 *p*-C*H*), 7.71 (8H, s, BAr^F_4 *o*-C*H*). ^{19}F NMR (376 MHz, $CDCl_3$): δ: -62.22 (s, BAr^F_4 C*F*$_3$). Elemental analysis, calculated for $C_{67}H_{57}N_3OZnClF_{24}B$ (%): C, 54.09; H, 3.86; N, 2.82; Zn, 4.39; Cl, 2.38. Found: C, 53.63; H, 3.89; N, 2.68; Zn, 4.08; Cl, 2.34. MS (MALDI) *m/z*: 622-629 [(L^8)ZnCl]$^+$. IR: 1661, 1639, 1625, 1593, 1577 cm^{-1} ($\nu_{C=N}$, $\nu_{C=C(Ar)}$).

[(L^{10})ZnCl][BAr^F_4]: **L^{10}** (0.267 g, 0.000497 mol), $ZnCl_2$ (0.069 g, 0.000507 mol) and $NaBAr^F_4$ (0.472 g, 0.000532 mol) were used; colourless crystals (0.417 g, 57%). ^{1}H NMR (400 MHz, $CDCl_3$): δ 1.11-1.17 (9H, 3 overlapping d, CH(C*H*$_3$)$_2$), 1.20 (3H, d, $^3J_{HH}$ = 6.8 Hz, CH(C*H*$_3$)$_2$), 1.23 (9H, s, C(C*H*$_3$)$_3$), 1.25-1.31 (6H, 2 overlapping d, CH(C*H*$_3$)$_2$), 2.39 (3H, s, C*H*$_3$C=N), 2.43 (3H, s, C*H*$_3$C=N), 2.48 (1H, septet, $^3J_{HH}$ = 6.9 Hz, C*H*(CH$_3$)$_2$), 2.54 (1H, septet, $^3J_{HH}$ = 6.8 Hz, C*H*(CH$_3$)$_2$), 2.63 (1H, septet, $^3J_{HH}$ = 6.9 Hz, C*H*(CH$_3$)$_2$), 5.84 (1H, s, α-C*H*), 6.53 (1H, d, $^3J_{HH}$ = 8.0 Hz, *o*-C*H*), 6.56 (1H, d, $^3J_{HH}$ = 7.9 Hz, *o*-C*H*), 6.60 (1H, d, $^3J_{HH}$ = 7.9 Hz, *o*-C*H*), 7.24-7.53 (9H, non-first-order m, other aromatic C*H*), 7.54 (4H, s, BAr^F_4 *p*-C*H*), 7.71 (8H, s, BAr^F_4 *o*-C*H*). ^{19}F NMR (376 MHz, $CDCl_3$): δ -62.20 (s, BAr^F_4 C*F*$_3$). Elemental analysis, calculated for $C_{69}H_{61}N_3ZnClF_{24}B$ (%): C, 55.26; H, 4.10; N, 2.80; Zn, 4.36; Cl, 2.36. Found: C, 54.79; H, 4.17; N, 2.63; Zn, 3.95; Cl, 2.77. MS MALDI) *m/z*: 634-641 [(L^{10})ZnCl]$^+$. IR: 1651, 1627, 1610, 1575 cm^{-1} ($\nu_{C=N}$, $\nu_{C=C(Ar)}$).

[(L^{11})ZnCl][BAr^F_4]: **L^{11}** (0.289 g, 0.000501 mol), $ZnCl_2$ (0.070 g, 0.000515 mol) and $NaBAr^F_4$ (0.481 g, 0.000542 mol) were used; colourless crystals (0.575 g, 74%). ^{1}H NMR (400 MHz, $CDCl_3$): δ 0.71 (6H, d, $^3J_{HH}$ = 6.7 Hz, CH(C*H*$_3$)$_2$), 1.04 (6H, d, $^3J_{HH}$ = 6.7 Hz, CH(C*H*$_3$)$_2$), 1.09 (9H, s, C(C*H*$_3$)$_3$), 1.22 (6H, d, $^3J_{HH}$ = 6.9 Hz, CH(C*H*$_3$)$_2$), 1.39 (6H, d, $^3J_{HH}$ = 6.7 Hz, CH(C*H*$_3$)$_2$), 2.20 (2H, septet, $^3J_{HH}$ = 6.9 Hz, C*H*(CH$_3$)$_2$), 2.41 (6H, s, C*H*$_3$C=N), 2.85 (2H, septet, $^3J_{HH}$ = 6.7 Hz, C*H*(CH$_3$)$_2$), 5.81 (1H, s, α-C*H*), 6.40 (2H, dd, $^3J_{HH}$ = 7.9 Hz, $^4J_{HH}$ = 1.0 Hz, Ar^{iPr} *o*-C*H*), 7.05 (2H, d, $^3J_{HH}$ = 7.7 Hz, Ar^{iPr2} *m*-C*H*), 7.20-

7.50 (7H, non-first-order m, other aromatic C*H*), 7.44 (4H, s, BAr^F_4 *p*-C*H*), 7.61 (8H, s, BAr^F_4 *o*-C*H*). ^{19}F NMR (376 MHz, $CDCl_3$): δ -62.19 (s, BAr^F_4 CF_3). Elemental analysis, calculated for $C_{72}H_{67}N_3ZnClF_{24}B$ (%): C, 56.08; H, 4.38; N, 2.73; Zn, 4.24; Cl, 2.30. Found: C, 55.97; H, 4.36; N, 2.63; Zn, 3.94; Cl, 2.26. MS (MALDI) *m/z*: 674-681 $[(L^{11})ZnCl]^+$. IR: 1643, 1610 ($\nu_{C=N}$, $\nu_{C=C(Ar)}$).

[(L^{12})ZnCl][BAr^F_4]: **L^{12}** (0.268 g, 0.000501 mol), $ZnCl_2$ (0.069 g, 0.000507 mol) and $NaBAr^F_4$ (0.447 g, 0.000505 mol) were used; colourless crystals (0.585 g, 78%). ^{1}H NMR (400 MHz, $CDCl_3$): δ 1.10 (3H, d, $^3J_{HH}$ = 6.9 Hz, CH(CH_3)$_2$), 1.13 (3H, d, $^3J_{HH}$ = 6.9 Hz, CH(CH_3)$_2$), 1.14 (3H, d, $^3J_{HH}$ = 6.8 Hz, CH(CH_3)$_2$), 1.18 (9H, s, C(CH_3)$_3$), 1.31 (3H, d, $^3J_{HH}$ = 6.8 Hz, CH(CH_3)$_2$), 2.00 (3H, s, Mes-CH_3), 2.12 (3H, s, Mes-CH_3), 2.31 (3H, s, Mes-CH_3), 2.41 (3H, s, CH_3C=N), 2.44 (3H, s, CH_3C=N), 2.50 (1H, septet, $^3J_{HH}$ = 6.9 Hz, C*H*(CH$_3$)$_2$), 2.67 (1H, septet, $^3J_{HH}$ = 6.8 Hz, C*H*(CH$_3$)$_2$), 5.82 (1H, s, α-C*H*), 6.53 (1H, dd, $^3J_{HH}$ = 7.9 Hz, $^4J_{HH}$ = 1.1 Hz, Ar^{iPr} *o*-C*H*), 6.54 (1H, dd, $^3J_{HH}$ = 7.9 Hz, $^4J_{HH}$ = 1.1 Hz, Ar^{iPr} *o*-C*H*), 6.90 (1H, br s, Mes-C*H*), 6.96 (1H, br s, Mes-C*H*), 7.29-7.36 (2H, non-first-order m, Ar^{iPr} *p*-C*H*), 7.42-7.55 (4H, non-first-order m, Ar^{iPr} *m*- and *m'*-C*H*), 7.54 (4H, s, BAr^F_4 *p*-C*H*), 7.71 (8H, s, BAr^F_4 *o*-C*H*). ^{19}F NMR (376 MHz, $CDCl_3$): δ -62.21 (s, BAr^F_4 CF_3). Elemental analysis, calculated for $C_{69}H_{61}N_3ZnClF_{24}B$ (%): C, 55.26; H, 4.10; N, 2.80; Zn, 4.36; Cl, 2.36. Found: C, 55.37; H, 4.05; N, 2.76; Zn, 4.33; Cl, 2.70. MS (MALDI) *m/z*: 634-641 $[(L^{12})ZnCl]^+$. IR: 1647, 1612 cm^{-1} ($\nu_{C=N}$, $\nu_{C=C(Ar)}$).

[(η^4-L^{16})ZnCl][BAr^F_4]: **L^{16}** (0.236 g, 0.000427 mol), $ZnCl_2$ (0.058 g, 0.000426 mol) and $NaBAr^F_4$ (0.378 g, 0.000427 mol) were used; colourless crystals (0.432 g, 67%). Crystals suitable for X-ray diffraction were obtained by vapour diffusion of hexane into a saturated 1,2-difluorobenzene solution of **[(η^4-L^{16})ZnCl][BAr^F_4]**. ^{1}H NMR (400 MHz, $CDCl_3$): δ 1.05 (3H, br d, CH(CH_3)$_2$), 1.11 (6H, d, $^3J_{HH}$ = 6.8 Hz, CH(CH_3)$_2$), 1.18 (3H, br d, CH(CH_3)$_2$), 1.24 (9H, br s, C(CH_3)$_3$), 2.25 (1H, poorly defined septet, C*H*(CH$_3$)$_2$), 2.29 (6H, s, CH_3C=N), 2.40 (1H, poorly defined septet, C*H*(CH$_3$)$_2$), 3.53 (3H, br s, OCH_3), 3.64 (3H, br s, OCH_3), 5.70 (1H, br s, α-C*H*), 6.71-7.48 (11H, non-first-order m, aromatic C*H*), 7.54 (4H, s, BAr^F_4 *p*-C*H*), 7.72 (8H, s, BAr^F_4 *o*-C*H*); peaks at 2.45 (br s, CH_3C=N) and 3.34, 3.91 (2 × v br s, OCH_3) indicate the presence of a minor isomeric component in solution (~20%), but due to the broadened nature of the spectrum as a whole it was not possible to identify any other peaks due to this isomer. ^{19}F NMR (376 MHz, $CDCl_3$): δ -62.27 (s, BAr^F_4 CF_3). Elemental analysis, calculated for $C_{68}H_{59}N_3O_2ZnClF_{24}B$ (%): C,

53.81; H, 3.92; N, 2.77; Zn, 4.31; Cl, 2.34. Found: C, 53.42; H, 3.81; N, 2.71; Zn, 4.14; Cl, 2.40. MS (MALDI) *m/z*: 652-659 $[(L^{16})ZnCl]^+$. IR: 1660, 1639, 1632, 1612, 1594 cm^{-1} ($\nu_{C=N}$, $\nu_{C=C(Ar)}$).

[(L^1)ZnCl][OTf]: In a typical procedure, THF (20 cm^3) was added to a solid mixture of $\mathbf{L^1}$ (0.493 g, 0.001 mol), $ZnCl_2$ (0.137 g, 0.00101 mol) and AgOTf (0.257 g, 0.001 mol) in a foil-wrapped Schlenk tube, forming a yellow solution. This was stirred at room temperature for approximately 1 hour, after which time the THF was removed under vacuum. The orange coloured residue was digested with DCM (40 cm^3), and the resultant cloudy bright-yellow solution was filtered through celite under N_2. The celite pad was washed with DCM (2 × 20 cm^3), and the volume of the filtrate was reduced under vacuum to ~8 cm^3. Layering of this solution with Et_2O caused slow formation of colourless crystals, which were collected by filtration in air and washed with excess Et_2O. Yield: 0.307 g, 41%. ^{1}H NMR (400 MHz, $CDCl_3$): δ 1.09 (18H, br d, $CH(CH_3)_2$), 2.57 (3H, septet, $^3J_{HH}$ = 6.7 Hz, $CH(CH_3)_2$), 2.62 (9H, s, CH_3C=N), 6.58 (3H, d, $^3J_{HH}$ = 7.9 Hz, *o*-C*H*), 6.80 (1H, s, α-C*H*), 7.21 (3H, td, $^3J_{HH}$ = 7.7 Hz, $^4J_{HH}$ = 1.5 Hz, *p*-C*H*), 7.29 (3H, td, $^3J_{HH}$ = 7.3 Hz, $^4J_{HH}$ = 1.0 Hz, *m*-C*H*), 7.35 (3H, dd, $^3J_{HH}$ = 7.9 Hz, $^4J_{HH}$ = 1.3 Hz, *m'*-C*H*). ^{19}F NMR (376 MHz, $CDCl_3$): δ -78.32 (s, O_3SCF_3). Elemental analysis, calculated for $C_{35}H_{43}N_3O_3ZnClSF_3$ (%): C, 56.54; H, 5.83; N, 5.65; Zn, 8.79; Cl, 4.77. Found: C, 54.85; H, 5.86; N, 5.34; Zn, 8.27; Cl, 4.04. MS (MALDI) *m/z*: 592-599 $[(L^1)ZnCl]^+$. IR: 1664, 1633, 1598, 1577, 1557, 1534 cm^{-1} ($\nu_{C=N}$, $\nu_{C=C(Ar)}$).

[(L^3)ZnCl][OTf]: $\mathbf{L^3}$ (0.254 g, 0.000501 mol), $ZnCl_2$ (0.071 g, 0.000522 mol) and AgOTf (0.127 g, 0.000494 mol) were used; white powder obtained by rapid precipitation with Et_2O (0.226 g, 60%). ^{1}H NMR (400 MHz, $CDCl_3$): δ 0.98-1.28 (12H, non-first-order m, $CH(CH_3)_2$), 1.21 (9H, s, $C(CH_3)_3$), 2.50-2.76 (11H, non-first-order m, CH_3C=N and $CH(CH_3)_2$), 6.43 (1H, d, $^3J_{HH}$ = 7.6 Hz, Ar^{tBu} *o*-C*H*), 6.63 (2H, v br m, Ar^{iPr} *o*-C*H*), 6.79 (1H, s, α-C*H*), 7.07-7.41 (8H, non-first order m, Ar^{iPr} *m*-, *p*- and *m'*-C*H*, Ar^{tBu} *m*- and *p*-C*H*), 7.47 (1H, d, $^3J_{HH}$ = 7.8 Hz, Ar^{tBu} *m'*-C*H*). Elemental analysis, calculated for $C_{36}H_{45}N_3O_3ZnClSF_3$ (%): C, 57.07; H, 5.99; N, 5.55; Zn, 8.63; Cl, 4.68. Found: C, 55.36; H, 5.93; N, 5.30; Zn, 8.53; Cl, 4.36. MS (MALDI) *m/z*: 606-612 $[(L^3)ZnCl]^+$. IR: 1662, 1635, 1625, 1598, 1577, 1560, 1530 cm^{-1} ($\nu_{C=N}$, $\nu_{C=C(Ar)}$).

[(L^8)ZnCl][OTf]: $\mathbf{L^8}$ (0.266 g, 0.000509 mol), $ZnCl_2$ (0.079 g, 0.000581 mol) and AgOTf (0.129 g, 0.000502 mol) were used; colourless crystals (0.264 g, 68%). ^{1}H NMR (400

MHz, $CDCl_3$): δ 1.01 (3H, d, $^3J_{HH}$ = 6.8 Hz, CH(CH_3)$_2$), 1.04 (3H, d, $^3J_{HH}$ = 6.7 Hz, CH(CH_3)$_2$), 1.09 (3H, d, $^3J_{HH}$ = 6.8 Hz, CH(CH_3)$_2$), 1.14 (3H, d, $^3J_{HH}$ = 6.7 Hz, CH(CH_3)$_2$), 1.36 (9H, s, C(CH_3)$_3$), 2.44 (1H, septet, $^3J_{HH}$ = 6.8 Hz, CH(CH$_3$)$_2$), 2.56 (1H, septet, $^3J_{HH}$ = 6.8 Hz, CH(CH$_3$)$_2$), 2.61 (6H, s, CH_3C=N), 3.65 (3H, s, OCH_3), 6.58 (1H, d, $^3J_{HH}$ = 7.8 Hz, *o*-C*H*), 6.61 (1H, d, $^3J_{HH}$ = 7.8 Hz, *o*-C*H*), 6.66 (1H, dd, $^3J_{HH}$ = 7.8 Hz, $^4J_{HH}$ = 1.3 Hz, *o*-C*H*), 6.76 (1H, s, α-C*H*), 6.91 (1H, br d, Ar^{OMe} *m'*-C*H*), 6.96 (1H, td, $^3J_{HH}$ = 7.7 Hz, $^4J_{HH}$ = 1.0 Hz, Ar^{OMe} *p*-C*H*), 7.19-7.34 (6H, non-first-order m, Ar^{iPr} *m*-, *p*- and 1 × *m'*-C*H*, Ar^{OMe} *m*-C*H*), 7.37 (1H, dd, $^3J_{HH}$ = 7.9 Hz, $^4J_{HH}$ = 1.2 Hz, 1 × Ar^{iPr} *m'*-C*H*). ^{19}F NMR (376 MHz, $CDCl_3$): δ -78.25 (s, O_3SCF_3). Elemental analysis, calculated for $C_{36}H_{45}N_3O_4ZnClSF_3$ (%): C, 55.89; H, 5.86; N, 5.43; Zn, 8.45; Cl, 4.58. Found: C, 54,89; H, 5.90; N, 5.30; Zn, 8.68; Cl, 4.60. MS (MALDI) *m/z*: 622-629 [(L^8)ZnCl]$^+$. IR: 1661, 1639, 1625, 1594, 1577 cm^{-1} ($\nu_{C=N}$, $\nu_{C=C(Ar)}$).

[(L^{10})ZnCl][OTf]: **L^{10}** (0.537 g, 0.001 mol), $ZnCl_2$ (0.136 g, 0.001 mol) and AgOTf (0.258 g, 0.001 mol) were used; white powder obtained by rapid precipitation with Et_2O (0.466 g, 59%). Crystals suitable for X-ray diffraction were obtained by vapour diffusion of Et_2O into a saturated DCM solution of **[(L^{10})ZnCl][OTf]**. ^{1}H NMR (400 MHz, $CDCl_3$): δ 1.04-1.12 (12H, 4 × overlapping d, CH(CH_3)$_2$), 1.16 (3H, d, $^3J_{HH}$ = 6.7 Hz, CH(CH_3)$_2$), 1.21 (3H, d, $^3J_{HH}$ = 6.9 Hz, CH(CH_3)$_2$), 1.34 (9H, s, C(CH_3)$_3$), 2.50 (1H, septet, $^3J_{HH}$ = 6.8 Hz, CH(CH$_3$)$_2$), 2.55 (1H, septet, $^3J_{HH}$ = 6.8 Hz, CH(CH$_3$)$_2$), 2.61 (1H, septet, $^3J_{HH}$ = 6.8 Hz, CH(CH$_3$)$_2$), 2.69 (6H, 2 × s, CH_3C=N), 6.49 (1H, d, $^3J_{HH}$ = 8.0 Hz, *o*-C*H*), 6.55 (1H, $^3J_{HH}$ = 7.9 Hz, *o*-C*H*), 6.61 (1H, dd, $^3J_{HH}$ = 7.9 Hz, $^4J_{HH}$ = 1.0 Hz, *o*-C*H*), 6.85 (1H, s, α-C*H*), 7.12-7.39 (9H, non-first-order m, *m*-, *p*- and *m'*-C*H*). ^{19}F NMR (376 MHz, $CDCl_3$): δ -78.23 (s, O_3SCF_3). Elemental analysis, calculated for $C_{38}H_{49}N_3O_3ZnClSF_3$ (%): C, 58.09; H, 6.29; N, 5.35; Zn, 8.32; Cl, 4.51. Found: C, 57.59; H, 6.28; N, 5.25; Zn, 8.50; Cl, 5.09. MS (MALDI) *m/z*: 635-642 [(L^{10})ZnCl]$^+$. IR: 1654, 1632, 1620, 1597, 1575 cm^{-1} ($\nu_{C=N}$, $\nu_{C=C(Ar)}$).

[(L^{11})ZnCl][OTf]: **L^{11}** (0.578 g, 0.001 mol), $ZnCl_2$ (0.134 g, 0.000985 mol) and AgOTf (0.259 g, 0.00101 mol) were used; colourless crystals (0.649 g, 80%). ^{1}H NMR (400 MHz, $CDCl_3$): δ 0.75 (6H, d, $^3J_{HH}$ = 6.7 Hz, CH(CH_3)$_2$), 1.07 (6H, d, $^3J_{HH}$ = 6.9 Hz, CH(CH_3)$_2$), 1.24 (6H, d, $^3J_{HH}$ = 6.8 Hz, CH(CH_3)$_2$), 1.29 (9H, s, C(CH_3)$_3$), 1.36 (6H, $^3J_{HH}$ = 6.8 Hz, CH(CH_3)$_2$), 2.33 (2H, septet, $^3J_{HH}$ = 6.7 Hz, CH(CH$_3$)$_2$), 2.77 (6H, s, CH_3C=N), 2.87 (2H, septet, $^3J_{HH}$ = 6.9 Hz, CH(CH$_3$)$_2$), 6.49 (2H, dd, $^3J_{HH}$ = 8.0 Hz, $^4J_{HH}$ = 1.1 Hz, Ar^{iPr} *o*-C*H*),

6.97 (1H, s, α-C*H*), 7.02 (2H, d, $^{3}J_{HH}$ = 7.8 Hz, Ar^{iPr2} *m*-C*H*), 7.15-7.24 (3H, non-first-order m, Ar^{iPr} *p*-C*H* and Ar^{iPr2} *p*-C*H*), 7.32-7.38 (2H, non-first-order m, Ar^{iPr} *m*-C*H*), 7.43 (2H, dd, $^{3}J_{HH}$ = 8.0 Hz, $^{4}J_{HH}$ = 1.4 Hz, Ar^{iPr} *m'*-C*H*). ^{19}F NMR (376 MHz, $CDCl_3$): δ -78.21 (s, O_3SCF_3). Elemental analysis, calculated for $C_{41}H_{55}N_3O_3ZnClSF_3$ (%): C, 59.49; H, 6.70; N, 5.08; Zn, 7.90; Cl, 4.38. Found: C, 59.39; H, 6.69; N, 5.03; Zn, 7.93; Cl, 4.47. MS (MALDI) *m/z*: 676-683 $[(L^{11})ZnCl]^+$. IR: 1637, 1614, 1593, 1580 cm^{-1} ($\nu_{C=N}$, $\nu_{C=C(Ar)}$).

[(L^{12})ZnCl][OTf]: **L^{12}** (0.535 g, 0.001 mol), $ZnCl_2$ (0.137 g, 0.00102 mol) and AgOTf (0.252 g, 0.000981 mol) were used; colourless crystals (0.559 g, 73%). ^{1}H NMR (400 MHz, $CDCl_3$): δ 1.11 (3H, d, $^{3}J_{HH}$ = 6.9 Hz, CH(CH_3)$_2$), 1.14 (3H, d, $^{3}J_{HH}$ = 6.8 Hz, CH(CH_3)$_2$), 1.15 (3H, d, $^{3}J_{HH}$ = 6.8 Hz, CH(CH_3)$_2$), 1.30 (3H, d, $^{3}J_{HH}$ = 6.8 Hz, CH(CH_3)$_2$), 1.38 (9H, s, C(CH_3)$_3$), 2.04 (3H, s, Mes-CH_3), 2.14 (3H, s, Mes-CH_3), 2.29 (3H, s, Mes-CH_3), 2.57 (1H, septet, $^{3}J_{HH}$ = 6.8 Hz, C*H*(CH$_3$)$_2$), 2.74 (1H, septet, $^{3}J_{HH}$ = 6.8 Hz, C*H*(CH$_3$)$_2$), 2.78 (3H, s, CH_3C=N), 2.80 (3H, s, CH_3C=N), 6.60 (1H, dd, $^{3}J_{HH}$ = 7.9 Hz, $^{4}J_{HH}$ = 1.0 Hz, Ar^{iPr} *o*-C*H*), 6.68 (1H, dd, $^{3}J_{HH}$ = 8.0 Hz, $^{4}J_{HH}$ = 1.0 Hz, Ar^{iPr} *o*-C*H*), 6.87 (1H, br s, Mes-C*H*), 6.92 (1H, br s, Mes-C*H*), 6.95 (1H, s, α-C*H*), 7.24-7.52 (6H, non-first-order m, Ar^{iPr} *m*-, *p*- and *m'*-C*H*). ^{19}F NMR (376 MHz, $CDCl_3$): -78.23 (s, O_3SCF_3). Elemental analysis, calculated for $C_{38}H_{49}N_3O_3ZnClSF_3$ (%): C, 58.09; H, 6.29; N, 5.35; Zn, 8.32; Cl, 4.51. Found: C, 58.18; H, 6.42; N, 5.27; Zn, 8.27; Cl, 4.64. MS (MALDI) *m/z*: 634-641 $[(L^{12})ZnCl]^+$. IR: 1652, 1630, 1614, 1580 cm^{-1} ($\nu_{C=N}$, $\nu_{C=C(Ar)}$).

[(L^{16})ZnCl][OTf]: **L^{16}** (0.522 g, 0.000998 mol), $ZnCl_2$ (0.134 g, 0.000985 mol) and AgOTf (0.254 g, 0.000988 mol) were used; white powder obtained by rapid precipitation with Et_2O (0.222 g, 28%). ^{1}H NMR (400 MHz, $CDCl_3$), peaks due major isomeric component (~80%): δ 0.87 (3H, d, $^{3}J_{HH}$ = 6.8 Hz, CH(CH_3)$_2$), 1.07 (3H, d, $^{3}J_{HH}$ = 6.8 Hz, CH(CH_3)$_2$), 1.10 (3H, $^{3}J_{HH}$ = 6.9 Hz, CH(CH_3)$_2$), 1.18 (3H, $^{3}J_{HH}$ = 6.8 Hz, CH(CH_3)$_2$), 1.30 (9H, s, C(CH_3)$_3$), 2.28 (1H, septet, $^{3}J_{HH}$ = 6.8 Hz, C*H*(CH$_3$)$_2$), 2.41 (1H, septet, $^{3}J_{HH}$ = 6.8 Hz, C*H*(CH$_3$)$_2$), 2.46 (3H, s, CH_3C=N), 2.74 (3H, s, CH_3C=N), 3.49 (3H, s, OCH_3), 3.52 (3H, s, OCH_3), 6.69 (1H, s, α-C*H*); peaks due to minor isomeric component: 0.83 (3H, d, $^{3}J_{HH}$ = 6.8 Hz, CH(CH_3)$_2$), 1.02-1.12 (6H, 2 × d, overlapped with peaks due to major isomer, CH(CH_3)$_2$), 1.22 (3H, d, $^{3}J_{HH}$ = 6.8 Hz, CH(CH_3)$_2$), 1.34 (9H, s, C(CH_3)$_3$), 2.20 (1H, poorly defined septet, C*H*(CH$_3$)$_2$), 2.58 (1H, poorly defined septet, C*H*(CH$_3$)$_2$), 2.47 (3H, s, CH_3C=N), 2.73 (3H, s, CH_3C=N), 3.23 (3H, s, OCH_3), 3.81 (3H, s, OCH_3), 6.71 (1H, s, α-C*H*); peaks due to both isomers: 6.77-6.89 (2H, non-first-order m, Ar^{OMe} *o*-

C*H*), 6.90-7.33 (9H, non-first-order m, other aromatic C*H*). ^{19}F NMR (376 MHz, $CDCl_3$): δ -78.19 (s, O_3SCF_3). Elemental analysis, calculated for $C_{37}H_{47}N_3O_5ZnClSF_3$ (%): C, 55.40; H, 5.89; N, 5.23; Zn, 8.14; Cl, 4.41. Found: C, 54.68; H, 5.99; N, 5.07; Zn, 7.62; Cl, 4.77. MS (MALDI) *m/z*: 652-659 $[(L^{16})ZnCl]^+$. IR: 1659, 1631, 1621, 1593 cm^{-1} ($\nu_{C=N}$, $\nu_{C=C(Ar)}$).

$[(L^1)Zn\{OCH(CF_3)_2\}][BAr^F_4]$: DCM (6 cm^3) was added to a solid mixture of **$[(L^1)ZnCl][BAr^F_4]$** (0.290 g, 0.000193 mol) and $NaOCH(CF_3)_2$ (0.043 g, 0.000226 mol), forming a cloudy, colourless mixture. This was stirred at room temperature for 2 hours, after which time a bright-yellow colouration had developed. The mixture was then filtered through celite, and the celite pad was washed with DCM (3 × 6 cm^3). The clear yellow filtrate was reduced in volume under vacuum to ~2 cm^3, and layered with hexane (12 cm^3). A white solid precipitated rapidly, which was collected by filtration under N_2, washed with excess hexane, dried under vacuum and stored in the glovebox. Yield: 0.181 g, 57%. ^{1}H NMR (400 MHz, CD_2Cl_2), peaks due to major isomeric species only: δ 0.47-1.33 (18H, m, $CH(CH_3)_2$), 1.94 (9H, s CH_3C=N), 2.09 (3H, poorly defined septet, $CH(CH_3)_2$), 5.05 (1H, 2 × s, α-C*H*), 6.10 (3H, br d, *o*-C*H*), 7.19-7.45 (9H, non-first-order m, *p*-, *m*- and *m'*-C*H*), 7.47 (4H, s, BAr^F_4 *p*-C*H*), 7.63 (8H, m, BAr^F_4 *p*-C*H*). ^{19}F NMR (376 MHz, CD_2Cl_2): δ -62.80 (s, BAr^F_4 CF_3). Elemental analysis, calculated for $C_{69}H_{56}N_3OZnF_{30}B$ (%): C, 52.14; H, 3.55; N, 2.64; Zn, 4.11. Found: C, 52.37; H, 3.48; N, 2.64; Zn, 4.06; Cl, 0.0. MS (MALDI) *m/z*: 782-788 $[(L^1)Zn\{OCH(CF_3)_2\} + KF]^+$. IR: 1670, 1636, 1610 cm^{-1} ($\nu_{C=N}$, $\nu_{C=C(Ar)}$).

6.9 Synthesis of β-Triketimine Thallium Complexes

$[(L^1)Tl][BAr^F_4]$: In a typical procedure, **$[(L^1)ZnCl][BAr^F_4]$** (0.100 g, 0.0000687 mol) was dissolved in DCM (10 cm^3), forming a clear, colourless solution. To this was then added TlOEt (0.32 cm^3 of a 0.21M solution in DCM, 0.0000672 mol), causing the instantaneous formation of a dense, white precipitate. The resulting mixture was stirred at room temperature overnight, then filtered through celite under N_2. The celite pad was washed with DCM (2 × 10 cm^3), and the volume of the filtrate was reduced to ~5 cm^3 under vacuum. Layering of this solution with hexane (10 cm^3) caused the slow formation of large, block-shaped crystals, which were collected by filtration in air and washed with a

large amount of hexane. Yield: 0.030 g, 29%. Elemental analysis, calculated for $C_{66}H_{55}N_3TlF_{24}B$ (%): C, 50.77; H, 3.55; N, 2.69. Found: C, 51.17; H, 3.75; N, 2.56. MS (MALDI) *m/z*: 696-699 $[(L^1)Tl]^+$.

$[(L^8)Tl][BAr^F{}_4]$: **$[(L^8)ZnCl][BAr^F{}_4]$** (0.112 g, 0.0000753 mol) and TlOEt (0.36 cm^3, 0.0000756 mol) were used; small colourless crystals (0.071 g, 59%). Elemental analysis, calculated for $C_{67}H_{57}N_3OTlF_{24}B$ (%): C, 50.56; H, 3.61; N, 2.64. Found: C, 50.47; H, 3.50; N, 2.58. MS (MALDI) *m/z*: 726-730 $[(L^8)Tl]^+$. IR: 1670, 1649, 1610, 1596, 1573 cm^{-1} ($\nu_{C=N}$, $\nu_{C=C(Ar)}$).

6.10 Synthesis of β-Triketimine Nickel Complexes

$[(L^8)NiBr]_2[NiBr_4]$: DCM (15 cm^3) was added to a mixture of **L^8** (0.261 g, 0.000499 mol) and $NiBr_2$(DME) (0.227 g, 0.000737 mol), forming a dark red-brown coloured solution which became light brown-yellow after a few minutes stirring. Stirring was continued for 3 days, after which time the solution was filtered through celite under N_2. The celite pad was washed with DCM (3 × 10 cm^3), and the filtrate was reduced in volume under vacuum to ~5 cm^3. The solution was layered with hexane (10 cm^3), causing red-brown crystals to form rapidly. The product was collected by filtration in air, and washed with hexane. Yield: 0.359 g, 86%. Elemental analysis, calculated for $C_{70}H_{90}N_6O_2Br_6Ni_3$ (%): C, 49.38; H, 5.33; N, 4.93, Ni, 10.34; Br, 28.15. Found: C, 49.05; H, 5.34; N, 5.05; Ni, 10.05; Br, 27.88. MS (MALDI) *m/z*: 660-667 $[(L^8)NiBr]^+$. IR: 1654, 1635, 1625, 1589 cm^{-1} ($\nu_{C=N}$, $\nu_{C=C(Ar)}$).

$[(L^{10})NiBr]_2[NiBr_4]$: **L^{10}** (0.267 g, 0.000499 mol) and $NiBr_2$(DME) (0.241 g, 0.000782 mol) were used; red-brown crystals (0.400 g, 93%). Elemental analysis, calculated for $C_{74}H_{98}N_6Br_6Ni_3$ (%): C, 51.46; H, 5.72; N, 4.86; Ni, 10.20; Br, 27.76. Found: C, 49.64; H, 5.71; N, 4.60; Ni, 9.73; Br, 28.06. MS (MALDI) *m/z*: 672-679 $[(L^{10})NiBr]^+$. IR: 1651, 1632, 1620, 1597, 1577 cm^{-1} ($\nu_{C=N}$, $\nu_{C=C(Ar)}$).

$[(L^{11})NiBr]_2[NiBr_4]$: **L^{11}** (0.291 g, 0.000504 mol) and $NiBr_2$(DME) (0.227 g, 0.000737 mol) were used; yellow-brown solid obtained by rapid precipitation with hexane (0.399 g, 88%). Elemental analysis, calculated for $C_{80}H_{110}N_6Br_6Ni_3$ (%): C, 53.04; H, 6.12; N, 4.64;

Ni, 9.72; Br, 26.47. Found: C, 51.60; H, 6.18; N, 4.47; Ni, 9.80; Br, 26.40. MS (MALDI) *m/z*: 714-721 $[(L^{11})NiBr]^+$. IR: 1665, 1638, 1618, 1598, 1530 cm^{-1} ($\nu_{C=N}$).

$[(L^{12})NiBr]_2[NiBr_4]$: **L^{12}** (0.271 g, 0.000507 mol) and $NiBr_2$(DME) (0.226 g, 0.000734 mol); yellow-brown solid obtained by rapid precipitation with hexane (0.404 g, 96%). Elemental analysis, calculated for $C_{74}H_{98}N_6Br_6Ni_3$ (%): C, 51.46; H, 5.72; N, 4.87; Ni, 10.20; Br, 27.76. Found: C, 50.85; H, 5.83; N, 4.70; Ni, 9.42; Br, 26.55. MS (MALDI) *m/z*: 672-678 $[(L^{12})NiBr]^+$. IR: 1650, 1634, 1614, 1598, 1580 cm^{-1} ($\nu_{C=N}$, $\nu_{C=C(Ar)}$).

$[(L^{16})NiBr]_2[NiBr_4]$: **L^{16}** (0.279 g, 0.000505 mol) and $NiBr_2$(DME) (0.233 g, 0.000756 mol) were used; green-yellow solid obtained by rapid precipitation with hexane (0.330 g, 74%). Elemental analysis, calculated for $C_{72}H_{94}N_6O_4Br_6Ni_3$ (%): C, 49.05; H, 5.37; N, 4.77; Ni, 9.99; Br, 27.19. Found: C, 47.91; H, 5.24; N, 4.58; Ni, 9.12; Br, 26.43. MS (MALDI) *m/z*: 690-697 $[(L^{16})NiBr]^+$. IR: 1653, 1629, 1614, 1590 cm^{-1} ($\nu_{C=N}$, $\nu_{C=C(Ar)}$).

$[\{(L^1)Ni(\mu\text{-}Br)\}_2][BAr^F{}_4]_2$: In a typical procedure, THF (20 cm^3) was added to a solid mixture of **L^1** (0.260 g, 0.000527 mol), $NiBr_2$(DME) (0.165 g, 0.000536 mol) and $NaBAr^F{}_4$ (0.516 g, 0.000582 mol), forming a green solution. This was stirred at room temperature for ~2 hours, after which time the THF was removed under vacuum. The brown coloured residue was digested with DCM (20 cm^3), and the resultant opaque green-brown solution was filtered through celite under N_2. The celite pad was washed with DCM (3 × 15 cm^3) and the volume of the filtrate was reduced under vacuum to ~5 cm^3. Layering of this solution with hexane (20 cm^3) caused the rapid formation of green crystals, which were collected by filtration in air and washed with a large amount of hexane. Yield: 0.621g, 79%. Elemental analysis, calculated for $C_{132}H_{110}N_6Br_2Ni_2F_{48}B_2$ (%): C, 53.01; H, 3.71; N, 2.81; Ni, 3.93; Br, 5.34. Found: C, 52.22; H, 3.66; N, 2.72; Ni, 3.49; Br, 5.05. MS (MALDI) *m/z*: 630-637 $[(L^1)NiBr]^+$. IR: 1669, 1635, 1609, 1596 cm^{-1} ($\nu_{C=N}$, $\nu_{C=C(Ar)}$).

$[\{(L^3)Ni(\mu\text{-}Br)\}_2][BAr^F{}_4]_2$: **$L^3$** (0.166 g, 0.000327 mol), $NiBr_2$(DME) (0.104 g, 0.000338 mol) and $NaBAr^F{}_4$ (0.296 g, 0.000334 mol) were used; dark-green crystals (0.331, 67%). Crystals of **$[\{(L^3)Ni(\mu\text{-}Br)(OH_2)\}_2][BAr^F{}_4]_2$** suitable for X-ray diffraction were obtained by vapour diffusion of hexane into a saturated 1,2-difluorobenzene solution of **$[\{(L^3)Ni(\mu\text{-}Br)\}_2][BAr^F{}_4]_2$**. Elemental analysis, calculated for $C_{134}H_{114}N_6Ni_2Br_2F_{48}B_2$ (%): C, 53.31; H, 3.81; N, 2.78; Ni, 3.89; Br, 5.29. Found: C, 52.91; H, 3.85; N, 2.70; Ni, 3.69; Br, 5.37.

MS (MALDI) *m/z*: 644-650 $[(L^3)NiBr]^+$. IR: 1666, 1659, 1632, 1610, 1593 cm^{-1} ($\nu_{C=N}$, $\nu_{C=C(Ar)}$).

$[\{(L^5)Ni(\mu\text{-}Br)\}_2][BAr^F{}_4]_2$: **$L^5$** (0.269 g, 0.000503 mol), $NiBr_2$(DME) (0.153 g, 0.000497 mol) and $NaBAr^F{}_4$ (0.445 g, 0.000502 mol) were used; pale-green powder obtained by rapid precipitation with hexane (0.517 g, 68%). Crystals of **$[\{(L^5)Ni(\mu\text{-}Br)(OH_2)\}_2][BAr^F{}_4]_2$** suitable for X-ray diffraction were obtained by vapour diffusion of hexane into a saturated 1,2-difluorobenzene solution of **$[\{(L^5)Ni(\mu\text{-}Br)\}_2][BAr^F{}_4]_2$**. Elemental analysis, calculated for $C_{138}H_{122}N_6Ni_2Br_2F_{48}B_2$ (%): C, 53.90; H, 4.00; N, 2.73; Ni, 3.82; Br, 5.20. Found: C, 51.61; H, 3.81; N, 2.47; Ni, 3.52; Br, 5.64. MS (MALDI) *m/z*: 672-679 $[(L^5)NiBr]^+$. IR: 1656, 1630, 1609, 1591 cm^{-1} ($\nu_{C=N}$, $\nu_{C=C(Ar)}$).

$[(\eta^2\text{-}L^6)NiBr(THF)][BAr^F{}_4]$: **$L^6$** (0.149 g, 0.000258 mol), $NiBr_2$(DME) (0.077 g, 0.000250 mol) and $NaBAr^F{}_4$ (0.227 g, 0.000256 mol) were used; olive-green crystals (0.227 g, 55%). Elemental analysis, calculated for $C_{76}H_{75}N_3ONiBrF_{24}B$ (%): C, 55.26; H, 4.57; N, 2.54; Ni, 3.55; Br, 4.84. Found: C, 53.70; H, 4.31; N, 2.41; Ni, 3.46; Br, 5.35. IR: 1648, 1609, 1591, 1561, 1555 cm^{-1} ($\nu_{C=N}$, $\nu_{C=C(Ar)}$).

$[\{(L^7)Ni(\mu\text{-}Br)\}_2][BAr^F{}_4]_2$: **$L^7$** (0.494 g, 0.001 mol), $NiBr_2$(DME) (0.309 g, 0.001 mol) and $NaBAr^F{}_4$ (0.886 g, 0.001 mol) were used; dark-green crystals (0.715 g, 48%). IR: 1632, 1659, 1610 cm^{-1} ($\nu_{C=N}$, $\nu_{C=C(Ar)}$).

$[\{(L^8)Ni(\mu\text{-}Br)\}_2][BAr^F{}_4]_2$: **$L^8$** (0.135 g, 0.000258 mol), $NiBr_2$(DME) (0.100 g, 0.000324 mol) and $NaBAr^F{}_4$ (0.242 g, 0.000273 mol) were used; bright-green crystals (0.293 g, 75%). Elemental analysis, calculated for $C_{134}H_{114}N_6O_2Br_2F_{48}Ni_2B_2$ (%): C, 52.75; H, 3.77; N, 2.75; Ni, 3.85; Br, 5.24. Found: C, 52.02; H, 3.71; N, 2.71; Ni, 3.68; Br, 5.23. MS (MALDI) *m/z*: 661-667 $[(L^8)NiBr]^+$. IR: 1661, 1638, 1628, 1609, 1595 cm^{-1} ($\nu_{C=N}$, $\nu_{C=C(Ar)}$).

$[(L^{10})NiBr][BAr^F{}_4]$: **$L^{10}$** (0.136 g, 0.000254 mol), $NiBr_2$(DME) (0.092 g, 0.000299 mol) and $NaBAr^F{}_4$ (0.248 g, 0.000279 mol) were used; yellow powder obtained by rapid precipitation with hexane (0.188 g, 48%). Bright-red single crystals suitable for X-ray diffraction were obtained by careful layering of hexane onto a saturated DCM solution of **$[(L^{10})NiBr][BAr^F{}_4]$**. Elemental analysis, calculated for $C_{69}H_{61}N_3NiBrF_{24}B$ (%): C, 53.90; H, 4.00; N, 2.73; Ni, 3.82; Br, 5.20. Found: C, 53.43; H, 3.73; N, 2.69; Ni, 3.49; Br, 5.09. MS (MALDI) *m/z*: 671-677 $[(L^{10})NiBr]^+$. IR: 1655, 1638, 1612 cm^{-1} ($\nu_{C=N}$, $\nu_{C=C(Ar)}$).

[(L^{11})NiBr][BAr^F_4]: $\mathbf{L^{11}}$ (0.147 g, 0.000255 mol), $NiBr_2$(DME) (0.089 g, 0.000289 mol) and $NaBAr^F_4$ (0.251 g, 0.000283 mol); bright-red crystals (0.329 g, 82%). Elemental analysis, calculated for $C_{72}H_{67}N_3NiBrF_{24}B$ (%): C, 54.74; H, 4.27; N, 2.66; Ni, 3.72; Br, 5.06. Found: C, 54.69; H, 4.35; N, 2.55; Ni, 3.36; Br, 5.10. MS (MALDI) *m/z*: 711-718 $[(L^{11})NiBr]^+$. IR: 1644, 1610 cm^{-1} ($\nu_{C=N}$, $\nu_{C=C(Ar)}$).

[{(L^{12})Ni(μ-Br)}$_2$][BAr^F_4]$_2$: $\mathbf{L^{12}}$ (0.139 g, 0.000260 mol), $NiBr_2$(DME) (0.099 g, 0.000321 mol) and $NaBAr^F_4$ (0.240 g, 0.000271 mol) were used; green powder obtained by rapid precipitation with hexane (0.310 g, 78%). Single crystals of **[{(L^{12})Ni(μ-Br)(OH_2)}$_2$][BAr^F_4]$_2$** suitable for X-ray diffraction were obtained by vapour diffusion of hexane into a saturated DCM solution of **[{(L^{12})Ni(μ-Br)}$_2$][BAr^F_4]**. Elemental analysis, calculated for $C_{138}H_{122}N_6Ni_2Br_2F_{48}B_2$ (%): C, 53.90; H, 4.00; N, 2.73; Ni, 3.82; Br, 5.20. Found: C, 52.73; H, 4.01; N, 2.77; Ni, 3.74; Br, 5.53. MS (MALDI) *m/z*: 669-675 $[(L^{12})NiBr]^+$. IR: 1654, 1623, 1609, 1585 cm^{-1} ($\nu_{C=N}$, $\nu_{C=C(Ar)}$).

[(η^4-L^{15})NiBr][BAr^F_4]: $\mathbf{L^{15}}$ (0.141 g, 0.000250 mol), $NiBr_2$(DME) (0.077 g, 0.000250 mol) and $NaBAr^F_4$ (0.226 g, 0.000255 mol) were used; dark-green crystals (0.171 g, 44%). Elemental analysis, calculated for $C_{70}H_{63}N_3ONiBrF_{24}B$ (%): C, 53.63; H, 4.05; N, 2.68; Ni, 3.75; Br, 5.10. Found: C, 51.63; H, 3.77; N, 2.49; Ni, 3.74; Br, 5.49. MS (MALDI) *m/z*: 702-709 $[(L^{15})NiBr]^+$. IR: 1656, 1631, 1610, 1589 cm^{-1} ($\nu_{C=N}$, $\nu_{C=C(Ar)}$).

[(η^4-L^{16})NiBr][BAr^F_4]: $\mathbf{L^{16}}$ (0.281 g, 0.000508 mol), $NiBr_2$(DME) (0.160 g, 0.000519 mol) and $NaBAr^F_4$ (0.449 g, 0.000507 mol) were used; green solid obtained by rapid precipitation with hexane (0.256 g, 32%). Single crystals suitable for X-ray diffraction were obtained by careful layering of hexane onto a saturated DCM solution of **[(η^4-L^{16})NiBr][BAr^F_4]**. Elemental analysis, calculated for $C_{68}H_{59}N_3O_2NiBrF_{24}B$ (%): C, 52.50; H, 3.82; N, 2.70; Ni, 3.77; Br, 5.14. Found: C, 52.09; H, 3.72; N, 2.59; Ni, 3.34; Br, 4.98. MS (MALDI) *m/z*: 690-698 $[(L^{16})NiBr]^+$. IR: 1655, 1626, 1611, 1594 cm^{-1} ($\nu_{C=N}$, $\nu_{C=C(Ar)}$).

[(L^1)NiBr][OTf]: In a typical procedure, DCM (40 cm^3) was added to a solid mixture of $\mathbf{L^1}$ (0.246 g, 0.000499 mol), $NiBr_2$(DME) (0.157 g, 0.000510 mol) and AgOTf (0.127 g, 0.000494 mol) in a foil-wrapped Schlenk tube, forming a dark-brown solution with a large amount of dense precipitate. This was stirred at room temperature for ~24 hours, after which time the colour had become lighter yellow-brown. The mixture was then filtered through celite under N_2, and the celite pad was washed with DCM (2 × 15 cm^3). The

volume of the filtrate was reduced under vacuum to ~5 cm^3, and the solution was layered with Et_2O (40 cm^3). A large mass of small, pale-red crystals formed slowly, which were collected by filtration in air and washed with Et_2O. Yield: 0.252 g, 65%. Elemental analysis, calculated for $C_{35}H_{43}N_3O_3NiBrSF_3$ (%): C, 53.80; H, 5.55; N, 5.38; Ni, 7.51; Br, 10.23. Found: C, 53.25; H, 5.37; N, 5.30; Ni, 7.30; Br, 10.39. MS (MALDI) *m/z*: 630-636 $[(L^1)NiBr]^+$. IR: 1662, 1638, 1598, 1577 cm^{-1} ($\nu_{C=N}$, $\nu_{C=C(Ar)}$).

$[\{(L^3)Ni(\mu\text{-}Br)\}_2][OTf]_2$: **$L^3$** (0.154 g, 0.000304 mol), $NiBr_2$(DME) (0.094 g, 0.000305 mol) and AgOTf (0.082 g, 0.000319 mol) were used; pale-green powder obtained by rapid precipitation with Et_2O (0.103 g, 43%). Elemental analysis, calculated for $C_{72}H_{90}N_6O_6Ni_2Br_2S_2F_6$ (%): C, 54.36; H, 5.70; N, 5.28; Ni, 7.38; Br, 10.05. Found: C, 52.08; H, 5.88; N, 4.72; Ni, 7.17; Br, 10.86. MS (MALDI) *m/z*: 644-650 $[(L^3)NiBr]^+$. IR: 1657, 1630, 1591, 1573, 1555, 1534 cm^{-1} ($\nu_{C=N}$, $\nu_{C=C(Ar)}$).

$[\{(L^5)Ni(\mu\text{-}Br)\}_2][OTf]_2$: **$L^5$** (0.270 g, 0.000505 mol), $NiBr_2$(DME) (0.160 g, 0.000519 mol) and AgOTf (0.128 g, 0.000498 mol) were used; green precipitate formed upon reduction in volume of DCM solution, further precipitation caused by addition of Et_2O (0.275 g, 67%). Elemental analysis, calculated for $C_{76}H_{98}N_6O_6Ni_2Br_2S_2F_6$ (%): C, 55.42; H, 6.00; N, 5.10; Ni, 7.13; Br, 9.70. Found: C, 52.69; H, 5.69; N, 4.70; Ni, 7.06; Br, 10.63. MS (MALDI) *m/z*: 672-678 $[(L^5)NiBr]^+$. IR: 1653, 1629, 1591 cm^{-1} ($\nu_{C=N}$, $\nu_{C=C(Ar)}$).

$[(L^8)NiBr][OTf]$: **L^8** (0.262 g, 0.000501 mol), $NiBr_2$(DME) (0.155 g, 0.000503 mol) and AgOTf (0.135 g, 0.000525 mol) were used; yellow powder obtained by rapid precipitation with Et_2O (0.233 g, 59%). Single crystals suitable for X-ray diffraction were obtained by vapour diffusion of Et_2O into a saturated DCM solution of **$[(L^8)NiBr][OTf]$**. Elemental analysis, calculated for $C_{36}H_{45}N_3O_4NiBrSF_3$ (%): C, 53.29; H, 5.59; N, 5.18; Ni, 7.24; Br, 9.85. Found: C, 53.28; H, 5.59; N, 5.10; Ni, 6.93; Br, 10.12. MS (MALDI) 660-666 $[(L^8)NiBr]^+$. IR: 1656, 1636, 1591 cm^{-1} ($\nu_{C=N}$, $\nu_{C=C(Ar)}$).

$[(L^{10})NiBr][OTf]$: **L^{10}** (0.270 g, 0.000505 mol), $NiBr_2$(DME) (0.157 g, 0.000510 mol) and AgOTf (0.130 g, 0.000506 mol) were used; orange-red crystals obtained using hexane in place of Et_2O (0.322 g, 77%). Single crystals suitable for X-ray diffraction were obtained by vapour diffusion of Et_2O into a saturated DCM solution of **$[(L^{10})NiBr][OTf]$**. Elemental analysis, calculated for $C_{38}H_{49}N_3O_3NiBrSF_3$ (%): C, 55.42; H, 6.00; N, 5.10; Ni,

7.13; Br, 9.70. Found: C, 54.80; H, 6.10; N, 4.92; Ni, 7.02; Br, 9.92. MS (MALDI) *m/z*: 672-678 $[(L^{10})NiBr]^+$. IR: 1653, 1634, 1618, 1593, 1575 cm^{-1} ($\nu_{C=N}$, $\nu_{C=C(Ar)}$).

$[(L^{11})NiBr][OTf]$: **L^{11}** (0.288 g, 0.000499 mol), $NiBr_2$(DME) (0.156 g, 0.000506 mol) and AgOTf (0.127 g, 0.000494 mol) were used; bright-red crystals obtained using hexane in place of Et_2O (0.358 g, 84%). Single crystals suitable for X-ray diffraction were obtained by slow diffusion of Et_2O into a saturated $CHCl_3$ solution of **$[(L^{11})NiBr][OTf]$**. Elemental analysis, calculated for $C_{41}H_{55}N_3O_3NiBrSF_3$ (%): C, 56.90; H, 6.40; N, 4.85; Ni, 6.78; Br, 9.23. Found: C, 55.63; H, 6.23; N, 4.74; Ni, 6.53; Br, 9.17. MS (MALDI) *m/z*: 714-720 $[(L^{11})NiBr]^+$. IR: 1644, 1606, 1587, 1555 cm^{-1} ($\nu_{C=N}$, $\nu_{C=C(Ar)}$).

$[(L^{12})NiBr][OTf]$: **L^{12}** (0.272 g, 0.000508 mol), $NiBr_2$(DME) (0.163 g, 0.000529 mol) and AgOTf (0.133 g, 0.000518 mol) were used; bright-red crystals obtained using hexane in place of Et_2O (0.279 g, 67%). Single crystals suitable for X-ray diffraction were obtained by slow diffusion of Et_2O into a saturated DCM solution of **$[(L^{12})NiBr][OTf]$**. Elemental analysis, calculated for $C_{38}H_{49}N_3O_3NiBrSF_3$ (%): C, 55.42; H, 6.00; N, 5.10; Ni, 7.13; Br, 9.70. Found: C, 54.93; H, 5.80; N, 4.99; Ni, 6.99; Br, 9.59. MS (MALDI) *m/z*: 672-679 $[(L^{12})NiBr]^+$. IR: 1648, 1630, 1611, 1599, 1577 cm^{-1} ($\nu_{C=N}$, $\nu_{C=C(Ar)}$).

$[(\eta^4\text{-}L^{15})NiBr][OTf]$: **$L^{15}$** (0.144 g, 0.000255 mol), $NiBr_2$(DME) (0.073 g, 0.000237 mol) and AgOTf (0.064 g, 0.000249 mol) were used; bright-green crystals (0.096 g, 48%). Elemental analysis, calculated for $C_{39}H_{51}N_3O_4NiBrSF_3$ (%): C, 54.89; H, 6.02; N, 4.92; Ni, 6.88; Br, 9.36. Found: C, 53.76; H, 5.88; N, 4.72; Ni, 6.60; Br, 9.09. MS (MALDI) *m/z*: 702-708 $[(L^{15})NiBr]^+$. IR: 1655, 1650, 1632, 1588 cm^{-1} ($\nu_{C=N}$, $\nu_{C=C(Ar)}$).

$[(\eta^4\text{-}L^{16})NiBr][OTf]$: **$L^{16}$** (0.279 g, 0.000505 mol), $NiBr_2$(DME) (0.157 g, 0.000510 mol) and AgOTf (0.129 g, 0.000502 mol) were used, green-yellow solid obtained by rapid precipitation with Et_2O (0.128 g, 30%). Single crystals suitable for X-ray diffraction were obtained by vapour diffusion of hexane into a saturated $CHCl_3$ solution of **$[(\eta^4\text{-}L^{16})NiBr][OTf]$**. Elemental analysis, calculated for $C_{37}H_{47}N_3O_5NiBrSF_3$ (%): C, 52.82; H, 5.63; N, 4.99; Ni, 6.98; Br, 9.50. Found: C, 50.99; H, 5.38; N, 4.74; Ni, 7.04; Br, 8.65. MS (MALDI) *m/z*: 690-697 $[(L^{16})NiBr]^+$. IR: 1659, 1639, 1614, 1591 cm^{-1} ($\nu_{C=N}$, $\nu_{C=C(Ar)}$).

$(\eta^2\text{-}L^6)NiBr_2$: DCM (15 cm^3) was added to a solid mixture of **L^6** (0.145 g, 0.000251 mol) and $NiBr_2$(DME) (0.079 g, 0.000256 mol), forming an orange suspension which turned deep purple-red upon stirring at room temperature for ~1 hour. After stirring for a further

~24 hours, the mixture was filtered through celite under N_2. The celite pad was then washed with DCM (2 × 15 cm^3), and the volume of the filtrate was reduced under vacuum to ~5 cm^3. Layering of this solution with hexane (40 cm^3) caused the formation of extremely dark violet-coloured crystals, which were collected by filtration in air and washed with hexane. Yield: 0.104 g, 52%. Elemental analysis, calculated for $C_{40}H_{55}N_3NiBr_2$ (%): C, 60.32; H, 6.96; N, 5.28; Ni, 7.37; Br, 20.07. Found: C, 59.98; H, 6.83; N, 5.08; Ni, 6.76; Br, 20.07. MS (MALDI) *m/z*: 714-720 $[(L^6)NiBr]^+$. IR: 1604, 1589, 1554 cm^{-1} ($\nu_{C=N}$, $\nu_{C=C(Ar)}$).

6.11 General Procedure for Ethylene Polymerisation Experiments

A large Schlenk tube was loaded with the appropriate nickel complex (~6 μmol) and equipped with a Suba-Seal. Freshly distilled toluene (200 cm^3) was then added (aside from **$(L^6)NiBr_2$**, none of the complexes tested has any appreciable solubility in toluene), followed by MAO (4 cm^3 of a 10% solution in toluene, ~1000 molar equiv. per Ni) which invariably caused a rapid colour change to pale orange-brown and the formation of small black particles. After stirring for 5 minutes, ethylene was added directly from a cylinder, by means of a long needle attached to a length of PVC tubing. Ethylene addition was continued for a period of 120 minutes, after which time the reaction was terminated by transferral of all the contents of the reaction flask to a mixture of methanol (1800 cm^3) and conc. HCl (200 cm^3). The resulting mixture was stirred overnight, and any polymer was collected by filtration and washed with copious amounts of methanol. The polymer was then dried under high vacuum for a period of ~3 days. Analytical data for a number of the polyethylene samples prepared in this work are presented in **section 4.2.2.2**.

7. References

1. A. Werner, W. Spruck, W. Megerle, J. Pastor, *Z. Anorg. Chem.*, 1899, **21**, 201.
2. G. Bähr, *Z. Anorg. Allg. Chem.*, 1951, **267**, 137.
3. S. G. McGeachin, *Can. J. Chem.*, 1968, **46**, 1903.
4. M. C. Barral, E. Delgado, E. Gutiérrez-Puebla, R. Jimenez-Aparicio, A. Monge, C. Del Pino, A. Santos, *Inorg. Chim. Acta*, 1983, **74**, 101.
5. G. B. Jameson, H. R. Oswald, H. R. Beer, *J. Am. Chem. Soc.*, 1984, **106**, 1669.
6. C. L. Honeybourne, G. A. Webb, *Chem. Commun.*, 1968, 739.
7. R. Diercks, J. Kopf, H. T. Dieck, *Acta Crystallog., Sect. C: Cryst. Struct. Commun.*, 1984, 1984, **C40**, 363.
8. D. Walther, *Z. Anorg. Allg. Chem.*, 1977, **431**, 17.
9. J. E. Parks, R. H. Holm, *Inorg. Chem.*, 1968, **7**, 1408.
10. L. K. Johnson, C. M. Killian, M. Brookhart, *J. Am. Chem. Soc.*, 1995, **117**, 6414.
11. R. van Asselt, C. J. Elsevier, W. J. J. Smeets, A. L. Spek, R. Benedix, *Recl. Trav. Chim. Pays-Bas*, 1994, **113**, 88.
12. J. Feldman, S. J. McLain, A. Parthasarathy, W. J. Marshall, J. C. Calabrese, S. D. Arthur, *Organometallics*, 1997, **16**, 1514.
13. W. Clegg, E. K. Cope, A. J. Edwards, F. S. Mair, *Inorg. Chem.*, 1998, **37**, 2317.
14. A SciFinder Scholar search on 17/02/2010 for N-carbon substituted β-diimine and β-diiminate complexes yielded 3485 substances across 833 references, of which 743 were published post-1997.
15. S. Trofimenko, *J. Am. Chem. Soc.*, 1966, **88**, 1842.
16. S. Trofimenko, *Chem. Rev.*, 1993, **93**, 943; S. Trofimenko, *Scorpionates: The Coordination Chemistry of Polypyrazolylborate Ligands*, Imperial College Press, London, 1999; S. Trofimenko, *Polyhedron*, 2004, **23**, 197; C. Pettinari, *Scorpionates II: Chelating Borate Ligands*, Imperial College Press, London, 2008.
17. A. Antiñolo, F. Carillo-Hermosilla, A. E. Corrochano, J. Fernández-Baeza, M. Lanfranchi, A. Otero, M. A. Pellinghelli, *J. Organomet. Chem.*, 1999, **577**, 174.
18. E. Kime-Hunt, K. Spartalian, M. DeRusha, C. M. Nunn, C. J. Carrano, *Inorg. Chem.*, 1989, **28**, 4392.
19. C.-H. Li, J.-D. Chen, L.-S. Liou, J.-C. Wang, *Inorg. Chim. Acta*, 1998, **269**, 302.
20. A. Kayal, J. Kuncheria, S. C. Lee, *Chem. Commun.*, 2001, 2482.
21. P. Dapporto, F. Mani, C. Mealli, *Inorg. Chem.*, 1978, **17**, 1323.
22. P. Burchill, M. G. H. Wallbridge, *Inorg. Nucl. Chem. Lett.*, 1976, **12**, 93.
23. M. J. Abrams, R. Faggiani, C. J. L. Lock, *Inorg. Chim. Acta*, 1985, **106**, 69.
24. M. K. Chan, W. H. Armstrong, *Inorg. Chem.*, 1989, **28**, 3777.
25. M. R. Churchill, B. G. DeBoer, F. J. Rotella, O. M. Abu Salah, M. I. Bruce, *Inorg. Chem.*, 1975, **14**, 2051.
26. G. G. Lobbia, C. Pettinari, F. Marchetti, *Polyhedron*, 1996, **15**, 881.
27. J. S. Thompson, T. J. Marks, J. A. Ibers, *J. Am. Chem. Soc.*, 1979, **101**, 4180.
28. J. S. Thompson, T. Sorrell, T. J. Marks, J. A. Ibers, *J. Am. Chem. Soc.*, 1979, **101**, 4193; D. M. Jenkins, J. C. Peters, *J. Am. Chem. Soc.*, 2005, **127**, 7148.
29. U. Brand, M. Rombach, H. Vahrenkamp, *Chem. Commun.*, 1998, 2717; A. Beheshti, W. Clegg, S. H. Dale, R. Hyvadi, *Acta Crystallogr., Sect. C: Cryst. Struct. Commun.*, 2009, **C65**, m314.
30. P. J. Desrochers, S. LeLievre, R. J. Johnson, B. T. Lamb, A. L. Phelps, A. W. Cordes, W. Gu, S. P. Cramer, *Inorg. Chem.*, 2003, **42**, 7945.
31. A. Looney, G. Parkin, *Inorg. Chem.*, 1994, **33**, 1234.
32. C. E. Ruggiero, S. M. Carrier, W. B. Tolman, *Angew. Chem. Int. Ed. Engl.*, 1994, **33**, 895.

33. S. Hikichi, Y. Sasakura, M. Yoshizawa, Y. Ohzu, Y. Moro-oka, M. Akita, *Bull. Chem. Soc. Jpn.*, 2002, **75**, 1255.
34. D. Li, C. Ruschman, S. Parkin, R. Clérac, S. M. Holmes, *Chem. Commun.*, 2006, 4036.
35. S. G. N. Roundhill, D. M. Roundhill, D. R. Bloomquist, C. Landee, R. D. Willett, D. M. Dooley, H. B. Gray, *Inorg. Chem.*, 1979, **18**, 831; S. Wang, Y.-Z. Li, J.-L. Zuo, X.-Z. You, *Acta Crystallogr., Sect. E: Struct. Rep. Online*, 2004, **E60**, m376.
36. N. Kitajima, T. Koda, S. Hashimoto, T. Kitagawa, Y. Moro-oka, *Chem. Commun.*, 1988, 151; N. Kitajima, T. Koda, S. Hashimoto, T. Kitagawa, Y. Moro-oka, *J. Am. Chem. Soc.*, 1991, **113**, 5664.
37. J. Pérez, L. García, R. Carrascosa, E. Pérez, J. L. Serrano, G. Sánchez, G. García, M. D. Santana, L. López, J. García, *Z. Anorg. Allg. Chem.*, 2007, **633**, 1869.
38. C. Di Nicola, F. Marchetti, M. Monari, L. Pandolfo, C. Pettinari, *Inorg. Chem. Commun.*, 2008, **11**, 665.
39. J. E. Joachim, C. Apostolidis, B. Kanellakopulos, R. Maier, N. Marques, D. Meyer, J. Müller, A. P. de Matos, B. Nuber, J. Rebizant, M. L. Ziegler, *J. Organomet. Chem.*, 1993, **448**, 119.
40. D. Li, S. Parkin, G. Wang, G. T. Yee, S. M. Holmes, *Inorg. Chem.*, 2006, **45**, 1951.
41. Y.-J. Sun, P. Cheng, S.-P. Yan, Z.-H. Jiang, D.-Z. Liao, P.-W. Shen, *Inorg. Chem. Commun.*, 2000, **3**, 289.
42. W. H. Armstrong, S. J. Lippard, *J. Am. Chem. Soc.*, 1983, **105**, 4837; W. H. Armstrong, A. Spool, G. C. Papaefthymiou, R. B. Frankel, S. J. Lippard, *J. Am. Chem. Soc.*, 1984, **106**, 3653; W. H. Armstrong, S. J. Lippard, *J. Am. Chem. Soc.*, 1984, **106**, 4632; J. E. Sheets, R. S. Czernuszewicz, G. C. Dismukes, A. L. Rheingold, V. Petrouleas, J. Stubbe, W. H. Armstrong, R. H. Beer, S. J. Lippard, *J. Am. Chem. Soc.*, 1987, **109**, 1435.
43. (a) J. C. Calabrese, S. Trofimenko, J. S. Thompson, *Chem. Commun.*, 1986, 1122; (b) J. C. Calabrese, S. Trofimenko, J. S. Thompson, *Inorg. Chem.*, 1987, **26**, 1507.
44. I. B. Gorrell, G. Parkin, *Inorg. Chem.*, 1990, **29**, 2452.
45. S. M. Carrier, C. E. Ruggiero, W. B. Tolman, G. B. Jameson, *J. Am. Chem. Soc.*, 1992, **114**, 4407.
46. W. B. Tolman, *Inorg. Chem.*, 1991, **30**, 4880.
47. I. B. Gorrell, A. Looney, G. Parkin, *Chem. Commun.*, 1990, 220.
48. R. Alsfasser, A. K. Powell, H. Vahrenkamp, *Angew. Chem.*, 1990, **102**, 939.
49. R. Han, I. B. Gorrell, A. Looney, G. Parkin, *Chem. Commun.*, 1991, 717.
50. J. L. Kisko, T. Hascall, G. Parkin, *J. Am. Chem. Soc.*, 1998, **120**, 10561.
51. J. D. Jewson, L. M. Liable-Sands, G. P. A. Yap, A. L. Rheingold, K. H. Theopold, *Organometallics*, 1999, **18**, 300.
52. J. W. Egan, Jr., B. S. Haggerty, A. L. Rheingold, S. C. Sendlinger, K. H. Theopold, *J. Am. Chem. Soc.*, 1990, **112**, 2445.
53. C. Bergquist, T. Fillebeen, M. M. Morlok, G. Parkin, *J. Am. Chem. Soc.*, 2003, **125**, 6189.
54. J. L. Detrich, R. Konečný, W. M. Vetter, D. Doren, A. L. Rheingold, K. H. Theopold, *J. Am. Chem. Soc.*, 1996, **118**, 1703.
55. J. C. Calabrese, S. Trofimenko, *Inorg. Chem.*, 1992, **31**, 4810.
56. D. T. Shay, G. P. A. Yap, L. N. Zakharov, A. L. Rheingold, K. H. Theopold, *Angew. Chem. Int. Ed. Engl.*, 2005, **44**, 1508.
57. R. Alsfasser, S. Trofimenko, A. Looney, G. Parkin, H. Vahrenkamp, *Inorg. Chem.*, 1991, **30**, 4098.

58. (a) A. Looney, G. Parkin, R. Alsfasser, M. Ruf, H. Vahrenkamp, *Angew. Chem. Int. Ed. Engl.*, 1992, **31**, 92; (b) R. Han, A. Looney, K. McNeill, G. Parkin, A. L. Rheingold, B. S. Haggerty, *J. Inorg. Biochem.*, 1993, **49**, 105.
59. A. Looney, R. Han, K. McNeill, G. Parkin, *J. Am. Chem. Soc.*, 1993, **115**, 4690.
60. C. Bergquist, G. Parkin, *J. Am. Chem. Soc.*, 1999, **121**, 6322.
61. J. L. Kersten, R. R. Kucharczyk, G. P. A. Yap, A. L. Rheingold, K. H. Theopold, *Chem. Eur. J.*, 1997, **3**, 1668.
62. A. Hess, M. R. Hörz, L. M. Liable-Sands, D. C. Lindner, A. L. Rheingold, K. H. Theopold, *Angew. Chem. Int. Ed. Engl.*, 1999, **38**, 166.
63. K. Qin, C. D. Incarvito, A. L. Rheingold, K. H. Theopold, *Angew. Chem. Int. Ed. Engl.*, 2002, **41**, 2333.
64. K. Qin, C. D. Incarvito, A. L. Rheingold, K. H. Theopold, *J. Am. Chem. Soc.*, 2002, **124**, 14008.
65. K. Fujisawa, M. Tanaka, Y. Moro-oka, N. Kitajima, *J. Am. Chem. Soc.*, 1994, **116**, 12079.
66. K. Fujisawa, T. Kobayashi, K. Fujita, N. Kitajima, Y. Moro-oka, Y. Miyashita, Y. Yamada, K. Okamoto, *Bull. Chem. Soc. Jpn.*, 2000, **73**, 1797.
67. H. Komatsuzaki, N. Sakamoto, M. Satoh, S. Hikichi, M. Akita, Y. Moro-oka, *Inorg. Chem.*, 1998, **37**, 6554.
68. S. Hikichi, H. Komatsuzaki, M. Akita, Y. Moro-oka, *J. Am. Chem. Soc.*, 1998, **120**, 4699.
69. S. Hikichi, T. Ogihara, K. Fujisawa, N. Kitajima, M. Akita, Y. Moro-oka, *Inorg. Chem.*, 1997, **36**, 4539.
70. T. Ogihara, S. Hikichi, M. Akita, T. Uchida, T. Kitagawa, Y. Moro-oka, *Inorg. Chim. Acta*, 2000, **297**, 162.
71. M. Nabika, Y. Seki, T. Miyatake, Y. Ishikawa, K. Okamoto, K. Fujisawa, *Organometallics*, 2004, **23**, 4335.
72. M. Nabika, S. Kiuchi, T. Miyatake, K. Fujisawa, *J. Polym. Sci., Part A: Polym. Chem.*, 2009, **47**, 5720.
73. C. M. Dowling, D. Leslie, M. H. Chisholm, G. Parkin, *Main Group Chem.*, 1995, **1**, 29.
74. M. C. Kuchta, G. Parkin, *J. Am. Chem. Soc.*, 1995, **117**, 12651; M. C. Kuchta, J. B. Bonanno, G. Parkin, *J. Am. Chem. Soc.*, 1996, **118**, 10914.
75. M. C. Kuchta, G. Parkin, *Main Group Chem.*, 1996, **1**, 291.
76. J. C. Green, J. L. Suter, *Dalton Trans.*, 1999, 4087.
77. (a) S. Trofimenko, J. C. Calabrese, P. J. Domaille, J. S. Thompson, *Inorg. Chem.*, 1989, **28**, 1091; (b) S. Trofimenko, J. C. Calabrese, J. K. Kochi, S. Wolowiec, F. B. Hulsbergen, J. Reedijk, *Inorg. Chem.*, 1992, **31**, 3943.
78. M. Cano, J. V. Heras, S. Trofimenko, A. Monge, E. Gutierrez, C. J. Jones, J. A. McCleverty, *Dalton Trans.*, 1990, 3577.
79. O. M. Reinaud, A. L. Rheingold, K. H. Theopold, *Inorg. Chem.*, 1994, **33**, 2306.
80. O. M. Reinaud, K. H. Theopold, *J. Am. Chem. Soc.*, 1994, **116**, 6979.
81. O. M. Reinaud, G. P. A. Yap, A. L. Rheingold, K. H. Theopold, *Angew. Chem. Int. Ed. Engl.*, 1995, **34**, 2051.
82. J. L. Detrich, O. M. Reinaud, A. L. Rheingold, K. H. Theopold, *J. Am. Chem. Soc.*, 1995, **117**, 11745.
83. S. Thyagarajan, D. T. Shay, C. D. Incarvito, A. L. Rheingold, K. H. Theopold, *J. Am. Chem. Soc.*, 2003, **125**, 4440.
84. N. Kitajima, K. Fujisawa, Y. Moro-oka, *J. Am. Chem. Soc.*, 1989, **111**, 8975; N. Kitajima, K. Fujisawa, C. Fujimoto, Y. Moro-oka, S. Hashimoto, T. Kitagawa, K. Toriumi, K. Tatsumi, A. Nakamura, *J. Am. Chem. Soc.*, 1992, **114**, 1277.

85. N. Kitajima, K. Fujisawa, M. Tanaka, Y. Moro-oka, *J. Am. Chem. Soc.*, 1992, **114**, 9232; D. Qiu, L. Kilpatrick, N. Kitajima, T. G. Spiro, *J. Am. Chem. Soc.*, 1994, **116**, 2585.
86. N. Kitajima, K. Fujisawa, Y. Moro-oka, *J. Am. Chem. Soc.*, 1990, **112**, 3210.
87. K. Fujisawa, K. Fujita, T. Takahashi, N. Kitajima, Y. Moro-oka, Y. Matsunaga, Y. Miyashita, K. Okamoto, *Inorg. Chem. Commun.*, 2004, **7**, 1188.
88. K. Fujisawa, Y. Moro-oka, N. Kitajima, *Chem. Commun.*, 1994, 623.
89. K. Fujisawa, Y. Iwata, N. Kitajima, H. Higashimura, M. Kubota, Y. Miyashita, Y. Yamada, K. Okamoto, Y. Moro-oka, *Chem. Lett.*, 1999, 739.
90. N. Kitajima, T. Katayama, K. Fujisawa, Y. Iwata, Y. Moro-oka, *J. Am. Chem. Soc.*, 1993, **115**, 7872.
91. K. Fujisawa, N. Lehnert, Y. Ishikawa, K. Okamoto, *Angew. Chem. Int. Ed. Engl.*, 2004, **43**, 4944.
92. F. Paulat, N. Lehnert, Y. Ishikawa, K. Okamoto, K. Fujisawa, *Inorg. Chim. Acta*, 2008, **361**, 901.
93. N. Kitajima, S. Hikichi, M. Tanaka, Y. Moro-oka, *J. Am. Chem. Soc.*, 1993, **115**, 5496.
94. N. Kitajima, U. P. Singh, H. Amagai, M. Osawa, Y. Moro-oka, *J. Am. Chem. Soc.*, 1991, **113**, 7757.
95. N. Kitajima, M. Osawa, M. Tanaka, Y. Moro-oka, *J. Am. Chem. Soc.*, 1991, **113**, 8952.
96. S. Hikichi, M. Yoshizawa, Y. Sasakura, M. Akita, Y. Moro-oka, *J. Am. Chem. Soc.*, 1998, **120**, 10567.
97. S. Hikichi, M. Yoshizawa, Y. Sasakura, H. Komatsuzaki, Y. Moro-oka, M. Akita, *Chem. Eur. J.*, 2001, **7**, 5011.
98. S. Hikichi, H. Okuda, Y. Ohzu, M. Akita, *Angew. Chem. Int. Ed. Engl.*, 2009, **48**, 188.
99. S. Yoshimitsu, S. Hikichi, M. Akita, *Organometallics*, 2002, **21**, 3762.
100. N. Kitajima, H. Komatsuzaki, S. Hikichi, M. Osawa, Y. Moro-oka, *J. Am. Chem. Soc.*, 1994, **116**, 11596.
101. U. P. Singh, A. K. Sharma, S. Hikichi, H. Komatsuzaki, Y. Moro-oka, M. Akita, *Inorg. Chim. Acta*, 2006, **359**, 4407.
102. M. Osawa, K. Fujisawa, N. Kitajima, Y. Moro-oka, *Chem. Lett.*, 1997, 919.
103. H. Komatsuzaki, Y. Nagasu, K. Suzuki, T. Shibasaki, M. Satoh, F. Ebina, S. Hikichi, M. Akita, Y. Moro-oka, *Dalton Trans.*, 1998, 511.
104. Y. Matsunaga, K. Fujisawa, N. Ibi, Y. Miyashita, K. Okamoto, *Inorg. Chem.*, 2005, **44**, 325.
105. M. S. Varonka, T. H. Warren, *Inorg. Chem.*, 2009, **48**, 5605.
106. N. Kitajima, H. Fukui, Y. Moro-oka, *J. Am. Chem. Soc.*, 1990, **112**, 6402; N. Kitajima, N. Tamura, H. Amagai, H. Fukui, Y. Moro-oka, Y. Mizutani, T. Kitagawa, R. Mathur, K. Heerwegh, C. A. Reed, C. R. Randall, L. Que, Jr., K. Tatsumi, *J. Am. Chem. Soc.*, 1994, **116**, 9071.
107. N. Kitajima, H. Amagai, N. Tamura, M. Ito, Y. Moro-oka, K. Heerwegh, A, Pénicaud, R. Mathur, C. A. Reed, P. D. W. Boyd, *Inorg. Chem.*, 1993, **32**, 3583.
108. K. Kim, S. J. Lippard, *J. Am. Chem. Soc.*, 1996, **118**, 4914.
109. (a) N. Kitajima, M. Ito, H. Fukui, Y. Moro-oka, *J. Am. Chem. Soc.*, 1993, **115**, 9335; (b) M. Ito, H. Amagai, H. Fukui, N. Kitajima, Y. Moro-oka, *Bull. Chem. Soc. Jpn.*, 1996, **69**, 1937.
110. T. Ogihara, S. Hikichi, M. Akita, Y. Moro-oka, *Inorg. Chem.*, 1998, **37**, 2614.
111. M. Akita, N. Shirasawa, S. Hikichi, Y. Moro-oka, *Chem. Commun.*, 1998, 973; N. Shirasawa, M. Akita, S. Hikichi, Y. Moro-oka, *Chem. Commun.*, 1999, 417; N. Shirasawa, T. T. Nguyet, S. Hikichi, Y. Moro-oka, M. Akita, *Organometallics*, 2001, **20**, 3582.
112. D. M. Eichhorn, W. H. Armstrong, *Inorg. Chem.*, 1990, **29**, 3607.
113. C. J. Siemer, F. A. McKee, W. H. Armstrong, D. M. Eichhorn, *Polyhedron*, 2001, **20**, 2637.

114. A. Kramer-Aach, W. Kläui, R. Bell, A. Strerath, H. Wunderlich, D. Mootz, *Inorg. Chem.*, 1997, **36**, 1552.
115. F. Hartmann, W. Kläui, A. Kramer-Aach, D. Mootz, A. Strerath, H. Wunderlich, *Z. Anorg. Allg. Chem.*, 1993, **619**, 2071.
116. B. Domhöver, W. Kläui, A. Kramer-Aach, R. Bell, D. Mootz, *Angew. Chem. Int. Ed. Engl.*, 1998, **37**, 3050.
117. M. A. Halcrow, L. M. L. Chia, X. Liu, E. J. L. McInnes, L. J. Yellowlees, F. E. Mabbs, J. E. Davies, *Chem. Commun.*, 1998, 2465; M. A. Halcrow, L. M. L. Chia, X. Liu, E. J. L. McInnes, L. J. Yellowlees, F. E. Mabbs, I. J. Scowen, M. McPartlin, J. E. Davies, *Dalton Trans.*, 1999, 1753.
118. I. Sylvestre, J. Wolowska, E. J. L. McInnes, C. A. Kilner, M. A. Halcrow, *Inorg. Chim. Acta*, 2005, **358**, 1337.
119. M. A. Halcrow, E. J. L. McInnes, F. E. Mabbs, I. J. Scowen, M. McPartlin, H. R. Powell, J. E. Davies, *Dalton Trans.*, 1997, 4025.
120. X. Liu, L. M. L. Chia, C. A. Kilner, L. J. Yellowlees, M. Thornton-Pett, S. Trofimenko, M. A. Halcrow, *Chem. Commun.*, 2000, 1947.
121. S. Dhar, A. R. Chakravarty, *Inorg. Chem.*, 2005, **44**, 2582; S. Roy, A. K. Patra, S. Dhar, A. R. Chakravarty, *Inorg. Chem.*, 2008, **47**, 5625.
122. A. L. Rheingold, R. L. Ostrander, B. S. Haggerty, S. Trofimenko, *Inorg. Chem.*, 1994, **33**, 3666.
123. P. J. Desrochers, R. W. Cutts, P. K. Rice, M. L. Golden, J. B. Graham, T. M. Barclay, A. W. Cordes, *Inorg. Chem.*, 1999, **38**, 5690.
124. K. Uehara, S. Hikichi, M. Akita, *Dalton Trans.*, 2002, 3529.
125. A. V. Yakovenko, S. V. Kolotilov, A. W. Addison, S. Trofimenko, G. P. A Yap, V. Lopushanskaya, V. V. Pavlishchuk, *Inorg. Chem. Commun.*, 2005, **8**, 932.
126. S. Chattopadhyay, T. Deb, H. Ma, J. L. Petersen, V. G. Young, Jr., M. P. Jensen, *Inorg. Chem.*, 2008, **47**, 3384.
127. H. Ma, S. Chattopadhyay, J. L. Petersen, M. P. Jensen, *Inorg. Chem.*, 2008, **47**, 7966.
128. M. Ruf, B. C. Noll, M. D. Groner, G. T. Yee, C. G. Pierpont, *Inorg. Chem.*, 1997, **36**, 4860.
129. M. Ruf, C. G. Pierpont, *Angew. Chem. Int. Ed. Engl.*, 1998, **37**, 1736.
130. M. L. Kirk, D. A. Shultz, E. C. Depperman, C. L. Brannen, *J. Am. Chem. Soc.*, 2007, **129**, 1937 and references therein.
131. H. Higashimura, K. Fujisawa, Y. Moro-oka, M. Kubota, A. Shiga, A. Terahara, H. Uyama, S. Kobayashi, *J. Am. Chem. Soc.*, 1998, **120**, 8529; H. Higashimura, M. Kubota, A. Shiga, K. Fujisawa, Y. Moro-oka, H. Uyama, S. Kobayashi, *Macromolecules*, 2000, **33**, 1986.
132. C. L. Foster, X. Liu, C. A. Kilner, M. Thornton-Pett, M. A. Halcrow, *Dalton Trans.*, 2000, 4563.
133. E. L. Hegg, R. Y. N. Ho, L. Que, Jr., *J. Am. Chem. Soc.*, 1999, **121**, 1972; M. P. Mehn, K. Fujisawa, E. L. Hegg, L. Que, Jr., *J. Am. Chem. Soc.*, 2003, **125**, 7828.
134. T. K. Paine, H. Zheng, L. Que, Jr., *Inorg. Chem.*, 2005, **44**, 474.
135. A. Mukherjee, M. Martinho, E. L. Bominaar, E. Münck, L. Que, Jr., *Angew. Chem. Int. Ed. Engl.*, 2009, **48**, 1780.
136. M. P. Mehn, S. D. Brown, T. K. Paine, W. W. Brennessel, C. J. Cramer, J. C. Peters, L. Que, Jr., *Dalton Trans.*, 2006, 1347.
137. D. J. Harding, P. Harding, R. Daengngern, S. Yimklan, H. Adams, *Dalton Trans.*, 2009, 1314.
138. D. J. Harding, P. Harding, H. Adams, T. Tuntulani, *Inorg. Chim. Acta*, 2007, **360**, 3335.

139. D. Aguilà, E. Escribano, S. Speed, D. Talancón, L. Yermán, S. Alvarez, *Dalton Trans.*, 2009, 6610.
140. W. Hückel, H. Bretschneider, *Ber. Dtsch. Chem. Ges.*, 1937, **70**, 2024.
141. J. P. Jesson, *J. Chem. Phys.*, 1966, **45**, 1049.
142. S. Juliá, J. M. del Mazo, L. Avila, J. Elguero, *Org. Prep. Proced. Int.*, 1984, **16**, 299.
143. C. Titze, J. Hermann, H. Vahrenkamp, *Chem. Ber.*, 1995, **128**, 1095.
144. D. L. Reger, J. E. Collins, A. L. Rheingold, L. M. Liable-Sands, *Organometallics*, 1996, **15**, 2029.
145. S. Trofimenko, *J. Am. Chem. Soc.*, 1970, **92**, 5118.
146. F. Mani, *Inorg. Nucl. Chem. Lett.*, 1979, **15**, 297.
147. M. A. Mesubi, P. I. Ekemenzie, *Transition Met. Chem.*, 1984, **9**, 91.
148. D. J. O'Sullivan, F. J. Lalor, *J. Organomet. Chem.*, 1973, **57**, C58.
149. M. A. Mesubi, F. O. Anumba, *Transition Met. Chem.*, 1985, **10**, 5.
150. G. G. Lobbia, D. Leonesi, A. Cingolani, A. Lorenzotti, F. Bonati, *Synth. React. Inorg. Met.-Org. Chem.*, 1987, **17**, 909.
151. A. Cingolani, D. Martini, F. Marchetti, C. Pettinari, M. Ricciutelli, B. W. Skelton, A. H. White, *Inorg. Chim. Acta*, 2003, **350**, 641.
152. M. Cvetkovic, S. R. Batten, B. Moubaraki, K. S. Murray, L. Spiccia, *Inorg. Chim. Acta*, 2001, **324**, 131.
153. W. Kaim, C. Titze, T. Schurr, M. Sieger, M. Lawson, J. Jordanov, D. Rojas, A. M. Garciá, J. Manzur, *Z. Anorg. Allg. Chem.*, 2005**, 631**, 2568.
154. K. Fujisawa, T. Ono, H. Aoki, Y. Ishikawa, Y. Miyashita, K. Okamoto, H. Nakazawa, H. Higashimura, *Inorg. Chem. Commun.*, 2004, **7**, 330.
155. N. Lehnert, U. Cornelissen, F. Neese, T. Ono, Y. Noguchi, K. Okamoto, K. Fujisawa, *Inorg. Chem.*, 2007, **46**, 3916.
156. K. Fujisawa, H. Iwamoto, K. Tobita, Y. Miyashita, K. Okamoto, *Inorg. Chim. Acta*, 2009, **362**, 4500.
157. K. Yoon, G. Parkin, *Polyhedron*, 1995, **14**, 811.
158. K. Fujisawa, Y. Miyashita, Y. Yamada, K. Okamoto, *Bull. Chem. Soc. Jpn.*, 2001, **74**, 1065.
159. K. Fujisawa, T. Ono, Y. Ishikawa, N. Amir, Y. Miyashita, K. Okamoto, N. Lehnert, *Inorg. Chem.*, 2006, **45**, 1698.
160. K. Fujisawa, A. Tateda, Y. Miyashita, K. Okamoto, F. Paulat, V. K. K. Praneeth, A. Merkle, N. Lehnert, *J. Am. Chem. Soc.*, 2008, **130**, 1205.
161. M. Kujime, C. Izumi, M. Tomura, M. Hada, H. Fujii, *J. Am. Chem. Soc.*, 2008, **130**, 6088.
162. T. F. S. Silva, G. S. Mishra, M. F. G. da Silva, R. Wanke, L. M. D. R. S. Martins, A. J. L. Pombeiro, *Dalton Trans.*, 2009, 9207.
163. D. L. Reger, T. C. Grattan, K. J. Brown, C. A. Little, J. J. S. Lamba, A. L. Rheingold, R. D. Sommer, *J. Organomet. Chem.*, 2000, **607**, 120.
164. J. Niesel, A. Pinto, H. W. P. N'Dongo, K. Merz, I. Ott, R. Gust, U. Schatzschneider, *Chem. Commun.*, 2008, 1798.
165. H. Pfeiffer, A. Rojas, J. Niesel, U. Schatzschneider, *Dalton Trans.*, 2009, 4292.
166. K. Meister, J. Niesel, U. Schatzschneider, N. Metzler-Nolte, D. A. Schmidt, M. Havenith, *Angew. Chem. Int. Ed. Engl.*, 2010, **49**, 3310.
167. M. Nabika, S. Kiuchi, T. Miyatake, K. Okamoto, K. Fujisawa, *J. Mol. Catal. A: Chem.*, 2007, **269**, 163.
168. D. L. Reger, C. A. Little, A. L. Rheingold, R. Sommer, G. J. Long, *Inorg. Chim. Acta*, 2001, **316**, 65.
169. P. G. Edwards, A. Harrison, P. D. Newman, W. Zhang, *Inorg. Chim. Acta*, 2006, **359**, 3549.

170. S. R. Batten, J. Bjernemose, P. Jensen, B. A. Leita, K. S. Murray, B. Moubaraki, J. P. Smith, H. Toftlund, *Dalton Trans.*, 2004, 3370.
171. A. A. Salaudeen, C. A. Kilner, M. A. Halcrow, *Polyhedron*, 2008, **27**, 2569.
172. T. Dhanalakshmi, E. Suresh, M. Palaniandavar, *Dalton Trans.*, 2009, 8317.
173. C.-C. Shi, C.-S. Chen, S. C. N. Hsu, W.-Y. Yeh, M. Y. Chiang, T.-S. Kuo, *Inorg. Chem. Commun.*, 2008, **11**, 1264 and references therein.
174. A. Michaud, F.-G. Fontaine, D. Zargarian, *Inorg. Chim. Acta*, 2006, **359**, 2592.
175. M.-C. Nolet, A. Michaud, C. Bain, D. Zargarian, C. Reber, *Photochem. Photobiol.*, 2006, **82**, 57.
176. B. Ding, L. Yi, W.-Z. Shen, P. Cheng, D.-Z. Liao, S.-P. Yan, Z.-H. Jiang, *J. Mol. Struct.*, 2006, **784**, 138.
177. P. J. Desrochers, A. L. Corken, R. M. Tarkka, B. M. Besel, E. E. Mangum, T. N. Linz, *Inorg. Chem.*, 2009, **48**, 3535.
178. I. García, R. Quijada, K. Vera, M. Valderrama, *J. Mol. Catal. A: Chem.*, 2006, **260**, 70.
179. (a) S. C. Lawrence, M. E. G. Skinner, J. C. Green, P. Mountford, *Chem. Commun.*, 2001, 705; (b) H. R. Bigmore, S. R. Dubberley, M. Kranenburg, S. C. Lawrence, A. J. Sealey, J. D. Selby, M. A. Zuideveld, A. R. Cowley, P. Mountford, *Chem. Commun,*, 2006, 436.
180. H. R. Bigmore, M. A. Zuideveld, R. M. Kowalczyk, A. R. Cowley, M. Kranenburg, E. J. L. McInnes, P. Mountford, *Inorg. Chem.*, 2006, **45**, 6411.
181. T. B. Parsons, N. Hazari, A. R. Cowley, J. C. Green, P. Mountford, *Inorg. Chem.*, 2005, **44**, 8442.
182. F. Breher, J. Grunenberg, S. C. Lawrence, P. Mountford, H. Rüegger, *Angew. Chem. Int. Ed. Engl.*, 2004, **43**, 2521.
183. I. Krummenacher, H. Rüegger, F. Breher, *Dalton Trans.*, 2006, 1073.
184. H. R. Bigmore, J. Meyer, I. Krummenacher, H. Rüegger, E. Clot, P. Mountford, F. Breher, *Chem. Eur. J.*, 2008, **14**, 5918.
185. M. G. Cushion, J. Meyer, A. Heath, A. D. Schwarz, I. Fernández, F. Breher, P. Mountford, *Organometallics*, 2010, **29**, 1174.
186. I. Kuzu, I. Krummenacher, I. J. Hewitt, Y. Lan, V. Mereacre, A. K. Powell, P. Höfer, J. Harmer, F. Breher, *Chem. Eur. J.*, 2009, **15**, 4350.
187. W. Kläui, M. Berghahn, G. Rheinwald, H. Lang, *Angew. Chem. Int. Ed. Engl.*, 2000, **39**, 2464.
188. W. Kläui, D. Schramm, W. Peters, G. Rheinwald, H. Lang, *Eur. J. Inorg. Chem.*, 2001, 1415.
189. C. Santini, M. Pellei, G. G. Lobbia, A. Cingolani, R. Spagna, M. Camalli, *Inorg. Chem. Commun.*, 2002, **5**, 430.
190. C. Santini, M. Pellei, G. G. Lobbia, D. Fedeli, G. Falcioni, *J. Inorg. Biochem.*, 2003, **94**, 348; M. Pellei, G. G. Lobbia, C. Santini, R. Spagna, M. Camalli, D. Fedeli, G. Falcioni, *Dalton Trans.*, 2004, 2822.
191. W. Kläui, M. Berghahn, W. Frank, G. J. Reiß, T. Schönherr, G. Rheinwald, H. Lang, *Eur. J. Inorg. Chem.*, 2003, 2059.
192. E. T. Papish, M. T. Taylor, F. E. Jernigan, III, M. J. Rodig, R. R. Shawhan, G. P. A. Yap, F. A. Jové, *Inorg. Chem.*, 2006, **45**, 2242.
193. R. Wanke, P. Smoleński, M. F. C. G. da Silva, L. M. D. R. S. Martins, A. J. L. Pombeiro, *Inorg. Chem.*, 2008, **47**, 10158.
194. T. F. S. Silva, E. C. B. A. Alegria, L. M. D. R. S. Martins, A. J. L. Pombeiro, *Adv. Synth. Catal.*, 2008, **350**, 706.
195. C. C. McClauchlan, M. P. Weberski, Jr., B. A. Greiner, *Inorg. Chim. Acta*, 2009, **362**, 2662.

196. J. Hoyano, L. K. Peterson, *Can. J. Chem.*, 1976, **54**, 2697.
197. H. B. Davis, J. K. Hoyano, P. Y. Leung, L. K. Peterson, B. Wolstenholme, *Can. J. Chem.*, 1980, **58**, 151.
198. V. S. Joshi, V. K. Kale, K. M. Sathe, A. Sarkar, S. S. Tavale, C. G. Suresh, *Organometallics*, 1991, **10**, 2898.
199. C. J. Tokar, P. B. Kettler, W. B. Tolman, *Organometallics*, 1992, **11**, 2737.
200. K. R. Breakell, S. J. Rettig, D. L. Singbeil, A. Storr, J. Trotter, *Can. J. Chem.*, 1978, **56**, 2099.
201. K. S. Chong, S. J. Rettig, A. Storr, J. Trotter, *Can. J. Chem.*, 1979, **57**, 3107.
202. K. R. Breakall, S. J. Rettig, A. Storr, J. Trotter, *Can. J. Chem.*, 1979, **57**, 139.
203. S. A. Cortes-Llamas, M.-Á. Muñoz-Hernández, *Organometallics*, 2007, **26**, 6844.
204. S. Vepachedu, R. T. Stibrany, S. Knapp, J. A. Potenza, H. J. Schugar, *Acta Crystallogr., Sect. C: Cryst. Struct. Commun.*, 1995, **C51**, 423.
205. E. E. Pullen, A. L. Rheingold, D. Rabinovich, *Inorg. Chem. Commun.*, 1999, **2**, 194.
206. E. E. Pullen, D. Rabinovich, C. D. Incarvito, T. E. Concolino, A. L. Rheingold, *Inorg. Chem.*, 2000, **39**, 1561.
207. C. S. Tredget, S. C. Lawrence, B. D. Ward, R. G. Howe, A. R. Cowley, P. Mountford, *Organometallics*, 2005, **24**, 3136.
208. R. G. Howe, C. S. Tredget, S. C. Lawrence, S. Subongkoj, A. R. Cowley, P. Mountford, *Chem. Commun.*, 2006, 223.
209. F. Armbruster, I. Fernández, F. Breher, *Dalton Trans*, 2009, 5612.
210. A. Steiner, D. Stalke, *Chem. Commun.*, 1993, 1702.
211. A. Steiner, D. Stalke, *Inorg. Chem.*, 1995, **34**, 4846.
212. I. Fernández, P. Oña-Burgos, F. Armbruster, I. Krummenacher, F. Breher, *Chem. Commun.*, 2009, 2586.
213. G. G. Lobbia, F. Bonati, P. Cecchi, *Synth. React. Inorg. Met.-Org. Chem.*, 1991, **21**, 1141.
214. C. Janiak, *Chem. Commun.*, 1994, 545.
215. C. Janiak, T. G. Scharmann, H. Hemling, D. Lentz, J. Pickardt, *Chem. Ber.*, 1995, **128**, 235.
216. C. Janiak, *Chem. Ber.*, 1994, **127**, 1379.
217. C. Janiak, H. Hemling, *Dalton Trans.*, 1994, 2947.
218. K.-B. Shiu, J. Y. Lee, Y. Wang, M.-C. Cheng, S.-L. Wang, F.-L. Liao, *J. Organomet. Chem.*, 1993, **453**, 211.
219. I. T. Macleod, E. R. T. Tiekink, C. G. Young, *J. Organomet. Chem.*, 1996, **506**, 301.
220. F. E. Jernigan, III, N. A. Sieracki, M. T. Taylor, A. S. Jenkins, S. E. Engel, B. W. Rowe, F. A. Jové, G. P. A. Yap, E. T. Papish, G. M. Ferrence, *Inorg. Chem.*, 2007, **46**, 360.
221. S. R. Gardner, E. T. Papish, W. H. Monillas, G. P. A. Yap, *J. Inorg. Biochem.*, 2008, **102**, 2179.
222. E. T. Papish, T. M. Donahue, K. R. Wells, G. P. A. Yap, *Dalton Trans.*, 2008, 2923.
223. S. Kiani, J. R. Long, P. Stavropoulos, *Inorg. Chim. Acta*, 1997, **263**, 357.
224. M. Kumar, E. T. Papish, M. Zeller, A. D. Hunter, *Dalton Trans.*, 2010, 59.
225. F. J. Lalor, S. Miller, N. Garvey, *J. Organomet. Chem.*, 1988, **356**, C57
226. C. Santini, M. Pellei, G. G. Lobbia, S. Alidori, M. Berrettini, D. Fedeli, *Inorg. Chim. Acta*, 2004, **357**, 3549.
227. K.-B. Shiu, F.-M. Shen, S.-L. Wang, S.-C. Wei, *J. Organomet. Chem.*, 1989, **372**, 251.
228. S. G. A. van Assema, C. G. J. Tazelaar, G. B. de Jong, J. H. van Maarseveen, M. Schakel, M. Lutz, A. L. Spek, J. C. Slootweg, K. Lammertsma, *Organometallics*, 2008, **27**, 3210.
229. T. N. Sorrell, A. S. Borovik, *J. Am. Chem. Soc.*, 1987, **109**, 4255.
230. T. Rüther, N. Brassaud, K. J. Cavell, *Organometallics*, 2001, **20**, 1247.

231. B. A. Greiner, N. M. Marshall, A. A. N. Sarjeant, C. C. McClauchlan, *Inorg. Chim. Acta*, 2007, **360**, 3132.
232. L. P. Wu, Y. Yamagiwa, I. Ino, K. Sugimoto, T. Kuroda-Sowa, T. Kamikawa, M. Munakata, *Polyhedron*, 1999, **18**, 2047.
233. L. Zhou, D. Powell, K. M. Nicholas, *Inorg. Chem.*, 2007, **46**, 2316.
234. J. Volkman, K. M. Nicholas, *Org. Lett.*, 2004, **6**, 4301.
235. M. Kujime, T. Kurahashi, M. Tomura, H. Fujii, *Inorg. Chem.*, 2007, **46**, 541.
236. F.-J. Wu, D. M. Kurtz, Jr., K. S. Hagen, P. D. Nyman, P. G. Debrunner, V. A. Vankai, *Inorg. Chem.*, 1990, **29**, 5174.
237. V. A. Vankai, M. G. Newton, D. M. Kurtz, Jr., *Inorg. Chem.*, 1992, **31**, 341.
238. W. E. Lynch, D. M. Kurtz, Jr., S. Wang, R. A. Scott, *J. Am. Chem. Soc.*, 1994, **116**, 11030.
239. T. N. Sorrell, W. E. Allen, P. S. White, *Inorg. Chem.*, 1995, **34**, 952.
240. W. E. Allen, T. N. Sorrell, *Inorg. Chem.*, 1997, **36**, 1732.
241. C. Kimblin, V. J. Murphy, G. Parkin, *Chem. Commun.*, 1996, 235.
242. C. Kimblin, V. J. Murphy, T. Hascall, B. M. Bridgewater, J. B. Bonanno, G. Parkin, *Inorg. Chem.*, 2000, **39**, 967.
243. C. Kimblin, B. M. Bridgewater, D. G. Churchill, G. Parkin, *Dalton Trans.*, 2000, 2191.
244. T. Rüther, K. J. Cavell, N. C. Brassaud, B. W. Skelton, A. H. White, *Dalton Trans.*, 2002, 4684.
245. W. Kläui, C. Piefer, G. Rheinwald, H. Lang, *Eur. J. Inorg. Chem.*, 2000, 1549.
246. A. Schiller, R. Scopelliti, M. Benmelouka, K. Severin, *Inorg. Chem.*, 2005, **44**, 6482.
247. P. C. Kunz, G. J. Reiß, W. Frank, W. Kläui, *Eur. J. Inorg. Chem.*, 2003, 3945.
248. P. C. Kunz, M. U. Kassack, A. Hamacher, B. Spingler, *Dalton Trans.*, 2009, 7741.
249. P. C. Kunz, A. Zribi, W. Frank, W. Kläui, *Z. Anorg. Allg. Chem.*, 2007, **633**, 955.
250. P. C. Kunz, A. Zribi, W. Frank, W. Kläui, *Z. Anorg. Allg. Chem.*, 2008, **634**, 724.
251. S. Bellemin-Laponnaz, L. H. Gade, *Chem. Commun.*, 2002, 1286.
252. S. Bellemin-Laponnaz, L. H. Gade, *Angew. Chem. Int. Ed. Engl.*, 2002, **41**, 3473.
253. L. H. Gade, G. Marconi, C. Dro, B. D. Ward, M. Poyatos, S. Bellemin-Laponnaz, H. Wadepohl, L. Sorace, G. Poneti, *Chem. Eur. J.*, 2007, **13**, 3058.
254. C. G. Young, M. S. Malarek, D. J. Evans, C. J. Doonan, V. W. L. Ng, J. M. White, *Inorg. Chem.*, 2009, **48**, 1960.
255. J. F. Dunne, J. Su, A. Ellern, A. D. Sadow, *Organometallics*, 2008, **27**, 2399.
256. A. V. Pawlikowski, A. Ellern, A. D. Sadow, *Inorg. Chem.*, 2009, **48**, 8020.
257. D. Mukherjee, A. Ellern, A. D. Sadow, *J. Am. Chem. Soc.*, 2010, **132**, 7582.
258. B. Baird, A. V. Pawlikowski, J. Su, J. W. Wiench, M. Pruski, A. D. Sadow, *Inorg. Chem.*, 2008, **47**, 10208.
259. J. F. Dunne, K. Manna, J. W. Wiench, A. Ellern, M. Pruski, A. D. Sadow, *Dalton Trans.*, 2010, 641.
260. P. A. Brauner, G. Schwarzenbach, *Helv. Chim. Acta*, 1962, **45**, 2030.
261. G. Schwarzenbach, H.-B. Bürgi, W. P. Jensen, G. A. Lawrance, L. Mønsted, A. M. Sargeson, *Inorg. Chem.*, 1983, **22**, 4029.
262. L. Hausherr-Primo, K. Hegetschweiler, H. Rüegger, L. Odier, R. D. Hancock, H. W. Schmalle, V. Gramlich, *Dalton Trans.*, 1994, 1689.
263. Y. Fujii, T. Kiss, T. Gadja, X. S. Tan, T. Sato, Y. Nakano, Y. Hayashi, M. Yashiro, *J. Biol. Inorg. Chem.*, 2002, **7**, 843.
264. J. Y. Yang, M. P. Shores, J. J. Sokol, J. R. Long, *Inorg. Chem.*, 2003, **42**, 1403.
265. U. Brand, H. Vahrenkamp, *Inorg. Chim. Acta*, 1992, **198-200**, 663.

266. G. Park, J. Shao, F. H. Lu, R. D. Rogers, N. D. Chasteen, M. W. Brechbiel, R. P. Planalp, 2001, **40**, 4167.
267. H. Arii, Y. Saito, S. Nagatomo, T. Kitagawa, Y. Funahashi, K. Jitsukawa, H. Masuda, *Chem. Lett.*, 2003, **32**, 156; Y. Kajita, H. Arii, T. Saito, Y. Saito, S. Nagatomo, T. Kitagawa, Y. Funahashi, T. Ozawa, H. Masuda, *Inorg. Chem.*, 2007, **46**, 3322.
268. L. Q. Hatcher, M. A. Vance, A. A. N. Sarjeant, E. I. Solomon, K. D. Karlin, *Inorg. Chem.*, 2006, **45**, 3004 and references therein.
269. B. Greener, M. H. Moore, P. H. Walton, *Chem. Commun.*, 1996, 27.
270. B. Greener, L. Cronin, G. D. Wilson, P. H. Walton, *Dalton Trans.*, 1996, 401; L. Cronin, B. Greener, S. P. Foxon, S. L. Heath, P. H. Walton, 1997, **36**, 2594.
271. M. Cushion, P. Ebrahimpour, M. F. Haddow, A. J. Hallett, S. M. Mansell, A. G. Orpen, D. F. Wass, *Dalton Trans.*, 2009, 1632.
272. L. Cronin, B. Greener, M. H. Moore, P. H. Walton, *Dalton Trans.*, 1996, 3337.
273. C. J. Boxwell, P. H. Walton, *Chem. Commun.*, 1999, 1647.
274. B. Greener, P. H. Walton, *Dalton Trans.*, 1997, 3733.
275. S. J. Archibald, S. P. Foxon, J. D. Freeman, J. E. Hobson, R. N. Perutz, P. H. Walton, *Dalton Trans.*, 2002, 2797.
276. L. Cronin, P. H. Walton, *Inorg. Chim. Acta*, 1998, **269**, 241.
277. B. Greener, S. P. Foxon, P. H. Walton, *New J. Chem.*, 2000, **24**, 269.
278. L. Cronin, S. P. Foxon, P. J. Lusby, P. H. Walton, *J. Biol. Inorg. Chem.*, 2001, **6**, 367.
279. A. K. Nairn, S. J. Archibald, R. Bhalla, C. J. Boxwell, A. C. Whitwood, P. H. Walton, *Dalton Trans.*, 2006, 1790.
280. L. Bourget-Merle, M. F. Lappert, J. R. Severn, *Chem. Rev.*, 2002, **102**, 3031.
281. C. Cui, H. W. Roesky, H.-G. Schmidt, M. Noltemeyer, H. Hao, F. Cimpoesu, *Angew. Chem. Int. Ed. Engl.*, 2000, **39**, 4274.
282. N. J. Hardman, B. E. Eichler, P. P. Power, *Chem. Commun.*, 2000, 1991.
283. M. S. Hill, P. B. Hitchcock, *Chem. Commun.*, 2004, 1818.
284. P. L. Holland, W. B. Tolman, *J. Am. Chem. Soc.*, 1999, **121**, 7270; D. W. Randall, S. D. George, P. L. Holland, B. Hedman, K. O. Hodgson, W. B. Tolman, E. I. Solomon, *J. Am. Chem. Soc.*, 2000, **122**, 11632.
285. J. M. Smith, R. J. Lachicotte, P. L. Holland, *Chem. Commun.*, 2001, 1542; P. L. Holland, T. R Cundari, L. L. Perez, N. A. Eckert, R. J. Lachicotte, *J. Am. Chem. Soc.*, 2002, **124**, 14416.
286. J. M. Smith, R. J. Lachicotte, K. A. Pittard, T. R. Cundari, G. Lukat-Rogers, K. R. Rogers, P. L. Holland, *J. Am. Chem. Soc.*, 2001, **123**, 9222; J. M. Smith, A. R. Sadique, T. R. Cundari, K. R Rogers, G. Lukat-Rogers, R. J. Lachicotte, C. J. Flaschenriem, J. Vela, P. L. Holland, *J. Am. Chem. Soc.*, 2006, **128**, 756.
287. S. Pfirrmann, C. Limberg, C. Herwig, R. Stößer, B. Ziemer, *Angew. Chem. Int. Ed. Engl.*, 2009, **48**, 3357.
288. J. Chai, H. Zhu, A. C. Stückl, H. R. Roesky, J. Magull, A. Bencini, A. Caneschi, D. Gatteschi, *J. Am. Chem. Soc.*, 2005, **127**, 9201.
289. Y. Wang, B. Quillian, P. Wei, H. Wang, X.-J. Yang, Y. Xie, R. B. King, P. V. R. Schleyer, H. F. Schaefer, III, G. H. Robinson, *J. Am. Chem. Soc.*, 2005, **127**, 11944.
290. S. P. Green, C. Jones, A. Stasch, *Science*, 2007, **318**, 1754.
291. E. Kogut, H. L. Wiencko, L. Zhang, D. E. Cordeau, T. H. Warren, *J. Am. Chem. Soc.*, 2005, **127**, 11248.
292. Y. M. Badiei, A. Krishnaswamy, M. M. Melzer, T. H. Warren, *J. Am. Chem. Soc.*, 2006, **128**, 15056.

293. S. Yao, E. Bill, C. Milsmann, K. Wieghardt, M. Driess, *Angew. Chem. Int. Ed. Engl.*, 2008, **47**, 7110.
294. D. T. Carey, E. K. Cope-Eatough, E. Vilaplana-Mafé, F. S. Mair, R. G. Pritchard, J. E. Warren, R. J. Woods, *Dalton Trans.*, 2003, 1083.
295. E. K. Cope-Eatough, F. S. Mair, R. G. Pritchard, J. E. Warren, R. J. Woods, *Polyhedron*, 2003, **22**, 1447.
296. C. Hillairet, G. Michaud, S. Sirol, Patent No. WO 2007/006740 A1, 2007; G. Michaud, C. Hillairet, S. Sirol, Patent No. EP 1 925 620 A1, 2008.
297. D. J. Doyle, P. B. Hitchcock, M. F. Lappert, G. Li, *J. Organomet. Chem.*, 2009, **694**, 2611.
298. P. J. Ragogna, N. Burford, M. D'eon, R. McDonald, *Chem. Commun.*, 2003, 1052; P. B. Hitchcock, M. F. Lappert, J. E. Nycz, *Chem. Commun.*, 2003, 1142; N. Burford, M. D'eon, P. J. Ragogna, R. McDonald, M. J. Ferguson, *Inorg. Chem.*, 2004, **43**, 734.
299. C. Shimokawa, S. Itoh, *Inorg. Chem.*, 2005, **44**, 3010.
300. G. B. Nikiforov, H. W. Roesky, P. G. Jones, R. B. Oswald, M. Noltemeyer, *Dalton Trans.*, 2007, 4149.
301. S. Yokata, Y. Tachi, S. Itoh, *Inorg. Chem.*, 2002, **41**, 1342.
302. J. D. Azoulay, R. S. Rojas, A. V. Serrano, H. Ohtaki, G. B. Galland, G. Wu, G. C. Bazan, *Angew. Chem. Int. Ed. Engl.*, 2009, **48**, 1089.
303. E. A. Gregory, R. J. Lachicotte, P. L. Holland, *Organometallics*, 2005, **24**, 1803.
304. F. Basuli, J. C. Huffman, D. J. Mindiola, *Inorg. Chem.*, 2003, **42**, 8003.
305. F. Basuli, B. C. Bailey, L. A. Watson, J. Tomaszewski, J. C. Huffman, D. J. Mindiola, *Organometallics*, 2005, **24**, 1886.
306. N. M. West, P. S. White, J. L. Templeton, J. F. Nixon, *Organometallics*, 2009, **28**, 1425.
307. A. D. Phillips, G. Laurenczy, R. Scopelliti, P. J. Dyson. *Organometallics*, 2007, **26**, 1120.
308. C. E. Radzewich, M. P. Coles, R. F. Jordan, *J. Am. Chem. Soc.*, 1998, **120**, 9384.
309. M. Goto, Y. Ishikawa, T. Ishihara, C. Nakatake, T. Higuchi, H. Kurosaki, V. L. Goedken, *Chem. Commun.*, 1997, 539; M. Goto, Y. Ishikawa, T. Ishihara, C. Nakatake, T. Higuchi, H. Kurosaki, V. L. Goedken, *Dalton Trans.*, 1998, 1213; H. Kurosaki, Y. Ishikawa, T. Ishihara, T. Yamamoto, Y. Yamaguchi, M. Goto, *Dalton Trans.*, 2005, 1086.
310. K. Bowman, D. P. Riley, D. H. Busch, P. W. R. Corfield, *J. Am. Chem. Soc.*, 1975, **97**, 5036; D. P. Riley, J. A. Stone, D. H. Busch, *J. Am. Chem. Soc.*, 1976, **98**, 1752; D. P. Riley, J. A. Stone, D. H. Busch, *J. Am. Chem. Soc.*, 1977, **99**, 767; K. Bowman-Mertes, P. W. R. Corfield, D. H. Busch, *Inorg. Chem.*, 1977, **16**, 3226.
311. M. C. Weiss, V. L. Goedken, *J. Am. Chem. Soc.*, 1976, **98**, 3389.
312. J.-M. Giraudon, D. Mandon, J. Sala-Pala, J. E. Guerchais, J.-M. Kerbaol, Y. Le Mest, P. L'Haridon, *Inorg. Chem.*, 1990, **29**, 707.
313. R. Knorr, A. Weiß, *Chem. Ber.*, 1982, **115**, 139.
314. R. Knorr, F. Ruf, *Angew. Chem. Int. Ed. Engl.*, 1984, **23**, 368.
315. A. P. Dove, V. C. Gibson, E. L. Marshall, A. J. P. White, D. J. Williams, *Dalton Trans.*, 2004, 570.
316. H. Ulrich, *The Chemistry of Imidoyl Halides*, Plenum Press, New York, 1968.
317. P. H. M. Budzelaar, A. B. van Oort, A. G. Orpen, *Eur. J. Inorg. Chem.*, 1998, 1485.
318. C. Elschenbroich, A. Salzer, *Organometallics: A Concise Introduction*, Wiley VCH, Weinheim, 1992.
319. S. Trofimenko, *J. Am. Chem. Soc.*, 1969, **91**, 588.
320. E. C. Onyiriuka, A. Storr, *Can. J. Chem.*, 1987, **65**, 2464.
321. A. Solladié-Cavallo, G. Solladié, E. Tsamo, *J. Organomet. Chem.*, 1978, **144**, 181.
322. J. S.-Y. Wong, Y.-J. Gu, L. Szeto, W.-T. Wong, *Cryst. Eng. Comm.*, 2008, **10**, 29.

323. D. Braga, F. Grepioni, K. Biradha, V. R. Pedireddi, G. R. Desiraju, *J. Am. Chem. Soc.*, 1995, **117**, 3156.
324. C. Janiak, *Dalton Trans.*, 2000, 3885.
325. C. A. Hunter, J. K. M. Sanders, *J. Am. Chem. Soc.*, 1990, **112**, 5525.
326. R. J. Read, M. N. G. James, *J. Am. Chem. Soc.*, 1981, **103**, 6947.
327. J. Huguet, R. S. Brown, *J. Am. Chem. Soc.*, 1980, **102**, 7571; R. S. Brown, N. J. Curtis, J. Huguet, *J. Am. Chem. Soc.*, 1981, **103**, 6953; H. Slebocka-Tilk, J. L. Cocho, Z. Frakman, R. S. Brown, *J. Am. Chem. Soc.*, 1984, **106**, 2421.
328. S. Hikichi, M. Tanaka, Y. Moro-oka, N. Kitajima, *Chem. Commun.*, 1992, 814.
329. (a) M. Ruf, K. Weis, H. Vahrenkamp, *Chem. Commun.*, 1994, 135; (b) M. Ruf, H. Vahrenkamp, *Chem. Ber.*, 1996, **129**, 1025.
330. K. Weis, M. Rombach, M. Ruf, H. Vahrenkamp, *Eur. J. Inorg. Chem.*, 1998, 263; K. Weis, H. Vahrenkamp, *Eur. J. Inorg. Chem.*, 1998, 271.
331. M. Ruf, R. Burth, K. Weis, H. Vahrenkamp, *Chem. Ber.*, 1996, **129**, 1251.
332. M. Ruf, K. Weis, H. Vahrenkamp, *J. Am. Chem. Soc.*, 1996, **118**, 9288.
333. D. T. Puerta, S. M. Cohen, *Inorg. Chim. Acta*, 2002, **337**, 459.
334. S. Ramaswamy, H. Eklund, B. V. Plapp, *Biochemistry*, 1994, **33**, 5230.
335. R. Walz, K. Weis, M. Ruf, H. Vahrenkamp, *Chem. Ber.*, 1997, **130**, 975.
336. M. Ruf, H. Vahrenkamp, *Inorg. Chem.*, 1996, **35**, 6571; M. Ruf, F. A. Schell, R. Walz, H. Vahrenkamp, *Chem. Ber.*, 1997, **130**, 101.
337. C. Bergquist, G. Parkin, *Inorg. Chem.*, 1999, **38**, 422; C. Bergquist, H. Storrie, L. Koutcher, B. M. Bridgewater, R. A. Friesner, G. Parkin, *J. Am. Chem. Soc.*, 2000, **122**, 12651.
338. H. Brombacher, H. Vahrenkamp, *Inorg. Chem.*, 2004, **43**, 6042; H. Brombacher, H. Vahrenkamp, *Inorg. Chem.*, 2004, **43**, 6050; H. Brombacher, H. Vahrenkamp, *Inorg. Chem.*, 2004, **43**, 6054.
339. H. Boerzel, M. Koeckert, W. Bu, B. Spingler, S. Lippard, *Inorg. Chem.*, 2003, **42**, 1604.
340. C. Kimblin, W. E. Allen, G. Parkin, *Chem. Commun.*, 1995, 1813.
341. T. Itoh, Y. Fujii, T. Tada, Y. Yoshikawa, H. Hisada, *Bull. Chem. Soc. Jpn.*, 1996, **69**, 1265.
342. L. Cronin. P. H. Walton, *Chem. Commun.*, 2003, 1572.
343. C. Dro, S. Bellemin-Laponnaz, R. Welter, L. H. Gade, *Angew. Chem. Int. Ed. Engl.*, 2004, **43**, 4479.
344. F. Basolo, *Coord. Chem. Rev.*, 1968, **3**, 213.
345. (a) M. Brookhart, B. Grant, A. F. Volpe, Jr., *Organometallics*, 1992, **11**, 3920; (b) E. Hauptman, S. Sabo-Etienne, P. S. White, M. Brookhart, J. M. Garner, P. J. Fagan, J. C. Calabrese, *J. Am. Chem. Soc.*, 1994, **116**, 8038; (c) D. L. Sunick, P. S. White, C. K. Schauer, *Angew. Chem. Int. Ed. Engl.*, 1994, **33**, 75.
346. A. W. Addison, T. N. Rao, J. Reedijk, J. van Rijn, G. C. Verschoor, *Dalton Trans.*, 1984, 1349.
347. B. J. Coe, S. J. Glenwright, *Coord. Chem. Rev.*, 2000, **203**, 5; K. M. Anderson, A. G. Orpen, *Chem. Commun.*, 2001, 2682.
348. A search of the Cambridge Structural Database (CSD) on 29/08/10 for five-coordinate N_3OZnCl complexes yielded 25 hits, of which 11 are cationic.
349. M. A. Shipman, C. Price, A. E. Gibson, M. R. J. Elsegood, W. Clegg, A. Houlton, *Chem. Eur. J.*, 2000, **6**, 4371.
350. A search of the CSD on 29/08/10 for five-coordinate zinc complexes with a coordinated methoxyaryl group yielded 9 hits.
351. E. Bukhaltsev, I. Goldberg, A. Vigalok, *Organometallics*, 2005, **24**, 5732.
352. A. L. Spek, *J. Appl. Cryst.*, 2003, **36**, 7.

353. G. R. Desiraju, T. Steiner, *The Weak Hydrogen Bond in Structural Chemistry and Biology*, Oxford University Press, Oxford, 1999.
354. K. Yoon, G. Parkin, *J. Am. Chem. Soc.*, 1991, **113**, 8414.
355. K. Fujisawa, Y. Matsunaga, N. Ibi, N. Amir, Y. Miyashita, K. Okamoto, *Bull. Chem Soc. Jpn.*, 2006, **79**, 1894.
356. J. S. Klitzke, T. Roisnel, J.-F. Carpentier, O. L. Casagrande, Jr., *Inorg. Chim. Acta*, 2009, **362**, 4585.
357. Y. D. M. Champouret, W. J. Nodes, J. A. Scrimshire, K. Singh, G. A. Solan, I. Young, *Dalton Trans.*, 2007, 4565.
358. R. J. Wright, A. D. Phillips, S. Hino, P. P. Power, *J. Am. Chem. Soc.*, 2005, **127**, 4794.
359. For reviews see: (a) C. Janiak, *Coord. Chem. Rev.*, 1997, **163**, 107; (b) P. Ghosh, A. L. Rheingold, G. Parkin, *Inorg. Chem.*, 1999, **38**, 5464; (c) L. H. Gade, *Dalton Trans.*, 2003, 267; (d) K. Akhbari, A. Morsali, *Coord. Chem. Rev.*, 2010, **254**, 1977; (e) R. C. Fischer, P. P. Power, *Chem. Rev.*, 2010, **110**, 3877. For a theoretical discussion of thallophilic interactions, see: (f) P. Pyykkö, M. Straka, T. Tamm, *Phys. Chem. Chem. Phys.*, 1999, **1**, 3441; (g) C. Janiak, R. Hoffmann, *J. Am. Chem. Soc.*, 1990, **112**, 5924.
360. A. L. Rheingold, L. M. Liable-Sands, S. Trofimenko, *Chem. Commun.*, 1997, 1691.
361. G. Ferguson, M. C. Jennings, F. J. Lalor, C. Shanahan, *Acta Crystallog., Sect. C: Cryst. Struct. Commun.*, 1991, **C47**, 2079.
362. P. L. Jones, K. L. V. Mann, J. C. Jeffery, J. A. McCleverty, M. D. Ward, *Polyhedron*, 1997, **16**, 2435.
363. W. Kaminsky, A. Funck, H. Hähnsen, *Dalton Trans.*, 2009, 8803.
364. K. W. Doak in *Encyclopaedia of Polymer Science and Engineering*, H. F. Mark, Ed., Wiley-Interscience, New York, 1986, Vol. 6, pg 386.
365. L. L. Böhm, *Angew. Chem. Int. Ed. Engl.*, 2003, **42**, 5010; V. Busico, *Macromol. Chem. Phys.*, 2007, **208**, 26; V. Busico, *Dalton Trans.*, 2009, 8794.
366. M. P. McDaniel, *Adv. Catal.*, 2010, **53**, 123.
367. W. Kaminsky, *J. Polym. Sci., Part A: Polym. Chem.*, 2004, **42**, 3911.
368. J. F. Hagman, J. W. Crary in *Encyclopaedia of Polymer Science and Engineering*, H. F. Mark, N. M. Bikales, C. G. Overberger, G. Menges, J. I. Kroschwitz, Eds., Wiley-Interscience, New York, 1985, Vol. 1, pg 325.
369. A. M. Al-Jarallah, J. A. Anabtawi, M. A. B. Siddiqui, A. M. Aitani, A. W. Al-Sa'doun, *Catal. Today*, 1992, **14**, 1.
370. For reviews of late transition metal-catalysed olefin polymerisation see: (a) G. J. P. Britovsek, V. C. Gibson, D. F. Wass, *Angew. Chem. Int. Ed. Engl.*, 1999, **38**, 428; (b) S. D. Ittel, L. K. Johnson, M. Brookhart, *Chem. Rev.*, 2000, **100**, 1169; (c) V. C. Gibson, S. K. Spitzmesser, *Chem. Rev.*, 2003, **103**, 283; (d) J.-Y. Dong, Y. Hu, *Coord. Chem. Rev.*, 2006, **250**, 47; (e) Z. Guan, C. S. Popeney, *Top. Organomet. Chem.*, 2009, **26**, 179; (f) D. Takeuchi, *Dalton Trans.*, 2010, 311.
371. L. K. Johnson, S. Mecking, M. Brookhart, *J. Am. Chem. Soc.*, 1996, **118**, 267.
372. S. A. Svejda, L. K. Johnson, M. Brookhart, *J. Am. Chem. Soc.*, 1999, **121**, 10634; M. D. Leatherman, S. A. Svejda, L. K. Johnson, M. Brookhart, *J. Am. Chem. Soc.*, 2003, **125**, 3068.
373. Z. Guan, *Chem. Eur. J.*, 2002, **8**, 3087.
374. G. J. Domski, J. M. Rose, G. W. Coates, A. D. Bolig, M. Brookhart, *Prog. Polym. Sci.*, 2007, **32**, 30.
375. J. D. Azoulay, Y. Schneider, G. B. Galland, G. C. Bazan, *Chem. Commun.*, 2009, 6177.

376. S. Zai, F. Liu, H. Gao, C. Li, G. Zhou, S. Cheng, L. Guo, L. Zhang, F. Zhu, Q. Wu, *Chem. Commun.*, 2010, 4321.
377. R. D. Shannon, *Acta Crystallogr., Sect. A: Found. Crystallogr.*, 1976, **A32**, 751.
378. F. A. Kunrath, R. F. de Souza, O. L. Casagrande, Jr., N. R. Brooks, V. G. Young, Jr., *Organometallics*, 2003, **22**, 4739.
379. S. Senda, Y. Ohki, T. Hirayama, D. Toda, J.-L. Chen, T. Matsumoto, H. Kawaguchi, K. Tatsumi, *Inorg. Chem.*, 2006, **45**, 9914.
380. P. C. Junk, J. W. Steed, *Inorg. Chim. Acta*, 2007, **360**, 1661.
381. H.-T. Wang, Y.-Y. Song, M. Y. Chiang, W.-F. Zeng, *Acta Crystallogr., Sect. E: Struct. Rep. Online*, 2006, **E62**, m2464.
382. A search of the CSD on 27/10/10 for four-coordinate N_2ONiX complexes yielded 3 hits.
383. J. Li, D. Tian, H. Song, C. Wang, X. Zhu, C. Cui, J.-P. Cheng, *Organometallics*, 2008, **27**, 1605.
384. A search of the CSD on 27/10/10 for hydrogen-bonding interactions between $CHCl_3$ and triflate yielded 94 hits, with CH---O distances in the range 1.640-2.716 Å.
385. P. J. Desrochers, J. Telser, S. A. Zvyagin, A. Ozarowski, J. Krzystek, D. A. Vicic, *Inorg. Chem.*, 2006, **45**, 8930.
386. D. J. Harding, P. Harding, H. Adams, *Acta Crystallogr., Sect. E: Struct. Rep. Online*, 2009, **E65**, m773.
387. T. R. Belderraín, M. Paneque, E. Carmona, E. Gutiérrez-Puebla, M. A. Monge, C. Ruiz-Valero, *Inorg. Chem.*, 2002, **41**, 425.
388. A search of the CSD on 30/11/10 for five-coordinate N_3ONiX complexes yielded 6 hits.
389. Y. Shimazaki, S. Huth, S. Karasawa, S. Hirota, Y. Naruta, O. Yamauchi, *Inorg. Chem.*, 2004, **43**, 7816.
390. A search of the CSD on 30/11/10 for complexes of any coordination number bearing one or more nickel-methoxyaryl interactions yielded 23 hits, with Ni-O distances in the range 2.077-2.398 Å (mean = 2.222 Å).
391. C.-W. Yeh, H.-L. Hu, R.-H. Liang, K.-M. Wang, T.-Y. Yen, J.-D. Chen, J.-C. Wang, *Polyhedron*, 2005, **24**, 539.
392. S. Hazra, R. Koner, P. Lemoine, E. C. Sañudo, S. Mohanta, *Eur. J. Inorg. Chem.*, 2009, 3458.
393. R. Santi, A. M. Romano, A. Sommazzi, M. Grande, C. Bianchini, G. Mantovani, *J. Mol. Catal. A: Chem.*, 2005, **229**, 191.
394. J. Zhang, Z. Ke, F. Bao, J. Long, H. Gao, F. Zhu, Q. Wu, *J. Mol. Catal. A: Chem.*, 2006, **249**, 31.
395. Y. Li, L. Wang, H. Gao, F. Zhu, Q. Wu, *Appl. Organomet. Chem.*, 2006, **20**, 436.
396. G. B. Galland, R. F. de Souza, R. S. Mauler, F. F. Nunes, *Macromolecules*, 1999, **32**, 1620 and references therein.
397. A. Jurkiewicz, N. W. Eilerts, E. T. Hsieh, *Macromolecules*, 1999, **32**, 5471 and references therein.
398. A. J. Brandolini, D. Hills, *NMR Spectra of Polymers and Polymer Additives*, Marcel Dekker, New York, 2000.
399. J. A. Samuels, E. B. Lobkovsky, W. E. Streib, K. Folting, J. C. Huffman, J. W. Zwanziger, K. G. Caulton, *J. Am. Chem. Soc.*, 1993, **115**, 5093.
400. *CrysAlis PRO and CrysAlis RED*, Oxford Diffraction Ltd, Abingdon, UK, 2007.
401. *COLLECT*, Bruker-Nonius B.V. Delft, The Netherlands, 1999.
402. Z. Otwinowski, W. Minor, *Methods Enzymol.*, 1996, **276**, 307.
403. R. H. Blessing, *Acta Crystallogr., Sect. A: Found. Crystallogr.*, 1995, **A51**, 33.

404. G. M. Sheldrick, *Acta Crystallogr., Sect. A: Found. Crystallogr.*, 2008, **A64**, 112.
405. A. Altomare, G. Cascarano, C. Giacovazzo, A. Guagliardi, *J. Appl. Crystallogr.*, 1993, **26**, 343.
406. L. J. Farrugia, *J. Appl. Crystallogr.*, 1997, **30**, 565.
407. C. F. Macrae, I. J. Bruno, J. A. Chisholm, P. R. Edgington, P. McCabe, E. Pidcock, L. Rodriguez-Monge, R. Taylor, J. van de Streek, P. A. Wood, *J. Appl. Crystallogr.*, 2008, **41**, 466.

Appendix – Crystallographic Data Collection and Refinement Details

	L^1	L^{10}	L^{11}	$(L^1)Cr(CO)_3$	$(L^1)Mo(CO)_3$	$[(L^8)ZnCl]_2[Zn_2Cl_6]$
Formula	$C_{34}H_{43}N_3$	$C_{37}H_{49}N_3$	$C_{40}H_{55}N_3$	$C_{37}H_{43}CrN_3O_3$	$C_{37}H_{43}MoN_3O_3$	$C_{70}H_{90}Cl_8N_6O_2Zn_4$
Formula Weight	493.71	535.79	577.87	629.74	685.69	1592.64
Crystal System	Monoclinic	Monoclinic	Monoclinic	Trigonal	Trigonal	Orthorhombic
Space group	P21/c	P21/n	P21/n	P-3c1	P-3c1	Pna21
***a* [Å]**	13.7441(2)	9.8756(2)	9.7230(3)	14.5311(4)	14.8240(4)	16.9695(6)
***b* [Å]**	10.8258(2)	19.9334(4)	15.1749(4)	14.5311(4)	14.8240(4)	12.3728(4)
***c* [Å]**	20.3707(4)	17.1360(4)	24.1171(8)	18.4788(10)	18.5430(4)	35.8339(11)
α [°]	90	90	90	90	90	90
β [°]	102.621(1)	104.999(1)	90.548(1)	90	90	90
γ [°]	90	90	90	120	120	90
V [Å^3]	2957.74(9)	3258.37(12)	3558.21(19)	3379.1(2)	3528.92(15)	7523.7(4)
Z	4	4	4	4	4	4
D (calcd.) [gcm^{-3}]	1.109	1.092	1.079	1.238	1.315	1.406
μ [mm^{-1}]	0.064	0.063	0.062	0.315	0.410	1.590
T [K]	120	150	120	120	200	100
θ [°]	1.5-28.3	2.9-25.0	1.6-24.0	2.1-29.6	3.0-26.5	4.1-25.0
Reflections measured	7205	40515	10910	25211	4602	38922
Unique reflections (R_{int})	7205 (0)	5711 (0.065)	5590 (0.111)	3416 (0.085)	2450 (0.036)	12856 (0.063)
Obs. data [I > 2.0 σ(I)]	4610	4406	2742	3035	1721	12227
R	0.0508	0.0589	0.0573	0.0445	0.0395	0.0954
***wR*$_2$**	0.1882	0.1696	0.1297	0.1217	0.0882	0.2050
S	0.99	1.05	0.96	1.08	1.03	1.19

	$[(L^{12})ZnCl]_2[Zn_2Cl_6]$	$[(L^{16})ZnCl]_2[Zn_2Cl_6]$	$[(L^1)ZnCl][BAr^F_4].¼CH_2Cl_2$	$[(L^8)ZnCl][BAr^F_4].1½CH_2Cl_2$	$[(L^{12})ZnCl][BAr^F_4]$	$[(\eta^4\text{-}L^{16})ZnCl][BAr^F_4]$
Formula	½($C_{74}H_{98}Cl_8N_6Zn_4$)	½($C_{72}H_{94}Cl_8N_6O_4Zn_4$)	$C_{265}H_{222}B_4Cl_6F_{96}N_{12}Zn_4$	$C_{137}H_{120}Cl_8N_6O_2Zn_2B_2F_{48}$	$C_{69}H_{61}ClN_3ZnBF_{24}$	$C_{68}H_{59}ClN_3O_2ZnBF_{24}$
Formula Weight	808.37	826.35	5915.97	3228.37	1499.86	1517.83
Crystal System	Monoclinic	Monoclinic	Monoclinic	Triclinic	Orthorhombic	Monoclinic
Space group	C2/c	P21/c	P21/c	P-1	Pbca	P21/c
a	39.217(3)	12.3610(14)	35.024(1)	12.9161(4)	19.920(5)	20.1685(7)
b	12.0585(6)	26.651(2)	13.2240(4)	14.5491(4)	17.083(5)	19.3848(7)
c	16.8057(9)	12.6833(14)	30.8390(7)	19.2638(5)	40.861(5)	17.4715(7)
α [°]	90	90	90	78.466(2)	90	90
β [°]	97.262(5)	111.999(13)	105.838(1)	86.366(2)	90	94.974(3)
γ [°]	90	90	90	88.067(3)	90	90
V [Å^3]	7883.6(8)	3874.1(8)	13741.1(7)	3538.95(17)	13905(6)	6805.0(4)
Z	8	4	2	1	8	4
D (calcd.) [gcm^{-3}]	1.362	1.417	1.430	1.515	1.433	1.482
μ [mm^{-1}]	1.517	1.549	0.523	0.606	0.499	0.513
T [K]	100	100	150	100	100	100
θ [°]	3.0-24.0	2.9-23.3	3.0-22.0	2.7-23.3	2.8-23.3	2.6-28.3
Reflections measured	18411	13078	28891	16170	23264	33929
Unique reflections (R_{int})	5200 (0.077)	5395 (0.123)	16569 (0.155)	10136 (0.048)	9929 (0.065)	16844 (0.045)
Obs. data [I > 2.0 σ(I)]	3125	3578	5663	6159	5845	9654
R	0.0437	0.1051	0.0969	0.0450	0.0502	0.0391
***wR*$_2$**	0.0857	0.2319	0.2166	0.1003	0.1081	0.0744
S	0.91	1.17	1.25	0.87	0.90	0.82

	[(L^{8})ZnCl][OTf]	[(L^{10})ZnCl][OTf]	[(L^{11})ZnCl][OTf]	[(L^{12})ZnCl][OTf]	[(L^{1})Tl][BAr$^{F}_{4}$].½C$_6$H$_{14}$
Formula	$C_{36}H_{45}ClN_3O_4ZnF_3S$	$C_{38}H_{49}ClN_3O_3ZnF_3S$	$C_{41}H_{55}ClN_3O_3ZnF_3S$	$C_{38}H_{49}ClN_3O_3ZnF_3S$	$C_{69}H_{62}N_3TlBF_{24}$
Formula Weight	773.66	785.71	827.79	785.71	1604.41
Crystal System	Triclinic	Monoclinic	Monoclinic	Triclinic	Triclinic
Space group	P-1	P21/n	P21/n	P-1	P-1
***a* [Å]**	9.2958(5)	12.2019(6)	13.9663(3)	9.0319(4)	12.8319(4)
***b* [Å]**	12.8161(5)	16.8688(8)	14.4512(3)	11.6885(9)	16.0697(5)
***c* [Å]**	17.0823(7)	18.9293(8)	20.6065(5)	19.9915(16)	17.3854(6)
α [°]	82.290(3)	90	90	74.168(7)	98.692(3)
β [°]	89.416(4)	92.820(4)	92.323(2)	80.172(5)	105.005(3)
γ [°]	78.660(4)	90	90	70.766(6)	90.030(2)
V [Å^3]	1977.07(16)	3891.5(3)	4155.59(16)	1909.5(2)	3420.0(2)
Z	2	4	4	2	2
D (calcd.) [gcm^{-3}]	1.300	1.341	1.323	1.367	1.558
μ [mm^{-1}]	0.795	0.807	0.759	0.822	2.470
T [K]	100	100	100	100	100
θ [°]	2.7-26.4	2.9-26.4	2.8-26.4	2.5-30.5	2.7-26.4
Reflections measured	13853	15575	29648	19279	24638
Unique reflections (R_{int})	8079 (0.035)	7948 (0.047)	8485 (0.046)	11087 (0.040)	13958 (0.037)
Obs. data [I > 2.0 σ(I)]	6310	5263	5904	7445	10498
R	0.0338	0.0330	0.0307	0.0365	0.0346
wR$_2$	0.0881	0.0651	0.0771	0.0752	0.0611
S	0.98	0.85	0.89	0.87	0.88

	[(L^{8})Tl][BAr$^{F}_{4}$]	[(L^{8})NiBr]$_2$[NiBr$_4$].2CH$_2$Cl$_2$	[(L^{10})NiBr]$_2$[NiBr]$_4$	[{(L^{7})Ni(μ-Br)}$_2$][BAr$^{F}_{4}$]$_2$	[{(L^{8})Ni(μ-Br)}$_2$][BAr$^{F}_{4}$]$_2$.2CH$_2$Cl$_2$
Formula	$C_{67}H_{57}N_3OTlBF_{24}$	$C_{72}H_{94}N_6O_2Cl_4Br_6Ni_3$	$C_{74}H_{98}Br_6N_6Ni_3$	$C_{132}H_{110}Br_2N_6Ni_2B_2F_{48}$	$C_{136}H_{118}Br_2Cl_4N_6Ni_2O_2B_2F_{48}$
Formula Weight	1591.35	1872.80	1727.05	2991.06	3220.96
Crystal System	Triclinic	Monoclinic	Monoclinic	Triclinic	Triclinic
Space group	P-1	C2/c	P21/c	P-1	P-1
a	14.5773(6)	30.706(2)	17.3320(12)	14.5663(5)	13.5765(5)
b	15.7349(6)	14.3904(7)	12.2810(11)	14.8071(6)	15.2026(5)
c	16.0545(5)	21.5887(14)	36.282(3)	16.3965(6)	18.1596(6)
α [°]	116.290(3)	90	90	82.985(3)	109.331(3)
β [°]	90.363(3)	114.204(7)	102.003(3)	85.599(3)	91.585(3)
γ [°]	95.185(3)	90	90	69.118(4)	91.760(3)
V [Å^3]	3283.6(2)	8700.8(10)	7553.9(11)	3277.4(2)	3532.3(2)
Z	2	4	4	1	1
D (calcd.) [gcm^{-3}]	1.610	1.430	1.519	1.515	1.514
μ [mm^{-1}]	2.573	3.562	3.958	1.017	1.024
T [K]	100	100	120	100	100
θ [°]	2.5-28.3	2.7-22.0	4.1-23.3	2.9-26.4	2.7-23.3
Reflections measured	30023	11599	6920	19471	19917
Unique reflections (R_{int})	16258 (0.031)	5215 (0.039)	6920 (0)	13225 (0.033)	10004 (0.041)
Obs. data [I > 2.0 σ(I)]	12770	3313	3401	7889	6589
R	0.0329	0.0496	0.0981	0.0408	0.0468
wR$_2$	0.0681	0.1328	0.3082	0.0859	0.1359
S	0.93	0.95	1.03	0.86	1.04

	[{(L^3)Ni(μ-Br)(OH_2)}$_2$][BAr^F_4]$_2$	[{(L^5)Ni(μ-Br)(OH_2)}$_2$][BAr^F_4]$_2$.$C_6H_4F_2$	[{(L^{12})Ni(μ-Br)(OH_2)}$_2$][BAr^F_4]$_2$.CH_2Cl_2	[(L^{10})NiBr][BAr^F_4]	[(L^{11})NiBr][BAr^F_4]
Formula	$C_{134}H_{116}Br_2N_6Ni_2O_2B_2F_{48}$	$C_{144}H_{124}Br_2N_6O_2Ni_2B_2F_{50}$	$C_{139}H_{124}Br_2Cl_2N_6O_2Ni_2B_2F_{48}$	$C_{69}H_{61}N_3BrNiBF_{24}$	$C_{72}H_{67}BrN_3NiBF_{24}$
Formula Weight	1525.56	3217.28	3190.13	1537.61	1579.69
Crystal System	Monoclinic	Triclinic	Triclinic	Monoclinic	Triclinic
Space group	P21/c	P-1	P-1	P21/c	P-1
a **[Å]**	15.3634(5)	13.2515(4)	12.4628(6)	19.7184(8)	13.159(5)
b **[Å]**	15.9793(7)	16.3801(6)	16.3902(6)	19.8713(8)	16.366(5)
c **[Å]**	26.8567(12)	17.2248(6)	18.7126(9)	18.2731(6)	20.791(5)
α [°]	90	98.826(3)	69.855(4)	90	71.959(5)
β [°]	92.184(4)	94.171(3)	84.680(4)	104.515(3)	75.604(5)
γ [°]	90	108.203(3)	74.911(4)	90	66.375(5)
V [Å^3]	6588.4(5)	3480.6(2)	3464.8(3)	6931.4(5)	3861(2)
Z	4	1	1	4	2
D (calcd.) [gcm^{-3}]	1.538	1.535	1.529	1.474	1.359
μ [mm^{-1}]	1.015	0.967	1.005	0.964	0.867
T [K]	100	100	100	100	100
θ [°]	2.9-25.0	2.7-26.4	2.6-23.3	2.7-23.3	4.1-25.0
Reflections measured	20249	21486	21483	33294	33769
Unique reflections (*R*$_{int}$)	11588 (0.095)	14108 (0.043)	9727 (0.048)	9908 (0.052)	13587 (0.037)
Obs. data [I > 2.0 σ(I)]	7137	8148	6071	6268	8197
R	0.1071	0.0461	0.0585	0.0768	0.0670
***wR*$_2$**	0.2862	0.0987	0.1736	0.2267	0.2077
S	1.09	0.85	1.03	1.06	1.07

	[(η^4-L^{15})NiBr][BAr^F_4].¼CH_2Cl_2	[(η^4-L^{16})NiBr][BAr^F_4]	[(η^2-L^6)NiBr(THF)][BAr^F_4]	[(L^8)NiBr][OTf]	[(L^{10})NiBr][OTf]
Formula	$C_{281}H_{254}Cl_2Br_4N_{12}O_4Ni_4B_4F_{96}$	$C_{68}H_{59}BrN_3O_2NiBF_{24}$	$C_{76}H_{75}BrN_3ONiBF_{24}$	$C_{36}H_{45}BrN_3O_4NiF_3S$	$C_{38}H_{49}BrN_3O_3NiF_3S$
Formula Weight	6355.46	1555.58	1651.79	811.41	823.46
Crystal System	Monoclinic	Monoclinic	Monoclinic	Monoclinic	Monoclinic
Space group	P21/c	P21/c	C2/c	P21/n	P21/n
a	40.163(3)	19.9798(6)	42.832(5)	12.1179(4)	12.0868(4)
b	20.5896(8)	19.2155(4)	12.811(5)	17.0895(4)	17.1897(6)
c	34.4556(13)	17.6707(4)	34.536(5)	18.6212(5)	18.7371(7)
α [°]	90	90	90	90	90
β [°]	90.607(5)	95.133(2)	125.865(5)	91.703(2)	92.569(3)
γ [°]	90	90	90	90	90
V [Å^3]	28491(3)	6757.0(3)	15358(7)	3854.54(19)	3889.1(2)
Z	4	4	8	4	4
D (calcd.) [gcm^{-3}]	1.482	1.529	1.429	1.398	1.406
μ [mm^{-1}]	0.960	0.992	0.876	1.649	1.633
T [K]	100	100	100	100	100
θ [°]	2.7-25.0	2.7-26.4	2.8-20.8	2.6-26.4	2.6-26.4
Reflections measured	100661	26618	25616	24083	16395
Unique reflections (*R*$_{int}$)	50066 (0.097)	13773 (0.050)	8019 (0.061)	7869 (0.034)	7944 (0.057)
Obs. data [I > 2.0 σ(I)]	25931	8183	4725	6352	4957
R	0.0549	0.0380	0.0369	0.0765	0.0345
***wR*$_2$**	0.1031	0.0705	0.0697	0.1831	0.0613
S	0.86	0.86	0.84	1.24	0.82

	[(L^{11})NiBr][OTf].$CHCl_3$	[(L^{12})NiBr][OTf]	[(η^4-L^{15})NiBr][OTf].CH_2Cl_2	[(η^4-L^{16})NiBr][OTf]	(η^2-L^6)$NiBr_2$
Formula	$C_{42}H_{56}Cl_3BrN_3O_3NiF_3S$	$C_{38}H_{49}BrN_3O_3NiF_3S$	$C_{40}H_{53}Cl_2BrN_3O_4NiF_3S$	$C_{37}H_{47}BrN_3O_5NiF_3S$	$C_{40}H_{55}Br_2N_3Ni$
Formula Weight	984.91	823.46	938.41	841.44	796.36
Crystal System	Monoclinic	Triclinic	Triclinic	Orthorhombic	Monoclinic
Space group	P21/c	P-1	P-1	Pca21	P21/n
***a* [Å]**	13.430(5)	9.0561(4)	11.2197(10)	21.5889(6)	13.0327(6)
***b* [Å]**	21.372(5)	11.7027(5)	13.4063(8)	13.0631(6)	15.7007(7)
***c* [Å]**	16.275(5)	19.9835(8)	16.3188(7)	27.6430(12)	19.4141(10)
α [°]	90	73.858(4)	95.573(4)	90	90
β [°]	93.577(5)	80.437(4)	103.793(5)	90	95.918(4)
γ [°]	90	70.527(4)	109.530(7)	90	90
V [$Å^3$]	4662(3)	1911.69(15)	2204.3(3)	7795.8(5)	3951.4(3)
Z	4	2	2	8	4
D (calcd.) [gcm^{-3}]	1.403	1.431	1.414	1.434	1.339
μ [mm^{-1}]	1.541	1.661	1.569	1.635	2.543
T [K]	100	100	100	100	100
θ [°]	2.7-24.7	2.7-28.3	2.7-26.4	2.9-26.4	2.8-25.0
Reflections measured	14870	16397	15463	30670	12039
Unique reflections (R_{int})	7906 (0.051)	9457 (0.043)	8992 (0.057)	14443 (0.047)	6937 (0.051)
Obs. data [I > 2.0 σ(I)]	4621	6161	5958	9313	4130
R	0.0622	0.0388	0.0427	0.0541	0.0404
***wR*$_2$**	0.1651	0.0837	0.0999	0.1283	0.0858
S	0.94	0.86	0.90	0.93	0.83